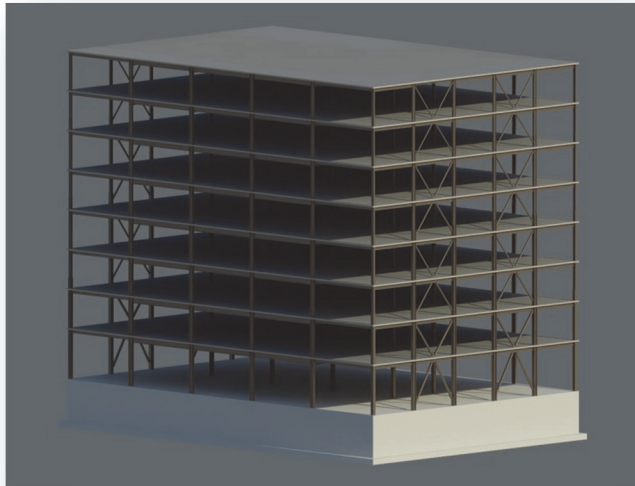


NIST Technical Note 1863-1



Assessment of First Generation Performance-Based Seismic Design Methods for New Steel Buildings

Volume 1: Special Moment Frames



John L. Harris III
Matthew S. Speicher

This publication is available free of charge from:
<http://dx.doi.org/10.6028/NIST.TN.1863-1>



NIST
National Institute of
Standards and Technology
U.S. Department of Commerce

NIST Technical Note 1863-1

Assessment of First Generation Performance- Based Seismic Design Methods for New Steel Buildings

Volume 1: Special Moment Frames

John L. Harris III

Matthew S. Speicher

Materials and Structural Systems Division

Engineering Laboratory

This publication is available free of charge from:
<http://dx.doi.org/10.6028/NIST.TN.1863-1>

February 2015



U.S. Department of Commerce
Penny Pritzker, Secretary

National Institute of Standards and Technology
*Willie May, Acting Under Secretary of Commerce for Standards
and Technology and Acting Director*

Disclaimers

Certain commercial software, equipment, instruments, or materials may have been used in the preparation of information contributing to this report. Identification in this report is not intended to imply recommendation or endorsement by NIST, nor is it intended to imply that such software, equipment, instruments, or materials are necessarily the best available for the purpose.

NIST policy is to use the International System of Units (metric units) in all its publications. In this report, however, information is presented in U.S. Customary Units (inch-pound), as this is the preferred system of units in the U.S. earthquake engineering industry.

**National Institute of Standards and Technology Technical Note 1863-1
Natl. Inst. Stand. Technol. Tech Note 1863-1, 300 pages (February 2015)
CODEN: NTNOEF**

**This publication is available free for charge from:
<http://dx.doi.org/10.6028/NIST.TN.1863-1>**

Preface

In June 2008, the National Earthquake Hazards Reduction Program (NEHRP) sponsored a Performance-Based Seismic Design (PBSD) workshop for leading practitioners and researchers from around the United States to develop a comprehensive list of research needs to foster full development and implementation of PBSD. From this workshop, the Building Seismic Safety Council (BSSC) reported a prioritized list of key PBSD research and implementation needs in NIST GCR 09-917-2: *Research Required to Support Full Implementation of Performance-Based Seismic Design* (NIST 2009a). The highest priority need identified in this report was to “benchmark” current PBSD methodologies (e.g., ASCE/SEI 41-06: *Seismic Rehabilitation of Existing Buildings* (ASCE 2006)—hereafter referred to as ASCE 41) with code procedures for design of new buildings. Two observations from the report were that among workshop participants (1) ASCE 41 procedures are perceived to be overly conservative and (2) existing PBSD methods are not accepted by practitioners as providing a uniform level of confidence. A supporting reason for these two observations was that no systematic effort had been undertaken to benchmark structural performance as determined using ASCE 41 procedures, together with widely accepted procedures for designing new buildings using ASCE/SEI 7-10: *Minimum Design Loads for Buildings and Other Structures* (ASCE 2010)—hereafter referred to as ASCE 7.

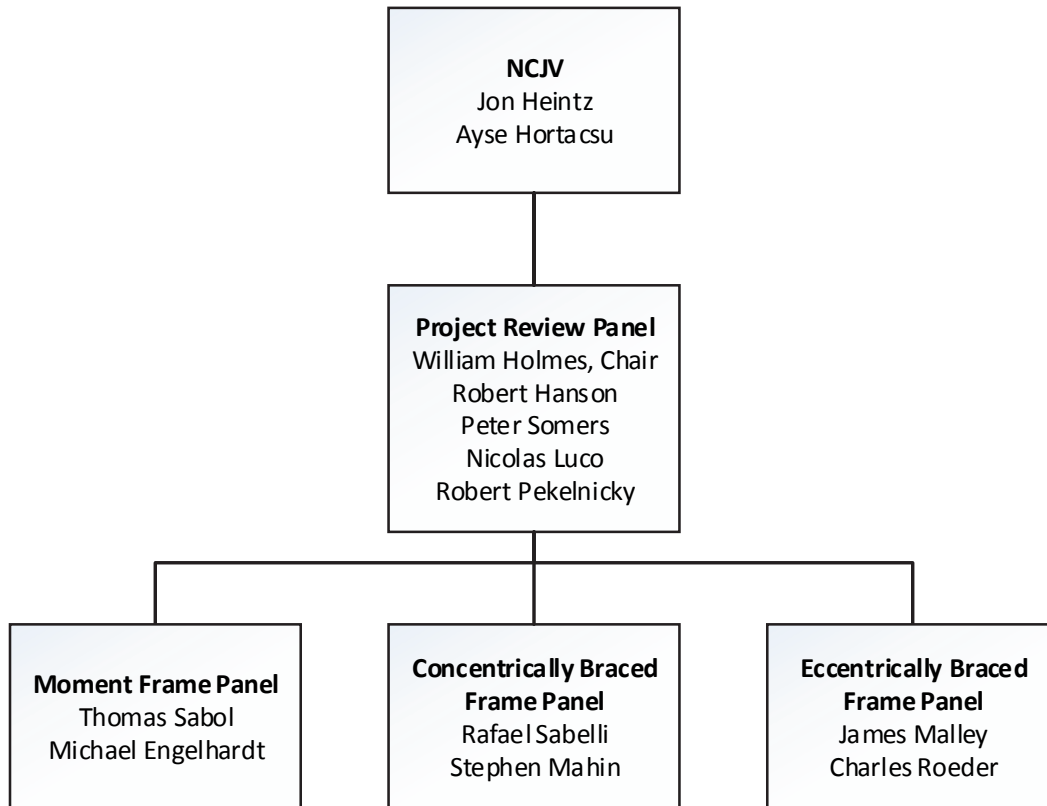
Work was initiated at the National Institute of Standards and Technology (NIST) to support this priority study under the *Assessment of Design Methods in Existing PBSD Standards Project*. This task was conducted by the Earthquake Risk Reduction in Buildings and Infrastructure group, the research division of the NEHRP Office at NIST. This research involves problem-focused studies in PBSD assessing the applicability and accuracy of implementing first-generation PBSD analysis methods now used for evaluating existing buildings in the performance-based design of new buildings. The current study focuses on buildings with lateral systems utilizing structural steel frames. This project evaluates the results of the studies and identifies changes to current model building codes and standards provisions that will encourage more universal use of PBSD. The volume of data required to illustrate the results and conclusions necessitated three separate reports, as follows:

- Volume 1: Special Moment Frames (this report)
- Volume 2: Special Concentrically Braced Frames
- Volume 3: Eccentrically Braced Frames

A fourth report, Volume 4: Buckling Restrained Braced Frames, is under development.

A peer review panel (PRP) was engaged under a contract with the NEHRP Consultants Joint Venture (NCJV)—www.nehrp-consultants.org. The PRP was tasked to complement the NIST project by providing, where needed, individual subject matter expert guidance to improve the technical detail and outcome of the project; provide technical support on specific topics on seismic hazard analysis, ground motion scaling for

varying return periods, nonlinear dynamic analysis, structural behavior and design of building structures; and provide peer review services. The review panel for this project was structured as follows:



Jon Heintz (Program Manager)
Applied Technology Council
201 Redwood Shores Parkway, Suite 240
Redwood City, California 94065

Ayse Hortacsu (Project Manager)
Applied Technology Council
201 Redwood Shores Parkway, Suite 240
Redwood City, California 94065

Michael Engelhardt
The University of Texas at Austin
Dept. of Civil, Arch. and Environ. Eng.
301 East Dean Keeton St., Stop C1747
Austin, TX 78712

Robert Hanson
University of Michigan, Emeritus
5885 Dunabbey Loop
Dublin, Ohio 43017

William Holmes (PRP Chair)
Rutherford + Chekene
55 Second Street, Suite 600
San Francisco, California 94105

Nicolas Luco
U.S. Geological Survey
Box 25046 – DFC – MS 966
Denver, Colorado 80225

Stephen Mahin
University of California, Berkeley
Dept. of Civil and Environ. Eng.
777 Davis Hall
Berkeley, California 94720

James Malley
Degenkolb Engineers
235 Montgomery St., Suite 500
San Francisco, California 94104

Robert Pekelnicky
Degenkolb Engineers
235 Montgomery St., Suite 500
San Francisco, California 94104

Charles Roeder
University of Washington
Dept. of Civil and Environ. Eng.
Box 352700
Seattle, WA 98195

Rafael Sabelli
Walter P. Moore
595 Market St., Suite 2130
San Francisco, California 94105

Thomas Sabol
Englekirk Institutional
2116 Arlington Ave.
Los Angeles, California 90018

Peter Somers
Magnusson Klemencic Associates
1301 Fifth Ave., Suite 3200
Seattle, WA 98101

The authors gratefully acknowledge the members of the PRP for their input and guidance during this project and in the preparation of report volumes 1-3. Further, the authors wish to thank Jon Heintz and Ayse Hortacsu at Applied Technology Council for management of Task Order 12. Special thanks are also extended to Jack Hayes (NEHRP Director), Steve McCabe (NEHRP Deputy Director), and Bob Pekelnicky for reviewing the final NIST reports.

John L. Harris III
Research Structural Engineer
jay.harris@nist.gov

Matthew S. Speicher
Research Structural Engineer
matthew.speicher@nist.gov

National Institute of Standards and Technology
Engineering Laboratory
National Earthquake Hazards Reduction Program Office
100 Bureau Dr., MS 8604
Gaithersburg, MD 20899

Table of Contents

Preface	iii
Table of Contents	vii
List of Tables	xiii
List of Figures	xvii
List of Abbreviations	xxv
Executive Summary	xxvii
Chapter 1 Introduction	1-1
1.1 Project Motivation and Background.....	1-3
1.2 Scope of Project	1-5
Chapter 2 Overview and Design of Archetype Buildings	2-1
2.1 General Information	2-1
2.2 Structural Design Loads	2-5
2.2.1 Load Combinations	2-5
2.2.2 Gravity Loads.....	2-5
2.2.3 Environmental Loads	2-6
2.2.3.1 Earthquake Forces	2-6
2.2.3.2 Wind Forces	2-9
2.3 Structural Analysis and Mathematical Model	2-9
2.4 SFRS Design	2-13
2.4.1 SMF Design.....	2-13
2.4.2 SCBF Design.....	2-22
Chapter 3 Seismic Assessment	3-1
3.1 Assessment Overview	3-1
3.1.1 Seismic Hazard.....	3-3
3.1.2 General Analysis Requirements	3-3
3.1.3 Analysis Procedures	3-5
3.1.3.1 Linear Analysis Procedures.....	3-5
3.1.3.1.1 Linear Static Procedure	3-7

	3.1.3.1.2	Linear Dynamic Procedure.....	3-8
	3.1.3.2	Nonlinear Analysis Procedures	3-8
	3.1.3.2.1	Nonlinear Static Procedure.....	3-9
	3.1.3.2.2	Nonlinear Dynamic Procedure	3-13
	3.1.4	Acceptance Criteria	3-14
	3.1.4.1	Linear Procedures.....	3-15
	3.1.4.1.1	Calculating Component Assessment Results	3-15
	3.1.4.2	Nonlinear Procedures	3-16
	3.1.4.2.1	Calculating Component Assessment Results	3-17
3.2		Moment Frame	3-19
	3.2.1	Assessment Methodology.....	3-19
	3.2.1.1	Linear Procedures.....	3-19
	3.2.1.2	Nonlinear Procedures	3-31
	3.2.2	Seismic Assessment Results.....	3-45
	3.2.2.1	Four-Story Moment Frame.....	3-46
	3.2.2.1.1	Linear Static Procedure	3-46
	3.2.2.1.1.1 BSE-1 Earthquake Hazard Level (LS BPL).....	3-46
	3.2.2.1.1.2 BSE-2 Earthquake Hazard Level (CP BPL).....	3-47
	3.2.2.1.2	Linear Dynamic Procedure.....	3-49
	3.2.2.1.2.1 BSE-1 Earthquake Hazard Level (LS BPL).....	3-49
	3.2.2.1.2.2 BSE-2 Earthquake Hazard Level (CP BPL).....	3-51
	3.2.2.1.3	Nonlinear Static Procedure.....	3-53
	3.2.2.1.4	Nonlinear Dynamic Procedure	3-58
	3.2.2.2	Eight-Story Moment Frame.....	3-66
	3.2.2.2.1	Linear Static Procedure	3-66
	3.2.2.2.1.1 BSE-1 Earthquake Hazard Level (LS BPL).....	3-66
	3.2.2.2.1.2 BSE-2 Earthquake Hazard Level (CP BPL).....	3-68
	3.2.2.2.2	Linear Dynamic Procedure.....	3-70
	3.2.2.2.2.1 BSE-1 Earthquake Hazard Level (LS BPL).....	3-70
	3.2.2.2.2.2 BSE-2 Earthquake Hazard Level (CP BPL).....	3-72
	3.2.2.2.3	Nonlinear Static Procedure.....	3-74
	3.2.2.2.4	Nonlinear Dynamic Procedure	3-82
	3.2.2.3	Sixteen-Story Moment Frame	3-89
	3.2.2.3.1	Linear Static Procedure	3-89
	3.2.2.3.1.1 BSE-1 Earthquake Hazard Level (LS BPL).....	3-89

	3.2.2.3.1.2	BSE-2 Earthquake Hazard Level (CP BPL)	3-92
	3.2.2.3.2	Linear Dynamic Procedure	3-95
	3.2.2.3.2.1	BSE-1 Earthquake Hazard Level (LS BPL).....	3-95
	3.2.2.3.2.2	BSE-2 Earthquake Hazard Level (CP BPL)	3-98
	3.2.2.3.3	Nonlinear Static Procedure	3-101
	3.2.2.3.4	Nonlinear Dynamic Procedure	3-110
3.2.3	Seismic Assessment Discussion.....		3-117
3.2.3.1	Linear Assessment Procedures.....		3-117
3.2.3.1.1	Beam-to-Column Connections.....		3-117
3.2.3.1.2	Panel Zones		3-119
3.2.3.1.3	Member Cross-section Strength (flexural hinge) and Global Strength (member stability).....		3-119
3.2.3.1.4	Summary		3-121
3.2.3.2	Nonlinear Assessment Procedures		3-122
3.2.3.2.1	Beam-to-Column Connections.....		3-122
3.2.3.2.2	Panel Zones		3-123
3.2.3.2.3	Member Cross-section Strength (flexural hinge) and Global Strength (member stability).....		3-124
3.2.3.2.4	Summary		3-126
3.2.3.3	Comparison between Linear and Nonlinear Assessment Results		3-127
Chapter 4	Summary, Conclusions, and Recommendations.....		4-1
4.1	Summary of Project Work.....		4-1
4.2	Assumptions and Limitations of this Study.....		4-3
4.3	Conclusions and Observations		4-5
4.3.1	ASCE 41.....		4-5
4.3.1.1	General		4-5
4.3.1.2	Special Moment Frames.....		4-6
4.4	Recommendations for Future Research.....		4-7
4.4.1	ASCE 41.....		4-7
4.4.1.1	General		4-7
4.4.1.2	Fully Restrained Moment Frames		4-8
4.4.2	ASCE 7.....		4-9
4.4.3	AISC 341 / 360 / 358.....		4-9
4.4.3.1	Special Moment Frames.....		4-9

Appendix A	Ground Motions for Response History Analysis	A-1
A.1	Ground Motion Record Set	A-1
A.2	Ground Motion Selection and Scaling	A-1
A.3	Four-Story Archetype Building.....	A-3
A.3.1	4-Story Special Moment Frame	A-3
A.4	Eight-Story Archetype Building.....	A-6
A.4.1	8-Story Special Moment Frame	A-6
A.5	Sixteen-Story Archetype Building	A-9
A.5.1	16-Story Special Moment Frame	A-9
A.6	FEMA P-695 Far-Field Record Set.....	A-12
Appendix B	Supplemental Design Information and Design Examples.....	B-1
B.1	Horizontal Design Forces.....	B-1
B.1.1	Wind Forces	B-1
B.1.2	Seismic Forces.....	B-3
B.1.2.1	Effective Seismic Weights and Story Gravity Forces	B-3
B.1.2.2	Horizontal Seismic Forces, E-W Direction.....	B-4
B.1.2.2.1	MC4 (Special Moment Frame)	B-4
B.1.2.2.2	MC8 (Special Moment Frame)	B-7
B.1.2.2.3	MC16 (Special Moment Frame)	B-10
B.1.2.3	Horizontal Seismic Forces, N-S Direction	B-13
B.1.2.3.1	MC4 (Special Concentrically Braced Frame)	B-13
B.1.2.3.2	MC8 (Special Concentrically Braced Frame)	B-15
B.1.2.3.3	MC16 (Special Concentrically Braced Frame)	B-18
B.2	Horizontal and Vertical Irregularities.....	B-21
B.2.1	Special Moment Frame	B-21
B.2.2	Special Concentrically Braced Frame	B-23
B.3	SMF AISC Frame Stability (Effective Length Method)	B-25
B.4	Example Design Calculations	B-29
B.4.1	Special Moment Frame Example	B-29
B.4.1.1	Member Selection	B-29
B.4.1.2	SMF Beam and RBS Beam-to-Column Connection	B-30
B.4.1.2.1	Flexural Demand.....	B-30
B.4.1.2.2	Flexural Strength.....	B-30
B.4.1.2.3	Fully Restrained Connection.....	B-31

B.4.1.3	SMF Column.....	B-31
B.4.1.3.1	Axial and Flexural Demand	B-32
B.4.1.3.2	Axial Strength	B-32
B.4.1.3.3	Flexural Strength.....	B-33
B.4.1.3.4	Strength Check	B-33
B.4.1.4	SMF Panel Zone.....	B-34
B.4.1.4.1	Shear Demand	B-34
B.4.1.4.2	Shear Strength	B-35
B.4.1.4.3	Strength Check	B-35
B.4.1.5	SMF Strong-Column / Weak-Beam	B-36
Appendix C	Example Assessment Calculations	C-1
C.1	Linear Assessment Examples.....	C-1
C.1.1	SMF Frame Beam and RBS Beam-to-Column Connection.....	C-1
C.1.1.1	Flexural Demand	C-1
C.1.1.1.1	Frame Beam	C-1
C.1.1.1.2	FR Connection	C-2
C.1.1.2	Flexural Strength.....	C-2
C.1.1.2.1	Beam	C-2
C.1.1.2.2	Fully Restrained Connection.....	C-2
C.1.1.3	Acceptance Criteria.....	C-3
C.1.1.3.1	Beam	C-3
C.1.1.3.2	Fully Restrained Connection.....	C-3
C.1.1.4	Acceptance Criteria Check.....	C-5
C.1.1.4.1	Beam	C-5
C.1.1.4.2	Fully Restrained Connection.....	C-6
C.1.2	SMF Column.....	C-6
C.1.2.1	Axial Demand	C-7
C.1.2.2	Axial Strength	C-7
C.1.2.3	Flexural Demand.....	C-8
C.1.2.4	Flexural Strength.....	C-8
C.1.2.5	Acceptance Criteria Check.....	C-9
C.1.3	SMF Panel Zone.....	C-9
C.1.3.1	Shear Demand	C-9
C.1.3.2	Shear Strength	C-9

	C.1.3.3 Acceptance Criteria	C-9
	C.1.3.4 Acceptance Criteria Check	C-10
C.2	Nonlinear Assessment Examples	C-10
	C.2.1 SMF Beam	C-10
	C.2.1.1 Deformation Demand	C-10
	C.2.1.2 Acceptance Criteria	C-11
	C.2.1.3 Acceptance Criteria Check	C-12
	C.2.2 SMF Column	C-13
	C.2.2.1 Axial Demand	C-13
	C.2.2.2 Axial Strength	C-13
	C.2.2.3 Deformation Demand	C-13
	C.2.2.4 Acceptance Criteria	C-13
	C.2.2.5 Acceptance Criteria Check	C-15
	C.2.3 SMF Panel Zone	C-15
	C.2.3.1 Deformation Demand	C-16
	C.2.3.2 Acceptance Criteria	C-16
	C.2.3.3 Acceptance Criteria Check	C-16
Appendix D References.....		D-1

List of Tables

Table 1-1. Comparison of Seismic Hazard and Associated Performance for ASCE 7 and ASCE 41	1-4
Table 1-2. Performance Comparison between IBC and ASCE 41 – (From IEBC Table 301.1.4.1)	1-4
Table 2-1. Structural Characteristics of Archetype Buildings.....	2-1
Table 2-2. Design Gravity Loads	2-6
Table 2-3. Spectral Response Acceleration Parameters	2-7
Table 2-4. Seismic Analysis and Design Parameters, E-W.....	2-8
Table 2-5. Seismic Analysis and Design Parameters, N-S.....	2-8
Table 3-1. Seismic Performance Targets (from ASCE 41-06).....	3-2
Table 3-2. Seismic Performance Targets (from ASCE 41-13).....	3-2
Table 3-3. Spectral Response Parameters.....	3-3
Table 3-4. Displacement Multiplier—E-W (SMF)	3-6
Table 3-5. Displacement Multiplier—N-S (SCBF).....	3-6
Table 3-6. Analytical Fundamental Periods (seconds).....	3-8
Table 3-7. Empirical Fundamental Periods (seconds).....	3-8
Table 3-8. Story Shear Ratio - ELF	3-12
Table 3-9. Story Shear Ratio - RSA	3-12
Table 3-10. Basic Acceptance Criteria for a W24×84.....	3-22
Table 3-11. Basic <i>m</i> -factors for Linear Procedures, SMF	3-26
Table 3-12. Plastic Rotation Angles for Improved WUF and Column Hinge for a W18×175	3-38
Table 3-13. NSP General Information, 4-Story SMF (kip, inch).....	3-53
Table 3-14. NSP Analysis Parameters, 4-Story SMF BSE-2 CP (kip, inch).....	3-53
Table 3-15. NSP Analysis Parameters— 4-Story SMF BSE-1 LS (kip, inch).....	3-53
Table 3-16. NSP General Information, 8-Story SMF (kip, inch).....	3-75
Table 3-17. NSP Analysis Parameters, 8-Story SMF BSE-2 CP (kip, inch).....	3-75
Table 3-18. NSP Analysis Parameters— 8-Story SMF BSE-1 LS (kip, inch).....	3-75
Table 3-19. NSP General Information, 16-Story SMF (kip, inch).....	3-102
Table 3-20. NSP Analysis Parameters, 16-Story SMF BSE-2 CP (kip, inch).....	3-102
Table 3-21. NSP Analysis Parameters, 16-Story SMF BSE-1 LS (kip, inch).....	3-102
Table 3-22. Performance Summary of FR Connections (BC) per Frame, Linear Procedures	3-118
Table 3-23. Performance Summary of Panel Zones (PZ) per Frame, Linear Procedures	3-119
Table 3-24. Performance Summary of Column Members (CM) per Frame, Linear Procedures	3-120

Table 3-25. BSO Performance Summary of Archetype Buildings, Linear Procedures	3-121
Table 3-26. Summary of Base Shears, Linear Procedures (kips).....	3-122
Table 3-27. Performance Summary of FR Connections (BC) per Frame, Nonlinear Procedures.....	3-123
Table 3-28. Performance Summary of Panel Zones (PZ) per Frame, Nonlinear Procedures.....	3-124
Table 3-29. Performance Summary of Column Hinges (CH) per Frame, Nonlinear Procedures	3-125
Table 3-30. Performance Summary of Column Members (CM) per Frame, Nonlinear Procedures....	3-126
Table 3-31. BSO Performance Summary of Archetype Buildings, Nonlinear Procedures.....	3-126
Table 3-32. BSO Performance Summary of Archetype Buildings.....	3-128
Table A-1. Ground Motion Records for E-W Direction of MC4.....	A-3
Table A-2. Ground Motion Records for E-W Direction of MC8.....	A-6
Table A-3. Ground Motion Records for E-W Direction of MC16.....	A-9
Table B-1. Wind Forces on MC4 (kips).....	B-2
Table B-2. Wind Forces on MC8 (kips).....	B-2
Table B-3. Wind Forces on MC 16 (kips).....	B-2
Table B-4. Effect Seismic Weights and Story Gravity Forces, MC4 (kips).....	B-3
Table B-5. Effect Seismic Weights and Story Gravity Forces, MC8 (kips).....	B-3
Table B-6. Effect Seismic Weights and Story Gravity Forces, MC16 (kips).....	B-4
Table B-7. Seismic Strength Design Forces, E-W MC4	B-4
Table B-8. Seismic Drift Forces, E-W MC4	B-5
Table B-9. ASCE 7 Allowable Drift and Stability Verification, E-W MC4 RSA	B-6
Table B-10. ASCE 7 Allowable Drift and Stability Verification, E-W MC4 ELF	B-7
Table B-11. Seismic Strength Design Forces, E-W MC8	B-7
Table B-12. Seismic Drift Forces, E-W MC8	B-8
Table B-13. ASCE 7 Allowable Drift and Stability Verification, E-W MC8 RSA	B-9
Table B-14. ASCE 7 Allowable Drift and Stability Verification, E-W MC8 ELF	B-9
Table B-15. Summary of Seismic Strength Design Forces, E-W MC16	B-10
Table B-16. Summary of Seismic Drift Forces, E-W MC16	B-11
Table B-17. ASCE 7 Allowable Drift and Stability Verification, E-W MC16 RSA	B-12
Table B-18. ASCE 7 Allowable Drift and Stability Verification, E-W MC16 RSA	B-13
Table B-19. Summary of Seismic Strength Design Forces, N-S MC4	B-13
Table B-20. Summary of Seismic Drift Forces, N-S MC4.....	B-14
Table B-21. ASCE 7 Allowable Drift and Stability Verification, N-S MC4 RSA.....	B-15
Table B-22. ASCE 7 Allowable Drift and Stability Verification, N-S MC4 ELF	B-15
Table B-23. Summary of Seismic Strength Design Forces, N-S MC8	B-16
Table B-24. Summary of Seismic Drift Forces, N-S MC8.....	B-16

Table B-25. ASCE 7 Allowable Drift and Stability Verification, N-S MC8 RSA.....	B-18
Table B-26. ASCE 7 Allowable Drift and Stability Verification, N-S MC8 ELF	B-18
Table B-27. Summary of Seismic Strength Design Forces, N-S MC16	B-18
Table B-28. Summary of Seismic Drift Forces, N-S MC16	B-19
Table B-29. ASCE 7 Allowable Drift and Stability Verification, N-S MC16 RSA.....	B-21
Table B-30. ASCE 7 Allowable Drift and Stability Verification, N-S MC16 ELF	B-21
Table B-31. Horizontal Irregularity Type 1 (a and b) Verification	B-22
Table B-32. Vertical Irregularity Type 1 (a and b) Verification (Exception 1).....	B-22
Table B-33. Vertical Irregularity Type 5 (a and b) Verification, ELF (kip, feet).....	B-23
Table B-34. Vertical Irregularity Type 5 (a and b) Verification, RSA (kip, feet).....	B-23
Table B-35. Horizontal Irregularity Type 1 (a and b) Verification	B-24
Table B-36. Vertical Irregularity Type 1 (a and b) Verification (Using Exception 1).....	B-24
Table B-37. Vertical Irregularity Type 5 (a and b) Verification, ELF (kip, feet).....	B-25
Table B-38. Vertical Irregularity Type 5 (a and b) Verification, RSA (kip, feet).....	B-25
Table B-39. AISC 360 Frame Stability (Effective Length Method), 4-Story SMF ELF (kip, inch).....	B-26
Table B-40. AISC 360 Frame Stability (Effective Length Method), 4-Story SMF RSA (kip, inch).....	B-26
Table B-41. AISC 360 Frame Stability (Effective Length Method), 8-Story SMF ELF (kip, inch).....	B-26
Table B-42. AISC 360 Frame Stability (Effective Length Method), 8-Story SMF RSA (kip, inch).....	B-26
Table B-43. AISC 360 Frame Stability (Effective Length Method), 16-Story SMF ELF (kip, inch).....	B-27
Table B-44. AISC 360 Frame Stability (Effective Length Method), 16-Story SMF RSA (kip, inch).....	B-27
Table B-45. Adjusted Effective Length Factors – 4-Story SMF	B-27
Table B-46. Adjusted Effective Length Factors – 8-Story SMF	B-28
Table B-47. Adjusted Effective Length Factors – 16-Story SMF	B-28
Table B-48. Controlling Load Combinations (kips, feet).....	B-32

List of Figures

Figure 2-1. Isometric View of MC4 Archetype Building	2-2
Figure 2-2. Isometric View of MC8 Archetype Building	2-2
Figure 2-3. Isometric View of MC16 Archetype Building	2-3
Figure 2-4. Typical Floor Framing Plan, MC4 and MC8.....	2-4
Figure 2-5. Typical Floor Framing Plan, MC16.....	2-4
Figure 2-6. Typical FR RBS Beam-to-Column Connection Assembly	2-10
Figure 2-7. FR RBS Beam-To-Column Connection Subassembly Model for Linear Analysis.....	2-11
Figure 2-8. Typical Brace-to-Beam / Column Connection Assembly	2-12
Figure 2-9. Brace-to-Beam / Column Connection Subassembly Model for Linear Analysis	2-12
Figure 2-10. Flow Chart of SMF Design Process	2-14
Figure 2-11. 4-Story SMF Schematic.....	2-17
Figure 2-12. 8-Story SMF Schematic.....	2-18
Figure 2-13. 16-Story SMF Schematic.....	2-20
Figure 2-14. Flow Chart of SCBF Design Process.....	2-22
Figure 2-15. 4-Story SCBF Schematic.....	2-24
Figure 2-16. 8-Story SCBF Schematic	2-25
Figure 2-17. 16-Story SCBF Schematic	2-27
Figure 3-1. Acceleration Response Spectra.....	3-3
Figure 3-2. Generalized Component Backbone Curve (adopted from ASCE 41 Figure C2-1)	3-9
Figure 3-3. NSP Process.....	3-11
Figure 3-4. P - M Interaction on Section m -factor (in-plane) and Member Instability (Primary Component)	3-23
Figure 3-5. Compactness Requirements as a Function of Axial Load Ratio, LS Acceptance Criteria ..	3-24
Figure 3-6. Acceptance Criteria as a Function of Axial Load Ratio and Section Compactness, LS Acceptance Criteria	3-25
Figure 3-7. Frame Capacity Schematic (m -factor), LS and CP, 4-Story SMF ELF.....	3-27
Figure 3-8. Frame Capacity Schematic (m -factor), LS and CP, 4-Story SMF RSA	3-27
Figure 3-9. Frame Capacity Schematic (m -factor), LS and CP, 8-Story SMF ELF	3-28
Figure 3-10. Frame Capacity Schematic (m -factor), LS and CP, 8-Story SMF RSA	3-28
Figure 3-11. Frame Capacity Schematic (m -factor), LS and CP, 16-Story SMF ELF	3-29
Figure 3-12. Frame Capacity Schematic (m -factor), LS and CP, 16-Story SMF RSA	3-30
Figure 3-13. SMF Beam-to-Column Subassembly Analytical Schematic	3-32

Figure 3-14. PERFORM-3D RBS Calibration	3-33
Figure 3-15. PERFORM-3D Panel Zone Calibration	3-34
Figure 3-16. In-plane Flexural Hinge Yield Surface Model (Including Force-Controlled Response) ...	3-36
Figure 3-17. Variation in Acceptance Criteria and Hinge Model for Axial Force	3-36
Figure 3-18. <i>P-M</i> Interaction on Plastic Rotation, LS Acceptance Criteria (Primary Component)	3-37
Figure 3-19. <i>P-M</i> Interaction Curve (Section Yield Surface).....	3-38
Figure 3-20. <i>P-M</i> Interaction Curve (Member Strength).....	3-39
Figure 3-21. Frame Capacity Schematic (Inelastic), YD, LS, and CP, 4-Story SMF ELF	3-40
Figure 3-22. Frame Capacity Schematic (Inelastic), YD, LS, and CP, 4-Story SMF RSA.....	3-40
Figure 3-23. Frame Capacity Schematic (Inelastic), YD, LS, and CP, 8-Story SMF ELF	3-41
Figure 3-24. Frame Capacity Schematic (Inelastic), YD, LS, and CP, 8-Story SMF RSA.....	3-42
Figure 3-25. Frame Capacity Schematic (Inelastic), YD, LS, and CP, 16-Story SMF ELF	3-43
Figure 3-26. Frame Capacity Schematic (inelastic), YD, LS and CP, 16-Story SMF RSA.....	3-44
Figure 3-27. LSP Assessment Results, 4-Story SMF ELF, BSE-1 LS.....	3-46
Figure 3-28. LSP Assessment Results, 4-Story SMF RSA, BSE-1 LS	3-47
Figure 3-29. LSP Assessment Results, Compression in Exterior Columns, 4-Story SMF, BSE-1	3-47
Figure 3-30. LSP Assessment Results, 4-Story SMF ELF, BSE-2 CP	3-48
Figure 3-31. LSP Assessment Results, 4-Story SMF RSA, BSE-2 CP	3-48
Figure 3-32. LSP Assessment Results, Compression in Exterior Columns, 4-Story SMF, BSE-2.....	3-49
Figure 3-33. LDP Assessment Results, 4-Story SMF ELF, BSE-1 LS	3-50
Figure 3-34. LDP Assessment Results, 4-Story SMF RSA, BSE-1 LS	3-50
Figure 3-35. LDP Assessment Results, Compression in Exterior Columns, 4-Story SMF, BSE-1	3-51
Figure 3-36. LDP Assessment Results, 4-Story SMF ELF, BSE-2 CP	3-52
Figure 3-37. LDP Assessment Results, 4-Story SMF RSA, BSE-2 CP	3-52
Figure 3-38. LDP Assessment Results, Compression in Exterior Columns, 4-Story SMF, BSE-2	3-52
Figure 3-39. 4-Story SMF ELF Pushover, BSE-2.....	3-54
Figure 3-40. 4-Story SMF RSA Pushover, BSE-2	3-54
Figure 3-41. 4-Story SMF ELF Pushover – Story Drift Ratios – BSE-2	3-55
Figure 3-42. 4-Story SMF RSA Pushover – Story Drift Ratios – BSE-2.....	3-55
Figure 3-43. Schematic of Flexural Actions in Columns, 4-Story SMF (NSP and NDP).....	3-56
Figure 3-44. NSP Assessment Results, 4-Story SMF ELF, BSE-1 LS (+push to right)	3-57
Figure 3-45. NSP Assessment Results, 4-Story SMF RSA, BSE-1 LS (+push to right)	3-57
Figure 3-46. NSP Assessment Results, 4-Story SMF ELF, BSE-2 CP (+push to right).....	3-57
Figure 3-47. NSP Assessment Results, 4-Story SMF RSA, BSE-2 CP (+push to right)	3-58
Figure 3-48. NDP Assessment Results, Beam Hinges, 4-Story SMF ELF, BSE-1 LS	3-59

Figure 3-49. NDP Assessment Results, Beam Hinges, 4-Story SMF RSA, BSE-1 LS	3-59
Figure 3-50. NDP Assessment Results, Beam Hinges, 4-Story SMF ELF, BSE-2 CP	3-60
Figure 3-51. NDP Assessment Results, Beam Hinges, 4-Story SMF RSA, BSE-2 CP	3-60
Figure 3-52. NDP Assessment Results, Column Hinges, 4-Story SMF ELF, BSE-2 CP	3-61
Figure 3-53. NDP Assessment Results, Column Hinges, 4-Story SMF RSA, BSE-2 CP	3-62
Figure 3-54. NDP Assessment Results, Column Hinges, 4-Story SMF ELF, BSE-2 Yield	3-62
Figure 3-55. NDP Assessment Results, Column Hinges, 4-Story SMF RSA, BSE-2 Yield	3-63
Figure 3-56. NDP Assessment Results, Column Members, 4-Story SMF ELF, BSE-2 CP	3-63
Figure 3-57. NDP Assessment Results, Column Members, 4-Story SMF RSA, BSE-2 CP	3-64
Figure 3-58. NDP Assessment Results, Panel Zones, 4-Story SMF ELF, BSE-2 CP	3-65
Figure 3-59. NDP Assessment Results, Panel Zones, 4-Story SMF RSA, BSE-2 CP	3-65
Figure 3-60. LSP Assessment Results, 8-Story SMF ELF, BSE-1 LS	3-67
Figure 3-61. LSP Assessment Results, 8-Story SMF RSA, BSE-1 LS	3-67
Figure 3-62. LSP Assessment Results, Compression in Exterior Columns, 8-Story SMF, BSE-1	3-68
Figure 3-63. LSP Assessment Results, 8-Story SMF ELF, BSE-2 CP	3-69
Figure 3-64. LSP Assessment Results, 8-Story SMF RSA, BSE-2 CP	3-69
Figure 3-65. LSP Assessment Results, Compression in Exterior Columns, 8-Story SMF, BSE-2	3-70
Figure 3-66. LDP Assessment Results, 8-Story SMF ELF, BSE-1 LS	3-71
Figure 3-67. LDP Assessment Results, 8-Story SMF RSA, BSE-1 LS	3-71
Figure 3-68. LDP Assessment Results, Compression in Exterior Columns, 8-Story SMF, BSE-1	3-72
Figure 3-69. LDP Assessment Results, 8-Story SMF ELF, BSE-2 CP	3-73
Figure 3-70. LDP Assessment Results, 8-Story SMF RSA, BSE-2 CP	3-73
Figure 3-71. LDP Assessment Results, Compression in Exterior Columns, 8-Story SMF, BSE-2	3-74
Figure 3-72. 8-Story SMF ELF Pushover, BSE-2	3-75
Figure 3-73. 8-Story SMF RSA Pushover, BSE-2	3-76
Figure 3-74. 8-Story SMF ELF Pushover – Story Drift Ratios – BSE-2	3-76
Figure 3-75. 8-Story SMF RSA Pushover – Story Drift Ratios – BSE-2	3-77
Figure 3-76. Story Shear Demand to Strength Comparison, ELF	3-78
Figure 3-77. Story Shear Demand to Strength Comparison, RSA	3-78
Figure 3-78. Schematic of Flexural Actions in Columns, 8-Story SMF (NSP and NDP)	3-79
Figure 3-79. NSP Assessment Results, 8-Story SMF ELF, BSE-1 LS (+push to right)	3-80
Figure 3-80. NSP Assessment Results, 8-Story SMF RSA, BSE-1 LS (+push to right)	3-80
Figure 3-81. NSP Assessment Results, 8-Story SMF ELF, BSE-2 CP (+push to right)	3-81
Figure 3-82. NSP Assessment Results, 8-Story SMF RSA, BSE-2 CP (+push to right)	3-81
Figure 3-83. NDP Assessment Results, Beam Hinges, 8-Story SMF ELF, BSE-1 LS	3-82

Figure 3-84. NDP Assessment Results, Beam Hinges, 8-Story SMF RSA, BSE-1 LS	3-83
Figure 3-85. NDP Assessment Results, Beam Hinges, 8-Story SMF ELF, BSE-2 CP	3-83
Figure 3-86. NDP Assessment Results, Beam Hinges, 8-Story SMF RSA, BSE-2 CP	3-84
Figure 3-87. NDP Assessment Results, Column Hinges, 8-Story SMF ELF, BSE-2 CP	3-85
Figure 3-88. NDP Assessment Results, Column Hinges, 8-Story SMF RSA, BSE-2 CP	3-85
Figure 3-89. NDP Assessment Results, Column Hinges, 8-Story SMF ELF, BSE-2 Yield	3-86
Figure 3-90. NDP Assessment Results, Column Hinges, 8-Story SMF RSA, BSE-2 Yield	3-86
Figure 3-91. NDP Assessment Results, Column Members, 8-Story SMF ELF, BSE-2	3-87
Figure 3-92. NDP Assessment Results, Column Members, 8-Story SMF RSA, BSE-2	3-87
Figure 3-93. NDP Assessment Results, Panel Zones, 8-Story SMF ELF, BSE-2 CP	3-88
Figure 3-94. NDP Assessment Results, Panel Zones, 8-Story SMF RSA, BSE-2 CP	3-88
Figure 3-95. LSP Assessment Results, 16-Story SMF ELF, BSE-1 LS	3-90
Figure 3-96. LSP Assessment Results, 16-Story SMF RSA, BSE-1 LS	3-91
Figure 3-97. LSP Assessment Results, Compression in Exterior Columns, 16-Story SMF, BSE-1	3-92
Figure 3-98. LSP Assessment Results, 16-Story SMF ELF, BSE-2 CP	3-93
Figure 3-99. LSP Assessment Results, 16-Story SMF RSA, BSE-2 CP	3-94
Figure 3-100. LSP Assessment Results, Compression in Exterior Columns, 16-Story SMF, BSE-2	3-95
Figure 3-101. LDP Assessment Results, 16-Story SMF ELF, BSE-1 LS	3-96
Figure 3-102. LDP Assessment Results, 16-Story SMF RSA, BSE-1 LS	3-97
Figure 3-103. LDP Assessment Results, Compression in Exterior Columns, 16-Story SMF, BSE-1	3-98
Figure 3-104. LDP Assessment Results, 16-Story SMF ELF, BSE-2 CP	3-99
Figure 3-105. LDP Assessment Results, 16-Story SMF RSA, BSE-2 CP	3-100
Figure 3-106. LDP Assessment Results, Compression in Exterior Columns, 16-Story SMF, BSE-2	3-101
Figure 3-107. 16-Story SMF ELF Pushover, BSE-2	3-102
Figure 3-108. 16-Story SMF RSA Pushover, BSE-2	3-103
Figure 3-109. 16-Story SMF ELF Pushover – Story Drift Ratios – BSE-2	3-103
Figure 3-110. 16-Story SMF RSA Pushover – Story Drift Ratios – BSE-2	3-104
Figure 3-111. Schematic of Flexural Actions in Columns, 16-Story SMF (NSP and NDP)	3-105
Figure 3-112. NSP Assessment Results, 16-Story SMF ELF, BSE-1 LS (+push to right)	3-106
Figure 3-113. NSP Assessment Results, 16-Story SMF RSA, BSE-1 LS (+push to right)	3-107
Figure 3-114. NSP Assessment Results, 16-Story SMF ELF, BSE-2 CP (+push to right)	3-108
Figure 3-115. NSP Assessment Results, 16-Story SMF RSA, BSE-2 CP (+push to right)	3-109
Figure 3-116. NDP Assessment Results, Beam Hinges, 16-Story SMF ELF, BSE-1 LS	3-110
Figure 3-117. NDP Assessment Results, Beam Hinges, 16-Story SMF RSA, BSE-1 LS	3-111
Figure 3-118. NDP Assessment Results, Beam Hinges, 16-Story SMF ELF, BSE-2 CP	3-111

Figure 3-119. NDP Assessment Results, Beam Hinges, 16-Story SMF RSA, BSE-2 CP	3-112
Figure 3-120. NDP Assessment Results, Column Hinges, 16-Story SMF ELF, BSE-2 CP	3-113
Figure 3-121. NDP Assessment Results, Column Hinges, 16-Story SMF RSA, BSE-2 CP	3-113
Figure 3-122. NDP Assessment Results, Column Hinges, 16-Story SMF ELF, BSE-2 Yield	3-114
Figure 3-123. NDP Assessment Results, Column Hinges, 16-Story SMF RSA, BSE-2 Yield	3-114
Figure 3-124. NDP Assessment Results, Column Members, 16-Story SMF ELF, BSE-2 CP	3-115
Figure 3-125. NDP Assessment Results, Column Members, 16-Story SMF RSA, BSE-2 CP	3-115
Figure 3-126. NDP Assessment Results, Panel Zones, 16-Story SMF ELF, BSE-2 CP	3-116
Figure 3-127. NDP Assessment Results, Panel Zones, 16-Story SMF RSA, BSE-2 CP	3-116
Figure A-1. Acceleration Response Spectra: Original, Scaled, and Scaled Average Spectrum for E-W Direction of MC4	A-4
Figure A-2. Acceleration Response Spectra: Original and Scaled for Each Selected Record for E-W Direction of MC4	A-5
Figure A-3. Acceleration Response Spectra: Original, Scaled, and Scaled Average Spectrum for E-W Direction of MC8	A-7
Figure A-4. Acceleration Response Spectra: Original and Scaled for Each Selected Record for E-W Direction of MC8	A-8
Figure A-5. Acceleration Response Spectra: Original, Scaled, and Scaled Average Spectrum for E-W Direction of MC16	A-10
Figure A-6. Acceleration Response Spectra: Original and Scaled for Each Selected Record for E-W Direction of MC16	A-11
Figure A-7. 1994 Northridge Earthquake at Beverly Hills, Mulholland Drive Station, Comp. 009	A-12
Figure A-8. 1994 Northridge Earthquake at Beverly Hills, Mulholland Drive Station, Comp. 279	A-12
Figure A-9. 1994 Northridge Earthquake at Canyon Country WLC Station, Comp. 000	A-13
Figure A-10. 1994 Northridge Earthquake at Canyon Country WLC Station, Comp. 270	A-13
Figure A-11. 1999 Duzce, Turkey Earthquake at Bolu Station, Comp. 000	A-14
Figure A-12. 1999 Duzce, Turkey Earthquake at Bolu Station, Comp. 090	A-14
Figure A-13. 1999 Hector Mine Earthquake at Hector Station, Comp. 000	A-15
Figure A-14. 1999 Hector Mine Earthquake at Hector Station, Comp. 090	A-15
Figure A-15. 1979 Imperial Valley Earthquake at Delta Station, Comp. 262	A-16
Figure A-16. 1979 Imperial Valley Earthquake at Delta Station, Comp. 352	A-16
Figure A-17. 1979 Imperial Valley Earthquake at El Centro Array Station #11, Comp. 140	A-17
Figure A-18. 1979 Imperial Valley Earthquake at El Centro Array Station #11, Comp. 230	A-17
Figure A-19. 1995 Kobe, Japan Earthquake at Nishi-Akashi Station, Comp. 000	A-18
Figure A-20. 1995 Kobe, Japan Earthquake at Nishi-Akashi Station, Comp. 090	A-18
Figure A-21. 1995 Kobe, Japan Earthquake at Shin-Osaka Station, Comp. 000	A-19

Figure A-22. 1995 Kobe, Japan Earthquake at Shin-Osaka Station, Comp. 090	A-19
Figure A-23. 1999 Kocaeli, Turkey Earthquake at Duzce Station, Comp. 180	A-20
Figure A-24. 1999 Kocaeli, Turkey Earthquake at Duzce Station, Comp. 270	A-20
Figure A-25. 1999 Kocaeli, Turkey Earthquake at Arcelik Station, Comp. 000.....	A-21
Figure A-26. 1999 Kocaeli, Turkey Earthquake at Arcelik Station, Comp. 090.....	A-21
Figure A-27. 1992 Landers Earthquake at Yermo Fire Station, Comp. 270	A-22
Figure A-28. 1992 Landers Earthquake at Yermo Fire Station, Comp. 360	A-22
Figure A-29. 1992 Landers Earthquake at Coolwater Station, Longitudinal Direction	A-23
Figure A-30. 1992 Landers Earthquake at Coolwater Station, Transverse Direction	A-23
Figure A-31. 1989 Loma Prieta Earthquake at Capitola Station, Comp. 000	A-24
Figure A-32. 1989 Loma Prieta Earthquake at Capitola Station, Comp. 090	A-24
Figure A-33. 1989 Loma Prieta Earthquake at Gilroy Array Station #3, Comp. 000	A-25
Figure A-34. 1989 Loma Prieta Earthquake at Gilroy Array Station #3, Comp. 090	A-25
Figure A-35. 1990 Manjil, Iran Earthquake at Abbar Station, Longitudinal Direction	A-26
Figure A-36. 1990 Manjil, Iran Earthquake at Abbar Station, Transverse Direction.....	A-26
Figure A-37. 1987 Superstition Hills Earthquake at El Centro, Imperial County, Comp. 000	A-27
Figure A-38. 1987 Superstition Hills Earthquake at El Centro, Imperial County, Comp. 090	A-27
Figure A-39. 1987 Superstition Hills Earthquake at Poe Road, Comp. 270	A-28
Figure A-40. 1987 Superstition Hills Earthquake at Poe Road, Comp. 360	A-28
Figure A-41. 1992 Cape Mendocino Earthquake at Rio Dell Overpass, Comp. 270.....	A-29
Figure A-42. 1992 Cape Mendocino Earthquake at Rio Dell Overpass, Comp. 360.....	A-29
Figure A-43. 1999 Chi-Chi, Taiwan Earthquake at CHY101 Station, E-W Component.....	A-30
Figure A-44. 1999 Chi-Chi, Taiwan Earthquake at CHY101 Station, N-S Component.....	A-30
Figure A-45. 1999 Chi-Chi, Taiwan Earthquake at TCU045 Station, E-W Component	A-31
Figure A-46. 1999 Chi-Chi, Taiwan Earthquake at TCU045 Station, N-S Component	A-31
Figure A-47. 1971 San Fernando Earthquake at Los Angeles Hollywood Store Station, Comp. 090 ..	A-32
Figure A-48. 1971 San Fernando Earthquake at Los Angeles Hollywood Store Station, Comp. 180 ..	A-32
Figure A-49. 1976 Friuli, Italy Earthquake at Tolmezzo Station, Comp. 000	A-33
Figure A-50. 1976 Friuli, Italy Earthquake at Tolmezzo Station, Comp. 270	A-33
Figure B-1. Strength Design Lateral Forces and Story Shears	B-5
Figure B-2. Drift Design Lateral Forces and Story Shears.....	B-5
Figure B-3. Story Drift Ratios and Deflected Shape	B-6
Figure B-4. Strength Design Lateral Forces and Story Shears	B-7
Figure B-5. Drift Design Lateral Forces and Story Shears.....	B-8
Figure B-6. Story Drift Ratios and Deflected Shape	B-9

Figure B-7. Strength Design Lateral Forces and Story Shears.....	B-10
Figure B-8. Drift Design Lateral Forces and Story Shears.....	B-11
Figure B-9. Story Drift Ratios and Deflected Shape	B-12
Figure B-10. Strength Design Lateral Forces and Story Shears.....	B-14
Figure B-11. Drift Design Lateral Forces and Story Shears.....	B-14
Figure B-12. Story Drift Ratios and Deflected Shape	B-15
Figure B-13. Strength Design Lateral Forces and Story Shears.....	B-16
Figure B-14. Drift Design Lateral Forces and Story Shears.....	B-17
Figure B-15. Story Drift Ratios and Deflected Shape	B-17
Figure B-16. Strength Design Lateral Forces and Story Shears.....	B-19
Figure B-17. Drift Design Lateral Forces and Story Shears.....	B-20
Figure B-18. Story Drift Ratios and Deflected Shape	B-20
Figure B-19. SMF Member Sizes, 8-story RSA.....	B-29

List of Abbreviations

AISC	American Institute of Steel Construction
ASCE	American Society of Civil Engineers
ASTM	American Society for Testing and Materials
ATC	Applied Technology Council
BPL	Building Performance Level
BSE	Basic Safety Earthquake
BSO	Basic Safety Objective
BSSC	Building Seismic Safety Council
CBF	Concentrically Braced Frame
CP	Collapse Prevention
DC	Deformation-Controlled
DCR	Demand to capacity ratio
EBF	Eccentrically Braced Frame
EHL	Earthquake Hazard Level
ELF	Equivalent Lateral Force
E-W	East-West
FC	Force-Controlled
FEMA	Federal Emergency Management Agency
FR	Fully Restrained
GSA	General Services Administration
GCR	Grant/Contract Report
HD	Highly Ductile
HSS	Hollow Structural Section
IBC	International Building Code
ICC	International Code Council
IEBC	International Existing Building Code
IO	Immediate Occupancy
LC	Load Combination
LDP	Linear Dynamic Procedure
LFRS	Lateral Force Resisting System
LRFD	Load and Resistance Factor Design

LS	Life Safety
LSP	Linear Static Procedure
LTB	Lateral Torsional Buckling
MC	Moment Curvature
MCE (MCE _R)	Maximum Considered Earthquake
MD	Moderately Ductile
MR	Moment Rotation
MRSA	Modal Response Spectrum Analysis
MWFRS	Main Wind Force Resisting System
NDP	Nonlinear Dynamic Procedure
NEHRP	National Earthquake Hazards Reduction Program
NIBS	National Institute of Building Sciences
NIST	National Institute of Standards and Technology
NPL	Nonstructural Performance Level
N-S	North-South
NSP	Nonlinear Static Procedure
PBS	Public Buildings Service
PBSD	Performance-Based Seismic Design
RBS	Reduced Beam Section
RHA	Response History Analysis
RSA	Response Spectrum Analysis
SCBF	Special Concentrically Braced Frame
SCWB	Strong Column Weak Beam
SDC	Seismic Design Category
SDOF	Single Degree of Freedom
SEAONC	Structural Engineers Association of Northern California
SEI	Structural Engineering Institute
SFRS	Seismic Force Resisting System
SMF	Special Moment Frame
SPL	Structural Performance Level
SRSS	Square Root Sum of the Squares
W.P.	Work Point

Executive Summary

This report presents the results of a study investigating the correlation between the seismic performance of an ASCE 7 code-compliant building and its performance as quantified using ASCE 41 analysis procedures and structural performance metrics. This investigation is performed by evaluating a suite of structural steel buildings in a high seismicity region that are designed using ASCE 7 and evaluated using ASCE 41. *The basic question is whether the standards for designing new steel buildings and assessing existing steel buildings provide consistent levels of performance.* An additional outcome of this research is to advance the state-of-knowledge in PBSO and assessment of buildings using ASCE 41. Further, results provide the technical background for provisions that target equivalent seismic performance between a new building and an existing building that is required to meet the seismic performance objective of a new building.

This report presents the results of a structural seismic performance assessment using ASCE 41 procedures and performance measures of buildings utilizing steel special moment frames (SMF) as the lateral force-resisting system (LFRS).

A suite of archetype buildings that incorporate SMFs along one principal direction of the buildings is designed in accordance with ASCE 7. The suite consists of 4-, 8-, and 16-story buildings designed using both the Equivalent Lateral Force (ELF) Procedure and Modal Response Spectrum Analysis (RSA). Both analysis procedures are used to provide a generally applicable range of LFRS strength within the selected seismic intensity region. As such, an LFRS may include significant overstrength to resist nonseismic loads or to satisfy other design criteria. A design space is created to investigate the effects of design methodology, building height and other LFRS-specific geometric modifications on seismic performance. In reality, the design space is infinitely large and many design choices made in this study can also have different configurations to evaluate the variation in performance specific to a design choice.

The seismic performance assessment of the building suite is conducted using both linear and nonlinear analysis procedures prescribed in ASCE 41:

- Linear Static Procedure (LSP)
- Linear Dynamic Procedure (Response Spectrum) (LDP)
- Nonlinear Static Procedure (NSP)
- Nonlinear Dynamic Procedure (NDP)

For this study, the performance assessment targets the Basic Safety Objective (BSO) prescribed in ASCE 41. This objective includes the interrelated goals of Life Safety (LS) Building Performance Level (BPL) at the Basic Safety Earthquake-1 (BSE-1) earthquake hazard level (EHL) and Collapse Prevention (CP) BPL at the BSE-2 EHL. This performance objective is chosen to align with the intended structural performance objective of an ordinary building in ASCE 7, which is qualitatively defined here as “life safety” provided by collapse prevention of the building, given a maximum considered earthquake (MCE) event.

To evaluate seismic assessment criteria, each component of the SMFs is designated as a *primary* or component in accordance with ASCE 41 §2.2.5 (and ASCE 41 §2.4.4.2). Similarly, quantitative performance measures (i.e., acceptance criteria) for *primary* components are used for all assessment procedures, although performance measures for *secondary* components are permitted by ASCE 41 for some primary components. The consistent use of primary acceptance criteria keeps all components and associated assessment results correlated among the assessment procedures for this study.

The goals of this research are as follows:

- Assess *new* structural steel buildings utilizing SMFs designed per ASCE 7 requirements and, in turn, evaluated using ASCE 41,
- Develop a qualitative link between the performance implied in ASCE 7 in light of the performance identified by ASCE 41 procedures and performance measures,
- Provide guidance or technical support for improved or new provisions in ASCE 41 (and to a lesser extent, ASCE 7),
- Reduce uncertainty in first-generation PBSD procedures for performance-based seismic assessment, and
- Identify any inconsistencies, ambiguities, and confusing provisions in ASCE 41.

The primary conclusions of this research can be divided into two parts: General Observations and Specific Observations about ASCE 41 analytical procedures.

A. *General Observations for Special Moment Frames:*

- The LSP generally results in more conservative normalized demand to capacity ratios, DCR_N , values than that of the LDP, because of the differences in the distribution of seismic demands and the lack of modal representation other than the fundamental mode in the LSP.
- The NSP generally results in less conservative DCR_N values than that of the NDP, contrary to what would be expected with increasing the analytical complexity, because of the differences in the distribution of seismic demands and the lack of modal representation other than the fundamental mode in the NSP.
- The nonlinear procedures provide a more rigorous assessment approach as compared to the linear procedures. The results from the LSP, and to a lesser extent the LDP, indicate more performance failures in components than identified using the nonlinear procedures. The results presented emphasize the inherent conservatism in the linear procedures. However, this conservatism is accompanied by a reduction in required analytical resources and proficiency of the analyst.
- The linear procedures can illustrate the trend in demands but may fail to highlight critical performance zones within a given frame.

B. *Specific Observations for Special Moment Frames:*

The following significant observations and conclusions are based on the collective results obtained from the assessment of the SMFs. More details about the specific items are in the relevant sections of the assessment discussion in Chapter 3.

- Analytical results based on component-level performances indicate that new SMFs designed in accordance with ASCE 7, and its referenced standards, have difficulty achieving the ASCE 41 BSO for an existing building intended to be equivalent to a new building. This observation is driven by the performance of the columns and beam-to-column connections.
- *Assuming* the archetype buildings meet the collapse performance objective of ASCE 7, the results of the assessment procedures indicate that ASCE 41 is generally conservative for SMFs. ASCE 41 analysis would require retrofit or replacement of specific components of a code-compliant SFRS to satisfy the CP BPL, given an MCE event. The results highlight that columns (i.e., beam-columns) with high axial and flexural demands and beam-to-column connections with a reduced beam section (RBS) have difficulty in satisfying the performance criteria in ASCE 41. Future research is needed to couple the collapse performance objectives of the two standards, as well as other performance objectives associated with a seismic hazard with a lower return period.
- A significant number of columns, primarily at the exterior of the frames, did not satisfy the ASCE 41 acceptance criteria. These failures are in beam-columns classified by analysis as “force-controlled”, which can be particularly problematic when the columns are located at the base of a frame. The results for columns can be enhanced by more mechanistically consistent assessment provisions and analytical modeling parameters for columns. Refinement of the relevant interaction equations to evaluate specific failure mechanisms could assist by allowing what would be a force-controlled column to be classified as “deformation-controlled”.
- A significant number of RBS beam-to-column connections, primarily at the exteriors of the frames, did not satisfy the ASCE 41 acceptance criteria for the LSP and NDP. Although the nonlinear acceptance criteria and detailing recommendations in ASCE 41 were derived from experimental test data, the rationale for the quantitative development of the cumulative reduction factors on these criteria (i.e., 0.8 multipliers in ASCE 41 §5.4.2.4.3-4) is unclear. The analytical results indicate that step function-based cumulative reduction factors can have a significant impact on the performance of a SMF. Further, reduction factors for the span-to-depth ratio limitations for beam-to-column connections have potentially opposing effects that could impact the results between linear and nonlinear assessment procedures.
- Assessment results illustrate that panel zones designed per ASCE 7 and its referenced standards, including the common practice of upsizing columns to offset the need for doubler plates and/or continuity plates, consistently satisfied the ASCE 41 acceptance criteria by a large margin. Consequently, the panel zones are deemed stronger than required by ASCE 41. Specifically, upsizing columns can impact the strength of panel zones in reference to the balance yield approach adopted by ASCE 41 and in turn can influence the performance of the beam-to-column connections.
- Components of the SMFs that do not satisfy the CP acceptance criteria would need to be strengthened to achieve the performance required by ASCE 41. However, the results from the various assessment procedures were seen to be inconsistent in some cases for a given design routine (i.e., LSP vs. NDP) or the same assessment procedure was inconsistent between design routines (i.e., ELF and RSA). This makes it difficult to definitively suggest that using ASCE 41 to design a new SMF would produce a system capable of achieving the seismic performance objective of ASCE 7. Future research is needed to evaluate the collapse probability of a new system strengthened by ASCE 41 relative to the seismic performance objective of ASCE 7. The same is required for a new system that has component strengths reduced from that required by ASCE 7 to meet an ASCE 41 performance objective. Further, the adequacy of the components of the enhanced

frame (those required to satisfy ASCE 41) would be dependent upon which analysis procedure is used to iterate between design and assessment, and therefore the fidelity of the analytical model and analysis parameters.

- Results of this study indicate that for ASCE 41 to be used as a seismic design procedure for new steel buildings, as a performance-based alternative to ASCE 7 (see ASCE 7 §1.3.1.3), acceptance criteria for the various analysis methods must be calibrated to each other to consistently result in a uniform collapse risk. Additionally, ASCE 41 would need to reference material-specific design standards (e.g., AISC 341) for their seismic design requirements, as well as consistent requirements for defining acceptance criteria for a component (e.g., plastic rotation).

Chapter 1 Introduction

In 1997, the Federal Emergency Management Agency (FEMA) published FEMA 273: *NEHRP Guidelines for the Seismic Rehabilitation of Buildings* (FEMA 1997) as a first step towards standardizing seismic performance assessment procedures for existing buildings. This effort, produced under the Applied Technology Council’s project 33 (ATC-33), was the first significant step in implementing performance-based seismic design (PBSD) into practice. Subsequently in 2000, FEMA and the American Society of Civil Engineers (ASCE) published FEMA 356: *Prestandard and Commentary for the Seismic Rehabilitation of Buildings* (FEMA 2000e). This publication introduced many changes to FEMA 273 to refine the accuracy and applicability of the provisions. The changes are chronicled in FEMA 357: *Global Topics Report on the Prestandard and Commentary for the Seismic Rehabilitation of Buildings* (FEMA 2000f). In 2006 ASCE published ASCE/SEI 41-06: *Seismic Rehabilitation of Existing Buildings* (ASCE 2006) as an ASCE Standard—hereafter referred to as ASCE 41. This document is referenced by the *International Existing Building Code* (IEBC) published by the International Code Council (ICC) (ICC 2012a).

ASCE 41 represents the current state-of-practice in seismic evaluation and rehabilitation of existing buildings. This standard is referenced by the California Building Standards Code (CBSC 2010), Federal government building standards (e.g., NIST 2011a), and a number of other local jurisdictions. ASCE 41 provides analytical procedures and criteria for evaluating buildings and designing seismic retrofits based on a defined performance goal (i.e., Life Safety and Collapse Prevention). This ability to explicitly define a performance goal and then assess a building design against that goal has led practitioners to adapt ASCE 41 methodology for use in new building design. The performance-based methodologies in ASCE 41 provide an alternative to the traditional prescriptive approaches used in the current standard for new buildings, ASCE/SEI 7-10: *Minimum Design Loads for Buildings and Other Structures* (ASCE 2010)—hereafter referred to as ASCE 7. Referenced by the *International Building Code* (IBC) (ICC 2012b), ASCE 7 is widely used throughout the country for seismic design of new buildings. However, with the trend toward performance-based design, the correlation between the performance of a building designed with the prescriptive provisions of ASCE 7 and assessed with the performance-based provisions of ASCE 41 is largely unknown.

The next version of ASCE 41 (ASCE 41-13¹) will offer a new track for application of the provisions to existing buildings whose performance goal is equivalent to that of a building designed with the new building standard. Consequently, this new track will allow direct seismic performance assessment of new buildings or, alternatively, a substitute seismic design approach via Chapter 1 of ASCE 7. For example, the PBS-P100: *Facility Standards for the Public Buildings Service* (GSA 2012) prescribes that ASCE 41-06 shall

¹ ASCE 41-13: *Seismic Evaluation and Retrofit of Existing Buildings* (ASCE 2014) was being developed during this project period. As such, new or updated provisions in ASCE 41-13 were not incorporated, except where changes were required to align with the seismic hazard prescribed in ASCE 7-10.

be used for the seismic design of new GSA facilities² and that the guidelines from ASCE 41 are intended to be applied to new buildings. This document does not permit a building to be designed for seismic performance below the minimum level specified by IBC. The National Institute of Building Sciences (NIBS) is using PBS-P100 as the basis for developing their *National Performance Based Design Guide* (NIBS 2013). Further, the Provisions Update Committee for the Building Seismic Safety Council is currently deliberating expanded provisions for performing nonlinear response history analysis (Chapter 16 in ASCE 7) for the 2015 edition of the *NEHRP Recommend Provisions for Seismic Regulations for New Buildings and Other Structures* (FEMA 2015). These expanded provisions reference ASCE 41-13 in the commentary for modeling and acceptance criteria for the design of new buildings.

This report presents the results of a study investigating the correlation between the seismic performance of an ASCE 7 code-compliant building and its performance as quantified using ASCE 41 analysis procedures and structural performance metrics. This investigation is performed by evaluating a suite of structural steel buildings in a high seismicity region that are designed using ASCE 7 and evaluated using ASCE 41. *The basic question is whether the standards for designing new steel buildings and assessing existing steel buildings provide consistent levels of performance.* The intended outcome of this research is to advance the state-of-knowledge in performance-based seismic design and assessment of buildings using ASCE 41. Further, results provide the technical background for provisions that target equivalent seismic performance between a new building and an existing building that is required to meet the seismic performance objective of a new building.

Applicability of ASCE 41-13 to this Study

During this project, ASCE/SEI 41-13, *Seismic Evaluation and Retrofit of Existing Buildings* (ASCE 2014), completed committee balloting and was sent out for public comment as well as for approval for inclusion in the IEBC. Any significant differences between ASCE 41-06 and ASCE 41-13 regarding assessment of steel structural systems will be highlighted in the discussions where applicable—unless otherwise noted, reference to ASCE 41 refers only to ASCE 41-06.

One significant addition to ASCE 41-13 is a process for applying the provisions for the seismic assessment of *existing* buildings where the intended performance is equivalent to that which is intended for new buildings designed in accordance with ASCE 7, including a correlation matrix between the two standards. While ASCE 41-06 is being used currently in practice to justify seismic performance of new buildings in compliance with ASCE 7 (as well as to identify noncompliance), this addition is the first step in conceptually aligning future editions of ASCE 41 and ASCE 7 so that ASCE 41 can be used for the seismic design of new buildings. Still, there are variations between material-specific provisions in ASCE 41 and provisions in material design standards referenced in ASCE 7 (e.g., AISC 360 and ACI 318) that need to be resolved.

² The seismic hazard used to characterize the design basis earthquake is that with a 10% probability of exceedence in 50 years. This differs from that used in ASCE/SEI 7-05 (ASCE 2005)—two-thirds of that with a 2% probability of exceedence in 50 years—and ASCE 7-10—two-thirds of that producing a 1% probability of collapse in 50 years.

In terms of assessment of steel systems, the technical content in ASCE 41-13 did not change in any significant manner that invalidates the results presented in this report. The few changes that would affect the results of individual components are highlighted where applicable. In fact, data from this study instigated some of these changes.

1.1 Project Motivation and Background

Traditional prescriptive seismic provisions for new buildings principally concentrate on the Life Safety objective applied to all-encompassing arrangements of similar lateral force-resisting systems. Little consideration is given to either the actual performance of individual buildings or the economic loss and occupancy interruption that may occur after an earthquake. Thus, a need arises for seismic provisions that allow engineers to design buildings and assess them against varying levels of performance associated with varying levels of earthquake hazard. So doing provides a method where desired building damage levels can be coupled to both quantitative and qualitative definitions of performance so that building and operational stakeholders are integrated into a project. Conceptually, PBSD was conceived to satisfy this need. The objective of PBSD is to provide a means of integrating additional performance objectives into the seismic design of new buildings that explicitly measure and account for risk of casualties, occupancy interruption, and economic loss including repair costs.

Prescriptive building code procedures, such as those found in ASCE 7, tend to restrict design innovation and can lead to inefficient structural designs and higher construction costs. In lieu of its prescriptive provisions, ASCE 7 allows alternative “rational” design methods, such as PBSD, to be used in new building design. PBSD affords the designer the freedom to bypass prescriptive building code provisions by demonstrating that a building performs to an explicitly defined performance target that equals or exceeds the life safety objective in prescriptive provisions. The use of such methods must be approved by the local authority having jurisdiction and typically requires rigorous structural analysis coupled with a high level of expertise.

Although ASCE 7 allows PBSD (see ASCE 7 §1.3.1.3) to be used in new building design, it provides no substantial guidance on implementing PBSD for this purpose. Therefore, many practitioners and local authorities have turned to the provisions in ASCE 41 as a way of implementing PBSD into new building design. These provisions, widely considered to be “first generation” PBSD principles, were originally intended to be used in the evaluation of existing buildings by assessing performance compliance with a selected rehabilitation objective. Since ASCE 41 is applicable to existing buildings, it does not provide a direct correlation between the rehabilitation objective and the intended performance of an ASCE 7 code-compliant new building (see Table 1-1). However, the IEBC does provide a correlation between ASCE 41 performance levels and IBC (and thus ASCE 7) Risk Categories, thus providing the link between the prescriptive requirements for new building design and the nonprescriptive requirements of existing building assessment and PBSD. A matrix showing this correlation is shown in Table 1-2. Still, this matrix has not been comprehensively validated nor have the seismic performance expectations for new buildings been quantitatively assessed to standardize acceptable performance within the framework of ASCE 41, or vice versa. ASCE 7 has not expressly adopted Table 1-2 for seismic design.

Table 1-1. Comparison of Seismic Hazard and Associated Performance for ASCE 7 and ASCE 41

		Target Building Performance Level ¹			
		Operational	Immediate Occupancy (IO)	Life Safety (LS)	Collapse Prevention (CP)
Earthquake Hazard Level	ASCE 41 50% / 50 year ²	ASCE 41 (nonstructural)	ASCE 41 Limited	ASCE 41 Limited	ASCE 41 Limited
	ASCE 41 20% / 50 year ²	ASCE 41 Enhanced	ASCE 41	ASCE 41 Limited	ASCE 41 Limited
	ASCE 7 "Frequent" ¹	ASCE 7 Risk Category III & IV	ASCE 7 Risk Category I & II (anticipated) ³	N.A.	N.A.
	ASCE 41 BSE-1 ~ 10% / 50 year ²	ASCE 41 Enhanced	ASCE 41 Enhanced	ASCE 41 BSO	ASCE 41 Limited
	ASCE 7 $\frac{2}{3} \times MCE_R$ ¹	N.A.	ASCE 7 Risk Category III & IV	ASCE 7 Risk Category I & II (design)	N.A.
	ASCE 41 BSE-2 ~ 2% / 50 year ²	ASCE 41 Enhanced	ASCE 41 Enhanced	ASCE 41 Enhanced	ASCE 41 BSO
ASCE 7 MCE_R ¹	N.A.	N.A.	ASCE 7 Risk Category III & IV	ASCE 7 Risk Category I & II (objective) ³	

1. Seismic hazard defined in ASCE 7-10.
2. Seismic hazard defined in ASCE 41-06.
3. See ASCE 7, Expanded Seismic Commentary (ASCE 7-10, 3rd printing).

Table 1-2. Performance Comparison between IBC and ASCE 41 – (From IEBC Table 301.1.4.1)

Risk Category (Based on IBC Table 1604.5)	Performance Level for use with ASCE 41 BSE-1 Earthquake Hazard Level	Performance Level for use with ASCE 41 BSE-2 Earthquake Hazard Level
I	Life Safety (LS)	Collapse Prevention (CP)
II	Life Safety (LS)	Collapse Prevention (CP)
III	Note a	Note a
IV	Immediate Occupancy (IO)	Immediate Occupancy (IO)

- a. Acceptance criteria for Risk Category III shall be taken as 80 percent of the acceptance criteria specified for Risk Category II performance levels, but need not be less than the acceptance criteria specified for Risk Category IV performance levels

In June 2008 the National Earthquake Hazards Reduction Program (NEHRP) sponsored a PBSO workshop for leading practitioners and researchers from around the United States to develop a comprehensive list of research needs to foster full development and implementation of PBSO. From this workshop, the Building Seismic Safety Council (BSSC) reported a prioritized list of key PBSO research and implementation needs in NIST GCR 09-917-2: *Research Required to Support Full Implementation of Performance-Based Seismic Design* (NIST 2009a). The highest priority need identified in this report was to “benchmark” current PBSO methodologies (e.g., ASCE 41) with code procedures for design of new buildings. Two observations from the report were that among workshop participants (1) ASCE 41 procedures are perceived to be overly

conservative and (2) existing PBSB methods are not accepted by practitioners as providing a uniform level of confidence. A supporting reason for these two observations was that no systematic effort had been undertaken to benchmark structural performance as determined using ASCE 41 procedures, together with widely accepted procedures for designing new buildings using ASCE 7.

Additionally, needs for the advancement of PBSB have been highlighted by other researchers and practitioners (Toranzo-Dianderas 2009, SEAONC 2010, Paret, Searer, and Freeman 2011, and Pekelnicky and Poland 2012). The needs identified include, but are not limited to the following:

- Calibration / comparison of ASCE 41 to ASCE 7
- Reduced conservatism in linear procedures and acceptance criteria
- Better clarification of provisions and intent

Therefore, the research study presented in this report was undertaken in an effort to address some of these needs.

1.2 Scope of Project

This report presents the results of a structural seismic performance assessment using ASCE 41 procedures and performance measures of buildings utilizing steel special moment frames (SMF) as the lateral force-resisting system (LFRS)³.

A suite of archetype buildings that incorporate SMFs along one principal direction of the buildings is designed in accordance with ASCE 7. The suite consists of 4-, 8-, and 16-story buildings designed using both the Equivalent Lateral Force (ELF) Procedure and Modal Response Spectrum Analysis (RSA). Both analysis procedures are used to provide a generally applicable range of LFRS strength within the selected seismic intensity region. As such, components of an LFRS may include significant overstrength⁴ to resist nonseismic loads or to satisfy other design criteria. A design space is created to investigate the effects of design methodology, building height, and other LFRS-specific geometric modifications on seismic performance. In reality, the design space is infinitely large and many design choices made in this study can also have different configurations to evaluate the variation in performance specific to a design choice (e.g., study of a range of doubler plate thicknesses in an SMF and the influence on frame column performance).

The seismic performance assessment of the building suite is conducted using both linear and nonlinear analysis procedures prescribed in ASCE 41:

- Linear Static Procedure (LSP)

³ Although the LFRS is a component of a cohesive three-dimensional building system that includes structural framing intended to primarily resist gravity loads and nonstructural components, only the performance of the LFRS as identified by ASCE 41 procedures and measures is presented. The performance of an LFRS can be influenced by the inclusion of gravity framing in a analysis. Based on the analytical modeling used in this study, this interaction is deemed to be negligible because the LFRS resists nearly all forces and deformations resulting from lateral loads and movement.

⁴ Overstrength is defined here as the additional elastic strength in a component that is in excess of the required minimum seismic strength.

- Linear Dynamic Procedure (Response Spectrum) (LDP)
- Nonlinear Static Procedure (NSP)
- Nonlinear Dynamic Procedure (NDP)

For this study, the performance assessment targets the Basic Safety Objective (BSO) prescribed in ASCE 41. This objective includes the interrelated goals of Life Safety (LS) Building Performance Level (BPL) at the Basic Safety Earthquake-1 (BSE-1) earthquake hazard level (EHL) and Collapse Prevention (CP) BPL at the BSE-2 EHL (see Table 1-2 above). This performance objective is chosen to align with the intended structural performance objective of an ordinary building⁵ in ASCE 7, which is qualitatively defined here as “life safety” provided by collapse prevention of the building, given a maximum considered earthquake (MCE) event.

To evaluate seismic assessment criteria, each component of the SMFs is designated as a *primary* component in accordance with ASCE 41 §2.2.5 (and ASCE 41 §2.4.4.2). Similarly, quantitative performance measures (i.e., acceptance criteria) for *primary* components are used for all assessment procedures, although performance measures for *secondary* components are permitted by ASCE 41 for some primary components. The consistent use of primary acceptance criteria keeps all components and associated assessment results correlated among the assessment procedures for this study.

The goals of this research are as follows:

- Assess *new* structural steel buildings utilizing SMFs designed per ASCE 7 requirements and, in turn, evaluated using ASCE 41,
- Develop a qualitative link between the performance implied in ASCE 7 in light of the performance identified by ASCE 41 procedures and performance measures,
- Provide guidance or technical support for improved or new provisions in ASCE 41 (and to a lesser extent, ASCE 7),
- Reduce uncertainty in first-generation PBSD procedures for performance-based seismic assessment, and
- Identify any inconsistencies, ambiguities, and confusing provisions in ASCE 41.

This report does not discuss the correlation between deterministic performance metrics for components (e.g., *m*-factor in ASCE 41) and the system (e.g., *R*-factor in ASCE 7)—a topic for future research and one that is required to establish the link between the performance of an ASCE 7 code-compliant design and the associated performance identified by ASCE 41 procedures and performance measures. Here, it is assumed that the acceptance criteria for each BPL in ASCE 41 Chapter 5 are quantitatively rational and accurate interpretations of what deformations / actions are appropriate for the intended structural performance (see ASCE 41 Tables C1-2, C1-3, and C1-4). Clearly, this is a subjective and, at times, controversial topic, as some component actions are physically qualified only by experimental test results (i.e., SAC project, see FEMA 351 (FEMA 2000b)), but not necessarily for all performance levels.

⁵ Buildings assigned Risk Category I or II.

In this report, the archetype building designs are presented in Chapter 2. Next, the results from the seismic assessment in accordance with ASCE 41 and supplementary discussions are presented in Chapter 3. In the discussion of the assessment results, special focus is given to highlighting any notable differences or similarities between ASCE 41 and ASCE 7 (including the referenced design standards in ASCE 7 for the design of structural steel buildings) and to making suggestions for improvements in ASCE 41. Conclusions are provided in Chapter 4. Selection and scaling of ground motions, including pertinent ground motion data, for the NDP are provided in Appendix A. Additional information applicable to the design of the archetype buildings and detailed design calculations for a few example members and connections are provided in Appendix B. Detailed assessment calculations for a few example members and connections are provided in Appendix C.

The hope is that other follow-on projects will be undertaken by NIST and / or other organizations to provide additional data sets that advance the state-of-practice and state-of-knowledge and facilitate the implementation of performance-based seismic engineering in design of buildings. Further studies of structural steel systems (e.g., buckling-restrained braced frames), as well as studies of reinforced concrete moment frame and shear wall buildings, are planned as next steps at NIST.

Chapter 2 Overview and Design of Archetype Buildings

This chapter presents the design of the archetype buildings. General discussions are provided in Section 2.1 on the geometry of the buildings and the design criteria, including sizes of structural members not considered to principally resist lateral loads. Section 2.2 discusses the structural design loads and associated design criteria specific to them. Section 2.3 presents information regarding the structural analysis and mathematical model used in the structural member selection process. Section 2.4 provides the design of the structural systems principally required to resist lateral loads and stabilize the buildings.

2.1 General Information

A suite of three steel-framed office buildings is investigated in this study. It is presumed that the archetype buildings will be constructed in a high seismicity area (e.g., somewhere along the west coast of the United States—see Earthquake Forces section below). Building stability and resistance to environmental loads and deformations is provided by special moment frames along the East-West (E-W) direction and special concentrically braced frames along the North-South (N-S) direction. All lateral force-resisting systems (LFRS) are symmetrically located at the perimeter of the building and orthogonal. For purposes of design, the identified LFRS acts as both the seismic force-resisting system (SFRS) and the main wind force-resisting system (MWFRS). For completeness of the full design of the archetype buildings, design of both LFRSs is presented below. However, only the assessment of the moment frames will be presented in this report. Assessment of the braced frames is presented in NIST TN 1863-2: *Assessment of First Generation Performance-Based Design Methods for New Steel Buildings, Volume 2: Special Concentrically Braced Frames* (Harris and Speicher 2015).

Each building is rectangular in plan, with five 30-foot bays in the E-W direction and generally five 20-foot bays in the N-S direction. The plan dimensions for all floors and roofs are 152 feet in the E-W direction and 102 feet in the N-S direction. For all buildings, the height of the first story is 18 feet and the remaining story heights are 14 feet. A summary of the geometric structural characteristics of each building is provided in Table 2-1. Building schematics are shown in Figure 2-1 through Figure 2-3. The typical floor framing plan is shown in Figure 2-4 and Figure 2-5. For brevity, the building schematics do not show symmetrical elevator core or stairwell diaphragm openings.

Table 2-1. Structural Characteristics of Archetype Buildings

Bldg. ID	Stories	E-W Dimension	N-S Dimension	E-W LFRS	N-S LFRS	Notes
MC4	4	150' = 5 bays @ 30'	100' = 5 bays @ 20'	SMF	SCBF	SMF: 3–30-foot bays SCBF: 1–20-foot bay inverted ‘V’ (Chevron) with HSS braces
MC8	8	150' = 5 bays @ 30'	100' = 5 bays @ 20'	SMF	SCBF	SMF: 3–30-foot bays SCBF: 1–20-foot bay two-story X-bracing with HSS braces
MC16	16	150' = 5 bays @ 30'	100' = Varies – see Figure 2-5	SMF	SCBF	SMF: 3–30-foot bays SCBF: 2–30-foot bays two-story X-bracing with HSS braces

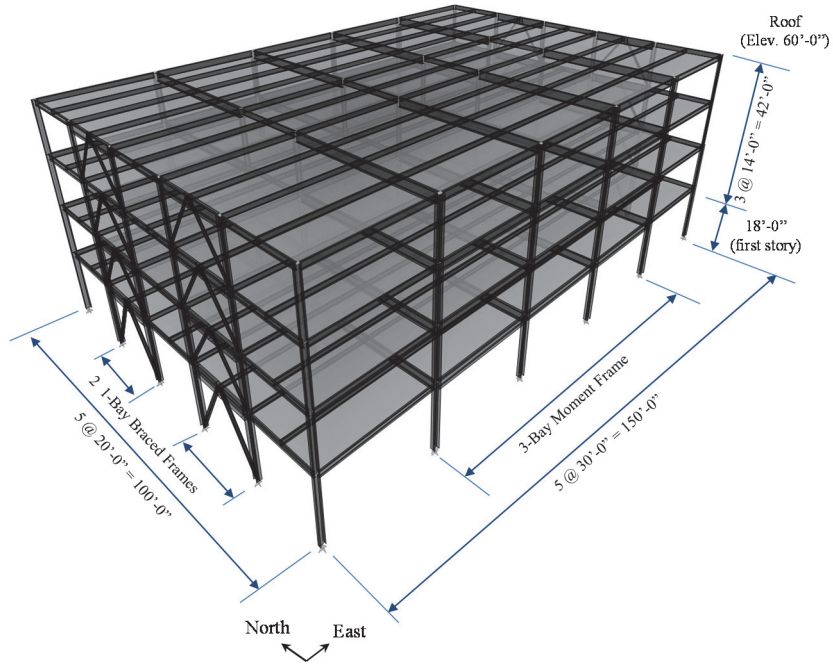


Figure 2-1. Isometric View of MC4 Archetype Building

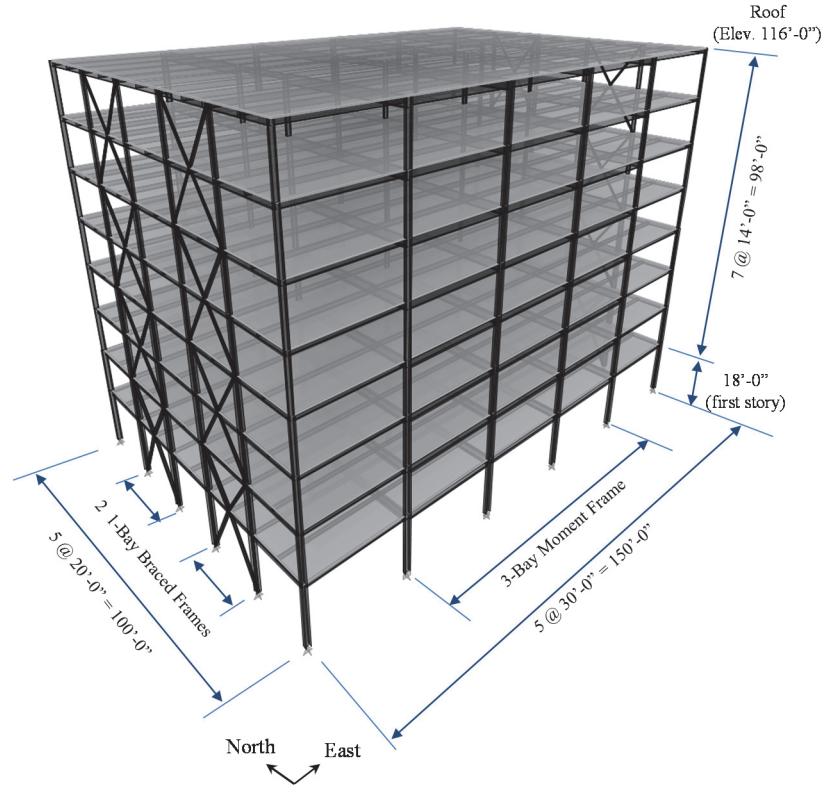


Figure 2-2. Isometric View of MC8 Archetype Building

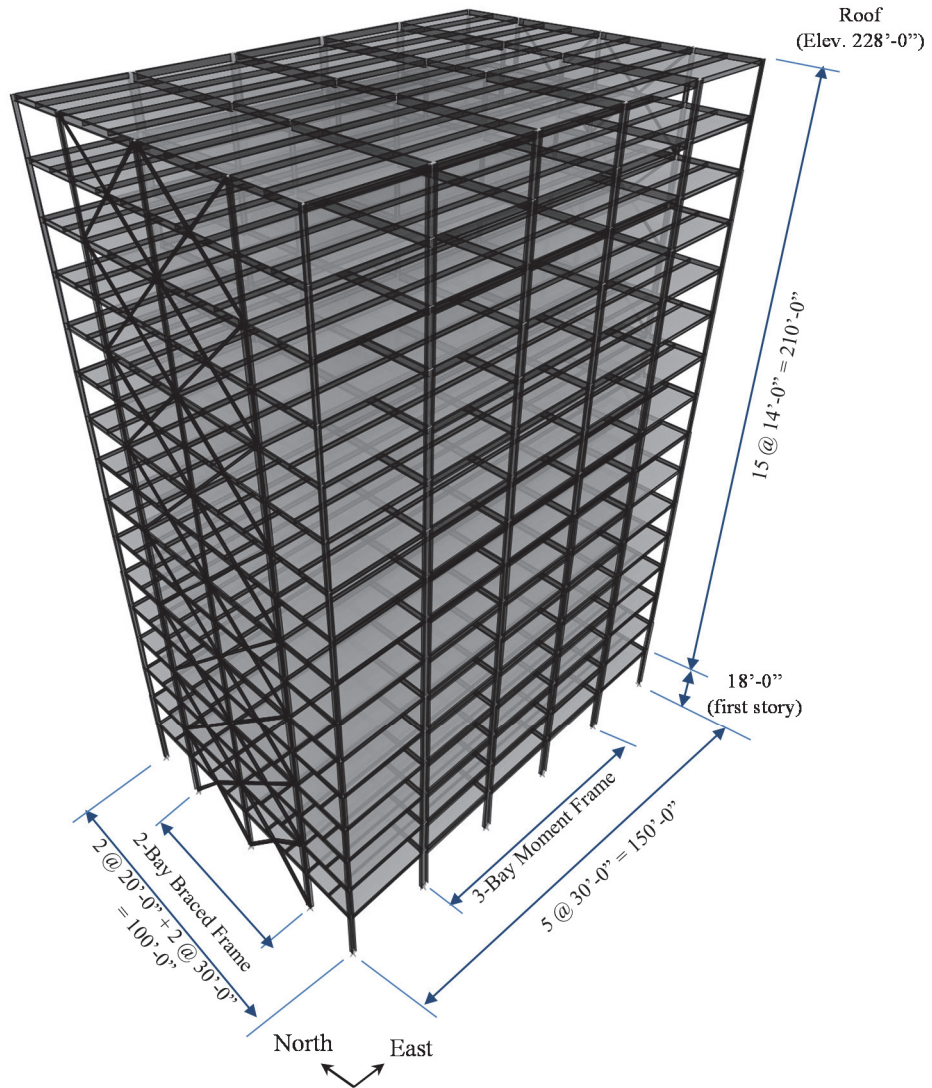


Figure 2-3. Isometric View of MC16 Archetype Building

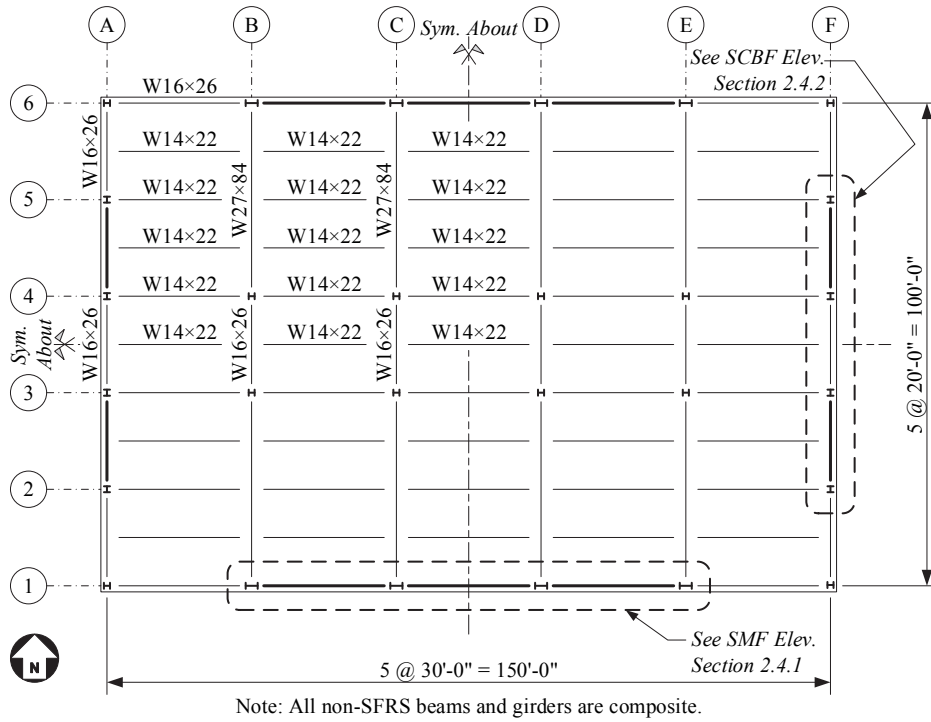


Figure 2-4. Typical Floor Framing Plan, MC4 and MC8

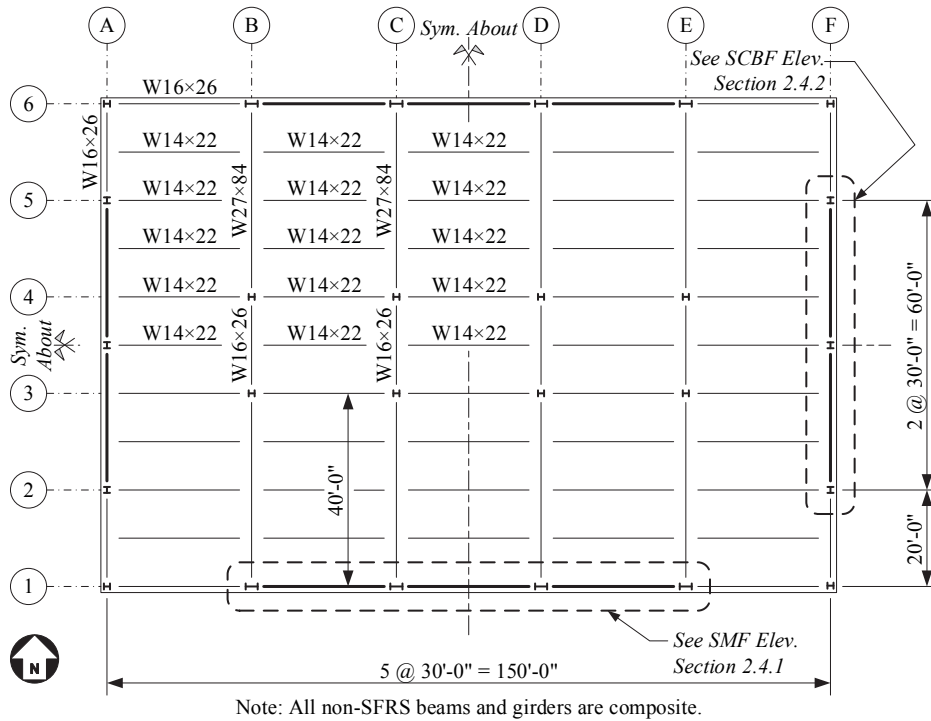


Figure 2-5. Typical Floor Framing Plan, MC16

The archetype buildings are analyzed and designed for all load effects in accordance with the following:

- IBC 2012: *International Building Code* (ICC 2012b)
- ASCE 7-10: *Minimum Design Loads for Buildings and Other Structures* (ASCE 2010)
- AISC 360-10: *Specification for Structural Steel Buildings* (AISC 2010a)
- AISC 341-10: *Seismic Provisions for Structural Steel Building* (AISC 2010b)
- AISC 358-10: *Prequalified Connections for Special and Intermediate Steel Moment Frames for Seismic Applications* (AISC 2010c)

The following material types and corresponding nominal properties were assumed in design:

- Wide-Flange Sections: A992 Grade 50, $F_y = 50$ ksi, $R_y = 1.1$
- HSS Sections: A500 Grade B, $F_y = 46$ ksi, $R_y = 1.4$
- Connections: A572 Grade 50, $F_y = 50$ ksi, $R_y = 1.1$
- $E = 29000$ ksi, $G = 11200$ ksi, $\nu = 0.3$

The archetype buildings do not contain any geometry-based or configuration-based horizontal irregularities, Type 2, 3, 4, or 5 as defined in ASCE 7 Table 12.3-1. Horizontal irregularity Type 1 is dependent on post-design analysis verification, and is presented in Appendix B. Similarly, the archetype buildings do not contain any geometry-based or configuration-based vertical irregularities, Type 2, 3, or 4 as defined in ASCE 7 Table 12.3-2. Vertical irregularity Types 1 and 5 are dependent on post-design analysis verification and are presented in Appendix B. The buildings are classified as Risk Category II structures in accordance with ASCE 7 §1.5.

2.2 Structural Design Loads

2.2.1 Load Combinations

Loads and load combinations used for analysis and strength design of members and connections are in accordance with ASCE 7 §2.3, including modifications to these combinations prescribed in ASCE 7 §12.4. This resulted in 189 load combinations for design of each component. Capacity design provisions for each SFRS type prescribed in AISC 341 as well as for beam-to-column connections in an SMF prescribed in AISC 358 provided several design load combinations in addition to those from ASCE 7.

Loads and load combinations for serviceability analysis and verification (e.g., wind drift), and seismic drift analysis and allowable drift compliance verification are discussed subsequently under Environmental Loads, §2.2.3.

2.2.2 Gravity Loads

The floor and roof dead load consists of the weight of the steel members, metal deck, and concrete slab weight (3¼ inch lightweight concrete at 110 pcf on 18-gage, 3 inch metal deck \approx 46 psf). Superimposed dead loads are taken as 15 psf for floors and 10 psf for the roof, representing mechanical, electrical, plumbing, and miscellaneous dead loads. A 250 plf superimposed dead load is also applied to the perimeter

horizontal framing to account for façade (curtain wall) weight. The edge of the slab is 1 foot from the perimeter framing. The design live load (unreduced) is 50 psf for floors and 30 psf for the roof (increased live load within egress areas is neglected in this study). A summary of the design gravity loads is presented in Table 2-2.

Table 2-2. Design Gravity Loads

Load	Load Type	Magnitude
Dead, D	Dead	46 psf ¹
Floor Superimposed Dead, SD	Dead	15 psf
Roof Superimposed Dead, SD	Dead	10 psf
Façade Dead (Curtain Wall), SD	Dead	250 plf
Unreduced Design Floor Live, L_o	Floor Live	50 psf (Office)
Unreduced Design Roof Live, L_o	Roof Live	30 psf ²

¹ Weight of slab and metal deck only. Self-weight of steel components is included automatically in the structural analysis.

² 10 psf was added to the roof live load to represent non-inertial service equipment weight.

Verification of serviceability criteria under gravity loads is performed per IBC §1604.3, ASCE 7 §1.3.2, and AISC 360 Chapter L.

2.2.3 Environmental Loads

2.2.3.1 Earthquake Forces

The archetype buildings are located where it is assumed they would be assigned a Seismic Design Category (SDC) at the upper limit of D (i.e., D_{max} —see footnote 6). Two designs are produced for each archetype building height and frame type as follows:

- One design using the ELF procedure per ASCE 7 §12.8 to determine the equivalent seismic effects.
- One design using the RSA procedure per ASCE 7 §12.9 to determine the equivalent seismic effects.

Two designs are performed to provide a common range of potential system strengths for seismic assessment using ASCE 41, and to a lesser extent, provide comparison points between the two design methodologies. There are cases when the two designs do not result in different member sizes because of material-specific minimum requirements. Further, wind effects are determined from statically applied design forces and thus the analysis method for wind does not vary between the two seismic analyses.

For the RSA procedure, enough modes are included in each principal direction to exceed 90 percent mass participation in both horizontal orthogonal directions. Masses were not modeled in the analysis to address vertical accelerations. Design forces determined from the RSA are scaled up so that the total modal base shear for design is equal to 85 percent of the corresponding base shear from applying the ELF procedure; story drifts are not scaled for verifying seismic drift compliance. Application of orthogonal seismic forces and accidental eccentricity prescribed in ASCE 7 §12.5 and ASCE 7 §12.8.4, respectively, are considered in the strength design analysis. The redundancy factor, ρ , is taken as 1.0 for each SFRS, and therefore does not affect the allowable seismic drift limits along the E-W direction (moment frames).

⁶ See FEMA P695: *Quantification of Building Seismic Performance Factors* (FEMA 2009a) for further information.

Effective seismic weights for computing the horizontal earthquake forces are determined from dead loads plus 20 percent of the unreduced design floor live loads to represent partition weight (i.e., $0.2 \times 50 \text{ psf} = 10 \text{ psf}$). The effective seismic weights (lumped at each level) are tabulated in Appendix B. It is assumed in this study that there is no snow load on the building.

The story gravity loads for seismic drift analysis prescribed in ASCE 7 §12.8.6 (including period calculation) and stability verification prescribed in ASCE 7 §12.8.7 are determined from dead loads plus 25 percent of the unreduced floor live loads (i.e., $0.25 \times L_o \approx 0.5L$ where L is the *reduced* floor live loads). Roof live loads are considered not to be present for seismic drift analysis. The effective lumped gravity load acting on a story is tabulated in Appendix B. Vertical seismic loads are considered for strength design but not for drift or stability compliance. Similarly, application of orthogonal seismic forces and accidental eccentricity are not considered in the drift analysis because story drifts are computed at the center of mass (which aligns with the center of stiffness) of each story because of building symmetry and regularity. The centers of mass for all stories are vertically aligned.

The seismic hazard in ASCE 7 is based on a risk-targeted design philosophy and is defined as ground motions having a one percent probability of causing total or partial structural collapse (i.e., “risk”) of an appropriately designed structure in 50 years (except in areas controlled by the deterministic cap⁷ on ground motions). This ground motion intensity is denoted in ASCE 7 as MCE_R . The following parameters summarize the seismic hazard used for design:

- Building Risk Category: II
- Site Soil Conditions: Site Class D, Stiff Soil – ASCE 7 Table 20.3-1
- Spectral Response Acceleration Parameters: shown in Table 2-3
- SDC: D—taken as D_{max} as used in FEMA P695

Table 2-3. Spectral Response Acceleration Parameters

SDC	S_s (g)	S_1 (g)	F_a	F_v	S_{MS} = $F_a S_s$ (g)	S_{M1} = $F_v S_1$ (g)	S_{DS} = $\frac{2}{5} S_{MS}$ (g)	S_{D1} = $\frac{2}{5} S_{M1}$ (g)	$3.5 \times T_s$ (sec)
D_{max}	1.50	0.60 ¹	1.00	1.50	1.50	0.90	1.00	0.60	2.1

1. S_1 is actually just under 0.60 (i.e., 0.599)

Allowable seismic drift limit is set to $h_{sx} / 50$ (for amplified story drifts, see ASCE 7 §12.12) where h_{sx} is the story height below the level under consideration. Composite action between the beams of the SFRS and the concrete slab is not considered for checking seismic drifts or when computing the fundamental period, T_1 . This action is commonly neglected in seismic analysis and design because research has shown that the slab does not contribute significantly to the strength or stiffness of the assembly at significant inelastic deformations (see FEMA 355D (FEMA 2000c)).

The seismic analysis and design parameters for each archetype building are provided in Table 2-4 for the E-W direction and Table 2-5 for the N-S direction. There is one archetype building system that is *not*

⁷ Regions where probabilistic-based ground motion parameters exceed those resulting from deterministic ground motions based on the characteristic magnitudes of earthquakes from well-defined active fault systems.

permitted to be designed with the ELF procedure because its design period, $C_u T_a$, is greater than $3.5 \times T_s$ (see ASCE 7 §12.6): E-W component of MC16 (SMF)—this system is shaded in Table 2-4. This frame is included to make a seismic performance comparison. Furthermore, ASCE 7 is vague about which T is referenced in ASCE 7 §12.6. For example, although the capped fundamental period ($T = C_u T_a$) may satisfy $3.5 \times T_s$, the actual fundamental period ($T = T_1$) may not, indicating that the ELF procedure may be used for strength design but not used for drift verification per ASCE 7 §12.8.6.2. Consequently, the same analysis procedure was used for both strength design and computation of the design story drifts in this study.

Table 2-4. Seismic Analysis and Design Parameters, E-W

Building	MC4		MC8		MC16	
SFRS	SMF		SMF		SMF	
R, C_d, Ω_o	8, 5.5, 3		8, 5.5, 3		8, 5.5, 3	
$C_u T_a$ (seconds)	1.04		1.76		3.02	
ELF Permitted?	Yes		Yes		No ⁸	
Height Limit (feet)	No Limit		No Limit		No Limit	
Analysis Procedure	ELF	RSA	ELF	RSA	ELF	RSA
W^1 (kips)	5172	5136	10618	10527	21782	21649
V_b^1 Design (kips)	374	316	467 ²	394 ²	958 ²	810 ²
V_b^1 Drift (kips)	213	166	273	192	375	295
RSA Scaling Factor ³	NA	Design = 93 Drift = 266	NA	Design = 101 Drift = 266	NA	Design = 134 Drift = 266
T_1^4 (seconds)	1.82	2.22	2.91	3.81	4.36	5.01
T_2^4 (seconds)	0.55	0.61	1.02	1.30	1.58	1.83
T_3^4 (seconds)	0.26	0.29	0.56	0.68	0.91	1.05
T_1^5 (seconds)	1.83	2.24	2.94	3.86	4.40	5.07
T_1^6 (seconds)	1.77	2.12	2.79	3.55	4.15	4.70
Steel Wgt. ⁷ (tons)	37	29	74	53	193	163

Notes:

- ¹ Inertial mass computed as Dead + Superimposed Dead + 0.2×Floor Live. W for ELF and RSA differ because of member size differences.
- ² $0.044 S_{DS} I_e$ min. controls strength design (not applied for drift).
- ³ Scaling for design = $g \times I_e / R \times (0.85 \times V_{b,ELF}) / V_{b,RSA}$. Scaling for drift = $g \times I_e / R \times C_u / I_e$. Scaling assumes the spectrum is defined as a function of g .
- ⁴ Computed from a second-order eigenvalue analysis with Dead + Superimposed Dead + 0.25×Floor Live gravity load.
- ⁵ Computed from a second-order eigenvalue analysis with 1.2×Dead + 1.2×Superimposed Dead + 0.25×Floor Live gravity load.
- ⁶ Computed from a first-order eigenvalue analysis.
- ⁷ Per single SFRS (see Table 1-1). Does not include connection or miscellaneous steel.
- ⁸ Analysis procedure not permitted per ASCE 7 §12.6. Shaded Area: design is included for seismic performance comparison purposes.

Table 2-5. Seismic Analysis and Design Parameters, N-S

Building	MC4		MC8		MC16	
SFRS	SCBF		SCBF		SCBF	
R, C_d, Ω_o	6, 5, 2		6, 5, 2		6, 5, 2	
$C_u T_a$ (seconds)	0.60		0.99		1.64	
ELF Permitted?	Yes		Yes		Yes	
Height Limit (feet)	240		240		240	
Analysis Procedure	ELF	RSA	ELF	RSA	ELF	RSA
W^1 (kips)	5172	5136	10618	10527	21782	21649
V_b^1 Design (kips)	857	723	1073	904	1326	1120
V_b^1 Drift (kips)	782	627	735	633	1089	945
RSA Scaling Factor ³	NA	Design = 74 Drift = 322	NA	Design = 92 Drift = 322	NA	Design = 76 Drift = 322
T_1^4 (seconds)	0.67	0.72	1.45	1.50	2.08	2.14
T_2^4 (seconds)	0.27	0.28	0.48	0.49	0.70	0.71
T_3^4 (seconds)	0.18	0.19	0.27	0.28	0.39	0.40
T_1^5 (seconds)	0.67	0.72	1.45	1.51	2.09	2.14
T_1^6 (seconds)	0.66	0.71	1.43	1.49	2.06	2.11
Steel Wgt. ⁷ (tons)	13	12	28	27	127	123

Notes:

- ¹ Inertial mass computed as Dead + Superimposed Dead + 0.2×Floor Live. W for ELF and RSA differ because of member size differences.
- ² $0.044 S_{DS} I_e$ min. controls strength design (not applied for drift).
- ³ Scaling for design = $g \times I_e / R \times (0.85 \times V_{b,ELF}) / V_{b,RSA}$. Scaling for drift = $g \times I_e / R \times C_u / I_e$. Scaling assumes the spectrum is defined as a function of g .
- ⁴ Computed from a second-order eigenvalue analysis with Dead + Superimposed Dead + 0.25×Floor Live gravity load.
- ⁵ Computed from a second-order eigenvalue analysis with 1.2×Dead + 1.2×Superimposed Dead + 0.25×Floor Live gravity load.
- ⁶ Computed from a first-order eigenvalue analysis.
- ⁷ Per single SFRS (see Table 1-1). Does not include connection or miscellaneous steel.

The difference in the stiffness and strength of the SCBFs provided by the ELF and RSA procedures is negligible. This is primarily due to design provisions prescribed in AISC 341 (e.g., minimum width-to-thickness ratios for highly ductile braces). A summary of the equivalent seismic forces for each archetype building is provided in Appendix B.

2.2.3.2 Wind Forces

Basic wind speeds are taken from the ASCE 7 wind maps based on locations along the west coast that would have a high probability of producing structures assigned to SDC D. The basic wind speed is taken to be 110 mph for the 700-year wind for strength design of components and 72 mph for the 10-year wind for verifying story drifts (serviceability). Each archetype building is assigned to Exposure B and is not considered rigid, with gust factors, G_f , for each principal direction computed assuming two percent damping. Torsional wind effects are considered, and the directionality factor, k_d , is 0.85. A summary of the wind forces for each archetype building is provided in Appendix B.

Allowable wind drift limit is set to $h_{sx} / 400$ (elastic) for the 10-year wind. Composite action between the beams of the MWFRS and the concrete slab is considered for checking wind drift and when computing the fundamental period, T_1 , for wind vibrations using an average I_{eff} as recommended in AISC 360 commentary for Chapter I. The same gravity load combination used for the seismic drift analysis is used in the wind drift analysis (see previous discussion under Earthquake Forces—§2.2.3.1).

Not all practitioners will use the 10-year wind to verify drift compliance (see ASCE 7 commentary for Appendix C); the 25-year or 50-year may be used, depending on project-specific requirements. The 10-year wind is considered appropriate for these structures, as the façade (curtain wall) is designed to accommodate large in-plane seismic movements, and period control (i.e., acceleration) is typically not a concern for building geometries in the range used for this investigation.

2.3 Structural Analysis and Mathematical Model

The archetype buildings are analyzed in ETABS, ver. 9.7.4 (CSI 2011a). A conventional *second-order* elastic analysis is used to determine the required strength of components, and member and story deformation demands (elastic and virtual inelastic). This type of analysis uses a constant reduced stiffness matrix based on an initial gravity (i.e., $P-\Delta$) load combination applied in a pre-analysis as follows:

- $P-\Delta$ load combination for strength analysis: $1.2 \times \text{Dead} + 0.25 \times \text{Floor Live}$
- $P-\Delta$ load combination for drift and stability verification analysis: $1.0 \times \text{Dead} + 0.25 \times \text{Floor Live}$

The analyses do not account for material nonlinearity or geometric imperfections (except for gravity-only load combinations—see AISC 360 Chapter C). Because the stiffness matrix remains constant for all loads, superposition of individual load effects in load combinations is applicable.

Each building is considered globally restrained horizontally, vertically, and rotationally at the seismic base (taken at grade level). The base columns of the LFRSs are embedded into the foundation wall. As such, column bases are modeled as rotationally restrained in the plane of the frames and rotationally unrestrained

out-of-plane. Non-SFRS gravity column bases are considered rotationally unrestrained in both orthogonal directions.

The mathematical models are based on centerline dimensions with rigid end offsets at the beam-to-column, brace-to-beam / column, and brace-to-beam joints with panel zones explicitly modeled based on column web and doubler plate (if required) geometry. The slabs are modeled as semi-rigid membrane diaphragms (no out-of-plane bending stiffness) with a 0.5 in-plane stiffness modifier to account for cracking at the design loads—see NIST GCR 11-917-10: *Seismic Design of Composite Steel Deck and Concrete-filled Diaphragms: A Guide for Practicing Engineers* (NIST 2011b).

In the moment frames, reduced beam sections (RBS) are explicitly modeled in all SMF beams by subdividing each member into seven segments; the RBS is modeled as two linearly-tapered sections. The typical fully restrained (FR) beam-to-column connection is illustrated in Figure 2-6, and the equivalent assembly model for linear analysis is shown in Figure 2-7.

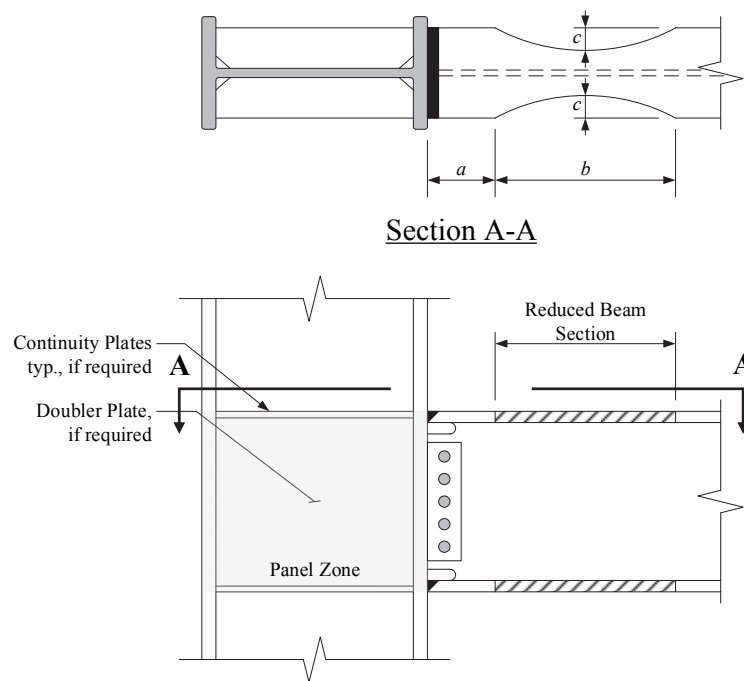


Figure 2-6. Typical FR RBS Beam-to-Column Connection Assembly

In the concentrically braced frames, member ends of the SCBF diagonal braces are rotationally unrestrained out-of-plane and restrained in-plane (though design forces do not vary significantly if modeled as unrestrained in both planes). Partially rigid end zones are included to capture gusset plate rigidity; the *tangible* length of SCBF diagonal braces is taken equal to 90 percent of the distance between work points (W.P.), L_{wp} .

The adopted brace-to-beam / column connection in the SCBF allows the beam to rotate near the edge of the gusset plate as shown in Figure 2-8—see AISC 341 Figure C-F2.8. The assembly model for linear analysis is shown in Figure 2-9. A rotationally unrestrained connection (adjacent to the gusset plate) was selected

because ASCE 41 does not prescribe flexural acceptance criteria for beam-to-column connections where a brace is present. This approach also provides a seismic design and assessment that does not rely on the contribution of non-brace assemblies for stiffness and strength. All other beam-to-column connections are simple-type connections (i.e., rotationally unrestrained).

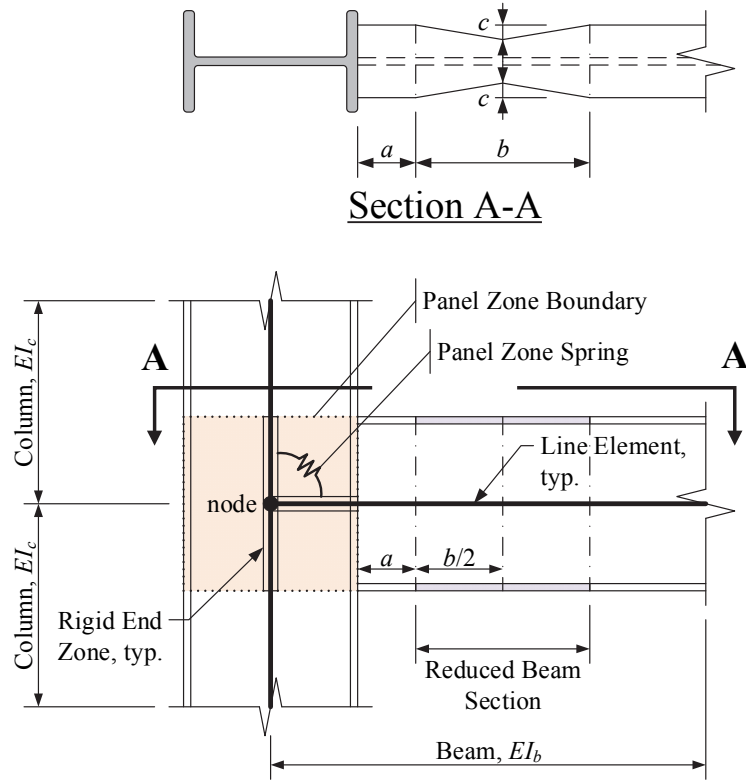


Figure 2-7. FR RBS Beam-To-Column Connection Subassembly Model for Linear Analysis

Diagonal braces were analyzed without gravity loads. Thus, two analyses were performed for each archetype building: (1) a gravity load-only model with braces removed and (2) a lateral force and gravity load model with braces in place. Load effects then were taken from the respective analysis for input into load combinations.

Non-LFRS framing that primarily supports gravity loads is included in the mathematical models to capture the “leaning column” effect. The gravity beams are modeled as composite beams with rotationally unrestrained member ends (i.e., shear tab connections). The gravity columns are modeled as continuous along the height of the building and designed for deformation compatibility. The increase in lateral stiffness along the two principal axes due to these columns is negligible. Other than the columns, no other forms of lateral stiffness attributed to non-SFRS framing (e.g., stairs) and nonstructural components are considered in the mathematical model.

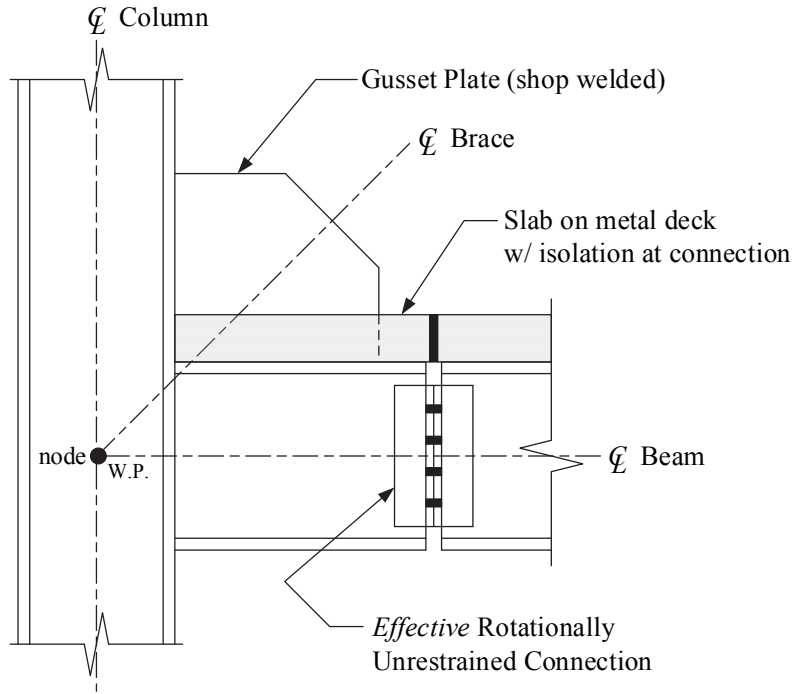


Figure 2-8. Typical Brace-to-Beam / Column Connection Assembly

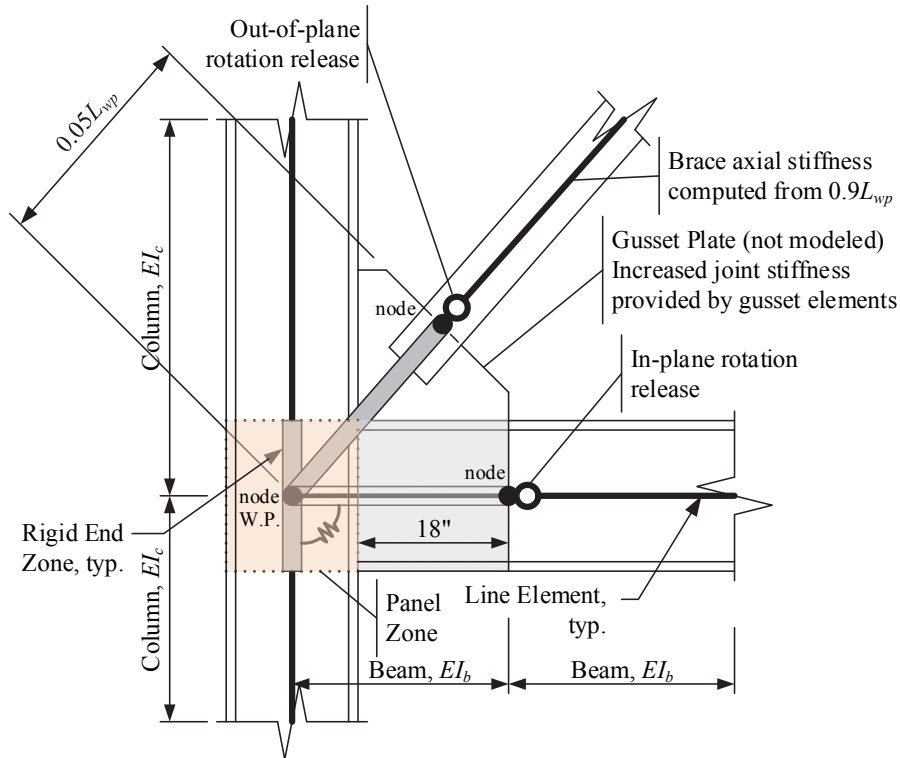


Figure 2-9. Brace-to-Beam / Column Connection Subassembly Model for Linear Analysis

2.4 SFRS Design

2.4.1 SMF Design

For the SMF designs, seismic drift criteria prescribed in ASCE 7 §12.12 tended to control member sizes for both 4-story archetype buildings and the 8-story ELF-designed archetype building. The seismic stability criteria prescribed in ASCE 7 §12.8.7 tended to control member sizes for the 8-story RSA-designed archetype building and both 16-story archetype buildings (ELF design was more drift controlled than the RSA design). The strong-column / weak-beam (SCWB) criteria using an amplified seismic load (axial) and section compactness requirements provided additional constraint on column sizes where required.

The RBS beam-to-column connections were designed in accordance with AISC 358 with the flange cut out dimensions optimized to produce the lowest *probable* moment, M_{pr} . Because the bay length did not change, the same beam depth was used for a given floor for uniform connection constructability and plastic hinge sequencing optimization (i.e., yield rotation is theoretically equal). The panel zones are designed for demands based on the *probable* moment of the RBS projected to the column face using nominal material properties. AISC 360 §J10.6 (b) is applicable for panel zone design because the effect of panel zone deformations on frame stability is explicitly considered in the analysis. The flow chart in Figure 2-10 illustrates the analysis and design process for an SMF. Additional details on design and construction of special moment frames can be found in NIST GCR 09-917-3: *Seismic Design of Steel Special Moment Frames: A Guide for Practicing Engineers* (NIST 2009b).

To reflect industry practice and reduce fabrication costs, column sizes were increased from that required by analysis rather than adding doubler plates. AISC Design Guide 13 (AISC 1999) and Troup (1999) showed that increasing the column size by up to 100 plf to eliminate both continuity plates and doubler plates was often the more economical alternative. Some seismic specifications (e.g., AISC 341), however, either require or suggest the use of transverse stiffeners in all high seismic applications. For these cases, eliminating the need for doubler plates alone may still prove to be the economical choice (Lee et al. 2002). In this study, this increase typically occurred at interior frame columns and on average was 100 plf for the frame as a whole.

The Effective Length Method (see AISC 360 §C1) is used for design of the SMF columns, with the Story Buckling Method (see commentary for AISC 360 Appendix 7) used to compute the effective length, $KL = K_2L$ (see footnote 8) for determining the nominal compression strength, P_n , of the column in the plane of the frame. In all but one SMF, at least one story had B_2 , as defined in AISC 360 Appendix 8, greater than 1.1; all stories were less than 1.5 (see AISC 360 Appendix 7). Tabulated values for B_2 are provided in Appendix B. $KL = L$ was adopted for determining P_n of the column out-of-plane of the frame.

⁸ AISC 360-05 (AISC 2005) used the term K_2 to define the in-plane effective length factor. AISC 360-10 Appendix 7 uses K in lieu of K_2 . However, K_2 is still used in the commentary of Appendix 7. Therefore, K_2 is also used here. Additional information can be found in *Steel Design Guide 28: Stability Design of Steel Buildings* (AISC 2013).

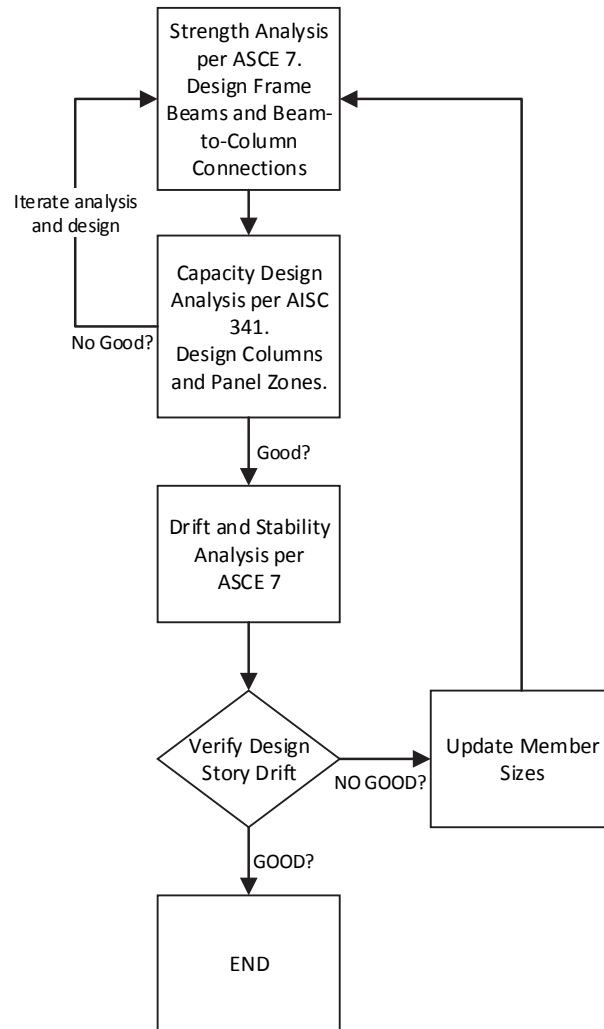


Figure 2-10. Flow Chart of SMF Design Process

Computation of in-plane effective length factors is *generally* considered to be not required for columns in regular moment frames in high seismicity areas (i.e., adopting $KL = L$). Seismic story drift and stability requirements in ASCE 7 typically result in significant in-plane story strength and stiffness above that required by the analysis. However, the concept of story drift control without consideration of its effects on a moment frame is a nontechnical rationale for neglecting the effective length factors for in-plane seismic design of frame columns. Essentially, the effects of drift control reduce the error in calculating the beam-column strength for load combinations including lateral forces because of the following (taken from White and Hajjar 1997):

- The in-plane, strong-axis radius of gyration, r_x , is increased thus lowering KL / r_x in the design equation. Column strength varies little with large variations of KL / r_x .
- The columns are heavily restrained at each end by deep beams, and subjected to nearly double-curvature bending under sideway of the frame.
- The beam-column interaction check for the lateral force-resisting columns is dominated by the moment term.

Designers must also consider the vertical strength of a story⁹ loaded only with gravity-type loads, as well as the correlation of the actual demand relative to this vertical strength (e.g., $P_{story} / P_{e,story}$ as defined in AISC 360 Appendix 8). This story strength would represent the minimum value of P_n (in the absence of moment) for construction of the P - M interaction diagram for the in-plane strength of a frame column in the story. Fundamentally, the effective length factor for a column is a function of the frame deformation demands and the loading on the column. Consequently, a P - M interaction diagram would need to be constructed for each category of load combination (e.g., vertical load, vertical plus horizontal loads) considering the influence of the ratio of vertical to horizontal loading demands as well as which loading is being incremented until incipient buckling. Theoretically, $KL = L$ should be adopted when the physical behavior of the column at its ultimate strength aligns with the theoretical definition of the compression strength. Future studies should investigate designing the selected frames using the Direct Analysis Method prescribed in AISC 360 Chapter C.

In proportioning frame members for this study, section depths were selected to maintain a low in-plane relative beam-to-column stiffness ratio, G . AISC 360 commentary for Appendix 7 defines G for bending about the strong-axis as Equation (2-1)—see AISC 360 for definitions of the variables and subscripts.

$$G = \frac{\sum \tau_b \frac{EI_{x,c}}{L_c}}{\sum \gamma \frac{EI_{x,b}}{L_b}} \quad (2-1)$$

Other relationships can be used to show that G can be computed as function of the in-plane flexural section strength, $Z_x \times F_y$, independent of the in-plane flexural stiffness, $E \times I_x$. Equation (2-2) shows that the strong-axis plastic section modulus, Z_x , is a function of the strong-axis moment of inertia, I_x , and section depth, d . Equation (2-3) rewrites the SCWB equation in AISC 341 (see §E3.4a) for a wide-flange section.

$$Z_x = \frac{2I_x}{d} \quad (2-2)$$

$$\frac{M_{p,c}}{M_{p,b}} = \frac{\min \left[1.18 \left(1 - \frac{P_{u,\Omega}}{P_y} \right), 1.0 \right] Z_{x,c} F_y}{Z_{x,b} F_y} \geq 1 \rightarrow \therefore Z_{x,b} \leq \min \left[1.18 \left(1 - \frac{P_{u,\Omega}}{P_y} \right), 1.0 \right] Z_{x,c} \quad (2-3)$$

$$\therefore G = \frac{\tau_b}{\min \left[1.18 \left(1 - \frac{P_{u,\Omega}}{P_y} \right), 1.0 \right]} \frac{d_c L_b}{d_b L_c} \quad (2-4)$$

⁹ The vertical story strength, $P_{e,story}$, is a function of the *elastic* lateral stiffness of the story.

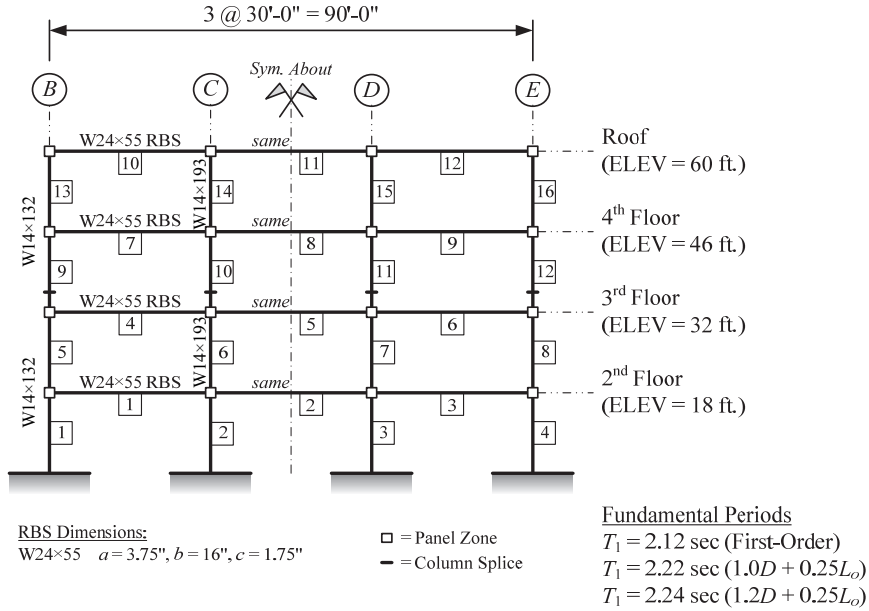
In the previous equations, $P_{u,\Omega}$ is the axial load demand in the column including the system overstrength factor, Ω_o , in ASCE 7 as required by AISC 341 §E3.4a. An additional rule of thumb is that $d_c \geq d_b / 2$ and $d_c \leq d_b$. For example, an 18-inch deep column and 24-inch deep beam were selected for the SMF in the 8-story building. Conservatively assuming a 15 percent reduction in plastic flexural strength of the column leads to $G = 1.9$ (see Equation (2-5)). A 27-inch deep column and 36-inch deep beam could also have been selected, but this would have been at the expense of architectural constraints and construction budget.

$$G = \frac{\tau_b}{1.18 \left(1 - \frac{P_{u,\Omega}}{P_y} \right)} \frac{d_c L_b}{d_b L_c} = \frac{1.0}{0.85} \frac{d_c}{d_b} \frac{360}{168} = 2.52 \frac{18}{24} = 1.9 \quad (2-5)$$

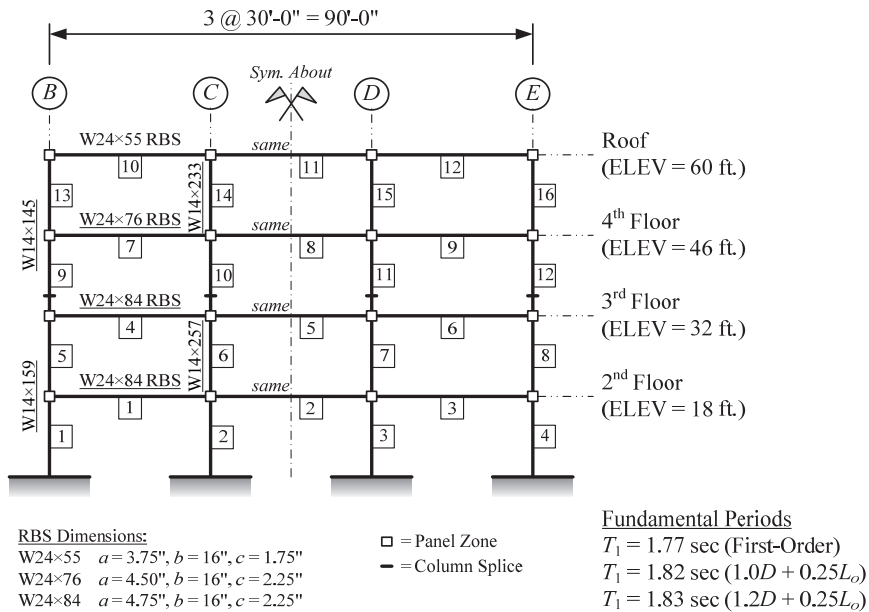
This approach assists in selecting member depths while attempting to minimize relative elastic flexural stiffness variations between the beams and columns within a story, and between adjacent stories. As discussed previously, computing G is not required unless the size of the frame column is governed by strength requirements and one is using the Effective Length Method; tabulated values for K are provided in Appendix B.

The lateral force distributions and story shears for each archetype building are provided in Appendix B. Allowable drift compliance verification is provided in Appendix B. Similarly, verification for drift amplification from global p-delta (P - Δ) effects and ASCE 7 stability verification are also provided in Appendix B. Design calculations for select members and connections are provided to illustrate the design process in Appendix B.

The 4-, 8-, and 16-story SMF frame designs are shown in Figure 2-11 through Figure 2-13. Each figure shows both the RSA design (a) and the ELF design (b)—underlined member sizes indicate changes from the RSA design. These figures also provide the RBS dimensions and fundamental periods of the archetype building for various gravity loads (e.g., drift and strength design).

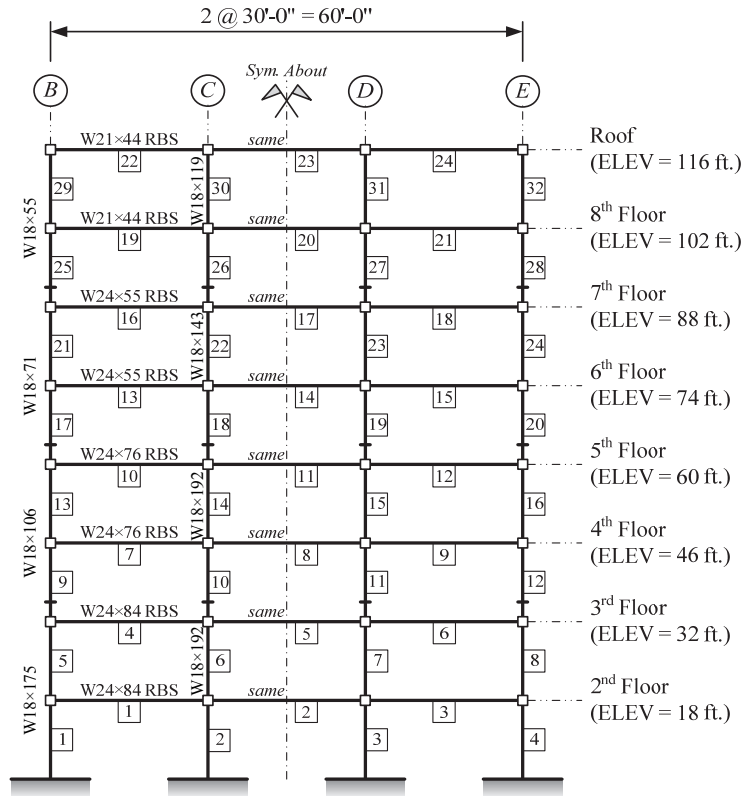


(a) RSA



(b) ELF

Figure 2-11. 4-Story SMF Schematic



RBS Dimensions:

RBS Dimensions:	W21x44	W24x55	W24x76	W24x84
a	3.25"	3.75"	4.50"	4.75"
b	14"	16"	16"	16"
c	1.50"	1.75"	2.25"	2.25"

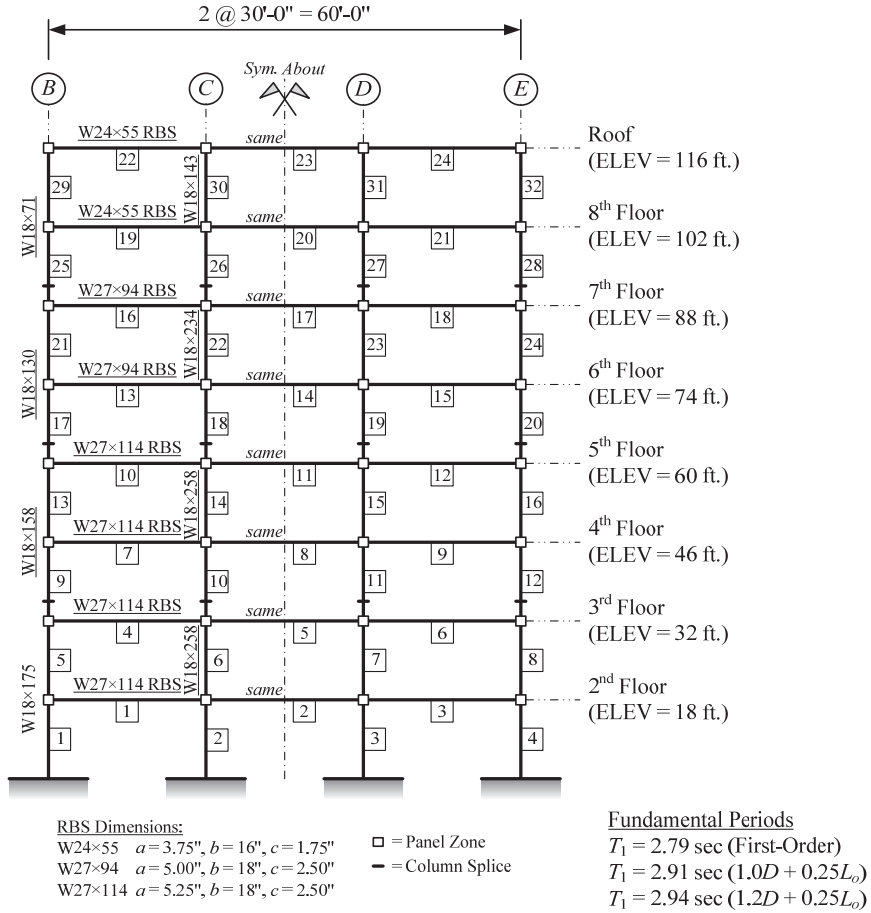
□ = Panel Zone
 — = Column Splice

Fundamental Periods

- $T_1 = 3.55$ sec (First-Order)
- $T_1 = 3.81$ sec ($1.0D + 0.25L_o$)
- $T_1 = 3.86$ sec ($1.2D + 0.25L_o$)

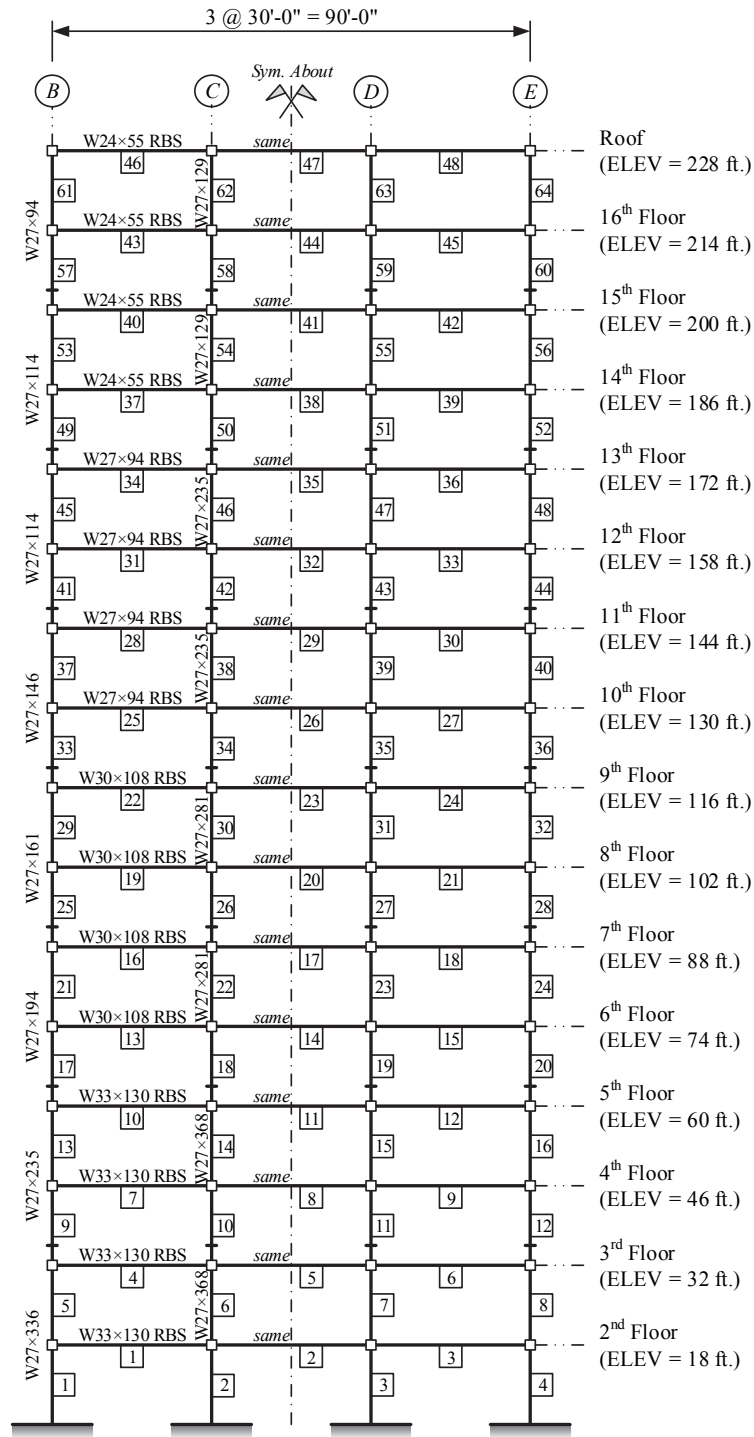
(a) RSA

Figure 2-12. 8-Story SMF Schematic



(b) ELF

Figure 2-12. 8-Story SMF Schematic, Cont'd



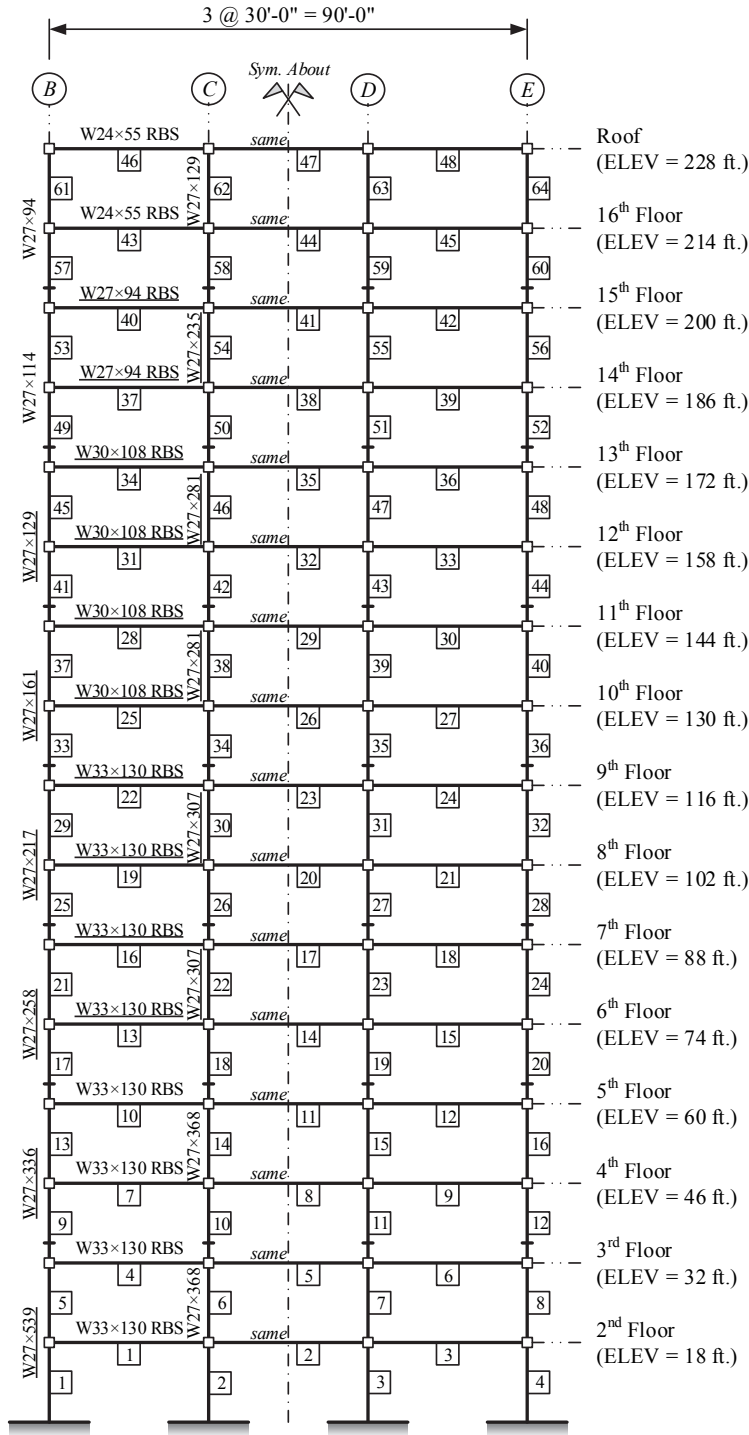
RBS Dimensions:
W24x55 $a = 3.75"$, $b = 16"$, $c = 1.75"$
W27x94 $a = 5.00"$, $b = 18"$, $c = 2.50"$
W30x108 $a = 5.25"$, $b = 20"$, $c = 2.50"$
W33x130 $a = 5.75"$, $b = 22"$, $c = 2.75"$

□ = Panel Zone
- - = Column Splice

Fundamental Periods
 $T_1 = 4.70$ sec (First-Order)
 $T_1 = 5.01$ sec ($1.0D + 0.25L_o$)
 $T_1 = 5.07$ sec ($1.2D + 0.25L_o$)

(a) RSA

Figure 2-13. 16-Story SMF Schematic



RBS Dimensions:

W24x55 $a = 3.75"$, $b = 16"$, $c = 1.75"$
W27x94 $a = 5.00"$, $b = 18"$, $c = 2.50"$
W30x108 $a = 5.25"$, $b = 20"$, $c = 2.50"$
W33x130 $a = 5.75"$, $b = 22"$, $c = 2.75"$

□ = Panel Zone
- - = Column Splice

Fundamental Periods

$T_1 = 4.15$ sec (First-Order)
 $T_1 = 4.36$ sec ($1.0D + 0.25L_o$)
 $T_1 = 4.40$ sec ($1.2D + 0.25L_o$)

(b) ELF

Figure 2-13. 16-Story SMF Schematic, Cont'd

2.4.2 SCBF Design

SCBF designs are included here to provide the required information of the building for SMF designs. For the SCBF designs, seismic strength requirements prescribed in ASCE 7 and seismic compactness requirements in AISC 341 controlled brace sizes for all archetype buildings. Section compactness and capacity design requirements in AISC 341 §F2.3 (i) and (ii)—exception 2(a) is not considered here—governed column and beam sizes. The beams in the 4-story frames are laterally braced per AISC 341 and designed for the unbalanced load created by a buckled brace. For the 8- and 16-story frames, except at the second floor, beam sizes were maintained at each floor based on the largest required strength (usually at the third and fourth floors). The beams on the second floor had an atypical change in required strength because of the variation in adjacent story heights. The flowchart in Figure 2-14 illustrates the analysis and design process for an SCBF. Additional details on design and construction of special concentrically braced frames can be found in NIST GCR 13-917-24: *Seismic Design of Steel Special Concentrically Braced Frame Systems: A Guide for Practicing Engineers* (NIST 2013).

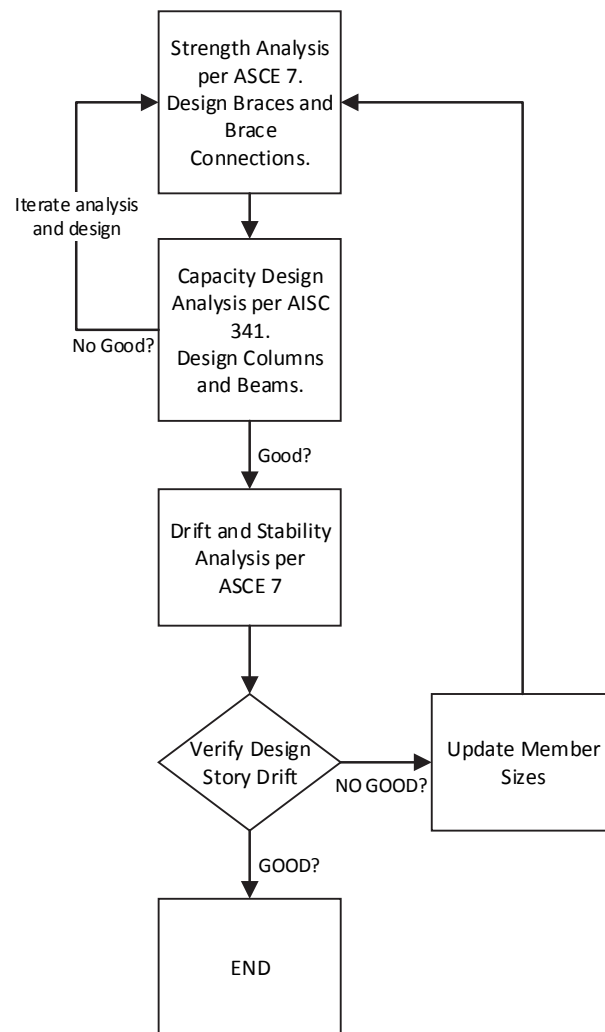


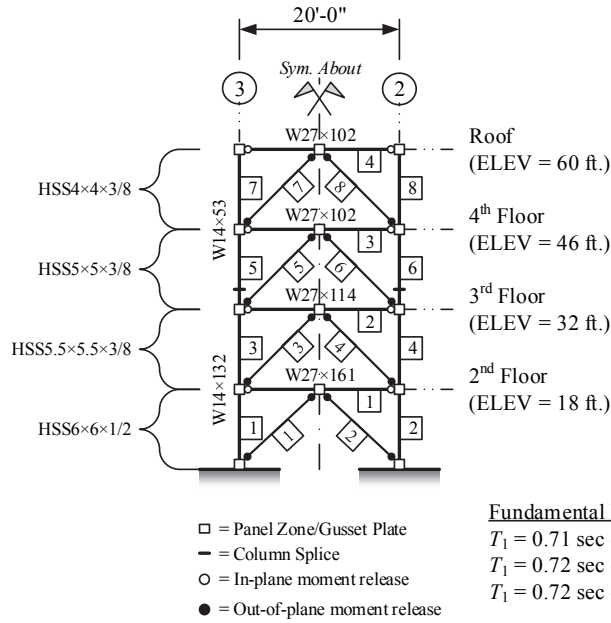
Figure 2-14. Flow Chart of SCBF Design Process

Wind drift criteria began to influence the 16-story SCBF when two isolated 20-foot two-story braced bays were used (as done in the 4- and 8-story archetype buildings). Therefore, a double 30-foot bay configuration was adopted to minimize nonseismic force contributions to member selections, as well as to allow seismic assessment of longer (potentially slender) braces.

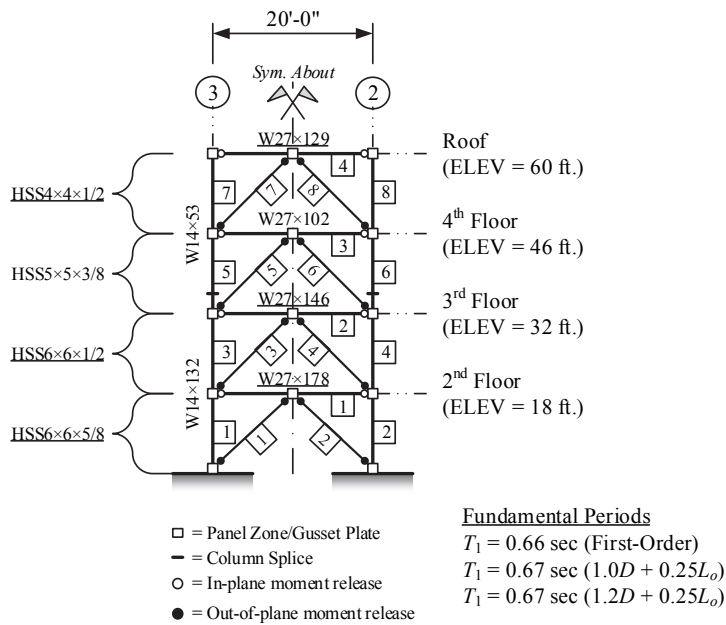
The Effective Length Method (see AISC 360 §C1) is used for design of the SCBF braces, beams, and columns. The effective length factor, K , was conservatively taken as unity for determining the nominal compression strength, P_n , of the SCBF members, although a lower value could be justified by analysis. Though the gusset plate connections are not fully designed and detailed in this study, a lower value of K could have been adopted where the rotational stiffness of the connection can influence the assumed boundary conditions of the adjacent braces (out-of-plane buckling controlled design). Hollow structural sections (HSS) are used as the diagonal braces in all archetype buildings while keeping face dimensions within the adjacent column flange widths. The *tangible* length of SCBF braces is taken equal to 90 percent of the distance between work points, L_{wp} . Diagonal braces are designed *not* to carry gravity loads—see §2.3.

The lateral force distributions and story shears for each archetype building are provided in Appendix B. Allowable drift compliance verification is provided in Appendix B. Similarly, verification for drift amplification from global p-delta ($P-\Delta$) effects and ASCE 7 stability verification are also provided in Appendix B. Design calculations for select members and connections are provided to illustrate the design process in Appendix B.

The 4-, 8-, and 16-story SCBF frame designs are shown in Figure 2-15 through Figure 2-17, respectively. Each figure shows both the RSA design (a) and the ELF design (b)—underlined member sizes indicate changes from the RSA design. These figures also provide the fundamental periods of the archetype building for various gravity loads (e.g., drift and strength design).

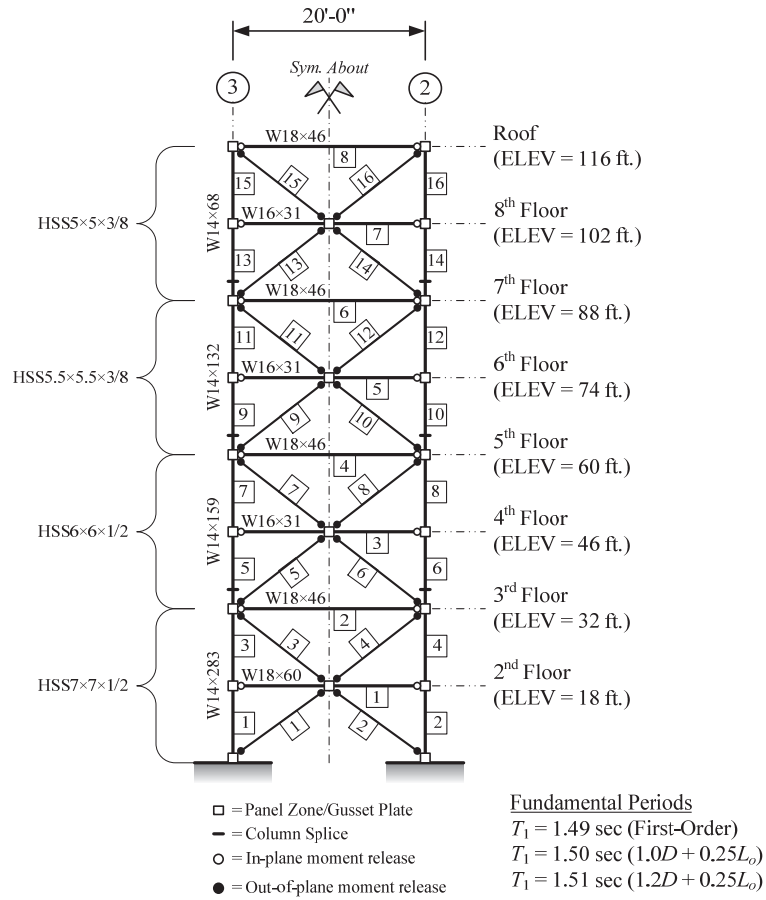


(a) RSA



(b) ELF

Figure 2-15. 4-Story SCBF Schematic



(a) RSA

Figure 2-16. 8-Story SCBF Schematic

Chapter 3 Seismic Assessment

This chapter presents the results of the seismic assessment of the special moment frames in accordance with ASCE 41. Section 3.1 provides general discussions on the global analysis requirements for assessment. Analysis requirements specific to moment frames and assessment results of *primary* components of the frames are provided in Section 3.2.

3.1 Assessment Overview

A seismic performance assessment of the special moment frames is conducted using both linear and nonlinear analysis procedures prescribed in ASCE 41 §2.4:

- Linear Static Procedure [ASCE 41 §3.3.1]
- Linear Dynamic Procedure (Response Spectrum) [ASCE 41 §3.3.2]¹⁰
- Nonlinear Static Procedure [ASCE 41 §3.3.3]¹¹
- Nonlinear Dynamic Procedure [ASCE 41 §3.3.4]

Seismic assessment analyses follow the guidelines outlined in ASCE 41 Chapters 1 through 3, and, where applicable, ASCE 41 Chapter 5. Foundations, including soil-structure interaction, and geological site hazards (ASCE 41 Chapter 4) are not considered in this study. Modeling and assessment requirements for steel structural systems follow the provisions in ASCE 41 Chapter 5. Any deviations from these guidelines are explained where applicable.

The seismic performance target (i.e., ‘rehabilitation objective’) for this study is selected as the Basic Safety Objective (BSO) in ASCE 41 §1.4.1. This selection allows the correlation between the seismic performance objective intended by ASCE 41 and the intended design objective of ASCE 7 for an ordinary building¹² to be evaluated. The BSO associated goals for Structural Performance Levels (SPLs) found in ASCE 41 §1.5.1 and Earthquake Hazard Levels (EHLs) found in ASCE 41 §1.6 are given in Table 3-1. Nonstructural Performance Levels (NPLs) found in ASCE 41 §1.5.2 are not considered in this study. The target Building Performance Levels (BPLs) found in ASCE 41 §1.5.3 are given in Table 3-1.

The only explicit connection between the target *structural* performance objectives (i.e., SPL) of the BSO in ASCE 41 and the intended *structural* design performance objective of ASCE 7 is ‘Collapse Prevention’ given an MCE event, assuming that the BSE-2 EHL is equivalent to the MCE defined by ASCE 7—see Table 1-1 and Table 3-1. It is presumed by ASCE 7 that an appropriately designed structure using a seismic hazard of $\frac{2}{3}\times$ MCE will achieve this *structural* design performance objective. ASCE 7 does not explicitly

¹⁰ The user can alternatively perform a linear response history analysis. This was not done in this study, although it would bypass the limitations of using modal response spectrum analysis.

¹¹ Simplified Nonlinear Static Procedure (NSP) is not considered.

¹² Structures assigned to Risk Category II or lower.

identify a target *structural* design performance objective for ‘Life Safety’ at $\frac{2}{3}\times$ MCE. Rather, ASCE 7 contains implicit life safety measures to protect against loss of life from nonstructural damage at the design-level event, $\frac{2}{3}\times$ MCE.

Table 3-1. Seismic Performance Targets (from ASCE 41-06)

Earthquake Hazard Level	Earthquake Intensity	Structural Performance Level	Nonstructural Performance Level	Building Performance Level
BSE-1 – §1.6.1.2	$\frac{2}{3}\times$ BSE-2	Life Safety (S-3)	Not Considered (N-E)	Life Safety (3-E)
BSE-2 – §1.6.1.1	Maximum Considered Earthquake (MCE)	Collapse Prevention (S-5)	Not Considered (N-E)	Collapse Prevention (5-E)

Prior to ASCE 7-10, the MCE was defined as a uniform seismic hazard associated with a two percent probability of being exceeded in 50 years, except near known faults where deterministic-based hazards controlled. ASCE 7-10 adopted a risk-targeted design philosophy that shifts from a uniform *hazard design basis* to a uniform *risk design basis*, and defines the MCE ground motion intensity (denoted as MCE_R) as ground motions having a one percent probability of causing total or partial structural collapse in 50 years. This risk has a conditional probability (‘anticipated reliability’) of ten percent probability of total or partial structural collapse conditioned on the occurrence of an MCE event—see ASCE 7 Table C.1.3.1b. Several reference documents are available for more information about this implementation (FEMA 2009b, commentary of ASCE 7-10 (3rd printing), and NIST 2012). Therefore, the approved MCE in ASCE 41-06 §1.6.1.1 (see BSE-2 in Table 3-1) should be taken as the MCE_R in ASCE 7-10 to maintain equivalency between the standards. ASCE 41-13 §2.2.4 prescribes using the MCE_R to define the BSE-2 EHL for the new building equivalency track. The seismic performance targets for this study are taken from ASCE 41-13 and are given in Table 3-2.

Table 3-2. Seismic Performance Targets (from ASCE 41-13)

Earthquake Hazard Level	Earthquake Intensity	Structural Performance Level	Nonstructural Performance Level	Building Performance Level
BSE-1N ¹ – §2.4.1.2	$\frac{2}{3}\times$ BSE-2N	Life Safety (S-3)	Not Considered (N-E)	Life Safety (3-E)
BSE-2N ¹ – §2.4.1.1	Maximum Considered Earthquake (MCE_R)	Collapse Prevention (S-5)	Not Considered (N-E)	Collapse Prevention (5-E)

¹ ASCE 41-13 expanded the term ‘BSE’ to include ‘N’ or ‘E’ depending on the chosen assessment track. For this project, the ‘N’ is dropped to follow the terminology used in ASCE 41-06.

This study does not evaluate assessment results for earthquake hazard levels with return periods shorter than identified above or building performance levels below Life Safety. Future research efforts may evaluate incorporating other performance levels for design in ASCE 7—see NIST GCR 12-917-20: *Tentative Framework for Development of Advanced Seismic Design Criteria for New Buildings* (NIST 2012).

3.1.1 Seismic Hazard

The seismic hazard is defined in ASCE 41 §1.6. The spectral response parameters for the BSE-2 (\equiv BSE-2N—see above) and BSE-1 (\equiv BSE-1N—see above) EHLs are given in Table 3-3. The parameters summarize the seismic hazard¹³ for Site Class D, Stiff Soil, in ASCE 41 §1.6.1.4.1.

Table 3-3. Spectral Response Parameters

EHL	S_S (g)	S_I (g)	F_a ³	F_v ³	S_{XS} (g)	S_{XI} (g)	T_s (sec)	T_o (sec)
BSE-2	1.5	0.60 ¹	1.0	1.50	1.50	0.90	0.60	0.12
BSE-1 ²	1.5	0.60 ¹	1.0	1.50	1.00	0.60	0.60	0.12

¹ S_I is actually just under 0.60 (i.e., 0.599)

² S_S and S_I do not include 2/3 reduction prior to site class modification

³ See ASCE 41 Table 1-4 and Table 1-5

Figure 3-1 illustrates the generalized response spectrum for BSE-1 and BSE-2.

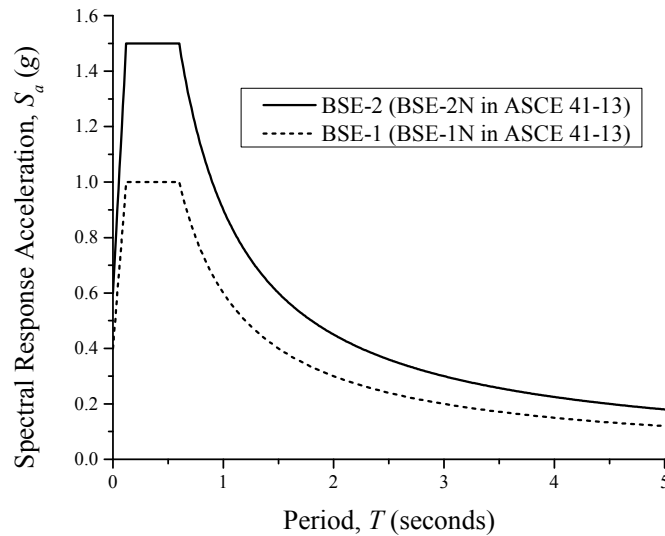


Figure 3-1. Acceleration Response Spectra

3.1.2 General Analysis Requirements

This section discusses the implementation of the general analysis requirements prescribed in ASCE 41 §3.2 in this study.

ASCE 41 §3.2.2—Mathematical Modeling: The archetype buildings are modeled in three-dimensions. Increased forces and displacements because of torsional demands are inherently addressed in the three-

¹³ The seismic hazard in ASCE 41-13 is the MCE_R, ground motion based on a risk-targeted design philosophy in which an appropriately designed structure will have a one percent probability of collapse (i.e., risk) in 50-years (except in areas controlled by the deterministic cap on ground motions—see ASCE 7 commentary for Chapter 11).

dimensional analysis. Because of building symmetry, the inherent torsional moment at each floor is *theoretically* zero. Accidental torsional moment (i.e., five percent mass offset) at each floor is not considered in the assessment analyses because the displacement modifier, η , associated with the applied loads including accidental torsion is less than 1.1 at every floor for all buildings (see Table 3-4 and Table 3-5). The values in these tables for determining torsional irregularity are based on floor displacements relative to the base and not story drifts as used in ASCE 7¹⁴.

All members and connections of the seismic force-resisting system (SFRS) are classified as *primary* components in accordance with ASCE 41 §2.4.4.2 for both linear and nonlinear assessment procedures. Gravity framing (non-SFRS members and shear tab connections) is assumed in this study to provide negligible analytical lateral stiffness and strength—see ASCE 41 §3.2.2.3. Therefore, components of the non-SFRS framing are classified as *secondary* components for both linear and nonlinear assessment procedures. Similar to the assumptions adopted for design, specific component stiffnesses (e.g., partially restrained composite shear tab connections and stairs) are not modeled explicitly in the mathematical model. This is done to minimize the influence of secondary components on the demands imposed on primary components. This will allow assessment results between linear and nonlinear analysis to be compared. Performance assessment of these secondary members is outside the scope of this study—though would need to be checked in a *real* retrofit design. In addition, foundation or soil flexibility is not included in the analysis. Models for anticipated component inelastic actions in nonlinear assessment procedures include both strength and stiffness degradation—discussed subsequently in §3.2.

ASCE 41 §3.2.3—Configuration: Building irregularities are discussed in ASCE 41 §3.1.3.1. Building irregularities defined in ASCE 41 are used only to determine whether the linear procedures are applicable.

ASCE 41 §3.2.4—Diaphragms: Floor diaphragms are modeled for analysis as semi-rigid membranes (i.e., *stiff* per ASCE 41). The same assumptions adopted in design are maintained for assessment.

ASCE 41 §3.2.5—P- Δ Effects: Global P - Δ effects are considered in the linear and nonlinear analyses, for both static and dynamic. Local P - δ effects are not addressed either explicitly or implicitly in the analyses.

ASCE 41 §3.2.6—Soil-Structure Interaction: Soil-Structure Interaction is not considered in the seismic assessment of the archetype buildings.

ASCE 41 §3.2.7—Multidirectional Seismic Effects: The *principal* axes of the archetype buildings align directly with the E-W and N-S directions (performance in the E-W direction is presented in this report). Seismic effects are determined by applying the seismic forces independently in each of the two orthogonal directions. Per ASCE 41 §3.2.7.1, concurrent seismic effects are addressed in the assessment by combining the effects along each principal axes.

¹⁴ Amplification of the accidental torsion, if required, is consistent between ASCE 41 and ASCE 7.

ASCE 41 §3.2.7—Vertical Seismic Effects: Vertical seismic effects are not considered for seismic assessment of the archetype buildings. Masses are input for horizontal accelerations only for dynamic analysis.

ASCE 41 §3.2.8—Gravity Loads: Gravity loads for the linear assessment procedures are applied using the following two load combinations (LC). Roof live loads are considered not to be present for seismic analysis. There is no snow load acting on the buildings.

- $LC1 = 1.1 \times (\text{Dead} + 0.25 \times \text{Unreduced Floor Live})$
- $LC2 = 0.9 \times \text{Dead}$

A P - Δ load combination based on LC1 above is used for the linear assessment analyses; consequently, this is conservative for analysis using LC2.

Both gravity load combinations above are used for the nonlinear static procedure. The average of the two combinations (LC1 and LC2) is applied in the nonlinear dynamic procedure.

- $LC3 = 1.0 \times \text{Dead} + 0.25 \times \text{Unreduced Floor Live}$

A P - Δ load combination based on LC3 above is used for the nonlinear assessment analyses.

ASCE 41 §3.2.9—Verification of Design Assumptions: The following design objectives are verified with the nonlinear dynamic procedure.

- SMF—Strong Column Weak Beam (SCWB) (AISC 341)
- SMF—adequate flexural and shear strength in beam at the face of column (AISC 358)
- SMF—adequate shear strength at the center of the RBS (AISC 358)
- SMF—in-plane and out-of-plane stability of columns (AISC 360)

ASCE 41 §3.2.10—Overturning: Overturning is not considered for design or seismic assessment of the archetype buildings.

3.1.3 Analysis Procedures

This section discusses the implementation of the specific analysis procedures prescribed in ASCE 41 §3.3 in this study.

3.1.3.1 Linear Analysis Procedures

The archetype buildings are modeled and analyzed in ETABS 9.7.4 (CSI 2011a) for the linear analyses. The assumptions used in the mathematical model and analysis techniques are the same as those adopted for design (see Chapter 2). Modeling and analysis considerations for the linear procedures are outlined in ASCE 41 §3.2.2 with supplemental information provided in ASCE 41 §3.3.2.2 for the Linear Dynamic Procedure (LDP). Gravity loads and load combinations assumed present during the earthquake are computed from

ASCE 41 §3.2.8 as discussed previously. The effective horizontal seismic weights, w , for analysis are computed in accordance with ASCE 41 §3.3.1, and are the same as those used for design (see Chapter 2). Global P - Δ effects (e.g., B_2 in AISC 360 Appendix 8) are addressed in the analysis by using a simplified algorithm—see ETABS User Manual. ETABS does not explicitly include local P - δ effects (e.g., B_1 in AISC 360 Appendix 8). System specific modeling assumptions and analysis techniques are described in their respective sections.

Table 3-4. Displacement Multiplier—E-W (SMF)

Floor	$\eta = \delta_{max} / \delta_{avg}$					
	MC4		MC8		MC16	
	ELF	RSA	ELF	RSA	ELF	RSA
Roof	-	-	-	-	1.010	1.008
16	-	-	-	-	1.009	1.007
15	-	-	-	-	1.009	1.007
14	-	-	-	-	1.009	1.007
13	-	-	-	-	1.009	1.007
12	-	-	-	-	1.009	1.007
11	-	-	-	-	1.008	1.007
10	-	-	-	-	1.008	1.007
9 (Roof MC8)	-	-	1.010	1.007	1.008	1.007
8	-	-	1.010	1.007	1.008	1.007
7	-	-	1.009	1.006	1.008	1.007
6	-	-	1.009	1.006	1.008	1.007
5 (Roof MC4)	1.006	1.006	1.008	1.005	1.008	1.007
4	1.006	1.006	1.008	1.005	1.008	1.007
3	1.005	1.005	1.007	1.005	1.008	1.007
2	1.005	1.005	1.007	1.005	1.008	1.007

Values shown to four significant figures are for comparison purposes only.

Table 3-5. Displacement Multiplier—N-S (SCBF)

Floor	$\eta = \delta_{max} / \delta_{avg}$					
	MC4		MC8		MC16	
	ELF	RSA	ELF	RSA	ELF	RSA
Roof	-	-	-	-	1.088	1.090
16	-	-	-	-	1.088	1.090
15	-	-	-	-	1.088	1.090
14	-	-	-	-	1.088	1.090
13	-	-	-	-	1.089	1.090
12	-	-	-	-	1.089	1.090
11	-	-	-	-	1.089	1.090
10	-	-	-	-	1.089	1.091
9 (Roof MC8)	-	-	1.087	1.091	1.089	1.091
8	-	-	1.087	1.091	1.089	1.091
7	-	-	1.088	1.091	1.089	1.091
6	-	-	1.088	1.092	1.090	1.091
5 (Roof MC4)	1.093	1.094	1.089	1.092	1.090	1.091
4	1.094	1.095	1.090	1.093	1.090	1.091
3	1.094	1.095	1.090	1.093	1.090	1.091
2	1.094	1.095	1.091	1.093	1.089	1.090

Values shown to four significant figures are for comparison purposes only.

ASCE 41 §2.4.1.1 prescribes restrictions on the use of the linear procedures. First, a *retrofitted*¹⁵ SFRS must not contain certain types of structural irregularities where the earthquake demands on the primary components of the SFRS fail to comply with the demand capacity ratio (DCR) limitations.

$$DCR = \frac{Q_{UD}}{Q_{CE}} \leq 2.0 \quad (3-1)$$

where Q_{UD} is the demand on a component due to gravity and earthquake loads and Q_{CE} is the expected strength of the component. The archetype buildings do not contain any configuration-based in-plane or out-of-plane irregularities. Further, a linear analysis procedure must be performed to determine whether a building contains a weak story or torsional strength irregularity. Because of plan symmetry and regularity of the archetype buildings, there are no torsional irregularities. The required weak story irregularity verifications are discussed subsequently in the linear static procedure for each specific system type.

3.1.3.1.1 Linear Static Procedure

The Linear Static Procedure (LSP) is outlined in ASCE 41 §3.3.1. The provisions of the LSP closely resemble those of the ELF procedure in ASCE 7; as such, no additional analysis details are presented here. However, one place where ASCE 7 and ASCE 41 differ is in the determination of the fundamental period, T , in the direction being analyzed. ASCE 41 does not place an upper-bound limit on the period used for assessment as ASCE 7 does for strength design. In this study, the fundamental periods are determined by eigenvalue analysis per ASCE 41 §3.3.1.2.1.

Further restrictions on the use of the LSP are prescribed in ASCE 41 §2.4.1.2. The LSP cannot be used if any of the following occur:

- The fundamental period of the building, T , is greater than $3.5 \times T_s$ ($= 3.5 \times 0.6 = 2.1$ seconds in this study). This trigger is similar to that used in ASCE 7; however, like ASCE 7, which computation method for T to be used in this evaluation is not clear. If the analytical method (ASCE 41 §3.3.1.2.1) is used, only the E-W component of the ELF-designed MC4 and N-S components of all the buildings satisfy this requirement—see Table 3-6 (directional components that fail this criteria are shaded). If the empirical method (ASCE 41 §3.2.1.2.2) is used, all building components satisfy this constraint except the E-W component of MC16. In this study, this analysis constraint is disregarded to allow an assessment comparison between methods—see Table 3-7 (directional components that fail this criteria are shaded).
- The building has a ratio of the horizontal dimension at any story to the corresponding dimension in an adjacent story that exceeds 1.4. In this study, this constraint is satisfied because the building plan does not change at any story.
- The building has a torsional stiffness irregularity. This limitation is satisfied as discussed previously under accidental torsion as well as in Chapter 2. In this study, this check is based on the individual story drift rather than the floor displacement relative to the base.
- The building has a vertical stiffness irregularity. In this study, this limitation is automatically satisfied by using ASCE 7 §12.3.2.2 Exception 1 for the design of the archetype buildings.

¹⁵ This term is now used in lieu of ‘rehabilitation’.

- The building has a non-orthogonal SFRS. In this study, this limitation is not applicable to the archetype buildings.

Regardless of the restrictions on using the LSP, results from applying the LSP to the archetype buildings are included for the purpose of seismic performance comparison between the various assessment methods in this study.

Table 3-6. Analytical Fundamental Periods (seconds)

Direction	SFRS	MC4		MC8		MC16	
		ELF	RSA	ELF	RSA	ELF	RSA
E-W	SMF	1.83	2.23	2.93	3.84	4.39	5.05
N-S	SCBF	0.67	0.72	1.45	1.51	2.09	2.14

Table 3-7. Empirical Fundamental Periods (seconds)

Direction	SFRS	MC4		MC8		MC16	
		ELF	RSA	ELF	RSA	ELF	RSA
E-W	SMF	0.93	0.93	1.57	1.57	2.69	2.69
N-S	SCBF	0.43	0.43	0.71	0.71	1.17	1.17

3.1.3.1.2 Linear Dynamic Procedure

The Linear Dynamic Procedure (LDP) is outlined in ASCE 41 §3.3.2. The LDP requires the use of either response spectrum analysis (RSA) or response history analysis (RHA)—only the RSA is presented in this report. Though there are significant benefits of using the RHA (e.g., maintaining sign convention on response), the RSA was selected to align with the design methodology. The provisions of the LDP closely resemble those of the RSA procedure in ASCE 7; as such, no additional analysis details are presented here, except that no base shear scaling is required by ASCE 41. Damping for analysis is taken as five percent of critical for all modes for dynamic analysis to match the response spectrum (see ASCE 41 §1.6.1.5.3). A sufficient number of modes is used in the analysis to capture at least 90 percent of the mass participation in each of the two horizontal principal directions. Masses were not modeled in the analysis to address vertical accelerations. Furthermore, the square root of the sum of the squares (SRSS) rule is used to combine the modal responses so as to obtain the maximum forces and deformations.

3.1.3.2 Nonlinear Analysis Procedures

The archetype buildings are modeled and analyzed in PERFORM-3D 5.0.0 (CSI 2011b) for the nonlinear procedures. Modeling and analysis considerations for the nonlinear procedures are outlined in ASCE 41 §3.2.2 with supplemental information provided in ASCE 41 §3.3.3.2 for the Nonlinear Static Procedure (NSP) and ASCE 41 §3.3.4.2 for the Nonlinear Dynamic Procedure (NDP). Primary components of the SFRS expected to experience inelastic deformations are modeled using a full “backbone” curve that includes strength and stiffness (applicable only for the NDP) degradation and residual strength. For this study, all nonlinear components are modeled with the anchor points (A to E) bounding the full backbone curve as shown in ASCE 41 Figure C2-1 and Figure 5-1—see Figure 3-2. This topic will be discussed further in the respective analysis and system-specific sections.

Gravity loads and corresponding load combination assumed to be present during the earthquake are computed from ASCE 41 §3.2.8 as discussed previously. The effective horizontal seismic weights, w , for analysis are computed in accordance with ASCE 41 §3.3.1 and are the same as those used for design (see Chapter 2). Global $P-\Delta$ effects (e.g., B_2 in AISC 360 Appendix 8) are addressed in the analysis by using a simplified algorithm—see PERFORM-3D *User Guide* (CSI 2011d). PERFORM-3D does not explicitly include local $P-\delta$ effects (e.g., B_1 in AISC 360 Appendix 8). Building specific modeling assumptions and analysis techniques are described in their respective sections.

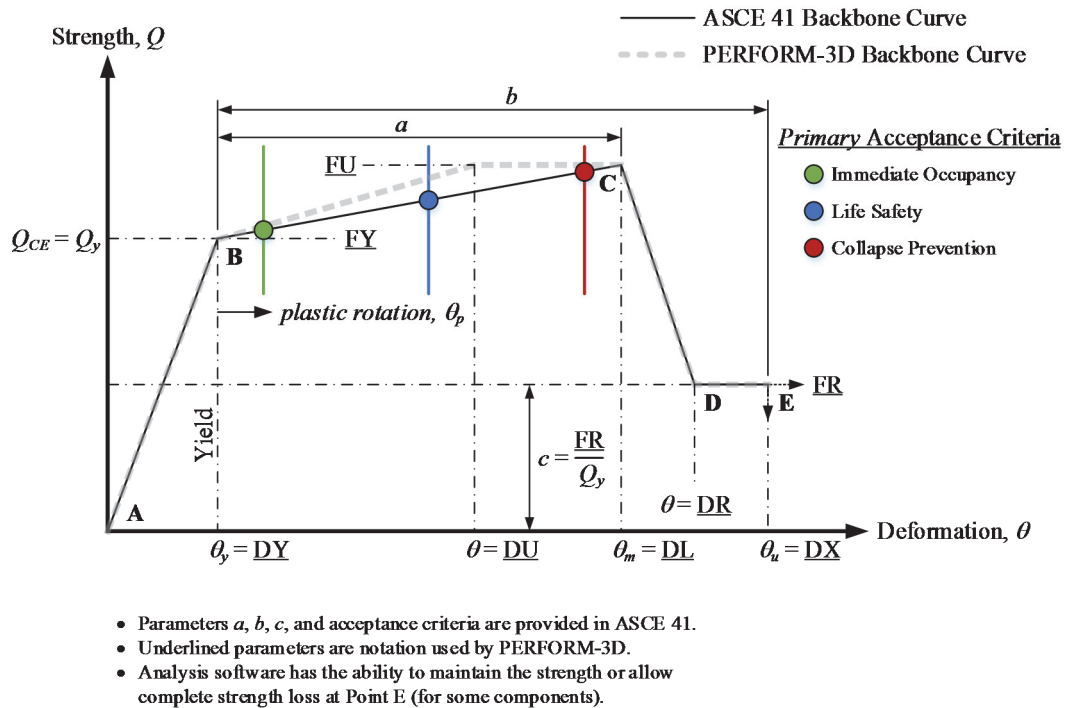


Figure 3-2. Generalized Component Backbone Curve (adopted from ASCE 41 Figure C2-1)

3.1.3.2.1 Nonlinear Static Procedure

The Nonlinear Static Procedure (NSP) is outlined in ASCE 41 §3.3.3. ASCE 41 places limitations on the use of the NSP in ASCE 41 §2.4.2. First, if higher modes are significant, the NSP is permitted with supplemental verifications required using the LDP. Higher mode effects are considered significant when the story shear computed by analysis with at least 90 percent horizontal mass participation is at least 1.3 times greater than that computed considering only response in the fundamental mode. This condition is generally triggered in multistory buildings with fundamental periods greater than 1.0 second in the direction being considered (see Table 3-8 and Table 3-9—story shear ratios that fail this criteria are shaded).

Second, if $R > R_{max}$ (as defined in ASCE 41 §3.3.3), dynamic instability is a potential failure mode and the NSP is not permitted. Information regarding this ductility criterion as applied to an idealized single-degree-of-freedom (SDOF) system is provided in FEMA 440: *Improvements of Nonlinear Static Seismic Analysis*

Procedures (FEMA 2005). However, this verification is computationally cumbersome because a nonlinear static analysis has to be conducted to determine both R and R_{max} , prior to knowing if the NSP is permitted. This verification is illustrated subsequently in the NSP assessment results. The NSP procedure is graphically illustrated in the flowchart of Figure 3-3.

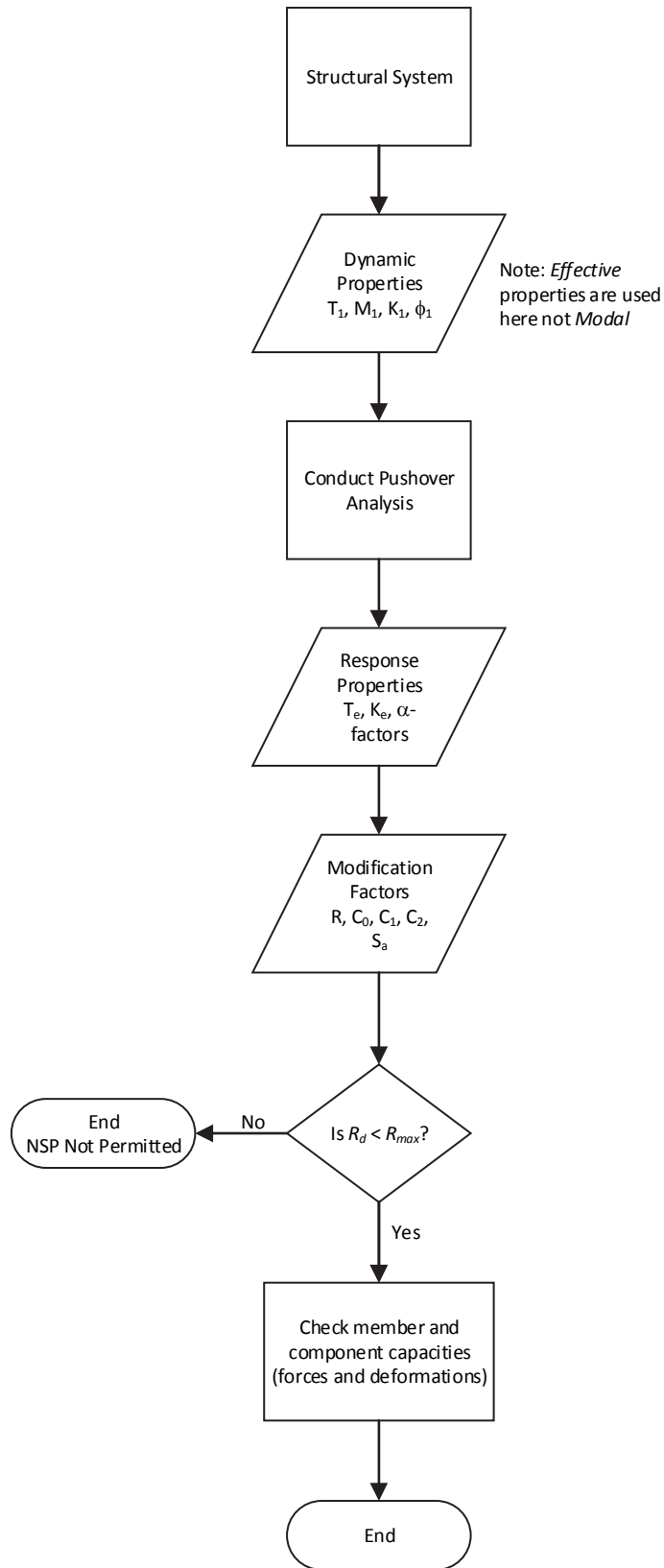


Figure 3-3. NSP Process

Table 3-8. Story Shear Ratio - ELF

Story	$V_{story} / V_{story,1st mode}$					
	MC4 E-W	MC8 E-W	MC16 E-W	MC4 N-S	MC8 N-S	MC16 N-S
Roof	-	-	2.96	-	-	2.07
16	-	-	2.03	-	-	1.83
15	-	-	1.61	-	-	1.61
14	-	-	1.41	-	-	1.43
13	-	-	1.29	-	-	1.28
12	-	-	1.20	-	-	1.17
11	-	-	1.14	-	-	1.09
10	-	-	1.09	-	-	1.05
9 (Roof)	-	1.98	1.07	-	1.57	1.04
8	-	1.41	1.07	-	1.31	1.05
7	-	1.19	1.06	-	1.13	1.07
6	-	1.10	1.07	-	1.03	1.12
5 (Roof)	1.45	1.05	1.08	1.07	1.02	1.17
4	1.10	1.03	1.11	1.01	1.06	1.22
3	1.01	1.05	1.15	1.00	1.13	1.26
2	1.06	1.10	1.19	1.02	1.20	1.29

Table 3-9. Story Shear Ratio - RSA

Story	$V_{story} / V_{story,1st mode}$					
	MC4 E-W	MC8 E-W	MC16 E-W	MC4 N-S	MC8 N-S	MC16 N-S
Roof	-	-	3.10	-	-	2.11
16	-	-	2.11	-	-	1.86
15	-	-	1.65	-	-	1.64
14	-	-	1.42	-	-	1.45
13	-	-	1.30	-	-	1.29
12	-	-	1.22	-	-	1.18
11	-	-	1.15	-	-	1.10
10	-	-	1.11	-	-	1.05
9 (Roof)	-	2.25	1.09	-	1.59	1.04
8	-	1.50	1.09	-	1.33	1.05
7	-	1.22	1.09	-	1.14	1.08
6	-	1.12	1.09	-	1.03	1.13
5 (Roof)	1.58	1.07	1.11	1.08	1.02	1.18
4	1.14	1.05	1.15	1.01	1.08	1.24
3	1.01	1.08	1.21	1.00	1.17	1.28
2	1.08	1.16	1.26	1.02	1.25	1.31

The mathematical model requirements for use with the NSP are outlined in ASCE 41 §3.2.2 and ASCE 41 §3.3.3.2. *Primary* components of the SFRS expected to experience inelastic deformations are modeled using full backbone curves that include strength degradation and residual strength (see ASCE 41 §3.2.2.3 and ASCE 41 §3.3.3.2). ASCE 41 §5.4.2.2.2 allows the *generalized* modeling parameters provided in ASCE 41 to model the full backbone curves of steel components for the NSP as an alternative to experimental calibration. In this study, all nonlinear components are modeled with the anchor points (A to E) bounding the full backbone curve as shown in Figure 3-2 and quantified in ASCE 41 Tables 5-6 and 5-7. Component strength at the ultimate deformation, point E on the backbone curve, retains residual strength

and does not experience complete strength loss. SFRS-specific modeling approaches are discussed in their respective sections.

For the nonlinear static analysis algorithm in PERFORM-3D, the following apply:

- The lateral force distribution is based on a non-adaptive first-mode shape (first-order elastic) and mass distribution.
- Damping is set to zero percent for all modes with no supplemental Rayleigh damping. All elements are assigned a beta- K damping stiffness reduction factor of unity (no reduction).
- Strength degradation is included in the analysis.
- Global P - Δ effects are directly included in the analysis. Local P - δ effects are not addressed in the analysis. Geometric nonlinearity is assigned to all elements.
- Number of Steps is taken as 100 and Maximum Number of Events is taken as 1,000.
- Roof displacement at the center of mass relative to the base is used as the target displacement. The reference drift is therefore taken as the roof drift; the maximum allowable drift is taken as 10 percent. All story drifts are included in the list of Controlled Drifts.
- See PERFORM-3D *User Guide* for additional information.

3.1.3.2.2 Nonlinear Dynamic Procedure

The Nonlinear Dynamic Procedure (NDP) is outlined in ASCE 41 §3.3.4. The NDP is intended to be the most rigorous of all the assessment procedures prescribed, with no limitations placed on types of buildings allowed for the assessment because of the intent of capturing the *true* behavior of the building subjected to strong ground motions.

The mathematical model requirements for use with the NDP are outlined in ASCE 41 §3.2.2 and ASCE 41 §3.3.4.2, except that the point-in-time gravity load present during strong ground motion is taken as $(D + SD) + 0.25 \times L_{o, floor}$, a slight but common alternative to ASCE 41 §3.2.8 (see ASCE 7 §16.2.3). Primary components of the SFRS expected to experience inelastic deformations are modeled using full backbone curves that include strength and stiffness degradation and residual strength (see ASCE 41 §3.2.2.3 and ASCE §3.3.4.2).

For the NSP, ASCE 41 §5.4.2.2.2 allows using the *generalized* modeling parameters provided in ASCE 41 Tables 5-6 and 5-7 to model the full backbone curves of steel components as an alternative to experimental calibration. However, for the NDP, ASCE 41 §5.4.2.2.3 requires all component hysteretic behavior be based on experimental data unless permitted by the authority have jurisdiction. The benefit of calibrating component models with experimental results is that the force-deformation relationship will more accurately reflect strength and stiffness degradation, both cyclic and in-cycle—see NIST GCR 10-917-5: *Nonlinear Structural Analysis for Seismic Design: A Guide for Practicing Engineers* (NIST 2010a) and FEMA P-440A: *Effects of Strength and Stiffness Degradation on Seismic Response* (FEMA 2009c). In this study, all nonlinear components are modeled with the anchor points (A to E) bounding the full backbone curve as shown in Figure 3-2 and quantified in ASCE 41 Tables 5-6 and 5-7. All nonlinear components are calibrated based on experimental results to determine cyclic and in-cycle stiffness degradation only; post-yield strength increases and strength degradation calibrations from experimental results were not included. Component strength at the ultimate deformation, point E on the backbone curve, retains the residual strength and does not experience complete strength loss. SFRS-specific modeling approaches are discussed in their

respective sections. Therefore, the same PERFORM-3D model used in the NSP is also used in the NDP; analytical results from the two procedures are thus consistent and directly comparable. Future ASCE 41 revisions should unify modeling practices for the NSP and NDP, as well as provide supporting data to the authority having jurisdiction. Future research should examine the response of these systems with hysteretic models calibrated completely to test results, including performing FEMA P695 analyses.

The nonlinear dynamic analysis algorithm in PERFORM-3D used the following parameters:

- Damping is taken as three percent of critical for all modes (elastic) and 0.3 percent of critical is added as Rayleigh damping (elastic stiffness component only, beta- K) for dynamic analysis. Damping computation in PERFORM-3D is not based on the tangent stiffness matrix. All elements are assigned a beta- K damping stiffness reduction factor of unity (no reduction).
- Strength and stiffness degradation are included in the analysis.
- Global P - Δ effects are directly included in the analysis. Local P - δ effects are not addressed in the analysis. Geometric nonlinearity is assigned to all elements.
- Maximum Number of Events for each time step is taken as 200.
- Time steps for analysis are taken as the time step of the input motion, ranging from 0.005 to 0.02 seconds—see FEMA P695 Appendix A.
- See PERFORM-3D *User Guide* for additional information.

A critical aspect of the NDP is the selection and scaling of input ground motions (free-field motions) which is described in ASCE 41 §1.6.2.2. The methodology adopted in this study is discussed in Appendix A.

In addition to the analysis routine terminating when a solution fails to converge, the routine was also set to terminate when an arbitrarily selected roof drift ratio of twenty percent¹⁶ is achieved (story drift ratios can be higher). While both of these methods are used to indicate and rationalize total or partial collapse of a system, the indicator of collapse used in this study is the component demands measured against the nonlinear modeling parameters and acceptance criteria. These component limits will typically be reached prior to an analysis routine failing to converge or an excessive roof drift is reached.

3.1.4 Acceptance Criteria

This section discusses the implementation of the acceptance criteria in ASCE 41 §3.4. Component actions are classified as *force-controlled* or *deformation-controlled* depending on the post-elastic behavior of the component (see ASCE 41 Table C2-1). Generally speaking, *deformation-controlled* actions are assigned to component actions capable of a ductile response (e.g., moment in a plastic hinge in a compact beam) and *force-controlled* actions are assigned to component actions with limited ductility (e.g., moment in a plastic hinge in a column with high axial load). Additionally, a knowledge factor, κ , is applied to account for uncertainties in the framing system and materials. Since the archetype buildings are new construction with quality control measures, κ is taken as unity in this study to represent *new component capacities or actions* as discussed in ASCE 41 §2.2.2 and ASCE 41 Tables 2-1, 2-2, and 2-3.

¹⁶ This value does not change the qualitative performance result of a component; however, it can influence the mean value of a performance response for a set of records. For example, mean values would be slightly larger than if ten percent was selected.

3.1.4.1 Linear Procedures

Acceptance criteria of components for linear assessment procedures are provided as m -factors. The m -factor is intended to account for the ductility associated with a specific action and depends on the SPL and component type. ASCE 41 Table 5-5 provides the m -factors for steel components for linear assessment procedures. Adjustments to the m -factors for member or connection characteristics are detailed in ASCE 41 Chapter 5. In this study, actions in force-controlled components are assigned $m = 1.0$ for simplicity and computational consistency in developed assessment spreadsheets. It should be noted that ASCE 41 does not assign an m -factor to force-controlled components.

3.1.4.1.1 Calculating Component Assessment Results

Component forces and deformations obtained by the LSP or LDP are referred to as design actions, Q_U (e.g., flexure in a component).

Component design actions classified as *deformation-controlled*, Q_{UD} , are computed by

$$Q_{UD} = Q_G \pm Q_E \quad (\text{ASCE 41 §3.4.2.1.1}) \quad (3-2)$$

Component design actions classified as *force-controlled*, Q_{UF} , are computed by

$$Q_{UF} = Q_G + \frac{Q_E}{C_1 C_2 J} \quad (\text{ASCE 41 §3.4.2.1.2}) \quad (3-3)$$

where Q_G is the action due to gravity loads and Q_E is the action due to earthquake effects. Elastic force-controlled demands from earthquake effects are divided by $C_1 C_2$ to remove the demand amplification for short period structures from non-ductile components (see ASCE 41 §3.3.1). Similarly, the demand is divided by J , which is the force-delivery reduction factor and is taken as the minimum demand capacity ration (DCR) of the components in the load path delivering force to the component. Alternatively, J can be taken as 2.0 when the system is located in a region of a high level of seismicity, independent of EHL. However, holding J constant for multiple performance levels (disregarding the change in intensity) is not consistent with a capacity design approach, resulting in potentially overly conservative estimates of component actions in force-controlled elements at the higher EHL, or vice versa.

ASCE 41 §3.4.2.2 requires that deformation-controlled and force-controlled actions in primary and secondary components satisfy:

$$\text{Deformation-controlled: } m\kappa Q_{CE} \geq Q_{UD} \quad (\text{ASCE 41 §3.4.2.2.1}) \quad (3-4)$$

$$\text{Force-controlled: } (m)\kappa Q_{CL} \geq Q_{UF} \quad (\text{ASCE 41 §3.4.2.2.2}) \quad (3-5)$$

where m is the component demand modification factor (taken as unity for force-controlled actions—see above), κ is the knowledge factor (taken as unity in this study), Q_{CE} is the expected strength of the component, and Q_{CL} is the lower-bound strength of the component.

The results of the linear assessment procedures are presented in this report as a *normalized* demand capacity ratio, DCR_N , so that the acceptance criteria verification becomes a unity check similar to that done in modern component design standards (e.g., AISC 360). DCR_N is computed by rearranging ASCE 41 Eq. 3-20 and ASCE 41 Eq. 3-21 as required. As such, a DCR_N value greater than unity indicates that the component does not satisfy the performance criteria for a given SPL. DCR_N is similar to, but different than, the DCR as used in ASCE 41. This approach is also a more consistent way to present results over the various types of assessment procedures used in this study. However, a slightly different interpretation is also taken in this study with regards to the DCR_N : in lieu of m and κ adjusting the apparent strength of a component, as illustrated in ASCE 41 §3.4.2.2, m and κ act to reduce the elastic demand to the *expected* demand given an EHL. Where required, the DCR_N is determined from an interaction equation from the appropriate equation.

$$\text{Deformation-controlled: } DCR_N = \frac{Q_{UD}}{m\kappa Q_{CE}} = \frac{DCR}{m\kappa} \quad (3-6)$$

$$\text{Force-controlled: } DCR_N = \frac{Q_{UF}}{(m)\kappa Q_{CL}} \quad [\text{with } m \text{ taken as } 1.0] \quad (3-7)$$

3.1.4.2 Nonlinear Procedures

Acceptance criteria of components for nonlinear assessment procedures are provided as plastic (inelastic) deformations dependent on the SPL and component type. ASCE 41 Tables 5-6 and 5-7 provide the plastic deformations limits for steel components for nonlinear assessment procedures. Adjustments to the acceptance criteria for member or connection characteristics are detailed in ASCE 41 Chapter 5.

Inelastic deformation parameters in ASCE 41 are provided for steel components in terms of plastic deformations rather than total deformations. The choice of whether to use plastic deformations or total deformations will depend on what nonlinear component model is adopted for each component action in the structural analysis (e.g., moment-curvature hinge or moment-rotation hinge). Consequently, yield and post-yield elastic deformations may need to be added to the values given in ASCE 41 to determine the total deformation for each SPL.

In this study, demands on *primary* components of new buildings are measured against acceptance criteria for *primary* components. ASCE 41 §3.4.3.2 allows *primary* component demands to be within the acceptance criteria for *secondary* components for the NSP if degradation effects are explicitly modeled—a change introduced in FEMA 356. This also includes NDP, although not explicitly stated. This allowance is neglected in this study for the following reasons:

- Bypassing nonlinear acceptance criteria set for primary components suggests that acceptance criteria for primary components for linear and nonlinear assessment procedures are not calibrated. In this study, acceptance criteria for primary components are maintained for all assessment methods to provide a uniform comparison basis.

- There is no technical justification provided in ASCE 41 as to why comprehensive component models for primary components, which are required to stabilize the structure after a large earthquake, will allow them to deform to the extent given for a secondary component and maintain the structural integrity of the system. Analytically speaking, it is debatable if collapse prevention can be reliably achieved if a concentrated few SFRS components are deformed past the deformation associated with their peak strength and lose a considerable amount of strength and stiffness. Available literature has indicated the difficulty in solution convergence in analysis when component response is following a negative stiffness branch. Still, some liberties are provided, debatably, for existing buildings, but transferring this allowance to new buildings is also of debatable validity. Engineering judgment must be applied. Broadly speaking, the function that separating existing buildings and new buildings into bins plays in developing a resilient community must be clarified.
- Reliability issues arise when adopting secondary acceptance criteria for primary components. For example, the acceptance criterion of an RBS beam-to-column connection taken as a secondary component for the Life Safety SPL is beyond the peak deformation (“*a*” in Figure 3-2). In ASCE 41, primary acceptance criteria for the Collapse Prevention SPL generally matches the deformation associated with the peak strength of a component.
- There is little empirical evidence supporting the acceptance criteria for secondary steel components permitted in ASCE 41 §3.4.3.2, other than for beam-to-column connections studied in the SAC project (see FEMA 350 series (FEMA 2000a through 2000d)). Experimental tests are rarely continued to achieve the peak deformations and the associated reserve strength of a component or subassembly after the required loading protocol is complete.

As a side note, ASCE 41-13 has removed all acceptance criteria for primary components for nonlinear assessment. Future research should be conducted to evaluate the systems by measuring demands against acceptance criteria for secondary components—which can be done by inspection with the analysis results presented in this study.

3.1.4.2.1 Calculating Component Assessment Results

Component forces and deformations obtained by the NSP or NDP are referred to as design actions, Q_U (e.g., plastic rotation in a plastic hinge). Component design actions are computed as the action in the member or connection at the target displacement for the NSP and as the maximum value for a given earthquake for the NDP. Subsequently, a statistical average is computed from the maximum values from the suite of ground motions. In specific cases, the maximum value must be coupled with other actions in the component at the instant of computation of the maximum response.

Component design actions classified as *deformation-controlled*, Q_{UD} , are computed by

$$Q_{UD} = Q_G \pm Q_E \quad (\text{ASCE 41 §3.4.3.2.1}) \quad (3-8)$$

Component design actions classified as *force-controlled*, Q_{UF} , are computed by

$$Q_{UF} = Q_G \pm Q_E \quad (\text{ASCE 41 §3.4.3.2.3}) \quad (3-9)$$

where Q_G is the action due to gravity loads (or associated deformation) and Q_E is the action due to earthquake effects (or associated deformations). Superposition of forces or deformations is not applicable

in a nonlinear analysis; thus, gravity loads are directly applied in the analysis. The above equations are numerical interpretations of ASCE 41 §3.4.3.2. They are used in this study to maintain computational consistency over the various types of assessment procedures.

ASCE 41 §3.4.3.2 requires that deformation-controlled and force-controlled actions in primary and secondary components satisfy:

$$\text{Deformation-controlled: } \kappa Q_{CE} \geq Q_{UD} \quad (\text{ASCE 41 §3.4.2.2.1}) \quad (3-10)$$

$$\text{Force-controlled: } \kappa Q_{CL} \geq Q_{UF} \quad (\text{ASCE 41 §3.4.2.2.2}) \quad (3-11)$$

where Q_{CE} is the expected strength or deformation demand of a component, Q_{CL} is the lower-bound strength of a component, and κ is the knowledge factor (taken as unity in this study). ASCE 41 Chapter 5 does not explicitly provide a relationship between Q_{CE} (or Q_{CL}) and Q_y on the force-deformation curve.

The results of the nonlinear assessment procedures are presented in this report as a normalized demand capacity ratio, DCR_N , where the plastic or total deformation demands are normalized with respect to the plastic or total acceptance criteria, modified by κ if required. The acceptance criteria verification then becomes a unity check similar to that done in modern component design standards (e.g., AISC 360). As such, a DCR_N value greater than unity indicates that the component does not satisfy the performance criteria for a given SPL. This approach is a consistent way to present results over the various types of assessment procedures used in this study.

$$\text{Deformation-controlled: } DCR_N = \frac{Q_{UD}}{\kappa Q_{CE}} = \begin{cases} \text{Total} & \frac{\theta_{plastic} + \theta_{elastic}}{\kappa(\theta_y + \theta_{pe} + \theta_{p,AC})} \\ \text{Plastic} & \frac{\theta_{plastic}}{\kappa\theta_{p,AC}} \end{cases} \quad (3-12)$$

$$\text{Force-controlled: } DCR_N = \frac{Q_{UF}}{\kappa Q_{CL}} \quad (3-13)$$

where $\theta_{plastic}$ is the plastic deformation of a component, $\theta_{elastic}$ is the elastic deformation of a component, θ_y is the yield deformation of a component, θ_{pe} is the post-yield elastic deformation of a component, and $\theta_{p,AC}$ is the acceptance criteria of a component based on plastic deformation.

3.2 Moment Frame

Seismic performance assessment of *steel moment frames* is performed in accordance with ASCE 41 §5.4. The moment frames in the archetype buildings are designed with fully restrained (FR) moment connections as identified in AISC 360 §B3.6b and as an SMF as identified in ASCE 7 §12.2 (item C.1 in Table 12.2-1) and AISC 341 §E3. This designation *aligns* with that prescribed in ASCE 41 §5.4.2, *Fully Restrained Moment Frames*. The FR beam-to-column moment connection used in each SMF is an RBS as identified in AISC 358 Table 2.1 and ASCE 41 Table 5-4.

3.2.1 Assessment Methodology

There are three primary characteristics of each component (i.e., member, connection, etc.) forming the structural model for each assessment method:

1. Stiffness, ASCE 41 §5.4.2.2
2. Strength, ASCE 41 §5.4.2.3
3. Acceptance Criteria, ASCE 41 §5.4.2.4, and whether or not the component *action* is force-controlled or deformation-controlled.

Each component characteristic is discussed in the appropriate linear and nonlinear assessment discussion.

The following component design actions are assessed in this study:

- Beam-to-column connection flexural force or deformation (RBS)
- Panel zone shear force or deformation
- Beam and column flexural force or deformation at potential plastic hinge zones (section strength)¹⁷
- Column axial-moment interaction strength (member strength)
- Beam and connection flexure and shear strength (e.g., moment at face of column)

3.2.1.1 Linear Procedures

This section discusses the three primary component characteristics listed in Section 3.2.1 and computation of the demand in the component for the linear assessment procedures.

Stiffness

The stiffnesses of all members and connections for linear assessment follow ASCE 41 §5.4.2.2.1. Panel zones at the beam-to-column joints are explicitly modeled; ETABS uses the scissor model—see *User Manual*. Explicit joint and connection modeling is not required because the beam-to-column connections are classified as FR. However, the stiffness of the frame beams must be modified to account for the reduced beam sections within the beam-to-column connections (see Chapter 2).

¹⁷ Beam hinges within the RBS are included in assessment of FR connection (controlling mechanism).

Strength

The strength of all members and connections for linear assessment follow ASCE 41 §5.4.2.3.2.

The expected flexural strength of a member, $Q_{CE} = M_{CE} (= Q_y)$, is computed as M_n from AISC 360 Chapter F¹⁸ with $\phi_b = 1.0$ and F_{ye} in lieu of F_y . For ASTM A992 steel, $F_{ye} = 1.1 \times F_y$ (see ASCE 41 Table 5-3), which corresponds to $R_y F_y$ in AISC 341. Composite action with the concrete slab is generally neglected in computing M_n for frame beams. In so doing, it is assumed that the plastic moment strength is achievable via adequate lateral bracing, thus $M_n = M_p$. If the flexural strength is less than M_p , then the available ductility of the member is significantly reduced because of member or cross-section instability (which also affects the acceptance criteria). ASCE 41 enforces section compactness requirements through the acceptance criteria—discussed subsequently.

The lower-bound flexural strength of a member, $Q_{CL} = M_{CL}$, is computed as M_n from AISC 360 Chapter F¹⁸ with $\phi_b = 1.0$ and F_{yLB} in lieu of F_y . For ASTM A992 steel, $F_{yLB} = 1.0 \times F_y$ (see ASCE 41 Table 5-2).

Although not explicitly identified in ASCE 41 §5.4.2.3.2, the expected shear strength of a member, $Q_{CE} = V_{CE} (= Q_v)$, is identical to that computed as V_n from AISC 360, Chapter G with $\phi_v = 1.0$ and F_{ye} in lieu of F_y . Web slenderness, h / t_w , is critical in developing a fully yielded cross-section. As such, there are cases when

$$\frac{418}{\sqrt{F_y}} = 2.45 \sqrt{\frac{E}{F_y}} < \frac{h}{t_w} \leq \frac{640}{\sqrt{F_y}} = 3.76 \sqrt{\frac{E}{F_y}} \quad (3-14)$$

and the web is still capable of achieving full yield strength in shear. However, if the web slenderness approaches the upper limit (taken as the ‘compact’ limit in AISC 360 Table B4.1) then the beam may have difficulty achieving its plastic moment strength, M_p . There is no lower-bound shear strength, V_{CL} , in ASCE 41 or shear-moment interaction.

The lower-bound compression strength of a member, $Q_{CL} = P_{CL}$, is computed as P_n from AISC 360 Chapter E¹⁸ with $\phi_c = 1.0$ and F_{yLB} in lieu of F_y . For ASTM A992 steel, $F_{yLB} = 1.0 \times F_y$ (see ASCE 41 Table 5-2).

Though identified in ASCE 41 §5.4.2.3.2-2, no explicit guidance is provided for computing the expected flexural strength, M_{CE} , of a compression member if the axial load demand, P , exceeds 10 percent of the *axial strength*. This guidance would be useful for computing the flexural DCR at a given location, such as at the column base where a plastic hinge is anticipated. The term *axial strength* of a compression member is also not well defined (i.e., is it P_{ye} or P_{CL} ?). Similarly, P is not defined except in an unrelated provision for the NSP. ASCE 41 §5.4.2.2.2 states that P for a linear analysis is P_{UF} . The flexural strength will also depend on the selected P - M interaction curve, which will use M_{CE} (or M_{CL}) at $P = 0$ as the anchor point. Further, there is little need to have triggering language based on 10 percent axial load ratio because it delineates no physical phenomenon and does not influence computing the yield chord rotation, θ_y . In fact

¹⁸ ASCE 41 inadvertently states AISC 341.

this trigger, it adds complexity, which will be discussed subsequently in the Acceptance Criteria section. ASCE 41 does not delineate between orthogonal buckling axes and non-flexural buckling limit states (e.g., torsional, local buckling) for its interaction verification. This can significantly affect the assessment of beam-column members where a high in-plane moment is associated with a buckling limit state other than in-plane flexural buckling. Beam-columns can be further penalized in linear assessment methods where P_{UF} is highly affected by selecting a value for J .

The expected tension strength of a member, $Q_{CE} = T_{CE} (= Q_y)$, is computed as $A_c \times F_{ye}$, where A_c is the cross-sectional area of the member. ASCE 41 does not provide other tensile strengths, potentially brittle, similar to AISC 360 Chapter D, e.g. net section fracture.

The expected shear strength of a panel zone, $Q_{CE} = V_{CE} (= Q_y)$, is computed as $0.55 F_{ye} \times d_b \times t_p$. (ASCE 41 Equation 5-5¹⁹). This strength equates to $0.92 \times V_y$ from AISC 360 Chapter J10.6 with $\phi_v = 1.0$ and F_{ye} in lieu of F_y . ASCE 41 does not provide additional panel zone strength to account for column flange bending.

ASCE 41 does not provide explicit guidance on computing the expected strength, Q_{CE} , of a FR beam-to-column connection. The RBS beam-to-column connections were designed in accordance with AISC 358. As such, the controlling mechanism is the moment at the center of the RBS. It is assumed that the acceptance criteria for FR beam-to-column connections (m -factor) translated from results from the SAC project are applicable at the face of the column—see below. Therefore, the moment at the face of the column is used as the demand, Q_{UD} , and the expected flexural strength of the connection, $Q_{CE} = M_{CE}$, is computed as M_p at the center of the RBS and projected to the face of the column (this value will always be less than using M_p taken at the column face). Alternatively, the demand and acceptance criteria could be adjusted to the hinge location (controlling mechanism) and the connection at the face of the column evaluated as force-controlled, see ASCE 41 §5.4.2.4.2-4. ASCE 41 should clarify the intent of ASCE 41 Eq. 5-14 and express that is the lower-bound strength of the connection evaluated at the column face compared to the expected strength of the connection at the hinge location projected to the column face. As noted, AISC 358 design provisions for an RBS connection satisfies this criteria. Because the plastic hinge is confined within the RBS and forms away from the face of the column, the flexural demand at the center of the RBS should also be used to check the plastic hinge as a “beam” hinge.

Acceptance Criteria

The acceptance criteria of members and connections for linear assessment follow ASCE 41 §5.4.2.4.2.

Flexure in Beams and Beam-to-Column Connections

The acceptance criteria for *flexural* action at expected locations of plastic hinging in beams (members with axial load ratio less than or equal to 10 percent) are provided in ASCE 41 Table 5-5 and are dependent on web and flange slenderness. The range of flange limits match AISC 341 limits for *highly* and *moderately* ductile unstiffened compression elements. The range of web limits match AISC 341 limits for *highly* and

¹⁹ The reason the shear yield stress for a column web (assuming it can be designated as a beam) being defined as $0.6 \times F_{ye}$ is not clear, but if the same column web is a panel zone, the shear yield stress is $0.55 \times F_{ye}$.

moderately ductile stiffened compression elements taking at $P = 0$. The flange and web slenderness limits for moderately ductile sections are taken as a ‘compact’ compression element in AISC 360 (i.e., λ_p). The lower-bound web slenderness limit is taken as that capable of full section yielding in shear. These web slenderness limits were introduced in FEMA 356 whereas flange limits were introduced in FEMA 273 and subsequently modified in FEMA 356 (upper-bound limit was changed from a pure axial compression limit to a compression from flexure limit).

In cases where the expected flexural strength of an unbraced segment is governed by instability (e.g., lateral-torsional buckling (LTB)) rather than full section yielding, the m -factors in ASCE 41 Table 5-5 shall be reduced accordingly. Again, ASCE 41 inadvertently references AISC 341 for these calculations as well as using the notation, M_r , which is no longer used in AISC 360.

The acceptance criteria for beam-to-column connections (flexural hinge is located within the connection) are taken from Fully Restrained Moment Connections in ASCE 41 Table 5-5 and are dependent on connection detailing, panel zone strength in a balanced yield condition, and member and cross-section slenderness (see ASCE 41 §5.4.2.4.2, 4.1 to 4.4). It is assumed that the acceptance criteria for FR beam-to-column connections (m -factor) translated from results from the SAC project are applicable at the face of the column—see §3.2.1.2. Furthermore, the m -factors for “beams” are not applicable for flexural plastic hinges within the region²⁰ demarcating the beam-to-column connection when connection components prevent the unobstructed spread of plasticity. However, because the plastic hinge is forced to develop in a prescribed location away from the column face, thus allowing essentially unobstructed spread of plasticity within the RBS zone, m -factors for a “beam” should also be used to check the performance of the hinge itself. Unless evaluating at the IO performance level, the m -factor for the beam-to-column connection will control over the m -factor for flexure in the RBS—see Table 3-10.

Table 3-10. Basic Acceptance Criteria for a W24×84

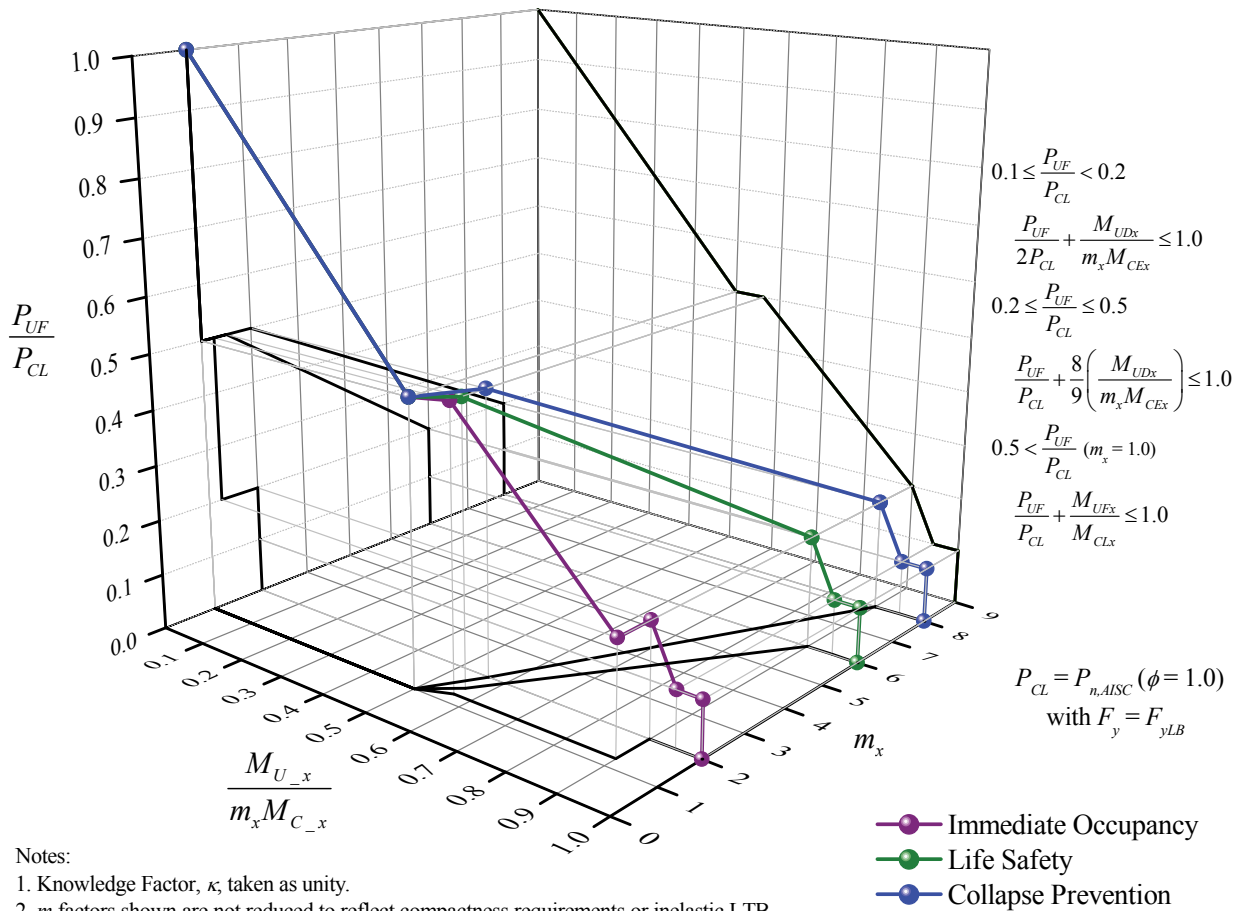
SPL	RBS Beam-to-Column Connection	Beam
CP	$6.2-0.032d = 5.4$	8
LS	$4.9-0.025d = 4.3$	6
IO	$3.5-0.016d = 3.1$	2

Flexure in Columns and Columns-to-Base Connections

The acceptance criteria for *flexural* action at expected locations of plastic hinging in columns (members with axial load ratio greater than 10 percent) are provided in ASCE 41 Table 5-5 and are dependent on the axial load ratio, P_{UF} / P_{CL} , and web and flange slenderness. As discussed above, ASCE 41 does not delineate between orthogonal buckling axes and non-flexural buckling limit states (e.g., torsional, local buckling) for computing P_{CL} . Consequently, this can significantly affect the assessment of beam-column members where a high in-plane moment is associated with a buckling limit state other than in-plane flexural buckling. If the axial load ratio is greater than 0.5, then flexural action is considered force-controlled and the flexural demand and strength are taken as M_{UF} and M_{CL} , respectively. Otherwise, the m -factor is adjusted for P - M

²⁰ This region is also used in AISC 341 to define the *protected zone*.

interaction as shown in Figure 3-4 and the flexural demand and strength are taken as M_{UD} and M_{CE} , respectively.



- Notes:
1. Knowledge Factor, κ , taken as unity.
 2. m factors shown are not reduced to reflect compactness requirements or inelastic LTB.
 3. Beam-Column with $P_{UF}/P_{CL} < 0.1$ can be treated as a beam.

Figure 3-4. P - M Interaction on Section m -factor (in-plane) and Member Instability (Primary Component)

The flange slenderness limits for columns are the same as those for beams and are *independent* of axial load. The lower-bound web slenderness range is essentially²¹ 75 percent of the slenderness limits in AISC 341-02 (AISC 2002)—taken from FEMA (2000c)—at distinct axial force ratios (0.2 and 0.5). These ratios are at the upper range of axial force ratios in ASCE 41, albeit P_{UF}/P_{ye} and P_{UF}/P_{CL} represent two physically different phenomena in regards to plate buckling. The upper-bound web slenderness range is essentially the slenderness limits in AISC 341-02 at distinct axial force ratios (0.1 and 0.2). These ratios are at the lower range of axial force ratio in ASCE 41. Using fixed axial limits on slenderness can lead to excessive conservatism because of step function triggers, as illustrated in Figure 3-5 for the LS SPL—AISC 341 web compactness limits for highly (HD) and moderately (MD) ductile compression elements are included for comparison. The spherical icons shown in the figure represent the web slenderness ratios for all wide-flange sections currently available. Essentially, 35 percent of these sections do not satisfy the lower-bound criteria

²¹ Work to develop FEMA 356 was conducted at the same time as the SAC project—see FEMA 350 series.

in ASCE 41 whereas this value reduces to 12 percent when using the AISC 341 criteria for highly ductile elements. Ultimately, the step functions created by both the axial load ratios and the section compactness requirements result in a highly complex formulation that is difficult to implement, as illustrated in Figure 3-6 for the LS SPL (plastic rotation is shown in lieu of m -factor). ASCE 41 could be simplified by combining the acceptance criteria for beams and columns into one set of criteria with no 10 percent axial load ratio trigger.

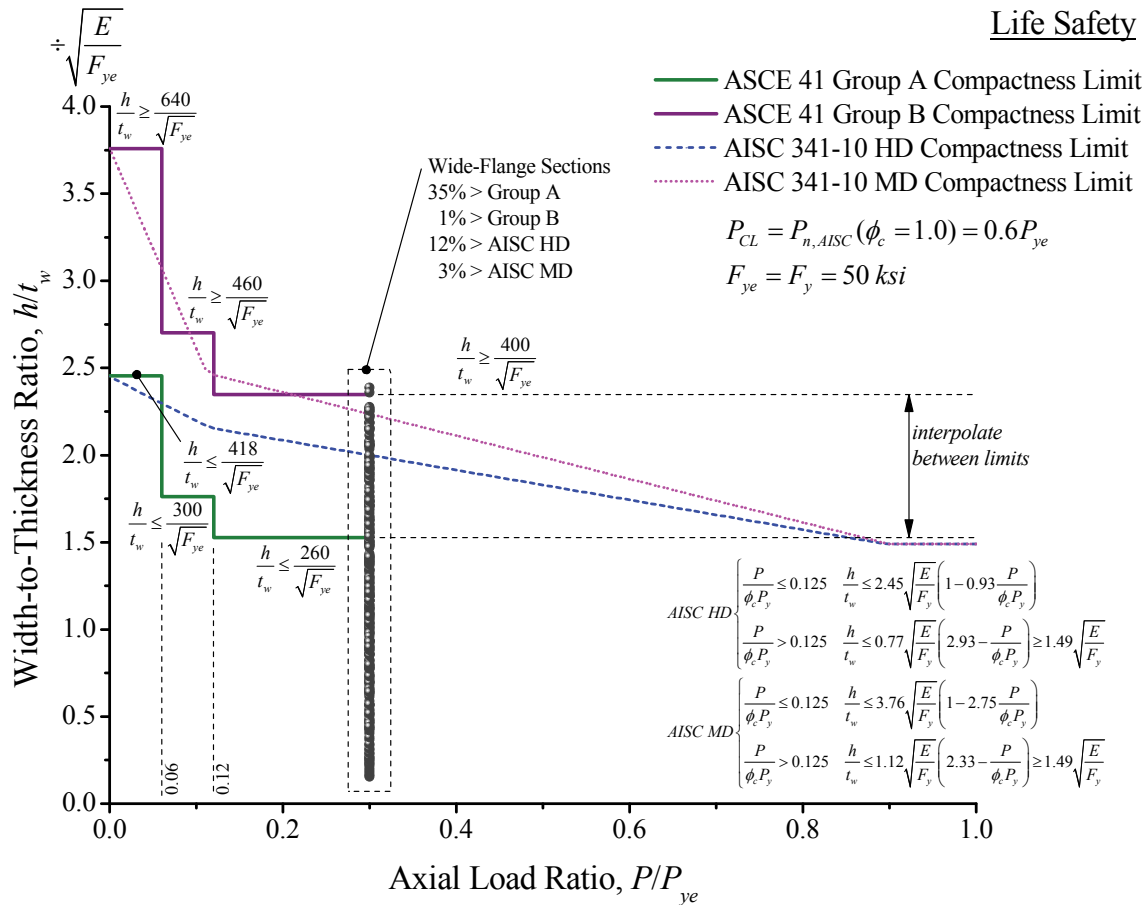


Figure 3-5. Compactness Requirements as a Function of Axial Load Ratio, LS Acceptance Criteria

In addition to the effect of P - M interaction on the m -factors (which is a section strength issue) for checking flexural actions in a column in accordance with ASCE 41 §3.4.2.2, member stability is also checked via global interaction equations in accordance with ASCE 41 §5.4.2.4, as shown in Figure 3-4—see projection of axial and moment ratios. The discontinuous curve is a result of variable P - M interaction equations, with the discontinuity at $P_{UF} / P_{CL} = 0.5$ being smallest when M_{CL} at $P_{UF} = 0$ equals M_p , and gets larger as M_{UD} / M_{UF} increases. Future efforts should simplify the ASCE 41 interaction curves for consistency and applicability, including eliminating $F_{y, LB}$ for a column that also uses F_{ye} .

Axial compression action in a column is always force-controlled due to significant reduction in ductility because of member and cross-sectional instability. Again, ASCE 41 is rather ambiguous when it comes to steel columns. First, there is no guidance on computing M_{CE} for a column. Although ASCE 41 §5.4.2.4.2-

2 provides some information, it is not consistent with that required to define the expected flexural strength, M_{CE} . Second, the m -factor is reduced for beams to account for LTB. Since this failure mode is also applicable to columns, the m -factor should similarly be reduced. However, a column that fails in LTB should be avoided, and $m = 1$ adopted since LTB is not a ductile phenomenon. Also, κ is not in the interaction equations similar to other verification procedures, and it is unclear if these equations have any physical meaning because member stability and section yielding effects are combined. Moreover, these equations can be conservative when weak-axis buckling is coupled with in-plane (strong-axis) bending.

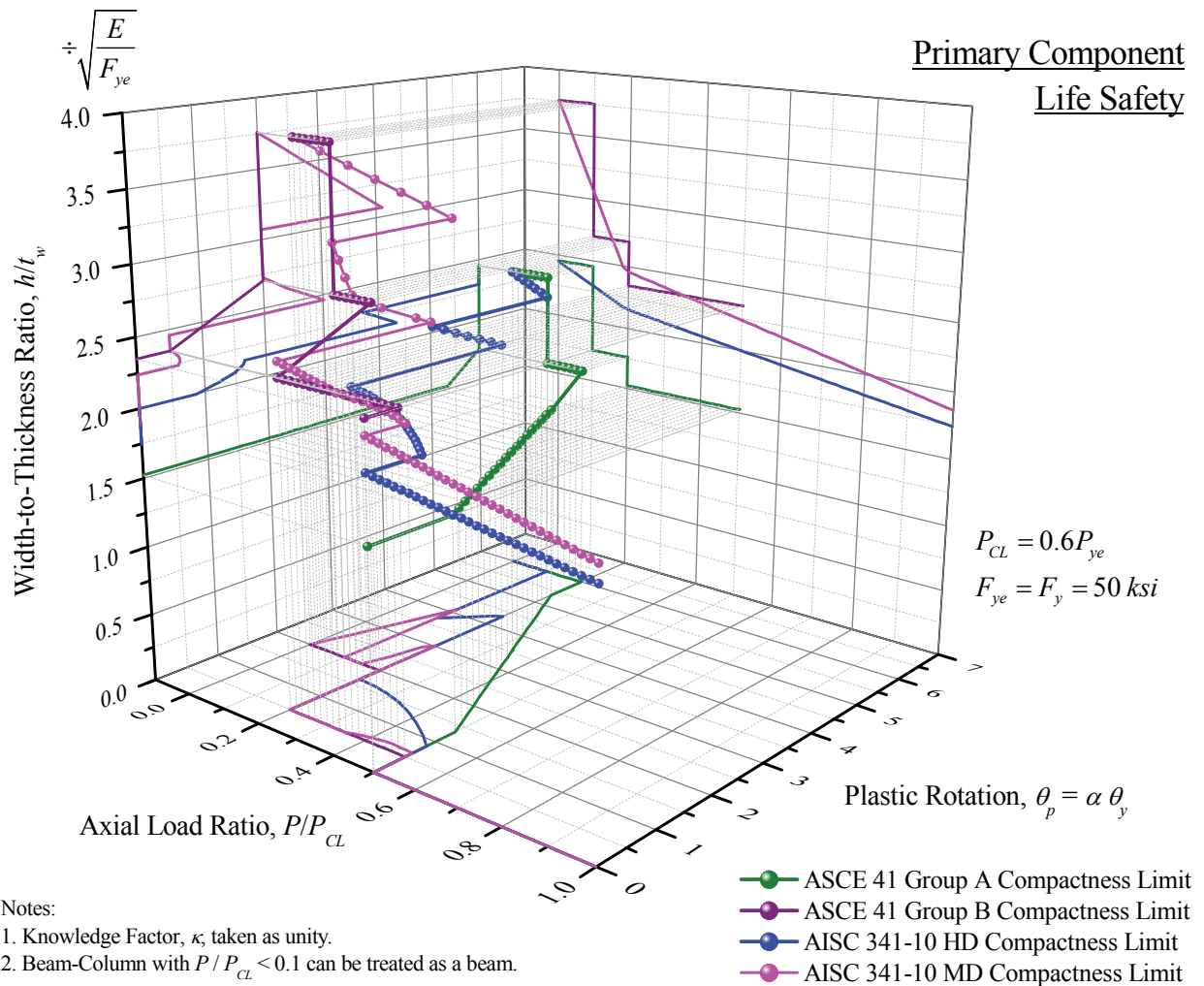


Figure 3-6. Acceptance Criteria as a Function of Axial Load Ratio and Section Compactness, LS Acceptance Criteria

In terms of assessment, ASCE 41 does not explicitly address column hinges near the column-to-base connections of a frame (similar to a beam-to-column connection). Columns are designed in accordance with capacity design provisions in AISC 341. However, ASCE 41 does not similarly adopt a capacity design approach for the assessment of MF columns.

Shear in Panel Zones

The acceptance criteria for *shear* action in panel zones are provided in ASCE 41 Table 5-5. The acceptance criteria are not a function of the axial force demand in the panel zone.

Demand

The flexural demand, M_{UD} , for the FR beam-to-column connections is taken as the moment at the face of the column. The flexural demand, M_{UD} , for the RBS (beam) is taken as the moment at the center of the RBS. The flexural demand, M_{UD} or M_{UF} , and axial force, P_{UF} , for the column are taken as the moment and axial force at the face of the each beam (top and bottom).

Table 3-11 summarizes the basic m -factors for the components of the SMF for the linear procedures. Figure 3-7 through Figure 3-12 provide the load-independent m -factors—taking in to account force-controlled and deformation-controlled classifications (force-controlled component actions are assigned an m -factor of unity, see §3.1.4.1). These figures are referred to herein as “Frame Capacity Schematics.” The two values given for a column represent the cases when $P_{UF} / P_{CL} = 0.2$ and 0.5 , adjusted for section compactness requirements. At $P_{UF} / P_{CL} = 0.2$ the interaction equation provides the same value when $P_{UF} / P_{CL} < 0.2$.

Table 3-11. Basic m -factors for Linear Procedures, SMF

Component - Action	Performance Level	
	LS	CP
Beam - Flexure		
a) $\frac{b_f}{2t_f} \leq \frac{52}{\sqrt{F_{ye}}}$ and $\frac{h}{t_w} \leq \frac{418}{\sqrt{F_{ye}}}$	6	8
b) $\frac{b_f}{2t_f} \geq \frac{65}{\sqrt{F_{ye}}}$ or $\frac{h}{t_w} \geq \frac{640}{\sqrt{F_{ye}}}$	2	3
c) other	linear interpolation	
Column - Flexure		
for $P_{UF} / P_{CL} < 0.2$		
a) $\frac{b_f}{2t_f} \leq \frac{52}{\sqrt{F_{ye}}}$ and $\frac{h}{t_w} \leq \frac{300}{\sqrt{F_{ye}}}$	6	8
b) $\frac{b_f}{2t_f} \geq \frac{65}{\sqrt{F_{ye}}}$ or $\frac{h}{t_w} \geq \frac{460}{\sqrt{F_{ye}}}$	1.25	2
c) other	linear interpolation	
for $0.2 \leq P_{UF} / P_{CL} \leq 0.5$		
a) $\frac{b_f}{2t_f} \leq \frac{52}{\sqrt{F_{ye}}}$ and $\frac{h}{t_w} \leq \frac{260}{\sqrt{F_{ye}}}$	$9 \left(1 - \frac{5}{3} \frac{P}{P_{CL}}\right)$	$12 \left(1 - \frac{5}{3} \frac{P}{P_{CL}}\right)$
b) $\frac{b_f}{2t_f} \geq \frac{65}{\sqrt{F_{ye}}}$ or $\frac{h}{t_w} \geq \frac{400}{\sqrt{F_{ye}}}$	1.25	1.5
c) other	linear interpolation	
Column Panel Zone - Shear	8	11
RBS - Flexure ¹	$4.9 - 0.025d$	$6.2 - 0.032d$

¹ m -factors shall be modified as indicated in ASCE 41 §5.4.2.2.2, item 4.

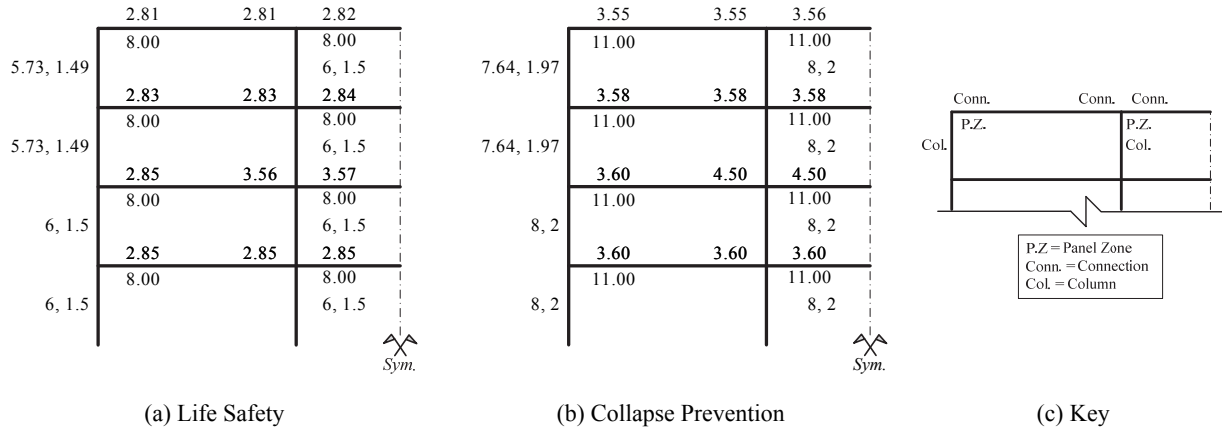


Figure 3-7. Frame Capacity Schematic (*m*-factor), LS and CP, 4-Story SMF ELF

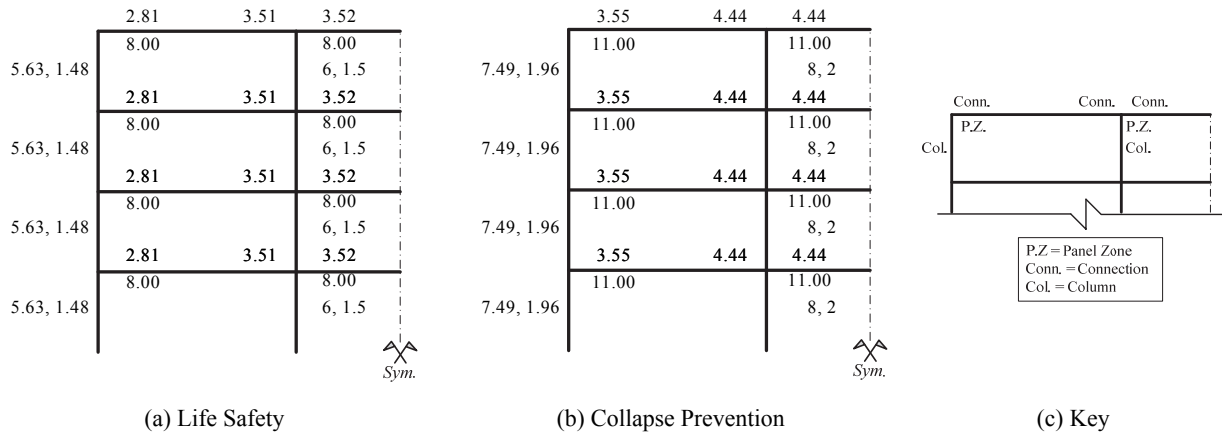


Figure 3-8. Frame Capacity Schematic (*m*-factor), LS and CP, 4-Story SMF RSA

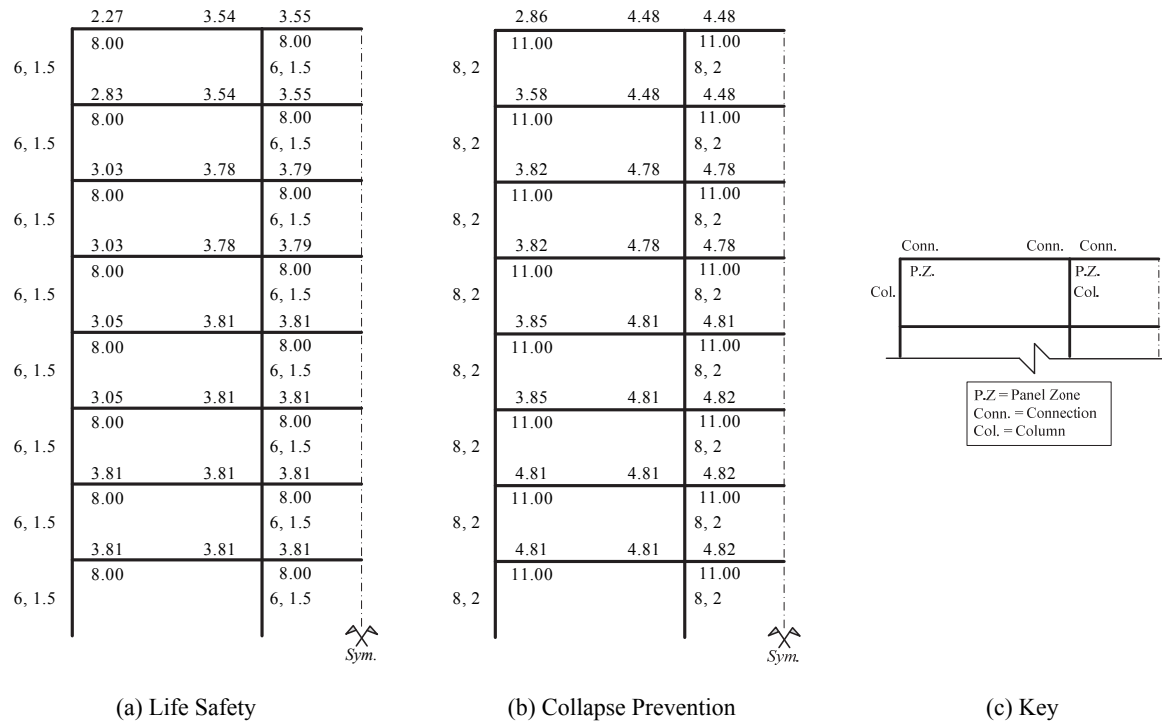


Figure 3-9. Frame Capacity Schematic (*m*-factor), LS and CP, 8-Story SMF ELF

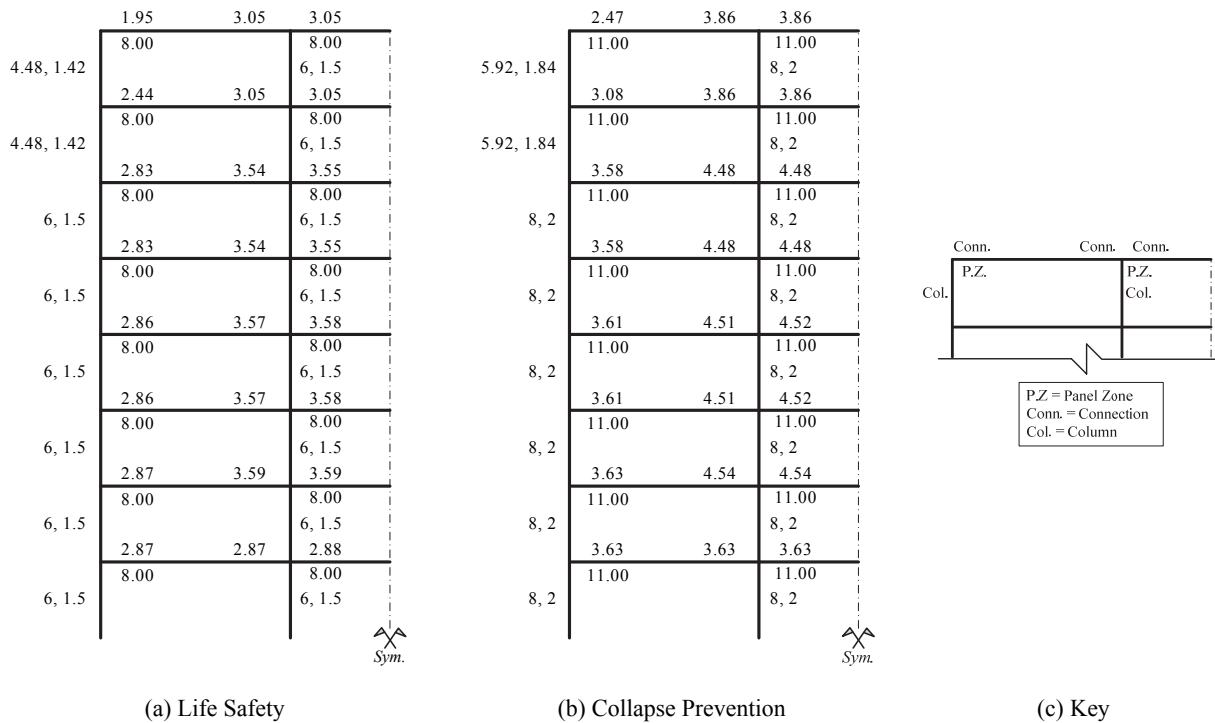


Figure 3-10. Frame Capacity Schematic (*m*-factor), LS and CP, 8-Story SMF RSA

	2.31	3.60	3.61
2.37, 1.31	8.00		8.00
	2.31	3.60	4.83, 1.44 3.61
2.37, 1.31	8.00		8.00
	2.31	3.60	4.83, 1.44 3.61
4.13, 1.4	8.00		8.00
	2.31	3.60	6, 1.5 3.61
4.13, 1.4	8.00		8.00
	3.07	3.83	6, 1.5 3.84
4.83, 1.44	8.00		8.00
	3.07	3.83	6, 1.5 3.84
4.83, 1.44	8.00		8.00
	3.07	3.83	6, 1.5 3.84
5.74, 1.49	8.00		8.00
	3.07	3.83	6, 1.5 3.84
5.74, 1.49	8.00		8.00
	3.17	3.97	6, 1.5 3.97
6, 1.5	8.00		8.00
	3.17	3.97	6, 1.5 3.97
6, 1.5	8.00		8.00
	2.54	3.97	6, 1.5 3.97
6, 1.5	8.00		8.00
	2.54	3.97	6, 1.5 3.97
6, 1.5	8.00		8.00
	2.61	4.07	6, 1.5 4.07
6, 1.5	8.00		8.00
	2.61	4.07	6, 1.5 4.07
6, 1.5	8.00		8.00
	3.26	4.07	6, 1.5 4.07
6, 1.5	8.00		8.00
	3.26	4.07	6, 1.5 4.07
6, 1.5	8.00		8.00
			6, 1.5

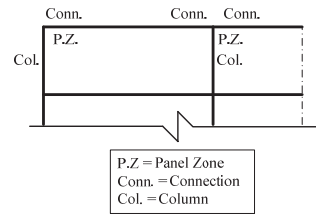
Sym.

(a) Life Safety

	2.91	4.55	4.56
3.03, 1.62	11.00		11.00
	2.91	4.55	6.4, 1.88 4.56
3.03, 1.62	11.00		11.00
	2.91	4.55	6.4, 1.88 4.56
5.44, 1.8	11.00		11.00
	2.91	4.55	8, 2 4.56
5.44, 1.8	11.00		11.00
	3.87	4.84	8, 2 4.84
6.4, 1.88	11.00		11.00
	3.87	4.84	8, 2 4.84
6.4, 1.88	11.00		11.00
	3.87	4.84	8, 2 4.84
7.64, 1.97	11.00		11.00
	3.87	4.84	8, 2 4.84
7.64, 1.97	11.00		11.00
	4.01	5.01	8, 2 5.02
8, 2	11.00		11.00
	4.01	5.01	8, 2 5.02
8, 2	11.00		11.00
	3.21	5.01	8, 2 5.02
8, 2	11.00		11.00
	3.21	5.01	8, 2 5.02
8, 2	11.00		11.00
	3.29	5.14	8, 2 5.14
8, 2	11.00		11.00
	3.29	5.14	8, 2 5.14
8, 2	11.00		11.00
	4.11	5.14	8, 2 5.14
8, 2	11.00		11.00
	4.11	5.14	8, 2 5.14
8, 2	11.00		11.00
			8, 2

Sym.

(b) Collapse Prevention



(c) Key

Figure 3-11. Frame Capacity Schematic (*m*-factor), LS and CP, 16-Story SMF ELF

3.2.1.2 Nonlinear Procedures

This section discusses the three primary component characteristics listed in Section 3.2.1 and computation of the demand in the component for the nonlinear assessment procedures.

Stiffness, Strength, Acceptance Criteria, and Demand

Component characteristics follow that outlined previously for the linear procedures. Although component stiffness is the primary characteristic in linear procedures, component strength is of equal importance in nonlinear procedures.

The stiffnesses of all members and connections for nonlinear assessment follow ASCE 41 §5.4.2.2.2 for the NSP and §5.4.2.2.3 for the NDP. The strength of all members and connections for nonlinear assessment follow ASCE 41 §5.4.2.3.3 for the NSP and §5.4.2.3.4 for the NDP. The same analytical model is used for both the NSP and NDP—see §3.1.3.2.

Compound elements with elastic and inelastic components are used for constructing all members in PERFORM-3D. Elastic stiffness and strength characteristics for each component follow that outlined for the linear procedures. Nonlinear components include the RBS beam-to-column connection modeled as a beam flexural hinge, the column flexural hinge modeled with axial-moment (P - M) interaction, and the panel zone modeled using the Krawinkler model (Krawinkler 1978). Figure 3-13 illustrates the analytical model of a beam-to-column subassembly for nonlinear assessment procedures. In the figure, Default End Zones are modeled with a flexural rigidity factor of two; a higher value is potentially too rigid to capture flexural deformations within the joint region. Detailed information concerning all aspects of the analytical model for nonlinear analysis can be found in PERFORM-3D *Components and Elements* (CSI 2011c).

The acceptance criteria in ASCE 41 for FR beam-to-column connections are derived from the results of the SAC project (see FEMA 351 (FEMA 2000b) and FEMA 355D (FEMA 2000c)). Therefore, plastic *rotation* is measured at the column face and the acceptance criteria include all effects inherent in the tested assemblies (e.g., panel zone and column yielding). This can be problematic when distinguishing between panel zone, beam, and column yielding effects. As the plastic rotation limits specified in ASCE 41 are average values for the tested assembly classes, it seems appropriate to separate yielding effects in a structural model. Therefore, beam and column hinge components and panel zone yielding components are individually modeled for nonlinear analysis in this study. Further, acceptance criteria for RBS beam-to-column connections do not address composite action with the floor slab, thus beam properties used in the nonlinear analysis model do not include this effect.

Flexural plasticity in beams and beam-columns is represented by nonlinear *moment-curvature* (MC) relationships which in turn are based on *moment-chord rotation* (MR) relationships provided by ASCE 41 Table 5-6. This shift in basis highlights a discrepancy between ASCE 41 §5.4.2.2.2-2 and the prescribed acceptance criteria. Conversion between plastic rotation and plastic curvature is done using a defined plastic hinge length, l_p . An MC hinge is preferred in lieu of an MR hinge, as yield rotation, θ_y , specified in ASCE 41 can lead to inconsistencies when beam models include rigid end offsets and when hinges are modeled away from the column faces. Further, ASCE 41 does not provide guidance on an appropriate beam length, l_b (ASCE 41 Equation 5-1). Theoretically, there is no difference between an MC hinge and an MR hinge

model as long as the conversion procedure for all nonlinear model parameters between the two is maintained. P - M interaction effects on a moment-curvature hinge are included in the analytical model (discussed subsequently).

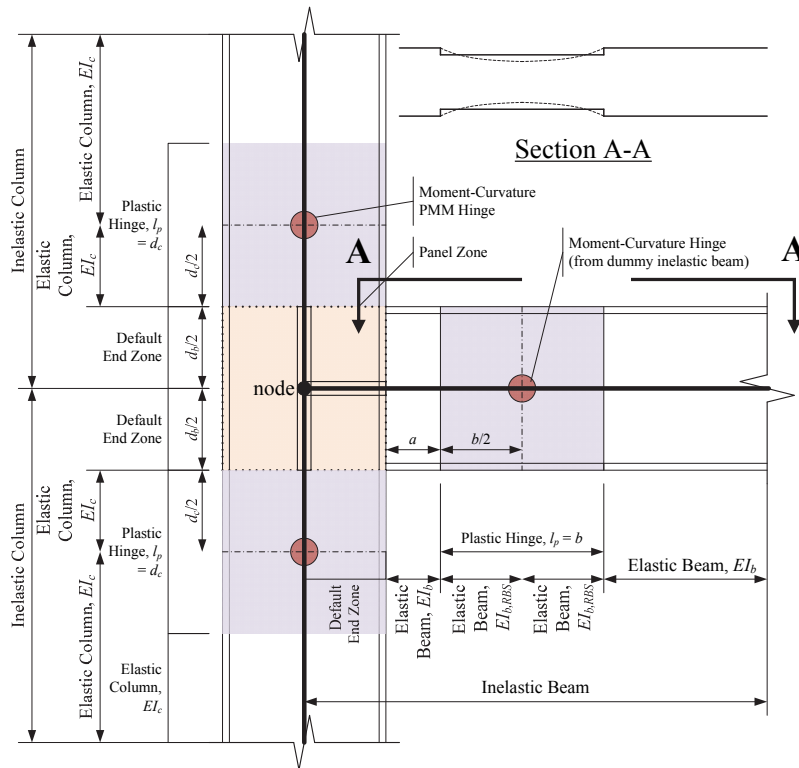


Figure 3-13. SMF Beam-to-Column Subassembly Analytical Schematic

Reduced beam sections are modeled within the beam member as elastic prismatic beam elements using the geometric cross-section properties at the outer two-thirds of the RBS. An MC hinge is placed at the center of the RBS with a plastic hinge length equal to the length of the RBS, b . Plastic rotation parameters modeling the backbone curve of the FR beam-to-column connection are taken from ASCE 41 Table 5-6. These values are converted to plastic curvature and subsequently adjusted from application at the column face to the center of the RBS and other FR connection adjustments discussed next. Stiffness and strength degradation are modeled based on calibrating the PERFORM-3D MODEL with experimental test data (see Figure 3-14—PERFORM-3D response is presented as “Analysis”). Intermediate anchor points defining the full backbone curve are determined from calibration with experimental test data (see Figure 3-14 and Figure 3-2). The ultimate flexural strength of the MC hinge is taken as $C_{pr} \times M_{CE}$ in accordance with AISC 358— C_{pr} is defined in AISC 358. The residual strength ratio (c in ASCE 41 Table 5-6) is normalized to the yield strength, M_{CE} , not the ultimate strength as required in PERFORM-3D.

The acceptance criteria for beam-to-column connections (flexural hinge is located within the connection) are taken from Fully Restrained Moment Connections in ASCE 41 Table 5-6 and are dependent on connection detailing, panel zone strength in a balanced yield condition, and member and cross-section slenderness (see ASCE 41 §5.4.2.4.3, 4.1 to 4.4). These reduction factors are also applied to the plastic rotation values defining the backbone curve. This is done because the CP acceptance criteria for a primary

FR connection was taken to match a —see Figure 3-2, and therefore any connection configuration that affects the value for a also affects the acceptance criteria. Similarly, the acceptance criteria are converted to plastic curvature and the application point is adjusted to the center of the RBS. Acceptance criteria for a beam hinge should also be used to verify the performance of the plastic hinge in the RBS; however, as discussed previously, it will not control unless evaluating the IO SPL. Therefore, this secondary check is not performed in this study. Expanded commentary on beam-to-column connection versus beam hinge acceptance criteria is needed in ASCE 41, as well as a discussion clarifying the reductions to the plastic rotation values defining the backbone curve and acceptance criteria.

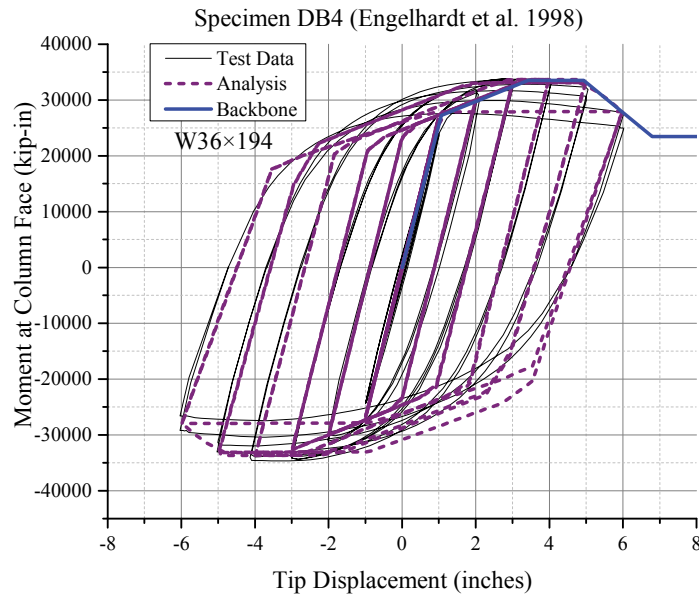


Figure 3-14. PERFORM-3D RBS Calibration

PERFORM-3D flexural section strength flags (used to verify a design strength at a given location) are placed at the column faces and at midspan of the beam to verify acceptable design of the beams and beam-to-column connections. Similarly, shear section strength flags are placed at the column faces and at the center of the RBS to verify acceptable design of the beam-to-column connections. These section strength flags are modified as needed for cross-section geometry, member strengths (does not typically control beams), and design-assessment criteria prescribed in ASCE 41.

Panel zones are explicitly modeled at all beam-to-column joints using the Krawinkler model. This model uses the force-deformation relationship intrinsic in the design equations prescribed in AISC 360 (see Figure 3-15—PERFORM-3D response is presented as “Analysis”). However, the yield stress in the panel zone model is taken as $0.55 \times F_{ye}$ in ASCE 41 in lieu of $0.6 \times F_y$ as used in design. Figure 3-15 shows the range of the expected demands on the panel zones (anchored to a shear strain ductility, γ / γ_s , of 4). This range is small because the probable flexural strength of the connection is used to check the panel zone strength in design, and this connection strength is associated with Collapse Prevention (CP) of the beam-to-column connection in ASCE 41. Only when an FR connection is strained past the CP level will the panel zone deform outside this range; nevertheless, the CP acceptance criteria for a panel zone in ASCE 41 is three times a shear strain ductility of 4.

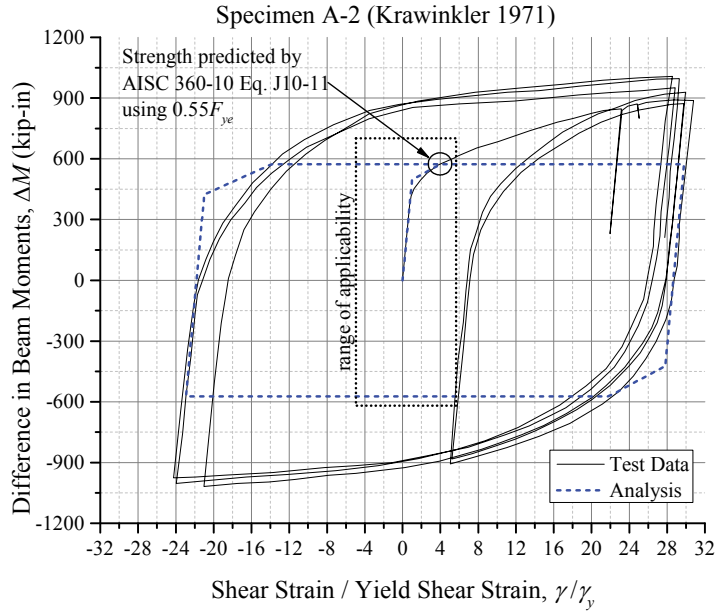


Figure 3-15. PERFORM-3D Panel Zone Calibration

Frame columns (i.e., beam-columns) are modeled similar to beams discussed previously, except that flexural *PMM* MC hinges that capture the combined effects of axial force and biaxial moments are placed near the joint region boundaries (see Figure 3-13). The plastic hinge length is assumed to be equal to the depth of the column, d_c . Out-of-plane moments are small relative to the in-plane moments in the SFRS members because each SFRS is an isolated planar frame in the direction of loading. Plastic rotation parameters of the flexural *PMM* hinges are taken from “columns” in ASCE 41 Table 5-6 and converted to plastic curvature (no adjustment for hinge location is needed). Criteria for flexural hinges based on member buckling strengths can be complex and problematic in capturing the in-plane nonlinear flexure behavior. For example, yield rotation, θ_y , for a column is based on section strength, P_{ye} , while modeling parameters and acceptance criteria (function of θ_y) are based on member strength, P_{CL} , without regard to the plane of buckling. ASCE 41-13 took the first step in resolving some issues concerning steel columns by permitting the modeling parameters to be determined using P / P_{CL} in the plane of buckling. Still, *P-M* interaction curves still require some clarification and guidance. In terms of assessment, ASCE 41 does not explicitly address column hinges near the column-to-base connections of a frame (similar to a beam-to-column connection).

In this study, modeling and acceptance criteria for the beam-column flexural hinges are taken as those provided for columns in ASCE 41 Table 5-6. The *P-M* interaction effect on the in-plane flexural strength of a column hinge, M_{CE_x} , where x denotes the in-plane bending axis, is modeled by the *section* strength of the member (i.e., yield surface) using P / P_{ye} in ASCE 41 Equation 5-4 (repeated below as Equation (3-15); see Figure 3-16, Figure 3-18, and Figure 3-19). *P-M* interaction relationships provided in PERFORM-3D for the yield surfaces of MC hinges in beam-columns are calibrated to approximate this curve as illustrated in Figure 3-19.

$$M_{CEx} = 1.18M_{pe,x} \left(1 - \frac{P}{P_{ye}} \right) \leq M_{pe,x} \quad (\text{ASCE 41 Equation 5-4}) \quad (3-15)$$

ASCE 41 Equation 5-4 is based on plastic design theory and applicable for the in-plane section strength (strong-axis bending) of a wide flange section. AISC 360 Equation H1-1 can also be applied for computing the in-plane section strength by using P / P_{ye} in lieu of P_r / P_c as defined in AISC 360. Plastic design theory also gives the out-of-plane section strength (weak-axis bending, with y denoting the out-of-plane bending axis) of a wide flange section as Equation (3-16).

$$M_{CEy} = 1.19M_{pe,y} \left(1 - \left(\frac{P}{P_{ye}} \right)^2 \right) \leq M_{pe,y} \quad (3-16)$$

P - M interaction effect on the plastic rotation parameters and acceptance criteria of a column hinge is modeled by *member* strength using P_{CL} , computed for buckling about any axis or failure mode independent of the effect it may have on the in-plane flexure response of the column hinge (see Figure 3-16).

First, ASCE 41 requires a column (i.e., flexural hinge in the column) to be force-controlled for flexure when $P / P_{CL} > 0.5$ for the nonlinear procedures and references the same equation used for linear assessment. This can be extremely problematic as separate strengths and interaction equations create discontinuities that cannot be effectively addressed in analysis software (see Figure 3-16). This elastic interaction equation is neglected in this study for nonlinear assessment and the hinge model obeys ASCE 41 Equation 5-4 independent of P_{CL} . ASCE 41 Equation 5-12 is more applicable for checking member stability than defining the section yield surface; Equation (3-17) rearranges ASCE 41 Equation 5-12 in terms of the moment strength.

$$M_{CE} = M_{CL} \left(1 - \frac{P}{P_{CL}} \right) \quad (\text{from ASCE 41 Equation 5-12}) \quad (3-17)$$

Second, flexural hinge model parameters and associated acceptance criteria are a function of the axial load ratio P / P_{CL} . Provisions for this interaction in ASCE 41, however, create a discontinuity in the curve, as shown in Figure 3-17, which cannot be effectively addressed in analysis software. PERFORM-3D provides a simplified curve to model the variation in acceptance criteria with axial force, also shown in Figure 3-17. The adopted curves in this study are conservative for $P / P_{CL} \leq 0.2$. Further, because of constraints on P - M hinge models in PERFORM-3D, the model parameters (a in ASCE 41 Table 5-6 plus the elastic component as shown in Figure 3-17, a plus elastic = DL in PERFORM-3D—see Figure 3-2 for a and DL) do not coincide for $P / P_{CL} > 0.2$. A column hinge with high axial load can reach its peak strength (a plus elastic = CP in this case) in regards to the provisions of ASCE 41 yet still be able to maintain its flexural strength. In general, column hinges are not expected to be significantly strained; however, demands may affect the performance of base hinges, which can have detrimental effects on the system upon loss of strength. More detailed information can be found in the PERFORM-3D *User Guide* (CSI 2011d) and PERFORM-3D *Components and Elements* (CSI 2011c). Lastly, it is of questionable validity to allow a primary column

component in a SFRS to have acceptance criteria based on a secondary component when based on a function of P / P_{CL} as was mentioned earlier

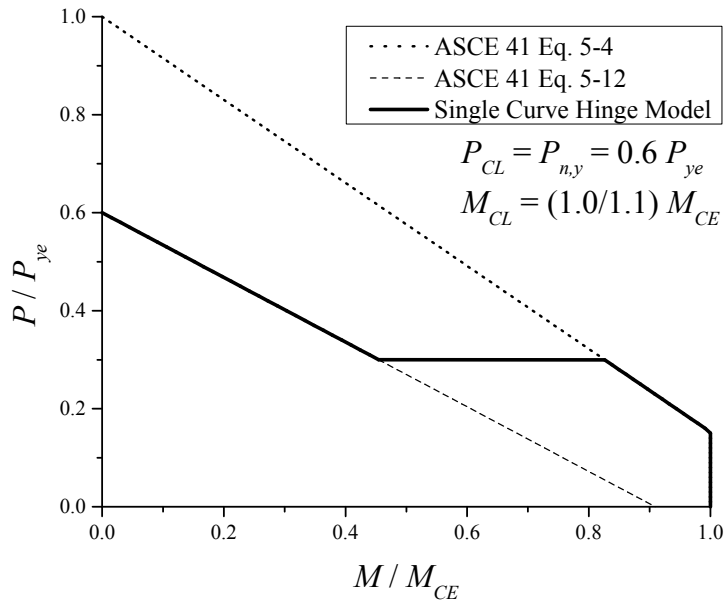


Figure 3-16. In-plane Flexural Hinge Yield Surface Model (Including Force-Controlled Response)

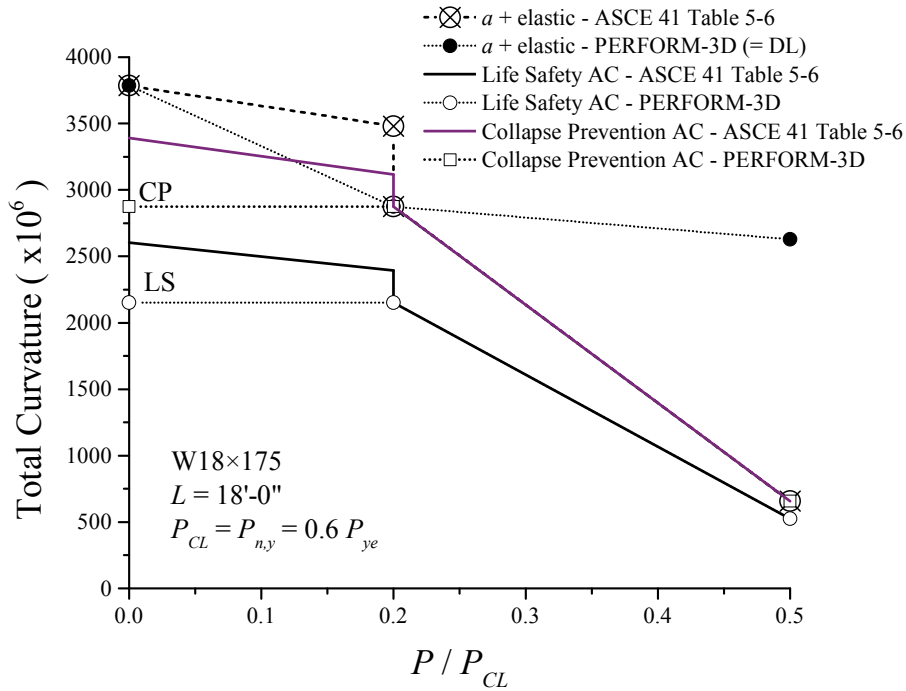


Figure 3-17. Variation in Acceptance Criteria and Hinge Model for Axial Force

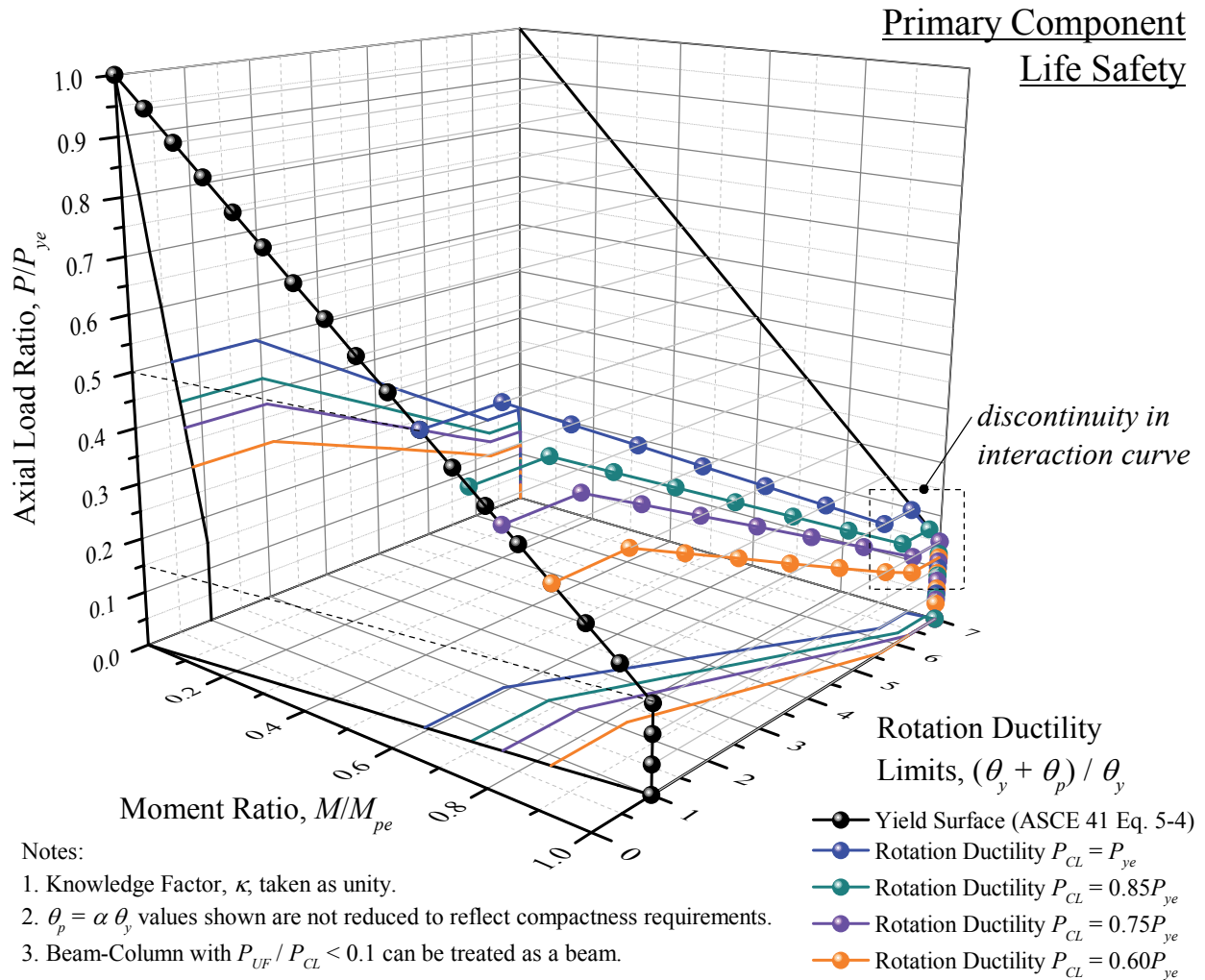


Figure 3-18. P - M Interaction on Plastic Rotation, LS Acceptance Criteria (Primary Component)

The ultimate flexural strength of the MC hinge is taken as 1.1 times M_{CE} at $P = 0$. This flexural strength increase is held constant for all values of axial force in PERFORM-3D. The residual strength ratio (c in ASCE 41 Table 5-6) is normalized to the yield strength, M_{CE} , at distinct P / P_{CL} values (not P / P_{ye} , which is used to compute M_{CE}) and not the ultimate strength as required in PERFORM-3D.

The column-to-base connection is modeled using an FR beam-to-column connection model in PERFORM-3D. It is reasonable to adopt an FR connection model (such as an improved welded WUF connection) to represent the base connection because doing so will provide a lower-bound estimate of the plastic rotations angle compared to that given explicitly for a column hinge, as shown in Table 3-12. Future research is needed to develop acceptance criteria and modeling parameters for column-to-base connections, including embedded connections.

Stability of a beam-column needs to be addressed in addition to capturing flexural plasticity. However, ASCE 41 does not provide explicit provisions to check member stability when $P / P_{CL} \leq 0.5$ for nonlinear

procedures. When $P / P_{CL} > 0.5$, ASCE 41 Equation 5-12 (primarily used for the linear procedures) can be used, but is not recommended as discussed previously.

Table 3-12. Plastic Rotation Angles for Improved WUF and Column Hinge for a W18×175

	$P = 0$	$P = 0.1999 \times P_{CL}$	$P = 0.2 \times P_{CL}$	$P = 0.5 \times P_{CL}$
WUF AC	0.041	0.038	0.031	0.0056
Column AC	0.071	0.065	0.053	0.0097
Ratio	0.58	0.58	0.58	0.58

In this study, section strength flags are applied to the frame columns as an indicator of member instability. For in-plane buckling and strong axis bending, a PM strength flag is placed at the ends of the column using AISC 360 §H1.3(a) for the interaction curve using $P_{n,x}$ as P_c . This approach closely aligns with ASCE 41 Equations 5-10, 5-11, and 5-12. The in-plane effective length of the column is taken as that computed for design (i.e., adjusted K factor (see Chapter 2)). This is considered a conservative practice as the analysis adjusts the stiffness matrix (only for material nonlinearity) at every time step and the leaning column effect is explicitly included. However, geometric imperfections (system and member), residual stresses, and epistemic uncertainties (i.e., ϕ factor) are not included in the mathematical model. Consequently, member strengths based on the actual unbraced length (i.e., $KL_x = L_x$) is of questionable validity, but so is using the design value based on a vertical load-only load combination. Research is needed concerning in-plane dynamic instability of inelastic members.

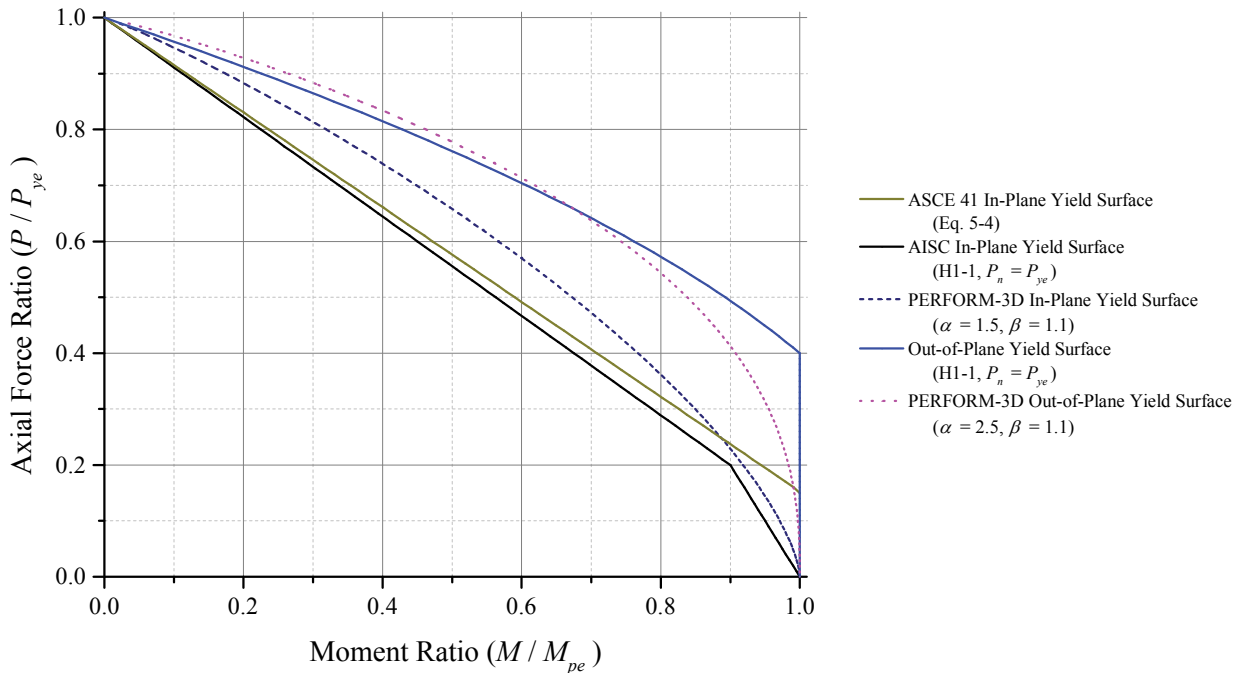


Figure 3-19. P - M Interaction Curve (Section Yield Surface)

For out-of-plane buckling and strong axis bending, a PM strength flag is placed at the ends of the column using AISC 360 §H1.3(b) for the interaction curve and the effective length is taken as the actual unbraced

length (i.e., $KL_y = L_y$). Adopting ASCE 41 Equations 5-10, 5-11, and 5-12 as an indicator of weak-axis instability coupled with in-plane bending can be highly conservative. PERFORM-3D uses a single continuous interaction curve as shown in Figure 3-20 which illustrates several interactions curves together with the approximations from PERFORM-3D. Similar to beams, section strengths are modified as needed based on cross-section geometry, member strengths (commonly controls columns in compression), and design-assessment criteria prescribed in ASCE 41.

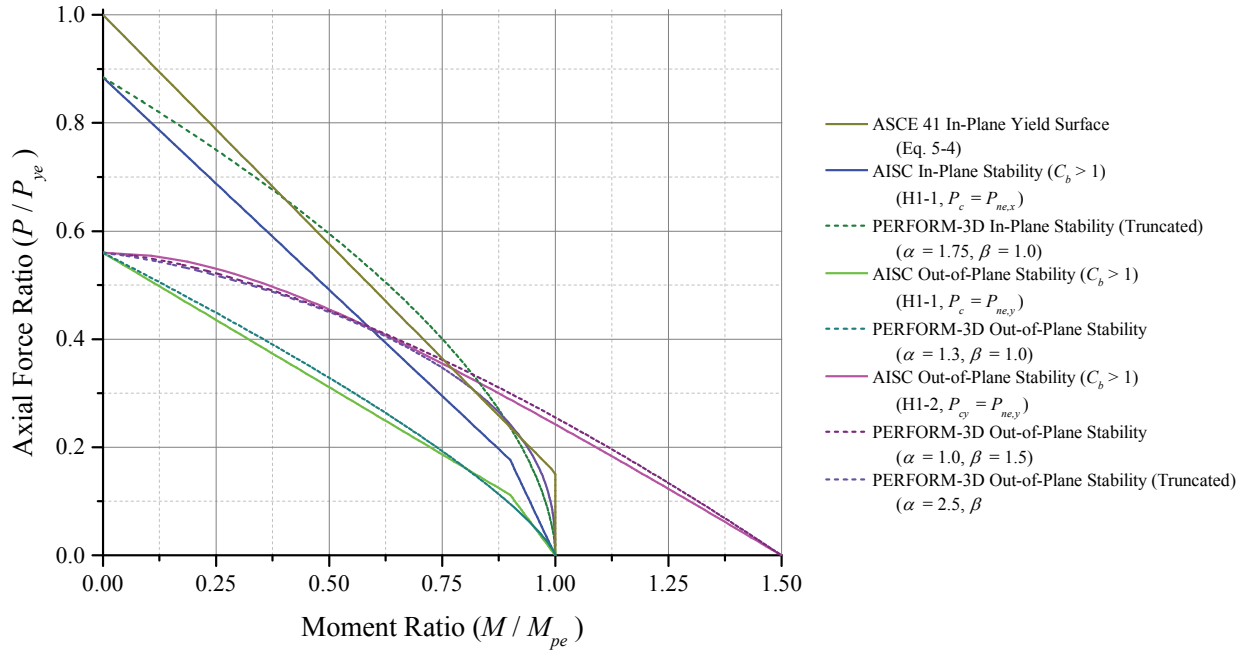
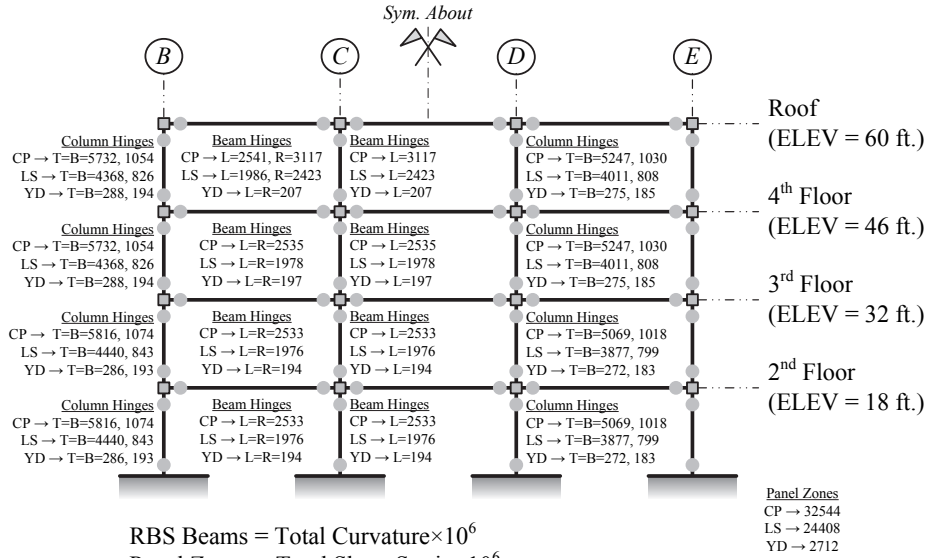


Figure 3-20. P - M Interaction Curve (Member Strength)

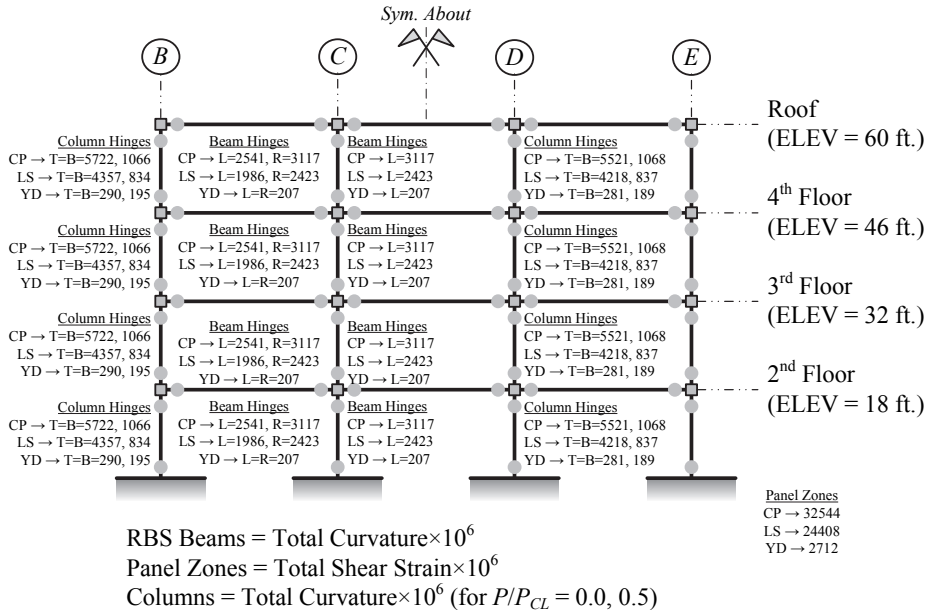
Figure 3-21 through Figure 3-26 provide the load-independent acceptance criteria—with consideration of force-controlled and deformation-controlled classifications. These figures are referred to herein as “Frame Capacity Schematics.” The two values given for a column represent the cases when $P_{UF} / P_{CL} = 0.2$ and 0.5 , adjusted for section compactness requirements. At $P_{UF} / P_{CL} = 0.2$, the interaction equation does not provide the same value when $P_{UF} / P_{CL} < 0.2$, as seen for the linear procedures.



RBS Beams = Total Curvature × 10⁶
 Panel Zones = Total Shear Strain × 10⁶
 Columns = Total Curvature × 10⁶ (for $P/P_{CL} = 0.0, 0.5$)

CP = Collapse Prevention, LS = Life Safety, YD = Yield
 L = Left Hinge, R = Right Hinge, T = Top Hinge, B = Bottom Hinge
 All values are for Primary Components

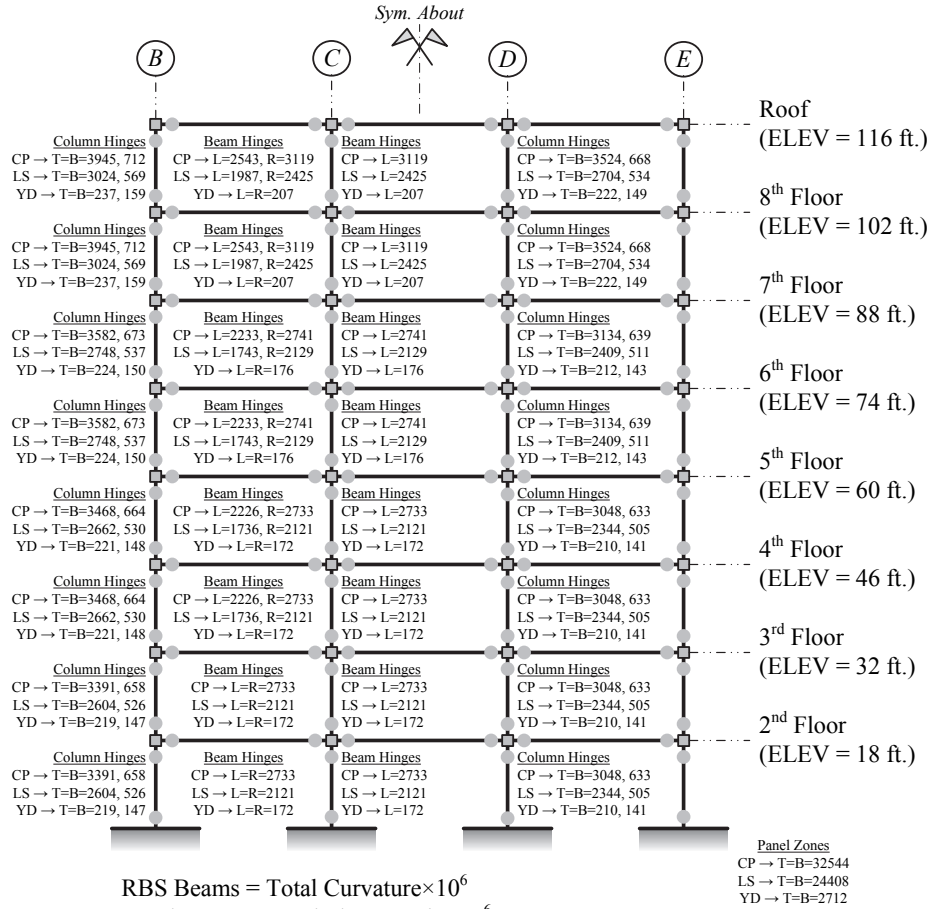
Figure 3-21. Frame Capacity Schematic (Inelastic), YD, LS, and CP, 4-Story SMF ELF



RBS Beams = Total Curvature × 10⁶
 Panel Zones = Total Shear Strain × 10⁶
 Columns = Total Curvature × 10⁶ (for $P/P_{CL} = 0.0, 0.5$)

CP = Collapse Prevention, LS = Life Safety, YD = Yield
 L = Left Hinge, R = Right Hinge, T = Top Hinge, B = Bottom Hinge
 All values are for Primary Components

Figure 3-22. Frame Capacity Schematic (Inelastic), YD, LS, and CP, 4-Story SMF RSA



RBS Beams = Total Curvature × 10⁶
 Panel Zones = Total Shear Strain × 10⁶
 Columns = Total Curvature × 10⁶ (for P/P_{CL} = 0.0, 0.5)

CP = Collapse Prevention, LS = Life Safety, YD = Yield
 L = Left Hinge, R = Right Hinge, T = Top Hinge, B = Bottom Hinge
 All values are for Primary Components

Figure 3-23. Frame Capacity Schematic (Inelastic), YD, LS, and CP, 8-Story SMF ELF

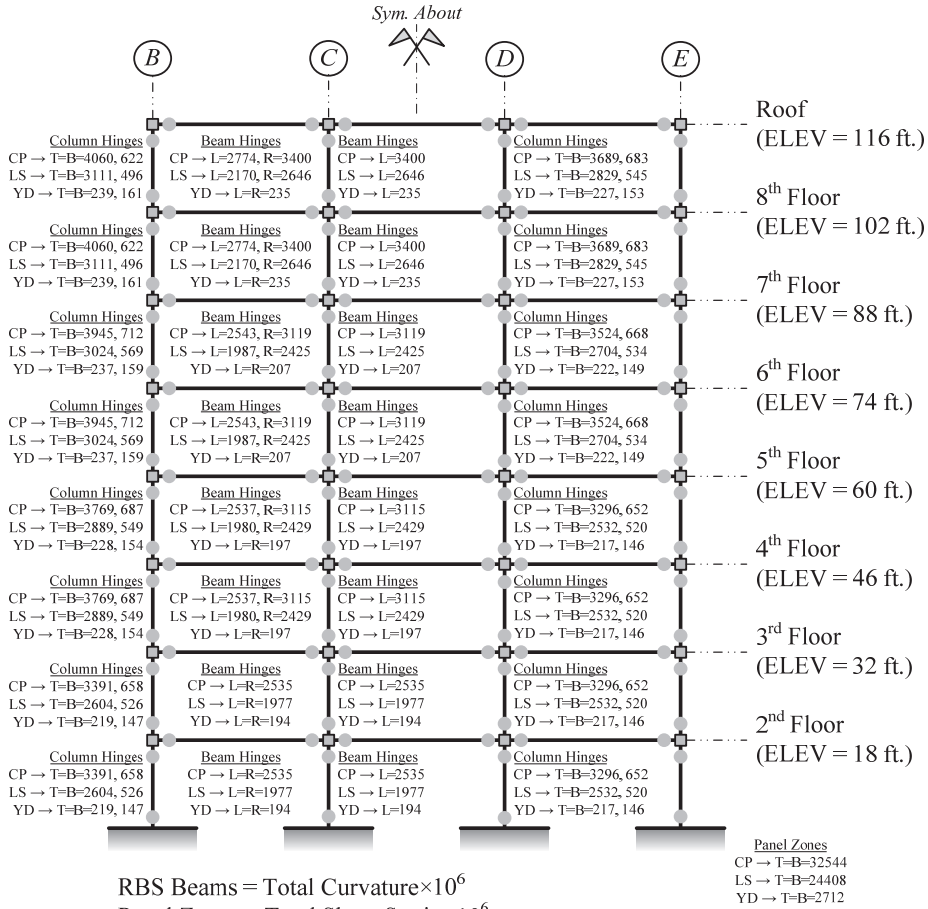
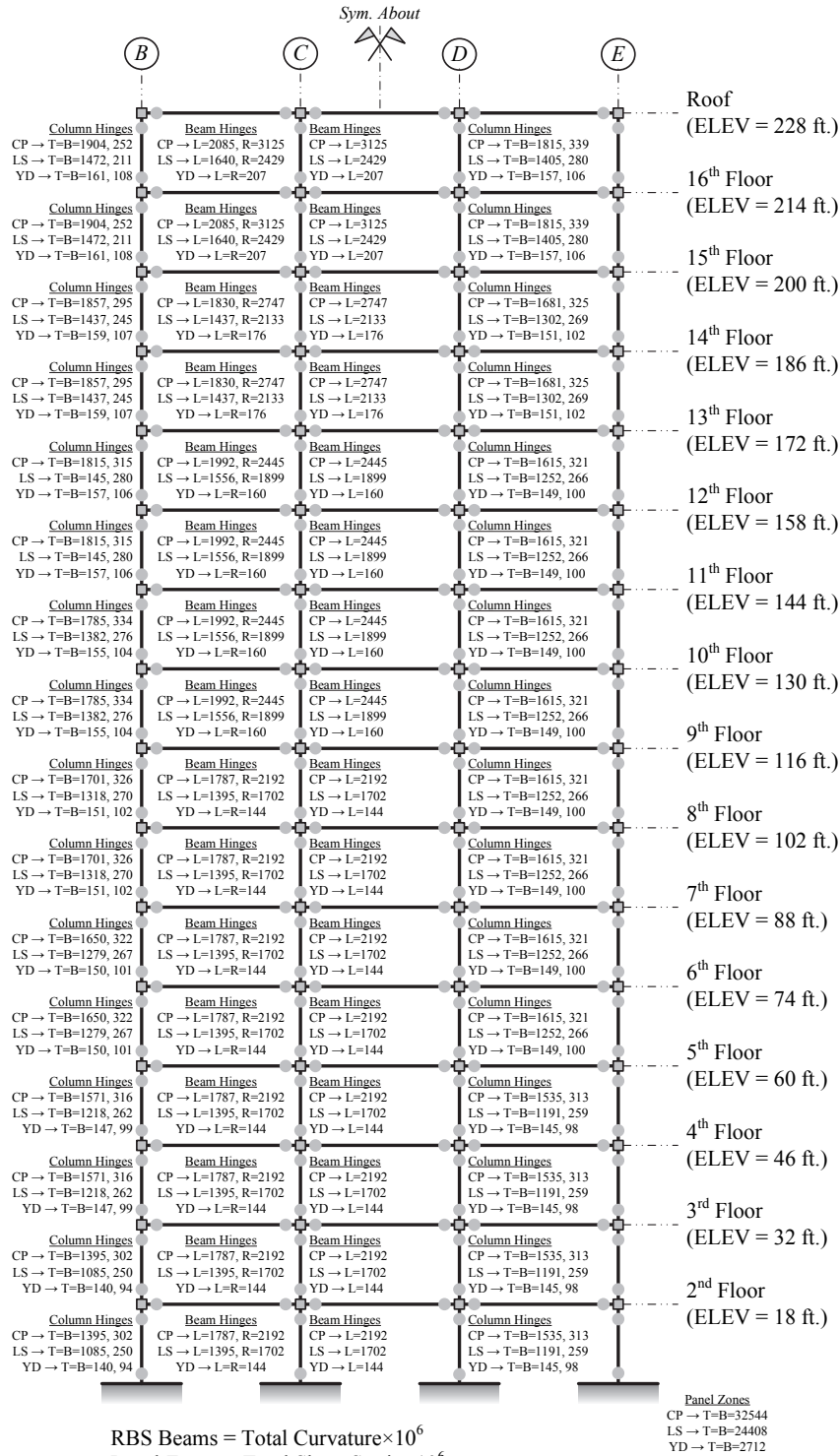


Figure 3-24. Frame Capacity Schematic (Inelastic), YD, LS, and CP, 8-Story SMF RSA



CP = Collapse Prevention, LS = Life Safety, YD = Yield
 L = Left Hinge, R = Right Hinge, T = Top Hinge, B = Bottom Hinge
 All values are for Primary Components

Figure 3-25. Frame Capacity Schematic (Inelastic), YD, LS, and CP, 16-Story SMF ELF

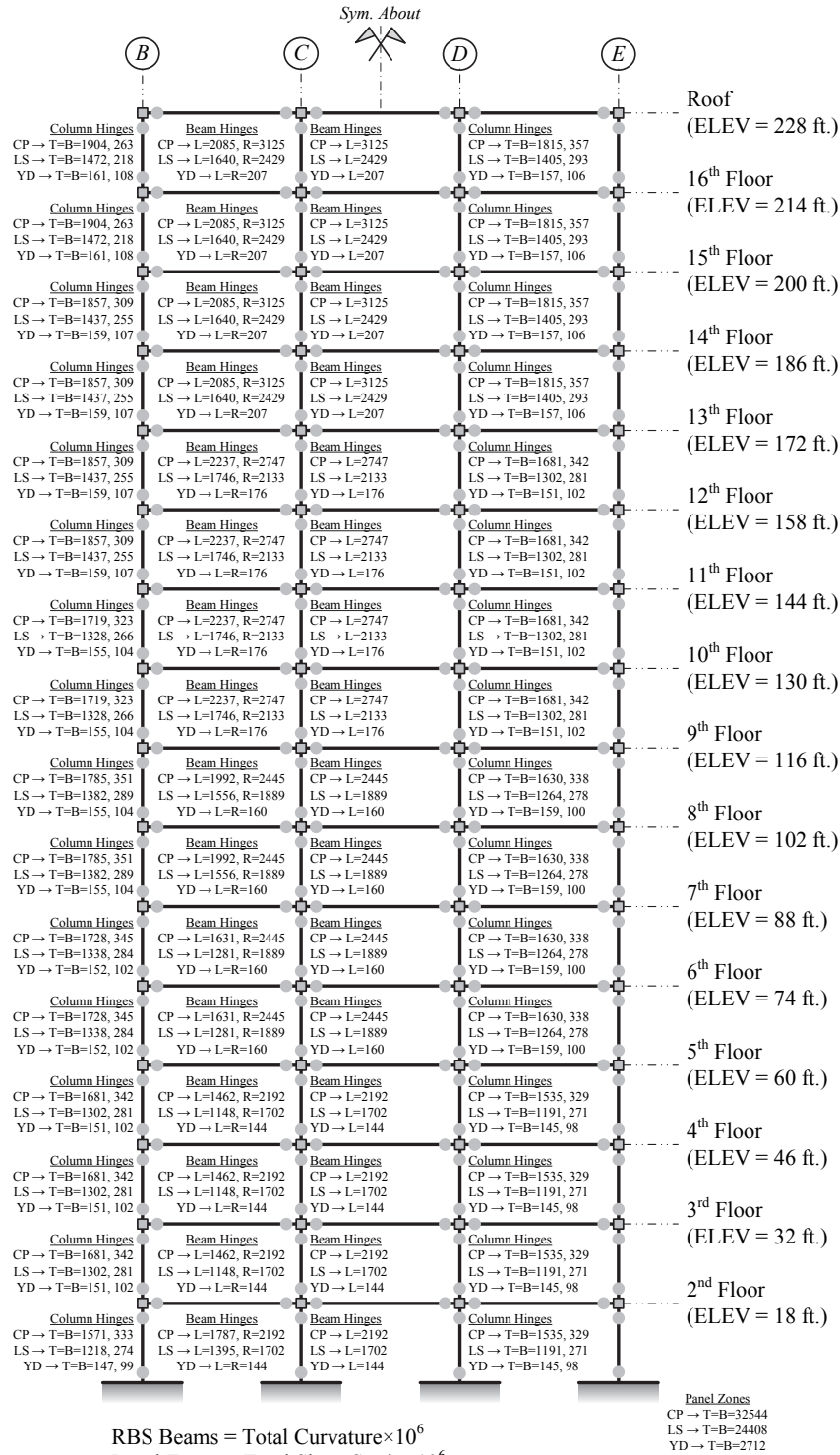


Figure 3-26. Frame Capacity Schematic (inelastic), YD, LS and CP, 16-Story SMF RSA

3.2.2 Seismic Assessment Results

The results for the SMFs assessed using each of the four analysis procedures are presented in this section. The following section highlights any failure to satisfy the acceptance criteria.

For the LSP and LDP, force-controlled column compression demands, P_{UF} , are computed by taking J in ASCE 41 §3.4.2.1.2-2 as the minimum DCR—as defined in ASCE 41—of the component(s) (i.e., beam hinges) delivering force to the member, but not less than 2.0. In this case, this method generally provides the least conservative axial force demand estimates than that determined from a *fully yielded* capacity design analysis per ASCE 41 §3.4.2.1.2-1. However, ASCE 41 does not provide explicit guidance on performing this capacity design analysis²² for a moment frame, as is done for an eccentrically braced frame in ASCE 41 §5.5.3.4. The capacity design procedure used in this study models all beam hinges adjacent to columns achieving M_{pr} . Axial force demand estimates from the capacity design procedure prescribed in AISC 341 for moment frames, which uses the system overstrength factor, Ω_o , in ASCE 7 are included with those determined from ASCE 41 in the respective analysis sections below. Force-controlled component actions are assigned an m -factor of unity, see §3.1.4.1.

Analysis results (e.g., DCR_N) for the NDP using the ground motion record set are statistically summarized by the median, mean, 84th percentile, and mean plus one standard deviation response for both the LS BPL (given the BSE-1 EHL) and the CP BPL (given the BSE-2 EHL). Mean and median response are presented because (1) ASCE 41 does not discuss how to process the results in the event of a structural collapse under a given record in the set, (2) new provisions under investigation for inclusion in the 2015 *NEHRP Provisions* are being debated as to how to process results from eleven records (an increase from seven in ASCE 7-10), and (3) the difference is small for well-performing systems that remain stable for all motions in a set. It is the goal here that showing the mean and median will assist in developing future code provisions.

For comparison purposes only, the DCR_N values obtained from the LSP, LDP, and NSP are superimposed on the figures showing the results obtained from the NDP. Results from the NSP and NDP can be directly compared because the basis of measurement is identical. However, caution should be used when comparing linear and nonlinear results by inspection because the nature of the analysis is fundamentally different; presenting them together here is not intended to imply they are equivalent. Results from the two are not always directly comparable as linear results would first need to be converted to total demand where applicable, and in certain cases not based on an interaction equation. Results from the linear assessment procedures are presented alongside results from the nonlinear assessment procedures primarily to highlight the distribution of performance predictions between the analytical methods.

For comparison purposes only, the base shears computed using the LSP and LDP are provided in §3.2.3.1.4.

²² ASCE 41 §3.4.2.1.2-1 refers to this type of analysis as a “limit state” analysis.

3.2.2.1 Four-Story Moment Frame

3.2.2.1.1 Linear Static Procedure

3.2.2.1.1.1 BSE-1 Earthquake Hazard Level (LS BPL)

In this section, the following apply:

- Figure 3-27 and Figure 3-28 provide the DCR_N and load-dependent m -factor values for the ELF and RSA designs, respectively, for the LSP at the BSE-1 EHL. In these figures, DCR_N values greater than unity are highlighted in red and underlined. DCR values, as defined by ASCE 41, can be obtained by multiplying DCR_N by m and κ , see Eq. 3-6.
- Figure 3-29 provides the maximum axial compression demands, P_{UF} , in the exterior column lines for various analysis methods and the column capacity, P_{CL} .

All component actions satisfy the LS BPL acceptance criteria except for the exterior beam-to-column connections in the RSA-designed frame on the second and third floors. These connection failures are primarily due to reduced m -factors as a result of the FR connection modifiers for panel zone strength and clear span-to-depth limitations. Assessment results for the panel zones all remained small compared to unity. This suggests that design rules and conventional practice (e.g., increase column sizes to offset the use of doubler plates) can produce strong panel zones with regard to ASCE 41 criteria, which can adversely affect the beam-to-column connection acceptance criteria. Current steel design practice, however, does not enforce a balanced yield condition between a beam hinge and the adjacent panel zone. Moreover, it is not logical that the FR connection reduction factors create a step function in performance. The 20 percent reduction between the interior connections in the ELF-designed frame on the second and third floors in Figure 3-27(b) is due to the change in the average story-height, h , when computing the panel zone demands—see ASCE 41 §5.4.2.4.2-4.2. Figure 3-27(b) and Figure 3-28(b) show that the frame columns are deformation-controlled for flexure.

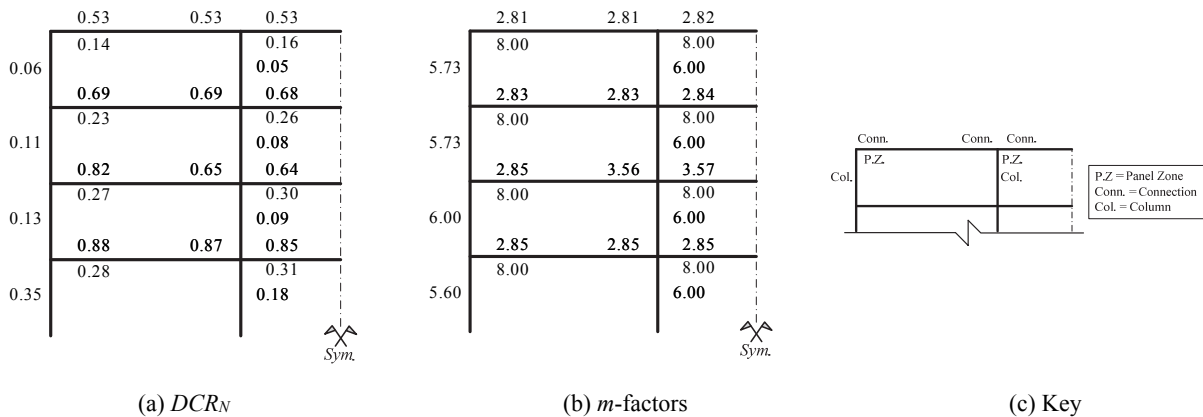


Figure 3-27. LSP Assessment Results, 4-Story SMF ELF, BSE-1 LS

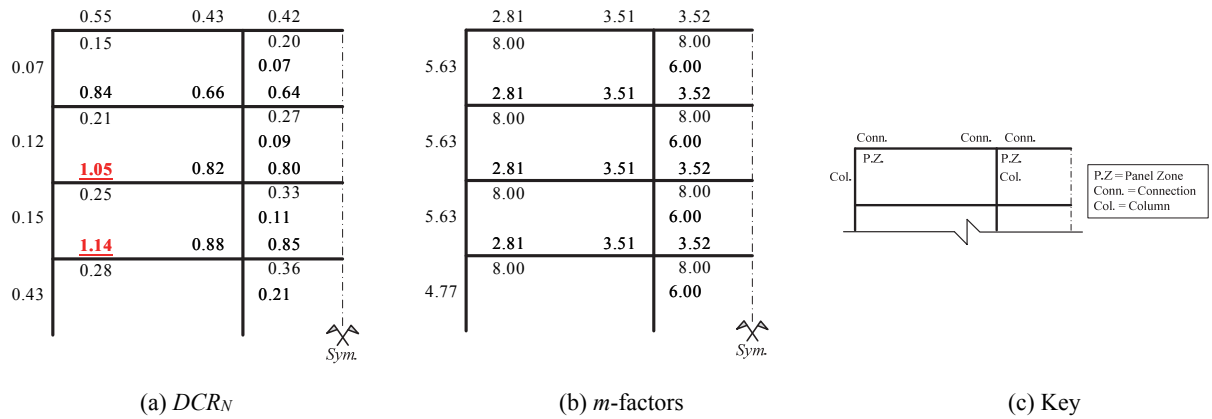


Figure 3-28. LSP Assessment Results, 4-Story SMF RSA, BSE-1 LS

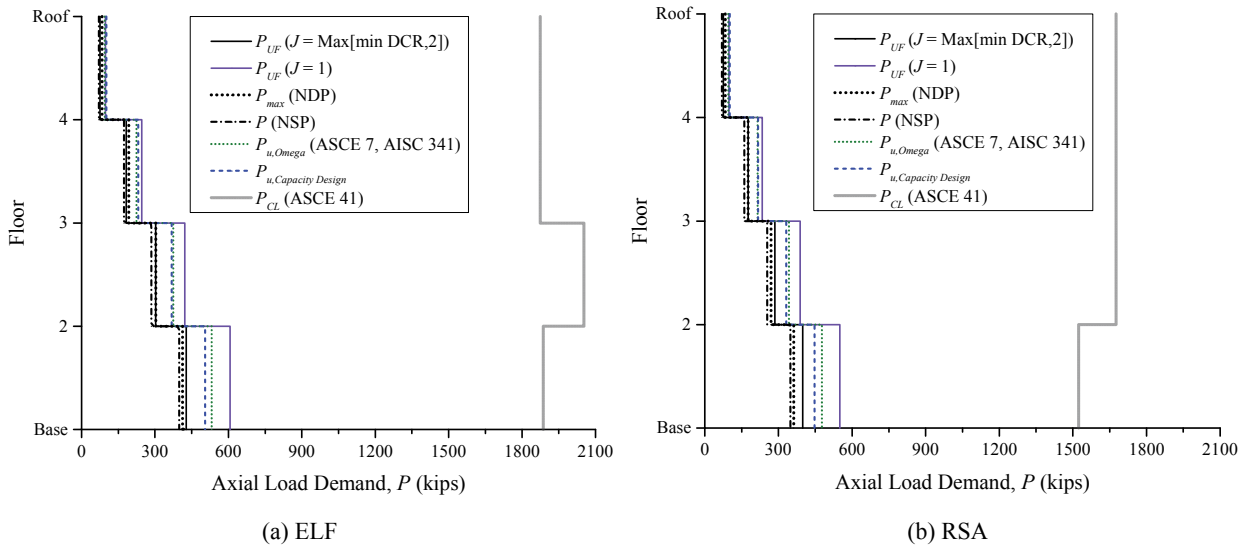


Figure 3-29. LSP Assessment Results, Compression in Exterior Columns, 4-Story SMF, BSE-1

3.2.2.1.1.2 BSE-2 Earthquake Hazard Level (CP BPL)

In this section, the following apply:

- Figure 3-30 and Figure 3-31 provide the DCR_N and load-dependent m -factor values for the ELF and RSA designs, respectively, at the LSP at the BSE-2 EHL. In these figures, DCR_N values greater than unity are highlighted in red and underlined. DCR values, as defined by ASCE 41, can be obtained by multiplying DCR_N by m and κ , see Eq. 3-6.
- Figure 3-32 provides the maximum axial compression demands, P_{UF} , in the exterior column lines for various analysis methods and the column capacity, P_{CL} .

All component actions satisfy the CP BPL acceptance criteria except for a few beam-to-column connections in the ELF- and RSA-designed frames on the second and third floors. As identified previously in §3.2.2.1.1.1, these connection failures are primarily due to reduced m -factors as a result of the FR connection modifiers for panel zone strength and clear span-to-depth limitations. Assessment results for the panel zones all remained small compared to unity—see §3.2.2.1.1.1. Figure 3-30(b) and Figure 3-31(b) show that the frame columns are deformation-controlled for flexure.

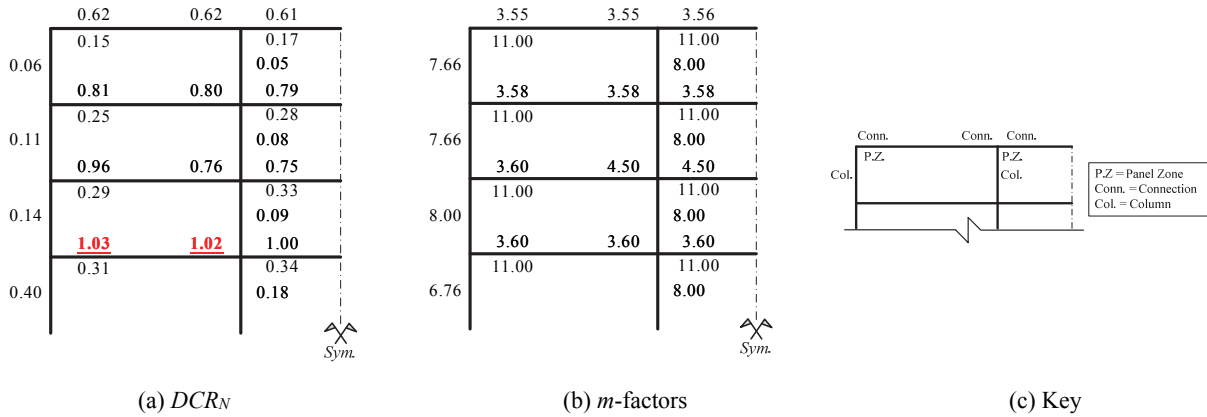


Figure 3-30. LSP Assessment Results, 4-Story SMF ELF, BSE-2 CP

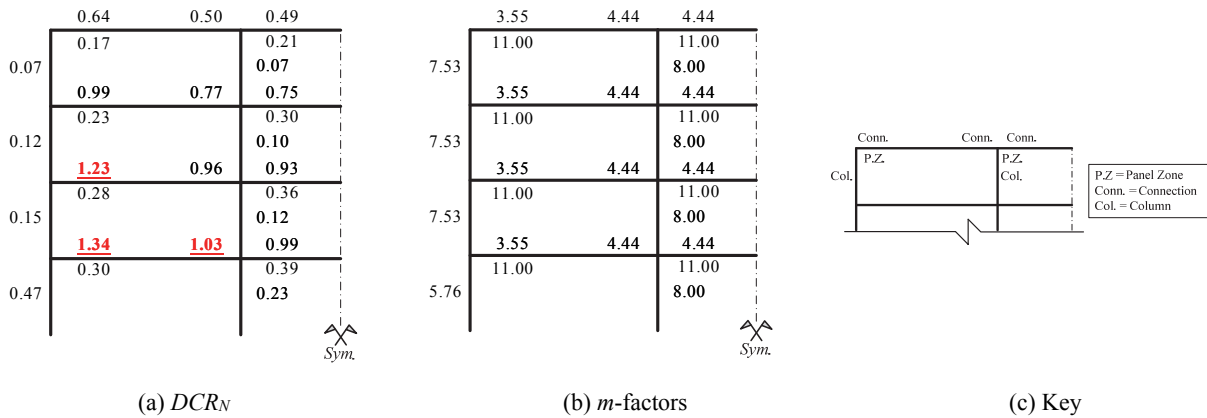


Figure 3-31. LSP Assessment Results, 4-Story SMF RSA, BSE-2 CP

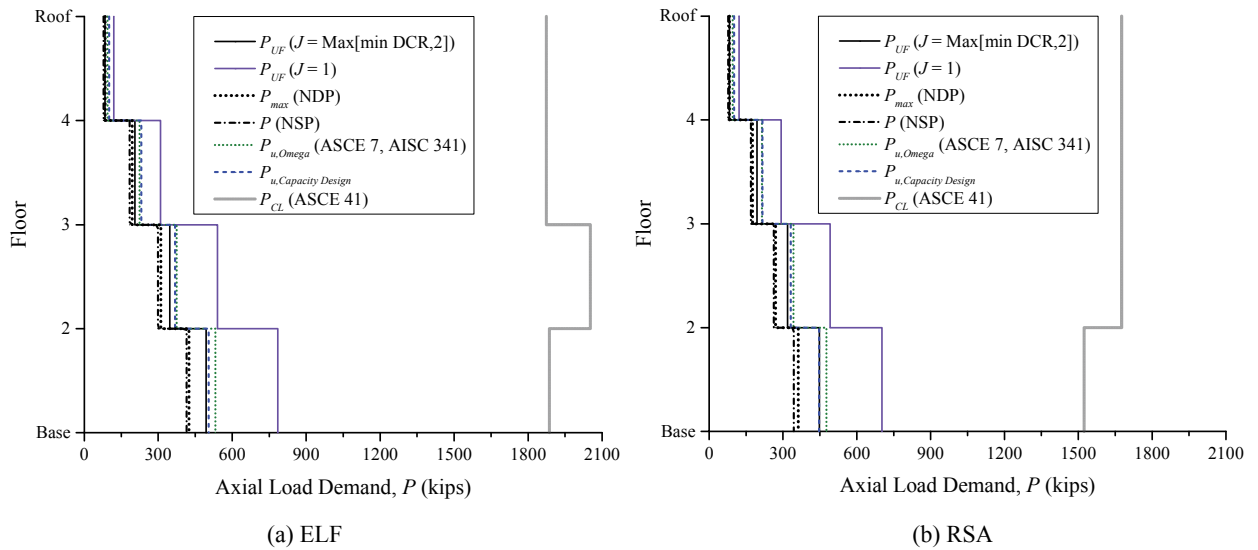


Figure 3-32. LSP Assessment Results, Compression in Exterior Columns, 4-Story SMF, BSE-2

3.2.2.1.2 Linear Dynamic Procedure

3.2.2.1.2.1 BSE-1 Earthquake Hazard Level (LS BPL)

In this section, the following apply:

- Figure 3-33 and Figure 3-34 provide the DCR_N and load-dependent m -factor values for the ELF and RSA designs, respectively, for the LDP at the BSE-1 EHL. In these figures, DCR_N values greater than unity are highlighted in red and underlined. DCR values, as defined by ASCE 41, can be obtained by multiplying DCR_N by m and κ , see Eq. 3-6.
- Figure 3-35 provides the maximum axial compression demands, P_{UF} , in the exterior column lines for various analysis methods and the column capacity, P_{CL} .

All component actions satisfy the LS BPL acceptance criteria. Assessment results for the panel zones all remained small compared to unity—see §3.2.2.1.1.1. Figure 3-33(b) and Figure 3-34(b) show that the frame columns are deformation-controlled for flexure.

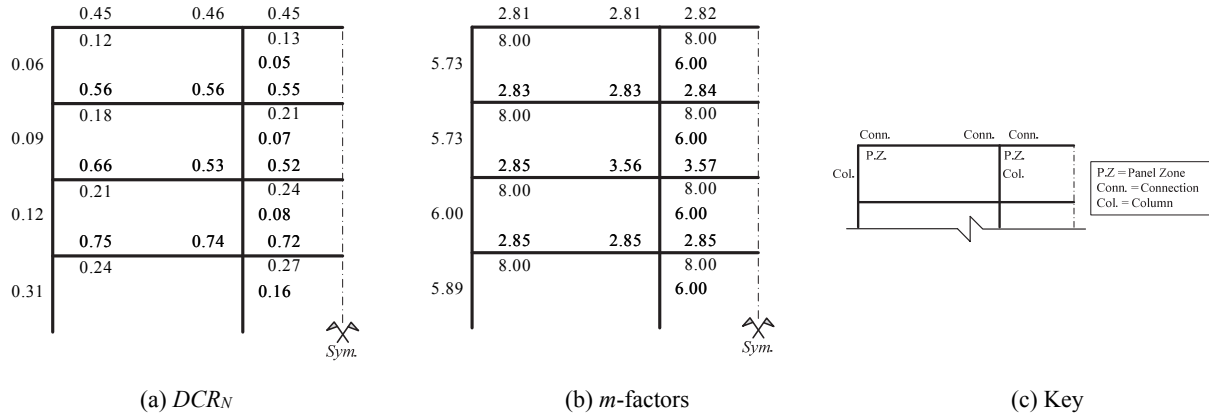


Figure 3-33. LDP Assessment Results, 4-Story SMF ELF, BSE-1 LS

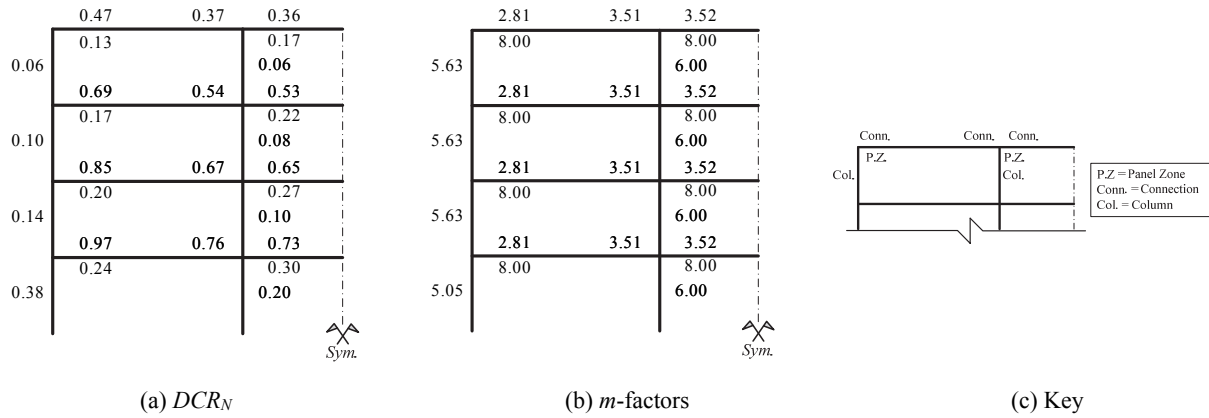


Figure 3-34. LDP Assessment Results, 4-Story SMF RSA, BSE-1 LS

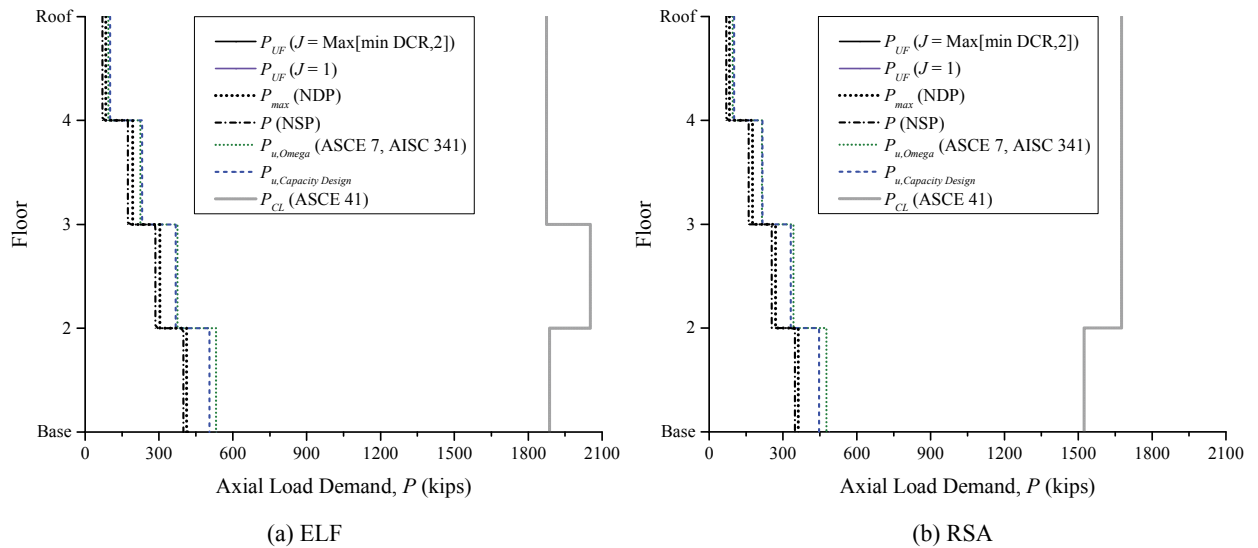


Figure 3-35. LDP Assessment Results, Compression in Exterior Columns, 4-Story SMF, BSE-1

3.2.2.1.2.2 BSE-2 Earthquake Hazard Level (CP BPL)

In this section, the following apply:

- Figure 3-36 and Figure 3-37 provide the DCR_N and load-dependent m -factor values for the ELF and RSA designs, respectively, for the LDP at the BSE-2 EHL. In these figures, DCR_N values greater than unity are highlighted in red and underlined. DCR values, as defined by ASCE 41, can be obtained by multiplying DCR_N by m and κ , see Eq. 3-6.
- Figure 3-38 provides the maximum axial compression demands, P_{UF} , in the exterior column lines for various analysis methods and the column capacity, P_{CL} .

All component actions satisfy the CP BPL acceptance criteria except the exterior beam-to-column connections in the RSA-designed frame on the second floor. As identified previously in §3.2.2.1.1.1, these connection failures are primarily due to reduced m -factors as a result of the FR connection modifiers for panel zone strength and clear span-to-depth limitations. Assessment results for the panel zones all remained small compared to unity—see §3.2.2.1.1.1. Figure 3-36(b) and Figure 3-37(b) show that the frame columns are deformation-controlled for flexure.

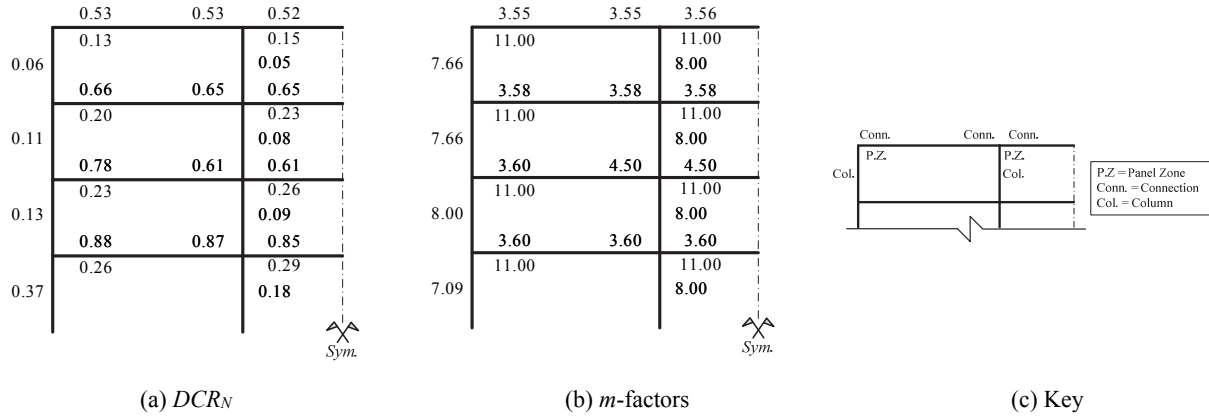


Figure 3-36. LDP Assessment Results, 4-Story SMF ELF, BSE-2 CP

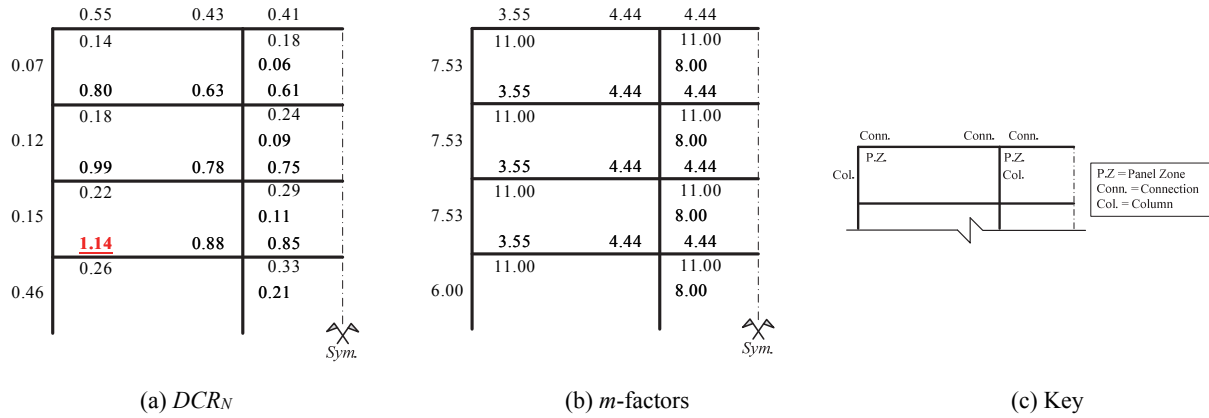


Figure 3-37. LDP Assessment Results, 4-Story SMF RSA, BSE-2 CP

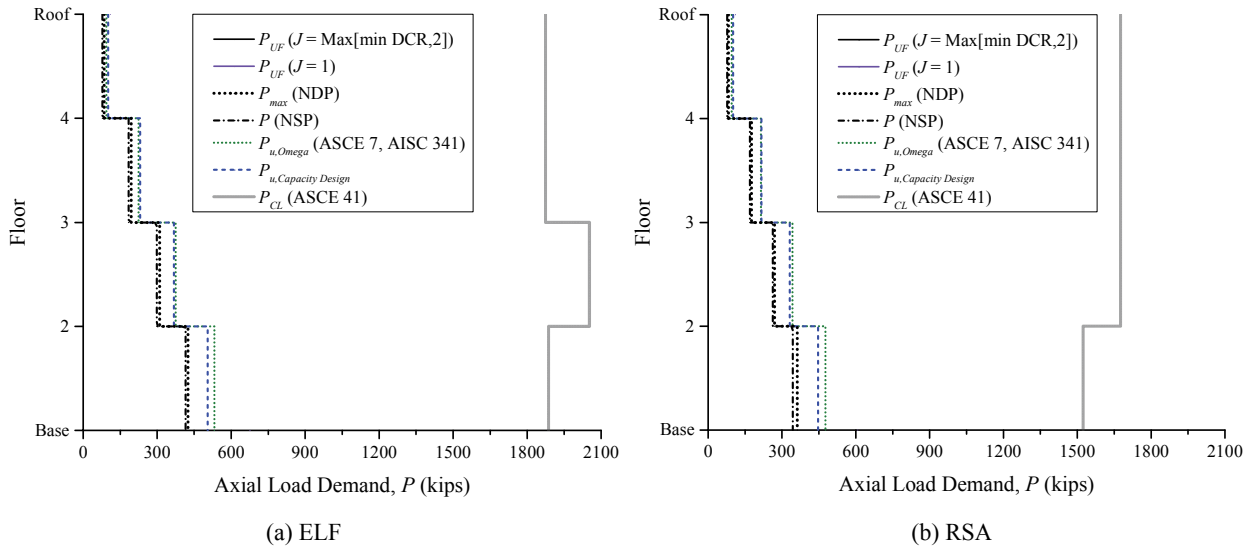


Figure 3-38. LDP Assessment Results, Compression in Exterior Columns, 4-Story SMF, BSE-2

3.2.2.1.3 Nonlinear Static Procedure

In this section, the following apply:

- Table 3-13 through Table 3-15 provide the computed NSP analysis and assessment parameters in accordance with ASCE 41 §3.3.3.
- Figure 3-39 and Figure 3-40 illustrate the monotonic pushover curves for the ELF and RSA-designed frames, respectively, at the BSE-2 EHL. Roof displacement is measured at the Center of Mass (CoM). A significant change in base shear is due to component strength loss (e.g., plastic hinges), notated in the figures. The softening of the pushover curve evident at about 12 inches of roof displacement for each frame is due to column hinges developing at the base of the frames. First-order and second-order responses, shown in these figures, aids in computing a physically meaningful value for $\alpha_{P-\Delta}$ used in ASCE 41 Equation 3-17.
- Figure 3-41 and Figure 3-42 illustrate the story drift ratios in terms of the roof drift ratio.

As discussed in §3.1.3.2.1, the NSP is permitted, but requires supplemental verification using the LDP—see §3.2.2.1.2. In this case, for both BSE-1 and BSE-2, the target displacement governs Δ_d for the ELF frame whereas the displacement at the maximum base shear governs Δ_d for the RSA frame. The change in Δ_d between BSE-1 and BSE-2 adds complexity to NSP process by changing the pushover variables. Axial compression force in the exterior columns at the target displacement are shown previously in the linear assessment sections.

Table 3-13. NSP General Information, 4-Story SMF (kip, inch)

Design	T_l	K_l	Δ_v	V_v	K_e	T_e	h	Δ_{peak}	V_{peak}	W	C_m	C_d
ELF	1.81	101.1	8.9	891	100.6	1.82	1.09	21.9	967.7	5172	1.00	1.28
RSA	2.19	67.6	8.4	570	67.7	2.18	1.12	15.3	637.3	5136	1.00	1.28

Table 3-14. NSP Analysis Parameters, 4-Story SMF BSE-2 CP (kip, inch)

Design	S_a	R	C_1	C_2	Δ_t	V_t	Δ_d	α_1	α_2	$\alpha_{P-\Delta}$	α_e	R_{max}	$R \leq R_{max}$
ELF	0.50	2.90	1.00	1.00	20.6	967.7	20.6	0.06	-0.28	-0.01	-0.06	7.61	OK
RSA	0.43	3.86	1.00	1.00	25.5	579.5	15.3	0.15	-0.20	-0.01	-0.05	9.33	OK

Table 3-15. NSP Analysis Parameters—4-Story SMF BSE-1 LS (kip, inch)

Design	S_a	R	C_1	C_2	Δ_t	V_t	Δ_d	α_1	α_2	$\alpha_{P-\Delta}$	α_e	R_{max}	$R \leq R_{max}$
ELF	0.33	1.93	1.00	1.00	13.8	945.4	13.8	0.11	-0.18	-0.01	-0.04	9.46	OK
RSA	0.29	2.57	1.00	1.00	17.0	636.6	15.3	0.15	-0.20	-0.01	-0.05	9.33	OK

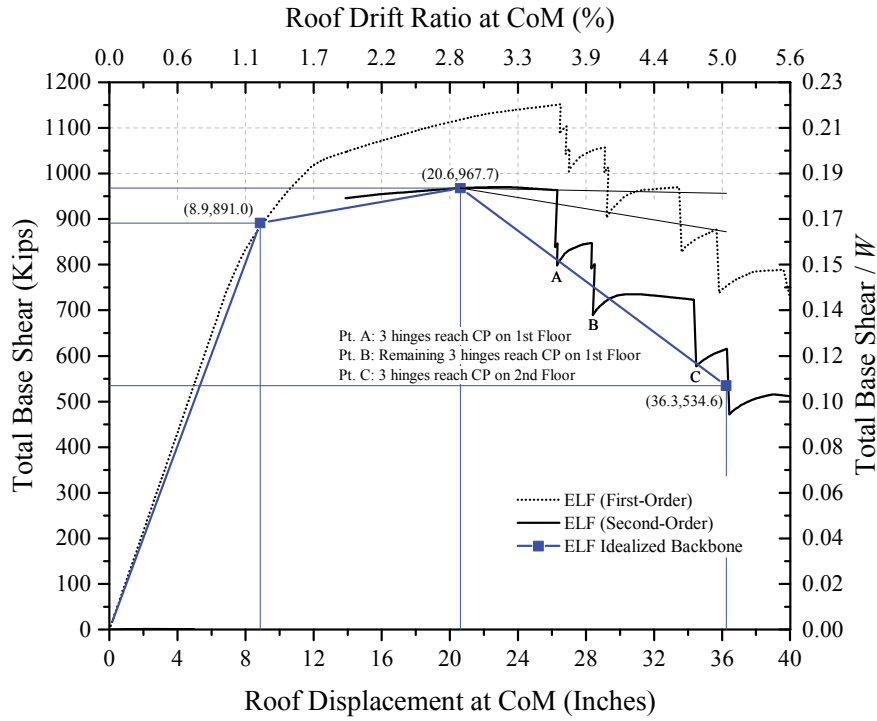


Figure 3-39. 4-Story SMF ELF Pushover, BSE-2

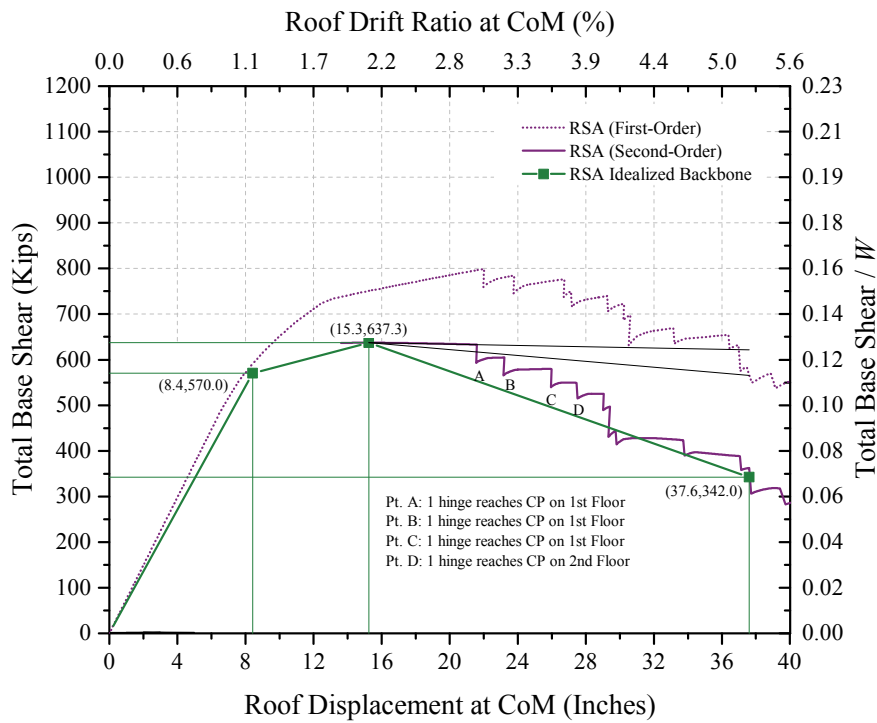


Figure 3-40. 4-Story SMF RSA Pushover, BSE-2

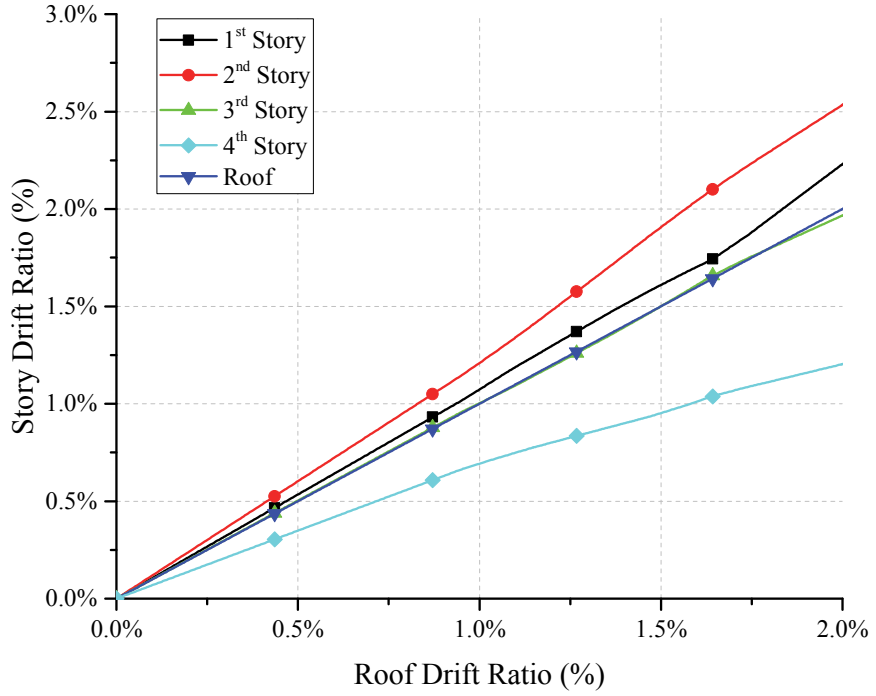


Figure 3-41. 4-Story SMF ELF Pushover – Story Drift Ratios – BSE-2

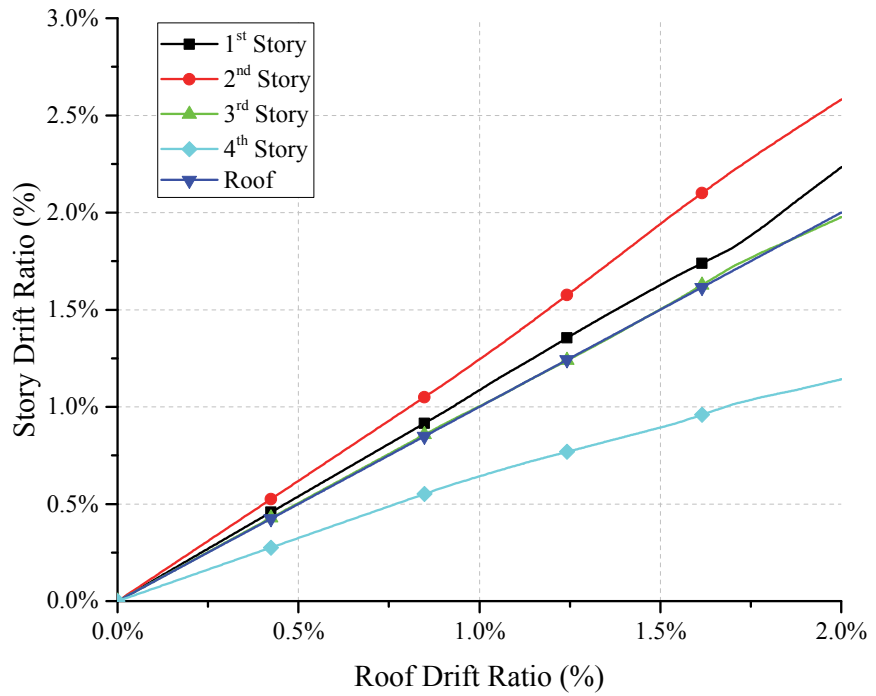


Figure 3-42. 4-Story SMF RSA Pushover – Story Drift Ratios – BSE-2

Of particular interest in the pushover curves is the large disparity between the peak base shears developed in the ELF- and RSA-designed buildings ($RSA / ELF = 637 / 968 = 0.66$), a 34 percent change. At first glance, this is greater than the 15 percent difference in design base shears allowed by ASCE 7. Upon further inspection, it can be reasoned that the primary contribution to this disparity is due to the increase in strength provided to the ELF-designed frame to satisfy drift provisions in ASCE 7 (i.e., 15 percent plus additional strength)—see NSP discussion in the 8-story results for more information.

Figure 3-43 illustrates which frame columns are force-controlled for flexure for both the NSP and NDP; all flexural actions are deformation-controlled in these frames. Figure 3-44 through Figure 3-47 illustrate the DCR_N values if greater than unity for the ELF- and RSA-designed frames at the target displacement for the LS BPL at the BSE-1 EHL and CP BPL at the BSE-2 EHL. These figures illustrate demands when the system is loaded to the right. The only performance concern observed is the exterior beam-to-column connections on the second floor in the RSA-designed frame at the BSE-2. As discussed previously in the linear assessment sections, the acceptance criteria of these components are impacted by the FR connection modifiers.

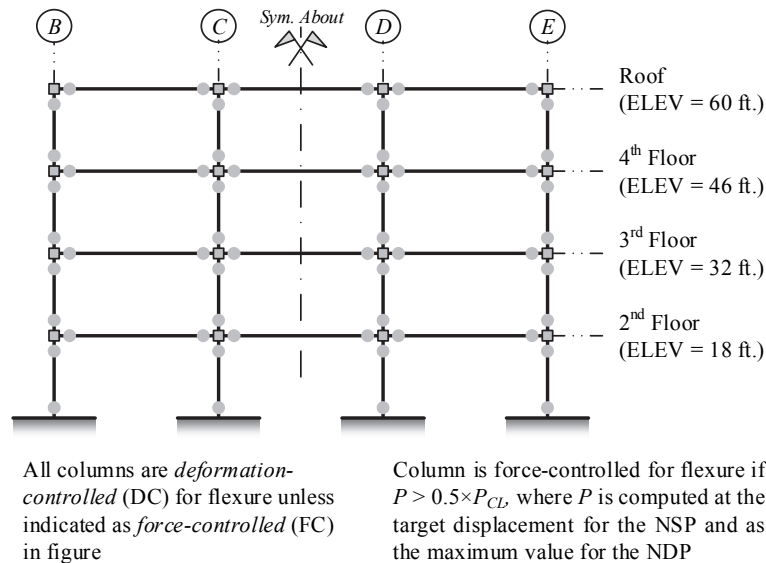


Figure 3-43. Schematic of Flexural Actions in Columns, 4-Story SMF (NSP and NDP)

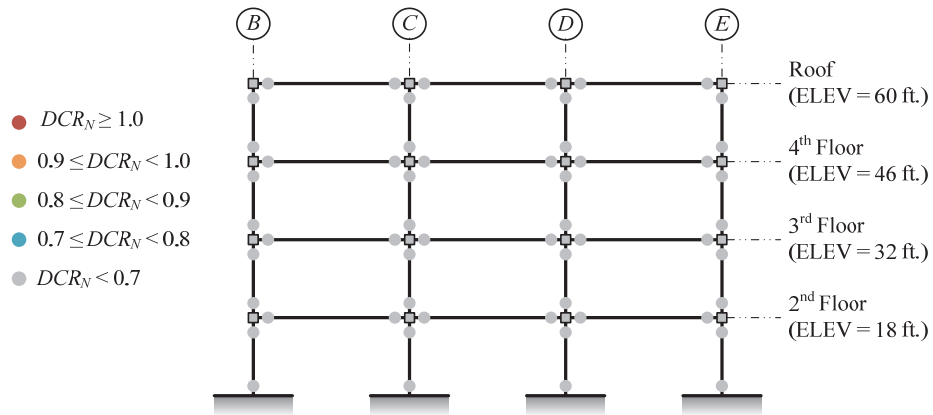


Figure 3-44. NSP Assessment Results, 4-Story SMF ELF, BSE-1 LS (+push to right)

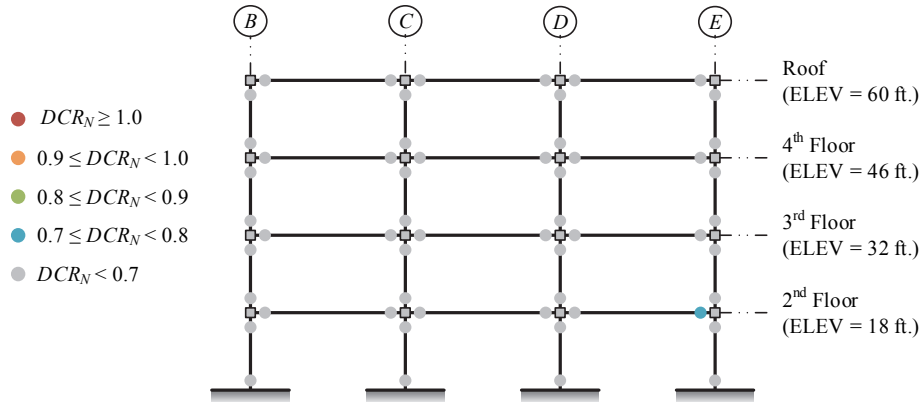


Figure 3-45. NSP Assessment Results, 4-Story SMF RSA, BSE-1 LS (+push to right)

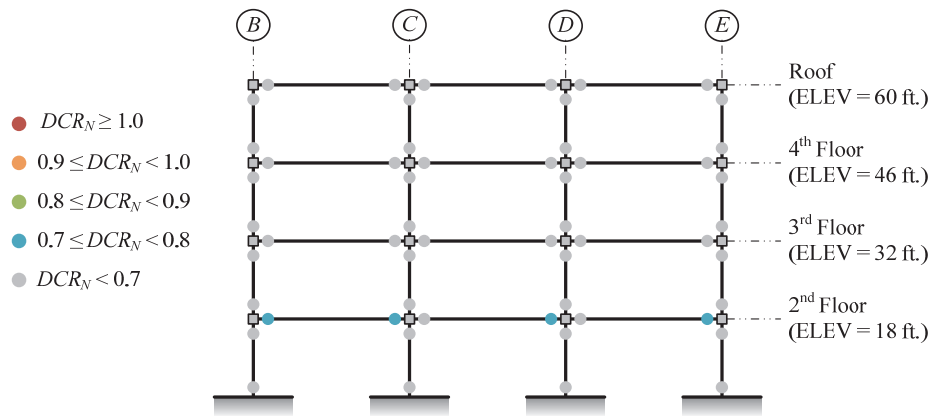


Figure 3-46. NSP Assessment Results, 4-Story SMF ELF, BSE-2 CP (+push to right)

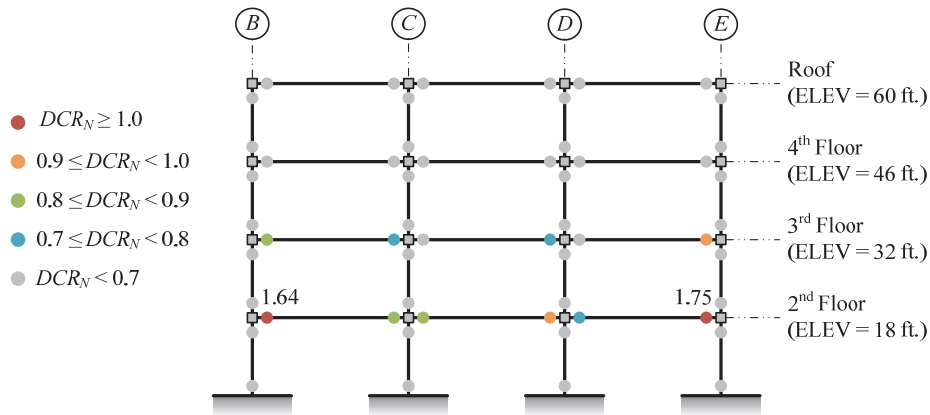


Figure 3-47. NSP Assessment Results, 4-Story SMF RSA, BSE-2 CP (+push to right)

3.2.2.1.4 Nonlinear Dynamic Procedure

The earthquake record set used to assess the E-W direction of MC4 is shown in Appendix A. For the ELF design, the analysis successfully completed for all 14 records at the BSE-1 and BSE-2 EHL. For the RSA design, the analysis successfully completed for all 14 records at the BSE-1 EHL; however, four analyses did not complete at the BSE-2 EHL due to excessive lateral drift. Maximum axial compression force in the exterior column lines from the record set are shown previously in the linear assessment sections.

Figure 3-48 through Figure 3-51 show the performance of the beam hinges (i.e., beam-to-column connections) at the BSE-1 (LS BPL) and BSE-2 (CP BPL) for the ELF- and RSA-designed frames, respectively. The results from the LSP, LDP, and NSP (loaded to the right) are included in the figures. Comparison discussions between the various procedures are addressed subsequently. As is evident from the figures, the ELF-designed frame performs better than the RSA-designed frame. Results for the RSA-designed frame indicate that the exterior beam-to-column connections have difficulty satisfying the CP BPL acceptance criteria at the BSE-2 EHL (primarily based on mean response). In contrast to the mean response, the median response generally indicates better performance because it is less influenced by large deformations resulting from component strength loss potentially resulting in collapse of the system. Consequently, the median is potentially a more stable performance metric when analyzing a large number of ground motion records, but should be restrained relative to a mean value.

The average ratio of secondary to primary component acceptance criteria for an RBS beam-to-column connection for all W18 sections and deeper is 1.49 for the CP SPL (1.47 for the LS SPL). The figures for the RSA-designed frame illustrate that this value is exceeded in the exterior beam-to-column connections at the BSE-2 EHL. This highlights the rapid analytical progression towards a collapsed state when several components are strained past the deformation associated with their peak strength—see §3.1.4.2.

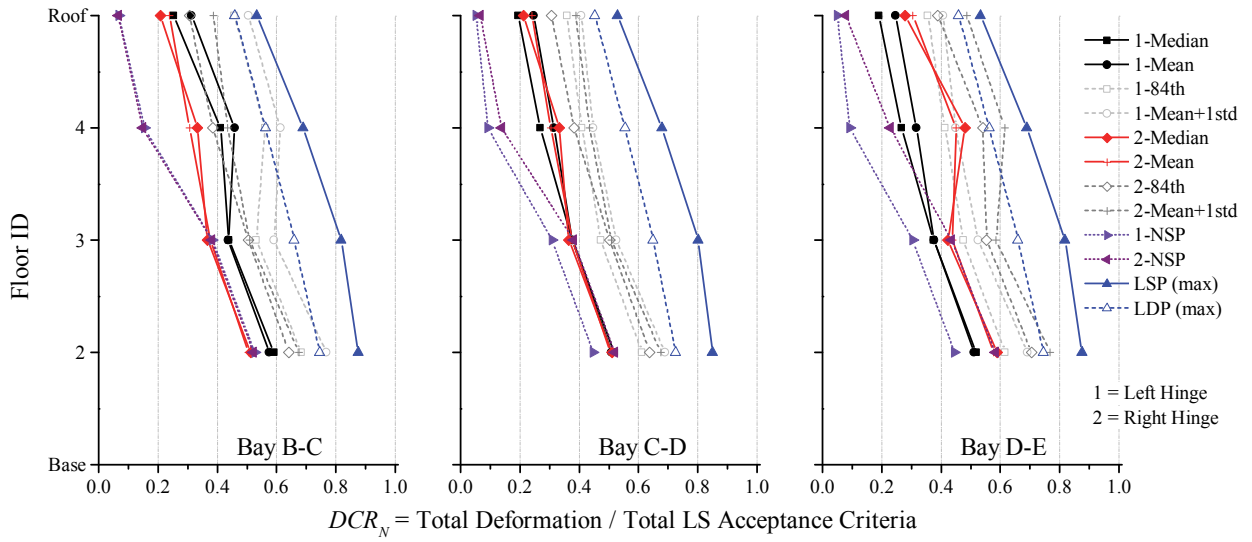


Figure 3-48. NDP Assessment Results, Beam Hinges, 4-Story SMF ELF, BSE-1 LS

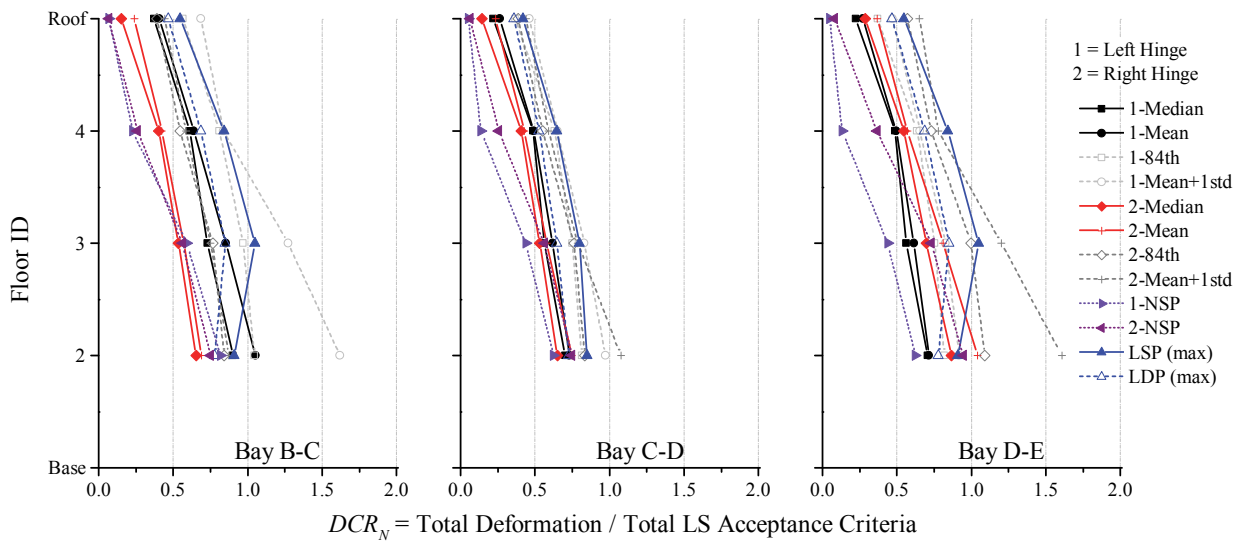


Figure 3-49. NDP Assessment Results, Beam Hinges, 4-Story SMF RSA, BSE-1 LS

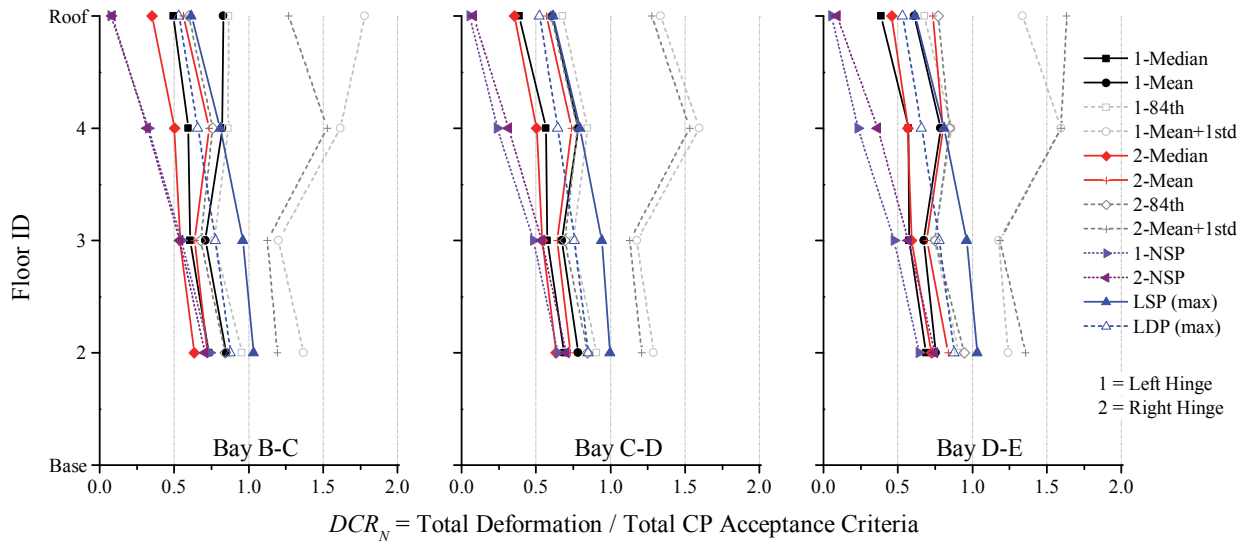


Figure 3-50. NDP Assessment Results, Beam Hinges, 4-Story SMF ELF, BSE-2 CP

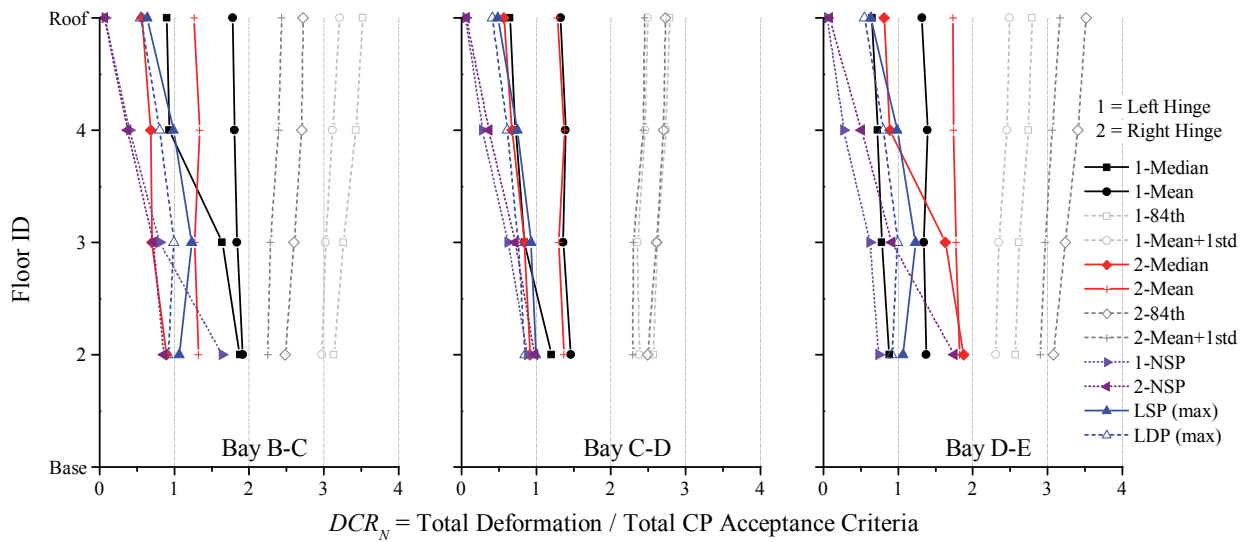


Figure 3-51. NDP Assessment Results, Beam Hinges, 4-Story SMF RSA, BSE-2 CP

The previous figures for the RSA-designed frame illustrate that the component strengths provided by drift control measures in ASCE 7 at $\frac{2}{3} \times MCE_R$ (equal to the BSE-1 here) are not significant enough to overcome the demands to satisfy the assessment criteria at the BSE-2 (taken here as MCE_R). In contrast, the ELF-designed frame satisfies the assessment criteria at the BSE-2. First, strong panel zones reduce the allowable deformations in the acceptance criteria and component model for the exterior beam-to-column connections. Second, the increase in hinge demands in the lower floors is attributed primarily to design choices, as drift is typically not a primary concern in these regions and thus beam strengths seldom get increased

significantly. Also contributing to this increase, to a lesser extent, is the distribution of the design forces from the MRSA. This effect highlights the change in story demands as column base hinges develop, an influence not addressed in elastic design analysis. However, a secondary design analysis to address the effects of “pinned” column bases could be conducted—not done in this study.

Figure 3-43 (see NSP section) illustrates which flexural actions in the frame columns are force-controlled for both the NSP and NDP; all flexural actions are deformation-controlled in these frames. Figure 3-52 and Figure 3-53 show the performance of the column hinges for the CP BPL criteria at the BSE-2 EHL (LS BPL for the BSE-1 is not shown). Column hinges at the base experience inelastic strain demands (yield corresponds to a $DCR_N \approx 0.15$ in the figures). However, the deformation demands are considerably lower than the primary CP acceptance criteria.

The DCR_N results for the LSP and LDP are based on an interaction equation and not from $M_{UD} / m \times M_{CE}$, or M_{UF} / M_{CL} , which would be a more physically consistent metric for comparison against the results from the nonlinear assessment procedures. Nonetheless, the linear results are applicable here because the columns are also deformation-controlled for flexure in the linear assessment procedures. Though there is a fundamental difference in how the DCR_N is computed for the linear and nonlinear procedures, the linear assessment results show similar distributions of demands and location of potential performance concerns.

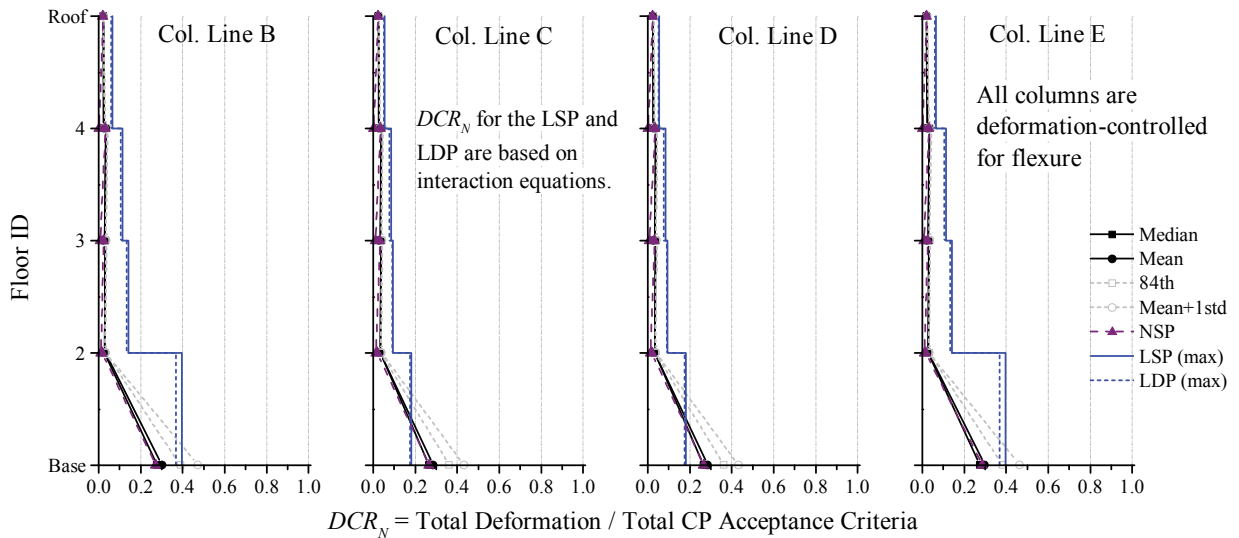


Figure 3-52. NDP Assessment Results, Column Hinges, 4-Story SMF ELF, BSE-2 CP

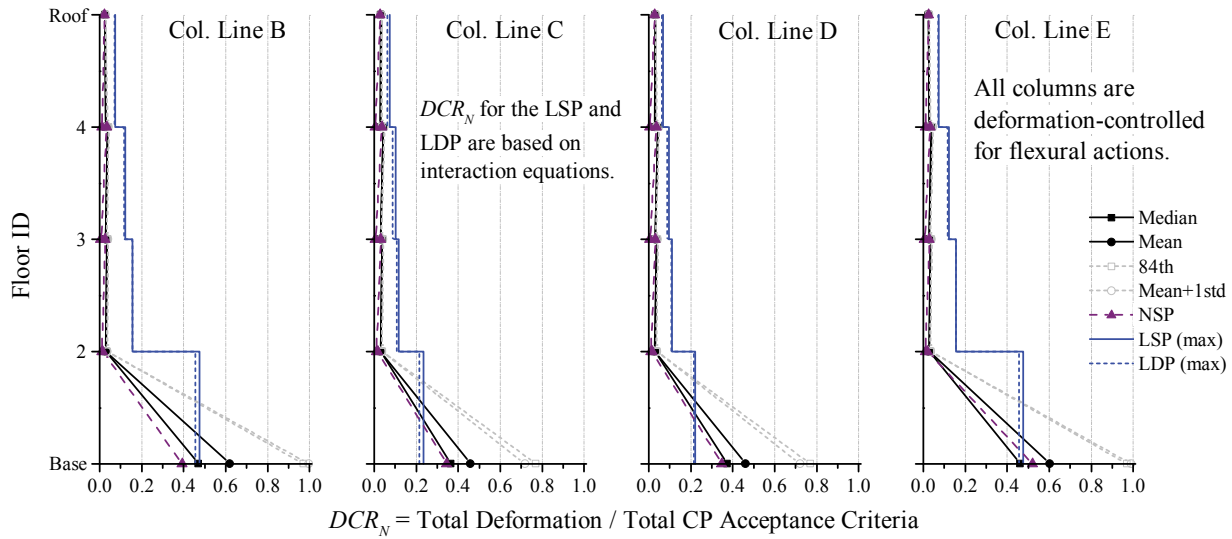


Figure 3-53. NDP Assessment Results, Column Hinges, 4-Story SMF RSA, BSE-2 CP

Figure 3-54 and Figure 3-55 show the curvature ductility demand of the column hinges (i.e., section strength) at the BSE-2 EHL. Figure 3-56 and Figure 3-57 show the elastic member strength interaction results at the BSE-2 EHL. The results indicate that the columns in the ELF- and RSA-designed frames satisfy the intended lower-bound acceptance criteria.

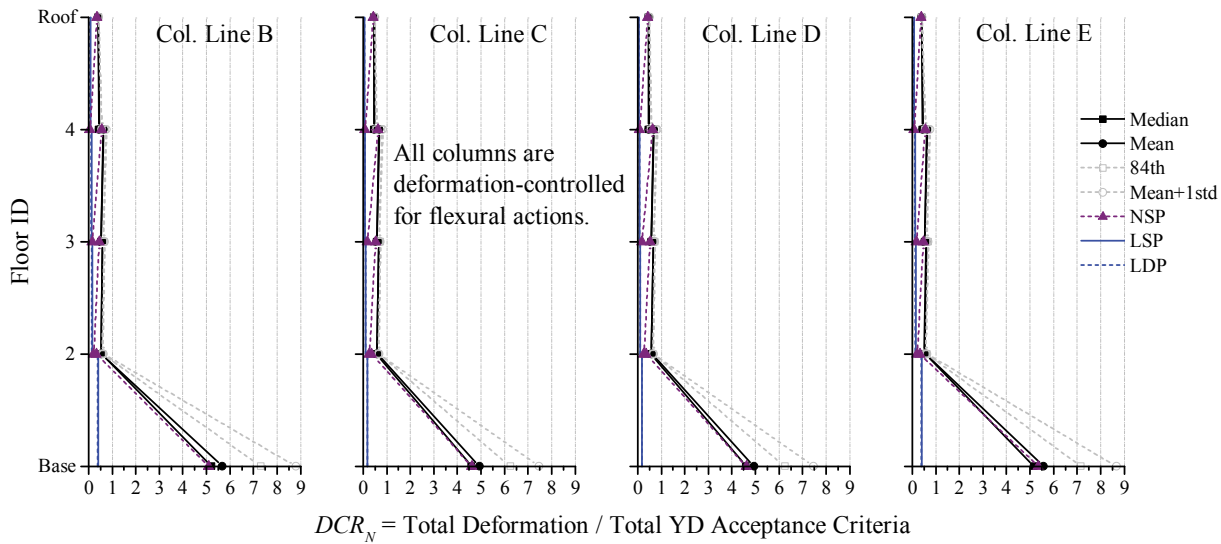


Figure 3-54. NDP Assessment Results, Column Hinges, 4-Story SMF ELF, BSE-2 Yield

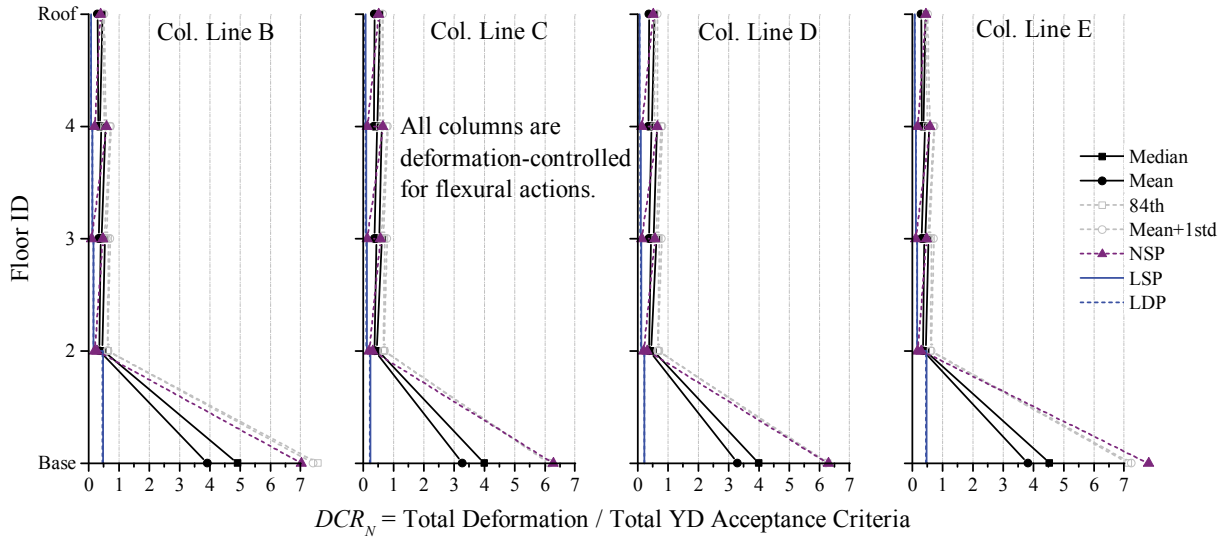


Figure 3-55. NDP Assessment Results, Column Hinges, 4-Story SMF RSA, BSE-2 Yield

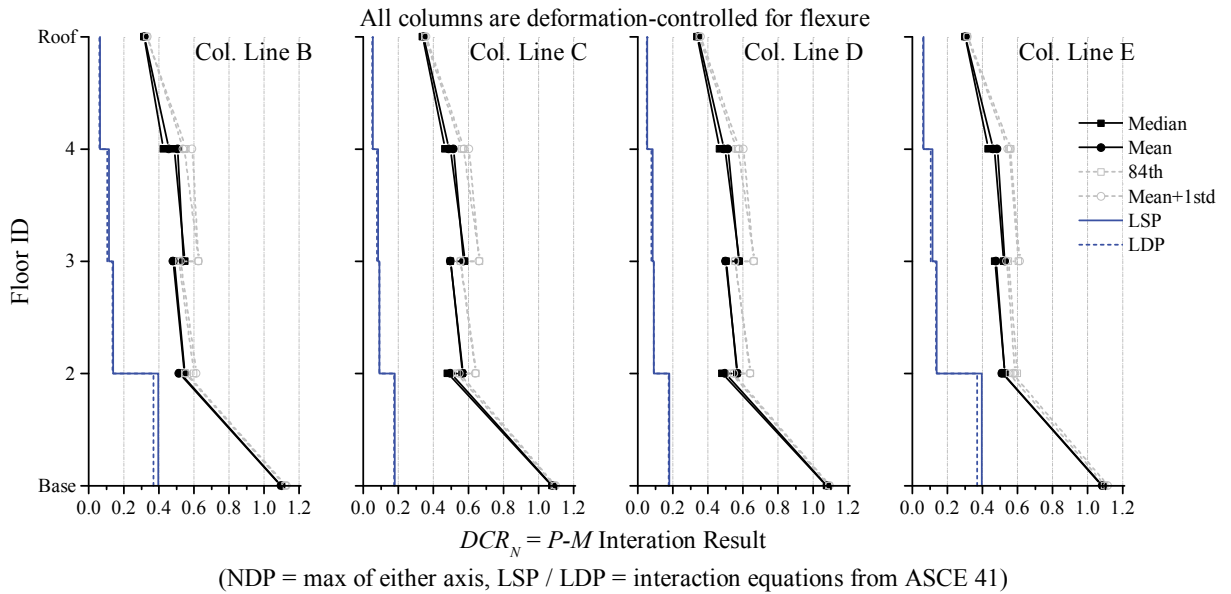


Figure 3-56. NDP Assessment Results, Column Members, 4-Story SMF ELF, BSE-2 CP

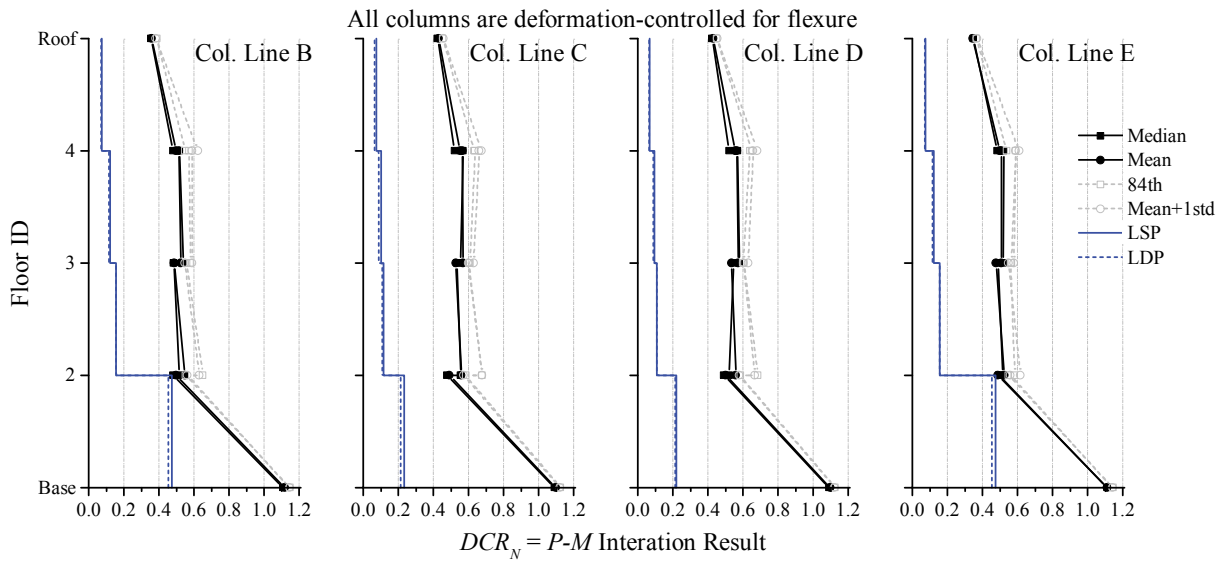


Figure 3-57. NDP Assessment Results, Column Members, 4-Story SMF RSA, BSE-2 CP

Figure 3-58 and Figure 3-59 show the performance of the panel zones for the CP BPL criteria at the BSE-2 EHL (LS BPL for the BSE-1 is not shown). The deformation demands are significantly lower than the CP acceptance criteria. Converting the results to total deformation / yield deformation indicates that the demands for the BSE-2 are consistently less than $4 \times \gamma_y$. These results illustrate that the panel zones are stronger than required by the assessment criteria, which may be the result of designing panel zones for the *probable* connection strength in lieu of the nominal yield strength (i.e., M_y) as recommended in FEMA 350. Also, upsizing column sizes to offset the need for doubler plates increases the shear strength of the panel zones. Future research should investigate alternative design procedures for panel zones as well as the variation in performance if columns sizes were not increased and doubler plates were added. This research would include the variation in the performance of column base hinges or column-to-base connections.

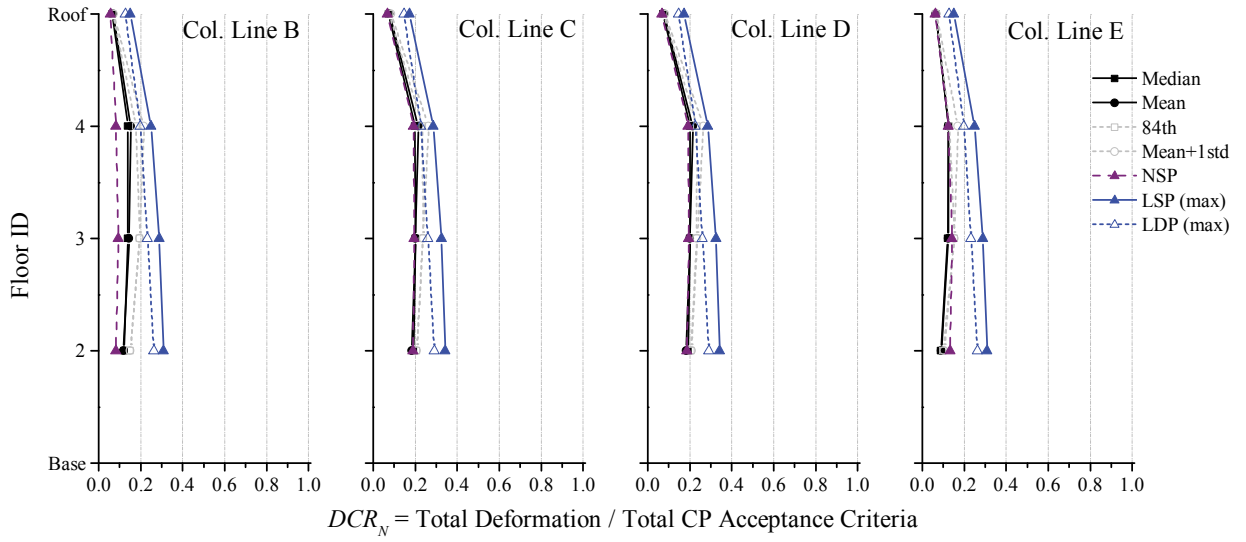


Figure 3-58. NDP Assessment Results, Panel Zones, 4-Story SMF ELF, BSE-2 CP

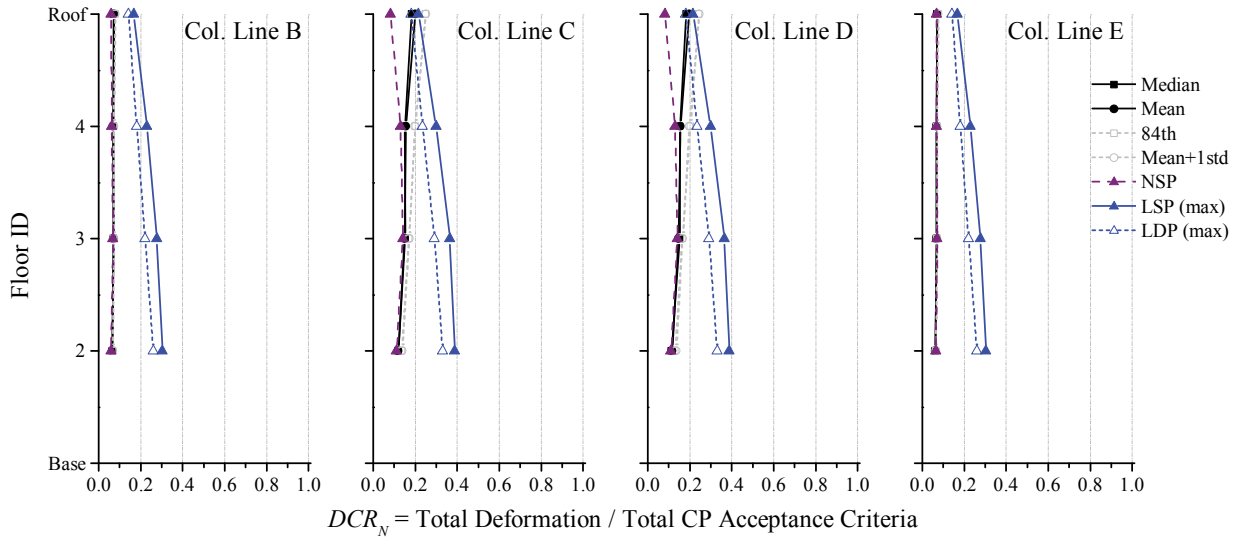


Figure 3-59. NDP Assessment Results, Panel Zones, 4-Story SMF RSA, BSE-2 CP

3.2.2.2 Eight-Story Moment Frame

3.2.2.2.1 Linear Static Procedure

3.2.2.2.1.1 BSE-1 Earthquake Hazard Level (LS BPL)

In this section, the following apply:

- Figure 3-60 and Figure 3-61 provide the DCR_N and load-dependent m -factor values for the ELF and RSA designs, respectively, for the LSP at the BSE-1 EHL. In these figures, DCR_N values greater than unity are highlighted in red and underlined. DCR values, as defined by ASCE 41, can be obtained by multiplying DCR_N by m and κ , see Eq. 3-6.
- Figure 3-62 provides the maximum axial compression demands, P_{UF} , in the exterior column lines for various analysis methods and the column capacity, P_{CL} .

All beam-to-column and panel zone component actions satisfy the LS BPL acceptance criteria except for the exterior beam-to-column connections in the RSA-designed frame on the third through sixth floors. These connection failures are primarily due to reduced m -factors as a result of the FR connection modifiers for panel zone strength and clear span-to-depth limitations. The 20 percent reduction between the interior connections in the RSA-designed frame on the second and third floors in Figure 3-61(b) is due to the change in the average story-height, h , when computing the panel zone demands—see ASCE 41 §5.4.2.4.2-4.2. These figures illustrate that drift and stability control in ASCE 7 provides a significant amount of member overstrength so that beam-to-column connections in the ELF-designed frame easily satisfy the LS BPL acceptance criteria. Assessment results for the panel zones all remained small compared to unity—see §3.2.2.1.1.1.

Several columns do not satisfy the LS BPL acceptance criteria using the interaction equation because they are designated as force-controlled for flexure since P_{UF} exceeds $0.5 \times P_{CL}$. Force-controlled designation can be particularly problematic for base columns where plastic hinges are expected to form. As discussed previously in §3.2.2, P_{UF} is determined by taking J (ASCE 41 §3.4.2.1.2-2) as the minimum DCR of the component(s) delivering force to the column, but not less than 2.0; interior columns are not applicable because P_E is essentially zero. This approach produces the least conservative P_{UF} as compared to AISC 341 SMF column design requirements and the fully yielded system as prescribed in ASCE 41 §3.4.2.1.2-1, as shown in Figure 3-62. It does not seem justified that force-controlled response be triggered by P_{UF} / P_{CL} in lieu of P_{UF} / P_{ye} , more so when P_{CL} is governed by any buckling mode other than in-plane flexural buckling. First, P_{CL} can be controlled by flexural buckling about the weak-axis, which is a failure mode that should be treated separately from the formation of a plastic hinge from in-plane bending. Second, P_{CL} varies based on the length of a member whereas P_{ye} is constant. ASCE 41-13 took the first step in resolving this inconsistency by permitting P_{UF} / P_{CL} to be computed in the plane of bending.

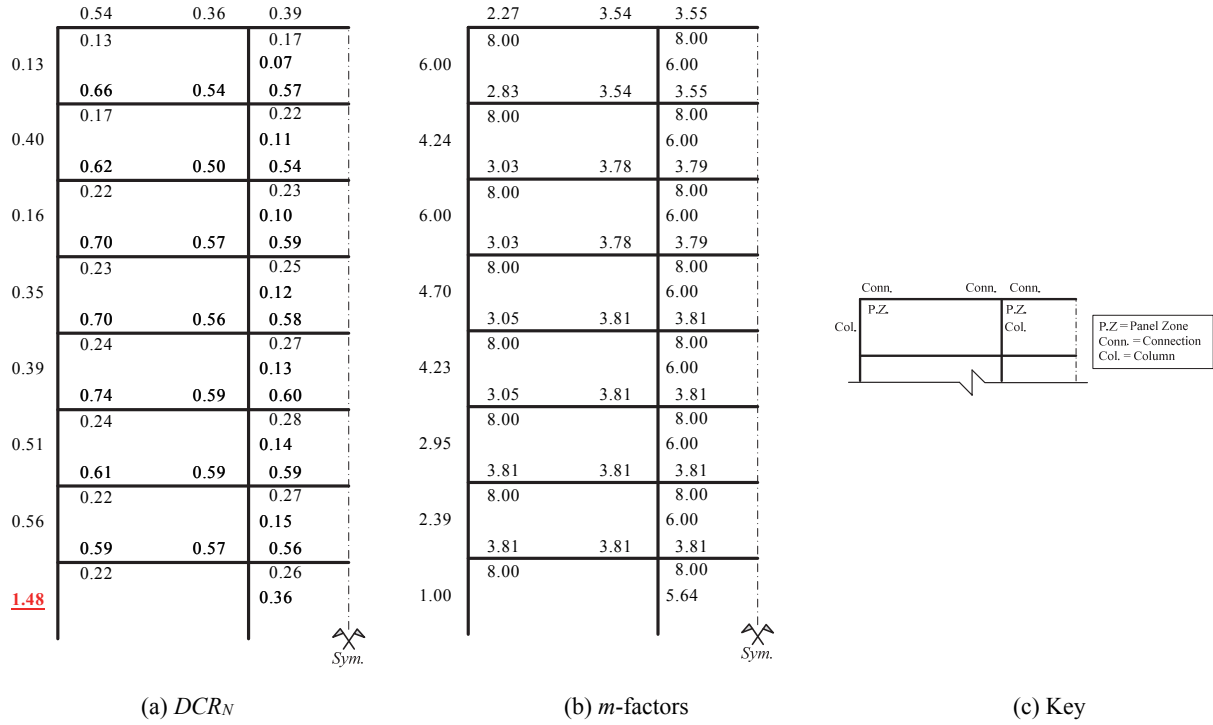


Figure 3-60. LSP Assessment Results, 8-Story SMF ELF, BSE-1 LS

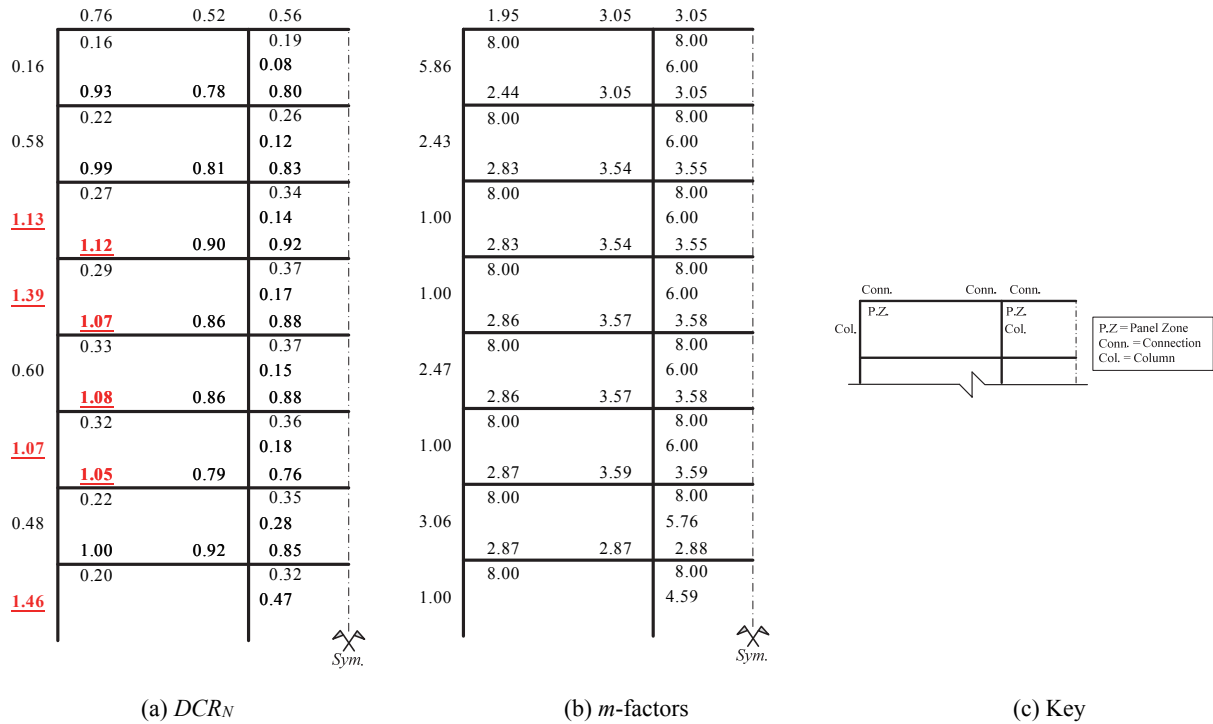


Figure 3-61. LSP Assessment Results, 8-Story SMF RSA, BSE-1 LS

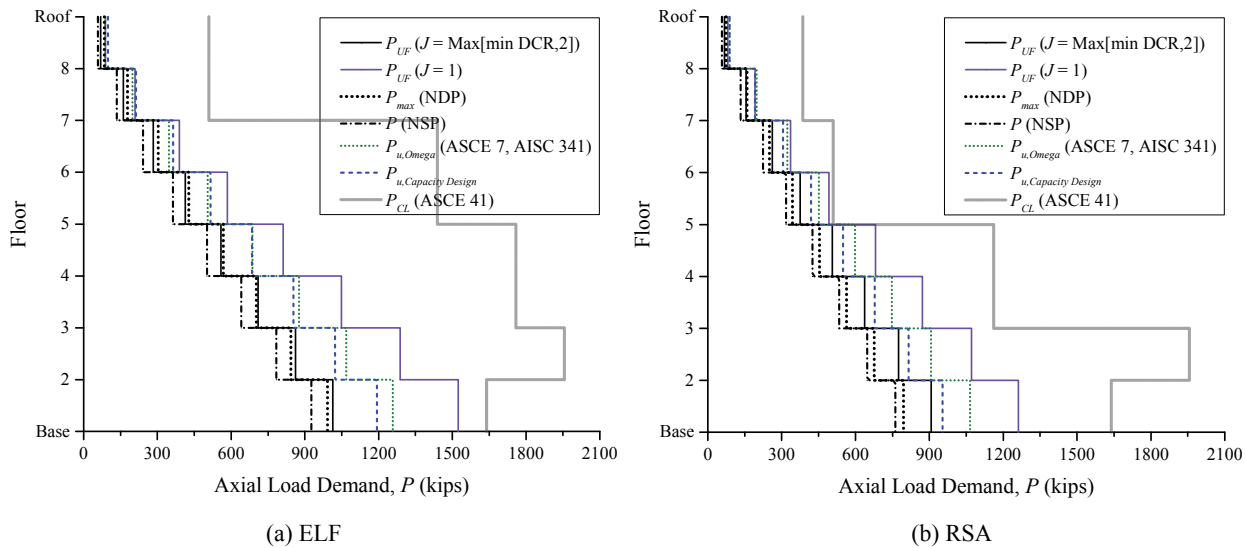


Figure 3-62. LSP Assessment Results, Compression in Exterior Columns, 8-Story SMF, BSE-1

3.2.2.2.1.2 BSE-2 Earthquake Hazard Level (CP BPL)

In this section, the following apply:

- Figure 3-63 and Figure 3-64 provide the DCR_N and load-dependent m -factor values for the ELF and RSA designs, respectively, for the LSP at the BSE-2 EHL. In these figures, DCR_N values greater than unity are highlighted in red and underlined. DCR values, as defined by ASCE 41, can be obtained by multiplying DCR_N by m and κ , see Eq. 3-6.
- Figure 3-65 provides the maximum axial compression demands, P_{UF} , in the exterior column lines for various analysis methods and the column capacity, P_{CL} .

All beam-to-column and panel zone component actions satisfy the CP BPL acceptance criteria except for the beam-to-column connections in the RSA-designed frame on the second through eighth floors. As identified previously, in §3.2.2.2.1 these connection failures are primarily due to reduced m -factors as a result of the FR connection modifiers for panel zone strength and clear span-to-depth limitations. Assessment results for the panel zones all remained small compared to unity—see §3.2.2.1.1.1.

Several columns do not satisfy the CP BPL acceptance criteria using the interaction equation because they are designated as force-controlled for flexure because of P_{UF} exceeding $0.5 \times P_{CL}$ (see previous discussion in §3.2.2.2.1.1). Further, comparing Figure 3-62 and Figure 3-65 illustrates that adopting a constant J factor of 2.0 for both performance levels is inconsistent with the intent of capacity design because of the change in the variation between P_{UF} and $P_{Capacity Design}$ in the figures. Although a column can satisfy the criteria for BSE-1, it may fail the criteria for BSE-2 because of an overly conservative value for P_{UF} . Consequently, J should vary between performance levels for consistency.

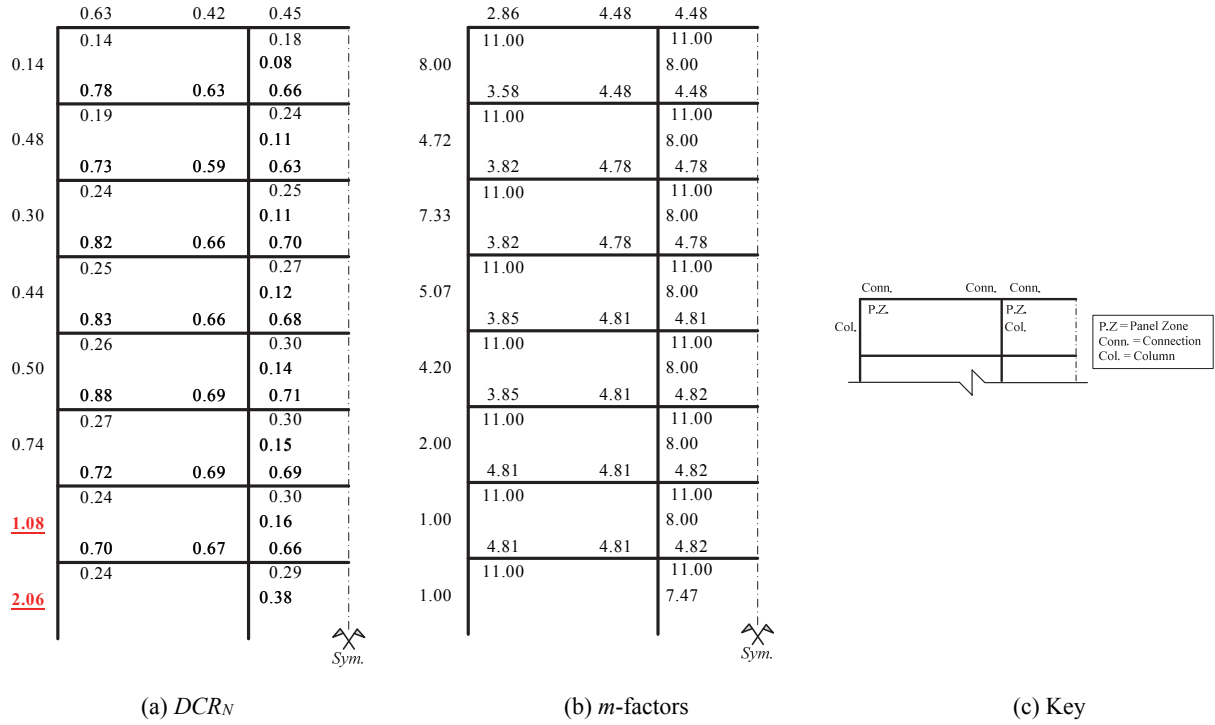


Figure 3-63. LSP Assessment Results, 8-Story SMF ELF, BSE-2 CP

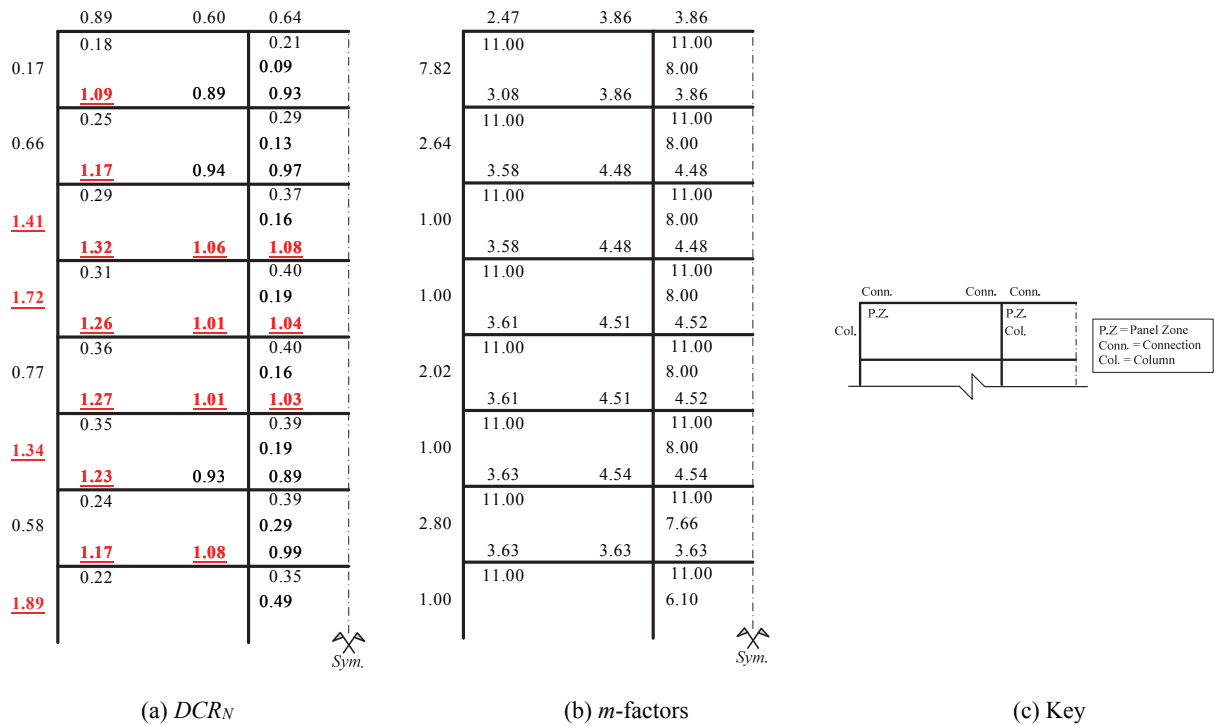


Figure 3-64. LSP Assessment Results, 8-Story SMF RSA, BSE-2 CP

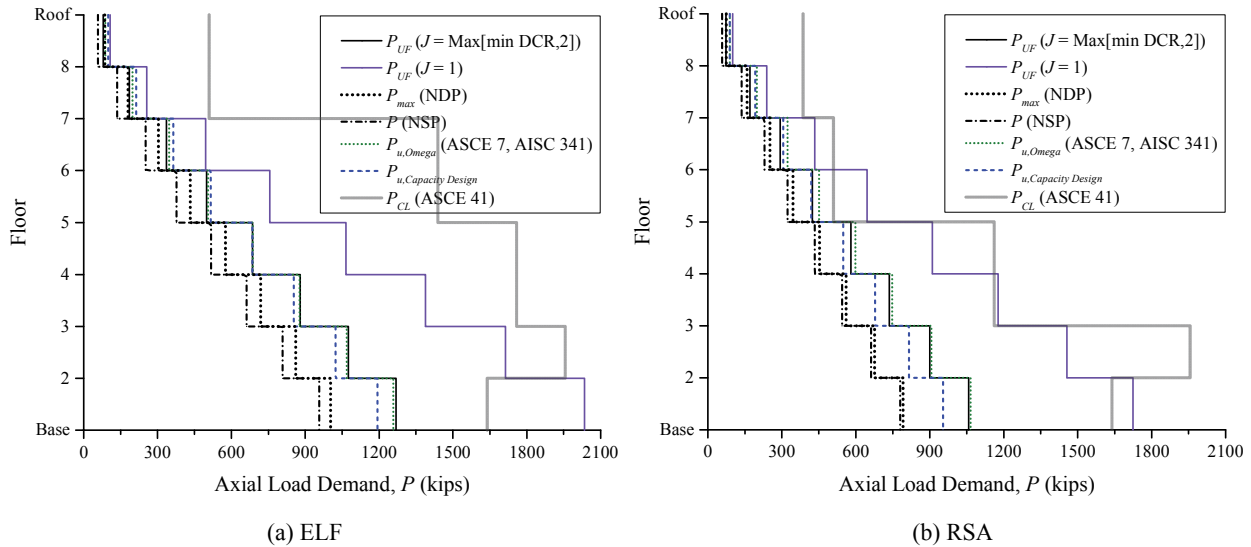


Figure 3-65. LSP Assessment Results, Compression in Exterior Columns, 8-Story SMF, BSE-2

3.2.2.2.2 Linear Dynamic Procedure

3.2.2.2.2.1 BSE-1 Earthquake Hazard Level (LS BPL)

In this section, the following apply:

- Figure 3-66 and Figure 3-67 provide the DCR_N and load-dependent m -factor values for the ELF and RSA designs, respectively, for the LDP at the BSE-1 EHL. In these figures, DCR_N values greater than unity are highlighted in red and underlined. DCR values, as defined by ASCE 41, can be obtained by multiplying DCR_N by m and κ , see Eq. 3-6.
- Figure 3-68 provides the maximum axial compression demands, P_{UF} , in the exterior column lines for various analysis methods and the column capacity, P_{CL} .

All beam-to-column connection and panel zone component actions satisfy the LS BPL for the ELF- and RSA-designed frames. Assessment results for the panel zones all remained small compared to unity—see §3.2.2.1.1.1.

Several columns do not satisfy the LS BPL acceptance criteria using the interaction equation as they are designated as force-controlled for flexure because of P_{UF} exceeding $0.5 \times P_{CL}$ (see previous discussion in §3.2.2.2.1.1).

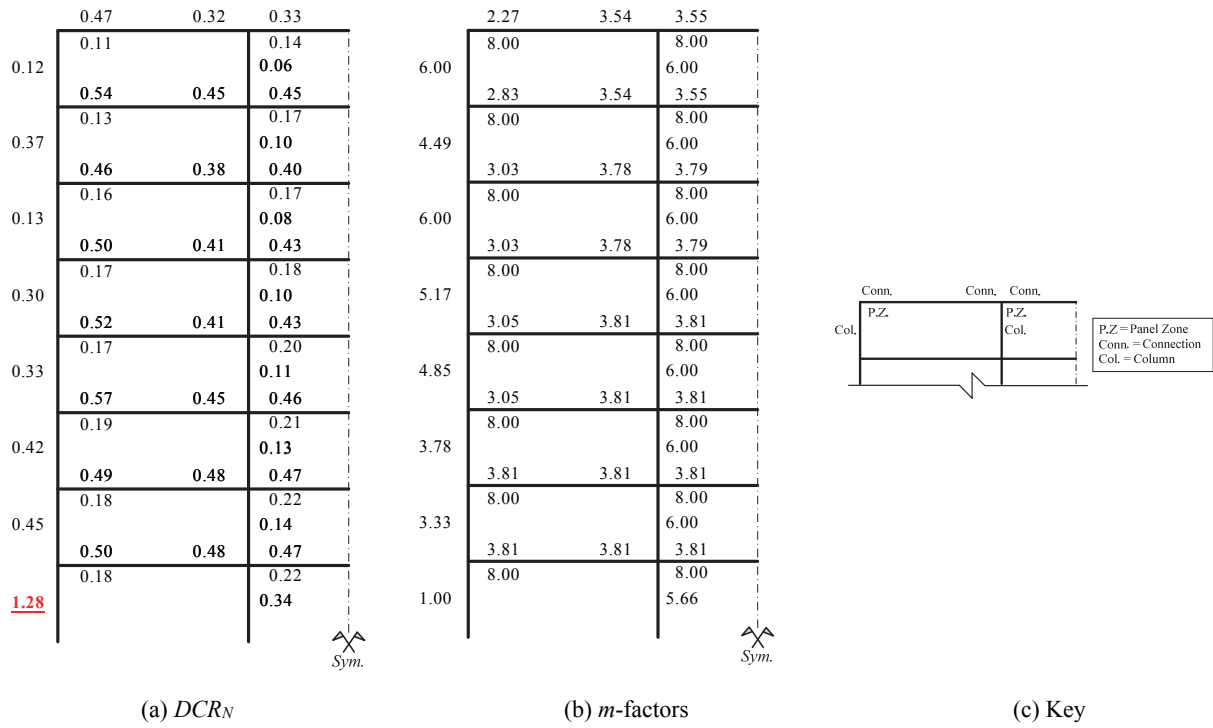


Figure 3-66. LDP Assessment Results, 8-Story SMF ELF, BSE-1 LS

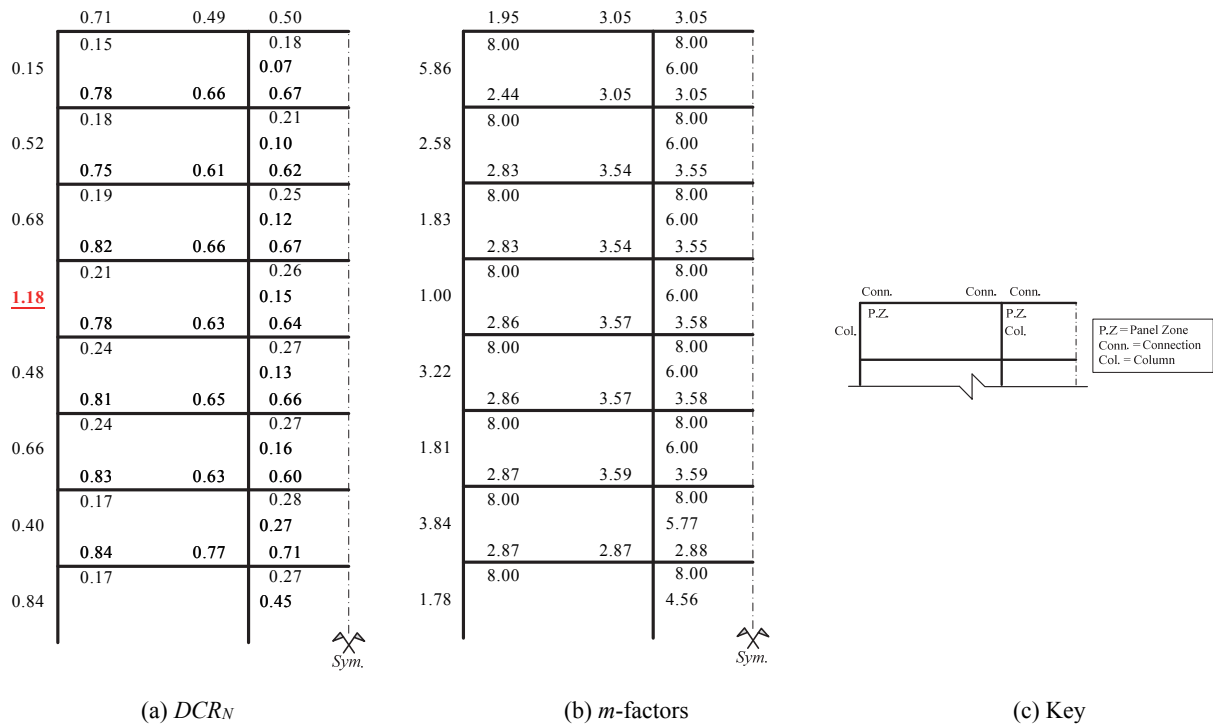


Figure 3-67. LDP Assessment Results, 8-Story SMF RSA, BSE-1 LS

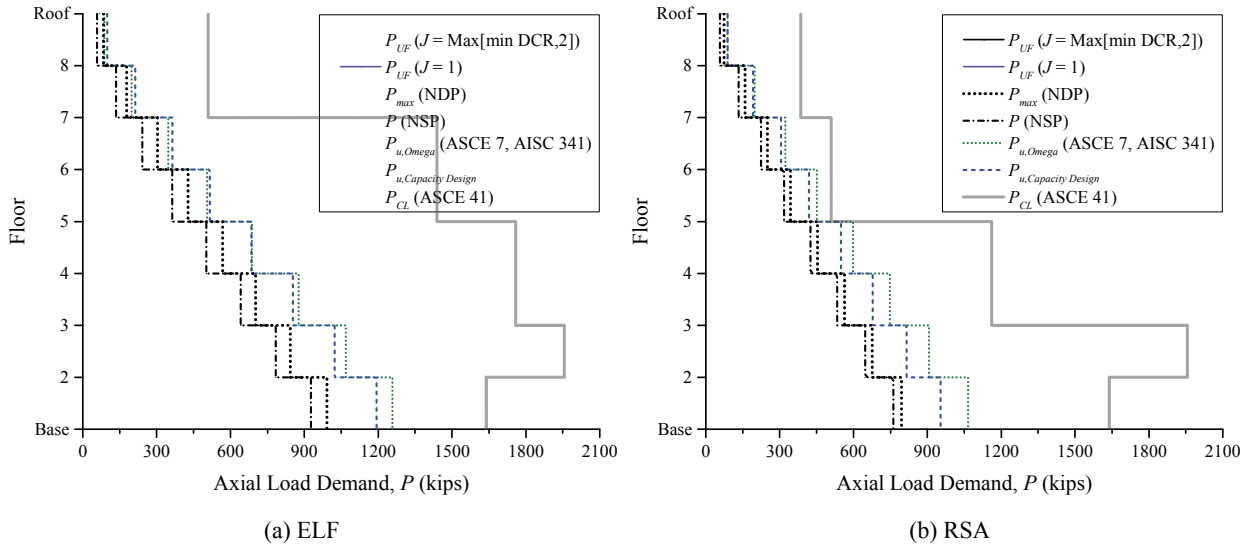


Figure 3-68. LDP Assessment Results, Compression in Exterior Columns, 8-Story SMF, BSE-1

3.2.2.2.2.2 BSE-2 Earthquake Hazard Level (CP BPL)

In this section, the following apply:

- Figure 3-69 and Figure 3-70 provide the DCR_N and load-dependent m -factor values for the ELF and RSA designs, respectively, for the LDP at the BSE-2 EHL. In these figures, DCR_N values greater than unity are highlighted in red and underlined. DCR values, as defined by ASCE 41, can be obtained by multiplying DCR_N by m and κ , see Eq. 3-6.
- Figure 3-71 provides the maximum axial compression demands, P_{UF} , in the exterior column lines for various analysis methods and the column capacity, P_{CL} .

All beam-to-column connection and panel zone component actions satisfy the CP BPL for the ELF- and RSA-designed frames. Assessment results for the panel zones all remained small compared to unity—see §3.2.2.1.1.1.

Several columns do not satisfy the CP BPL acceptance criteria using the interaction equation as they are designated as force-controlled for flexure because of P_{UF} exceeding $0.5 \times P_{CL}$ (see previous discussion in §3.2.2.1.1.1).

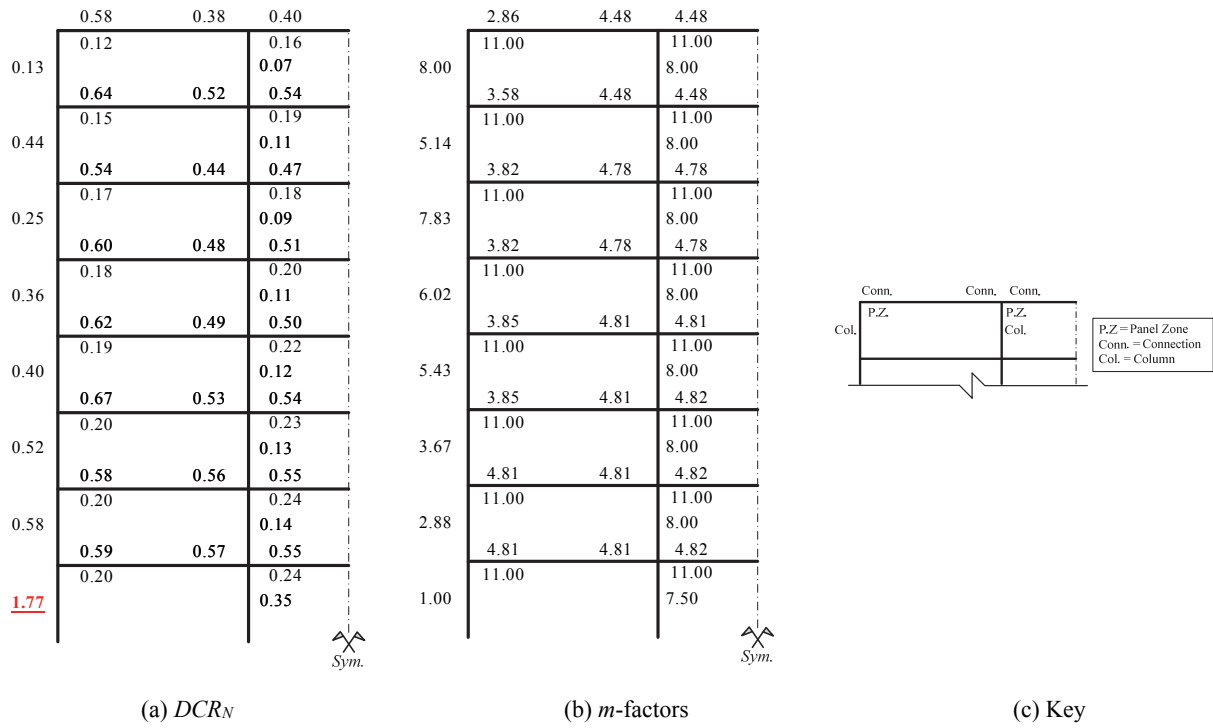


Figure 3-69. LDP Assessment Results, 8-Story SMF ELF, BSE-2 CP

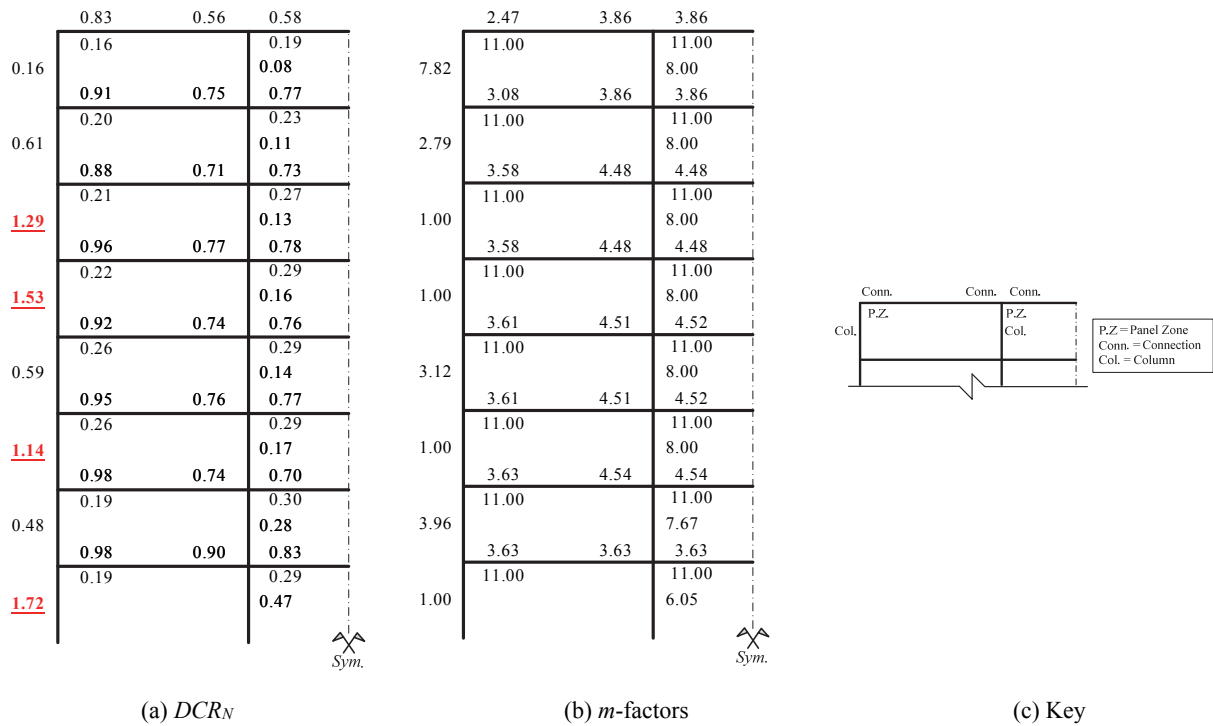


Figure 3-70. LDP Assessment Results, 8-Story SMF RSA, BSE-2 CP

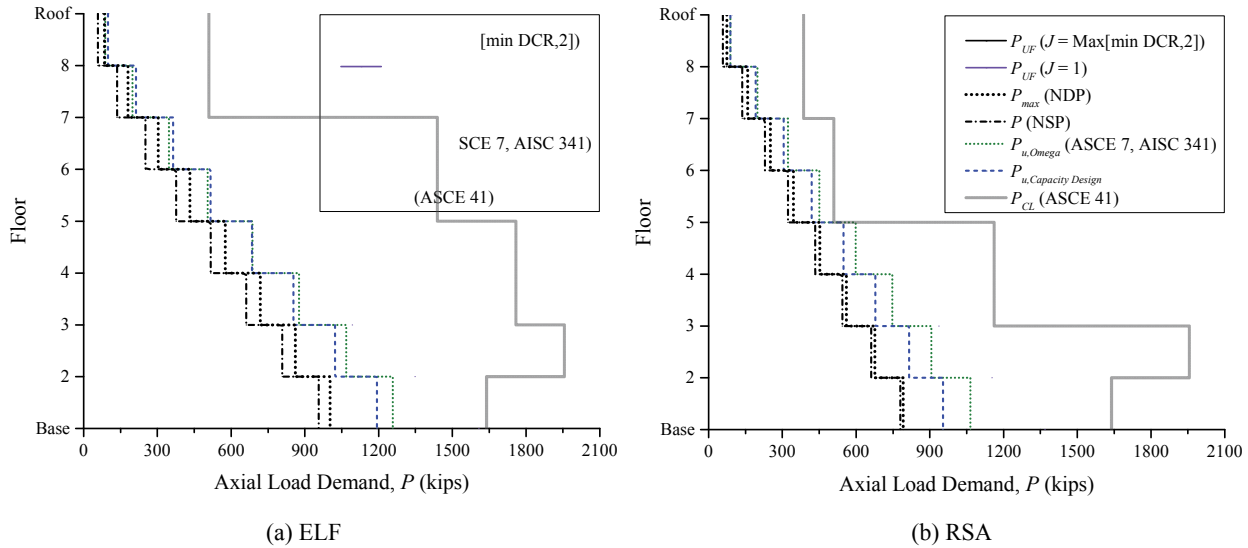


Figure 3-71. LDP Assessment Results, Compression in Exterior Columns, 8-Story SMF, BSE-2

3.2.2.2.3 Nonlinear Static Procedure

In this section, the following apply:

- Table 3-16 through Table 3-18 provide the computed NSP analysis and assessment parameters in accordance with ASCE 41 §3.3.3.
- Figure 3-72 and Figure 3-73 illustrate the monotonic pushover curves for the ELF- and RSA-designed frames, respectively, and the associated pushover parameters from ASCE 41 at the BSE-2 EHL. Roof displacement is measured at the Center of Mass (CoM). A significant change in base shear is due to component strength loss (e.g., plastic hinges), notated in the figures. The softening of the pushover curve evident at about 20 inches of roof displacement for each frame is due to column hinges developing at the base of the frames. First-order and second-order responses, shown in these figures, aids in computing a physically meaningful value for $\alpha_{P-\Delta}$ used in ASCE 41 Equation 3-17.
- Figure 3-74 and Figure 3-75 illustrate the story drift ratios in terms of the roof drift ratio.

As discussed in §3.1.3.2.1, the NSP is permitted, but requires supplemental verification using the LDP—see §3.2.2.2.2. In this case for both the BSE-1 and BSE-2 EHLs, the displacement at the maximum base shear governs Δ_d for both the ELF- and RSA-designed frames. Axial compression force in the exterior columns at the target displacement are shown previously in the linear assessment sections. Results indicate that the NSP generally results in a lower estimate of the axial force demands compared to the other methods used in this study. This is partly because the fundamental mode-based lateral force distribution does not adequately capture higher mode effects. Also, the target displacement at the roof computed based on fundamental mode properties may underestimate the story demands in the upper stories.

Figure 3-72 also includes a curve representing the force-displacement response if the column base hinges did not develop, such as for the case when columns are oversized. In this case, the target displacement

controls Δ_d and $\alpha_{P-\Delta}$ would be zero (or even positive). The second-order curves shown in the figure illustrate the potential sensitivity of NSP results when base column hinges develop in moment frames—including the effect of modeling parameters used for the hinges. Furthermore, the NSP is not permitted for assessment of the E-W direction of MC8 for the RSA-designed frame since $R > R_{max}$ for the BSE-2 EHL—results are provided here only for performance comparison between systems. However, the ratio of R / R_{max} ($= 1.01$) would likely be acceptable in practice.

Table 3-16. NSP General Information, 8-Story SMF (kip, inch)

Design	T_1	K_1	Δ_y	V_y	K_e	T_e	h	Δ_{peak}	V_{peak}	W	C_m	C_D
ELF	2.79	76.9	13.7	1050	76.9	2.79	1.15	19.1	1116.9	10618	1.00	1.32
RSA	3.60	41.5	14.9	623	41.7	3.59	1.19	26.3	664.8	10527	1.00	1.33

Table 3-17. NSP Analysis Parameters, 8-Story SMF BSE-2 CP (kip, inch)

Design	S_d	R	C_1	C_2	Δ_y	V_t	Δ_d	α_1	α_2	$\alpha_{P-\Delta}$	α_e	R_{max}	$R \leq R_{max}$
ELF	0.33	3.37	1.00	1.00	33.5	1092.3	19.1	0.16	-0.25	-0.02	-0.07	6.88	OK
RSA	0.26	4.35	1.00	1.00	43.3	593.2	26.3	0.09	-0.31	-0.10	-0.14	4.31	$R > R_{max}$

Table 3-18. NSP Analysis Parameters—8-Story SMF BSE-1 LS (kip, inch)

Design	S_d	R	C_1	C_2	Δ_y	V_t	Δ_d	α_1	α_2	$\alpha_{P-\Delta}$	α_e	R_{max}	$R \leq R_{max}$
ELF	0.22	2.25	1.00	1.00	22.4	1113.0	19.1	0.16	-0.25	-0.02	-0.07	6.88	OK
RSA	0.17	2.90	1.00	1.00	28.8	660.7	26.3	0.09	-0.31	-0.10	-0.14	4.31	OK

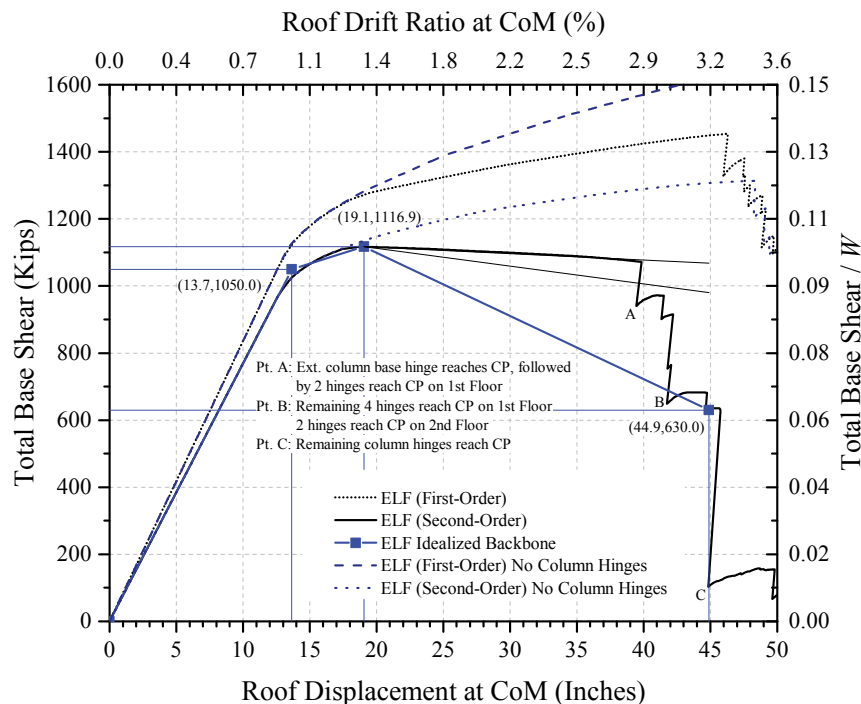


Figure 3-72. 8-Story SMF ELF Pushover, BSE-2

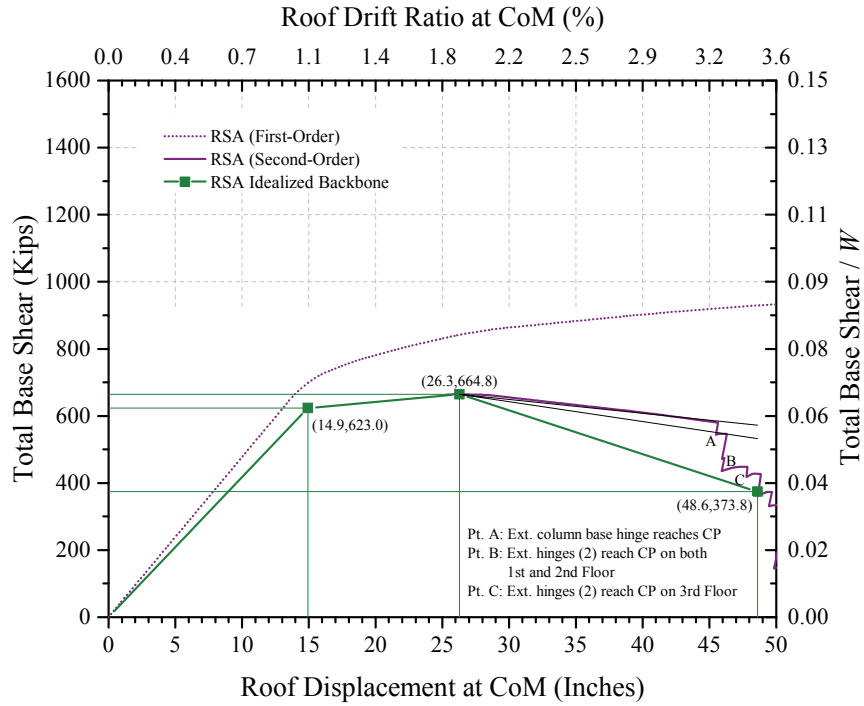


Figure 3-73. 8-Story SMF RSA Pushover, BSE-2

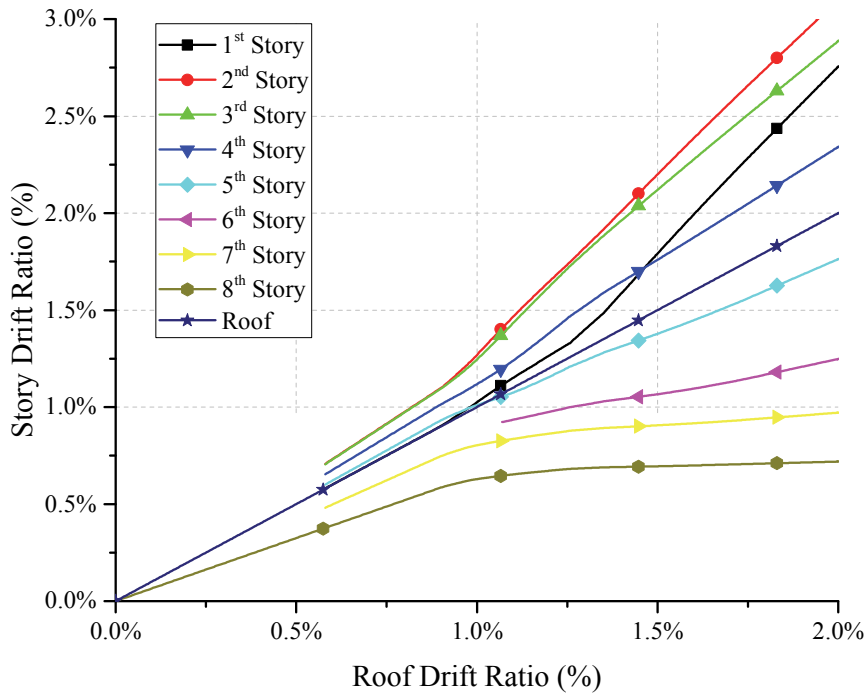


Figure 3-74. 8-Story SMF ELF Pushover – Story Drift Ratios – BSE-2

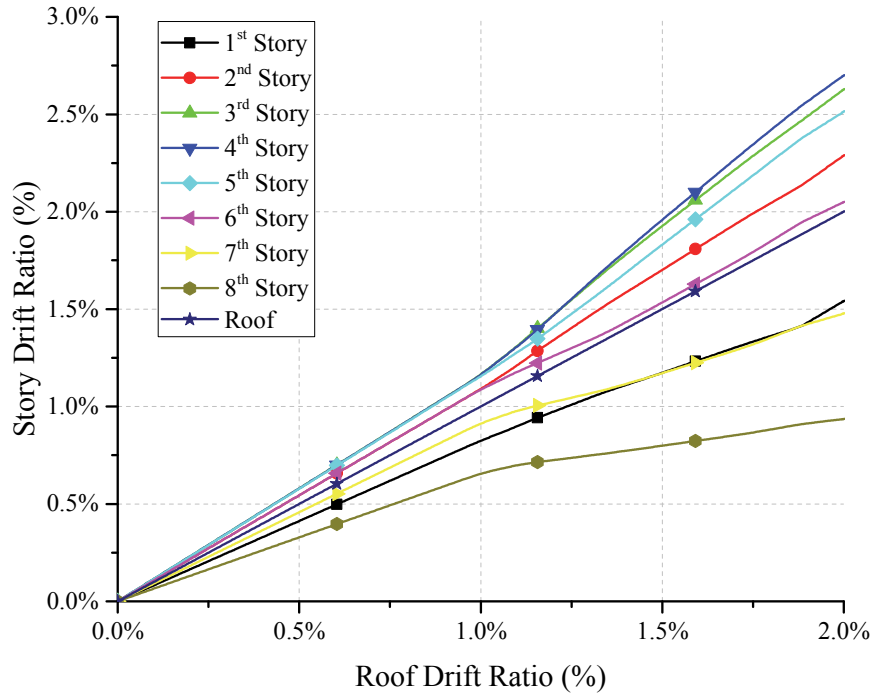


Figure 3-75. 8-Story SMF RSA Pushover – Story Drift Ratios – BSE-2

Of particular interest in the pushover curves is the large disparity between the peak base shears developed in the ELF- and RSA-designed buildings ($RSA / ELF = 665 / 1117 = 0.6$), a 40 percent change. At first glance, this is greater than the 15 percent difference in design base shears allowed by ASCE 7. Upon further inspection, it can be reasoned that the primary contribution to this disparity is due to the increase in strength provided to the ELF-designed frame to satisfy drift provisions in ASCE 7 (i.e., 15 percent plus additional strength). To a lesser extent, the distribution of the lateral forces in the NSP do not coincide with the allocation of the story shear yield strengths (as shown in Figure 3-76 and Figure 3-77), which results in capping the base shear if the initial story mechanism develops above the first story (as is the case for the RSA-designed frame). The oval in these figures illustrates the first floor to develop its defined yield strength, V_y , and the color-code for the expected plastic hinges match that provided in Figure 3-79.

Figure 3-78 illustrates which frame columns are force-controlled for flexure for both the NSP and NDP; red circles indicate anticipated plastic hinge locations that are force-controlled for flexure at the target displacement. As shown in the figure, the force-controlled columns do not align between the two frames—the axial load ratios, P / P_{CL} , for the exterior base columns are 0.58 and 0.48 for the ELF- and RSA-designed frames, respectively (0.26 and 0.64 at the fifth story). This illustrates the sensitivity of results due to variations between the non-adaptive loading profile in the NSP and that used for design. Figure 3-79 through Figure 3-82 illustrate the DCR_N values if greater than unity for the ELF- and RSA-designed frames at the target displacement for the LS BPL at the BSE-1 EHL and CP BPL at the BSE-2 EHL. These figures illustrate the demands when the system is loaded to the right. All component actions for the beam-to-column connections and panel zones satisfy the LS and CP BPL acceptance criteria at the target displacements. However, assuming deformation-controlled flexural actions, the exterior base column hinge for both frames fail the CP BPL primary acceptance criteria. This is a corollary to a column plastic hinge model (section

strength) being a function of P_{CL} (based on member stability) and not P_{ye} (based on section strength), as well as the adopted P - M interaction equation (see previous discussion on nonlinear model). This also indicates that this may be the first hinge to experience significant strength loss ($P / P_{CL} = 0.28$ for gravity loads alone—see summary section for calculations). As it is an exterior base column, this could be detrimental to the performance of the system.

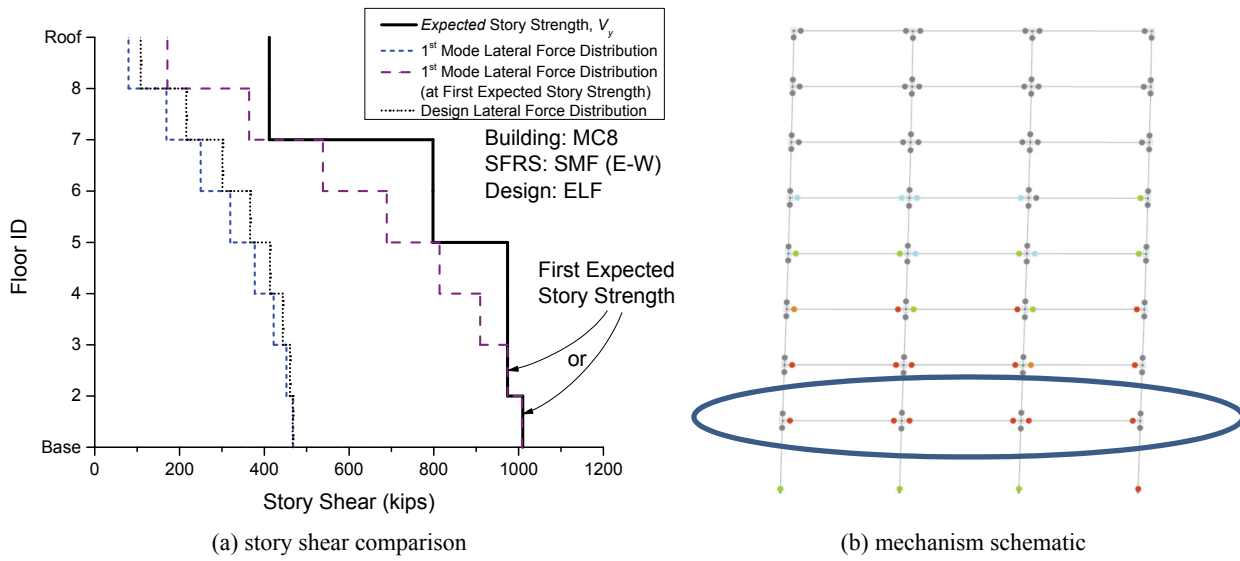


Figure 3-76. Story Shear Demand to Strength Comparison, ELF

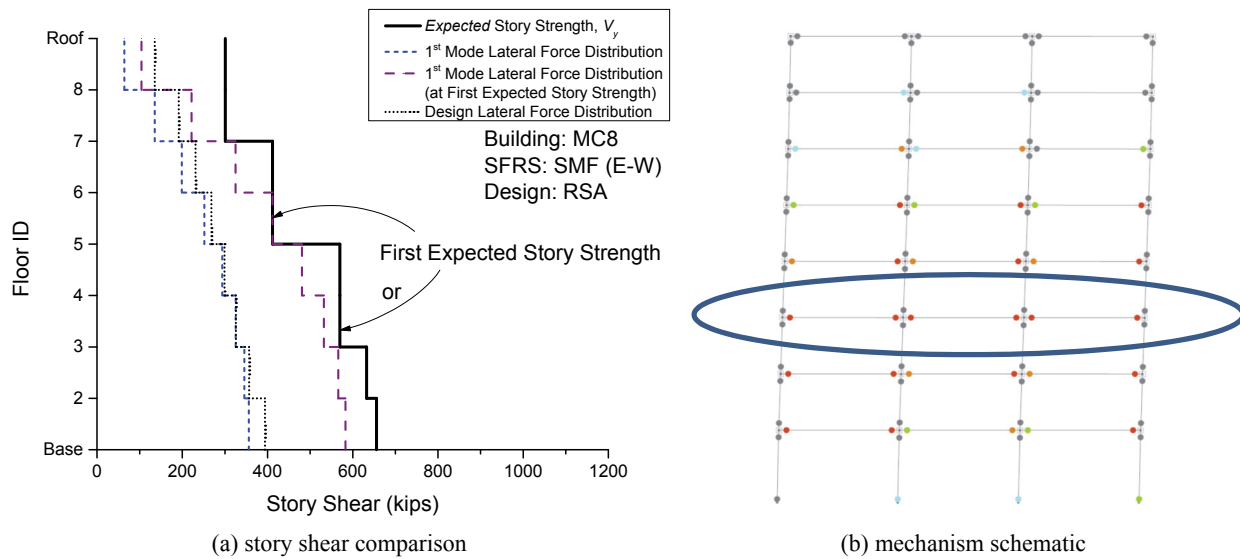


Figure 3-77. Story Shear Demand to Strength Comparison, RSA

Several exterior columns, including those at the base of the ELF-designed frame, are force-controlled for flexure at the target displacements. Force-controlled base columns are problematic for a region that is expected to experience inelastic strain demands. Therefore, the acceptance criterion for these flexural actions is based on the force-controlled lower-bound elastic P - M interaction (ASCE 41 Equation 5-12). As discussed previously, variations in P - M interaction curves add complexity to nonlinear flexural hinge model. Essentially, a nonlinear hinge based on the expected yield surface of the section must be accompanied by another model that can measure the lower-bound strength of the member (one for each axis of buckling). For simplicity, failing of the acceptance criteria (without computing interaction values) is self-evident because of the development of plastic hinges in the frame columns. Because plastic hinges have developed in the base columns in the ELF-design frame, flexural actions therefore do not satisfy the intended elastic acceptance criteria. Conversely, the force-controlled columns in the RSA frame satisfy the intended elastic acceptance criteria—member stability would still need to be verified.

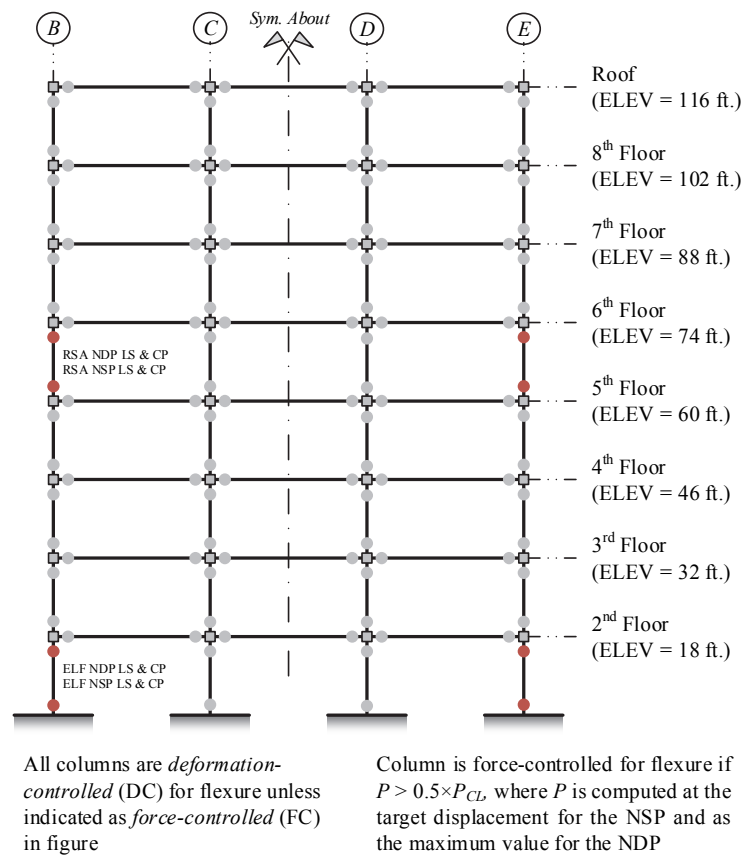


Figure 3-78. Schematic of Flexural Actions in Columns, 8-Story SMF (NSP and NDP)

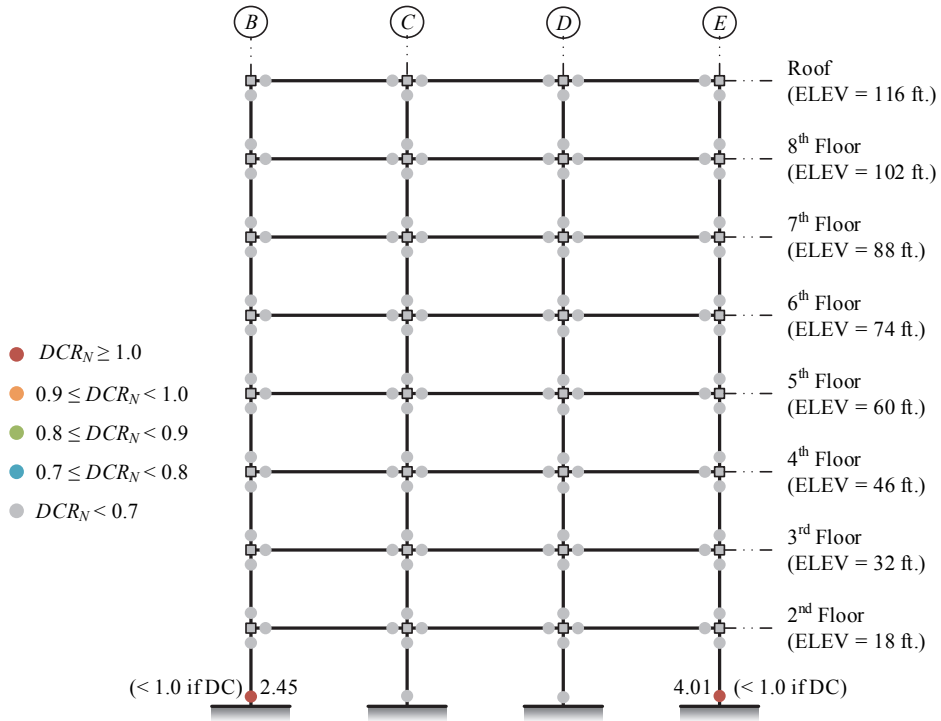


Figure 3-79. NSP Assessment Results, 8-Story SMF ELF, BSE-1 LS (+push to right)

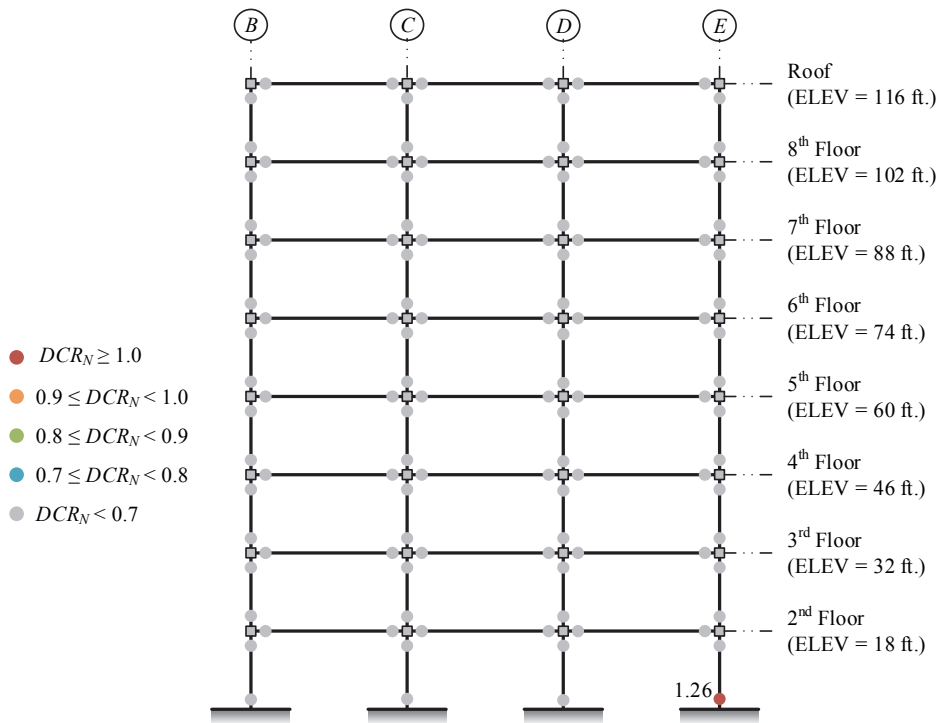


Figure 3-80. NSP Assessment Results, 8-Story SMF RSA, BSE-1 LS (+push to right)

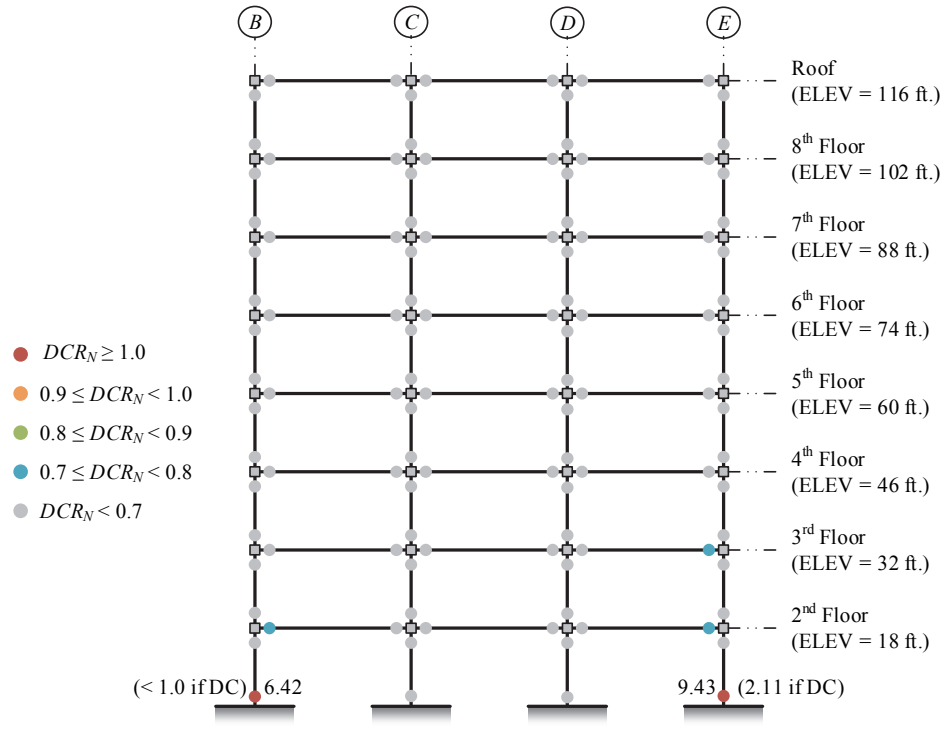


Figure 3-81. NSP Assessment Results, 8-Story SMF ELF, BSE-2 CP (+push to right)

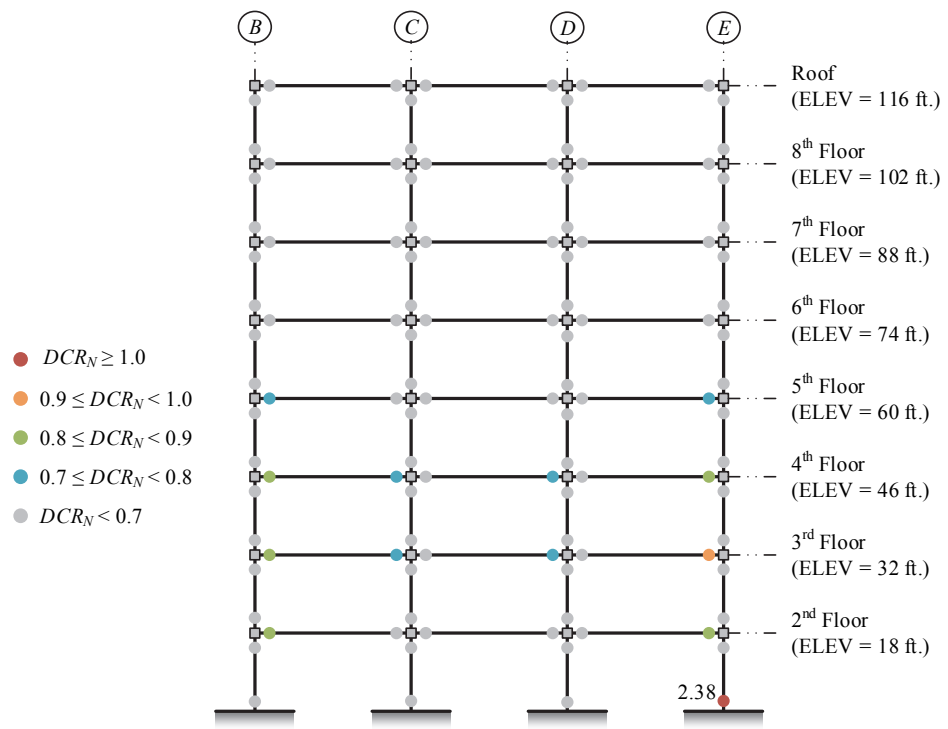


Figure 3-82. NSP Assessment Results, 8-Story SMF RSA, BSE-2 CP (+push to right)

3.2.2.2.4 Nonlinear Dynamic Procedure

The earthquake record set used to assess the E-W direction of MC8 is shown in Appendix A. For the ELF design, the analysis successfully completed for all 14 records at the BSE-1 EHL; however, three analyses did not complete at the BSE-2 EHL because of excessive lateral drift or solution non-convergence. For the RSA design, the analysis successfully completed for 12 records at the BSE-1 EHL; however, nine analyses did not complete at the BSE-2 EHL because of excessive lateral drift or solution non-convergence. Maximum axial compression force in the exterior column lines from the record set are shown previously in the linear assessment sections.

Figure 3-83 through Figure 3-86 show the performance of the beam hinges (i.e., beam-to-column connections) at the BSE-1 (LS BPL) and BSE-2 (CP BPL) for the ELF- and RSA-designed frames, respectively. The results from the LSP, LDP, and NSP (loaded to the right) are included in the figures. Comparison discussions between the various procedures are addressed subsequently. As is evident from the figures, the ELF-designed frame performs better than the RSA-designed frame. Results for the RSA-designed frame indicate that the beam-to-column connections have difficulty satisfying the CP BPL acceptance criteria at the BSE-2 EHL (primarily based on mean response). In contrast to the mean response, the median response indicates better performance at all stories because it is less influenced by large deformations resulting from component strength loss potentially resulting in collapse of the system. Consequently, the median is potentially a more stable performance metric when analyzing a large number of ground motion records, but should be restrained relative to a mean value. Further, there is a strong probability that system response is triggered by the performance of the exterior base column hinges—see previous discussion in NSP section.

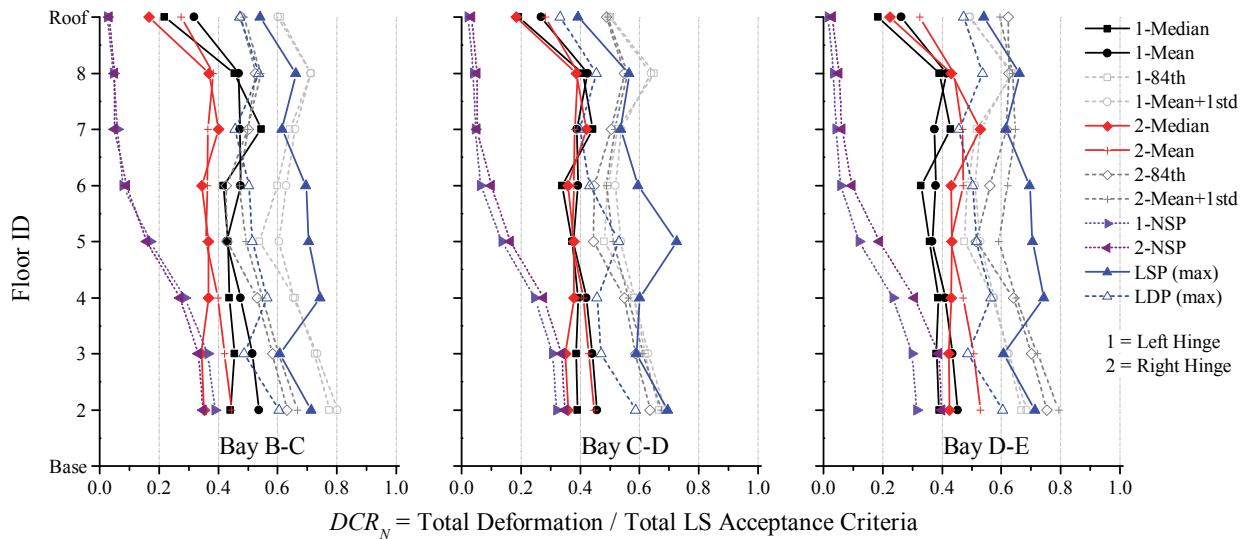


Figure 3-83. NDP Assessment Results, Beam Hinges, 8-Story SMF ELF, BSE-1 LS

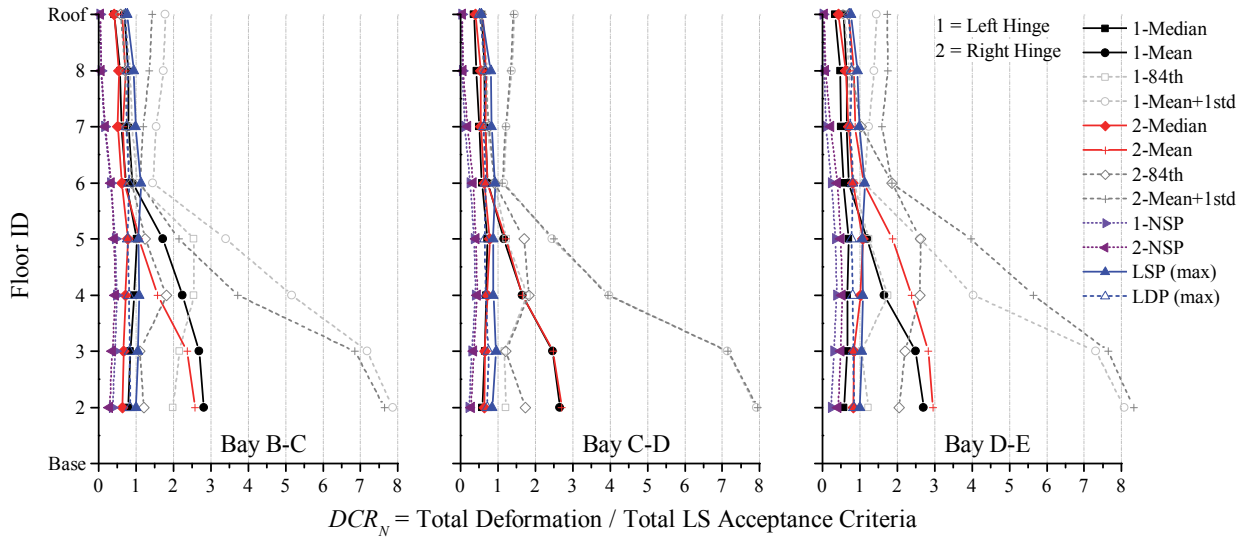


Figure 3-84. NDP Assessment Results, Beam Hinges, 8-Story SMF RSA, BSE-1 LS

The average ratio of secondary to primary component acceptance criteria for an RBS beam-to-column connection for all W18 sections and deeper is 1.49 for the CP SPL (1.47 for the LS SPL). The figures for the both frames illustrate that this value is exceeded in the beam-to-column connections at the BSE-2 EHL. This highlights the rapid progression towards a collapse state when several components are strained past the deformation associated with their peak strength—see §3.1.4.2.

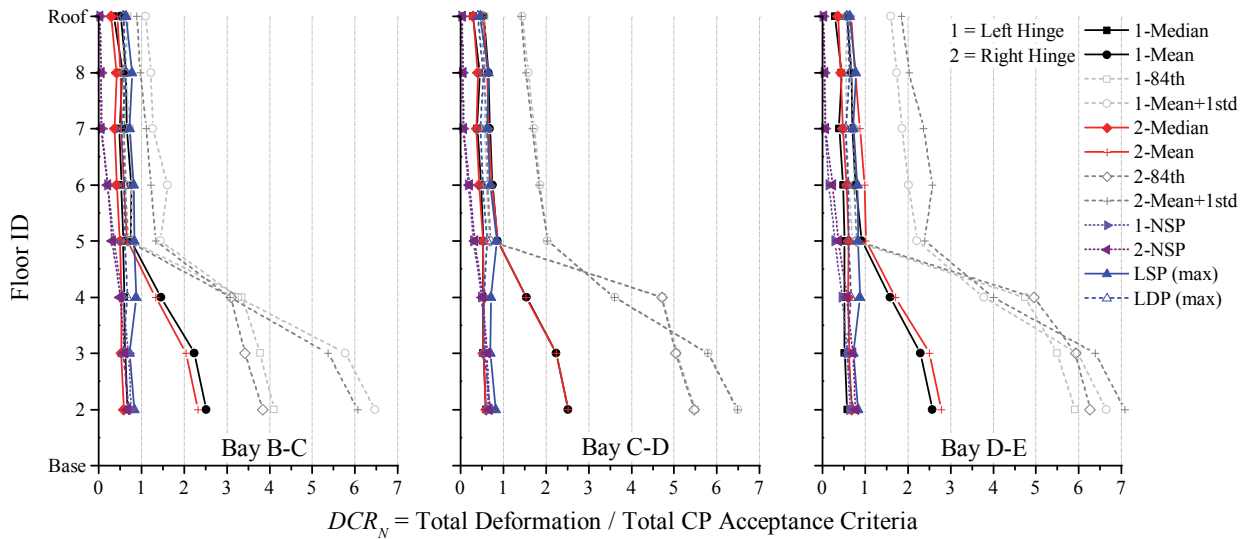


Figure 3-85. NDP Assessment Results, Beam Hinges, 8-Story SMF ELF, BSE-2 CP

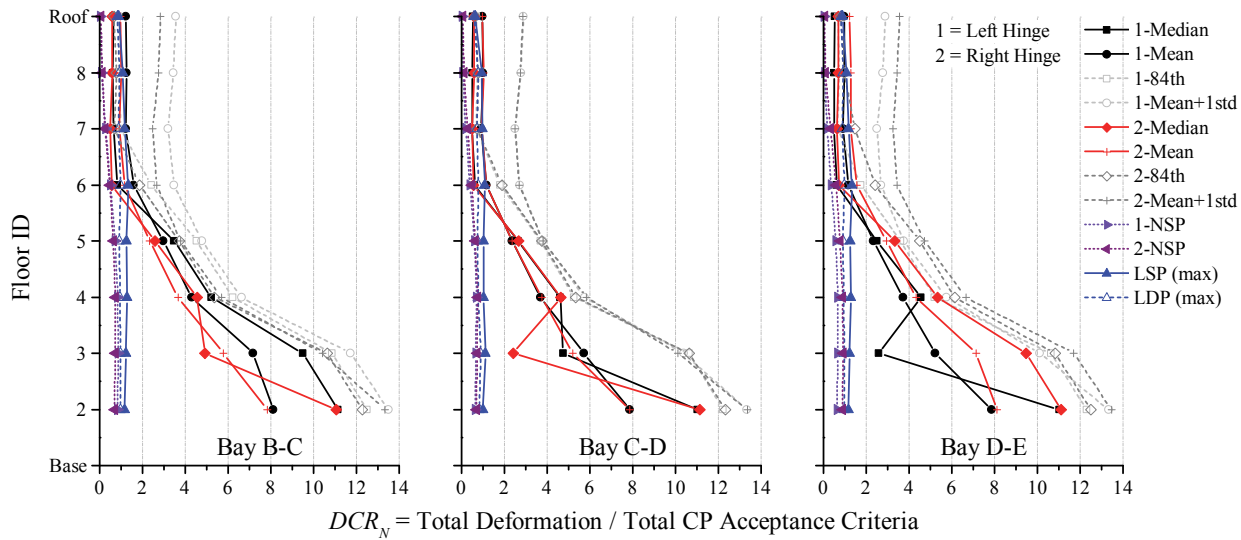


Figure 3-86. NDP Assessment Results, Beam Hinges, 8-Story SMF RSA, BSE-2 CP

The previous figures illustrate for both frames that the component strengths provided by drift and stability control measures in ASCE 7 at $\frac{2}{3} \times MCE_R$ (equal to the BSE-1 here) are not significant enough to overcome the demands to satisfy the assessment criteria at the BSE-2 (taken here as MCE_R). First, strong panel zones reduce the allowable deformations in the acceptance criteria and component model for the exterior beam-to-column connections. Second, base hinge modeling could have a drastic effect on the performance of the beam-to-column connections. This further highlights the change in story demands as column base hinges develop, an influence not addressed in elastic design analysis. However, a secondary design analysis to address the effects of “pinned” column bases could be conducted—not done in this study.

Figure 3-78 (see NSP section) illustrates which flexural actions in the frame columns are force-controlled for both the NSP and NDP. Figure 3-87 and Figure 3-88 show the performance of the column hinges for the CP BPL criteria for the BSE-2 assuming deformation-controlled flexural actions (LS BPL for the BSE-1 is not shown). Column hinges at the base experience inelastic strain demands (yield corresponds to a $DCR_N \approx 0.15$ in the figures). The deformation demands in these hinges are considerably higher than the CP primary acceptance criteria, indicating a significant performance concern of the frame columns and the SFRS. Similarly, the exterior base columns in the ELF-designed frame are force-controlled for flexure and therefore do not satisfy the lower-bound elastic acceptance criteria at the BSE-2 EHL. Moreover, the columns in the RSA-designed frame on the fifth floor do not satisfy the acceptance criteria because they are also force-controlled.

The DCR_N results for the LSP and LDP are based on an interaction equation and not from $M_{UD} / m \times M_{CE}$, or M_{UF} / M_{CL} , which would be a more physically consistent metric for comparison against the results from the nonlinear assessment procedures. Nonetheless, the linear results are generally not applicable here because most columns are force-controlled for flexure in the linear assessment procedures. Though there is a fundamental difference in how the DCR_N is computed for the linear and nonlinear procedures, the linear assessment results show similar distributions of demands and location of potential performance concerns.

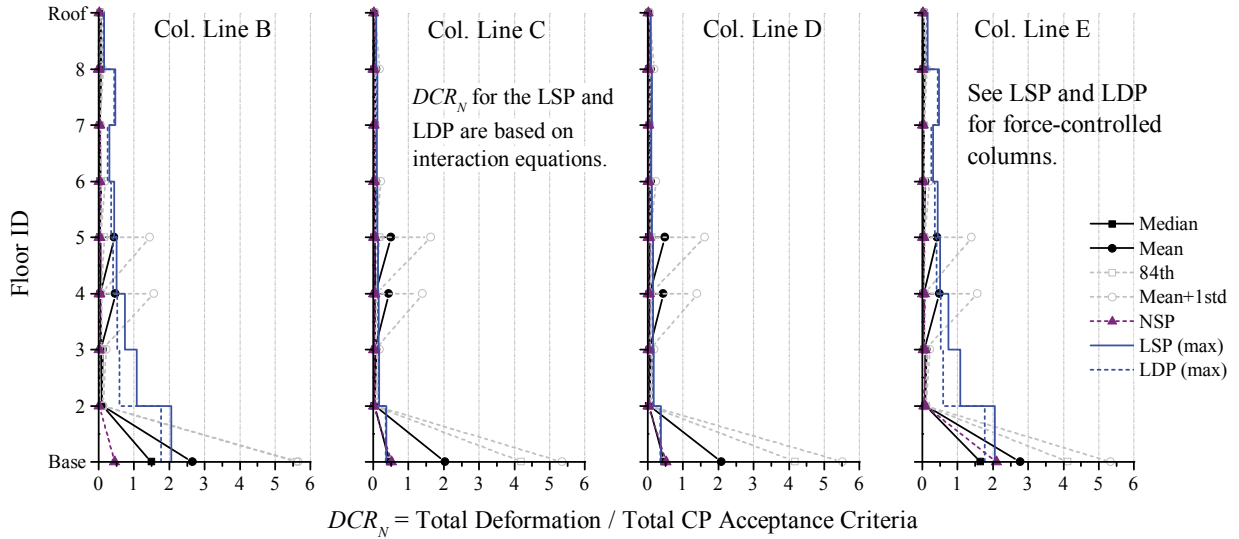


Figure 3-87. NDP Assessment Results, Column Hinges, 8-Story SMF ELF, BSE-2 CP

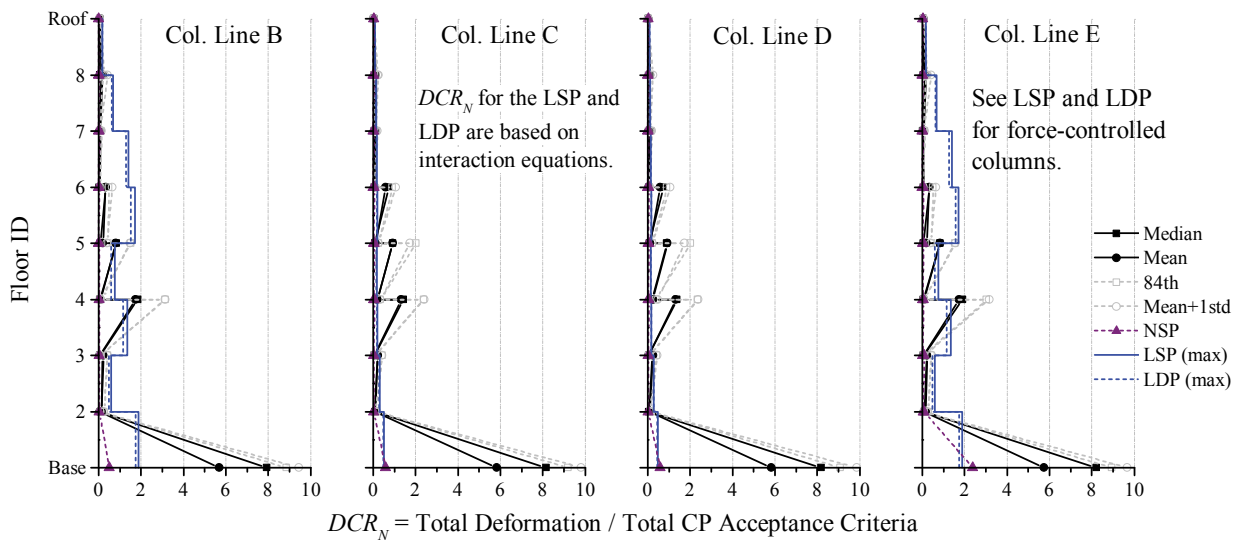


Figure 3-88. NDP Assessment Results, Column Hinges, 8-Story SMF RSA, BSE-2 CP

Figure 3-89 and Figure 3-90 show the curvature ductility demand of the column hinges (i.e., section strength) at the BSE-2 EHL. Figure 3-91 and Figure 3-92 show the elastic member strength interaction results at the BSE-2 EHL. The results indicate that the columns above the base in the ELF-designed frame satisfy the intended lower-bound acceptance criteria whereas the columns in the RSA-designed frame consistently do not satisfy these acceptance criteria—a result of the large number of analyses that did not complete.

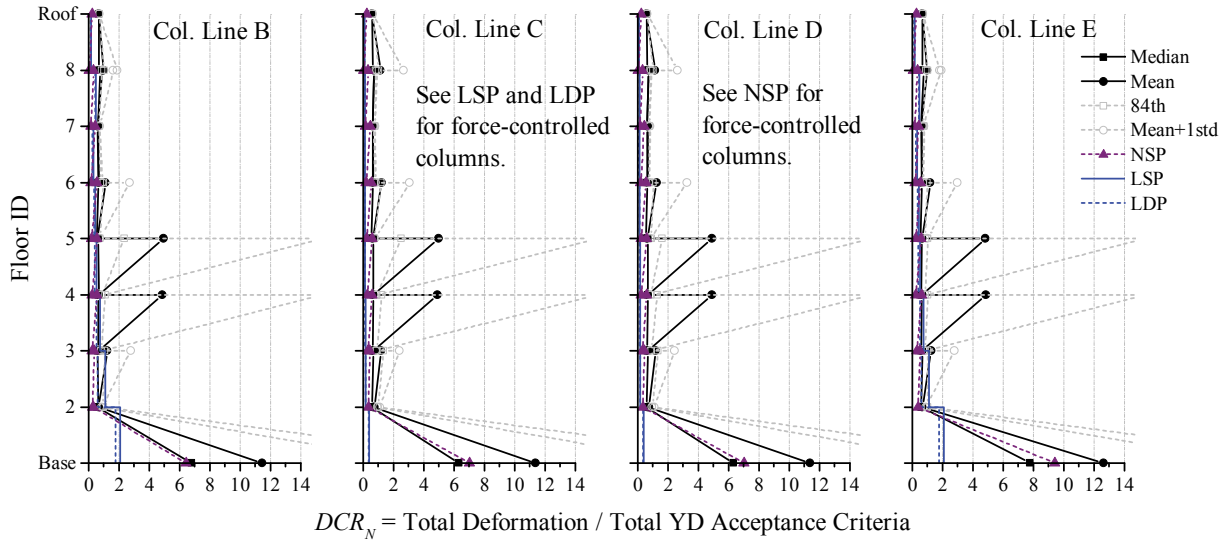


Figure 3-89. NDP Assessment Results, Column Hinges, 8-Story SMF ELF, BSE-2 Yield

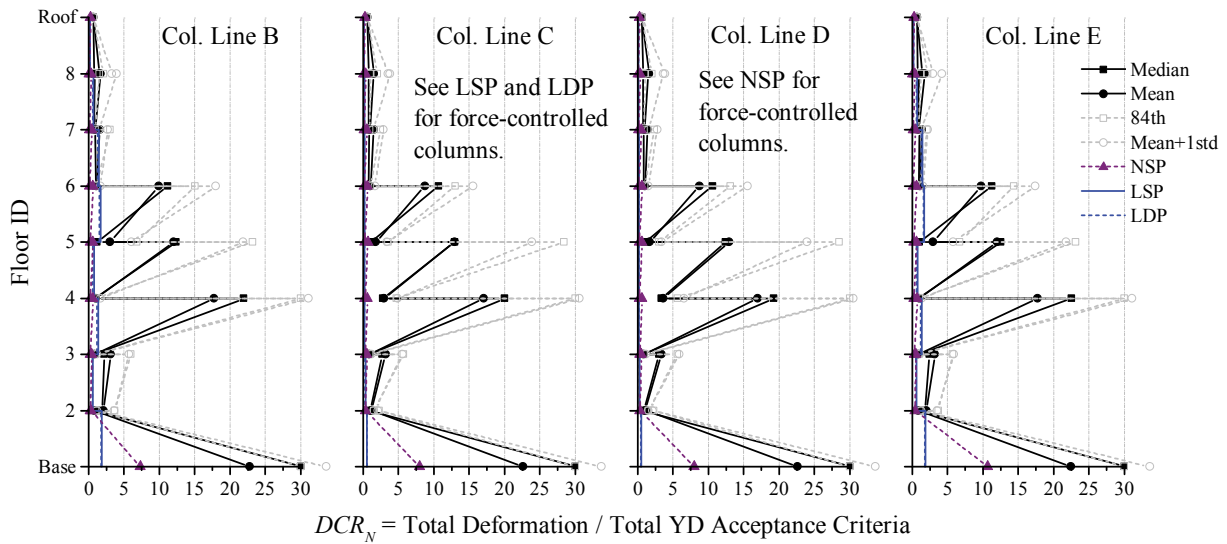


Figure 3-90. NDP Assessment Results, Column Hinges, 8-Story SMF RSA, BSE-2 Yield

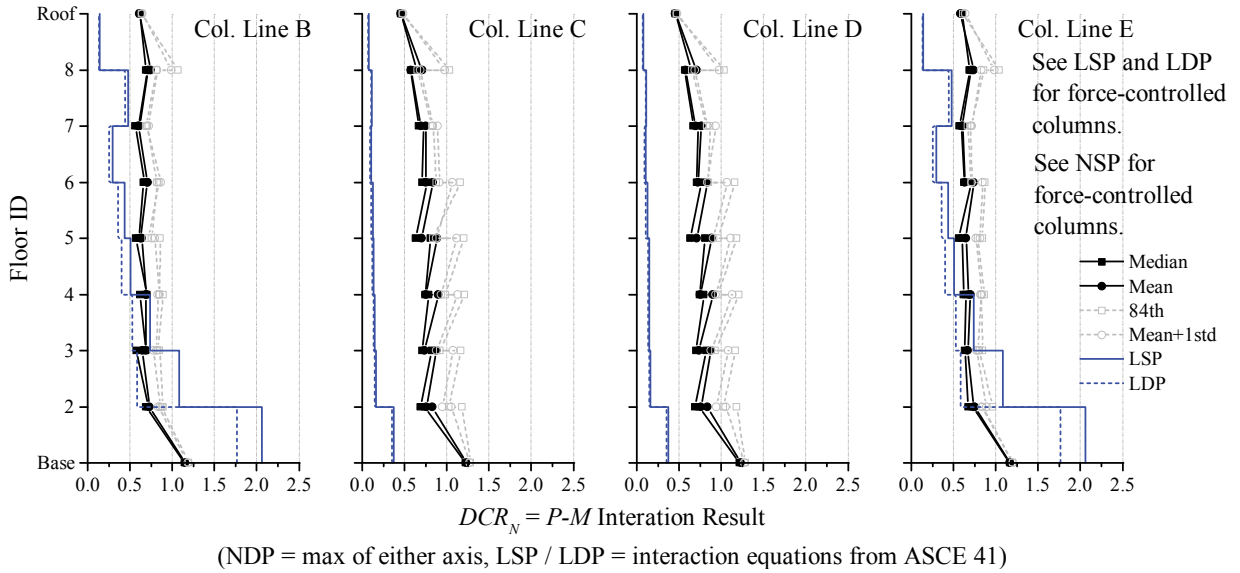


Figure 3-91. NDP Assessment Results, Column Members, 8-Story SMF ELF, BSE-2

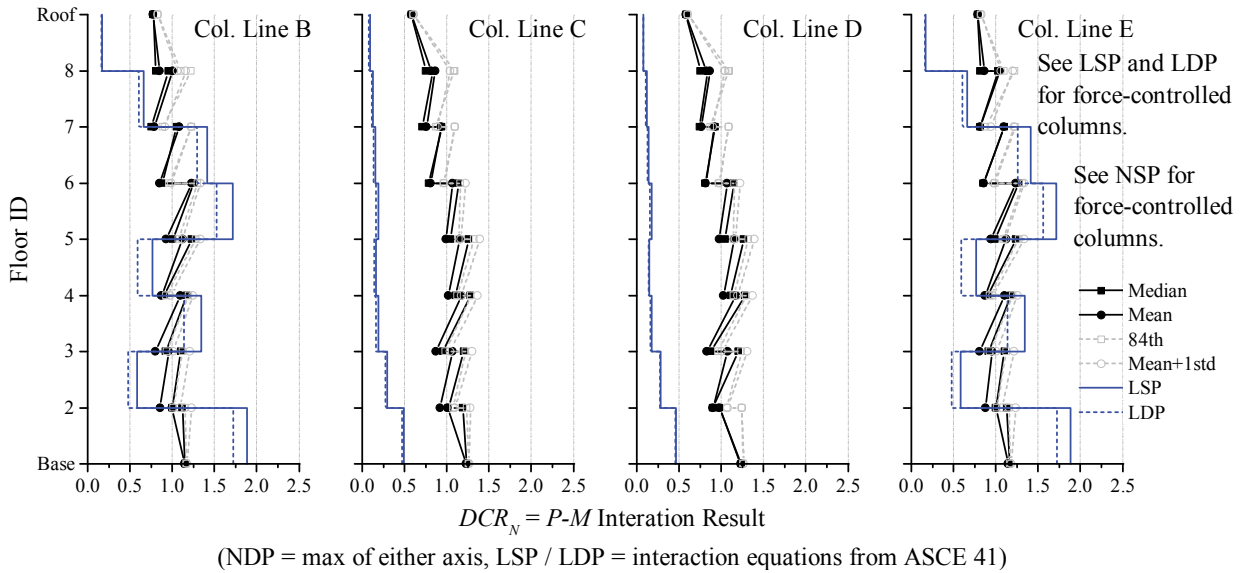


Figure 3-92. NDP Assessment Results, Column Members, 8-Story SMF RSA, BSE-2

Figure 3-93 and Figure 3-94 show the performance of the panel zones for the CP BPL criteria at the BSE-2 EHL (LS BPL for the BSE-1 is not shown). The deformation demands are significantly lower than the CP acceptance criteria. Converting the results to shear ductility (total deformation / yield deformation, γ_s) indicates that the demands for the BSE-2 are consistently less than $4 \times \gamma_y$. These results illustrate that the panel zones are stronger than required by the assessment criteria—see discussion in the 4-story NDP section. There is one outlier at the interior panel zones on the third floor in the RSA-designed frame. First,

the first hinges to form are on the third floor. Second, the mean results are biased toward the collapse state of the frame for a given record—a result of the large number of analyses that did not complete.

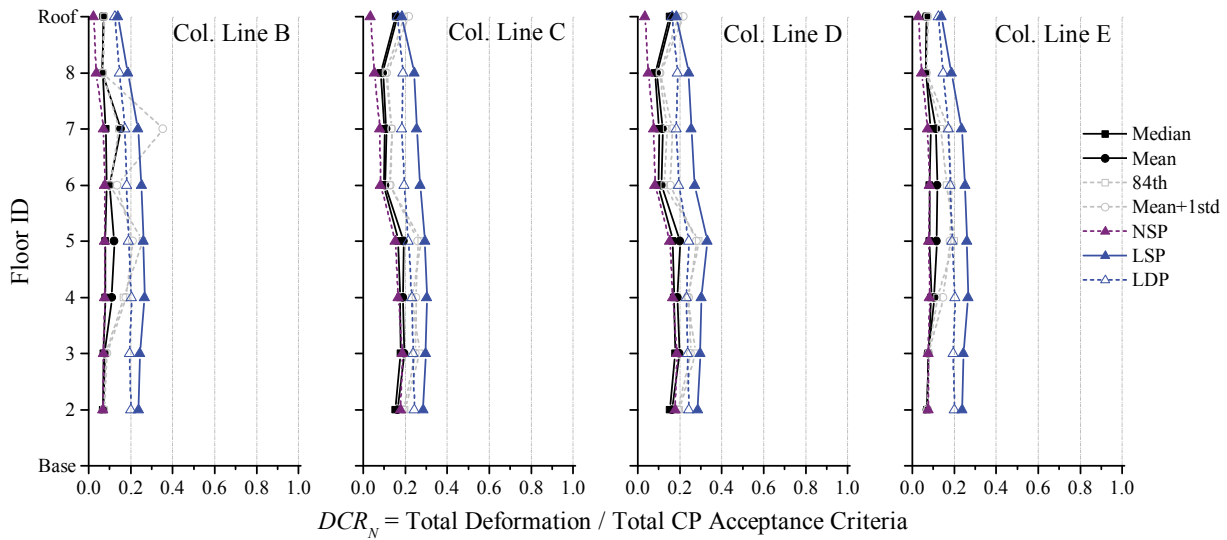


Figure 3-93. NDP Assessment Results, Panel Zones, 8-Story SMF ELF, BSE-2 CP

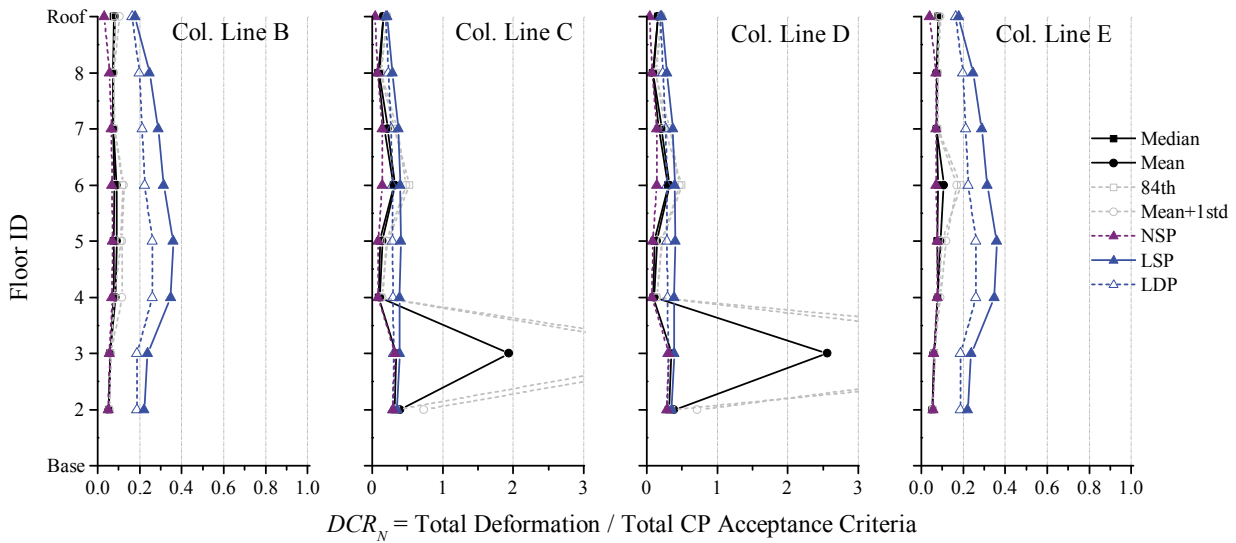


Figure 3-94. NDP Assessment Results, Panel Zones, 8-Story SMF RSA, BSE-2 CP

3.2.2.3 Sixteen-Story Moment Frame

3.2.2.3.1 Linear Static Procedure

3.2.2.3.1.1 BSE-1 Earthquake Hazard Level (LS BPL)

In this section, the following apply:

- Figure 3-95 and Figure 3-96 provide the DCR_N and load-dependent m -factor values for the ELF and RSA designs, respectively, for the LSP at the BSE-1 EHL. In these figures, DCR_N values greater than unity are highlighted in red and underlined. DCR values, as defined by ASCE 41, can be obtained by multiplying DCR_N by m and κ , see Eq. 3-6.
- Figure 3-97 provides the maximum axial compression demands, P_{UF} , in the exterior column lines for various analysis methods and the column capacity, P_{CL} .

All beam-to-column and panel zone component actions satisfy the LS BPL acceptance criteria except for the exterior beam-to-column connections in the RSA-designed frame on the 14th floor. These connection failures are primarily due to reduced m -factors as a result of the FR connection modifiers for panel zone strength and clear span-to-depth limitations. These figures illustrate that drift and stability control in ASCE 7 provides a significant amount of member overstrength so that beam-to-column connections in the ELF-designed frame easily satisfy the LS BPL acceptance criteria. Assessment results for the panel zones all remained small compared to unity—see §3.2.2.1.1.1.

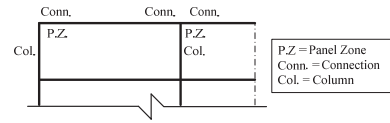
Several exterior frame columns in the RSA-designed frame do not satisfy the LS BPL acceptance criteria using the interaction equation because they are designated as force-controlled for flexure since P_{UF} exceeds $0.5 \times P_{CL}$ —see §3.2.2.2.1 for more discussion. As discussed previously in §3.2.2, P_{UF} is determined by taking J (ASCE 41 §3.4.2.1.2-2) as the minimum DCR of the component(s) delivering force to the column, but not less than 2.0; interior columns are not applicable because P_E is essentially zero. This approach produces the least conservative P_{UF} as compared to AISC 341 SMF column design requirements and the fully yielded system as prescribed in ASCE 41 §3.4.2.1.2-1, as shown in Figure 3-97.

	0.42	0.34	0.43
0.08	0.07		0.12
	0.60	0.39	0.06
			0.46
0.14	0.09		0.14
	0.47	0.38	0.10
	0.14		0.18
0.30			0.08
	0.55	0.44	0.53
	0.16		0.20
0.43			0.09
	0.55	0.44	0.54
	0.18		0.21
0.52			0.10
	0.61	0.49	0.58
	0.19		0.22
0.90			0.12
	0.68	0.53	0.61
	0.20		0.24
0.51			0.13
	0.70	0.54	0.61
	0.20		0.24
0.69			0.15
	0.82	0.49	0.54
	0.18		0.24
0.52			0.15
	0.82	0.49	0.53
	0.18		0.24
0.76			0.26
	0.69	0.50	0.53
	0.16		0.24
0.60			0.28
	0.69	0.50	0.52
	0.15		0.24
0.81			0.30
	0.72	0.52	0.53
	0.12		0.20
0.55			0.27
	0.70	0.51	0.50
	0.11		0.19
0.76			0.29
	0.67	0.47	0.44
	0.06		0.17
0.38			0.30
	0.56	0.39	0.35
	0.05		0.13
0.55			0.39

Sym.

	2.31	2.88	2.88
4.01	8.00		8.00
	2.31	3.60	6.00
			3.61
4.01	8.00		8.00
	3.07	3.83	6.00
			3.84
3.77	8.00		8.00
	3.07	3.83	6.00
			3.84
2.79	8.00		8.00
	3.17	3.97	6.00
			3.97
2.41	8.00		8.00
	3.17	3.97	6.00
			3.97
1.00	8.00		8.00
	3.17	3.97	6.00
			3.97
2.67	8.00		8.00
	3.17	3.97	6.00
			3.97
1.52	8.00		8.00
	2.61	4.07	6.00
			4.07
2.45	8.00		8.00
	2.61	4.07	6.00
			4.07
1.00	8.00		8.00
	3.26	4.07	5.84
			4.07
1.72	8.00		8.00
	3.26	4.07	5.56
			4.07
1.00	8.00		8.00
	3.26	4.07	5.29
			4.07
2.04	8.00		8.00
	3.26	4.07	5.70
			4.07
1.00	8.00		8.00
	3.26	4.07	5.49
			4.07
3.89	8.00		8.00
	3.26	4.07	5.31
			4.07
2.92	8.00		8.00
			4.67

Sym.



(a) DCR_N

(b) m -factors

(c) Key

Figure 3-95. LSP Assessment Results, 16-Story SMF ELF, BSE-1 LS

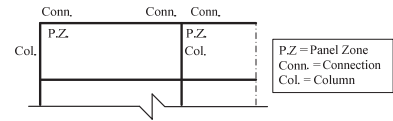
	0.44	0.37	0.48
0.08	0.07		0.13
	0.67	0.45	0.07
			0.53
0.16	0.11		0.17
	0.97	0.62	0.11
			0.69
0.29	0.12		0.22
	1.13	0.71	0.15
			0.78
0.43	0.14		0.25
	0.74	0.59	0.32
			0.68
0.58	0.21		0.27
	0.76	0.62	0.12
			0.72
0.96	0.22		0.27
	0.83	0.67	0.13
			0.75
0.55	0.23		0.29
	0.86	0.68	0.15
			0.76
0.89	0.23		0.29
	0.78	0.62	0.28
			0.69
0.86	0.23		0.28
	0.77	0.61	0.25
			0.68
0.96	0.23		0.27
	0.99	0.61	0.28
			0.66
0.91	0.20		0.26
	0.95	0.59	0.31
			0.62
1.05	0.19		0.25
	0.82	0.51	0.35
			0.55
0.88	0.17		0.20
	0.76	0.47	0.27
			0.50
0.95	0.15		0.18
	0.59	0.44	0.29
			0.44
0.73	0.10		0.16
	0.51	0.37	0.31
			0.36
1.15	0.08		0.13
			0.41

Sym.

(a) DCR_N

	2.31	2.88	2.88
4.01	8.00		8.00
	2.31	3.60	6.00
			3.61
4.01	8.00		8.00
	2.31	3.60	6.00
			3.61
3.84	8.00		8.00
	2.31	3.60	6.00
			3.61
2.97	8.00		8.00
	3.07	3.83	4.55
			3.84
1.85	8.00		8.00
	3.07	3.83	6.00
			3.84
1.00	8.00		8.00
	3.07	3.83	6.00
			3.84
2.17	8.00		8.00
	3.07	3.83	6.00
			3.84
1.00	8.00		8.00
	3.17	3.97	5.80
			3.97
1.00	8.00		8.00
	3.17	3.97	5.96
			3.97
1.00	8.00		8.00
	2.54	3.97	5.60
			3.97
1.00	8.00		8.00
	2.54	3.97	5.26
			3.97
1.00	8.00		8.00
	2.61	4.07	4.93
			4.07
1.00	8.00		8.00
	2.61	4.07	5.64
			4.07
1.00	8.00		8.00
	3.26	4.07	5.38
			4.07
1.00	8.00		8.00
	3.26	4.07	5.15
			4.07
1.00	8.00		8.00
	3.26	4.07	4.46
			4.46

Sym.

(b) m -factors

(c) Key

Figure 3-96. LSP Assessment Results, 16-Story SMF RSA, BSE-1 LS

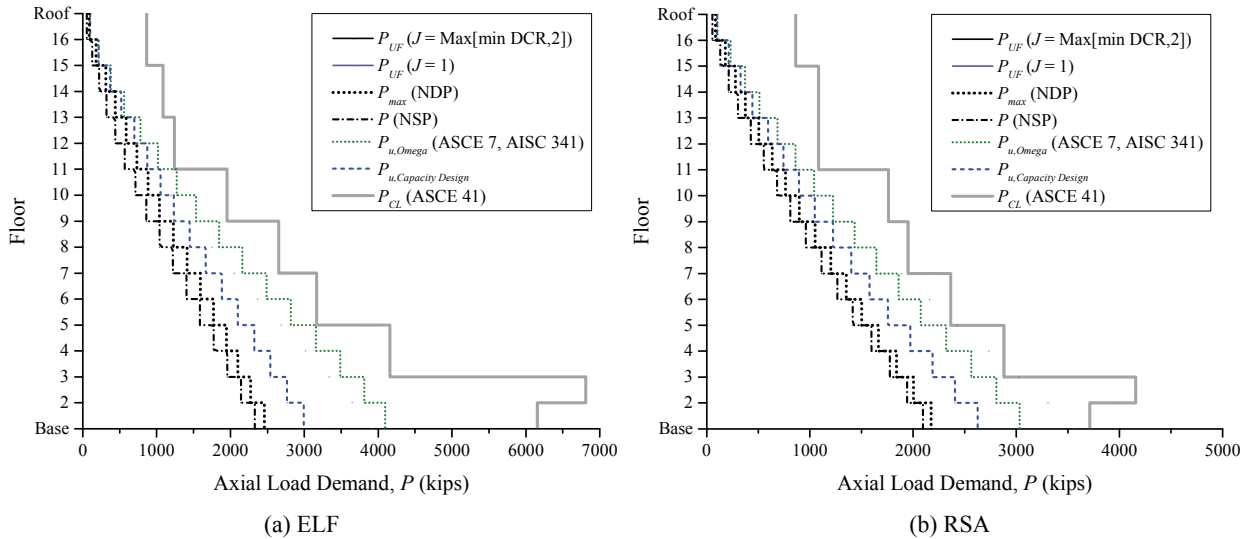


Figure 3-97. LSP Assessment Results, Compression in Exterior Columns, 16-Story SMF, BSE-1

3.2.2.3.1.2 BSE-2 Earthquake Hazard Level (CP BPL)

In this section, the following apply:

- Figure 3-98 and Figure 3-99 provide the DCR_N and load-dependent m -factor values for the ELF and RSA designs, respectively, for the LSP at the BSE-2 EHL. In these figures, DCR_N values greater than unity are highlighted in red and underlined. DCR values, as defined by ASCE 41, can be obtained by multiplying DCR_N by m and κ , see Eq. 3-6.
- Figure 3-100 provides the maximum axial compression demands, P_{UF} , in the exterior column lines for various analysis methods and the column capacity, P_{CL} .

All beam-to-column and panel zone component actions satisfy the CP BPL acceptance criteria except for several exterior beam-to-column connections in the RSA design on several floors. These connection failures are due to reduced m -factors as a result of the FR connection modifiers for panel zone strength and clear span-to-depth limitations. Assessment results for the panel zones all remained small compared to unity—see §3.2.2.1.1.1.

Several exterior frame columns in the ELF- and RSA-designed frames do not satisfy the CP BPL acceptance criteria using the interaction equation because they are designated as force-controlled for flexure since P_{UF} exceeds $0.5 \times P_{CL}$ —see §3.2.2.2.1 for more discussion. Further, comparing Figure 3-97 and Figure 3-100 illustrates that adopting a constant J factor of 2.0 for both performance levels is inconsistent with the intent of capacity design because of the change in the variation between P_{UF} and $P_{Capacity Design}$ in the figures—see §3.2.2.2.1 for more discussion.

	0.49	0.39	0.50
0.09	0.08		0.13
	0.70	0.44	0.07
			0.53
0.15	0.10		0.16
	0.56	0.45	0.10
			0.55
0.35	0.15		0.20
	0.65	0.51	0.09
			0.62
0.53	0.17		0.21
	0.65	0.52	0.10
			0.63
0.71	0.19		0.23
	0.72	0.57	0.11
			0.68
<u>1.19</u>	0.21		0.24
	0.80	0.62	0.13
			0.72
0.97	0.22		0.26
	0.83	0.64	0.14
			0.72
<u>1.17</u>	0.22		0.26
	0.97	0.58	0.17
			0.64
0.93	0.20		0.27
	0.97	0.57	0.25
			0.63
<u>1.02</u>	0.19		0.26
	0.81	0.59	0.28
			0.62
0.97	0.17		0.26
	0.82	0.59	0.30
			0.61
<u>1.09</u>	0.17		0.26
	0.85	0.62	0.33
			0.63
0.91	0.13		0.22
	0.82	0.60	0.28
			0.59
<u>1.02</u>	0.13		0.20
	0.79	0.56	0.30
			0.52
0.51	0.07		0.18
	0.66	0.46	0.31
			0.41
<u>1.29</u>	0.05		0.14
			0.41

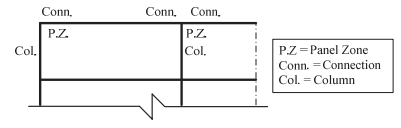
Sym.

(a) DCR_N

	2.91	3.64	3.64
5.48	11.00		11.00
	2.91	4.55	8.00
			4.56
5.48	11.00		11.00
	3.87	4.84	8.00
			4.84
4.50	11.00		11.00
	3.87	4.84	8.00
			4.84
2.91	11.00		11.00
	4.01	5.01	8.00
			5.02
1.90	11.00		11.00
	4.01	5.01	8.00
			5.02
1.00	11.00		11.00
	4.01	5.01	8.00
			5.02
1.00	11.00		11.00
	4.01	5.01	8.00
			5.02
1.00	11.00		11.00
	3.29	5.14	8.00
			5.14
1.00	11.00		11.00
	3.29	5.14	7.94
			5.14
1.00	11.00		11.00
	4.11	5.14	7.51
			5.14
1.00	11.00		11.00
	4.11	5.14	7.14
			5.14
1.00	11.00		11.00
	4.11	5.14	6.79
			5.14
1.00	11.00		11.00
	4.11	5.14	7.39
			5.14
1.00	11.00		11.00
	4.11	5.14	7.13
			5.14
3.24	11.00		11.00
	4.11	5.14	6.92
			5.14
1.00	11.00		11.00
			6.09

Sym.

(b) m -factors



(c) Key

Figure 3-98. LSP Assessment Results, 16-Story SMF ELF, BSE-2 CP

	0.51	0.42	0.55
0.09	0.08		0.14
	0.79	0.51	0.07
			0.62
0.33	0.12		0.19
			0.12
	1.15	0.72	0.80
0.34	0.13		0.25
			0.16
	1.33	0.83	0.91
0.52	0.15		0.27
			0.34
	0.88	0.69	0.80
0.98	0.23		0.30
			0.13
	0.90	0.73	0.85
1.28	0.24		0.30
			0.14
	0.99	0.78	0.88
1.00	0.25		0.32
			0.16
	1.02	0.80	0.89
1.20	0.25		0.32
			0.30
	0.92	0.72	0.82
1.15	0.25		0.30
			0.27
	0.91	0.72	0.80
1.28	0.25		0.29
			0.30
	1.17	0.72	0.78
1.22	0.22		0.29
			0.33
	1.12	0.69	0.73
1.42	0.20		0.27
			0.38
	0.97	0.60	0.64
1.18	0.18		0.22
			0.29
	0.90	0.56	0.59
1.27	0.16		0.20
			0.31
	0.69	0.52	0.51
0.98	0.11		0.17
			0.33
	0.60	0.44	0.42
1.59	0.09		0.14
			0.44

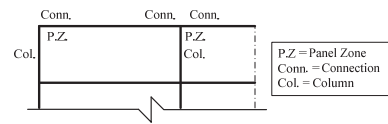
Sym.

(a) DCR_N

	2.91	3.64	3.64
5.48	11.00		11.00
			8.00
	2.91	4.55	4.56
3.02	11.00		11.00
			8.00
	2.91	4.55	4.56
4.63	11.00		11.00
			8.00
	2.91	4.55	4.56
3.24	11.00		11.00
			5.91
	3.87	4.84	4.84
1.00	11.00		11.00
			8.00
	3.87	4.84	4.84
1.00	11.00		11.00
			8.00
	3.87	4.84	4.84
1.00	11.00		11.00
			7.52
	4.01	5.01	5.02
1.00	11.00		11.00
			7.74
	4.01	5.01	5.02
1.00	11.00		11.00
			7.21
	3.21	5.01	5.02
1.00	11.00		11.00
			6.74
	3.21	5.01	5.02
1.00	11.00		11.00
			6.28
	3.29	5.14	5.14
1.00	11.00		11.00
			7.28
	3.29	5.14	5.14
1.00	11.00		11.00
			6.93
	4.11	5.14	5.14
1.00	11.00		11.00
			6.64
	4.11	5.14	5.14
1.00	11.00		11.00
			5.70

Sym.

(b) m -factors



(c) Key

Figure 3-99. LSP Assessment Results, 16-Story SMF RSA, BSE-2 CP

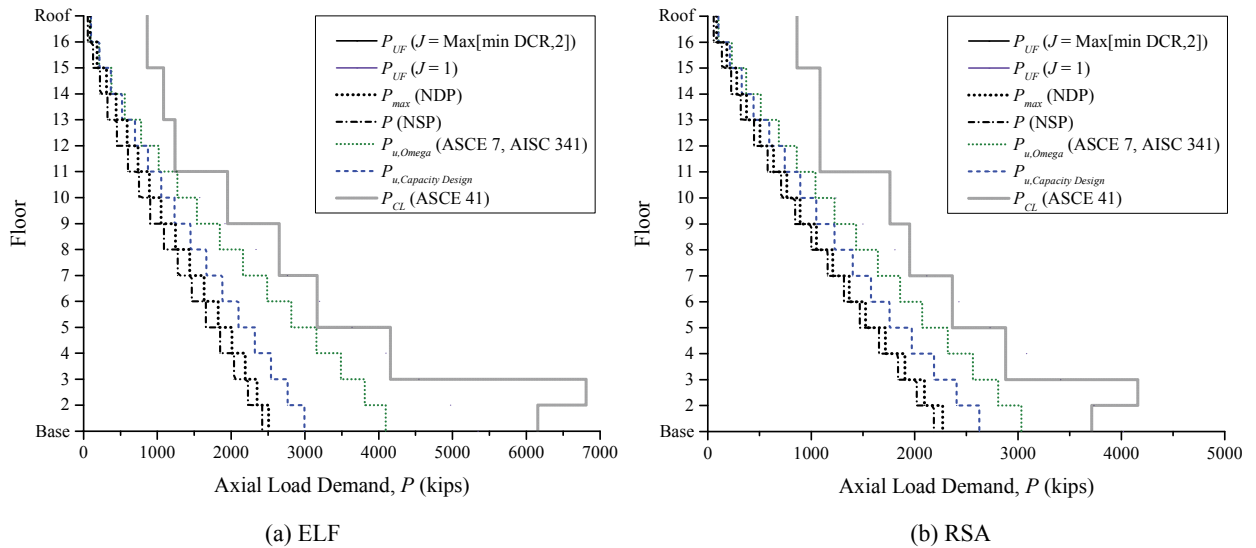


Figure 3-100. LSP Assessment Results, Compression in Exterior Columns, 16-Story SMF, BSE-2

3.2.2.3.2 Linear Dynamic Procedure

3.2.2.3.2.1 BSE-1 Earthquake Hazard Level (LS BPL)

In this section, the following apply:

- Figure 3-101 and Figure 3-102 provide the DCR_N and load-dependent m -factor values for the ELF and RSA designs, respectively, for the LDP at the BSE-1 EHL. In these figures, DCR_N values greater than unity are highlighted in red and underlined. DCR values, as defined by ASCE 41, can be obtained by multiplying DCR_N by m and κ , see Eq. 3-6.
- Figure 3-103 provides the maximum axial compression demands, P_{UF} , in the exterior column lines for various analysis methods and the column capacity, P_{CL} .

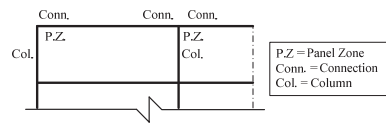
All beam-to-column connection, panel zone, and column component actions satisfy the LS BPL for the ELF- and RSA- designed frames. Contrary to the LSP results, all exterior frame columns in the ELF-designed frame are deformation-controlled for flexural action for the LDP, whereas only a few more are deformation-controlled for the RSA-designed frame. Assessment results for the panel zones all remained small compared to unity—see §3.2.2.1.1.1.

	0.50	0.41	0.43
0.09	0.08		0.13
	0.63	0.41	0.06
			0.43
0.15	0.09		0.13
	0.42	0.34	0.10
			0.39
0.28	0.12		0.15
	0.43	0.36	0.07
			0.41
0.40	0.12		0.15
	0.41	0.34	0.09
			0.39
0.45	0.13		0.15
	0.44	0.36	0.09
			0.41
0.60	0.14		0.16
	0.48	0.38	0.10
			0.43
0.42	0.14		0.16
	0.49	0.38	0.11
			0.43
0.51	0.14		0.16
	0.58	0.35	0.13
			0.38
0.41	0.13		0.17
	0.59	0.35	0.13
			0.38
0.48	0.13		0.17
	0.50	0.37	0.24
			0.38
0.45	0.11		0.17
	0.52	0.38	0.26
			0.38
0.52	0.11		0.17
	0.56	0.40	0.28
			0.40
0.42	0.09		0.15
	0.56	0.40	0.25
			0.40
0.47	0.09		0.15
	0.56	0.39	0.27
			0.36
0.30	0.05		0.14
	0.48	0.33	0.28
			0.30
0.42	0.04		0.11
			0.37

(a) DCR_N

	2.31	2.88	2.88
4.01	8.00		8.00
	2.31	3.60	6.00
			3.61
4.01	8.00		8.00
	3.07	3.83	6.00
			3.84
3.79	8.00		8.00
	3.07	3.83	6.00
			3.84
2.94	8.00		8.00
	3.17	3.97	6.00
			3.97
2.78	8.00		8.00
	3.17	3.97	6.00
			3.97
1.72	8.00		8.00
	3.17	3.97	6.00
			3.97
3.42	8.00		8.00
	3.17	3.97	6.00
			3.97
2.53	8.00		8.00
	2.61	4.07	6.00
			4.07
3.50	8.00		8.00
	2.61	4.07	6.00
			4.07
2.70	8.00		8.00
	3.26	4.07	5.97
			4.07
3.02	8.00		8.00
	3.26	4.07	5.69
			4.07
2.31	8.00		8.00
	3.26	4.07	5.42
			4.07
3.34	8.00		8.00
	3.26	4.07	5.80
			4.07
2.78	8.00		8.00
	3.26	4.07	5.58
			4.07
4.85	8.00		8.00
	3.26	4.07	5.37
			4.07
4.05	8.00		8.00
			4.69

(b) m -factors



(c) Key

Figure 3-101. LDP Assessment Results, 16-Story SMF ELF, BSE-1 LS

	0.51	0.43	0.46
0.09	0.09		0.13
	0.69	0.46	0.07
			0.49
0.16	0.10		0.16
			0.11
	0.86	0.56	0.57
0.28	0.10		0.19
			0.14
	0.90	0.58	0.60
0.41	0.10		0.19
			0.30
	0.55	0.45	0.49
0.51	0.16		0.20
			0.10
	0.55	0.45	0.51
0.81	0.16		0.19
			0.12
	0.58	0.47	0.52
0.45	0.16		0.20
			0.13
	0.60	0.48	0.52
0.55	0.16		0.20
			0.25
	0.54	0.43	0.48
0.56	0.16		0.19
			0.14
	0.54	0.44	0.48
0.77	0.16		0.19
			0.26
	0.71	0.45	0.47
0.61	0.14		0.19
			0.28
	0.70	0.44	0.45
0.83	0.14		0.18
			0.32
	0.62	0.39	0.41
0.61	0.12		0.15
			0.25
	0.60	0.37	0.39
0.76	0.12		0.14
			0.27
	0.49	0.36	0.36
0.47	0.08		0.13
			0.29
	0.44	0.32	0.30
0.97	0.07		0.11
			0.38

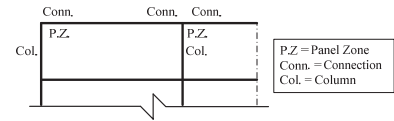

Sym.

(a) DCR_N

	2.31	2.88	2.88
4.01	8.00		8.00
			6.00
	2.31	3.60	3.61
4.01	8.00		8.00
			6.00
	2.31	3.60	3.61
3.85	8.00		8.00
			6.00
	2.31	3.60	3.61
3.07	8.00		8.00
			4.60
	3.07	3.83	3.84
2.16	8.00		8.00
			6.00
	3.07	3.83	3.84
1.00	8.00		8.00
			6.00
	3.07	3.83	3.84
2.81	8.00		8.00
			6.00
	3.07	3.83	3.84
2.06	8.00		8.00
			5.91
	3.17	3.97	3.97
1.96	8.00		8.00
			6.00
	3.17	3.97	3.97
1.00	8.00		8.00
			5.73
	2.54	3.97	3.97
1.60	8.00		8.00
			5.40
	2.54	3.97	3.97
1.00	8.00		8.00
			5.07
	2.61	4.07	4.07
1.51	8.00		8.00
			5.76
	2.61	4.07	4.07
1.00	8.00		8.00
			5.50
	3.26	4.07	4.07
2.78	8.00		8.00
			5.27
	3.26	4.07	4.07
1.00	8.00		8.00
			4.58


Sym.

(b) m -factors



(c) Key

Figure 3-102. LDP Assessment Results, 16-Story SMF RSA, BSE-1 LS

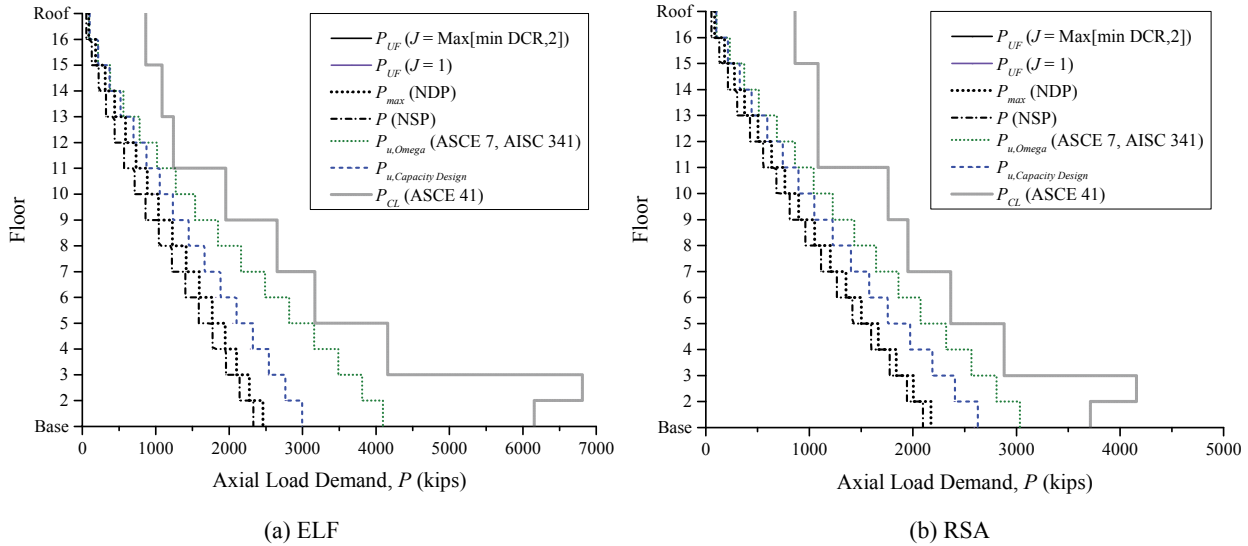


Figure 3-103. LDP Assessment Results, Compression in Exterior Columns, 16-Story SMF, BSE-1

3.2.2.3.2.2 BSE-2 Earthquake Hazard Level (CP BPL)

In this section, the following apply:

- Figure 3-104 and Figure 3-105 provide the DCR_N and load-dependent m -factor values for the ELF and RSA designs, respectively, for the LDP at the BSE-2 EHL. In these figures, DCR_N values greater than unity are highlighted in red and underlined. DCR values, as defined by ASCE 41, can be obtained by multiplying DCR_N by m and κ , see Eq. 3-6.
- Figure 3-106 provides the maximum axial compression demands, P_{UF} , in the exterior column lines for various analysis methods and the column capacity, P_{CL} .

All beam-to-column and panel zone component actions satisfy the CP BPL acceptance criteria except for several exterior beam-to-column connections in the RSA- designed frame in the upper floors. As identified previously in §3.2.2.3.1.1, these connection failures are primarily due to reduced m -factors as a result of the FR connection modifiers for panel zone strength and clear span-to-depth limitations. Assessment results for the panel zones all remained small compared to unity—see §3.2.2.1.1.1.

Several exterior frame columns in the RSA-designed frames do not satisfy the CP BPL acceptance criteria using the interaction equation because they are designated as force-controlled for flexure since P_{UF} exceeds $0.5 \times P_{CL}$ —see §3.2.2.2.1 for more discussion.

	0.58	0.46	0.50
0.09	0.09		0.14
	0.73	0.47	0.07
			0.50
0.32	0.09		0.15
	0.50	0.40	0.11
			0.45
0.33	0.13		0.16
	0.51	0.41	0.07
			0.47
0.48	0.13		0.16
	0.49	0.39	0.09
			0.46
0.56	0.14		0.16
	0.52	0.42	0.10
			0.48
0.97	0.15		0.17
	0.57	0.44	0.11
			0.50
0.52	0.15		0.18
	0.58	0.45	0.12
			0.50
0.92	0.15		0.18
	0.68	0.41	0.14
			0.45
0.52	0.14		0.18
	0.69	0.41	0.14
			0.45
0.82	0.14		0.18
	0.59	0.43	0.25
			0.45
0.59	0.12		0.19
	0.61	0.45	0.27
			0.45
0.85	0.12		0.19
	0.66	0.48	0.30
			0.48
0.54	0.10		0.17
	0.65	0.48	0.26
			0.47
0.80	0.10		0.16
	0.65	0.46	0.28
			0.42
0.38	0.06		0.15
	0.56	0.39	0.30
			0.35
0.55	0.04		0.12
			0.39

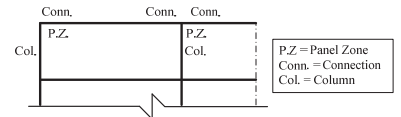
Sym.

(a) DCR_N

	2.91	3.64	3.64
5.48	11.00		11.00
	2.91	4.55	8.00
			4.56
3.02	11.00		11.00
	3.87	4.84	8.00
			4.84
4.55	11.00		11.00
	3.87	4.84	8.00
			4.84
3.19	11.00		11.00
	4.01	5.01	8.00
			5.02
2.65	11.00		11.00
	4.01	5.01	8.00
			5.02
1.00	11.00		11.00
	4.01	5.01	8.00
			5.02
3.22	11.00		11.00
	4.01	5.01	8.00
			5.02
1.00	11.00		11.00
	3.29	5.14	8.00
			5.14
3.14	11.00		11.00
	3.29	5.14	8.00
			5.14
1.00	11.00		11.00
	4.11	5.14	7.78
			5.14
2.28	11.00		11.00
	4.11	5.14	7.41
			5.14
1.00	11.00		11.00
	4.11	5.14	7.05
			5.14
2.72	11.00		11.00
	4.11	5.14	7.59
			5.14
1.00	11.00		11.00
	4.11	5.14	7.31
			5.14
5.15	11.00		11.00
	4.11	5.14	7.04
			5.14
3.83	11.00		11.00
			6.14

Sym.

(b) m -factors



(c) Key

Figure 3-104. LDP Assessment Results, 16-Story SMF ELF, BSE-2 CP

	0.60	0.49	0.53
0.10	0.09		0.15
	0.82	0.53	0.07
0.32	0.11		0.57
	0.11		0.17
0.33	<u>1.02</u>	0.64	0.11
	0.11		0.20
0.49	<u>1.07</u>	0.67	0.14
	0.11		0.21
0.64	0.65	0.52	0.32
	0.17		0.21
1.04	0.65	0.53	0.11
	0.17		0.21
0.56	0.69	0.55	0.12
	0.17		0.22
0.95	0.71	0.56	0.14
	0.17		0.22
0.90	0.64	0.51	0.26
	0.17		0.21
0.99	0.64	0.51	0.24
	0.17		0.20
0.94	0.84	0.52	0.27
	0.16		0.20
1.09	0.83	0.51	0.30
	0.15		0.20
0.91	0.74	0.46	0.33
	0.14		0.17
0.99	0.71	0.44	0.26
	0.13		0.15
0.77	0.58	0.43	0.28
	0.09		0.14
1.31	0.51	0.38	0.30
	0.07		0.12
			0.41

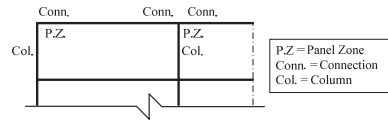
Sym.

(a) DCR_N

	2.91	3.64	3.64
5.48	11.00	11.00	11.00
	2.91	4.55	8.00
3.00	11.00	11.00	4.56
	11.00	11.00	8.00
4.66	2.91	4.55	8.00
	11.00	11.00	4.56
3.45	11.00	11.00	8.00
	3.87	4.84	6.02
1.97	11.00	11.00	4.84
	11.00	11.00	8.00
1.00	3.87	4.84	4.84
	11.00	11.00	8.00
2.62	11.00	11.00	8.00
	3.87	4.84	4.84
1.00	11.00	11.00	7.74
	4.01	5.01	5.02
1.00	11.00	11.00	5.02
	4.01	5.01	7.96
1.00	11.00	11.00	5.02
	11.00	11.00	7.47
1.00	3.21	5.01	5.02
	11.00	11.00	7.02
1.00	3.21	5.01	5.02
	11.00	11.00	6.58
1.00	3.29	5.14	5.14
	11.00	11.00	7.52
1.00	3.29	5.14	5.14
	11.00	11.00	7.18
1.00	4.11	5.14	5.14
	11.00	11.00	6.88
1.00	4.11	5.14	5.14
	11.00	11.00	5.94
1.00	11.00	11.00	5.94

Sym.

(b) m -factors



(c) Key

Figure 3-105. LDP Assessment Results, 16-Story SMF RSA, BSE-2 CP

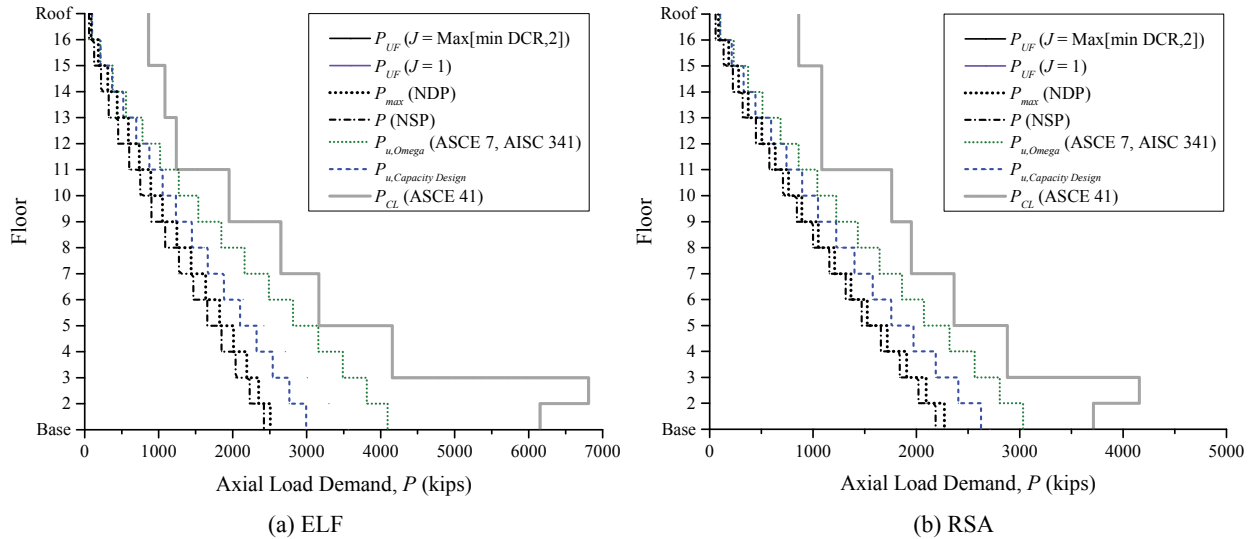


Figure 3-106. LDP Assessment Results, Compression in Exterior Columns, 16-Story SMF, BSE-2

3.2.2.3.3 Nonlinear Static Procedure

In this section, the following apply:

- Table 3-19 through Table 3-21 provide the computed NSP analysis and assessment parameters in accordance with ASCE 41 §3.3.3.
- Figure 3-107 and Figure 3-108 illustrate the monotonic pushover curves for the ELF- and RSA-designed frames, respectively, and the associated pushover parameters from ASCE 41 at the BSE-2 EHL. Roof displacement is measured at the Center of Mass (CoM). A significant change in base shear is due to component strength loss (e.g., plastic hinges), notated in the figures. The softening of the pushover curve evident at about 30 inches of roof displacement for each frame is due to column hinges developing at the base of the frames. First-order and second-order responses, shown in these figures, aids in computing a physically meaningful value for $\alpha_{p-\Delta}$ used in ASCE 41 Equation 3-17.
- Figure 3-109 and Figure 3-110 illustrate the story drift ratios in terms of the roof drift ratio.

As discussed in §3.1.3.2.1, the NSP is permitted, but requires supplemental verification using the LDP—see §3.2.2.3.2. In this case, the target displacement governs Δ_d for the ELF-designed frame for both BSE-1 and BSE-2 and the RSA-designed frame for BSE-1, whereas the displacement at the maximum base shear governs the RSA-designed frame for BSE-2. The change in Δ_d between BSE-1 and BSE-2 adds complexity to NSP process by changing the pushover variables. Further, when Δ_d is governed by the target displacement, the system can show decreased values for R_{max} between BSE-1 and BSE-2. Axial compression force in the exterior columns at the target displacement are shown previously in the linear assessment sections. Results indicate that the NSP generally results in a lower estimate of the axial force demands compared to the other methods used in this study. This is partly because of the fundamental mode-based lateral force distribution not capturing higher mode effects. Also, the target displacement at the roof computed based on fundamental mode properties may underestimate the story demands in the upper stories.

Table 3-19. NSP General Information, 16-Story SMF (kip, inch)

Design	T_1	K_1	Δ_y	V_y	K_e	T_e	h	Δ_{peak}	V_{peak}	W	C_m	C_D
ELF	4.12	64.0	24.6	1571	63.8	4.13	1.21	62.3	1617.0	21782	1.00	1.29
RSA	4.67	45.5	25.8	1177	45.6	4.66	1.23	41.1	1203.6	21649	1.00	1.36

Table 3-20. NSP Analysis Parameters, 16-Story SMF BSE-2 CP (kip, inch)

Design	S_a	R	C_1	C_2	Δ_t	V_t	Δ_d	α_1	α_2	$\alpha_{P-\Delta}$	α_e	R_{max}	$R \leq R_{max}$
ELF	0.22	3.04	1.00	1.00	47.4	1617.0	47.4	0.03	-0.45	0.00	-0.09	6.58	OK
RSA	0.20	3.60	1.00	1.00	56.7	1196.3	41.1	0.04	-0.34	-0.02	-0.08	7.09	OK

Table 3-21. NSP Analysis Parameters, 16-Story SMF BSE-1 LS (kip, inch)

Design	S_a	R	C_1	C_2	Δ_t	V_t	Δ_d	α_1	α_2	$\alpha_{P-\Delta}$	α_e	R_{max}	$R \leq R_{max}$
ELF	0.15	2.03	1.00	1.00	31.6	1581.9	31.6	0.02	-0.25	0.00	-0.05	10.53	OK
RSA	0.13	2.40	1.00	1.00	37.8	1202.9	37.8	0.05	-0.31	-0.02	-0.07	7.54	OK

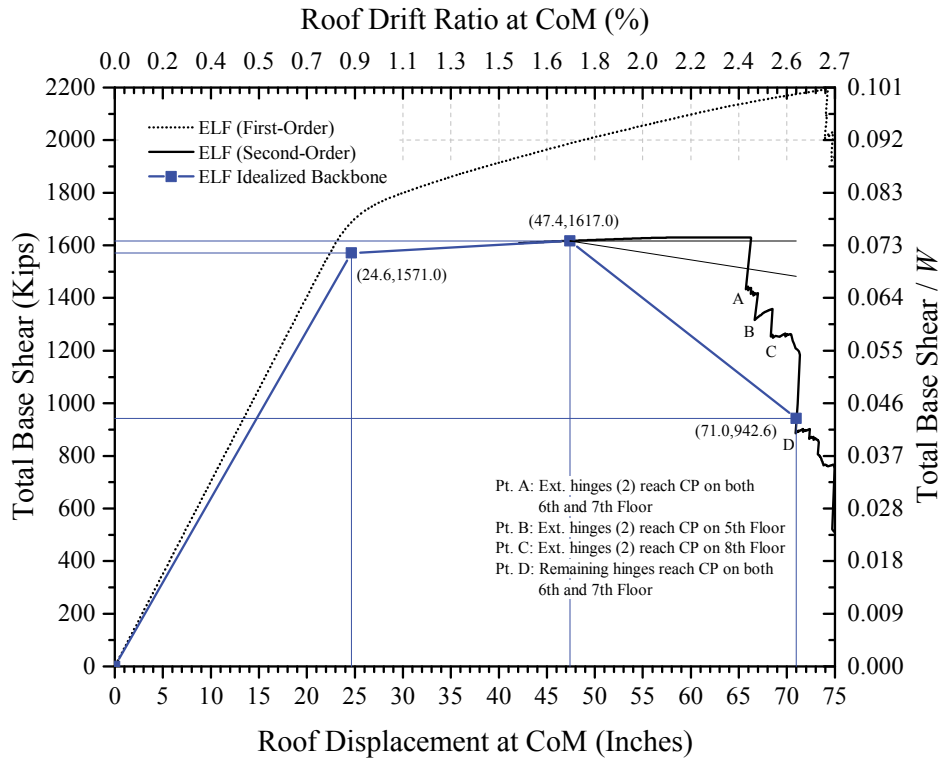


Figure 3-107. 16-Story SMF ELF Pushover, BSE-2

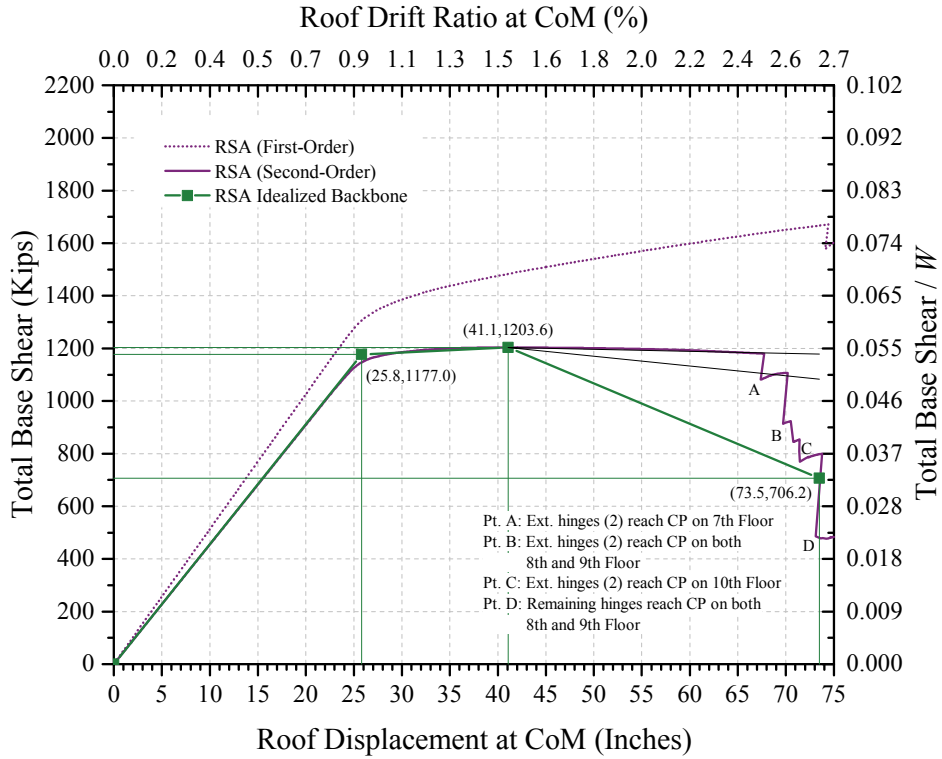


Figure 3-108. 16-Story SMF RSA Pushover, BSE-2

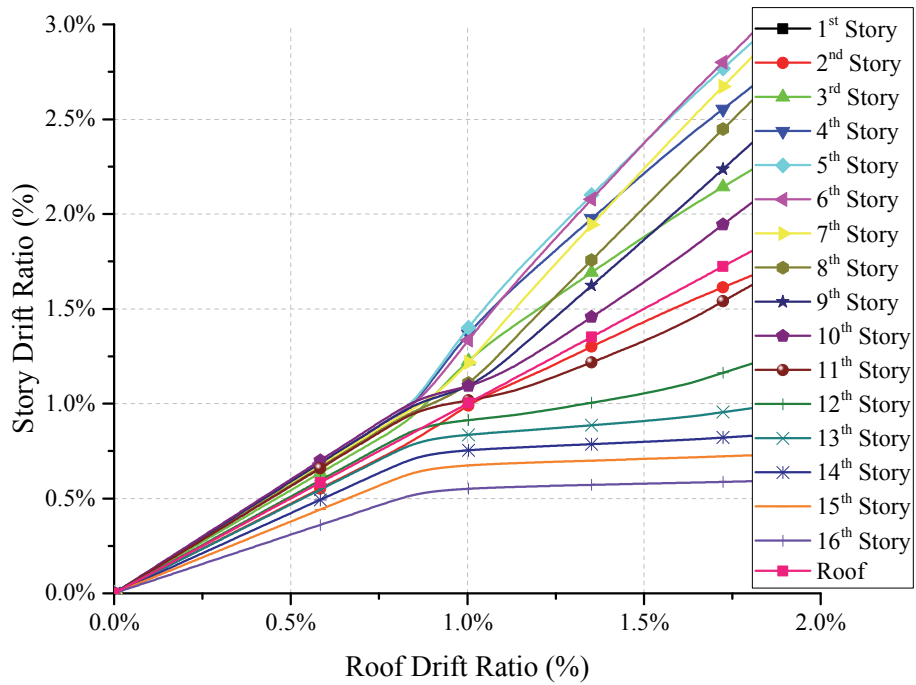


Figure 3-109. 16-Story SMF ELF Pushover – Story Drift Ratios – BSE-2

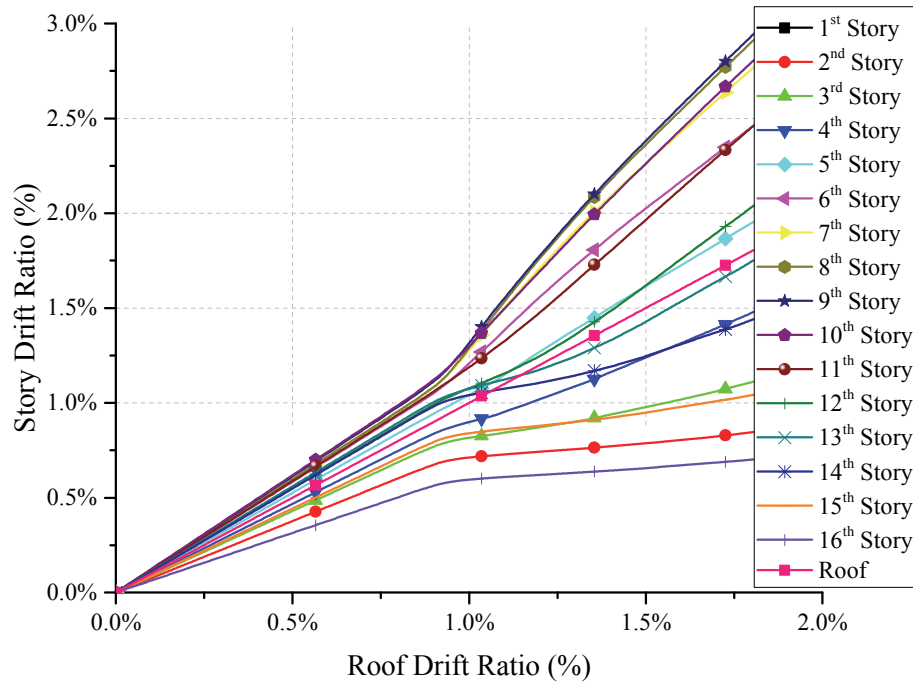


Figure 3-110. 16-Story SMF RSA Pushover – Story Drift Ratios – BSE-2

Of particular interest in the pushover curves is the large disparity between the peak base shears developed in the ELF- and RSA-designed buildings ($RSA / ELF = 1204 / 1617 = 0.74$), a 26 percent change. At first glance, this is greater than the 15 percent difference in design base shears allowed by ASCE 7. Upon further inspection, it can be reasoned that the primary contribution to this disparity is due to the increase in strength provided to the ELF-designed frame to satisfy drift provisions in ASCE 7 (i.e., 15 percent plus additional strength). See NSP discussion in the 8-story results for more information.

Figure 3-111 illustrates which frame columns are force-controlled for flexure for both the NSP and NDP; red circles indicate anticipated plastic hinge locations that are force-controlled for flexure at the target displacement. As shown in the figure, the force-controlled columns do not align between the two frames—the axial load ratios for the exterior base columns are 0.39 and 0.59 for the ELF- and RSA-designed frames, respectively. This illustrates the sensitivity of results due to variations between the non-adaptive loading profile in the NSP and that used for design. Figure 3-112 through Figure 3-115 illustrate the DCR_N values if greater than unity for the ELF- and RSA-designed frames at the target displacement for the LS BPL at the BSE-1 EHL and CP BPL at the BSE-2 EHL. These figures illustrate the demands when the system is loaded to the right. All component actions for the beam-to-column connections, columns (assuming deformation-controlled), and panel zones satisfy the LS and CP BPL acceptance criteria at the target displacements for both designs.

Several exterior columns, including those at the base of the frame for the RSA-designed frame, are force-controlled for flexure at the target displacement. Force-controlled base columns are problematic for a region that is expected to experience inelastic strain demands. Therefore, the acceptance criterion for these flexural actions is based on the force-controlled lower-bound elastic $P-M$ interaction (ASCE 41 Equation 5-12). As discussed previously, variations in $P-M$ interaction curves add complexity to nonlinear flexural hinge

model. Essentially, a nonlinear hinge based on the expected yield surface of the section must be accompanied by another model that can measure the lower-bound strength of the member (one for each axis of buckling). For simplicity, failing of the acceptance criteria (without computing interaction values) is self-evident because of the development of plastic hinges in the frame columns. Because plastic hinges have developed in the base columns in the ELF-design frame, flexural actions therefore do not satisfy the intended elastic acceptance criteria. Conversely, the force-controlled columns in the RSA frame satisfy the intended elastic acceptance criteria; however, member stability would still need to be verified.

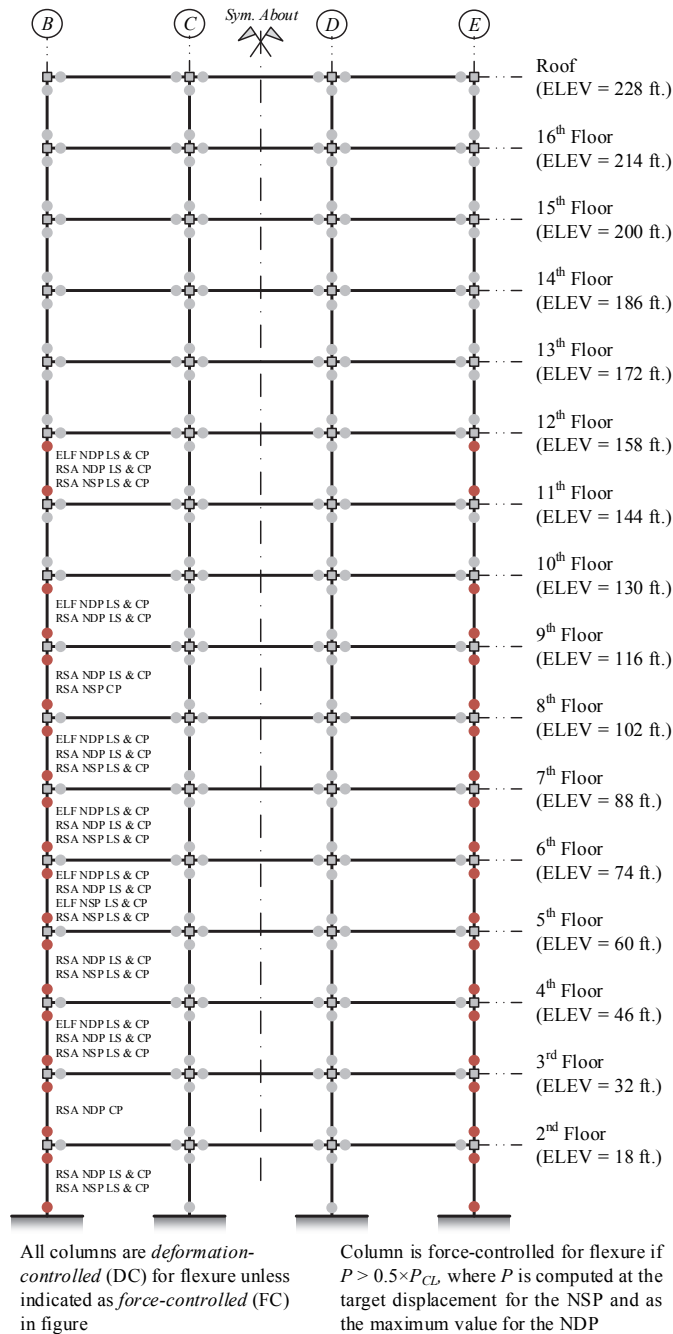


Figure 3-111. Schematic of Flexural Actions in Columns, 16-Story SMF (NSP and NDP)

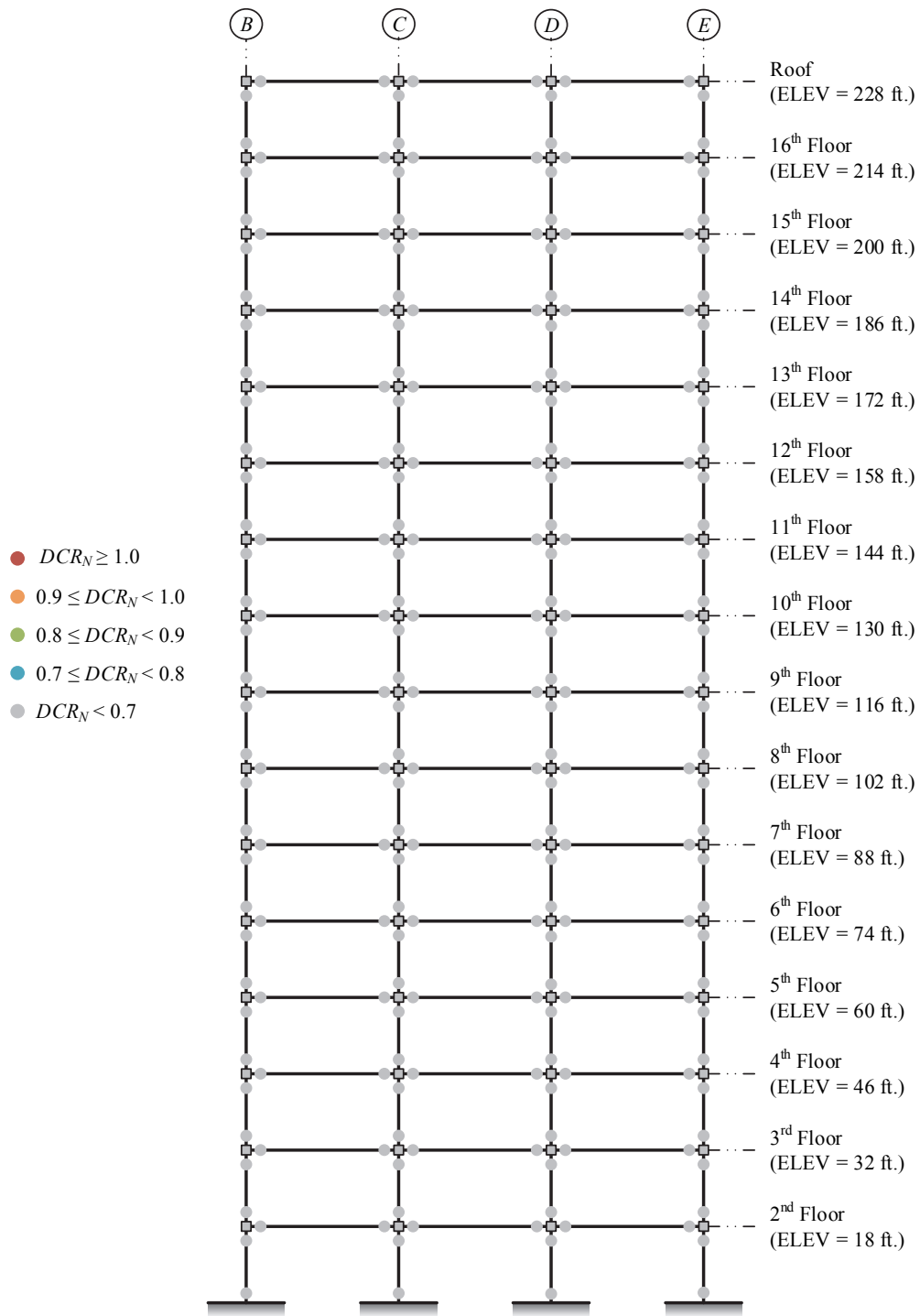


Figure 3-112. NSP Assessment Results, 16-Story SMF ELF, BSE-1 LS (+push to right)

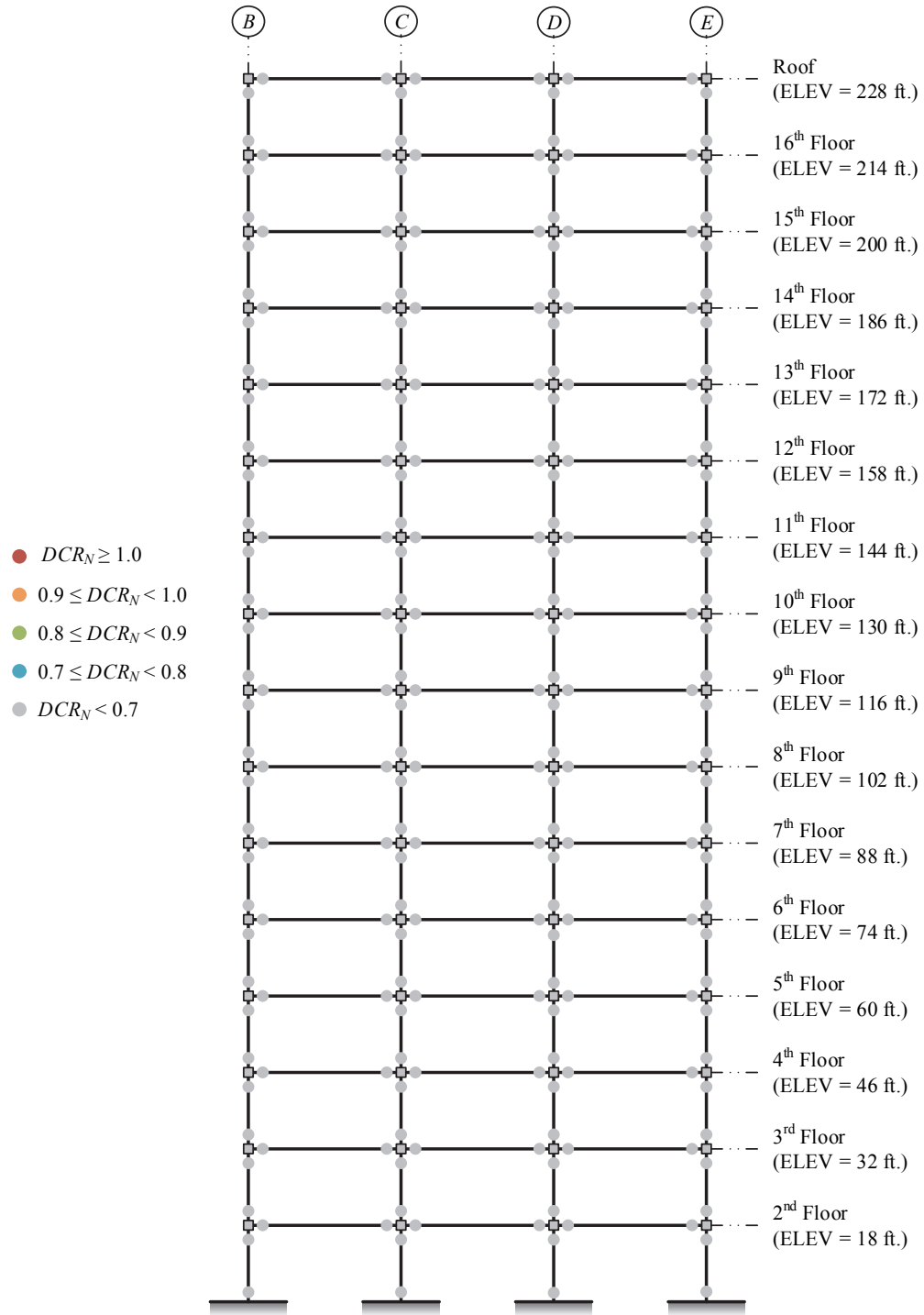


Figure 3-113. NSP Assessment Results, 16-Story SMF RSA, BSE-1 LS (+push to right)

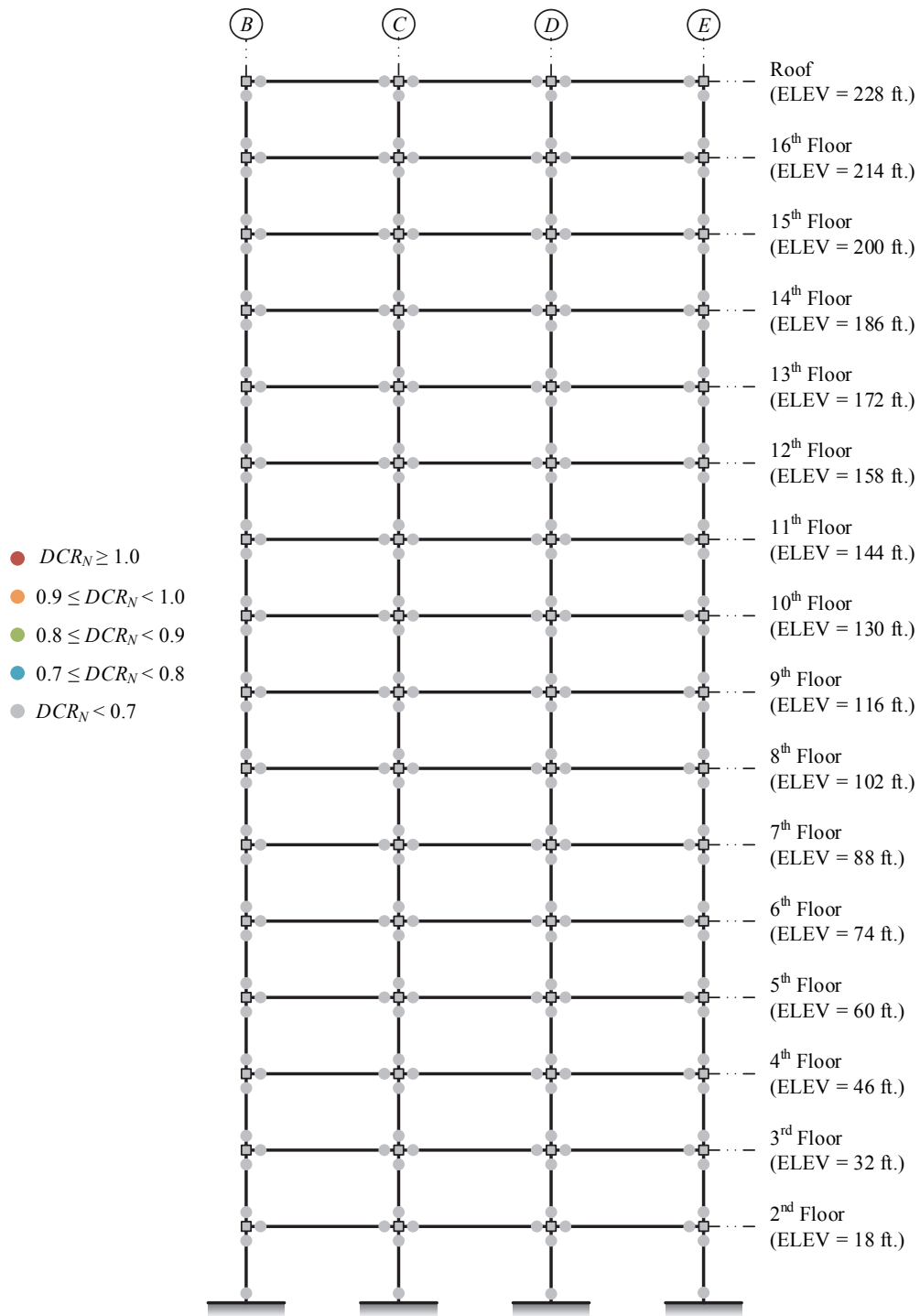


Figure 3-114. NSP Assessment Results, 16-Story SMF ELF, BSE-2 CP (+push to right)

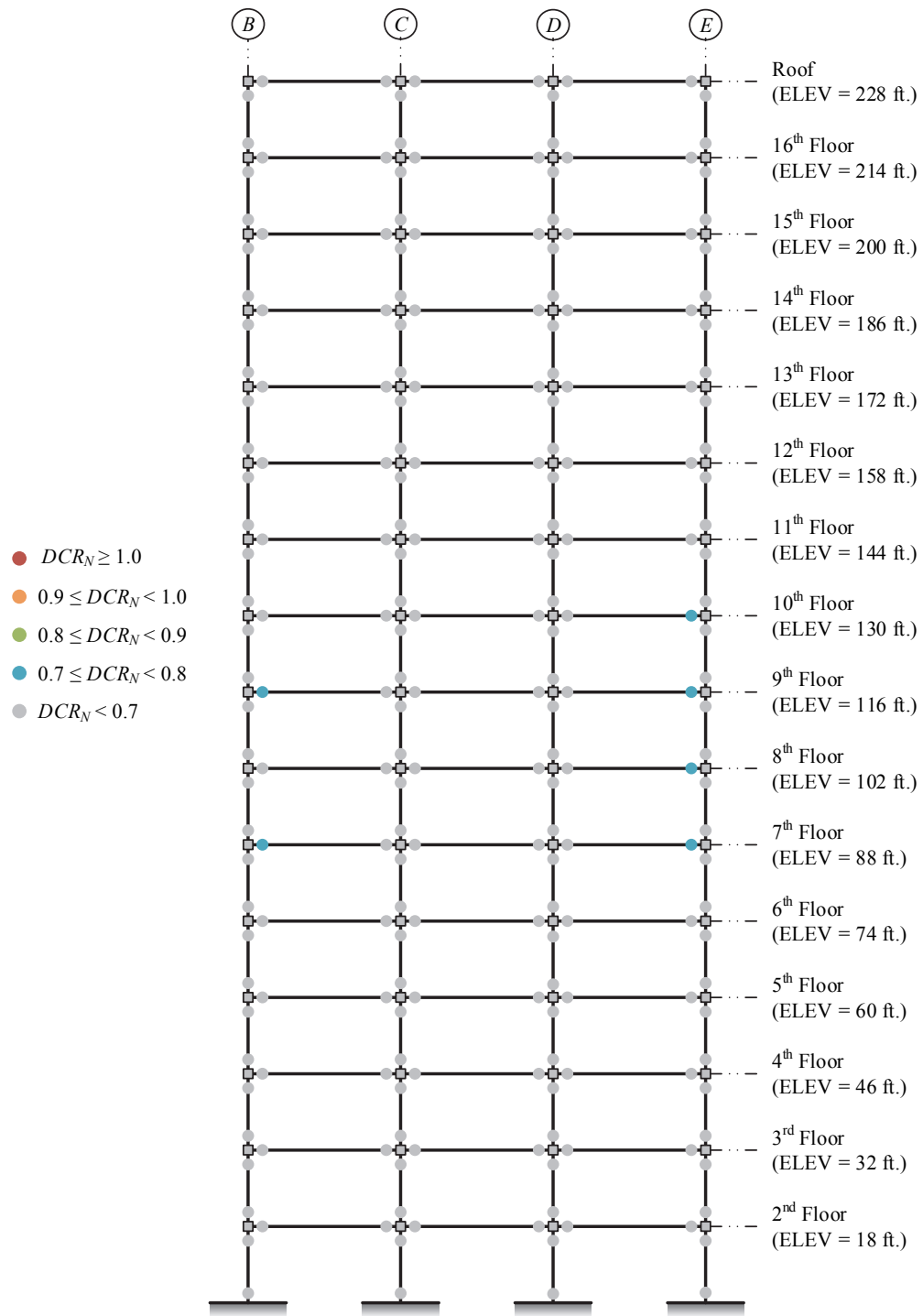


Figure 3-115. NSP Assessment Results, 16-Story SMF RSA, BSE-2 CP (+push to right)

3.2.2.3.4 Nonlinear Dynamic Procedure

The earthquake record set used to assess the E-W direction of MC16 is shown in Appendix A. For the ELF design, the analysis successfully completed for all 14 records at the BSE-1 and BSE-2 EHL. For the RSA design, the analysis successfully completed for all 14 records for the BSE-1 EHL; however, four analyses did not complete at the BSE-2 EHL because of excessive lateral drift or solution non-convergence. Maximum axial compression force in the exterior column lines from the record set are shown previously in the linear assessment sections.

Figure 3-116 through Figure 3-119 show the performance of the beam hinges (i.e., beam-to-column connections) at the BSE-1 (LS BPL) and BSE-2 (CP BPL) for the ELF- and RSA-designed frames, respectively. The results from the LSP, LDP, and NSP (loaded to the right) are included in the figures. Comparison discussions between the various procedures are addressed subsequently. As is evident from the figures, the ELF-designed frame performs better than the RSA-designed frame; however, recall that the ELF procedure is not permitted in this case. Results of the RSA-designed frame indicate that the beam-to-column connections have difficulty satisfying the CP BPL acceptance criteria at the BSE-2 EHL (based on mean response). In contrast to the mean response, the median response indicates better performance because it is less influenced by large deformations resulting from component strength loss potentially resulting in collapse of the system. Consequently, the median is potentially a more stable performance metric when analyzing a large number of ground motion records, but should be restrained relative to a mean value.

The average ratio of secondary to primary component acceptance criteria for an RBS beam-to-column connection for all W18 sections and deeper is 1.49 for the CP SPL (1.47 for the LS SPL). The figures for the RSA-designed frame illustrate that this value is exceeded in the beam-to-column connections at the BSE-2 EHL. This highlights the rapid progression towards a collapse state when several components are strained past the deformation associated with their peak strength—see §3.1.4.2.

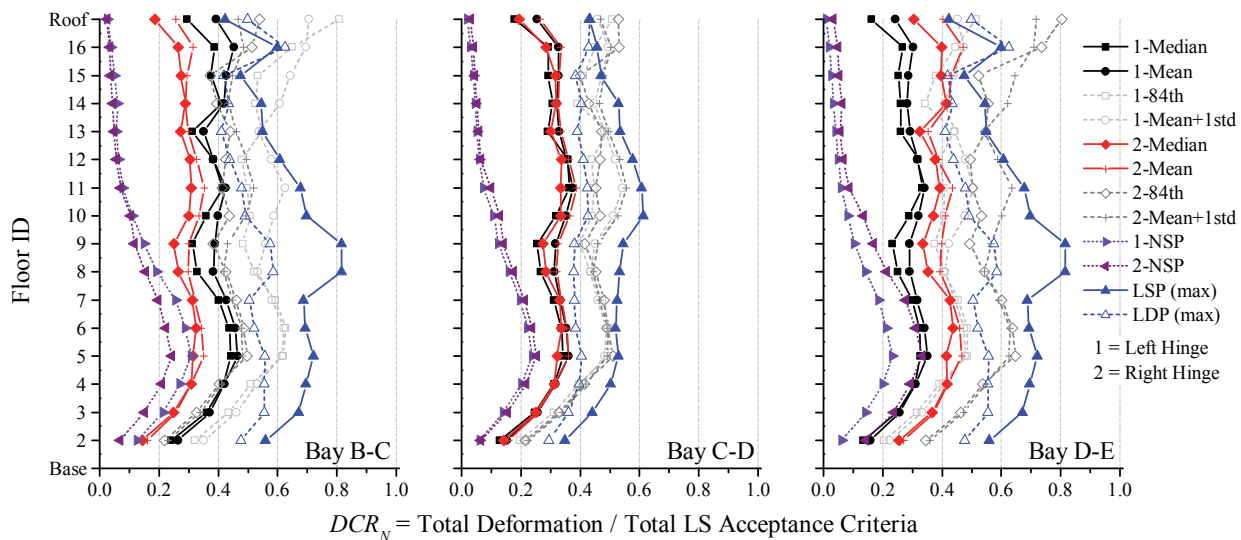


Figure 3-116. NDP Assessment Results, Beam Hinges, 16-Story SMF ELF, BSE-1 LS

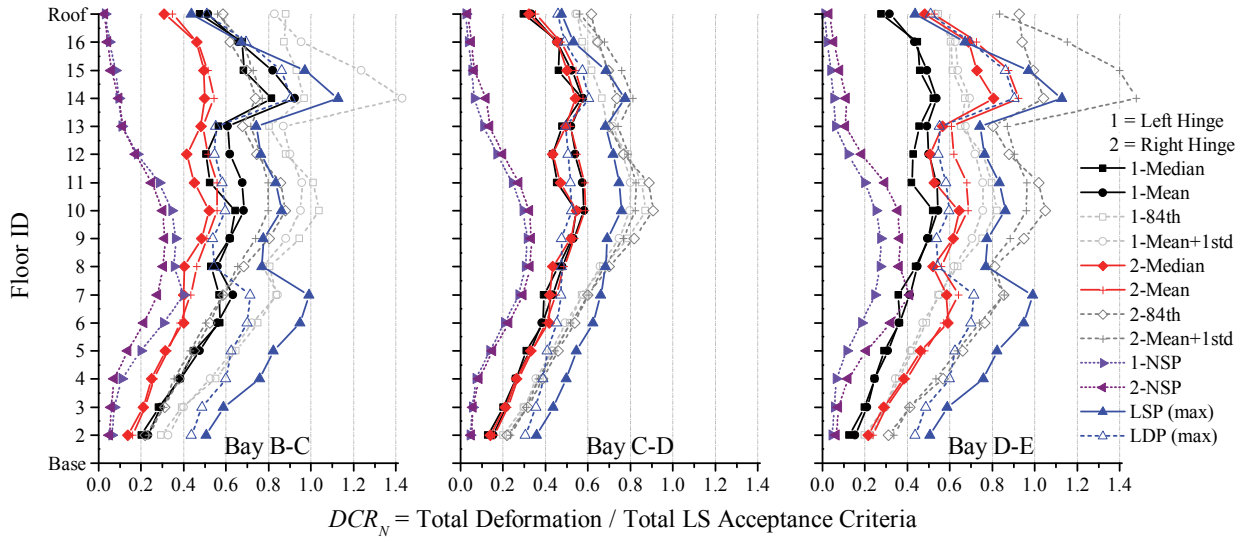


Figure 3-117. NDP Assessment Results, Beam Hinges, 16-Story SMF RSA, BSE-1 LS

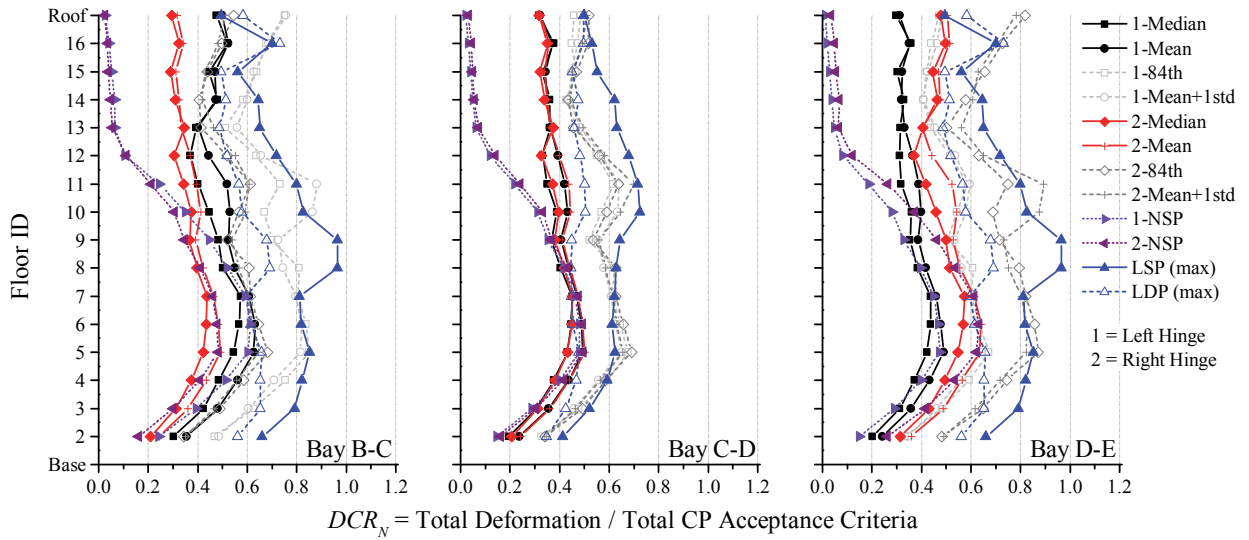


Figure 3-118. NDP Assessment Results, Beam Hinges, 16-Story SMF ELF, BSE-2 CP

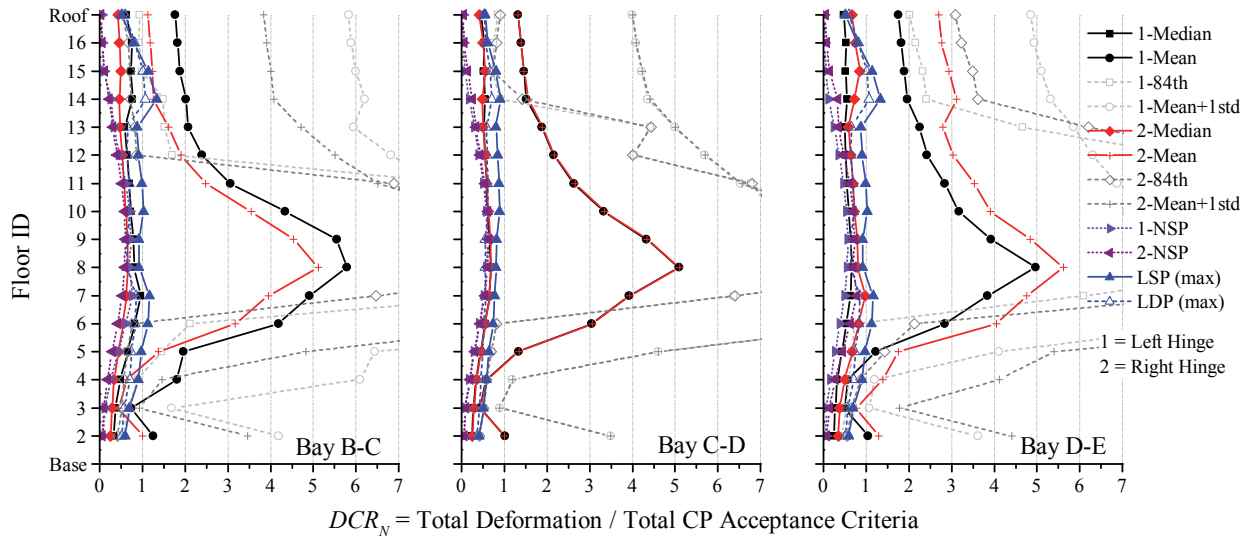


Figure 3-119. NDP Assessment Results, Beam Hinges, 16-Story SMF RSA, BSE-2 CP

The previous figures illustrate for the RSA-designed frame that the component strengths provided by drift and stability control measures in ASCE 7 at $\frac{2}{3} \times MCE_R$ (equal to the BSE-1 here) are not significant enough to overcome the demands to satisfy the assessment criteria at the BSE-2 (taken here as MCE_R). First, strong panel zones reduce the allowable deformations in the acceptance criteria and component model for the exterior beam-to-column connections. Second, base hinge modeling could have a drastic effect on the performance of the beam-to-column connections. This further highlights the change in story demands as column base hinges develop, an influence not addressed in elastic design analysis. In contrast, the results indicate that the ELF-designed frame satisfies the criteria by a considerable margin.

Figure 3-111 (see NSP section) illustrates which flexural actions in the frame columns are force-controlled for both the NSP and NDP. Figure 3-120 and Figure 3-121 show the performance of the column hinges for the CP BPL criteria at the BSE-2 EHL assuming deformation-controlled flexural actions (LS BPL for the BSE-1 is not shown unless assessment at BSE-2 illustrates performance concerns). Column hinges at the base experience inelastic strain demands (yield corresponds to a $DCR_N \approx 0.15$ in the figures). Mean response results also indicate column hinges develop up the height of the frame. However, this phenomenon is more likely associated to the number of collapses rather than a trigger mechanism initiating a structural collapse; median results may be a more stable metric in this case. Similarly, the exterior base columns in the RSA frame are force-controlled for flexure. The DCR_N results for the LSP and LDP are based on an interaction equation and not from $M_{UD} / m \times M_{CE}$, or M_{UF} / M_{CL} , which would be a more physically consistent metric for comparison against the results from the nonlinear assessment procedures. Nonetheless, the linear results are generally not applicable here because most columns are force-controlled for flexure in the linear assessment procedures. Though there is a fundamental difference in how the DCR_N is computed for the linear and nonlinear procedures, the linear assessment results show similar distributions of demands and location of potential performance concerns.

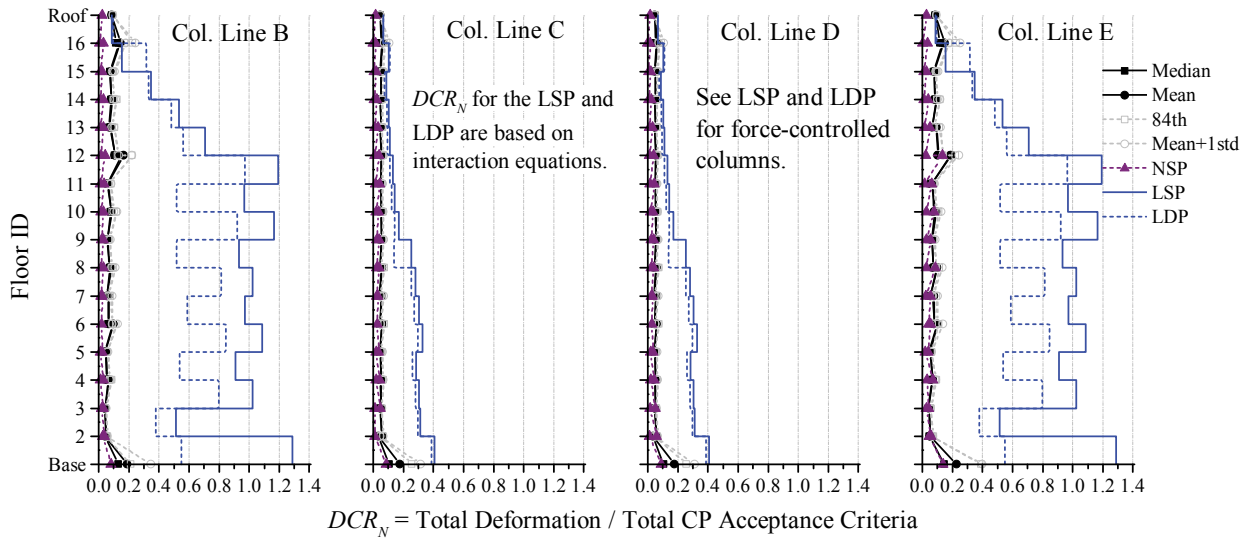


Figure 3-120. NDP Assessment Results, Column Hinges, 16-Story SMF ELF, BSE-2 CP

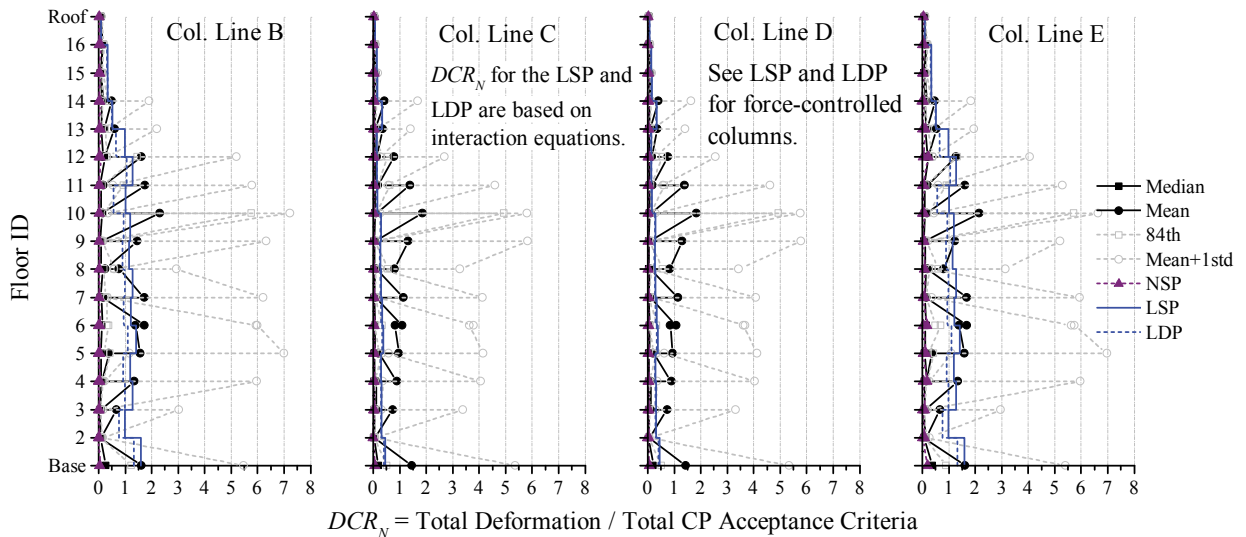


Figure 3-121. NDP Assessment Results, Column Hinges, 16-Story SMF RSA, BSE-2 CP

Figure 3-122 and Figure 3-123 show the curvature ductility demand of the column hinges (i.e., section strength) at the BSE-2 EHL. Figure 3-124 and Figure 3-125 show the elastic member strength interaction results at the BSE-2 EHL. The results indicate that the columns above the base in the ELF-designed frame satisfy the intended lower-bound acceptance criteria whereas the columns in the RSA-designed frame consistently do not satisfy these acceptance criteria—a result of the number of analyses that did not complete.

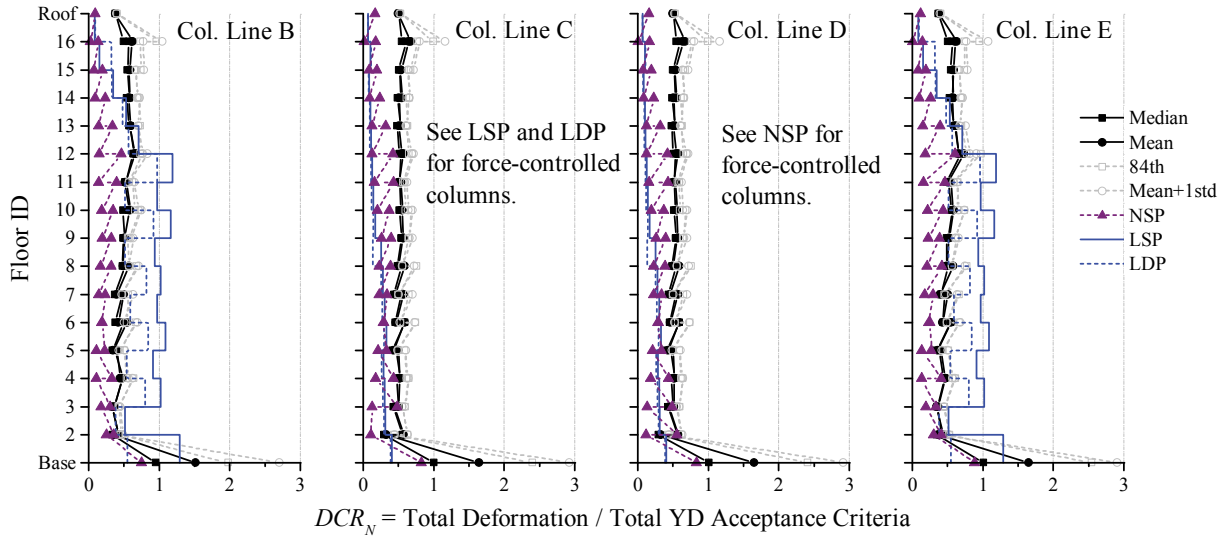


Figure 3-122. NDP Assessment Results, Column Hinges, 16-Story SMF ELF, BSE-2 Yield

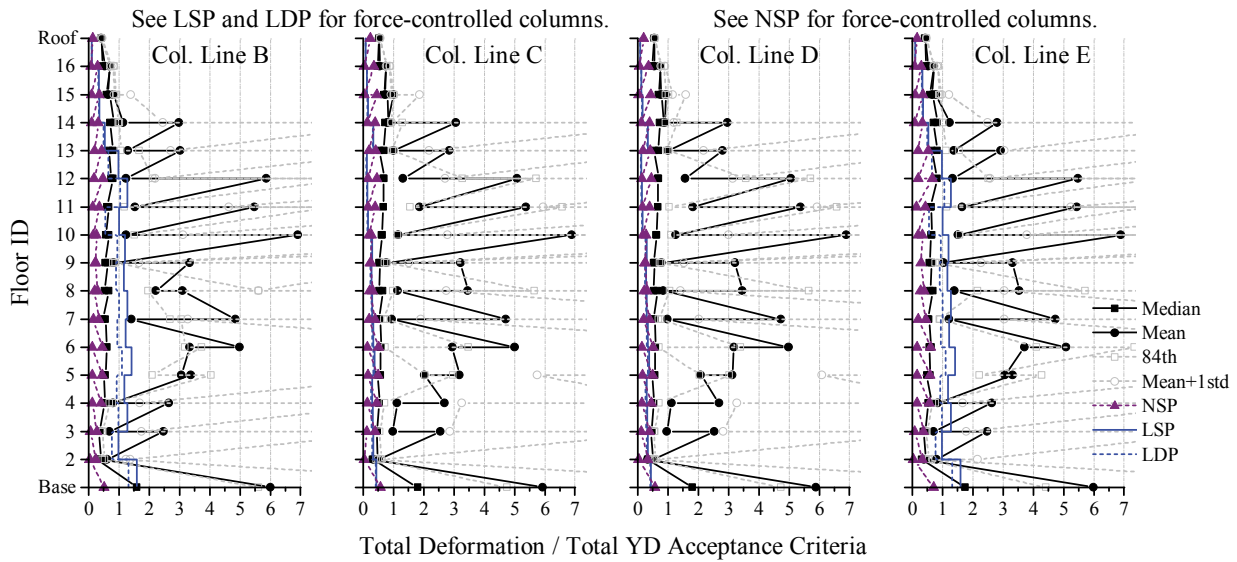


Figure 3-123. NDP Assessment Results, Column Hinges, 16-Story SMF RSA, BSE-2 Yield

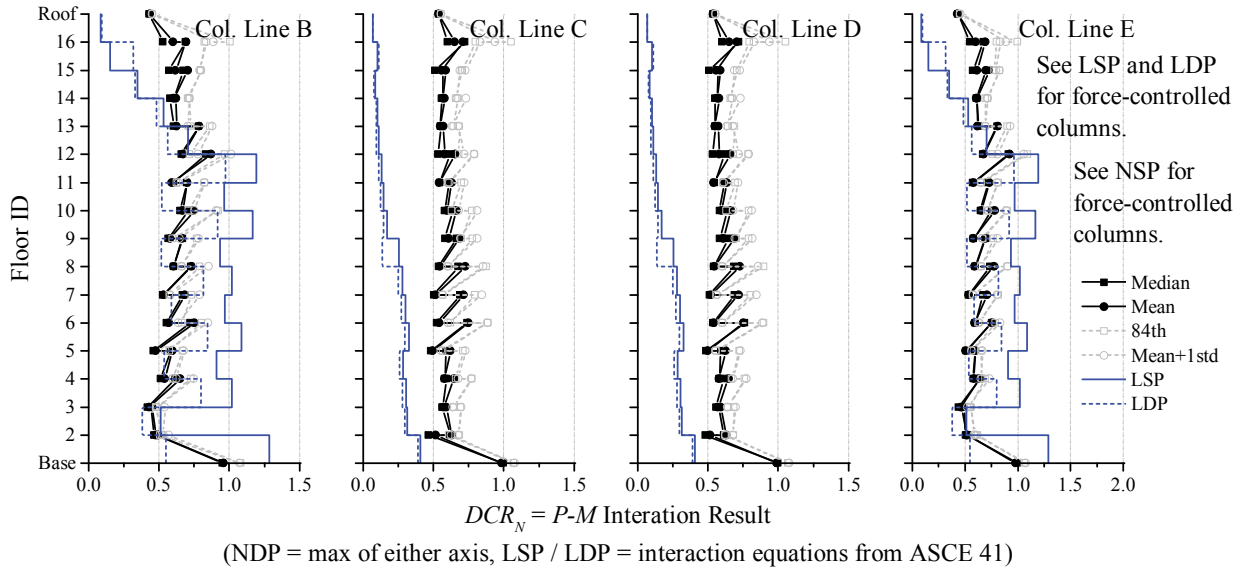


Figure 3-124. NDP Assessment Results, Column Members, 16-Story SMF ELF, BSE-2 CP

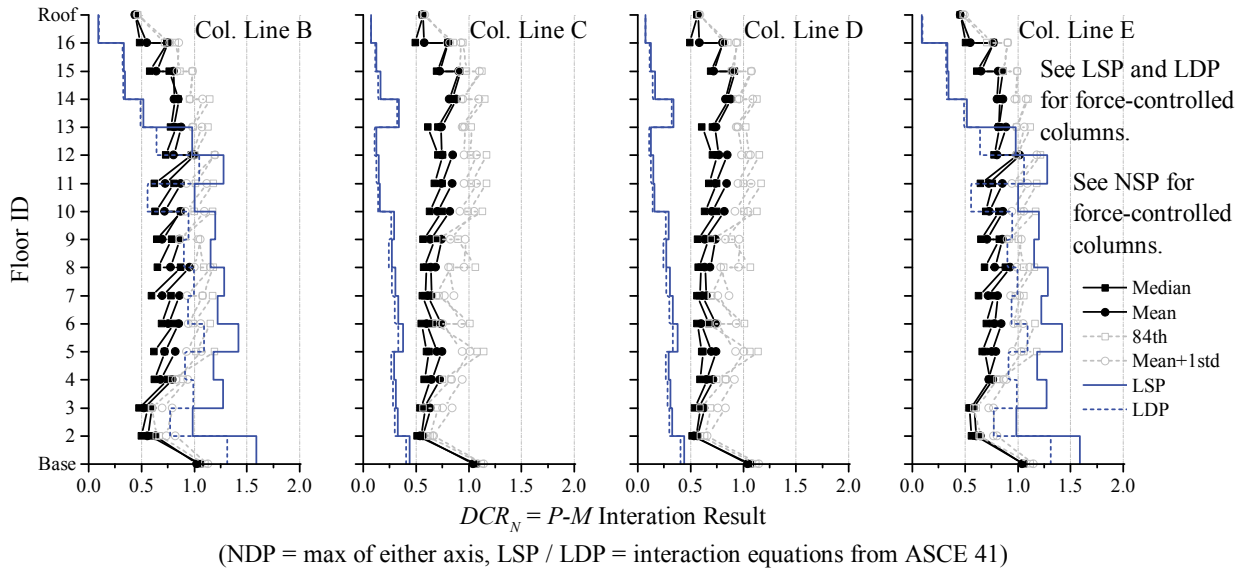


Figure 3-125. NDP Assessment Results, Column Members, 16-Story SMF RSA, BSE-2 CP

Figure 3-126 and Figure 3-127 show the performance of the panel zones for the CP BPL criteria at the BSE-2 (LS BPL for the BSE-1 is not shown). The deformation demands are significantly lower than the CP acceptance criteria. Converting the results to total deformation / yield deformation indicates that the demands for the BSE-2 are consistently less than $4 \times \gamma_y$. These results illustrate that the panel zones are stronger than required by the assessment criteria—see discussion in the 4-story NDP section.

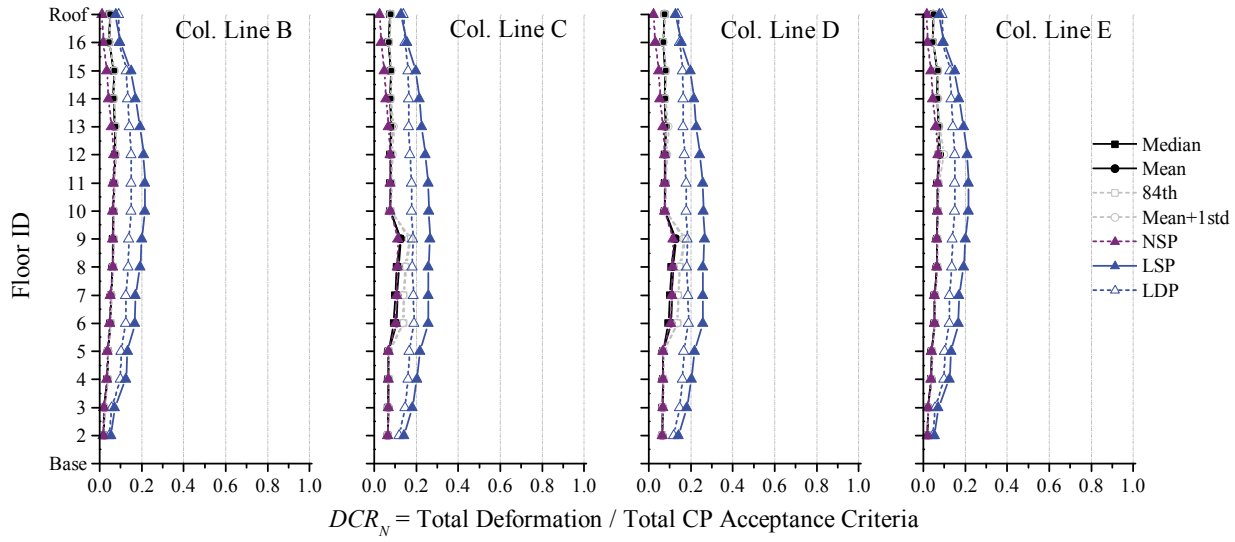


Figure 3-126. NDP Assessment Results, Panel Zones, 16-Story SMF ELF, BSE-2 CP

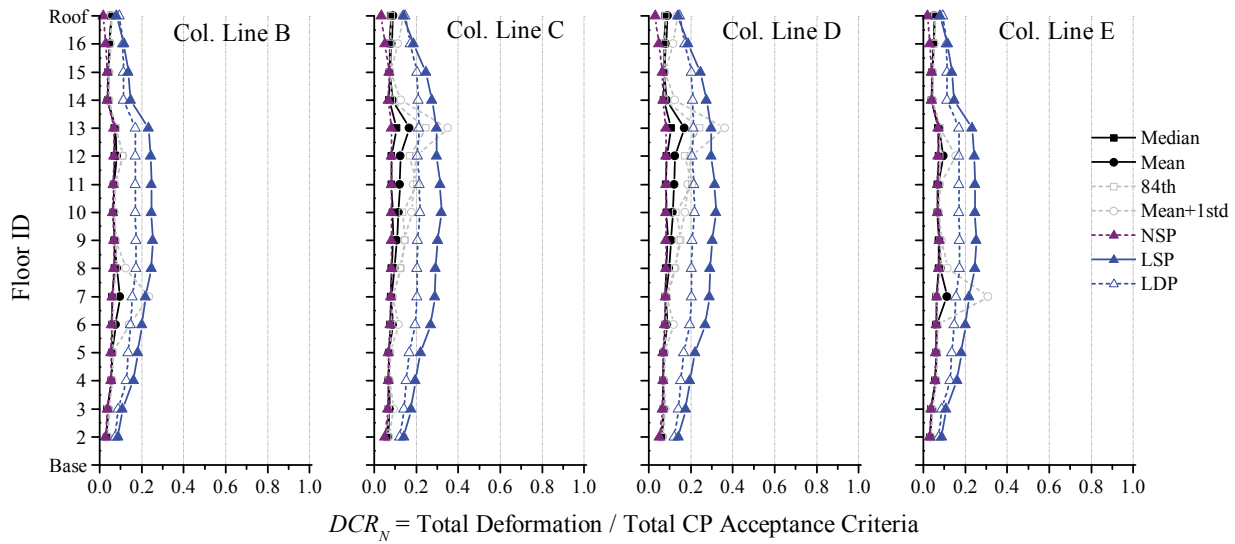


Figure 3-127. NDP Assessment Results, Panel Zones, 16-Story SMF RSA, BSE-2 CP

3.2.3 Seismic Assessment Discussion

The discussion in this section focuses on the following component design actions:

- Beam-to-column connection flexure (e.g., RBS)
- Panel zone shear
- Beam and column flexure within anticipated plastic hinge zones (section strength)²³
- Column axial-moment interaction strength (e.g., member strength)

ASCE 41 requires all frame components that do not satisfy the acceptance criteria to be retrofitted or replaced, even if only a small percentage of the total components fail the criteria (see ASCE 41 §5.4.2.5). Therefore, a building can only satisfy a selected BPL when all structural components satisfy the corresponding SPL. Building behavior is rarely governed by the response of a single component, with the one notable exception being collapse resulting from failure of a column. It can be argued that a shortcoming of ASCE 41 is the focus on component performance to ensure that all elements pass the evaluation, when failures of individual elements may not lead to catastrophic failure.

Design choices, constructability considerations, code requirements, nonseismic loads, analytical modeling assumptions, and other project specific requirements may add strength to critical components in a frame. Further, allocation of component strengths within the frame because of the lateral force distribution adopted in design can cause deviations of the component strengths from one story to another. Thus, capturing all possible permutations, in essence, would create an infinitely large design space. Nonetheless, the change in component strengths can significantly influence the DCR_N values obtained from the ASCE 41 assessments.

3.2.3.1 Linear Assessment Procedures

The following discusses the analytical results for the noted components from the linear procedures for each archetype building.

As noted previously, the LSP cannot be used to assess the E-W component of MC16. This assessment is included for comparison purposes and the results are shown as shaded in the tables in this section.

3.2.3.1.1 Beam-to-Column Connections

Table 3-22 provides a summary of the performance of the FR beam-to-column connections (RBS) for each linear assessment procedure and each BPL. The number listed in parentheses denotes the number of failed components in the frame—shown as bolded text. Also shown in the table is the percentage of failed components compared to the total number of similar components. The results indicate that the RSA-designed frame has difficulty satisfying the acceptance criteria when using the LSP for both the LS and CP BPL whereas only the 4-story ELF-designed frame fails the CP BPL. In contrast, the performance of both

²³ Beam hinges within the RBS are included in assessment of Type FR connection (controlling mechanism).

frames improves when using the LDP, although the 4- and 16-story RSA-designed frames fail the CP BPL acceptance criteria by a slight margin.

Table 3-22. Performance Summary of FR Connections (BC) per Frame, Linear Procedures

Archetype	Design	LSP		LDP	
		LS	CP	LS	CP
4-Story	ELF	All BC Pass	Ext. BC Fail (2) Int. BC Fail (2) 17%	All BC Pass	All BC Pass
	RSA	Ext. BC Fail (4) Int. BC Pass 17%	Ext. BC Fail (4) Int. BC Fail (2) 25%	All BC Pass	Ext. BC Fail (2) Int. BC Pass 8%
8-Story	ELF	All BC Pass	All BC Pass	All BC Pass	All BC Pass
	RSA	Ext. BC Fail (8) Int. BC Pass 17%	Ext. BC Fail (14) Int. BC Fail (14) 58%	All BC Pass	All BC Pass
16-Story	ELF	All BC Pass	All BC Pass	All BC Pass	All BC Pass
	RSA	Ext. BC Fail (2) Int. BC Pass 2%	Ext. BC Fail (10) Int. BC Pass 10%	All BC Pass	Ext. BC Fail (4) Int. BC Pass 4%

Performance failures are generally increased by reduced acceptance criteria (i.e., m -factors) attributed to panel zones strength, connection detailing, and span-to-depth ratio, L_c / d_b . Section compactness requirements in ASCE 41 match that required for design of highly ductile elements in AISC 341—except ASCE 41 uses *expected* in lieu of *nominal* material properties. As such, section compactness *generally* will not trigger a reduction in new building designs. However, continuity plates in one-sided connections designed in accordance with AISC 341 and AISC 360 can trigger a reduction if $t_{cp} < b_{bf} / 7$ with $t_{cp} \geq t_{bf} / 2$, but also $t_{cp} < t_{bf}$. Further, AISC 358 requires that $L_c / d_b \geq 7$ for an RBS beam-to-column connection in an SMF, but ASCE 41 requires a reduction in acceptance criteria when $L_c / d_b > 10$. Additionally, increasing column sizes to offset the need for doubler plates can be problematic with regards to connection performance (assuming adjacent beams are not similarly increased). Nonetheless, it is debatable if reduction factors based on (cumulative) step functions are appropriate for components expected to experience inelastic straining. Further research is needed to justify the fixed reductions to acceptance criteria for beam-to-column connections. The commentary for ASCE 41 should reference FEMA 355D (FEMA 2000c) in lieu of FEMA 355F (FEMA 2000d) for connection detailing recommendations.

The results for the 16-story archetype buildings indicate that drift and strength control (via stability verification) in ASCE 7 provides a significant amount of member overstrength so that beam-to-column connections more easily satisfy the acceptance criteria (compared to the 8-story which was primarily drift controlled).

The easiest retrofit option for these frames is to increase the flexural strength (and hinge strength in the beam) of the distressed connections so to offset any reductions due to panel zone strength and continuity plates (see Rehabilitation Strategies in ASCE 41 §2.5). However, this may adversely affect the performance of other components of the frame (e.g., columns). In terms of ASCE 41 assessment performance, using

doubler plates in lieu of upsizing the columns and keeping the beam span-to-depth ratio less than 10 (but greater than 7 if using linear procedures or 8 if using nonlinear procedures) may be more effective. Additional cost-benefit analyses are needed to validate the seismic performance of an SMF with these constraints (assuming performance metrics and analysis are reflective of realistic conditions).

3.2.3.1.2 Panel Zones

Table 3-23 provides a summary of the performance of the panel zones for each linear assessment procedure and each BPL. The results indicate that the panel zones consistently satisfy the performance criteria for the LS and CP BPL for both procedures. The DCR_N values all remained low, 0.1–0.3, indicating that panel zone design based on the probable connection strength, M_{pr} , as well as conventional practice (e.g., increase column sizes to offset the need for doubler plates) may tend toward producing strong panel zones under ASCE 41. As noted above, this can adversely affect the beam-to-column connection acceptance criteria.

Table 3-23. Performance Summary of Panel Zones (PZ) per Frame, Linear Procedures

Archetype	Design	LSP		LDP	
		LS	CP	LS	CP
4-Story	ELF	All PZ Pass	All PZ Pass	All PZ Pass	All PZ Pass
	RSA	All PZ Pass	All PZ Pass	All PZ Pass	All PZ Pass
8-Story	ELF	All PZ Pass	All PZ Pass	All PZ Pass	All PZ Pass
	RSA	All PZ Pass	All PZ Pass	All PZ Pass	All PZ Pass
16-Story	ELF	All PZ Pass	All PZ Pass	All PZ Pass	All PZ Pass
	RSA	All PZ Pass	All PZ Pass	All PZ Pass	All PZ Pass

Take for example a one-sided connection where a W24×76 beam frames to a W18×106 column. The ratio of shear in the panel zone at the probable flexural strength of the connection to shear yielding of the panel zone is conservatively 0.98 (see Equation (3-18)) and increase to 1.07 when using $0.55F_y$ for V_y . This indicates that the panel zone may not yield until the connection approaches its peak strength, generally associated with CP. Research (FEMA 350 (FEMA 2000a)) has suggested that a balanced yield condition between beam hinge and adjacent panel zone can increase the inelastic deformation capacity of a connection. This condition has been adopted in ASCE 41. Current steel design practice in accordance with AISC 341 does not impose a balanced yield condition.

$$\frac{V_{pr}}{V_y} \approx \frac{\left(\frac{C_{pr} Z_x (1.1F_y)}{0.95d_b} \right)}{0.6(1.1F_y)d_c t_{wc}} = \frac{594}{605} = 0.98 \quad (3-18)$$

3.2.3.1.3 Member Cross-section Strength (flexural hinge) and Global Strength (member stability)

Table 3-24 provides a summary of the performance of the *column* members for each linear assessment procedure and each BPL. Hinges in *beam* members that are part of the beam-to-column connection are discussed above and not addressed in this section. The number listed in parentheses denotes the number of failed components in the frame—shown as bolded text. Also shown in the table is the percentage of failed components compared to the total number of similar components. Recall that section strength and member strength of a column is combined into a single P - M interaction equation for linear assessment procedures in ASCE 41 (see ASCE 41 Equations 5-10, 5-11, and 5-12.) Consequently, identifying an efficient retrofit

option for a column can be challenging because understanding and isolating the failure mechanism of the column can be difficult.

Table 3-24. Performance Summary of Column Members (CM) per Frame, Linear Procedures

Archetype	Design	LSP		LDP	
		LS	CP	LS	CP
4-Story	ELF	All CM Pass	All CM Pass	All CM Pass	All CM Pass
	RSA	All CM Pass	All CM Pass	All CM Pass	All CM Pass
8-Story	ELF	Ext. CM Fail (2) Int. CM Pass 6%	Ext. CM Fail (4) Int. CM Pass 13%	Ext. CM Fail (2) Int. CM Pass 6%	Ext. CM Fail (2) Int. CM Pass 6%
	RSA	Ext. CM Fail (8) Int. CM Pass 25%	Ext. CM Fail (8) Int. CM Pass 25%	Ext. CM Fail (2) Int. CM Pass 6%	Ext. CM Fail (8) Int. CM Pass 25%
16-Story	ELF	All CM Pass	Ext. CM Fail (12) Int. CM Pass 19%	All CM Pass	All CM Pass
	RSA	Ext. CM Fail (4) Int. CM Pass 6%	Ext. CM Fail (20) Int. CM Pass 31%	All CM Pass	Ext. CM Fail (6) Int. CM Pass 9%

Several columns do not satisfy the assessment criteria using the interaction equation because of high axial force and moment in the 8-story and 16-story archetype buildings. These members are all force-controlled for both axial force and flexure because P_{UF} exceeds $0.5 \times P_{CL}$ —generally associated with weak-axis flexural buckling. As such, M_{UF} and M_{CL} are used in the interaction equation (ASCE 41 Equation 5-12). Determination of M_{UF} is subject to the same limitations as P_{UF} (see sections on assessment results). There are columns where the force-controlled requirement does not result in a performance failure (e.g., some 16-story SMF columns). As noted previously, the force distribution used in the LSP directly contributes to the increased column forces. However, generally speaking, the estimated axial load demands in the columns are the least conservative approximations, as compared to more rigorous analysis procedures (see the axial load figures, e.g., Figure 3-71). Exterior base columns in these frames consistently fail the acceptance criteria. This result is problematic because flexure hinges are *expected* to develop at the base of these columns. ASCE 41 does not provide guidance on how to assess column-to-base connections similar to beam-to-column connections.

As discussed previously, it is of debatable validity that force-controlled response be triggered with P_{UF} / P_{CL} in lieu of P_{UF} / P_{ye} , as was done in FEMA 273. The interaction equation in ASCE 41 used for the case of out-of-plane instability and in-plane flexure is also debatable; ASCE 41 would benefit from following AISC 360 in this regard (see AISC 360 §H1.3). ASCE 41 would also benefit from decoupling the single interaction curve for member stability and section strength into two separate interaction equations as done in AISC ASD Chapter N, Plastic Design (AISC 1989). Decoupling the stability and strength would provide a clearer picture of potential retrofit schemes for frame columns. Nonetheless, some member stability equations were derived from beam-columns test results where column ends did not translate relative to each other. Future research is required to justify updated interaction equations for assessment of beam-columns

with ASCE 41, as well as a critical examination of the acceptance criteria in regard to experimental test results.

In addition to the above performance observations, the effects of additional strengthening of columns in design should be recognized. The columns in the 4-story frames are somewhat oversized from that required from analysis to satisfy section compactness requirements in AISC 341, and therefore, the columns efficiently satisfy the acceptance criteria, regardless of estimation of P_{CL} . All the frame columns in the 4-story frames are deformation-controlled for flexure. As a side note, there is also considerably less scatter in the axial load demands in the columns from the various approximation methods.

3.2.3.1.4 Summary

Table 3-25 summarizes the performance of the archetype buildings in reference to the BSO for both linear procedures. Table 3-26 provides the base shears computed with the linear assessment procedures. Column performance (primarily at the base) from both assessment procedures controls the overall assessment of the SMF frames. Base column failure in this analytical context is more detrimental to the overall structural performance than beam-to-column connection performance. As noted above, additional research is needed concerning assessment criteria for beam-to-column connections and columns. The qualitative ratings are assigned primarily based on the performance of the column members and a few cases coupled with the performance of the beam-to-column connections. In the end, the 4- and 16-story ELF-designed frames satisfy the seismic performance objective only using the LDP (recall from Chapter 2 that the ELF procedure is not permitted for design of the 16-story SMF).

Table 3-25. BSO Performance Summary of Archetype Buildings, Linear Procedures

Archetype	Design	LSP			Design	LDP		
		BC	CM	PZ		BC	CM	PZ
4-Story	ELF	Fail	Pass	Pass	ELF	Pass	Pass	Pass
	RSA	Fail	Pass	Pass	RSA	Fail	Pass	Pass
8-Story	ELF	Pass	Fail	Pass	ELF	Pass	Fail	Pass
	RSA	Fail	Fail	Pass	RSA	Pass	Fail	Pass
16-Story	ELF	Pass	Fail	Pass	ELF	Pass	Pass	Pass
	RSA	Fail	Fail	Pass	RSA	Fail	Fail	Pass

The assessment results from the LSP and LDP illustrate that, on average, the ELF-designed SMF performs better than the RSA-designed SMF for all archetype buildings. This can be attributed to the increased strength and stiffness provided to the ELF-designed frames (see Table 2-4) by differences in the ELF and RSA procedures, including associated scaling provisions, in ASCE 7.

The LDP consistently results in lower DCR_N values than the LSP for both the ELF- and RSA-designed frames for all archetype buildings, an indication that a more accurate distribution of seismic demands (based on elastic modes) is better captured in taller frames. However, assessment of the RSA-designed frame consistently illustrates inferior performance using the LSP compared to the LDP because of the variation between the distribution of seismic demands and the allocation of component strengths within the frame. This variation is not as substantial when assessing the ELF-designed frame with the LDP. Moreover, the lateral force distribution in the LSP does not capture higher modes well, leading to conservative estimates

of column forces in the taller frames. This can be problematic for beam-columns due to the lower-bound estimate of compressive strength, P_{CL} .

Table 3-26. Summary of Base Shears, Linear Procedures (kips)

EHL	Routine	4-Story		8-Story		16-Story	
		ELF	RSA	ELF	RSA	ELF	RSA
BSE-1	LSP	1696	1380	2176	1646	2977	2574
	Ratio	0.93	0.97	0.91	0.94	0.91	0.93
BSE-2	LSP	2545	2070	3264	2470	4466	3862
	Ratio	0.93	0.97	0.92	0.94	0.91	0.93

Analytical results based on component-level performances obtained from the LSP and LDP suggest that special moment frames designed in accordance with ASCE 7 and its referenced standards have difficulty achieving the selected seismic performance objective of an existing building intended to be equivalent to a new building. This notion is driven by the performance of the columns and beam-to-column connections. The results for the columns can be enhanced by more mechanistically consistent column provisions and analytical modeling parameters. Although the acceptance criteria for a connection are derived from a highly vetted testing program, enhancement to the transference of nonlinear test results to linear acceptance criteria and the supplementary (cumulative) adjustment factors could be investigated.

3.2.3.2 Nonlinear Assessment Procedures

The following discusses the analytical results for the noted components from the nonlinear procedures for each archetype building.

As noted previously, the NSP is permitted for the frames but requires supplemental verification using the LDP. The following summaries for the NSP reflect results only from the NSP (see previous for the linear verification using the LDP). For the NDP, results are mainly discussed in reference to the *mean* response from the set of records except where noted otherwise.

3.2.3.2.1 Beam-to-Column Connections

Table 3-27 provides a summary of the performance of the FR beam-to-column connections (RBS) for each nonlinear assessment procedure and each BPL. The number listed in parentheses denotes the number of failed components in the frame—shown as bolded text. Also shown in the table is the percentage of failed components compared to the total number of similar components. Similar to the results from the linear procedures, the RSA-designed frames have difficulty satisfying the acceptance criteria when using the NDP for both the LS and CP BPL. Although the median response is biased less by a collapsed state of a given frame than the mean response, the results are not significantly improved, except for the 16-story SMF. The NDP consistently indicates poorer performance of the connections than that given by the NSP alone. The ELF-designed frames consistently satisfy the performance criteria for both the LS and CP BPL for both procedures, except for the 8-story frame under the BSE-2 EHL using the NDP, which has a special situation described subsequently.

The notable performance concerns of the beam-to-column connections is due to the cumulative penalty associated with strong panel zones and connection detailing per AISC 341 (i.e., continuity plate thickness in one-sided connections)—see LSP and LDP assessment results discussions. Further, the span-to-depth ratio requirements change between linear and nonlinear procedures. In many cases, the span-to-depth ratio triggered a reduction to the linear criteria but not similarly to the nonlinear criteria. Moreover, base hinges in the exterior columns in the 8-story frames directly influenced the rapid progression toward a collapsed state and, in turn, the poor performance of the beam-to-column connections.

Table 3-27. Performance Summary of FR Connections (BC) per Frame, Nonlinear Procedures

Archetype	Design	NSP		NDP (based on mean response of record set)	
		LS	CP	LS	CP
4-Story	ELF	All BC Pass	All BC Pass	All Pass	All Pass
	RSA	All BC Pass	Ext. BC Fail (2) Int. BC Pass 8%	Ext. BC Fail (2) Int. BC Pass 8%	Ext. BC Fail (8) Int. BC Fail (16) 100%
8-Story	ELF	All BC Pass	All BC Pass	All BC Pass	Ext. BC Fail (6) Int. BC Fail (12) 38%
	RSA	All BC Pass	All BC Pass	Ext. BC Fail (8) Int. BC Fail (16) 50%	Ext. BC Fail (10) Int. BC Fail (20) 63%
16-Story	ELF	All BC Pass	All BC Pass	All BC Pass	All BC Pass
	RSA	All BC Pass	All BC Pass	All BC Pass	Ext. BC Fail (30) Int. BC Fail (56) 90%

3.2.3.2.2 Panel Zones

Table 3-28 summarizes the performance of the panel zones for each nonlinear assessment procedure for the CP BPL. Similar to the results from the linear procedures, panel zones consistently satisfy the performance criteria for the LS and CP BPL for both procedures. The number listed in parentheses denotes the number of failed components in the frame—shown as bolded text. Also shown in the table is the percentage of failed components compared to the total number of similar components. The DCR_N values all remained small compared to unity (see LSP and LDP assessment results discussions). The panel zones consistently do not achieve four times the yield shear strain at BSE-2 EHL—the deformation associated with the panel zone strength given in AISC 360 §J. This strain level is associated with panel zone design given in AISC 360 §J at $2/3 \times MCE_R$ (taken here to be BSE-1 EHL) using M_{pr} . The third floor of the 8-story RSA-designed SMF is the only frame that shows a potential issue with panel zones. As discussed previously, this is a corollary of beam-to-column connection performance and base column hinging and not a panel zone performance concern. It is not yet fully understood whether good performance of panel zones is strictly due to increased strengths resulting from drift criteria, conservative design approaches (for the panel zones), or industry practice of increasing column size.

Table 3-28. Performance Summary of Panel Zones (PZ) per Frame, Nonlinear Procedures

Archetype	Design	NSP		NDP (based on mean response of record set)	
		LS	CP	LS	CP
4-Story	ELF	---	All PZ Pass	---	All PZ Pass
	RSA	---	All PZ Pass	---	All PZ Pass
8-Story	ELF	---	All PZ Pass	---	All PZ Pass
	RSA	---	All PZ Pass	---	Ext. PZ Pass Int. PZ Fail (2) 6%
16-Story	ELF	---	All PZ Pass	---	All PZ Pass
	RSA	---	All PZ Pass	---	All PZ Pass

3.2.3.2.3 Member Cross-section Strength (flexural hinge) and Global Strength (member stability)

Table 3-29 provides a summary of the performance of the *column* hinges for each nonlinear assessment procedure for the CP BPL Hinges in *beam* members that are part of the beam-to-column connection are discussed above and not addressed in this section. The number listed in parentheses denotes the number of failed components in the frame—shown as bolded text. Also shown in the table is the percentage of failed components compared to the total number of similar components. In addition to assessment results, the strong-column weak-beam (SCWB) philosophy prescribed in AISC 341 was verified to confirm locations of expected hinges at the BSE-2 EHL (CP BPL).

Base column hinges at the exterior of the 8-story frames consistently fail the performance criteria. These failures are a corollary of the modeling parameters for *P-M* hinges in ASCE 41 (see linear discussion). These columns are force-controlled for flexure in the 8-story ELF-designed frame and the 16-Story RSA-designed frame (shaded in the table) for the NSP and NDP. Still, the axial force demand, P_{max} , is from an individual record and is, therefore, biased by the behavior of the frame to that record. As such, it is difficult to capture record-to-record variability on force- and deformation-controlled response directly in the analysis for a set of ground motion records. Recall that the linear procedures also identified concerns with these columns.

Establishing the in-plane column hinge model and performance metrics as a function of the out-of-plane flexural buckling strength, when governs P_{CL} , can be problematic for wide-flange columns. More so, when the gravity load alone produces an axial force greater than $0.2 \times P_{CL}$, which is the case in the exterior base columns in the 8-story frames (see calculations below). These column base hinges reach the CP deformation limit prior to the adjacent beam-to-column connections. The maximum axial force from the NDP in this column (and hinge component) is 992 kips, which provides an axial load ratio, P / P_{CL} , of 0.6 (which would

require force-controlled action). The axial load ratio based on the section axial strength using expected material properties, P / P_{ye} , is 0.35 (which would require deformation-controlled action). Consequently, modeling the section flexural strength of a column hinge using the section axial strength of that section would not result in a force-controlled condition. This was the approach taken in FEMA 273, the predecessor of ASCE 41. Further, it is theoretically inconsistent to model the component strengths within the same column as a function of both P_{ye} and P_{CL} . As is evident in the 8-story frame response, base column failures can initiate a rapid progression towards a collapsed state, analytically speaking.

W18×175 (8-Story ELF-designed SMF Exterior Base Column):

$$P_{gravity} = \text{Dead} + \text{Superimposed Dead} + 0.25 \times \text{Unreduced Live Floor} = 457 \text{ kips}$$

$$P_{CL} = P_{n,y} = 1639 \text{ kips (1724 kips using } F_{ye})$$

$$P_{ye} = 2822 \text{ kips}$$

$$P_{gravity} / P_{CL} = 0.28 > 0.2 \quad (P_{gravity} / P_{CLe} = 0.27)$$

$$P_{gravity} / P_{ye} = 0.16$$

Table 3-29. Performance Summary of Column Hinges (CH) per Frame, Nonlinear Procedures

Archetype	Design	NSP		NDP (based on mean response of record set)	
		LS	CP	LS	CP
4-Story	ELF	---	All CH Pass SCWB ok	---	All CH Pass SCWB ok
	RSA	---	All CH Pass SCWB ok	---	All CH Pass SCWB ok
8-Story	ELF	---	Ext. CH Fail (2) Int. CH Pass 3% SCWB ok	---	Ext. CH Fail (4) Int. CH Pass 6% SCWB Not ok
	RSA	---	Ext. CH Fail (2) Int. CH Pass 3% SCWB ok	---	Ext. CH Fail (4) Int. CH Pass 6% SCWB Not ok
16-Story	ELF	---	All CH Pass SCWB ok	---	All CH Pass SCWB ok
	RSA	---	All CH Pass SCWB ok	---	Ext. CH Fail (22) Int. CH Fail (12) 27% SCWB ok

Table 3-30 summarizes the performance of the *column* member strength for each nonlinear assessment procedure for the CP BPL. ASCE 41 does not provide guidance on checking column member stability when using the nonlinear procedures unless the column is designated as force-controlled. It is mechanistically inconsistent to adjust material properties between section strength and member stability for a given column

(i.e., hinge uses P_{ye} and member uses P_{CL}). Except for the 8-story ELF- and RSA-designed frames, which indicate column hinges form in the upper stories using the NDP, analytical results of the member stability interaction curves indicate that column members satisfy the performance criteria. Nonetheless, the in-plane stability of a column with plastic hinges from in-plane flexure is highly complex and is a topic that is not well understood in the literature or implicitly or explicitly addressed in ASCE 41 for the nonlinear procedures. Experimental testing on deep wide-flanged steel beam-columns has illustrated that the weak-axis buckling strength of a wide-flange is not affected by plastic hinges from in-plane flexure.

Table 3-30. Performance Summary of Column Members (CM) per Frame, Nonlinear Procedures

Archetype	Design	NSP		NDP (based on mean response of record set)	
		LS	CP	LS	CP
4-Story	ELF	---	All CM Pass	---	All CM Pass
	RSA	---	All CM Pass	---	All CM Pass
8-Story	ELF	---	All CM Pass	---	All CM Pass
	RSA	---	All CM Pass	---	All CM Pass
16-Story	ELF	---	All CM Pass	---	All CM Pass
	RSA	---	All CM Pass	---	All CM Pass

3.2.3.2.4 Summary

Table 3-31 summarizes the performance of the archetype buildings in reference to the BSO for both nonlinear procedures. Column hinge performance, primarily in the base columns, from both assessment procedures controls the overall assessment of the frames. Base column failure is more detrimental to the overall structural performance than beam-to-column connection performance. As noted above, additional research is needed on assessment criteria for beam-to-column connections and columns. In the end, only the 4- and 16-story ELF-designed frames satisfy the seismic performance objective using either nonlinear procedure (recall from Chapter 2 that the ELF procedure is not permitted for design of the 16-story SMF). The shaded area in the table indicates which frames do not satisfy the NSP criteria due to supplemental verification using the LDP (see linear discussion above). The qualitative ratings are assigned primarily based on the performance of the column members and, for a few cases, the performance of the columns coupled with the performance of the beam-to-column connections.

Table 3-31. BSO Performance Summary of Archetype Buildings, Nonlinear Procedures

Archetype	Design	NSP			NDP (based on mean response of record set)			
		BC	CH	PZ	Design	BC	CH	PZ
4-Story	ELF	Pass	Pass	Pass	ELF	Pass	Pass	Pass
	RSA	Fail	Pass	Pass	RSA	Fail	Pass	Pass
8-Story	ELF	Pass	Fail	Pass	ELF	Fail	Fail	Pass
	RSA	Pass	Fail	Pass	RSA	Fail	Fail	Fail
16-Story	ELF	Pass	Pass	Pass	ELF	Pass	Pass	Pass
	RSA	Pass	Pass	Pass	RSA	Fail	Fail	Pass

The assessment results from the NSP and NDP illustrate that on average the ELF-designed SMF performs better than the RSA-designed SMF for all archetype buildings. This can be attributed to the increased

strength and stiffness provided to the ELF-designed frames (see Table 2-4 and Table 2-5) by differences in the ELF and RSA procedures, including associated scaling provisions, in ASCE 7.

The NSP (without supplemental verification) consistently results in lower DCR_N values than the NDP for both the ELF- and RSA-designed frames for all archetype buildings, an indication that a more accurate distribution of seismic demands is not well captured in taller frames using the NSP (LDP results are consistently greater than NSP, albeit a direct comparison is problematic as discussed previously). Nonlinear results indicate that the NSP has a tendency to underestimate the demands in the upper stories. This occurs primarily because of the differences in the distribution of seismic demands and the lack of modal representation other than the fundamental mode in the NSP. This effect was also noticed in NIST GCR 10-917-9: *Applicability of Nonlinear Multi-Degree-of-Freedom Modeling for Design* (NIST 2010c).

The results from the NDP are sensitive to excitation input, analysis parameters, and component modeling. In this study, generalized component models were incorporated with degradation effects calibrated to an experimental test. Future research should critically examine the applicability of the generalized modeling parameters for steel components in ASCE 41. Experimental research has shown that subassembly tests can have large scatter in acceptable performance given the stochastic variations in the type of loading, that being cyclical, near-fault, random, etc. (e.g., SAC project). Future research should investigate the influence of the loading protocol adopted to establish the deterministic acceptance criteria for connections and member hinges.

Analytical results based on component-level performances obtained from the NSP and NDP suggest that special moment frames designed in accordance with ASCE 7 and its referenced standards have difficulty achieving the selected seismic performance objective of an existing building intended to be equivalent to a new building. This notion is driven by the performance of the columns and beam-to-column connections. The results for the columns can be enhanced by more mechanistically consistent column provisions and analytical modeling parameters. Although the acceptance criteria for a connection are derived from a highly vetted testing program, enhancement to the (cumulative) adjustment factors to the criteria could be investigated.

3.2.3.3 Comparison between Linear and Nonlinear Assessment Results

Table 3-32 summarizes the performance of the archetype buildings for each analysis procedure. The results indicate that the linear procedures consistently provide DCR_N values greater than that given by the nonlinear procedures, highlighting the conservatism in the linear assessment procedures. As discussed previously, direct comparison of results between linear and nonlinear procedures can be problematic, except for direct comparison of the distribution of results. Still, on average, the LSP and LDP are capable of identifying potential performance concerns within critical areas of the frame as compared to the results from the NSP and NDP. Consistency is evident in the global performance rating of the 8-story SMF as well as frames designed per the MRSA procedure among the various assessment procedures. However, not all component performance failures align between the procedures. The conservatism of the linear procedures is also apparent, as expected.

The nonlinear procedures provide a more rigorous assessment approach as compared to the linear procedures. The results from the LSP, and to a lesser extent the LDP, indicate more performance failures in components than identified using the nonlinear procedures. The results presented emphasize the inherent conservatism in the linear procedures. However, this conservatism is coupled with a reduction in required resources and analytical proficiency. Certainly for the NDP, the effects of ground motion selection and scaling can be significant, including the number of records adopted to achieve a reasonable level of statistical confidence and the method by which the records were chosen with a bias to achieve an unfairly beneficial binary outcome. Moreover, some of the higher mode periods fall directly in localized high energy regions of the response spectrum resulting in increased demands that cannot be captured efficiently in a linear analysis using a smooth generalized spectrum. Furthermore for the NSP, the force distribution is potentially inadequate for frames that exhibit increased higher mode participation, either elastically or triggered by nonlinearity.

Table 3-32. BSO Performance Summary of Archetype Buildings

Archetype	Design	LSP	LDP	NSP	NDP (based on mean response of record set)
4-Story	ELF	Fail	Pass	Pass	Pass
	RSA	Fail	Fail	Fail	Fail
8-Story	ELF	Fail	Fail	Fail	Fail
	RSA	Fail	Fail	Fail	Fail
16-Story	ELF	Fail	Pass	Pass	Pass
	RSA	Fail	Fail	Fail	Fail

In contrast to the nonlinear procedures, the linear analysis model and assessment is implied to be less rigorous and more conservative. As already discussed, the linear procedures yielded more conservative results for the deformation-controlled components. The linear procedures can also illustrate the trend in demands but may fail to highlight critical performance zones within a given frame.

The columns that failed the linear criteria are typically force-controlled because of high axial loads, a result of using P_{UF} / P_{CL} in lieu of P_{UF} / P_{ye} to model flexural hinge strength and trigger force-controlled response. In comparison to the results from the NDP, the linear procedures produced conservative estimates of poor performance. On average, the linear procedures slightly overestimate the axial force demand in the exterior columns. Although there is general agreement between the procedures on which members may pose a risk, the results from the NDP illustrate that the column hinges can satisfy the performance criteria if the hinges were not force-controlled using P_{CL} , which is generally governed by out-of-plane flexural buckling. Enhancements to the assessment of beam-columns could consider using a dual assessment criterion that evaluates stability and flexural hinging separately (as is done for the NDP in this study).

Chapter 4 Summary, Conclusions, and Recommendations

This report presents the results of a study investigating the correlation between the seismic performance of an ASCE 7 code-compliant building and its performance as quantified using ASCE 41 analysis procedures and structural performance metrics. This investigation is performed by evaluating a suite of structural steel buildings in a high seismicity region that are designed using ASCE 7 and evaluated using ASCE 41. *The basic question is whether the standards for designing new steel buildings and assessing existing steel buildings provide consistent levels of performance.* An additional outcome of this research is to advance the state-of-knowledge in PBSD and assessment of buildings using ASCE 41. Further, results provide the technical background for provisions that target equivalent seismic performance between a new building and an existing building that is required to meet the seismic performance objective of a new building.

This chapter highlights significant observations and conclusions from the seismic assessment of the archetype buildings using four assessment procedures prescribed in ASCE 41. General findings and recommendations are based on the collective results for the seismic force-resisting system. More in-depth findings specific to the system are in the relevant subsections in this chapter, as well as in relevant sections of the assessment discussion in Chapter 3. Although the primary emphasis of this study is on benchmarking ASCE 41 assessment procedures, questions arise that may be more applicable to the design criteria used rather than to the assessment results—these items are identified in the section about future research.

4.1 Summary of Project Work

This report presents the results of the structural seismic performance assessment using ASCE 41 procedures and performance measures of buildings utilizing steel special moment frames (SMF) as the lateral force-resisting system (LFRS).

A suite of archetype buildings that incorporate SMFs along one principal direction of the buildings is designed in accordance with ASCE 7. The suite consists of 4-, 8-, and 16-story buildings designed using both the Equivalent Lateral Force Procedure and Modal Response Spectrum Analysis. Both analysis procedures are used to provide a generally applicable range of LFRS strength within the selected seismic intensity region. As such, a LFRS may include significant overstrength to resist nonseismic loads or satisfy other design criteria. A design space of varied building parameters is used to investigate the effects of building height, design methodology, and other LFRS-specific geometric modifications on seismic performance. In reality, the design space is infinitely large and many design choices made in this study can also have different configurations to evaluate the variation in performance specific to a design choice (e.g., study of a range of doubler plate thicknesses in an SMF and their influence on frame column performance).

The seismic performance assessment of the building suite is conducted using both linear and nonlinear analysis procedures prescribed in ASCE 41:

- Linear Static Procedure (LSP)
- Linear Dynamic Procedure (Response Spectrum) (LDP)
- Nonlinear Static Procedure (NSP)
- Nonlinear Dynamic Procedure (NDP)

For this study, the performance assessment targets the Basic Safety Objective (BSO) prescribed in ASCE 41 with the interrelated goals of Life Safety (LS) Building Performance Level (BPL) at the Basic Safety Earthquake-1 (BSE-1) earthquake hazard level (EHL) and Collapse Prevention (CP) BPL at the BSE-2 EHL. This performance objective is chosen to align with the intended structural performance objective of an ordinary building in ASCE 7, which is qualitatively defined here as “life safety” provided by collapse prevention of the building, given a maximum considered earthquake (MCE) event.

To evaluate seismic assessment criteria, each component of the SMFs is designated as a *primary* component in accordance with ASCE 41. Similarly, quantitative performance measures (i.e., acceptance criteria) for *primary* components are used for all assessment procedures, although performance measures for *secondary* components are permitted for some primary components. The consistent use of primary acceptance criteria keeps all components and associated assessment results correlated among the assessment procedures for this study.

As stated earlier, the goals of this research are as follows:

- Assess *new* structural steel buildings utilizing SMFs designed per ASCE 7 requirements and, in turn, evaluated using ASCE 41,
- Develop a qualitative link between the performance implied in ASCE 7 in light of the performance identified by ASCE 41 procedures and performance measures,
- Provide guidance or technical support for improved or new provisions in ASCE 41 (and to a lesser extent, ASCE 7),
- Reduce uncertainty in first-generation PBSD procedures for performance-based seismic assessment, and
- Identify any inconsistencies, ambiguities, and confusing provisions in ASCE 41

In reference to developing a link between ASCE 7 and ASCE 41, the primary difficulty in equating the two standards is rooted in their disjointed performance objectives. That is, acceptance criteria for a component in ASCE 41 are not directly calibrated to the seismic performance objective of ASCE 7, which is a 10 percent probability of partial or total collapse given an MCE event—that is MCE_R (or one percent probability of partial or total collapse in 50 years). Equating the two objectives of the standards would imply that only one structural performance level with an associated earthquake hazard level can be coupled: that being, CP at the MCE_R . However, this would be difficult based on a member-level binary performance solution. Consequently, the question becomes what percentage of components needs to fail the associated CP SPL to achieve a 10 percent probability of total or partial collapse given an MCE_R event? Future research should assess the archetype buildings in FEMA P695 analysis to ascertain the collapse probability in relation to the ASCE 7 performance objective. Results from that study can be used to probabilistically relate the R -factor in ASCE 7 to the m -factors and inelastic deformations using story drift. Clearly, the study presented in this report presumes that the R -factor used for design has been derived to provide the intended

collapse performance objective. As such, the analysis results do not necessarily reflect satisfactory or unsatisfactory performance in relation to the seismic performance objective of ASCE 7.

A consequence of a deterministic-type component evaluation (i.e., pass or fail) is that analytical results, depending on the accuracy of the model and analysis algorithms, can be independent of the behavior of the system. Individual member performance and the potential need to retrofit or replace it are therefore based on an analysis output rather than the influence of the component performance on the system performance. This is a challenging issue to overcome, and only recently has there been *some* progress made (e.g., FEMA P695 and FEMA P-58 (FEMA 2012)) toward having the ability to probabilistically correlate member performance to system performance. However, these efforts are not without their limitations and debatable performance metrics. It is still yet to be determined whether practitioners will accept these developing methods because of the time and resources needed to successfully apply their recommendations. However, ASCE 41 is available and being used for performance-based seismic engineering of building systems and components. In many cases, the acceptance criteria in ASCE 41 are being used to justify computed seismic performance to buildings officials as being satisfactory. The question is what seismic performance is being justified: the objective defined in ASCE 41 or that intended in ASCE 7? If satisfying ASCE 7, then this would infer that the CP SPL associated with the MCE_R (taken as the BSE-2) defined in ASCE 41 matches the intended collapse performance of ASCE 7. A significant effort is still needed to bring ASCE 41 to the state-of-the-art and equivalent to ASCE 7. In this regard, assessment provisions are meaningless without the technical support provided by experimental research and subsequent case studies that evaluate how the research findings affect component and system performance.

4.2 Assumptions and Limitations of this Study

The following discussion summarizes notable assumptions employed in this study and other limitations of the work that could impact the results, which form the basis for the conclusions and observations.

Building System and Component Characteristics for Design and Assessment

- The archetype buildings are representative of a specific type of building, which uses a seismically designed system to resist lateral loads and deformations. The selected system in this study represents one design option out of the many available for steel framed buildings. In designing the SFRS, there are many specific design assumptions made that play an important role in resisting lateral loads and deformations. Different selections for frame configuration, plan layout, bay spacing, height, connection details, and magnitude of non-seismic loads all could affect the assessment results.
- The buildings are *regular* in layout and configuration as defined in both ASCE 7 and ASCE 41. Irregular building configurations can affect seismic performance and are not addressed in this study, as they could complicate the comparisons that are being made.
- The archetype buildings are simple in concept and do not contain stairwells, elevator cores, architectural setbacks, atriums or other features found in typical buildings. The goal here is to study the basic performance of the SFRS in resisting lateral loads and deformations without the complexity posed by other attributes found in buildings today.

- Strength and stiffness of specific *secondary* components, as defined in ASCE 41, were not fully represented in the mathematical model for linear and nonlinear analyses (e.g., shear tab connection for gravity framing, façade, stairs, etc.). This assumption, while reasonable from an analysis standpoint, highlights a difference in requirements between ASCE 7 provisions for design and ASCE 41 provisions for assessment (ASCE 7 §12.7 and ASCE 41 §3.2.2).
- Composite action developed between primary and secondary structural components and the portion of slab they support was not included in the mathematical model for seismic design or assessment. This approach is consistent with that used by many practitioners and provides presumably conservative results because floor slabs are not active in providing composite action and added moment capacity. Composite action was included for the moment frame beams for verifying elastic story drifts under service-level wind loading.
- The column-to-base connections of the SFRS and the seismic base of the buildings were assumed to be horizontally, vertically, and rotationally restrained, resulting in a “fixed” connection to the ground. The base of non-SFRS columns were rotationally unrestrained. Soil-structure interaction effects, modeling the flexibility of the soil and / or the foundation components, and modelling partially-restrained column-to-base connections were not included in this study. Inclusion of these effects would likely affect the assessment results. However, inclusion of the effects of the soil-foundation flexibility into the analysis is complex and not well established at the present time. Moreover, current design practice commonly does not include soil-foundation effects; column-to-base connections to the building foundations are often idealized models, as is done in this study.
- No formal investigation was included in this study to evaluate the accuracy of the quantitative modeling parameters for nonlinear analysis or acceptance criteria for linear and nonlinear analysis provided in ASCE 41 for primary or secondary component models. There is a project currently ongoing with ATC (ATC-114: *Development of Accurate Models and Efficient Simulation Capabilities for Collapse Analysis to Support Implementation of Performance Based Seismic Engineering*) that will examine the component modelling parameters and acceptance criteria for specific components.

Structural Analysis

- No formal investigation was included in this study to evaluate the accuracy of the analysis algorithms in the software packages used for structural analysis. These software packages are the same as those used by practitioners. The stability of solution algorithms when the stiffness and strength of the component models have significantly degraded can vary between software packages. Therefore, any software accuracy limitations encountered in this study are consistent with those present in design offices.
- The methodology used in this study for ground motion selection and scaling resulted in a set of earthquake records that may not be applicable or suitable for a specific site. A different record set—selected by engineering judgment, selected by revising the parameters of the methodology, or developed from an alternative methodology—could affect the assessment results. However, the process employed here is consistent with that used in practice, representing a typical building site in an area with a high level of seismicity.

No formal investigation was included in this study to evaluate all potential sources of uncertainty or error, or whether multiple sources of error are correlated. The question of uncertainties in the analytical models, solution algorithms, material properties and even potential as-built final dimensions and positions of members are all beyond the scope of this study. The load and resistance factor design (LRFD) philosophy in use for structural design today are based on pioneering work on uncertainties in material and load characterizations performed starting in the 1950's. Whether a new similar large national effort to that conducted for LRFD is required today is not clear. Quantifying the effect of any source of uncertainty or error, as it relates to the design or assessment of buildings to resist earthquake motions, is a significant issue and would require its own research program to study all of the aspects.

4.3 Conclusions and Observations

This section highlights significant observations and conclusions from the seismic assessment of the archetype buildings. Topics are categorized as general or system specific. Additionally, more in-depth discussions of the observations and conclusions specific to the SFRS are in the relevant subsections in this chapter as well as in relevant summary sections of the assessment discussion.

4.3.1 ASCE 41

The following observations and conclusions can be drawn from this study. Topics are grouped by either general applicability to ASCE 41 assessment procedures or specific to the structural system.

4.3.1.1 General

The following general topics focus on observations identified by the assessment provisions for the selected assessment methods:

- The LSP generally results in more conservative normalized demand to capacity ratios, DCR_N , values than that of the LDP, because of the differences in the distribution of seismic demands and the lack of modal representation other than the fundamental mode in the LSP.
- The NSP generally results in less conservative DCR_N values than that of the NDP, contrary to what would be expected with increasing the analytical complexity, because of the differences in the distribution of seismic demands and the lack of modal representation other than the fundamental mode in the NSP.
- The nonlinear procedures provide a more rigorous assessment approach as compared to the linear procedures. The results from the LSP, and to a lesser extent the LDP, indicate more performance failures in components than identified using the nonlinear procedures. The results presented emphasize the inherent conservatism in the linear procedures. However, this conservatism is accompanied by a reduction in required analytical resources and proficiency of the analyst.
- The linear procedures can illustrate the trend in demands but may fail to highlight critical performance zones within a given frame.

4.3.1.2 Special Moment Frames

The following significant observations and conclusions are based on the collective results obtained from the assessment of the special moment frames. More details about the specific items are in the relevant sections of the assessment discussion in Chapter 3.

- Analytical results based on component-level performances indicate that new SMFs designed in accordance with ASCE 7, and its referenced standards, have difficulty achieving the ASCE 41 BSO for an existing building intended to be equivalent to a new building. This observation is driven by the performance of the columns and beam-to-column connections.
- *Assuming* the archetype buildings meet the collapse performance objective of ASCE 7, the results of the assessment procedures indicate that ASCE 41 is generally conservative for SMFs. ASCE 41 analysis would require retrofit or replacement of specific components of a code-compliant SFRS to satisfy the CP BPL given an MCE event. The results highlight that columns (i.e., beam-columns) with high axial and flexural demands and beam-to-column connections with a reduced beam section (RBS) have difficulty in satisfying the performance criteria in ASCE 41. Future research is needed to couple the collapse performance objectives of the two standards, as well as other performance objectives associated with a seismic hazard with a lower return period.
- A significant number of columns, primarily at the exterior of the frames, did not satisfy the ASCE 41 acceptance criteria. These failures are in beam-columns classified by analysis as “force-controlled”, which can be particularly problematic when the columns are located at the base of a frame. The results for columns can be enhanced by more mechanistically consistent assessment provisions and analytical modeling parameters for columns. Refinement of the relevant interaction equations to evaluate specific failure mechanisms could assist by allowing what would be a force-controlled column to be classified as “deformation-controlled”.
- A significant number of RBS beam-to-column connections, primarily at the exteriors of the frames, did not satisfy the ASCE 41 acceptance criteria for the LSP and NDP. Although the nonlinear acceptance criteria and detailing recommendations in ASCE 41 were derived from experimental test data, the rationale for the quantitative development of the cumulative reduction factors on these criteria (i.e., 0.8 multipliers in ASCE 41 §5.4.2.4.3-4) is unclear. The analytical results indicate that step function-based cumulative reduction factors can have a significant impact on the performance of an SMF. Further, reduction factors for the span-to-depth ratio limitations for beam-to-column connections have potentially opposing effects that could impact the results between linear and nonlinear assessment procedures.
- Assessment results illustrate that panel zones designed per ASCE 7 and its referenced standards, including the common practice of upsizing columns to offset the need for doubler plates and/or continuity plates, consistently satisfied the ASCE 41 acceptance criteria by a large margin. Consequently, the panel zones are deemed stronger than required by ASCE 41. Specifically, upsizing columns can impact the strength of panel zones in reference to the balance yield approach adopted by ASCE 41 and in turn can influence the performance of the beam-to-column connections.
- Components of the special moment frames that do not satisfy the CP acceptance criteria would need to be strengthened to achieve the performance required by ASCE 41. However, the results from the various assessment procedures were seen to be inconsistent in some cases for a given design routine (i.e., LSP vs. NDP) or the same assessment procedure was inconsistent between

design routines (i.e., ELF and RSA). This makes it difficult to definitively suggest that using ASCE 41 to design a new SMF would produce a system capable of achieving the seismic performance objective of ASCE 7. Future research is needed to evaluate the collapse probability of a new system strengthened by ASCE 41 relative to the seismic performance objective of ASCE 7. The same is required for a new system that has component strengths reduced from that required by ASCE 7 to meet an ASCE 41 performance objective. Further, the adequacy of the components of the enhanced frame (those required to satisfy ASCE 41) would be dependent upon which analysis procedure is used to iterate between design and assessment, and therefore the fidelity of the analytical model and analysis parameters.

- Results of this study indicate that for ASCE 41 to be used as a seismic design procedure for new steel buildings, as a performance-based alternative to ASCE 7 (see ASCE 7 §1.3.1.3), acceptance criteria for the various analysis methods must be calibrated to each other to consistently result in a uniform collapse risk. Additionally, ASCE 41 would need to reference material-specific design standards (e.g., AISC 341) for their seismic design requirements, as well as consistent requirements for defining acceptance criteria for a component (e.g., plastic rotation).

4.4 Recommendations for Future Research

The following sections identify items for future research. The recommendations are grouped by the applicable standard: ASCE 41, ASCE 7, and AISC 341 / 360 / 358.

4.4.1 ASCE 41

4.4.1.1 General

The following items are general considerations for future studies to enhance ASCE 41 assessment provisions:

- The archetype buildings should be analyzed using the methodology formulated in FEMA P695. This will provide the requisite data to identify the collapse probability of the systems (or frames) in relation to the intended collapse objective of ASCE 7. However, the same seismic performance factors as used in design should be used in the analysis. Results from this study can be used to probabilistically relate the R -factor in ASCE 7 to m -factors and inelastic deformations using story drift.
- Research should investigate the implementation of risk-targeted collapse assessment criteria into ASCE 41 similar to the design philosophy introduced in ASCE 7-10. As such, comparison of system fragility curves should be done to correlate the risk-target of ASCE 7 and the risk-target of an existing building intended to be equivalent to a new building.
- Research should evaluate the influence of gravity framing (e.g., partially restrained shear tab connections) on assessment results of the primary components of the SFRS.
- Research should investigate alternative lateral force distributions for taller systems for the NSP, including comparison between adaptive and non-adaptive loading.

- Research should be conducted to determine the number of components that do not need to satisfy the ASCE 41 component acceptance criteria while still permit the building to be classified as meeting a performance objective.
- Research should evaluate the systems used in this study by measuring demands against acceptance criteria for secondary components to quantify variations in performance results; for example, the RBS beam-to-column connections in the MC8 buildings. Even if secondary component criteria were implemented, the DCR_N values still indicate unsatisfactory performance in the lower floors. The primary acceptance criteria for the nonlinear procedures has been removed in ASCE 41-13. Based on some trends seen in this study, this should be done only if the acceptance criteria for linear and nonlinear procedures have been correlated and calibrated.
- Enhanced commentary is needed in ASCE 41, similar to the effort used to develop FEMA 274. Commentary can be used to explain differences in component strengths between ASCE 41 and ASCE 7 and its reference standards (e.g., AISC 341 and AISC 360). This effort would include cleaning up incorrect references (e.g., AISC 341 or AISC 360, FEMA 355F or FEMA 355D). Similarly, the commentary can detail the experimental tests used to derive the acceptance criteria.
- Consideration should be given to reorganize Chapter 5 (Chapter 9 in ASCE 41-13) to remove system-to-system references, most notably when they are not applicable. For example, a force-controlled column in an EBF cannot reference provisions for a column in a moment frame. This chapter would benefit with an outline similar to AISC 341, where the section on member strength is outlined similar to AISC 360. Therefore, the individual systems would reference a member strength in lieu of another system that may or may not be applicable.

4.4.1.2 Fully Restrained Moment Frames

The following items are considerations for future studies to enhance ASCE 41 assessment provisions for FR moment frames:

- Case studies should examine the seismic performance and cost of SMFs with lighter column sizes that include doubler plates. This cost-benefit analysis will shed light on relating construction costs to seismic performance and post-earthquake repair costs for various regions of the country.
- Research should investigate the assessment of panel zones in relation to the design methodology using AISC 341, as well as a critical examination of the acceptance criteria in regard to experimental test results. This research can be linked with the above study on the use of double plates and lighter columns.
- Case studies should investigate the frame design using the Direct Analysis Method in AISC 360 and the associated seismic assessment results. Some aspects of the Direct Analysis Method have been introduced in ASCE 41-13.
- Research is needed to develop acceptance criteria and modeling parameters for column-to-base connections, including embedded connections.
- Research is required to justify updated interaction equations for assessment of beam-columns using ASCE 41, as well as a critical examination of the acceptance criteria in regard to experimental test results. Decoupling interaction equations into specific failure mechanisms and referencing highly vetted design standards should be considered. Removing P_{CL} as the basis for force-controlled

response and acceptance criteria for a column hinges (i.e., revert back to FEMA 273) and using P_{CE} when F_{ye} is used to assess a flexure hinge in the same column should be considered.

- Research should critically examine the applicability of the generalized modeling parameters in ASCE 41 for plastic hinges in beams, beam-to-column connections, and columns for use in the nonlinear procedures.
- Research should investigate the influence of the loading protocol adopted to establish the deterministic acceptance criteria for connections and member hinges.
- Research is needed to justify the fixed reductions (i.e., 0.8 factor) to acceptance criteria of FR beam-to-column connections based on connection detailing.
- Research should investigate the correlation between acceptance criteria for the linear and nonlinear procedures.

4.4.2 ASCE 7

The following items are considerations for future studies to enhance ASCE 7 provisions:

- The assessment results illustrate that on average the ELF-designed frames perform better than the RSA-designed frames for all archetype buildings. However, the ELF procedure is not permitted in some cases. Research should investigate the applicability of the analysis limitations in terms of the intended collapse objective of ASCE 7.
- Research should investigate the lateral design force distributions in ASCE 7 and modal scaling provisions, and their influence on the allocation of component strengths within a frame. Research has indicated that higher modal base shear scaling may be warranted (NIST 2010b and NIST 2012). Potential modifications to the MRSA procedure could also include scaling provisions to additionally account for higher mode effects resulting from nonlinear response. Provisions can be directly transferred to the linear procedures in ASCE 41.
- Research efforts should evaluate incorporating other performance levels for design into ASCE 7 (NIST 2012).

4.4.3 AISC 341 / 360 / 358

4.4.3.1 Special Moment Frames

The following items are considerations for future studies to enhance AISC 341 provisions of special moment frames:

- In general, the SCWB provision in AISC 341 adequately limits column hinges (other than at the column-to-base connection) at the MCE_R . However, assessment results suggest that this provision may need adjustment for taller frames with increased participation of higher modes. Strictly speaking, assessment results depend on the design methodology adopted for the beam-columns (i.e., adjusted K factor that is dependent on the deformed shape of the column at buckling, computation of the *nominal* flexural capacity of the column, and interaction formula). Furthermore, column hinges above the base may have been produced by other phenomenon and thus column hinging is a supplementary indicator of frame collapse. Similarly, the yield surface model for the

section flexural strength of a wide-flange column adopted in the nonlinear analysis (as well as that prescribed in ASCE 41) is slightly different than that prescribed for the SCWB provision, which is a conservative yield surface to cover many different column types. Efforts could couple the two standards in terms of yield surfaces used to define the section flexural strength of a column.

- Analysis results indicate that the axial force demand prescribed in the SCWB provision (i.e., using Ω_o) is a reasonably conservative approximation compared to a full yield mechanism and results from the NDP. The conservatism increases as the aspect ratio of the frame increases. Research should investigate the applicability of a full yield mechanism for design.
- Design of the frame columns was based on two interaction equations in accordance with AISC 360 §H1.3 using the Effective Length Method. On average, this method provided acceptable minimum sizes for column strength. In the upper stories of taller frames where drift control was not as significant, a few (slender) column sizes were governed by out-of-plane stability (AISC 360 Equation H1-2) and also SCWB (i.e., $M_{nc} < M_{pc}$). However, research is needed to examine the effects of the Lateral-Torsional Buckling Modification Factor, C_b , including the influence of axial load and pre-curvature on C_b when computing the buckling strength of SMF columns. Similarly, research should investigate the influence of a plastic hinge on deep wide-flange column stability—see NIST GCR 11-917-13: *Research Plan for the Study of Seismic Behavior and Design of Deep, Slender Wide-Flange Structural Steel Beam-Column Members* (NIST 2011c).

Appendix A Ground Motions for Response History Analysis

A.1 Ground Motion Record Set

The far-field record set (22 records, each with two horizontal components) from FEMA P695 (FEMA 2009a) is selected as the input motion database for the NDP; 14 of the 44 horizontal component records are selected as the ground motion set for each archetype building, with no two records coming from the same station. The records are normalized for magnitude, distance, and source conditions as discussed in FEMA P695.

The *scaled* record set (see Ground Motion Selection and Scaling section below) for each archetype building is taken directly as the Basic Safety Earthquake-2 (BSE-2) earthquake hazard level (EHL). Although this EHL is not strictly the same as having a two percent probability of exceedance in 50 years, it is comparable, and anticipated future changes in ASCE 41-13 will likely match the seismic hazard defined in ASCE 7-10 (see Chapter 3). The scaled record set is factored by two-thirds to represent the BSE-1 EHL in lieu of explicitly determining the ground motion parameters with a ten percent probability of exceedance in 50 years. No spectral shape modifier, ε , is used to adjust the seismic demands for either BSEs (FEMA 2009a; Haselton et al. 2009), this is a topic of needed research.

As a side note, the goal initially was to analyze the archetype buildings using seven scaled pairs of ground motion records along each principal axis of the structure (14 records in each direction). However, because of complications in scaling orthogonal pairs for the maximum direction of response when a structure has significantly different periods along the principal axes, it was decided to analyze 14 unique records independently along each principal axis—see above. This is permitted by ASCE 41 since requirements for considering multidirectional seismic effects are not triggered in this study—see ASCE 41 §3.2.7. Further, there is no guidance regarding the application of scaled ground motion pairs for the maximum direction of response when a structure has significantly different periods along the principal axes. Future research is needed to provide provisions on scaling and application of ground motion pairs.

A.2 Ground Motion Selection and Scaling

The ground motion selection and scaling procedure for each archetype building is described below. This procedure was developed in consultation with select members of the peer review team. Each set of records (14 total) is used for both the equivalent lateral force (ELF) and response spectrum analysis (RSA) designs to gauge performance between the two. The process is as follows:

1. Determine the fundamental *lateral* mode period, T_1 , of the building in the direction being considered not including gravity load effects (i.e., first-order period) for both the ELF and RSA

designs. Second-order periods may also be computed with *expected point-in-time* gravity loads rather than *factored* loads. Determine the average (arithmetic mean) of the periods for the ELF and RSA designs, $T_{1,avg}$. This will keep the scaling of the two designs consistent.

2. For each of the 44 far-field component records (not the records computed from the square root of the sum of the squares (SRSS) of the two horizontal components of an event), compute the error between S_a from the recorded spectrum and S_a from the maximum considered earthquake (MCE_R) design spectrum at each period between $0.2 \times T_{1,avg}$ and $1.5 \times T_{1,avg}$. The period step used here is 0.01 second. The error at each period ranges from 0 to 1, with 0 being an identical match.
3. Sum the error values over the periods between $0.2 \times T_{1,avg}$ and $1.5 \times T_{1,avg}$ to get a single composite error value for each record.
4. Scale each record to minimize the total error from step 3.
5. Select the 14 records with least total error. If both horizontal components of a specific station are in the set, then remove the record with the larger error of the pair and select the next unique record from the remaining record set. This step is repeated as needed until all records selected are from different stations.
6. Compute the average spectrum from the record set (14 total) from step 5.
7. Scale the average spectrum from step 6 so that no value between $0.2 \times T_{1,avg}$ and $1.5 \times T_{1,avg}$ is less than the MCE_R spectrum. The 1.3 factor in ASCE 41 §1.6.2 is not included here, so as to address the change of spectrum parameters from geomean to maximum direction response in ASCE 7 (this factor will be removed in ASCE 41-13).
8. Scale the record set from step 5 by the value computed in step 7. Therefore, there are two scaling factors: step 4 and step 7.
9. Apply the total scaling factor (step 4 times step 7) to each component record in the set from step 5 and perform analysis.

For comparison purposes, the process in ASCE 41 §1.6.2.2 is summarized as follows:

1. Select a minimum of three recorded events (each event is a data set), each with two horizontal components.
2. Take the SRSS of the two horizontal components of each selected data set from step 1.
3. Select a *scaling factor* for each SRSS from step 2. Note that application of a scaling factor to the unscaled SRSS is equivalent to taking the SRSS of the similarly scaled components.
4. Compute the average of the scaled SRSS spectra from step 3 for all selected events.
5. Scale the average spectrum from step 4 so that no value between $0.2 \times T_{1,avg}$ and $1.5 \times T_{1,avg}$ is less than 1.3 times the *design* spectrum.
6. Apply the total scaling factor (step 3 times step 5) to each component record in an event and perform analysis.

The selection and scaling procedure in this study differs slightly from that found in ASCE 41. Because this study investigates a generalized SDC D_{max} analysis without a specific location, it is difficult to select a site and apply common selection and scaling processes typically performed by a geotechnical engineer. In lieu of taking the SRSS of the two horizontal components of an event and having 22 SRSS spectra and in turn computing the error of the SRSS records and associated scaling factor for the event, the error and scaling factor were computed for each component (44 spectra). 14 unique records were selected per principal

direction and the average of this set scaled to meet the target spectrum. In summary, steps 1 to 5 in the process identify the “best fit” to the ASCE 41 code spectrum (which matches ASCE 7). The average of this set is computed and scaled similarly to that in ASCE 41—without the 1.3 factor.

Other ground motion selection and scaling methods are discussed in NIST GCR 11-917-15: *Selecting and Scaling Earthquake Ground Motions for Performing Response-History Analyses* (NIST 2011d).

A.3 Four-Story Archetype Building

A.3.1 4-Story Special Moment Frame

Table A-1 summarizes the 14 strong motion records used for the nonlinear dynamic procedure (NDP) for the E-W direction of MC4 special moment frame (SMF). Figure A-1 illustrates the set of acceleration response spectra, original and scaled, and the scaled average spectrum. Figure A-2 illustrates the acceleration response spectra, original and scaled, for each select record. For comparison, the ASCE 41 code spectrum is shown in the figures. All records completed for the BSE-1 and BSE-2 for the ELF design. All records completed for the BSE-1 for the RSA design. All analyses except those using records 1, 4, 7, 9, and 12 completed for the BSE-2 for the RSA design.

Table A-1. Ground Motion Records for E-W Direction of MC4

ID	EQ No.	Event Name	Station	Comp. ¹	Error ²	BSE-2 Scaling ³	BSE-1 Scaling ³	Step ⁴	Time ⁵
1	34	Superstition Hills	Poe Road (temp)	2	28	3.055	2.037	0.010	23
2	12	Imperial Valley	El Centro Array #11	2	30	4.115	2.744	0.005	40
3	31	Superstition Hills	El Centro Imp. Co.	1	31	2.839	1.893	0.005	40
4	10	Imperial Valley	Delta	2	32	2.433	1.622	0.010	100
5	5	Duzce, Turkey	Bolu	1	34	2.021	1.347	0.010	56
6	28	Loma Prieta	Gilroy Array #3	2	39	2.018	1.345	0.005	40
7	17	Kocaeli, Turkey	Duzce	1	41	2.562	1.708	0.005	28
8	15	Kobe, Japan	Shin-Osaka	1	41	3.028	2.019	0.010	41
9	22	Landers	Yermo Fire Station	2	45	4.479	2.986	0.020	44
10	3	Northridge	Canyon Country-WLC	1	46	2.094	1.396	0.010	20
11	14	Kobe, Japan	Nishi-Akashi	2	47	3.020	2.013	0.010	41
12	41	San Fernando	LA - Hollywood Stor	1	51	5.010	3.340	0.010	28
13	29	Manjil, Iran	Abbar	1	52	2.839	1.893	0.020	54
14	7	Hector Mine	Hector	1	52	4.617	3.078	0.010	46

Notes:

1. Component Number. See FEMA P-695 Appendix A for additional parameters associated to each component of an event.
2. Single composite error value computed in Step 3.
3. Scaling factor for the component for the BSE-2 or BSE-1 EHL (BSE-1 = $\frac{2}{3}$ × BSE-2).
4. Time step in seconds.
5. Total time of record in seconds.

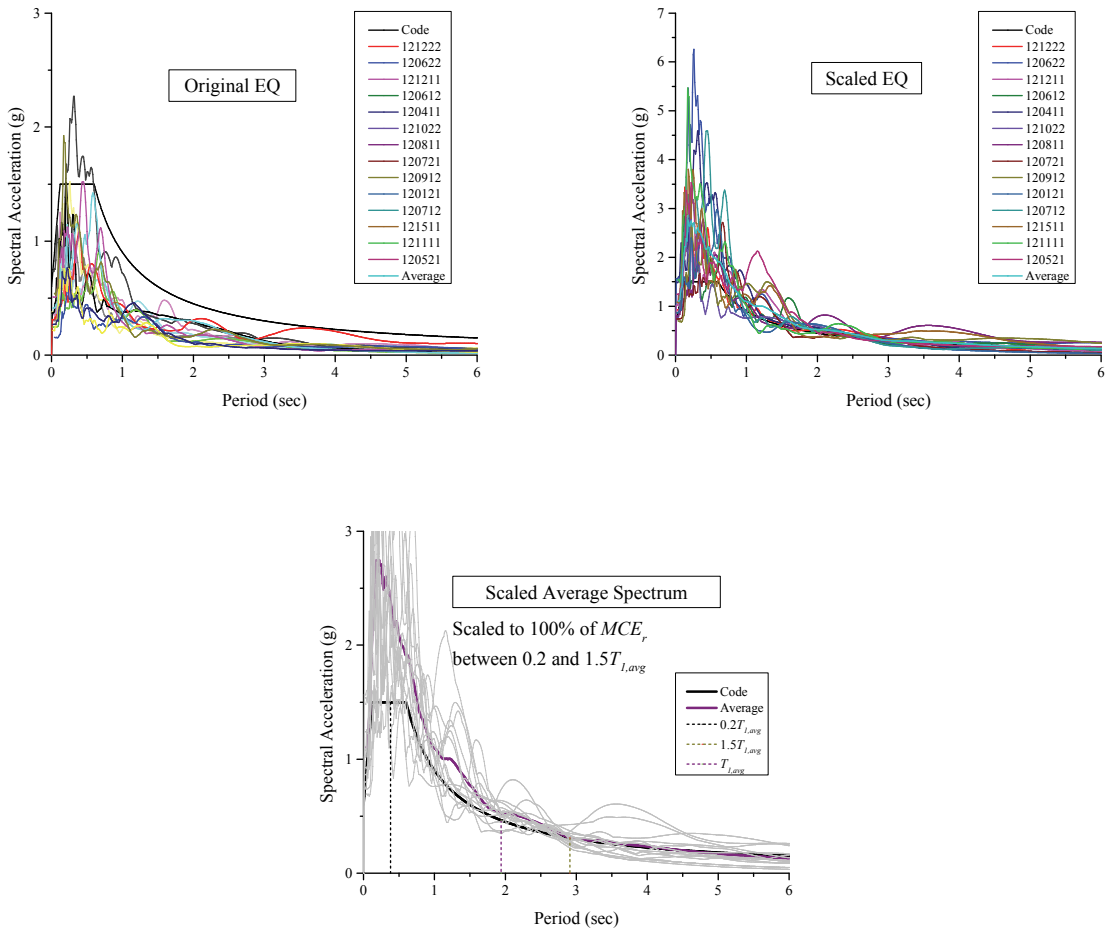


Figure A-1. Acceleration Response Spectra: Original, Scaled, and Scaled Average Spectrum for E-W Direction of MC4

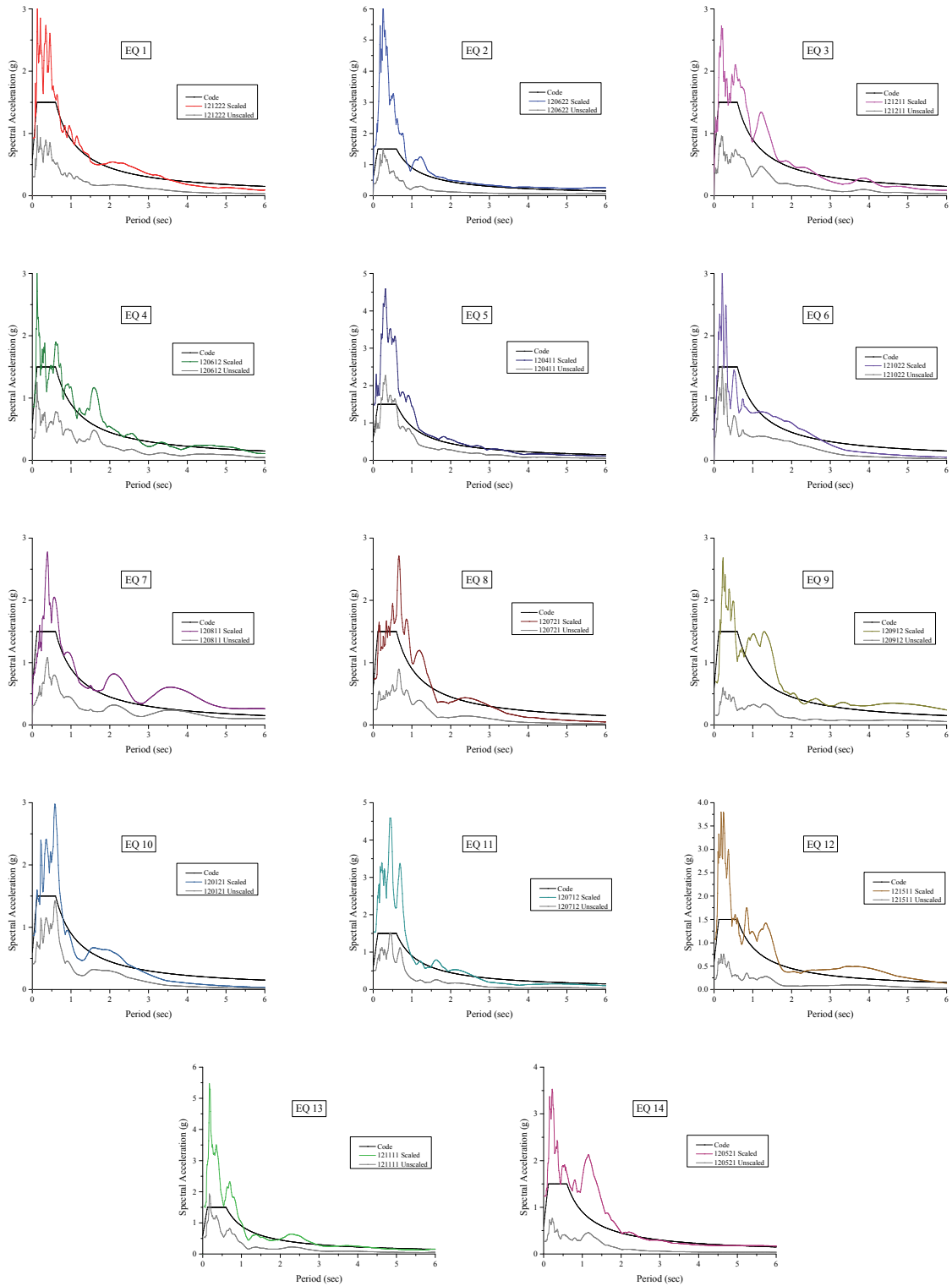


Figure A-2. Acceleration Response Spectra: Original and Scaled for Each Selected Record for E-W Direction of MC4

A.4 Eight-Story Archetype Building

A.4.1 8-Story Special Moment Frame

Table A-2 summarizes the 14 strong motion records used for the NDP for the E-W direction of MC8 (SMF). Figure A-3 illustrates the set of acceleration response spectra, original and scaled, and the scaled average spectrum. Figure A-4 illustrates the acceleration response spectra, original and scaled, for each select record. For comparison, the ASCE 41 code spectrum is shown in the figures. All records completed for the BSE-1 for the ELF design. All analyses with records except 8, 10, and 13 completed for the BSE-2 for the ELF design. All analyses except those using records 8 and 14 completed for the BSE-1 for the RSA design. All analyses except those using records 1, 2, 3, 4, 7, 8, 10, 12, 13, and 14 completed for the BSE-2 for the RSA design.

Table A-2. Ground Motion Records for E-W Direction of MC8

I D	EQ No.	Event Name	Station	Comp. ¹	Error ²	BSE-2 Scaling ³	BSE-1 Scaling ³	Step ⁴	Time ⁵
1	12	Imperial Valley	El Centro Array #11	2	29	3.862	2.575	0.005	40
2	21	Landers	Yermo Fire Station	1	56	2.842	1.894	0.020	44
3	10	Imperial Valley	Delta	2	58	2.371	1.581	0.010	100
4	27	Loma Prieta	Gilroy Array #3	1	59	5.483	3.656	0.005	40
5	5	Duzce, Turkey	Bolu	1	61	2.036	1.358	0.010	56
6	34	Superstition Hills	Poe Road (temp)	2	62	3.132	2.088	0.010	23
7	29	Manjil, Iran	Abbar	1	63	3.034	2.023	0.020	54
8	39	Chi-Chi, Taiwan	TCU045	1	63	4.768	3.179	0.005	90
9	42	San Fernando	LA - Hollywood Stor	2	66	6.846	4.564	0.010	28
10	19	Kocaeli, Turkey	Arcelik	1	67	8.760	5.840	0.005	30
11	7	Hector Mine	Hector	1	74	5.307	3.538	0.010	46
12	31	Superstition Hills	El Centro Imp. Co.	1	74	2.844	1.896	0.005	40
13	44	Friuli, Italy	Tolmezzo	2	80	9.476	6.318	0.005	37
14	38	Chi-Chi, Taiwan	CHY101	2	88	0.993	0.662	0.005	90

Notes:

1. Component Number. See FEMA P-695 Appendix A for additional parameters associated to each component of an event.
2. Single composite error value computed in Step 3.
3. Scaling factor for the component for the BSE-2 or BSE-1 EHL ($BSE-1 = \frac{2}{3} \times BSE-2$).
4. Time step in seconds.
5. Total time of record in seconds.

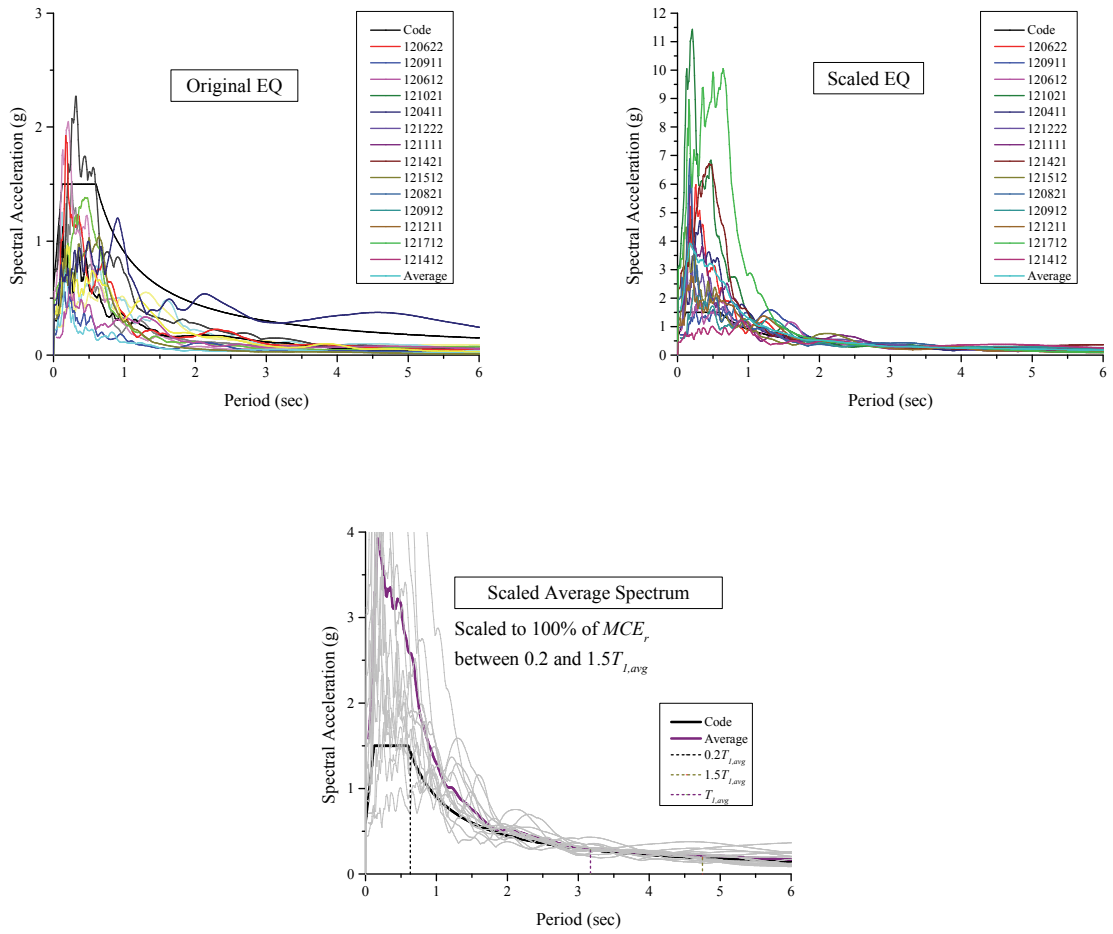


Figure A-3. Acceleration Response Spectra: Original, Scaled, and Scaled Average Spectrum for E-W Direction of MC8

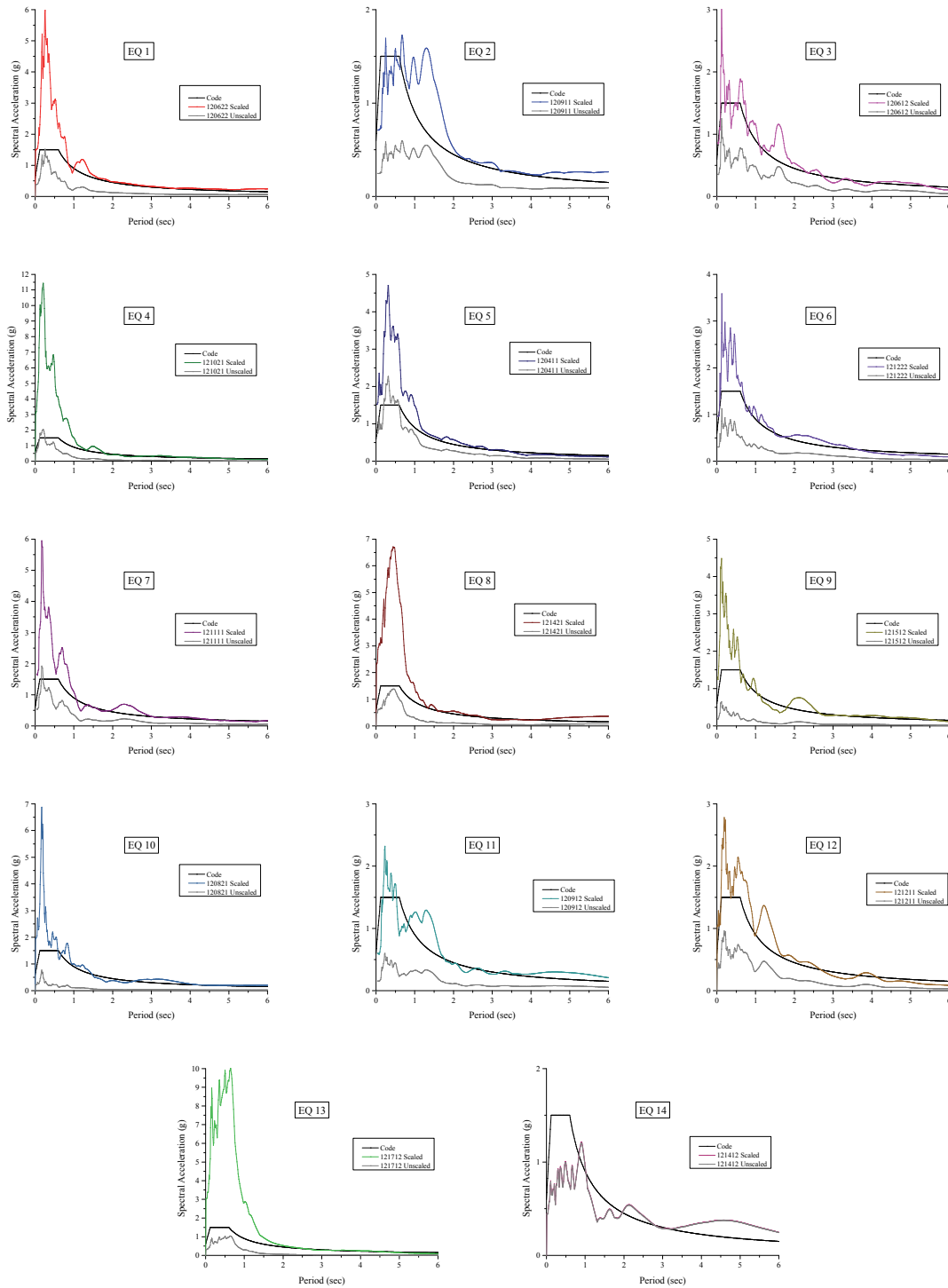


Figure A-4. Acceleration Response Spectra: Original and Scaled for Each Selected Record for E-W Direction of MC8

A.5 Sixteen-Story Archetype Building

A.5.1 16-Story Special Moment Frame

Table A-3 summarizes the 14 strong motion records used for the NDP for the E-W direction of MC16 (SMF). Figure A-5 illustrates the set of acceleration response spectra, original and scaled, and the scaled average spectrum. Figure A-6 illustrates the acceleration response spectra, original and scaled, for each select record. For comparison, the ASCE 41 code spectrum is shown in the figures. All analyses completed for the BSE-1 and BSE-2 for the ELF design. All records completed for the BSE-1 for the RSA design. All analyses except those using records 1, 2, 5, and 10 completed for the BSE-2 for the RSA design.

Table A-3. Ground Motion Records for E-W Direction of MC16

ID	EQ No.	Event Name	Station	Comp. 1	Error ²	BSE-2 Scaling ³	BSE-1 Scaling ³	Step ⁴	Time ⁵
1	12	Imperial Valley	El Centro Array #11	2	66	3.664	2.443	0.005	40
2	29	Manjil, Iran	Abbar	1	74	3.295	2.197	0.020	54
3	19	Kocaeli, Turkey	Arcelik	1	83	8.383	5.589	0.005	30
4	7	Hector Mine	Hector	1	88	4.992	3.328	0.010	46
5	9	Imperial Valley	Delta	1	93	3.061	2.041	0.010	100
6	22	Landers	Yermo Fire Station	2	94	3.089	2.059	0.020	44
7	5	Duzce, Turkey	Bolu	1	97	2.724	1.816	0.010	56
8	42	San Fernando	LA - Hollywood Stor	2	97	7.119	4.746	0.010	28
9	17	Kocaeli, Turkey	Duzce	1	103	1.673	1.115	0.005	28
10	32	Superstition Hills	El Centro Imp. Co.	2	105	2.940	1.960	0.005	40
11	14	Kobe, Japan	Nishi-Akashi	2	106	4.286	2.857	0.010	41
12	27	Loma Prieta	Gilroy Array #3	1	108	6.015	4.010	0.005	40
13	16	Kobe, Japan	Shin-Osaka	2	118	7.346	4.897	0.010	41
14	37	Chi-Chi, Taiwan	CHY101	1	121	1.241	0.827	0.005	90

Notes:

1. Component Number. See FEMA P-695 Appendix A for additional parameters associated to each component of an event.
2. Single composite error value computed in Step 3.
3. Scaling factor for the component for the BSE-2 or BSE-1 EHL ($BSE-1 = \frac{2}{3} \times BSE-2$).
4. Time step in seconds.
5. Total time of record in seconds.

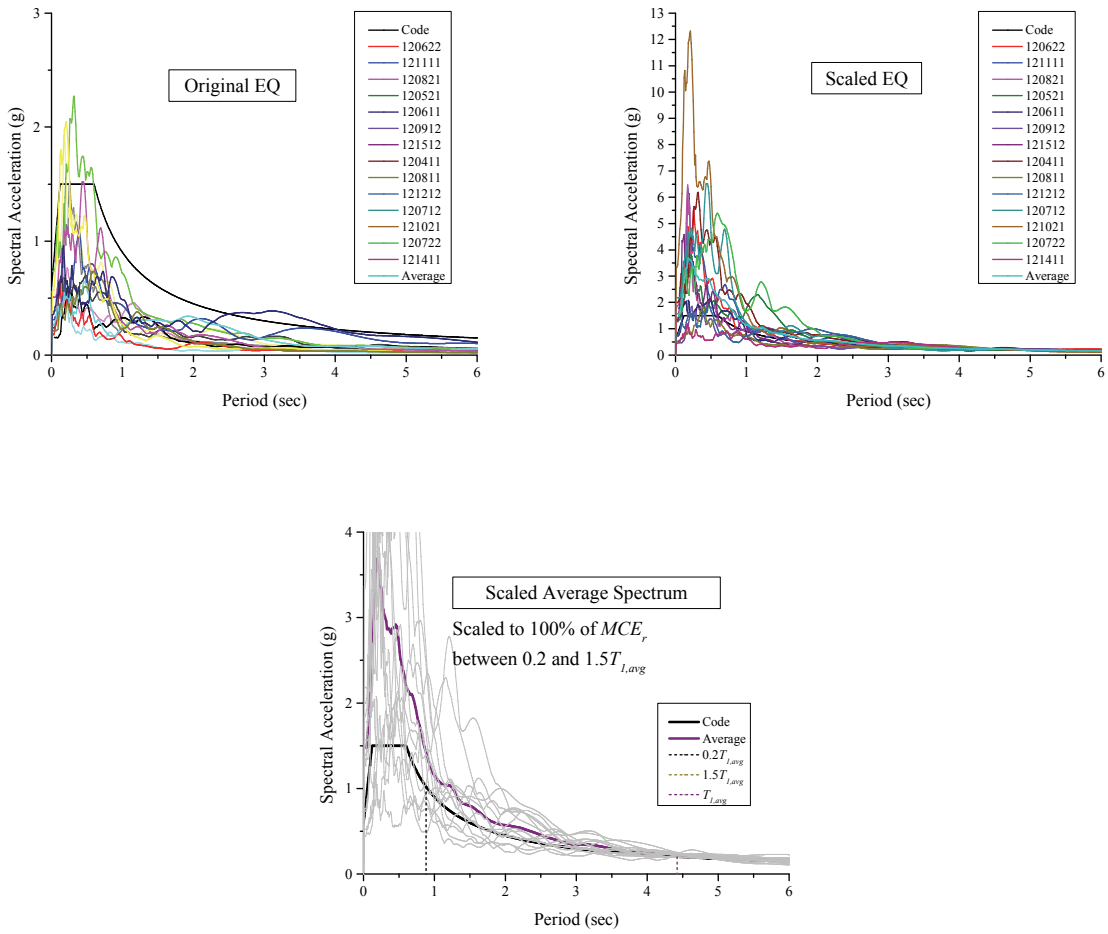


Figure A-5. Acceleration Response Spectra: Original, Scaled, and Scaled Average Spectrum for E-W Direction of MC16

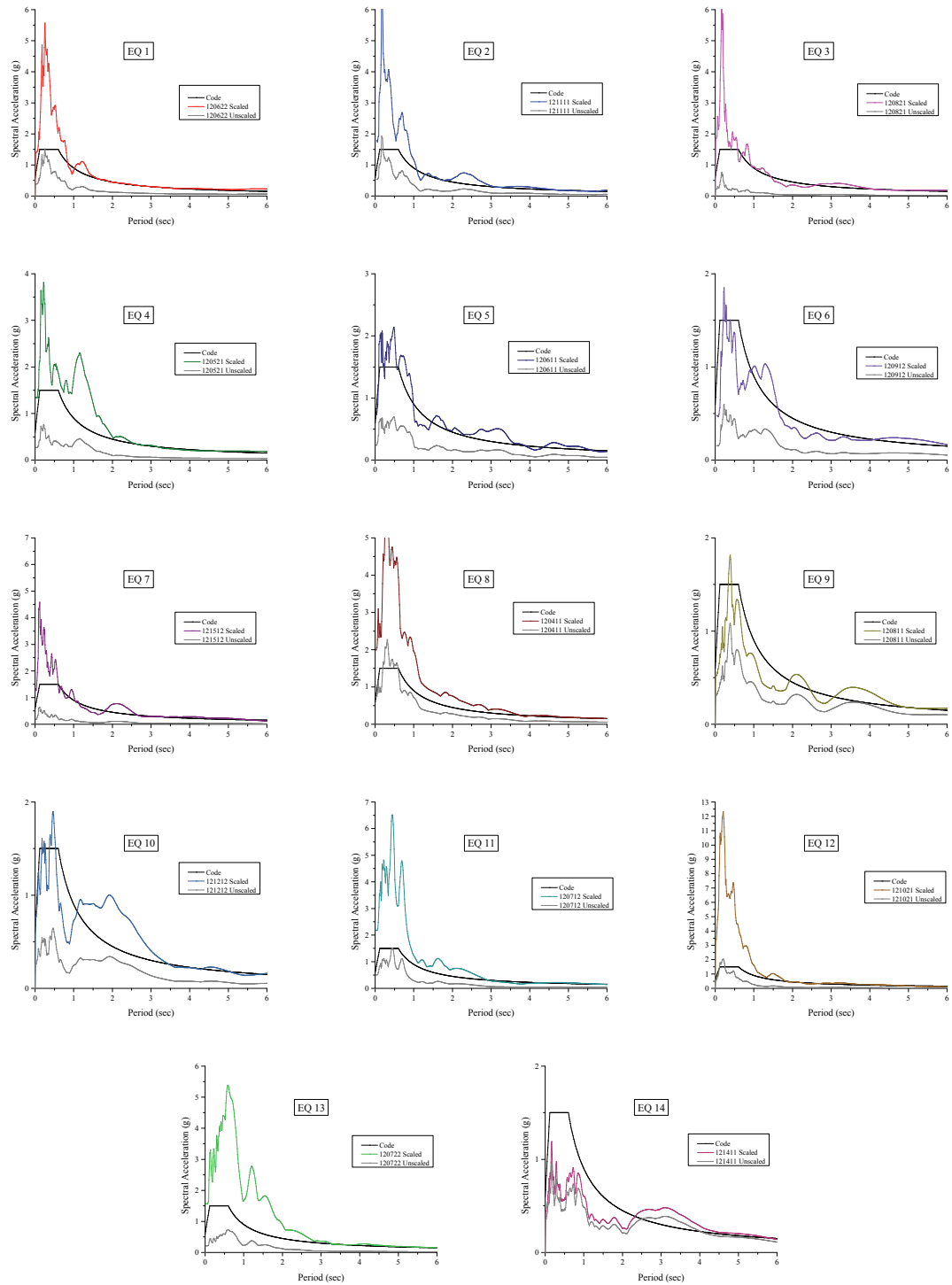


Figure A-6. Acceleration Response Spectra: Original and Scaled for Each Selected Record for E-W Direction of MC16

A.6 FEMA P-695 Far-Field Record Set

Figure A-7 through Figure A-50 illustrate the recorded ground motion, Fourier amplitude (frequency and period), and the five percent damped response spectra (displacement, velocity, acceleration) for each component.

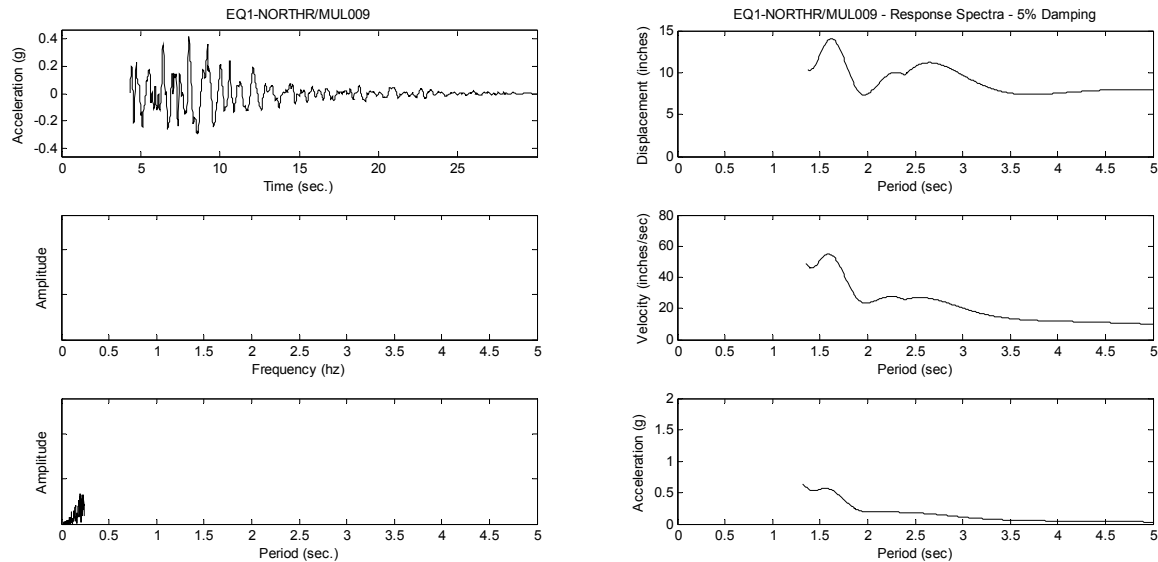


Figure A-7. 1994 Northridge Earthquake at Beverly Hills, Mulholland Drive Station, Comp. 009

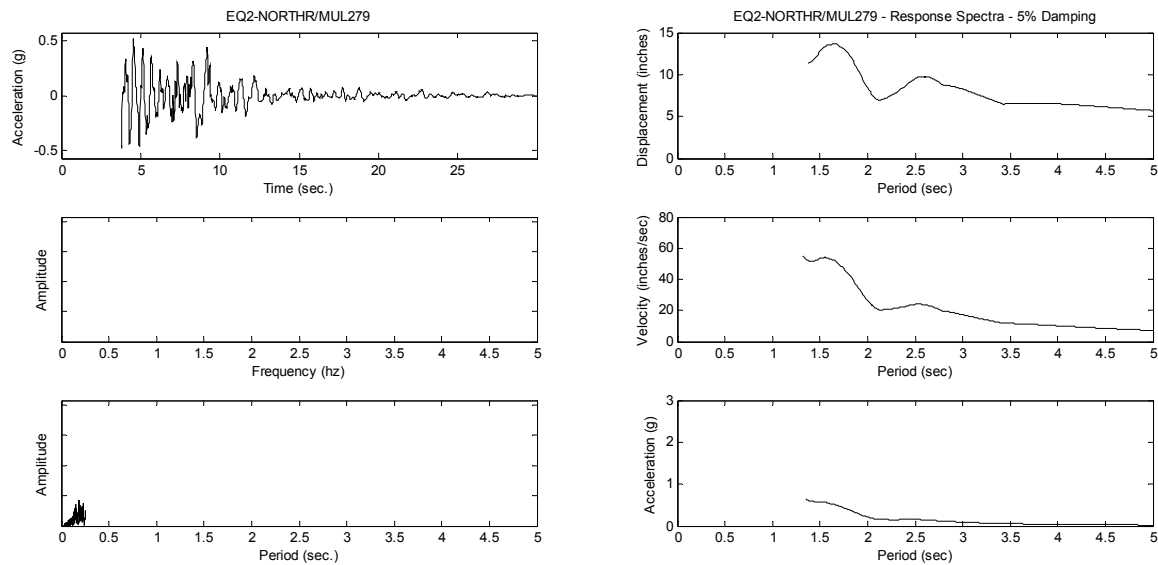


Figure A-8. 1994 Northridge Earthquake at Beverly Hills, Mulholland Drive Station, Comp. 279

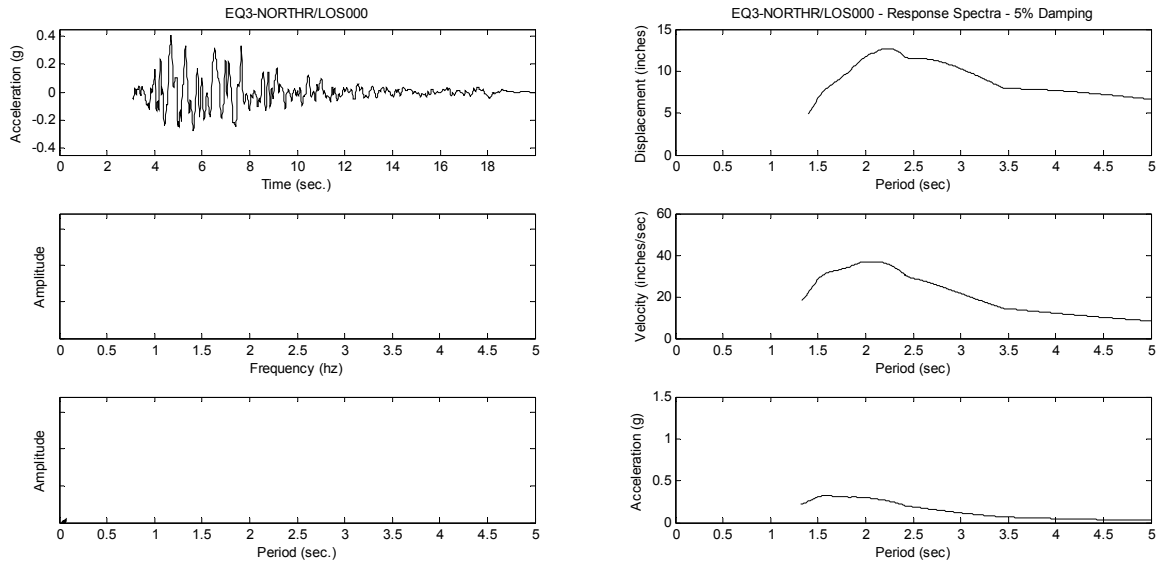


Figure A-9. 1994 Northridge Earthquake at Canyon Country WLC Station, Comp. 000

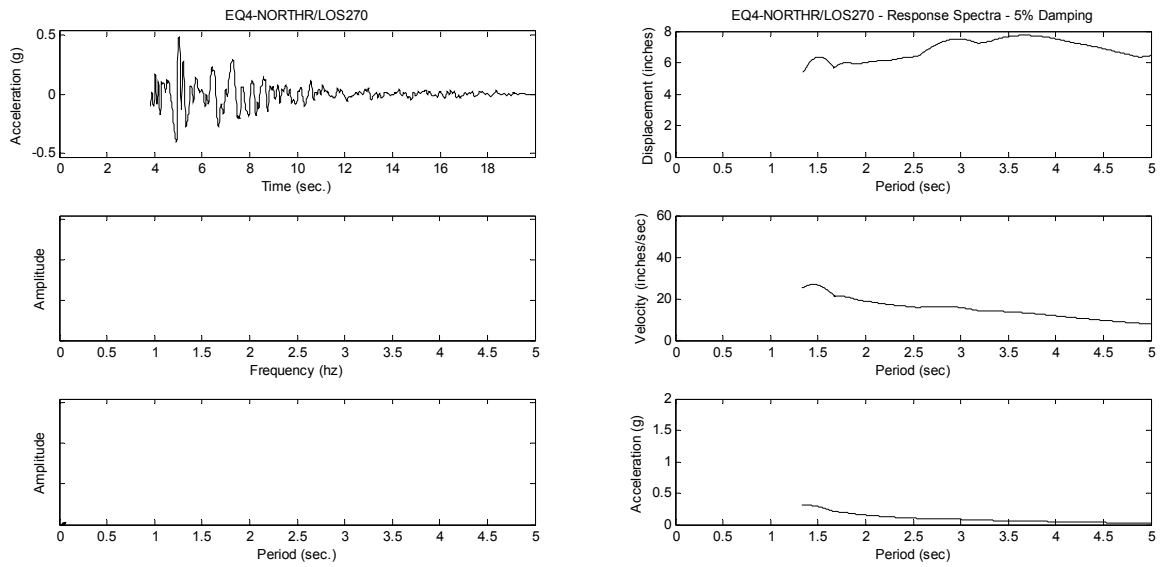


Figure A-10. 1994 Northridge Earthquake at Canyon Country WLC Station, Comp. 270

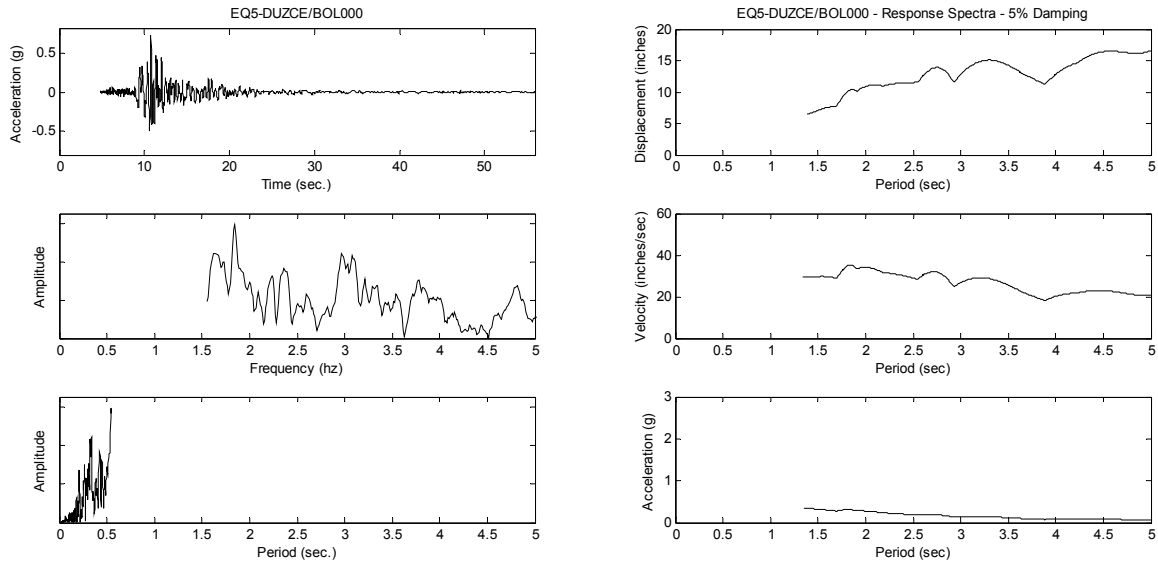


Figure A-11. 1999 Duzce, Turkey Earthquake at Bolu Station, Comp. 000

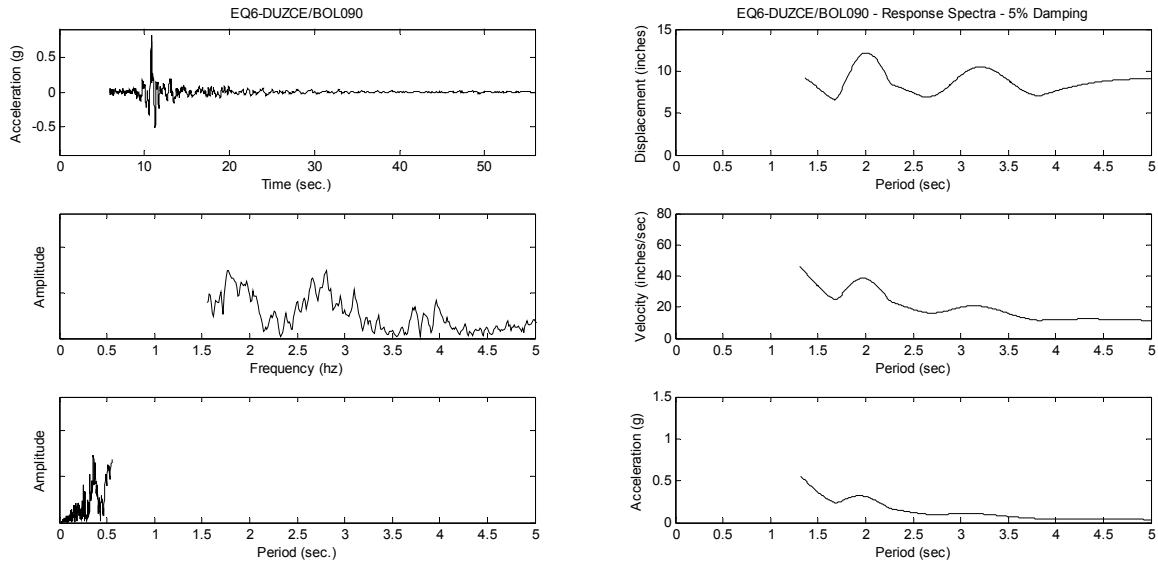


Figure A-12. 1999 Duzce, Turkey Earthquake at Bolu Station, Comp. 090

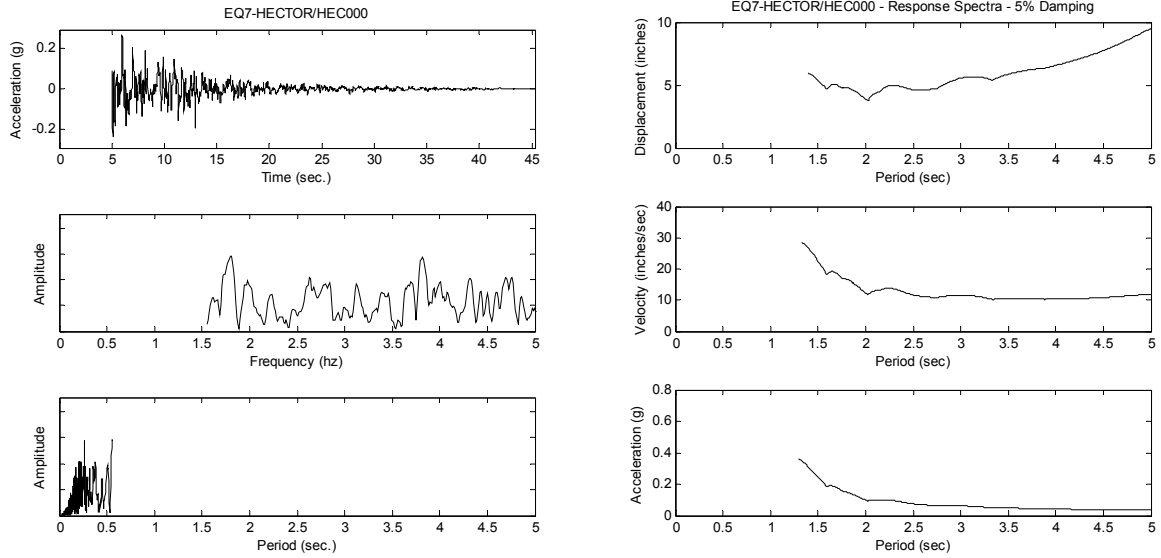


Figure A-13. 1999 Hector Mine Earthquake at Hector Station, Comp. 000

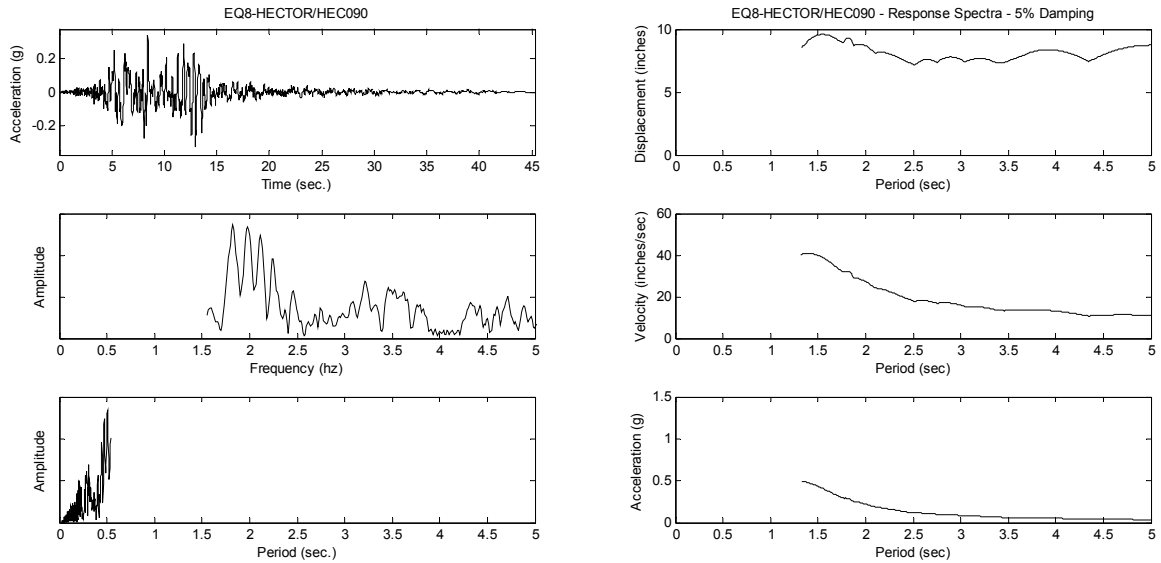


Figure A-14. 1999 Hector Mine Earthquake at Hector Station, Comp. 090

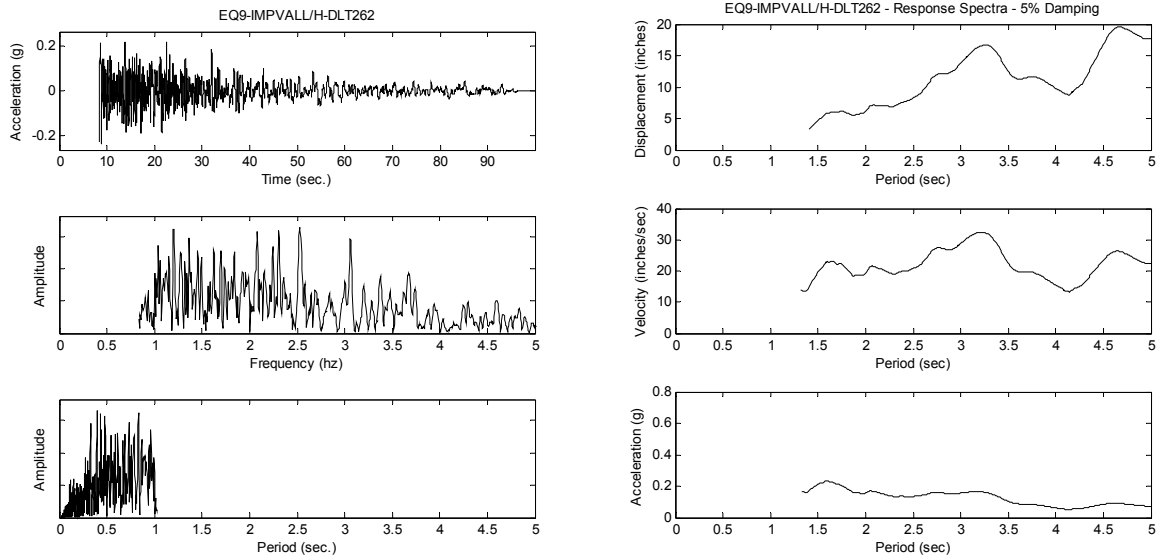


Figure A-15. 1979 Imperial Valley Earthquake at Delta Station, Comp. 262

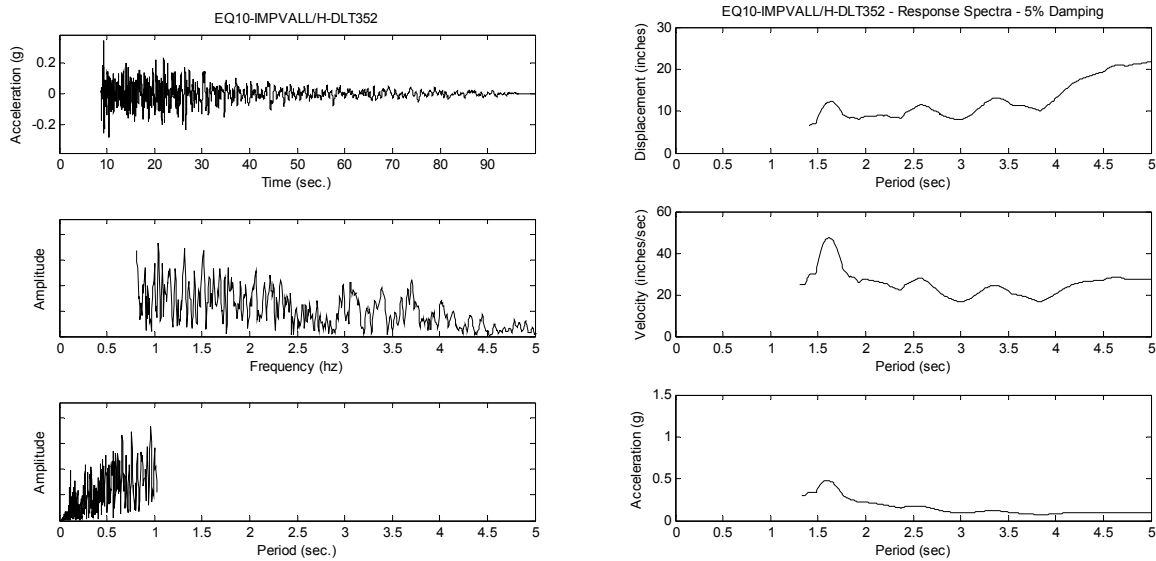


Figure A-16. 1979 Imperial Valley Earthquake at Delta Station, Comp. 352

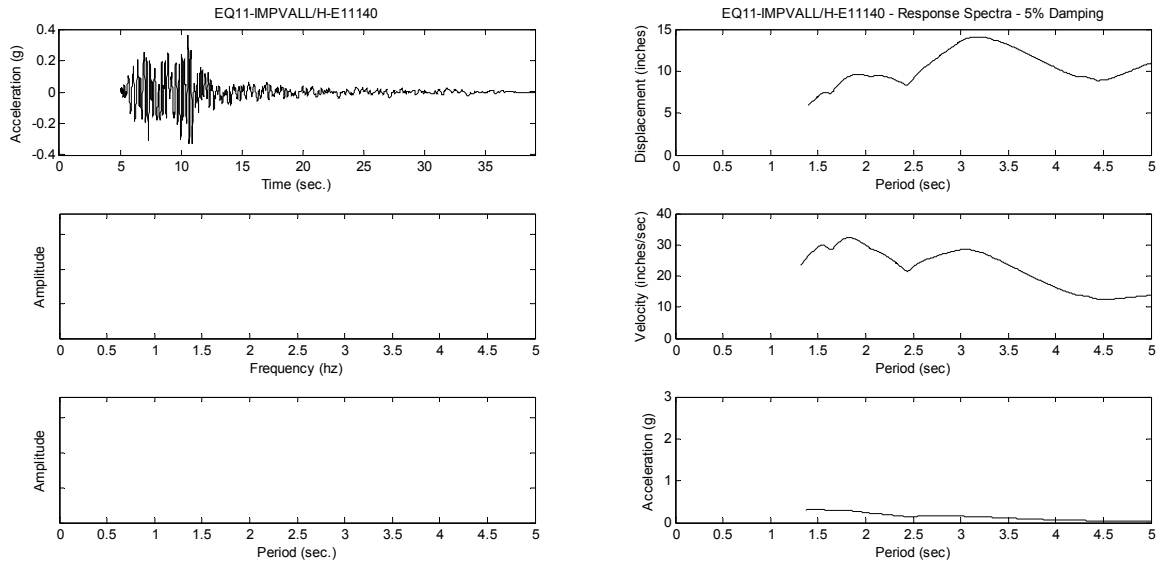


Figure A-17. 1979 Imperial Valley Earthquake at El Centro Array Station #11, Comp. 140

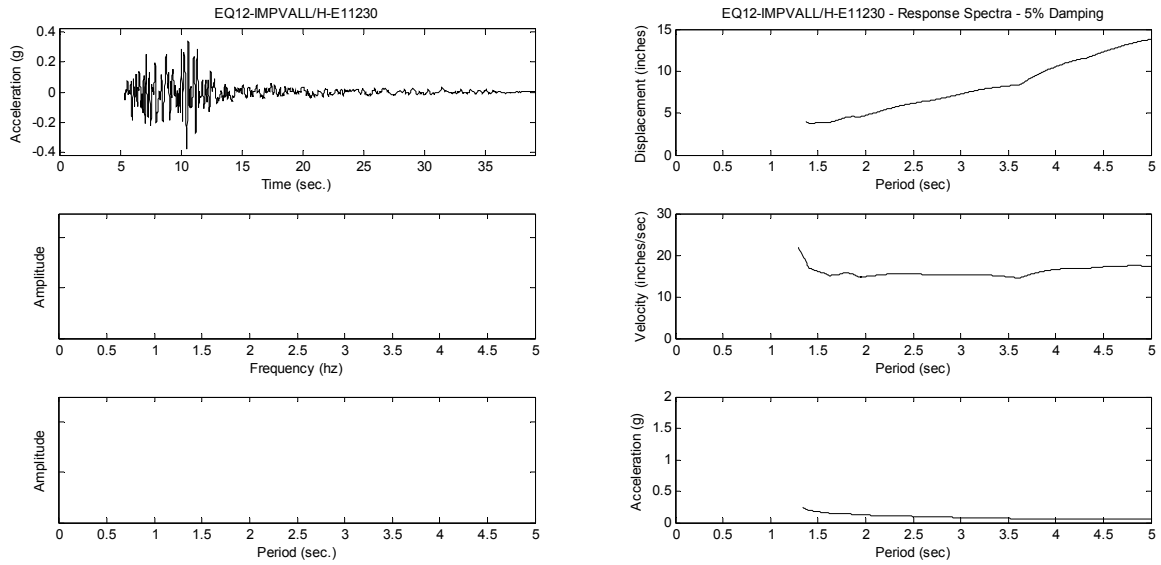


Figure A-18. 1979 Imperial Valley Earthquake at El Centro Array Station #11, Comp. 230

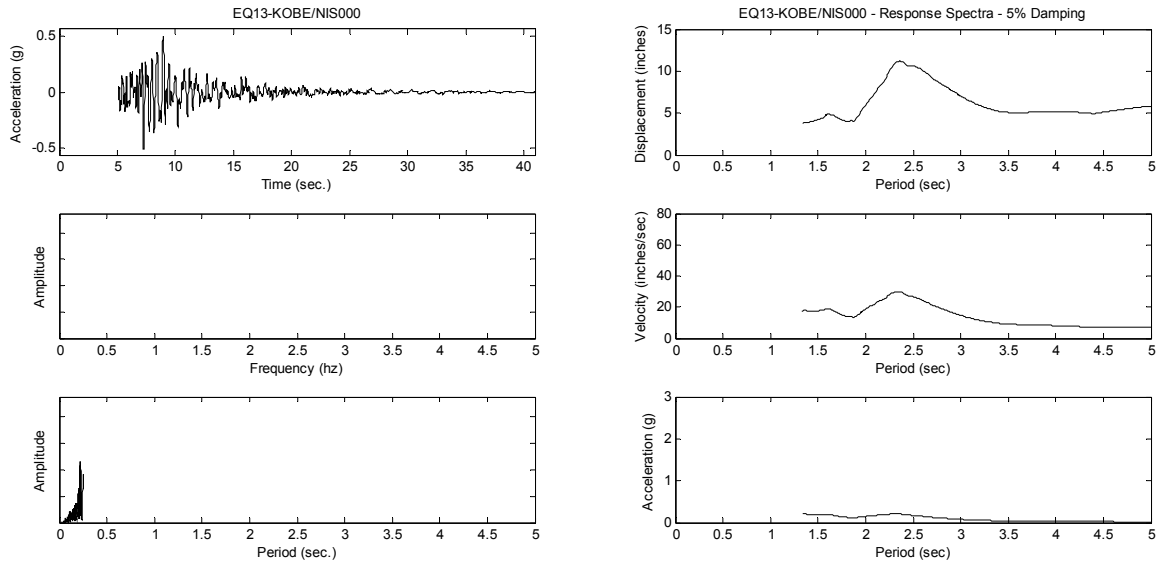


Figure A-19. 1995 Kobe, Japan Earthquake at Nishi-Akashi Station, Comp. 000

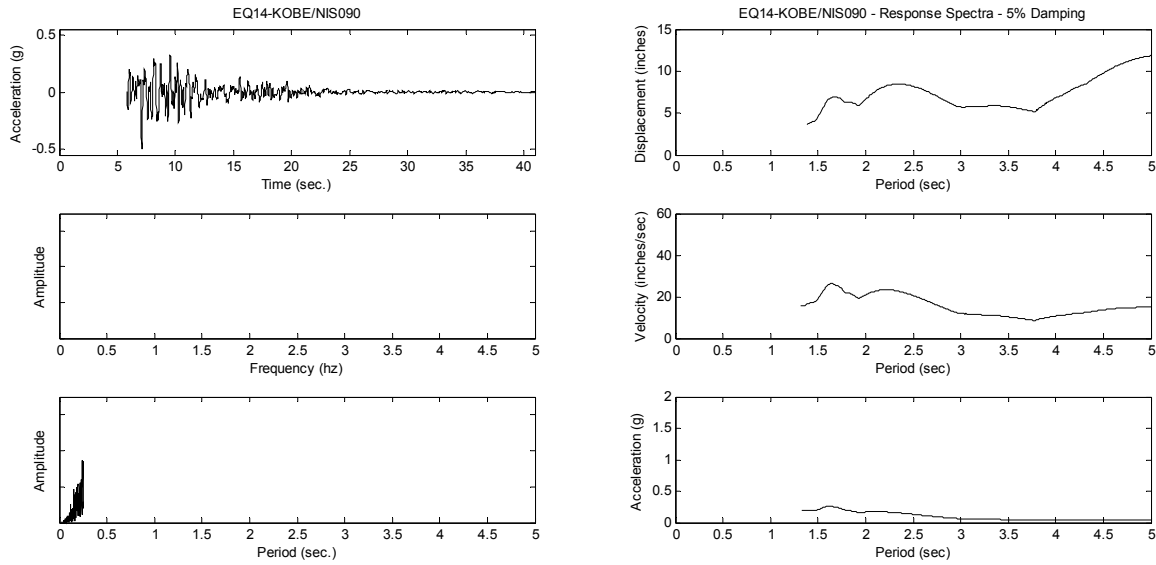


Figure A-20. 1995 Kobe, Japan Earthquake at Nishi-Akashi Station, Comp. 090

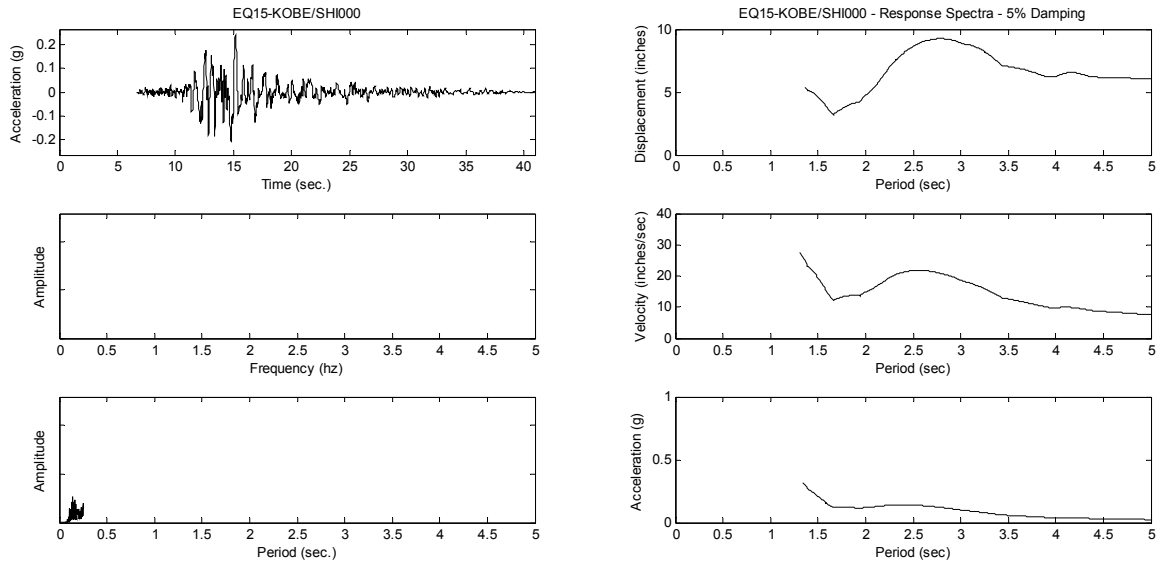


Figure A-21. 1995 Kobe, Japan Earthquake at Shin-Osaka Station, Comp. 000

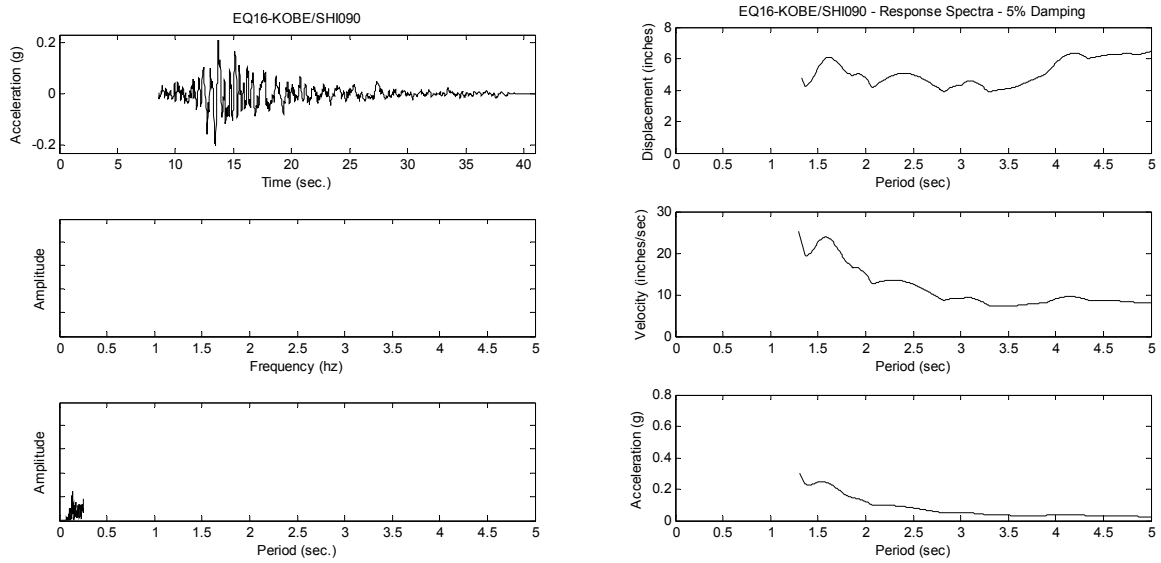


Figure A-22. 1995 Kobe, Japan Earthquake at Shin-Osaka Station, Comp. 090

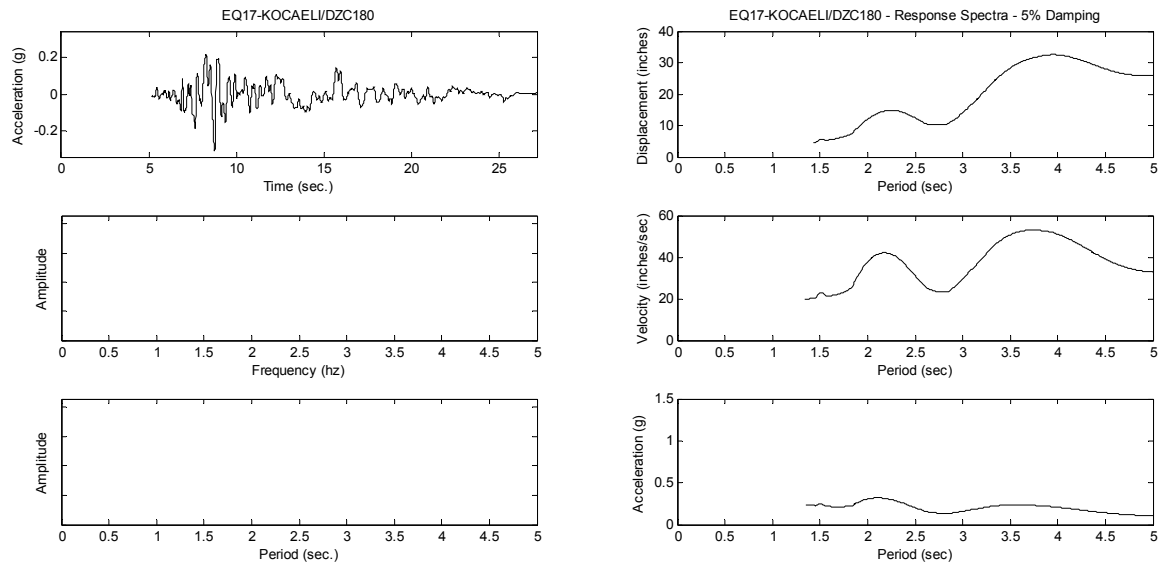


Figure A-23. 1999 Kocaeli, Turkey Earthquake at Duzce Station, Comp. 180

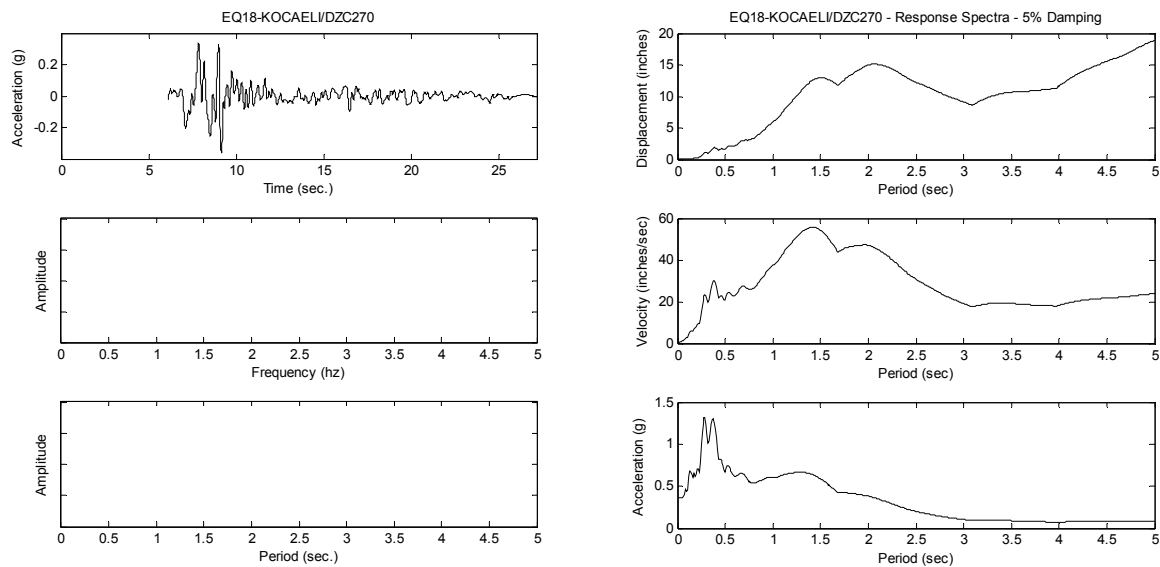


Figure A-24. 1999 Kocaeli, Turkey Earthquake at Duzce Station, Comp. 270

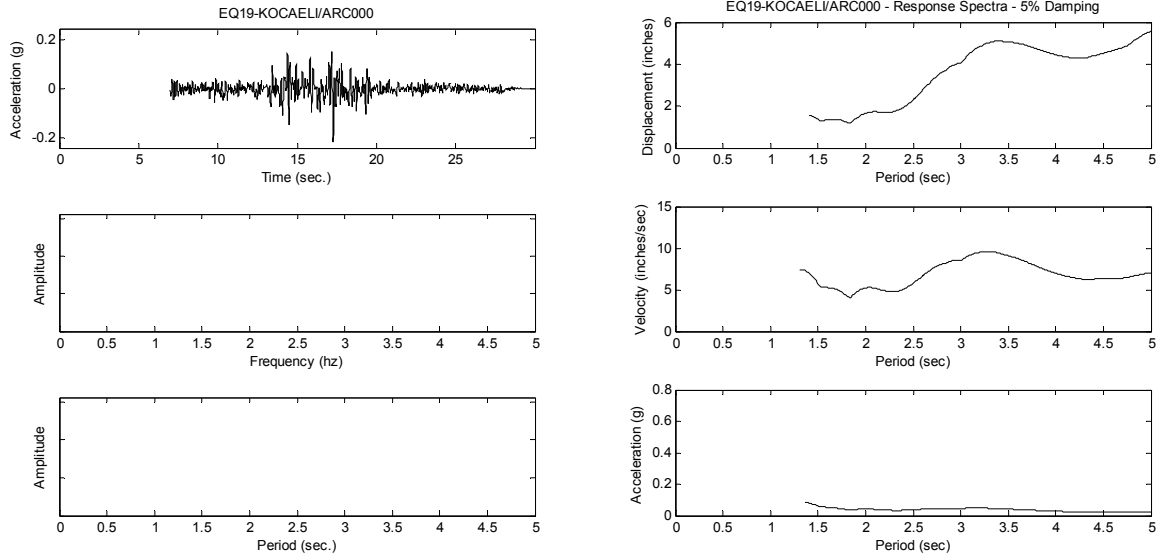


Figure A-25. 1999 Kocaeli, Turkey Earthquake at Arcelik Station, Comp. 000

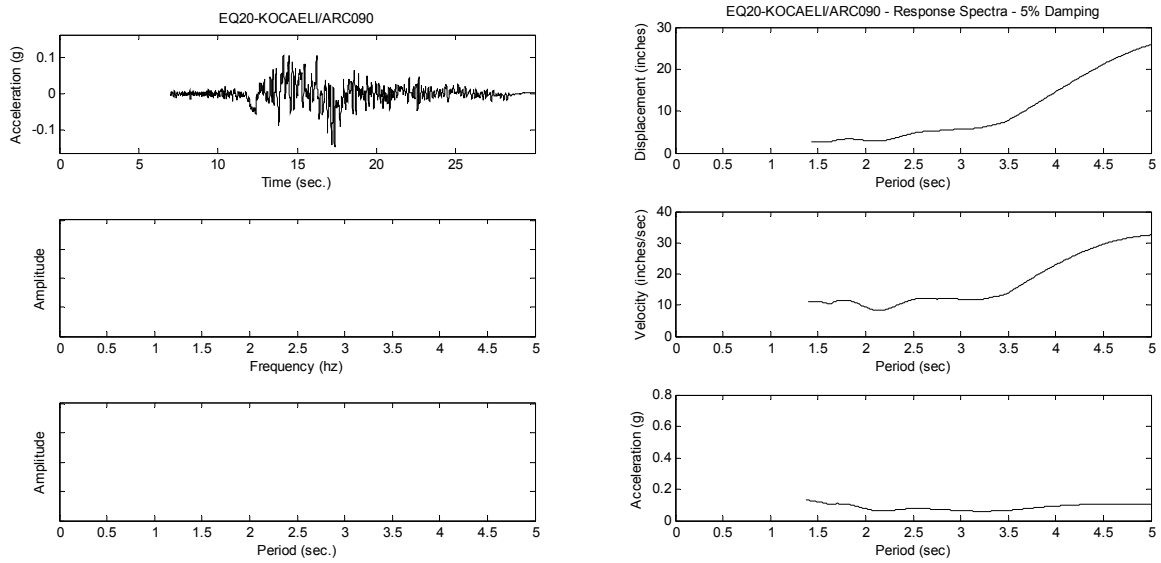


Figure A-26. 1999 Kocaeli, Turkey Earthquake at Arcelik Station, Comp. 090

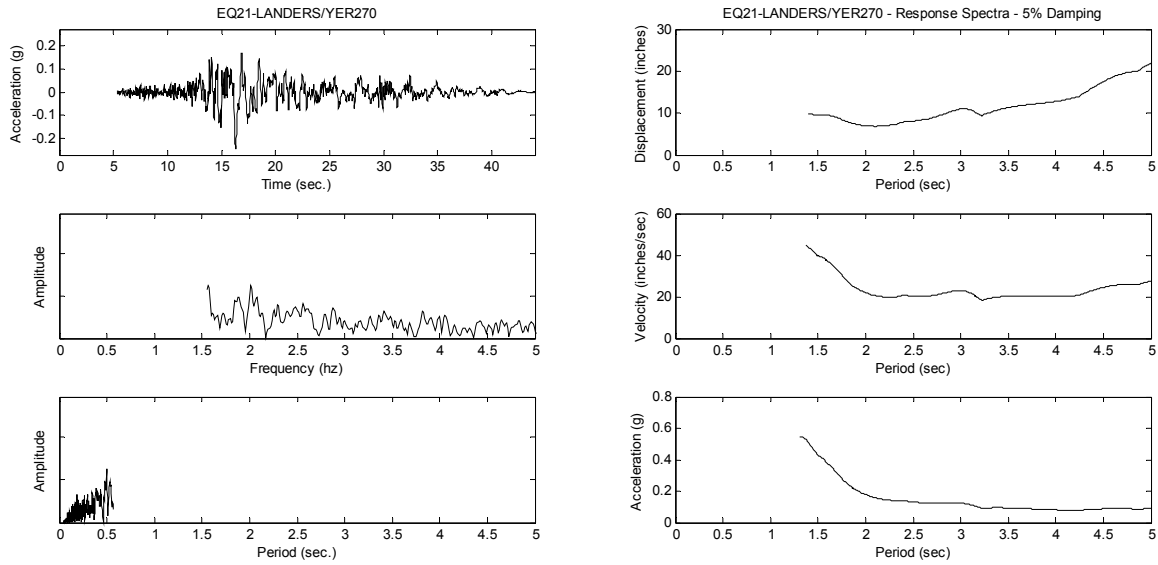


Figure A-27. 1992 Landers Earthquake at Yermo Fire Station, Comp. 270

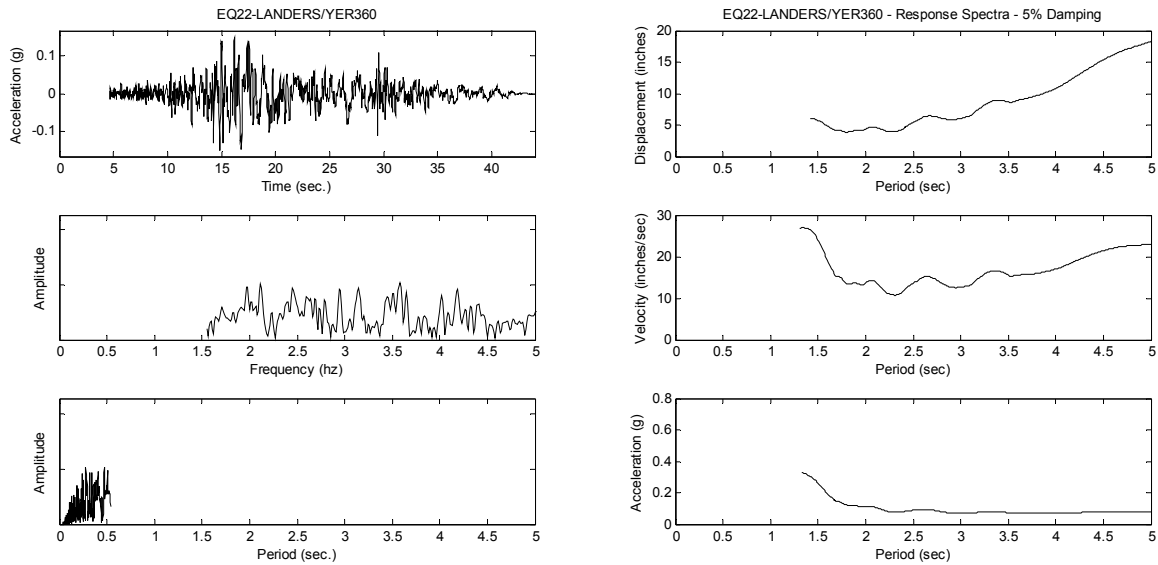


Figure A-28. 1992 Landers Earthquake at Yermo Fire Station, Comp. 360

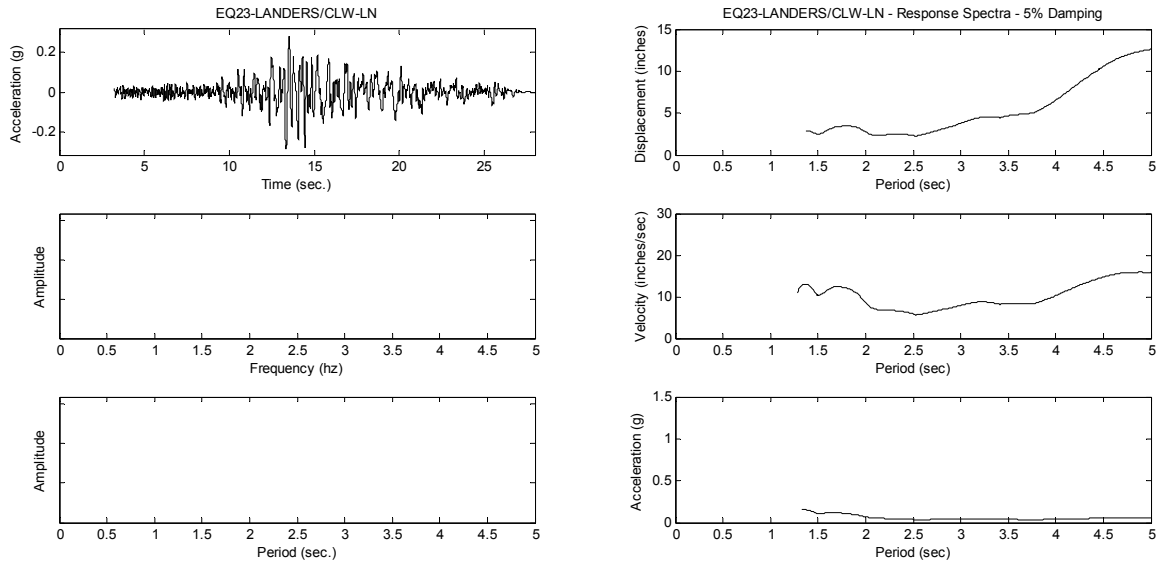


Figure A-29. 1992 Landers Earthquake at Coolwater Station, Longitudinal Direction

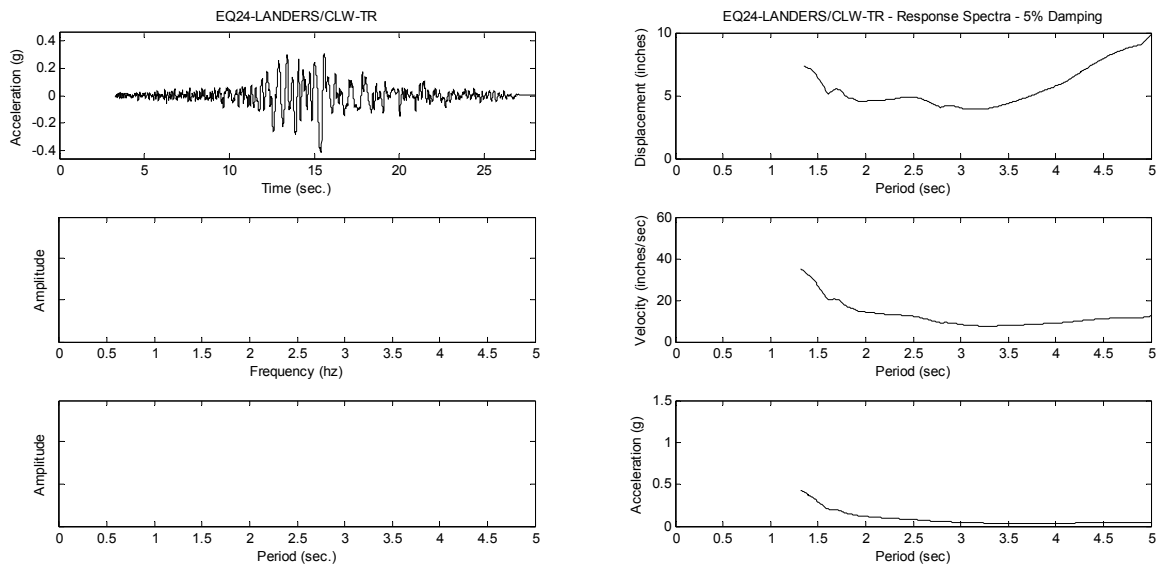


Figure A-30. 1992 Landers Earthquake at Coolwater Station, Transverse Direction

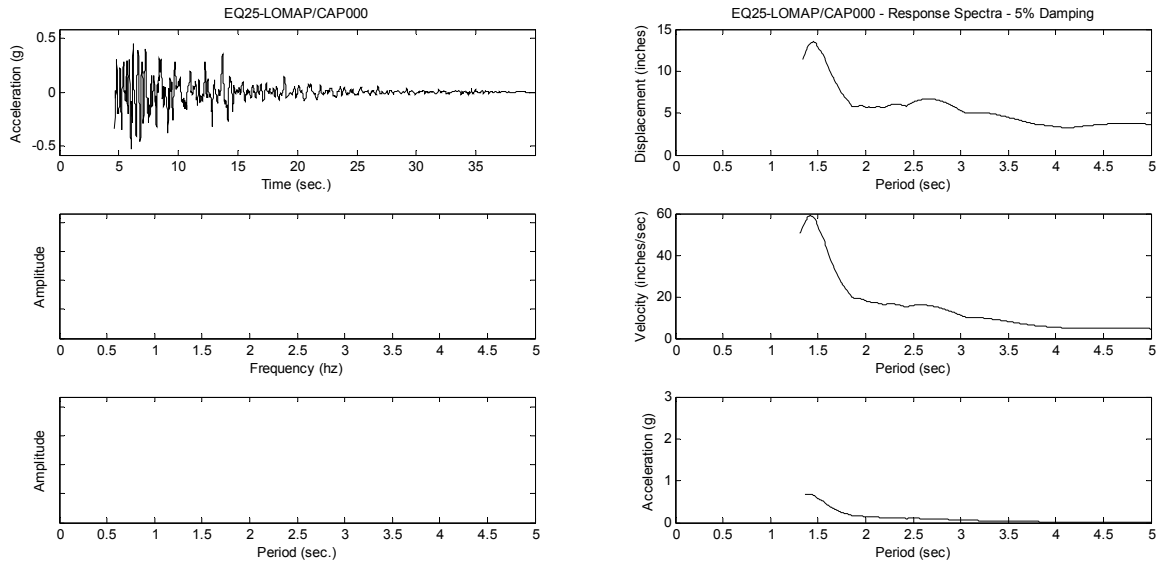


Figure A-31. 1989 Loma Prieta Earthquake at Capitola Station, Comp. 000

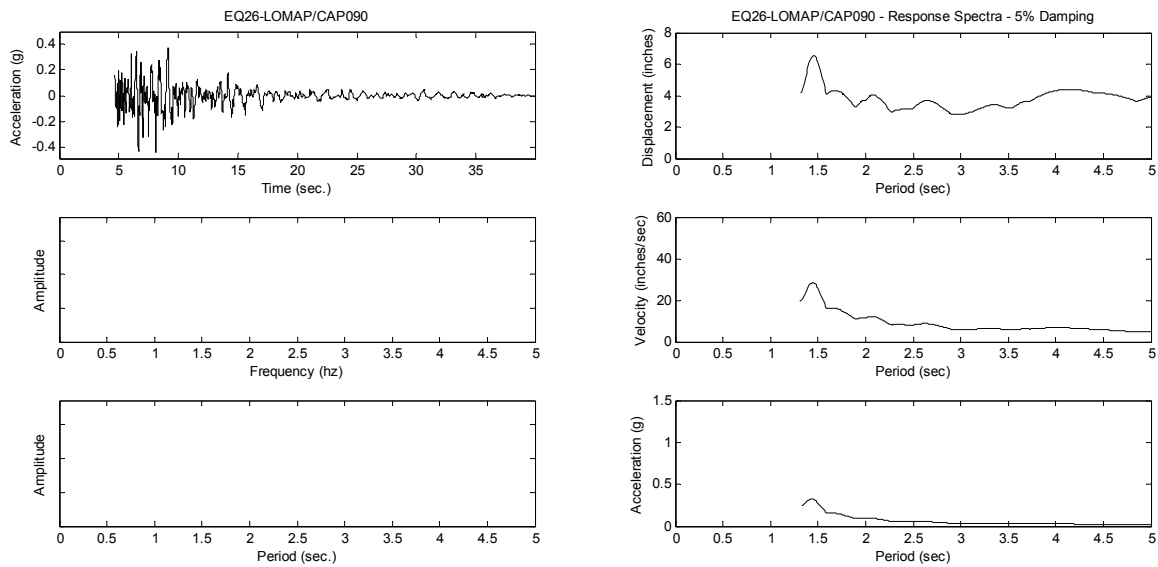


Figure A-32. 1989 Loma Prieta Earthquake at Capitola Station, Comp. 090

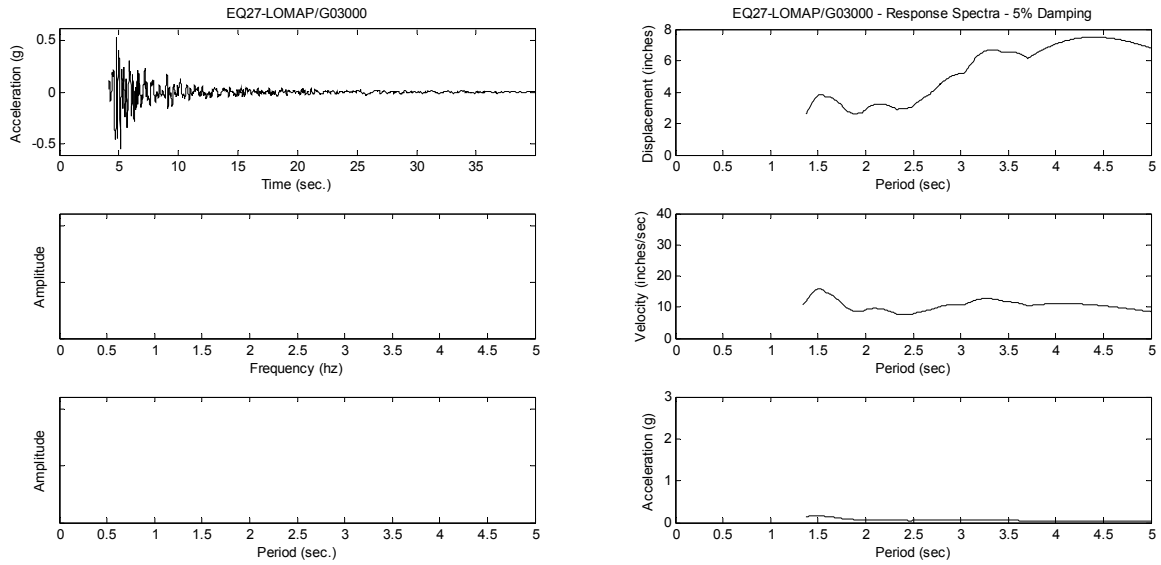


Figure A-33. 1989 Loma Prieta Earthquake at Gilroy Array Station #3, Comp. 000

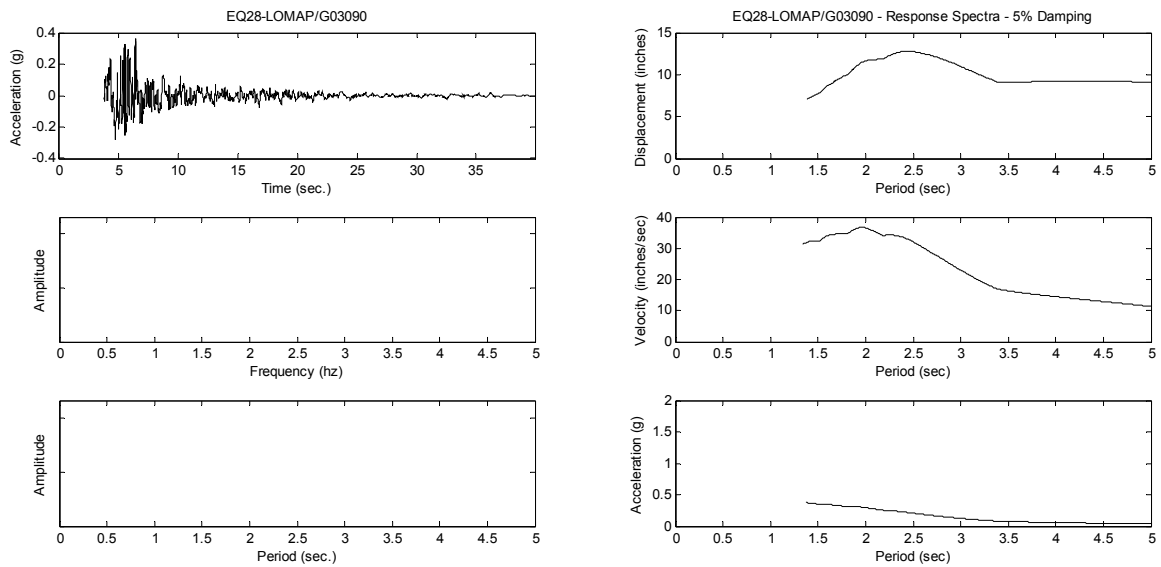


Figure A-34. 1989 Loma Prieta Earthquake at Gilroy Array Station #3, Comp. 090

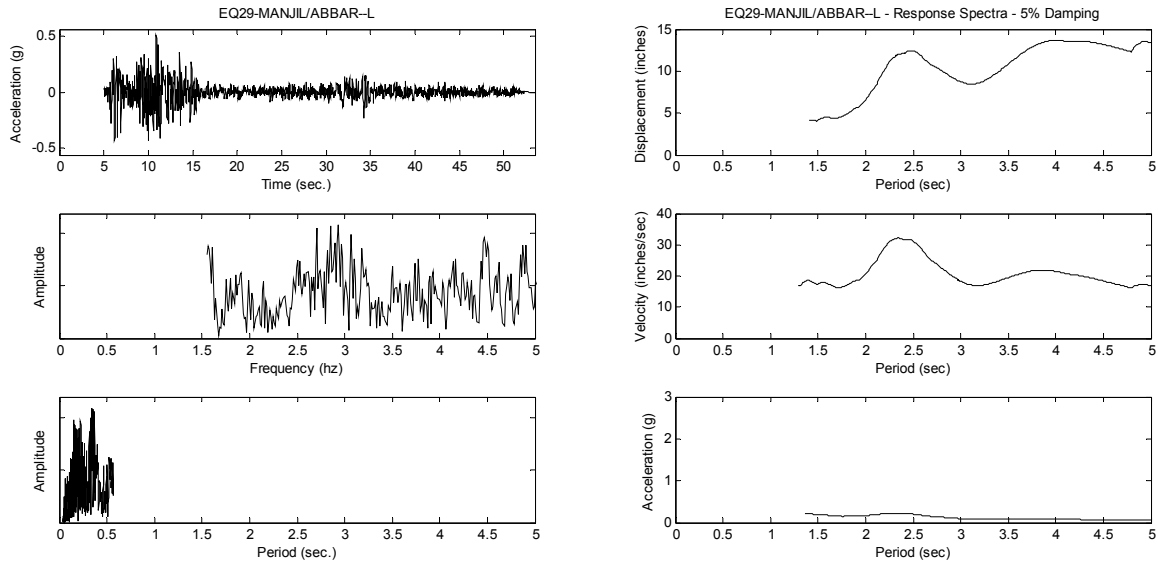


Figure A-35. 1990 Manjil, Iran Earthquake at Abbar Station, Longitudinal Direction

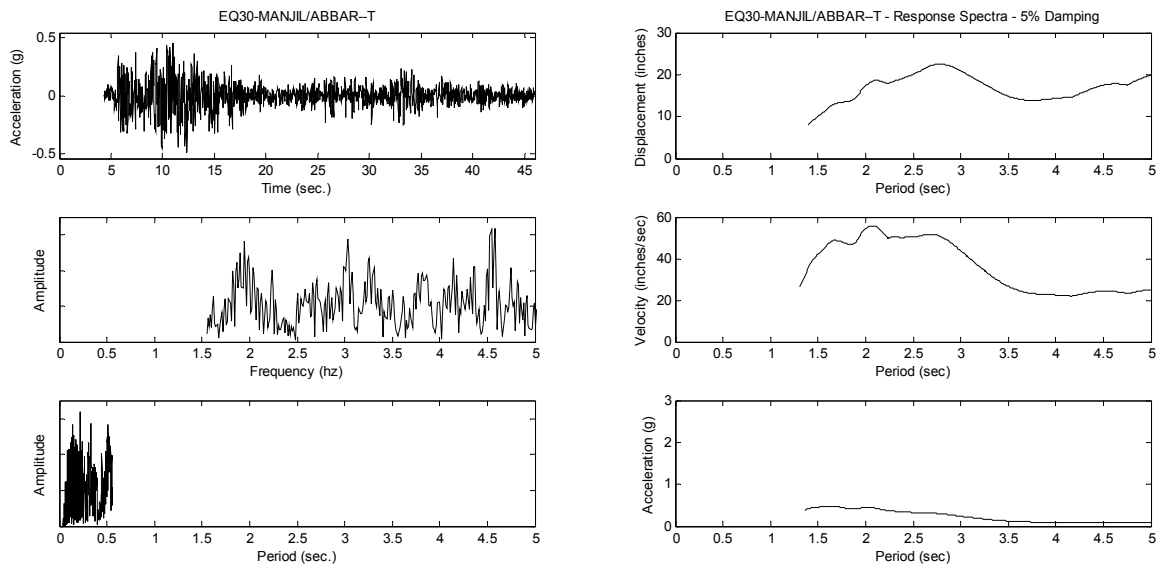


Figure A-36. 1990 Manjil, Iran Earthquake at Abbar Station, Transverse Direction

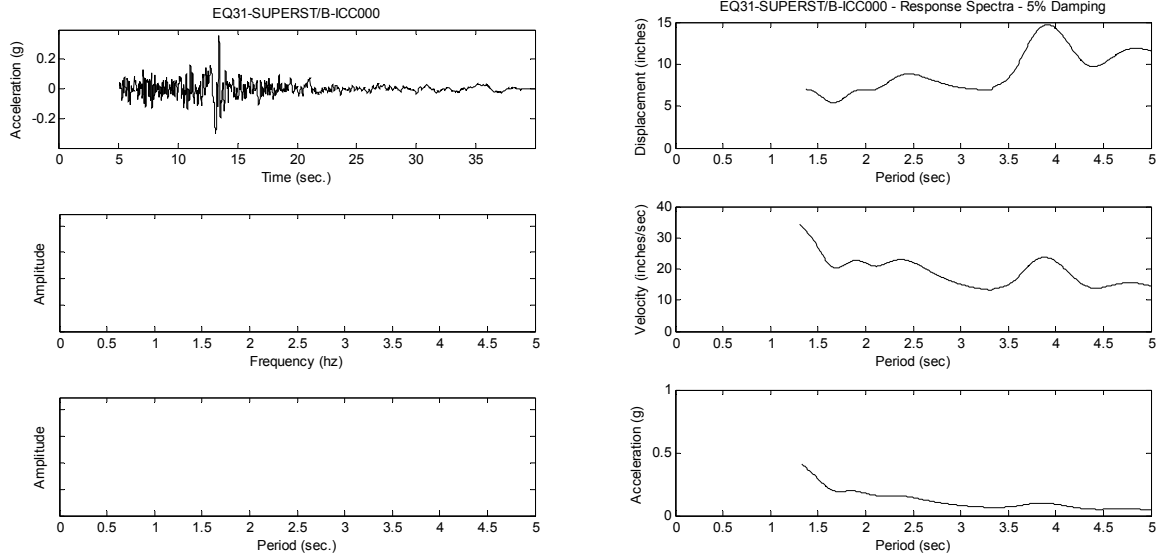


Figure A-37. 1987 Superstition Hills Earthquake at El Centro, Imperial County, Comp. 000

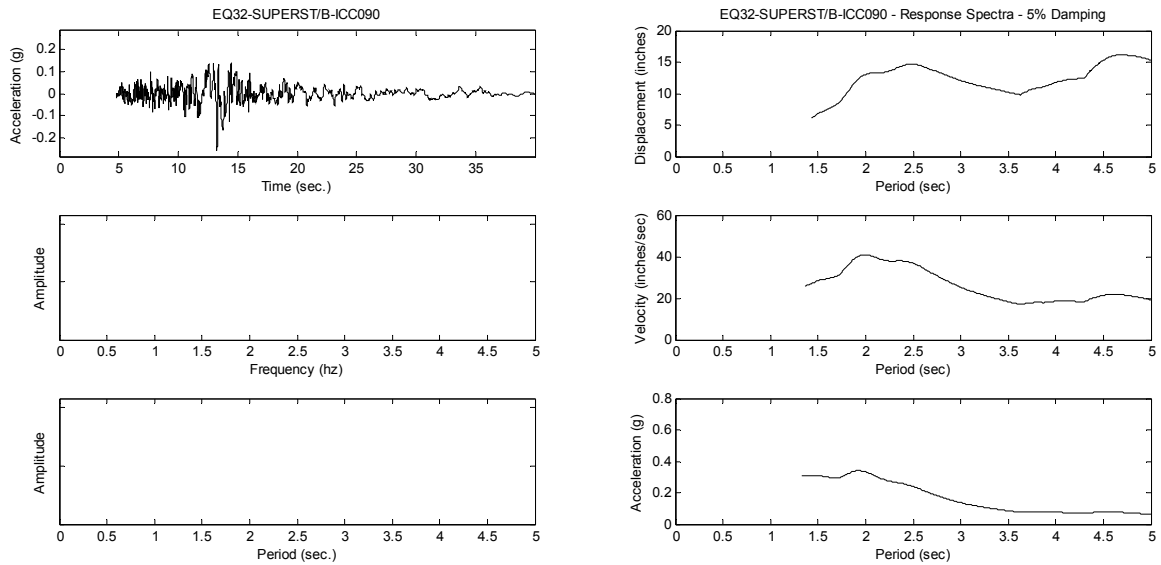


Figure A-38. 1987 Superstition Hills Earthquake at El Centro, Imperial County, Comp. 090

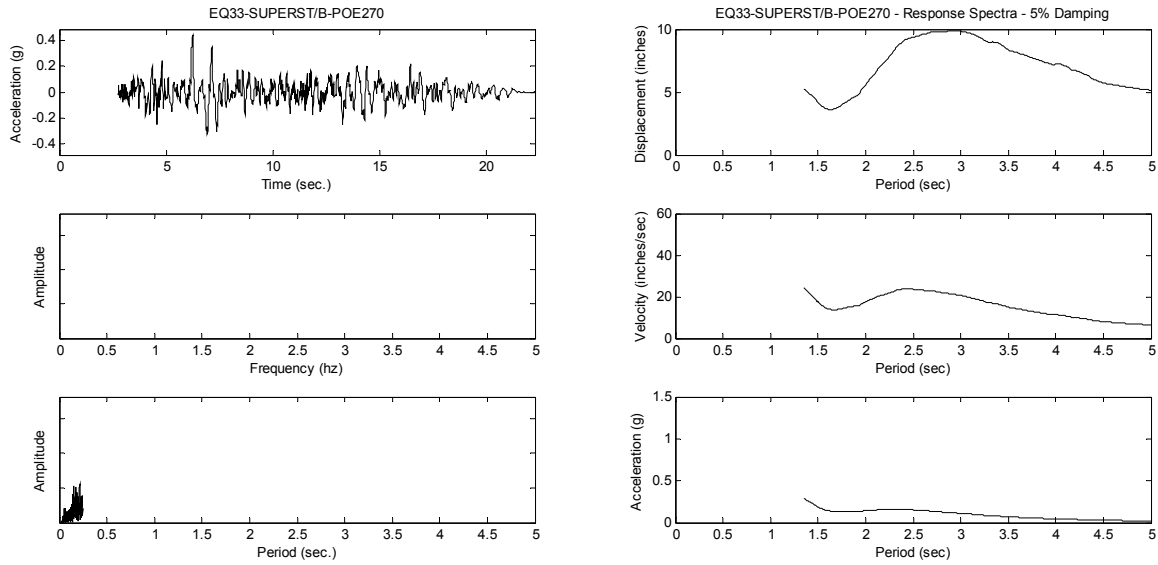


Figure A-39. 1987 Superstition Hills Earthquake at Poe Road, Comp. 270

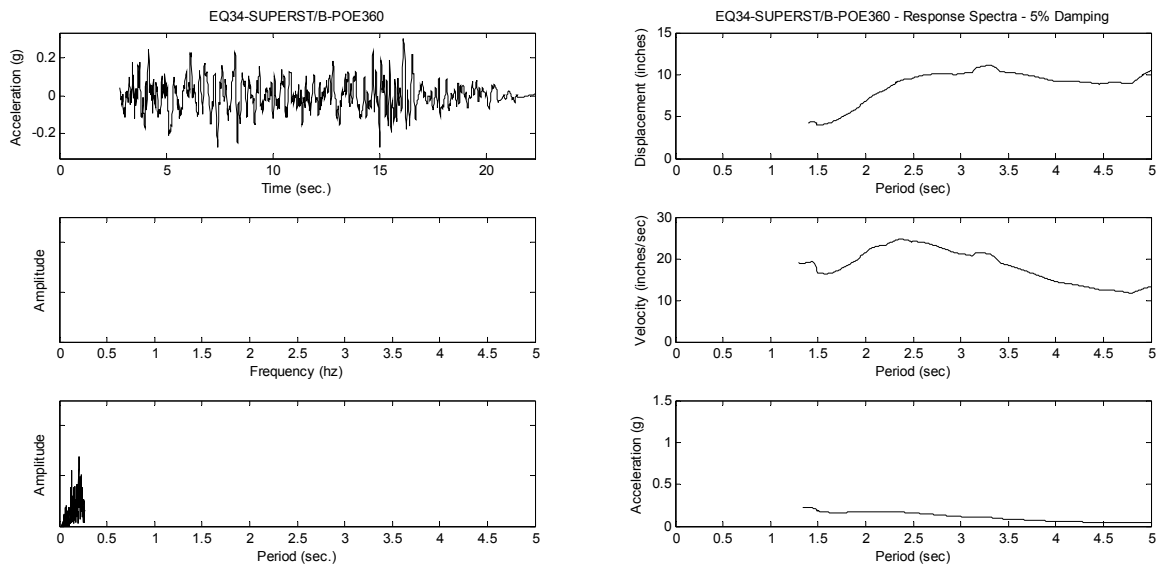


Figure A-40. 1987 Superstition Hills Earthquake at Poe Road, Comp. 360

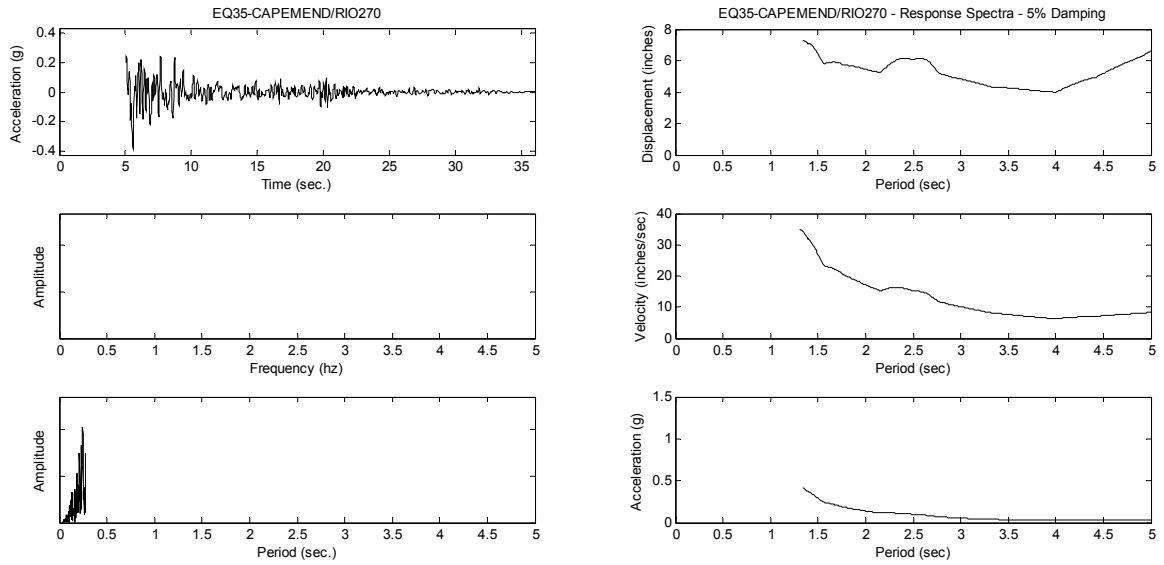


Figure A-41. 1992 Cape Mendocino Earthquake at Rio Dell Overpass, Comp. 270

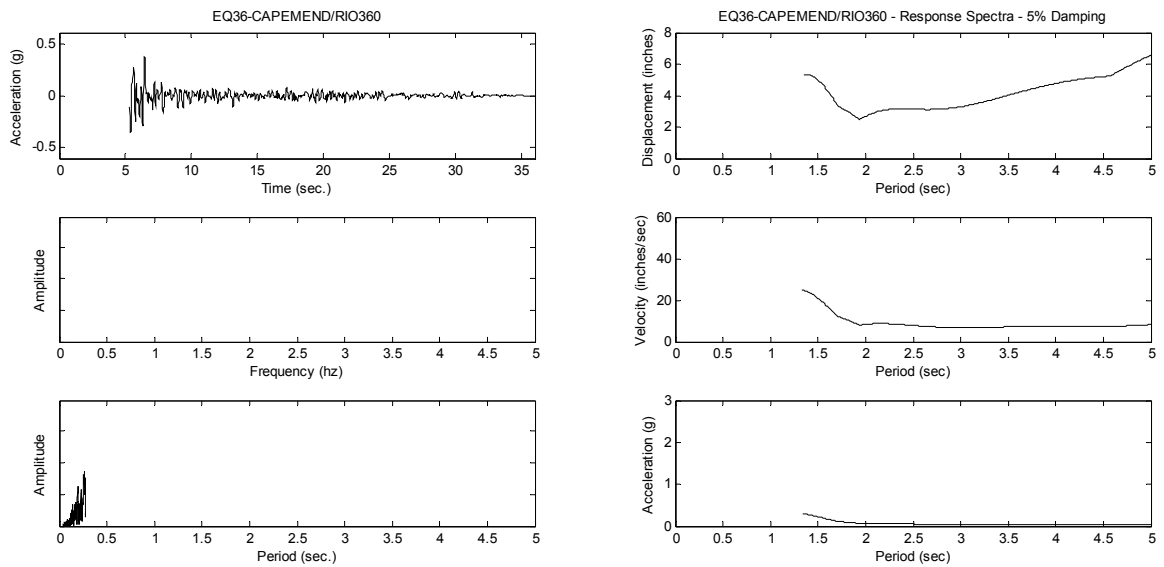


Figure A-42. 1992 Cape Mendocino Earthquake at Rio Dell Overpass, Comp. 360

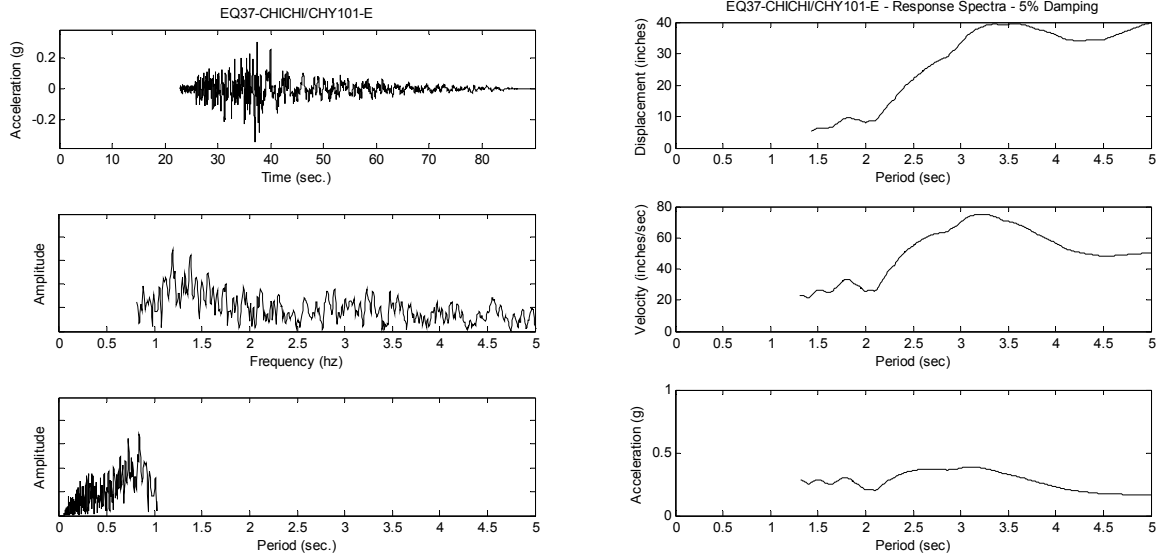


Figure A-43. 1999 Chi-Chi, Taiwan Earthquake at CHY101 Station, E-W Component

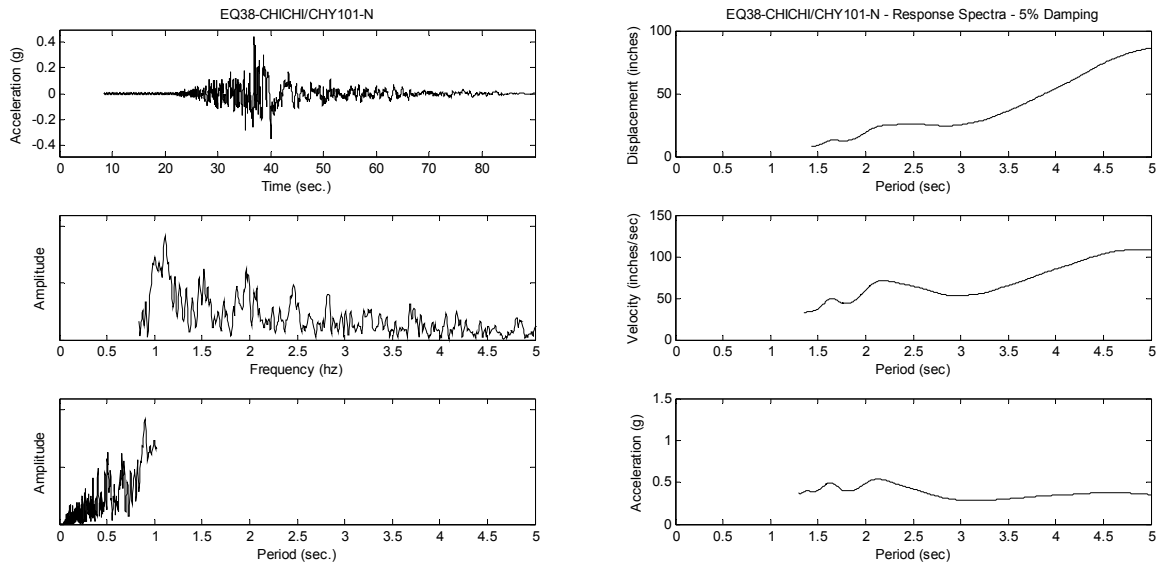


Figure A-44. 1999 Chi-Chi, Taiwan Earthquake at CHY101 Station, N-S Component

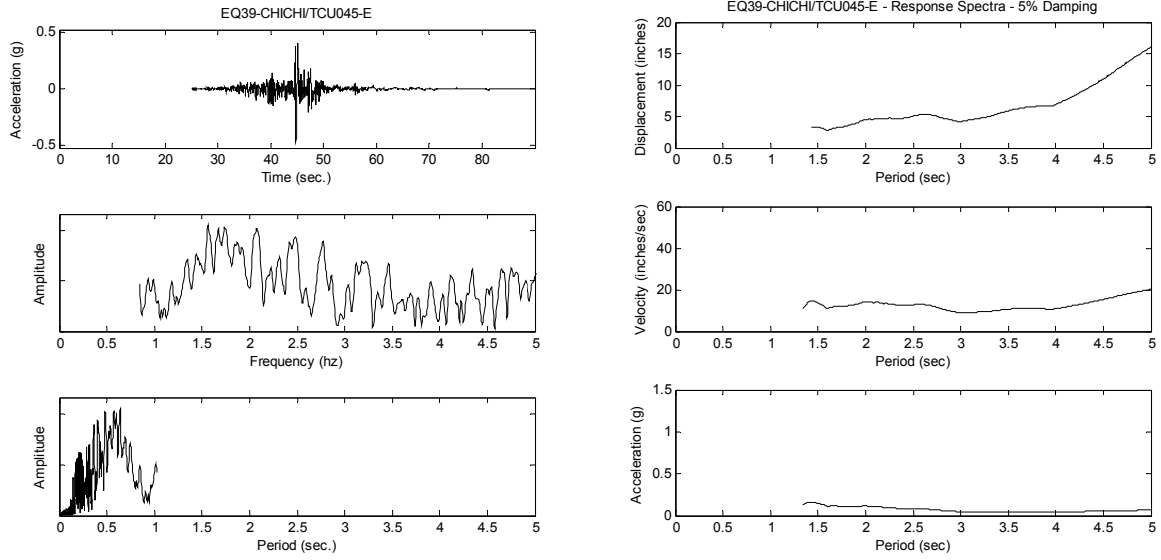


Figure A-45. 1999 Chi-Chi, Taiwan Earthquake at TCU045 Station, E-W Component

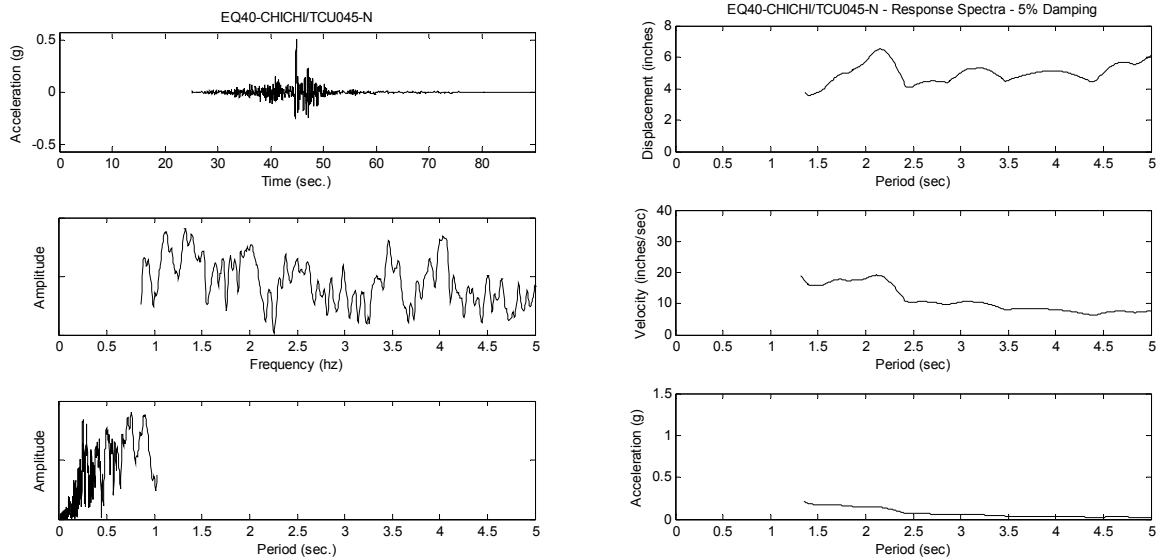


Figure A-46. 1999 Chi-Chi, Taiwan Earthquake at TCU045 Station, N-S Component

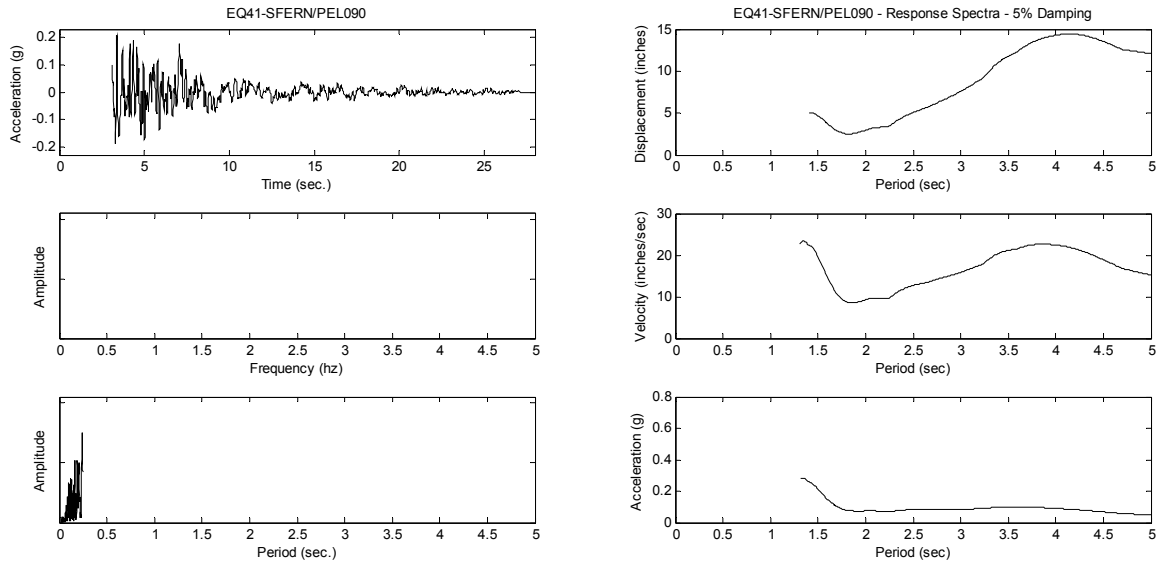


Figure A-47. 1971 San Fernando Earthquake at Los Angeles Hollywood Store Station, Comp. 090

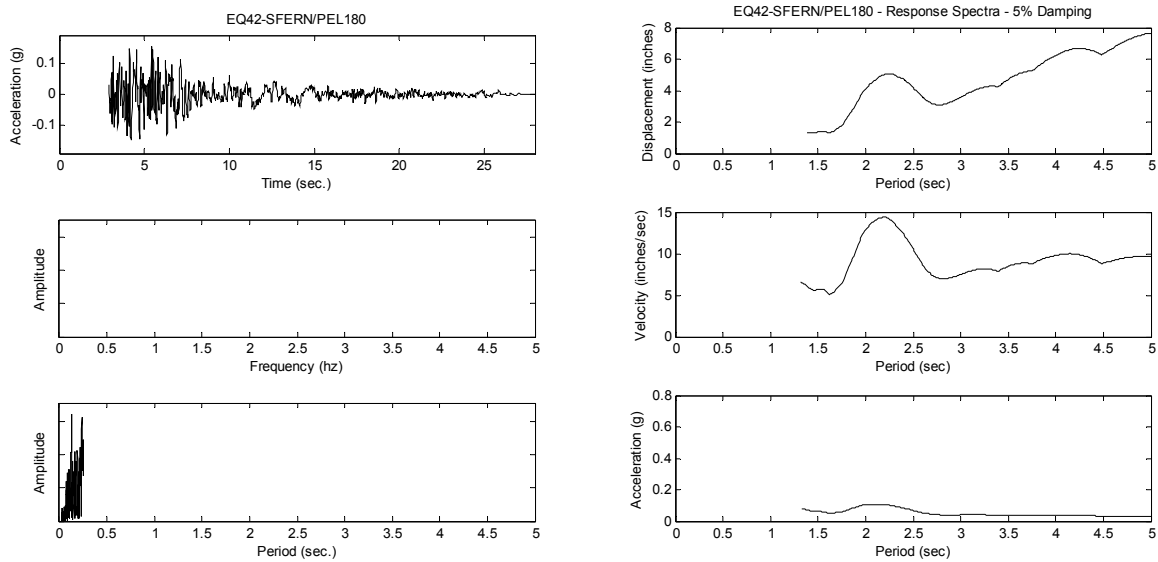


Figure A-48. 1971 San Fernando Earthquake at Los Angeles Hollywood Store Station, Comp. 180

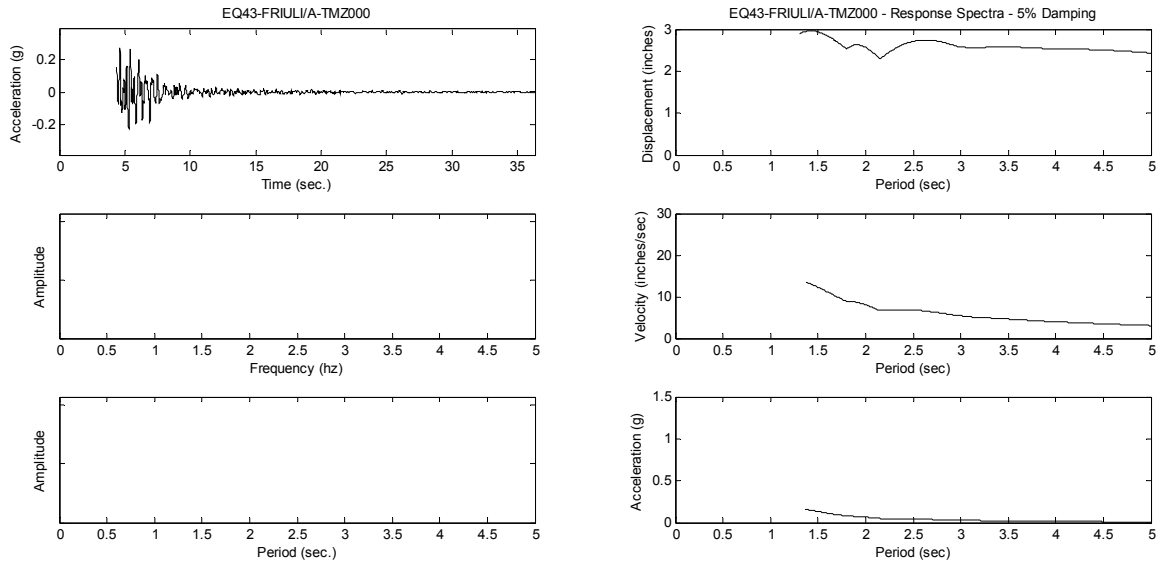


Figure A-49. 1976 Friuli, Italy Earthquake at Tolmezzo Station, Comp. 000

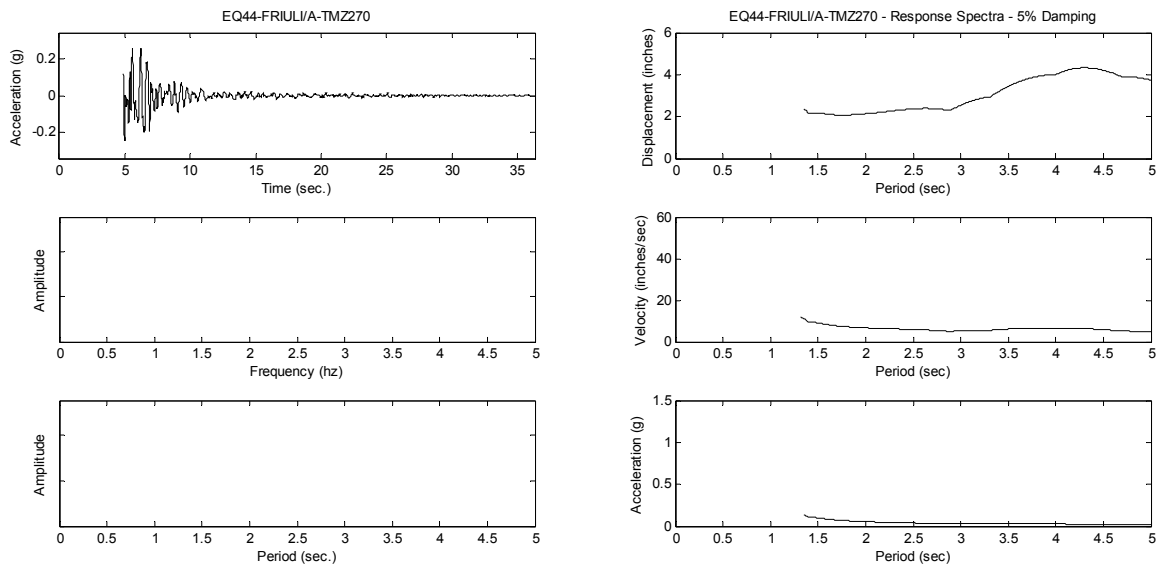


Figure A-50. 1976 Friuli, Italy Earthquake at Tolmezzo Station, Comp. 270

Appendix B Supplemental Design Information and Design Examples

This appendix presents supplemental information and details on the design of each archetype building.

Section B.1 provides information about the following:

- Wind forces both for strength and drift analyses
- Effective seismic weights and story gravity forces
- Seismic forces both for strength and drift analyses
- Lateral story drifts and displacements (ASCE 7 §2.8.6)
- ASCE 7 stability verification (ASCE 7 §12.8.7)

Section B.2 provides information regarding horizontal and vertical irregularities of the SFRS.

Section B.3 provides information regarding the AISC 360 frame stability calculation (B_2 for the effective length method) for the moment frame designs.

Section B.4 provides example calculations for the strength design of a few specific members and components:

- SMF beam and RBS beam-to-column connection
- SMF column
- SMF panel zone

B.1 Horizontal Design Forces

B.1.1 Wind Forces

Table B-1 through Table B-3 provide the horizontal wind forces for the 700-year wind for strength design of the members and components of the MWFRS and wind forces for the 10-year wind for verification of serviceability criteria for each archetype building. In these tables, F_x represents wind forces in the E-W direction and F_y represents wind in the N-S direction. Slight differences in applied wind forces are due to stiffness variations between the ELF and RSA designs.

Table B-1. Wind Forces on MC4 (kips)

Level	Elevation (ft)	Diaphragm Forces (kips), Applied at Geometric Center							
		700-Year Wind (Design)				10-Year Wind (Drift)			
		RSA		ELF		RSA		ELF	
		F_x	F_y	F_x	F_y	F_x	F_y	F_x	F_y
Roof	60	36.09	52.43	35.30	52.43	14.82	22.46	14.67	22.46
4	46	35.48	50.50	33.98	50.50	13.99	21.63	13.69	21.63
3	32	33.21	47.53	31.81	47.53	13.09	20.36	12.82	20.36
2	18	34.36	49.60	32.91	49.60	13.55	21.25	13.26	21.25
Base	0	139.14	200.06	134.01	200.06	55.46	85.71	54.44	85.71

Table B-2. Wind Forces on MC8 (kips)

Level	Elevation (ft)	Diaphragm Forces (kips), Applied at Geometric Center							
		700-Year Wind (Design)				10-Year Wind (Drift)			
		RSA		ELF		RSA		ELF	
		F_x	F_y	F_x	F_y	F_x	F_y	F_x	F_y
Roof	116	46.18	63.44	44.19	63.33	18.47	27.03	18.00	27.03
8	102	49.32	63.10	45.43	62.89	18.55	26.74	17.64	26.74
7	88	47.98	61.52	44.20	61.31	18.05	26.07	17.16	26.07
6	74	46.48	59.75	42.81	59.54	17.49	25.32	16.62	25.32
5	60	44.76	57.72	41.23	57.52	16.84	24.46	16.00	24.46
4	46	42.72	55.31	39.35	55.12	16.07	23.44	15.28	23.44
3	32	40.18	52.31	37.01	52.13	15.12	22.17	14.37	22.17
2	18	41.88	55.02	38.58	54.83	15.76	23.32	14.98	23.32
Base	0	359.49	468.19	332.81	466.67	136.35	198.54	130.04	198.54

Table B-3. Wind Forces on MC 16 (kips)

Level	Elevation (ft)	Diaphragm Forces (kips), Applied at Geometric Center							
		700-Year Wind (Design)				10-Year Wind (Drift)			
		RSA		ELF		RSA		ELF	
		F_x	F_y	F_x	F_y	F_x	F_y	F_x	F_y
Roof	228	56.78	77.60	55.35	77.48	22.58	32.73	22.22	32.73
16	214	62.23	78.96	59.41	78.72	23.22	32.81	22.50	32.81
15	200	61.44	78.03	58.66	77.80	22.93	32.42	22.22	32.42
14	186	60.61	77.06	57.86	76.83	22.62	32.02	21.92	32.02
13	172	59.74	76.04	57.03	75.81	22.29	31.59	21.60	31.59
12	158	58.81	74.95	56.14	74.73	21.95	31.14	21.27	31.14
11	144	57.82	73.79	55.20	73.58	21.58	30.66	20.91	30.66
10	130	56.76	72.55	54.19	72.34	21.18	30.15	20.53	30.15
9	116	55.62	71.21	53.10	71.00	20.76	29.59	20.11	29.59
8	102	54.37	69.75	51.91	69.54	20.29	28.98	19.66	28.98
7	88	53.00	68.14	50.60	67.94	19.78	28.31	19.16	28.31
6	74	51.46	66.33	49.12	66.13	19.20	27.56	18.61	27.56
5	60	49.69	64.26	47.44	64.07	18.54	26.70	17.97	26.70
4	46	47.60	61.81	45.44	61.62	17.76	25.68	17.21	25.68
3	32	44.98	58.74	42.94	58.57	16.79	24.41	16.26	24.41
2	18	47.26	62.28	45.12	62.09	17.64	25.88	17.09	25.88
Base	0	878.18	1131.51	839.50	1128.26	329.11	470.62	319.23	470.62

B.1.2 Seismic Forces

B.1.2.1 Effective Seismic Weights and Story Gravity Forces

Table B-4 through Table B-6 provide the effective seismic weights lumped at each story as well as the lumped gravity force acting on each story for each building design. The gravity force is computed using the two load combinations as discussed in Chapter 2.

Table B-4. Effect Seismic Weights and Story Gravity Forces, MC4 (kips)

Level, x	RSA			ELF		
	w_x^1	P_{story}^2	P_x^3	w_x^1	P_{story}^2	P_x^3
Roof	1091	1309	1091	1095	1314	1095
4	1339	2925	2470	1345	2936	2479
3	1346	4547	3854	1359	4574	3877
2	1364	6192	5257	1377	6235	5293
Total	5140	-	-	5176	-	-

¹ Inertial weight computed from Dead + Superimposed Dead + 0.2×Floor Live.

² Computed from 1.2×Dead + 1.2×Superimposed Dead + 0.25×Floor Live gravity load

³ Computed from Dead + Superimposed Dead + 0.25×Floor Live gravity load

Table B-5. Effect Seismic Weights and Story Gravity Forces, MC8 (kips)

Level, x	RSA			ELF		
	w_x^1	P_{story}^2	P_x^3	w_x^1	P_{story}^2	P_x^3
Roof	1081	1297	1081	1084	1300	1083
8	1324	2893	2443	1328	2901	2450
7	1333	4501	3815	1346	4525	3835
6	1338	6114	5192	1355	6158	5229
5	1349	7741	6580	1364	7803	6631
4	1353	9373	7973	1368	9452	8038
3	1367	11021	9378	1380	11115	9457
2	1390	12697	10807	1402	12806	10898
Total	10536	-	-	10627	-	-

¹ Inertial weight computed from Dead + Superimposed Dead + 0.2×Floor Live

² Computed from 1.2×Dead + 1.2×Superimposed Dead + 0.25×Floor Live gravity load

³ Computed from Dead + Superimposed Dead + 0.25×Floor Live gravity load

Table B-6. Effect Seismic Weights and Story Gravity Forces, MC16 (kips)

Level, x	RSA			ELF		
	w_x^1	P_{story}^2	P_x^3	w_x^1	P_{story}^2	P_x^3
Roof	1083	1296	1080	1083	1297	1081
16	1327	2893	2444	1327	2895	2444
15	1332	4496	3812	1342	4509	3822
14	1337	6105	5184	1349	6133	5208
13	1349	7728	6570	1357	7766	6601
12	1354	9358	7960	1360	9403	7997
11	1359	10993	9355	1366	11046	9399
10	1363	12634	10754	1370	12695	10806
9	1370	14282	12160	1379	14355	12221
8	1374	15936	13570	1384	16020	13641
7	1379	17595	14986	1389	17691	15066
6	1384	19260	16406	1394	19369	16496
5	1395	20939	17837	1402	21056	17935
4	1403	22627	19276	1410	22754	19381
3	1414	24328	20726	1425	24469	20843
2	1445	26067	22207	1462	26227	22341
Total	21667	-	-	21800	-	-

1. Inertial weight computed from Dead + Superimposed Dead + 0.2×Floor Live
2. Computed from 1.2×Dead + 1.2×Superimposed Dead + 0.25×Floor Live gravity load
3. Computed from Dead + Superimposed Dead + 0.25×Floor Live gravity load

B.1.2.2 Horizontal Seismic Forces, E-W Direction

B.1.2.2.1 MC4 (Special Moment Frame)

Table B-7 and Table B-8 provide the horizontal seismic forces and story shears for each building design for the seismic strength analysis and the drift analysis. The data are also graphically illustrated in Figure B-1 through Figure B-3. In these tables, F_x represents the seismic forces acting in the E-W direction only. The equivalent story forces for the RSA design are backed out from the story shears computed via a modal combination procedure. Although not theoretically correct, the forces provide a comparison basis for evaluating variations in the vertical distribution.

Table B-7. Seismic Strength Design Forces, E-W MC4

Level, x	RSA		ELF			Wind (700-Year)	
	F_x (kips)	V_i (kips)	F_x (kips)	V_i (kips)	V_{ELF} / V_{RSA}	F_x (kips)	V_i (kips)
Roof	145	145	138	138	1.05	36	36
4	68	213	121	259	0.82	35	72
3	46	259	77	336	0.77	33	105
2	56	316	38	374	0.84	34	139

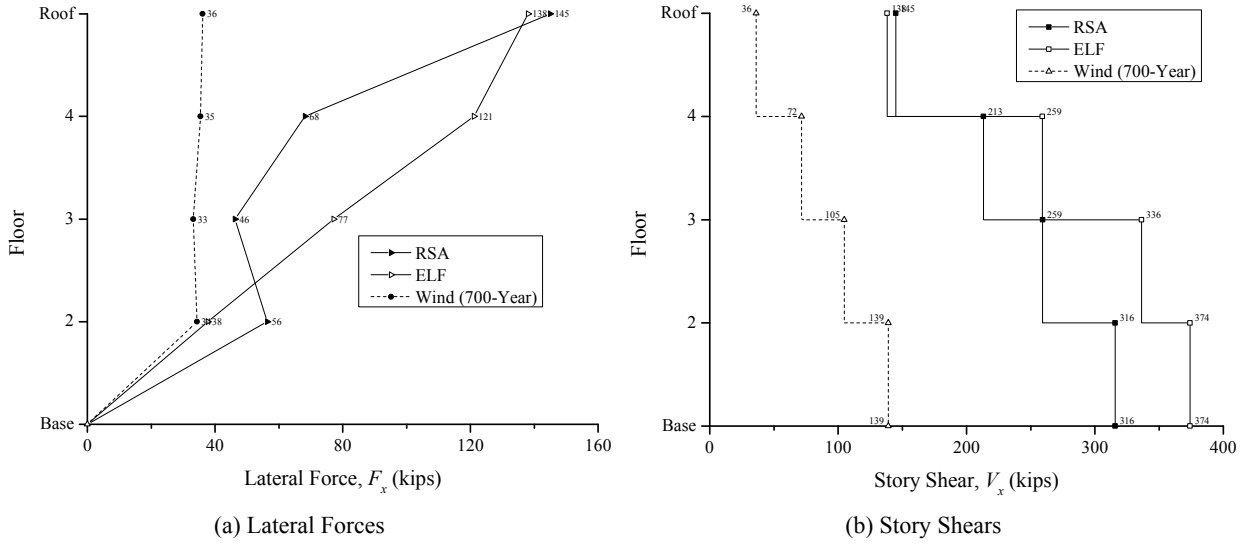


Figure B-1. Strength Design Lateral Forces and Story Shears

Table B-8. Seismic Drift Forces, E-W MC4

Level, x	F_x (kips)	V_i (kips)	RSA			F_x (kips)	V_i (kips)	ELF			Wind (10-Year)	
			δ_x (inch)	Δ_i (inch)	Δ_i / h_{sx}			δ_x (inch)	Δ_i (inch)	Δ_i / h_{sx}	F_x (kips)	V_i (kips)
Roof	76	76	11.82	1.88	0.011	89	89	12.13	2.28	0.014	15	15
4	36	112	9.94	2.73	0.016	70	159	9.85	3.00	0.018	14	29
3	24	136	7.21	3.39	0.020	39	198	6.85	3.33	0.020	13	42
2	30	166	3.82	3.82	0.018	15	213	3.51	3.51	0.016	14	55

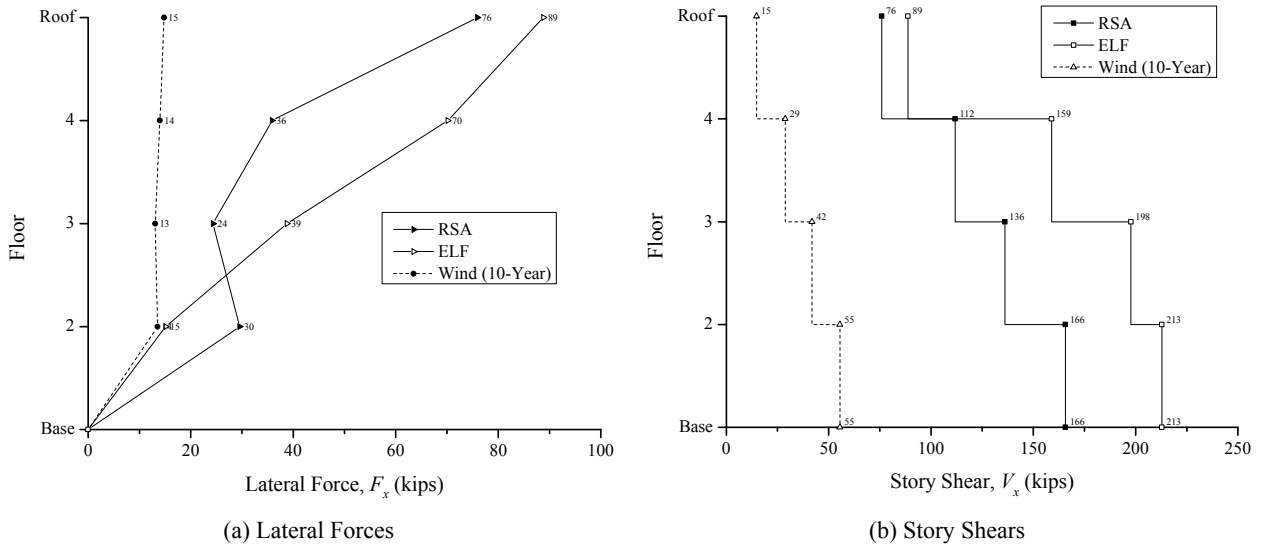


Figure B-2. Drift Design Lateral Forces and Story Shears

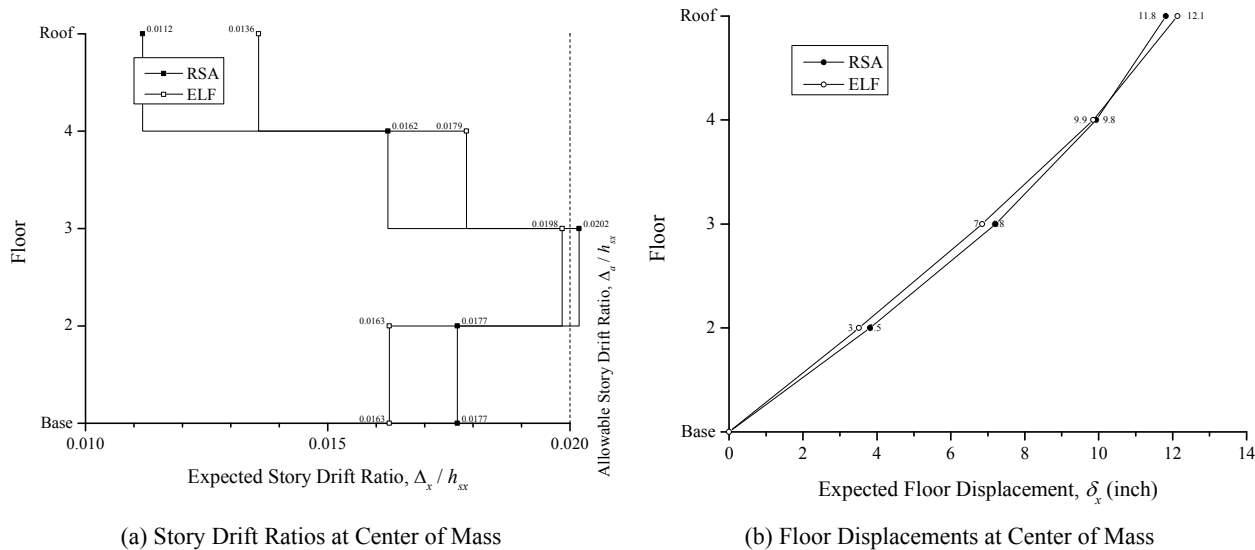


Figure B-3. Story Drift Ratios and Deflected Shape

Table B-9 and Table B-10 provide the tabulated data for verifying the allowable story drifts and the seismic stability coefficient per ASCE 7 §12.8.6 and ASCE §12.8.7 for each archetype building design. The following formulas were used in these calculations—see ASCE 7, where δ is the story drift and Δ is the story drift ratio as defined in ASCE 7.

$$\delta_x = \frac{C_d \delta_{xe}}{I_e} \quad (\text{B-1})$$

$$\Delta_i = \delta_x - \delta_{x-1} = \frac{C_d}{I_e} (\delta_{xe} - \delta_{(x-1)e}) \quad (\text{B-2})$$

$$\theta_{2i} = \frac{P_x \Delta_i I_e}{V_i h_{sx} C_d} = \frac{P_x (\delta_{xe} - \delta_{(x-1)e})}{V_i h_{sx}} \quad (\text{B-3})$$

$$\theta_{1i} = \frac{\theta_{2i}}{1 + \theta_{2i}} \quad (\text{B-4})$$

Table B-9. ASCE 7 Allowable Drift and Stability Verification, E-W MC4 RSA

Level, x	$V_i \times C_d$ (kips)	P_x (kips)	Δ_i (inch)	h_{sx} (inch)	Δ_i / h_{sx}	θ_{2i}	θ_{1i}	β_i	$\theta_{max,i}$
ROOF	418	1091	1.88	168	0.011	0.029	0.028	0.39	0.232
4	615	2470	2.73	168	0.016	0.065	0.061	0.54	0.168
3	749	3854	3.39	168	0.020	0.104	0.094	0.63	0.143
2	911	5257	3.82	216	0.018	0.102	0.093	0.70	0.129

Table B-10. ASCE 7 Allowable Drift and Stability Verification, E-W MC4 ELF

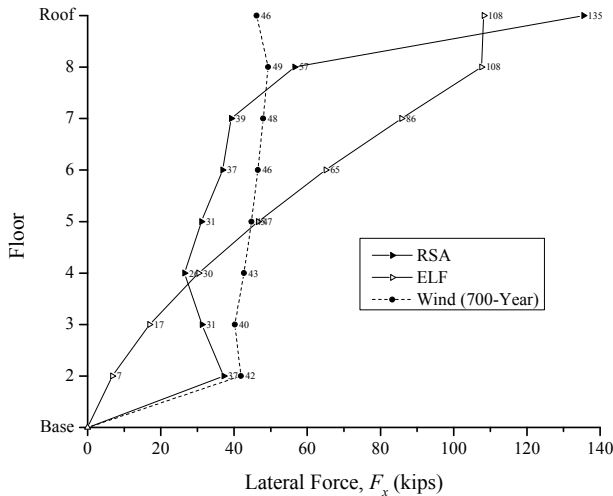
Level, x	$V_i \times C_d$ (kips)	P_x (kips)	Δ_i (inch)	h_{sx} (inch)	Δ_i / h_{sx}	θ_{2i}	θ_{1i}	β_i	$\theta_{max,i}$
ROOF	488	1095	2.28	168	0.014	0.030	0.030	0.39	0.231
4	874	2479	3.00	168	0.018	0.051	0.048	0.44	0.208
3	1088	3877	3.33	168	0.020	0.071	0.066	0.50	0.183
2	1171	5293	3.51	216	0.016	0.074	0.069	0.53	0.172

B.1.2.2.2 MC8 (Special Moment Frame)

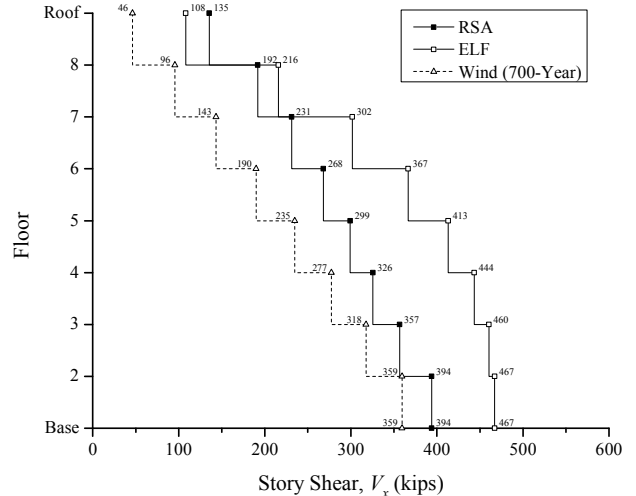
Table B-11 and Figure B-12 provide the horizontal seismic forces and story shears for each archetype building design for the seismic strength analysis and the drift analysis. The data are also graphically illustrated in Figure B-4 through Figure B-6. In these tables, F_x represents the seismic forces acting in the E-W direction only. The equivalent story forces for the RSA design are backed out from the story shears computed via a modal combination procedure. Although not theoretically correct, the forces provide a comparison basis for evaluating variations in the vertical distribution.

Table B-11. Seismic Strength Design Forces, E-W MC8

Level, x	RSA		ELF			Wind (700-Year)	
	F_x (kips)	V_i (kips)	F_x (kips)	V_i (kips)	V_{ELF} / V_{RSA}	F_x (kips)	V_i (kips)
Roof	135	135	108	108	1.25	46	46
8	57	192	108	216	0.89	49	96
7	39	231	86	302	0.77	48	143
6	37	268	65	367	0.73	46	190
5	31	299	47	413	0.72	45	235
4	26	326	30	444	0.73	43	277
3	31	357	17	460	0.77	40	318
2	37	394	7	467	0.84	42	359



(a) Lateral Forces

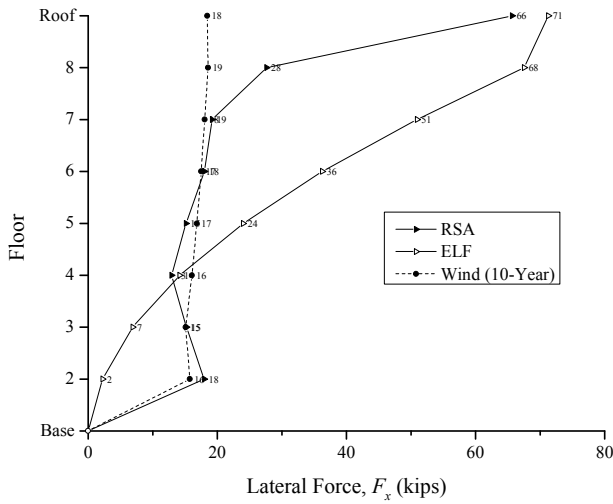


(b) Story Shears

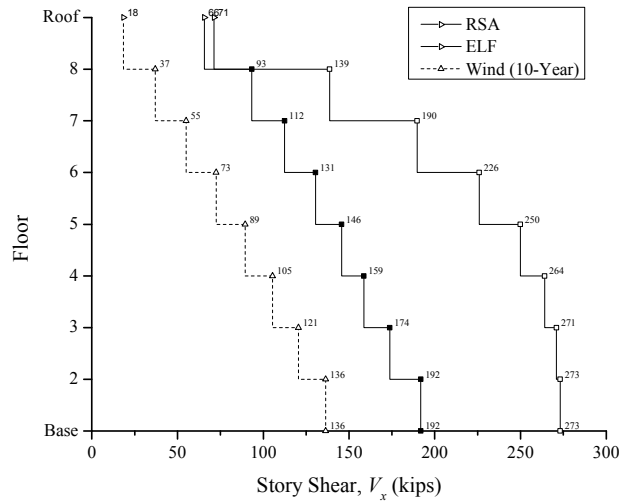
Figure B-4. Strength Design Lateral Forces and Story Shears

Table B-12. Seismic Drift Forces, E-W MC8

Level, x	F_x (kips)	V_i (kips)	RSA			ELF					Wind (10-Year)	
			δ_x (inch)	Δ_i (inch)	Δ_i / h_{sx}	F_x (kips)	V_i (kips)	δ_x (inch)	Δ_i (inch)	Δ_i / h_{sx}	F_x (kips)	V_i (kips)
Roof	66	66	21.48	1.84	0.011	71	71	22.95	2.25	0.013	18	18
8	28	93	19.64	2.38	0.014	68	139	20.70	2.83	0.017	19	37
7	19	112	17.26	2.75	0.016	51	190	17.87	2.81	0.017	18	55
6	18	131	14.52	2.92	0.017	36	226	15.06	3.00	0.018	17	73
5	15	146	11.59	2.90	0.017	24	250	12.06	3.06	0.018	17	89
4	13	159	8.69	2.99	0.018	14	264	9.00	3.11	0.019	16	105
3	15	174	5.70	2.86	0.017	7	271	5.89	2.96	0.018	15	121
2	18	192	2.84	2.84	0.013	2	273	2.93	2.93	0.014	16	136



(a) Lateral forces



(b) Story Shears

Figure B-5. Drift Design Lateral Forces and Story Shears

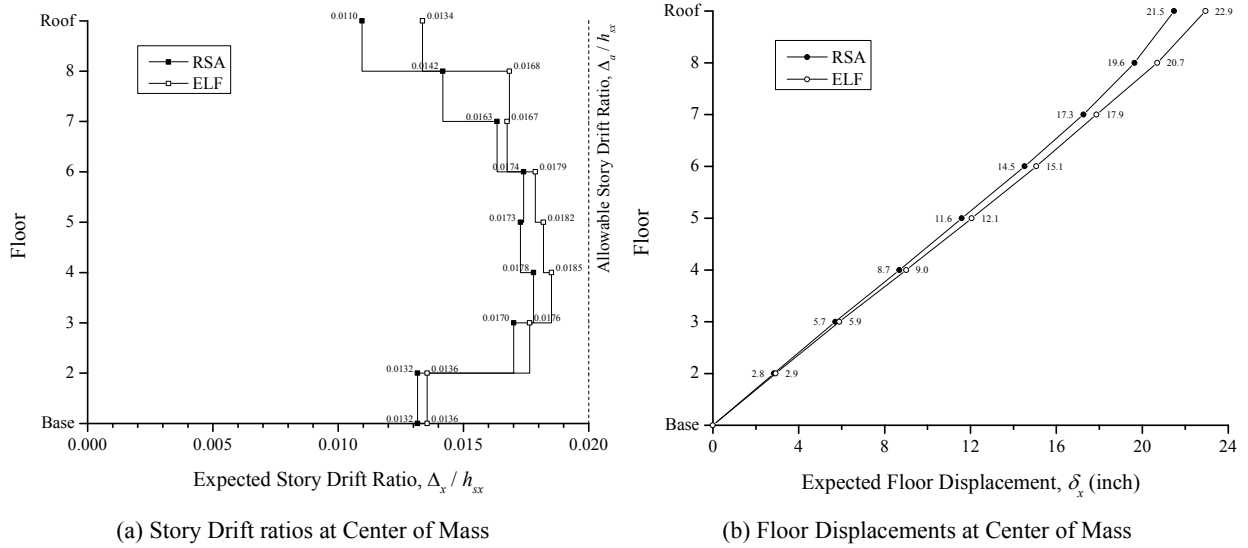


Figure B-6. Story Drift Ratios and Deflected Shape

Table B-13 and Table B-14 provide the tabulated data for verifying the allowable story drifts and the seismic stability coefficient per ASCE 7 §12.8.6 and §12.8.7 for each archetype building design.

Table B-13. ASCE 7 Allowable Drift and Stability Verification, E-W MC8 RSA

Level, x	$V_i \times C_d$ (kips)	P_x (kips)	Δ_i (inch)	h_{sx} (inch)	Δ_i / h_{sx}	θ_{2i}	θ_{1i}	β_i	$\theta_{max,i}$
ROOF	361	1081	1.84	168	0.011	0.033	0.032	0.53	0.172
8	513	2443	2.38	168	0.014	0.067	0.063	0.68	0.134
7	619	3815	2.75	168	0.016	0.101	0.092	0.67	0.136
6	718	5192	2.92	168	0.017	0.126	0.112	0.71	0.128
5	801	6580	2.90	168	0.017	0.142	0.124	0.62	0.147
4	872	7973	2.99	168	0.018	0.163	0.140	0.63	0.145
3	956	9378	2.86	168	0.017	0.167	0.143	0.60	0.151
2	1055	10807	2.84	216	0.013	0.135	0.119	0.60	0.152

Table B-14. ASCE 7 Allowable Drift and Stability Verification, E-W MC8 ELF

Level, x	$V_i \times C_d$ (kips)	P_x (kips)	Δ_i (inch)	h_{sx} (inch)	Δ_i / h_{sx}	θ_{2i}	θ_{1i}	β_i	$\theta_{max,i}$
ROOF	392	1083	2.25	168	0.013	0.037	0.036	0.37	0.246
8	763	2450	2.83	168	0.017	0.054	0.051	0.51	0.180
7	1043	3835	2.81	168	0.017	0.062	0.058	0.43	0.210
6	1243	5229	3.00	168	0.018	0.075	0.070	0.48	0.190
5	1375	6631	3.06	168	0.018	0.088	0.081	0.46	0.199
4	1453	8038	3.11	168	0.019	0.102	0.093	0.48	0.190
3	1491	9457	2.96	168	0.018	0.112	0.101	0.47	0.192
2	1503	10898	2.93	216	0.014	0.098	0.089	0.45	0.200

B.1.2.2.3 MC16 (Special Moment Frame)

Table B-15 and Table B-16 provide the horizontal seismic forces and story shears for each archetype building design for the seismic strength analysis and the drift analysis. The data are also graphically illustrated in Figure B-7 through Figure B-9. In these tables, F_x represents the seismic forces acting in the E-W direction only. The equivalent story forces for the RSA design are backed out from the story shears computed via a modal combination procedure. Although not theoretically correct, the forces provide a comparison basis for evaluating variations in the vertical distribution.

Table B-15. Summary of Seismic Strength Design Forces, E-W MC16

Level, x	RSA		ELF			Wind (700-Year)	
	F_x (kips)	V_i (kips)	F_x (kips)	V_i (kips)	V_{ELF} / V_{RSA}	F_x (kips)	V_i (kips)
Roof	196	196	133	133	1.47	57	57
16	95	292	144	278	1.05	62	119
15	54	346	127	405	0.85	61	180
14	46	391	111	515	0.76	61	241
13	45	436	95	611	0.71	60	301
12	41	477	80	691	0.69	59	360
11	33	510	67	758	0.67	58	417
10	31	541	55	813	0.67	57	474
9	33	573	44	857	0.67	56	530
8	33	607	34	891	0.68	54	584
7	29	636	26	917	0.69	53	637
6	26	662	18	935	0.71	51	689
5	29	691	12	947	0.73	50	738
4	38	729	7	954	0.76	48	786
3	44	773	3	957	0.81	45	831
2	37	810	1	958	0.85	47	878

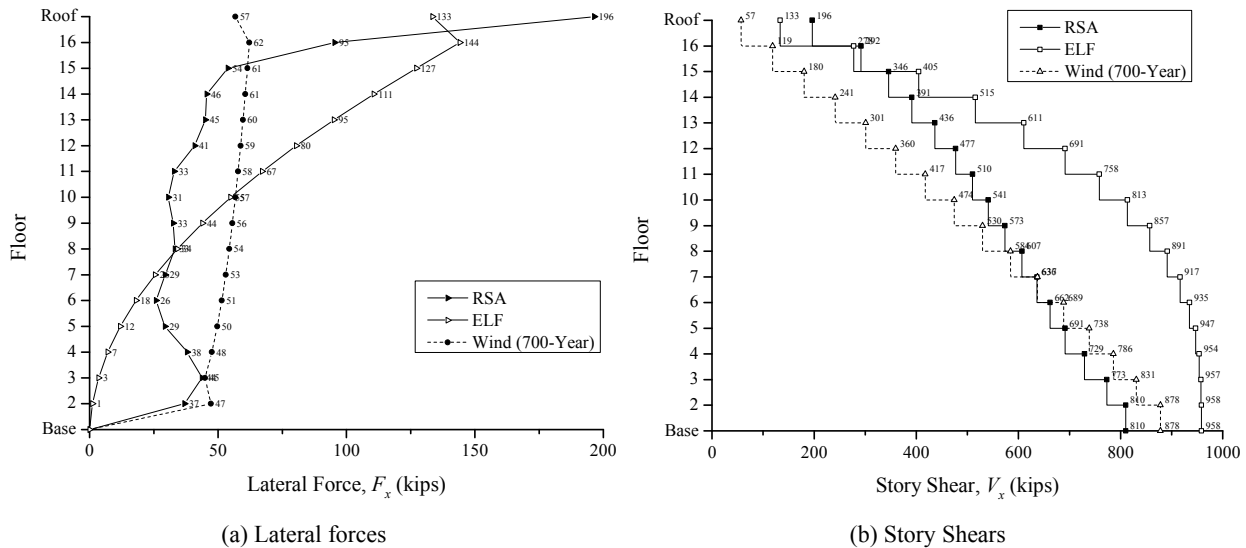


Figure B-7. Strength Design Lateral Forces and Story Shears

Table B-16. Summary of Seismic Drift Forces, E-W MC16

Level, x	RSA					ELF					Wind (10-Year)	
	F_x (kips)	V_i (kips)	δ_x (inch)	Δ_i (inch)	Δ_i / h_{sx}	F_x (kips)	V_i (kips)	δ_x (inch)	Δ_i (inch)	Δ_i / h_{sx}	F_x (kips)	V_i (kips)
Roof	71	71	29.39	1.28	0.008	52	52	38.12	1.76	0.010	23	23
16	35	106	28.11	1.69	0.010	56	109	36.36	2.16	0.013	23	46
15	20	126	26.42	2.00	0.012	50	158	34.20	2.30	0.014	23	69
14	17	142	24.42	2.02	0.012	43	202	31.89	2.51	0.015	23	91
13	16	159	22.41	1.89	0.011	37	239	29.39	2.62	0.016	22	114
12	15	174	20.51	1.99	0.012	31	270	26.77	2.81	0.017	22	136
11	12	186	18.52	2.09	0.012	26	296	23.96	2.92	0.017	22	157
10	11	197	16.43	2.10	0.012	21	318	21.05	2.84	0.017	21	178
9	12	209	14.33	2.04	0.012	17	335	18.21	2.64	0.016	21	199
8	12	221	12.29	2.07	0.012	13	348	15.57	2.60	0.015	20	219
7	11	232	10.22	2.07	0.012	10	358	12.97	2.57	0.015	20	239
6	9	241	8.15	1.94	0.012	7	365	10.40	2.51	0.015	19	258
5	11	252	6.21	1.75	0.010	5	370	7.89	2.37	0.014	19	277
4	14	266	4.47	1.67	0.010	3	373	5.52	2.20	0.013	18	295
3	16	282	2.80	1.49	0.009	1	374	3.32	1.83	0.011	17	311
2	13	295	1.31	1.31	0.006	0	375	1.49	1.49	0.007	18	329

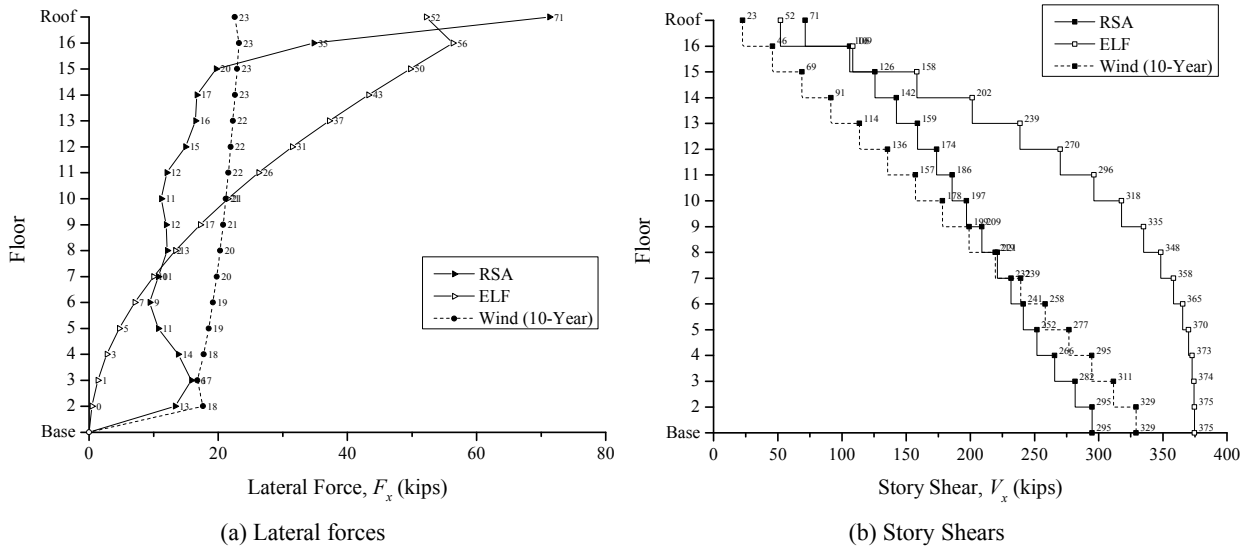


Figure B-8. Drift Design Lateral Forces and Story Shears

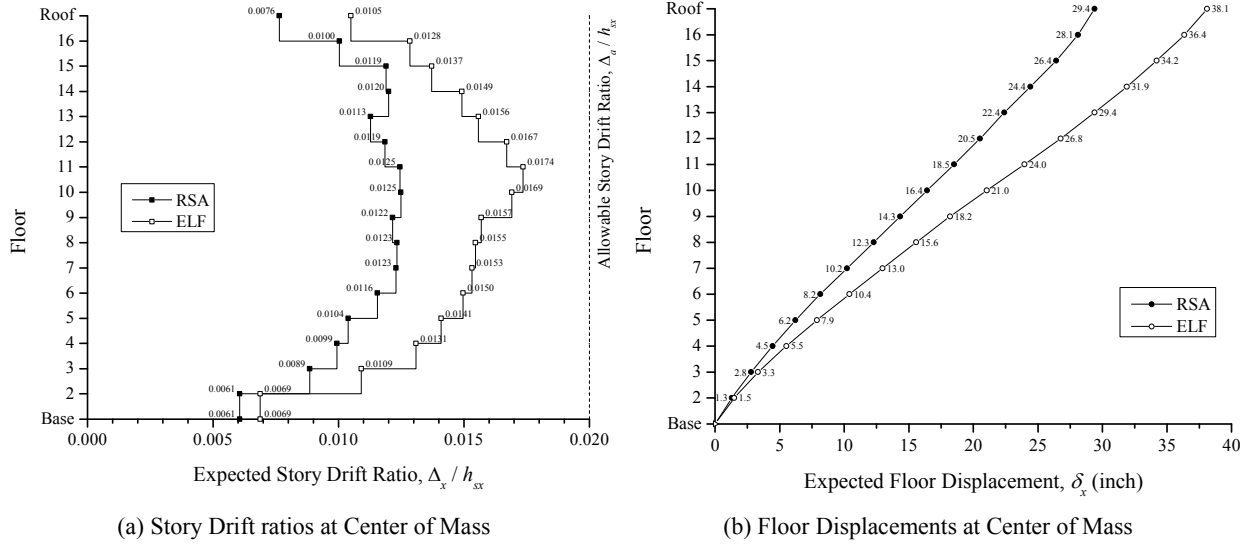


Figure B-9. Story Drift Ratios and Deflected Shape

Table B-17 and Table B-18 provide the tabulated data for verifying the allowable story drifts and the seismic stability coefficient per ASCE 7 §12.8.6 and ASCE 7 §12.8.7 for each building design.

Table B-17. ASCE 7 Allowable Drift and Stability Verification, E-W MC16 RSA

Level, x	$V_i \times C_d$ (kips)	P_x (kips)	Δ_i (inch)	h_{sx} (inch)	Δ_i / h_{sx}	θ_{2i}	θ_i	β_i	$\theta_{max,i}$
ROOF	392	1080	1.28	168	0.008	0.021	0.021	0.52	0.173
16	583	2444	1.69	168	0.010	0.042	0.040	0.68	0.133
15	692	3812	2.00	168	0.012	0.066	0.062	0.78	0.116
14	783	5184	2.02	168	0.012	0.079	0.074	0.81	0.112
13	874	6570	1.89	168	0.011	0.085	0.078	0.65	0.139
12	956	7960	1.99	168	0.012	0.099	0.090	0.67	0.137
11	1022	9355	2.09	168	0.012	0.114	0.102	0.68	0.134
10	1084	10754	2.10	168	0.012	0.124	0.110	0.68	0.134
9	1149	12160	2.04	168	0.012	0.129	0.114	0.67	0.135
8	1216	13570	2.07	168	0.012	0.138	0.121	0.67	0.135
7	1275	14986	2.07	168	0.012	0.145	0.126	0.68	0.133
6	1327	16406	1.94	168	0.012	0.143	0.125	0.68	0.134
5	1386	17837	1.75	168	0.010	0.134	0.118	0.63	0.143
4	1462	19276	1.67	168	0.010	0.131	0.116	0.61	0.149
3	1549	20726	1.49	168	0.009	0.118	0.106	0.60	0.150
2	1622	22207	1.31	216	0.006	0.083	0.077	0.54	0.169

Table B-18. ASCE 7 Allowable Drift and Stability Verification, E-W MC16 RSA

Level, x	$V_i \times C_d$ (kips)	P_x (kips)	Δ_i (inch)	h_{sx} (inch)	Δ_i / h_{sx}	θ_{2i}	θ_{1i}	β_i	$\theta_{max,i}$
ROOF	287	1081	1.76	168	0.010	0.040	0.038	0.47	0.194
16	597	2444	2.16	168	0.013	0.053	0.050	0.61	0.150
15	870	3822	2.30	168	0.014	0.060	0.057	0.58	0.157
14	1108	5208	2.51	168	0.015	0.070	0.065	0.64	0.142
13	1313	6601	2.62	168	0.016	0.078	0.073	0.69	0.131
12	1486	7997	2.81	168	0.017	0.090	0.082	0.74	0.123
11	1630	9399	2.92	168	0.017	0.100	0.091	0.78	0.117
10	1748	10806	2.84	168	0.017	0.104	0.095	0.78	0.116
9	1843	12221	2.64	168	0.016	0.104	0.094	0.71	0.128
8	1916	13641	2.60	168	0.015	0.110	0.099	0.69	0.131
7	1971	15066	2.57	168	0.015	0.117	0.105	0.71	0.127
6	2010	16496	2.51	168	0.015	0.123	0.109	0.72	0.126
5	2036	17935	2.37	168	0.014	0.124	0.110	0.75	0.121
4	2051	19381	2.20	168	0.013	0.124	0.110	0.73	0.125
3	2058	20843	1.83	168	0.011	0.110	0.099	0.71	0.128
2	2061	22341	1.49	216	0.007	0.075	0.069	0.59	0.154

B.1.2.3 Horizontal Seismic Forces, N-S Direction

B.1.2.3.1 MC4 (Special Concentrically Braced Frame)

Table B-19 and Table B-20 provide the horizontal seismic forces and story shears for each archetype building design for the seismic strength analysis and the drift analysis. The data are also graphically illustrated in Figure B-10 through Figure B-12. In these tables, F_y represents the seismic forces acting in the N-S direction only. Lastly, the equivalent story forces for the RSA design are backed out from the story shears computed via a modal combination procedure. Although not theoretically correct, the forces provide a comparison basis for evaluating variations in the vertical distribution.

Table B-19. Summary of Seismic Strength Design Forces, N-S MC4

Level, x	RSA		ELF			Wind (700-Year)	
	F_y (kips)	V_i (kips)	F_y (kips)	V_i (kips)	V_{ELF} / V_{RSA}	F_y (kips)	V_i (kips)
Roof	261	261	293	293	0.89	36	36
4	219	480	272	565	0.85	35	72
3	153	633	188	753	0.84	33	105
2	91	723	104	857	0.84	34	139

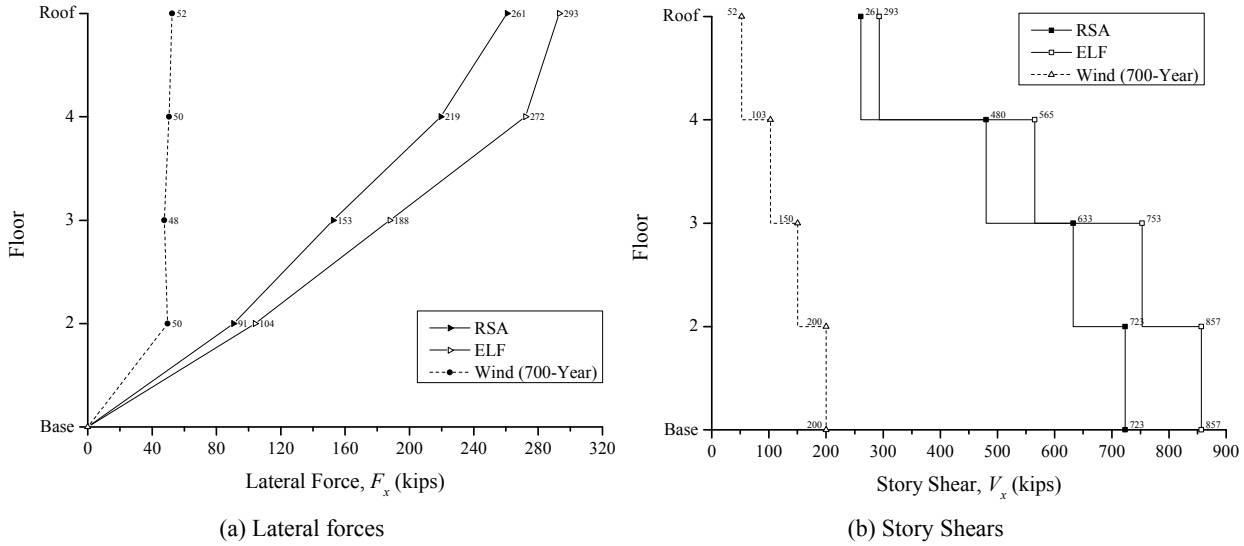


Figure B-10. Strength Design Lateral Forces and Story Shears

Table B-20. Summary of Seismic Drift Forces, N-S MC4

Level, x	RSA					ELF					Wind (10-Year)	
	F_y (kips)	V_i (kips)	δ_x (inch)	Δ_i (inch)	Δ_i / h_{sx}	F_y (kips)	V_i (kips)	δ_x (inch)	Δ_i (inch)	Δ_i / h_{sx}	F_y (kips)	V_i (kips)
Roof	226	226	4.88	1.02	0.006	270	270	5.41	1.20	0.007	15	15
4	190	416	3.85	1.22	0.007	249	519	4.21	1.51	0.009	14	29
3	132	549	2.63	1.28	0.008	170	689	2.70	1.31	0.008	13	42
2	78	627	1.35	1.35	0.006	93	782	1.39	1.39	0.006	14	55

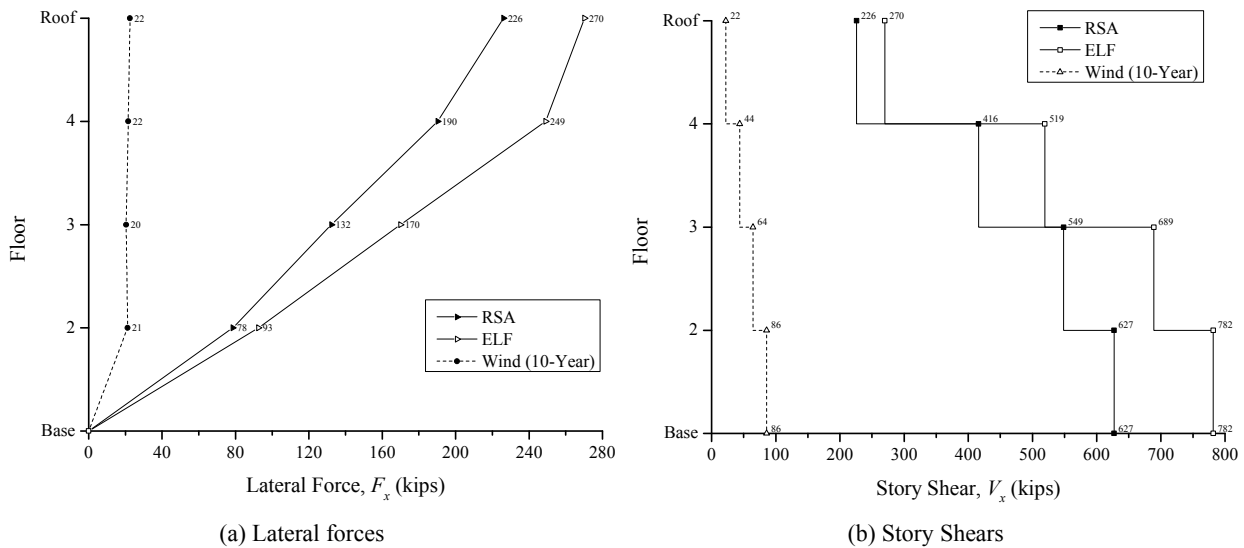


Figure B-11. Drift Design Lateral Forces and Story Shears

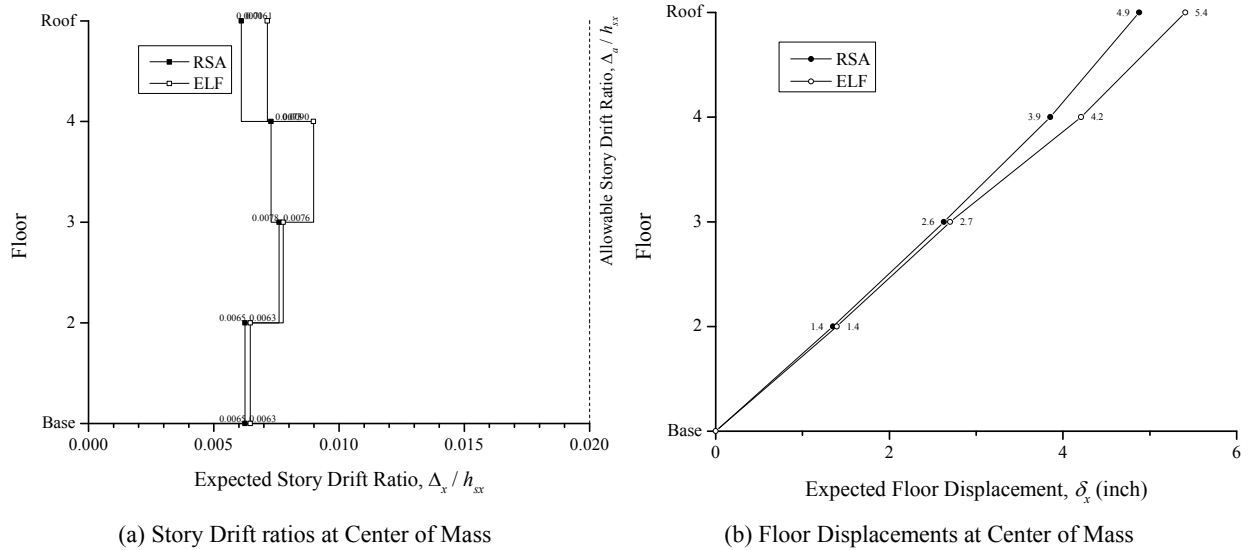


Figure B-12. Story Drift Ratios and Deflected Shape

Table B-21 and Table B-22 provide the tabulated data for verifying the allowable story drifts and the seismic stability coefficient per ASCE 7 §12.8.6 and ASCE §12.8.7 for each archetype building design.

Table B-21. ASCE 7 Allowable Drift and Stability Verification, N-S MC4 RSA

Level, x	$V_i \times C_d$ (kips)	P_x (kips)	Δ_i (inch)	h_{sx} (inch)	Δ_i / h_{sx}	θ_{2i}	θ_{1i}	β_i	$\theta_{max,i}$
ROOF	1130	1091	1.02	168	0.006	0.006	0.006	1.00	0.100
4	2082	2470	1.22	168	0.007	0.009	0.009	1.00	0.100
3	2743	3854	1.28	168	0.008	0.011	0.011	1.00	0.100
2	3135	5257	1.35	216	0.006	0.010	0.010	1.00	0.100

Table B-22. ASCE 7 Allowable Drift and Stability Verification, N-S MC4 ELF

Level, x	$V_i \times C_d$ (kips)	P_x (kips)	Δ_i (inch)	h_{sx} (inch)	Δ_i / h_{sx}	θ_{2i}	θ_{1i}	β_i	$\theta_{max,i}$
ROOF	1351	1095	1.20	168	0.007	0.006	0.006	1.00	0.100
4	2597	2479	1.51	168	0.009	0.009	0.008	1.00	0.100
3	3446	3877	1.31	168	0.008	0.009	0.009	1.00	0.100
2	3909	5293	1.39	216	0.006	0.009	0.009	1.00	0.100

B.1.2.3.2 MC8 (Special Concentrically Braced Frame)

Table B-23 and Table B-24 provide the horizontal seismic forces and story shears for each archetype building design for the seismic strength analysis and the drift analysis. The data are also graphically illustrated in Figure B-13 through Figure B-15. In these tables, F_y represents the seismic forces acting in the N-S direction only. Lastly, the equivalent story forces for the RSA design are backed out from the story

shears computed via a modal combination procedure. Although not theoretically correct, the forces provide a comparison basis for evaluating variations in the vertical distribution.

Table B-23. Summary of Seismic Strength Design Forces, N-S MC8

Level, x	RSA		ELF			Wind (700-Year)	
	F_y (kips)	V_i (kips)	F_y (kips)	V_i (kips)	V_{ELF} / V_{RSA}	F_y (kips)	V_i (kips)
Roof	239	239	216	216	1.11	46	46
8	174	414	225	441	0.94	49	96
7	94	508	190	631	0.80	48	143
6	59	566	154	785	0.72	46	190
5	70	636	119	904	0.70	45	235
4	93	729	86	990	0.74	43	277
3	100	829	55	1045	0.79	40	318
2	76	904	27	1073	0.84	42	359

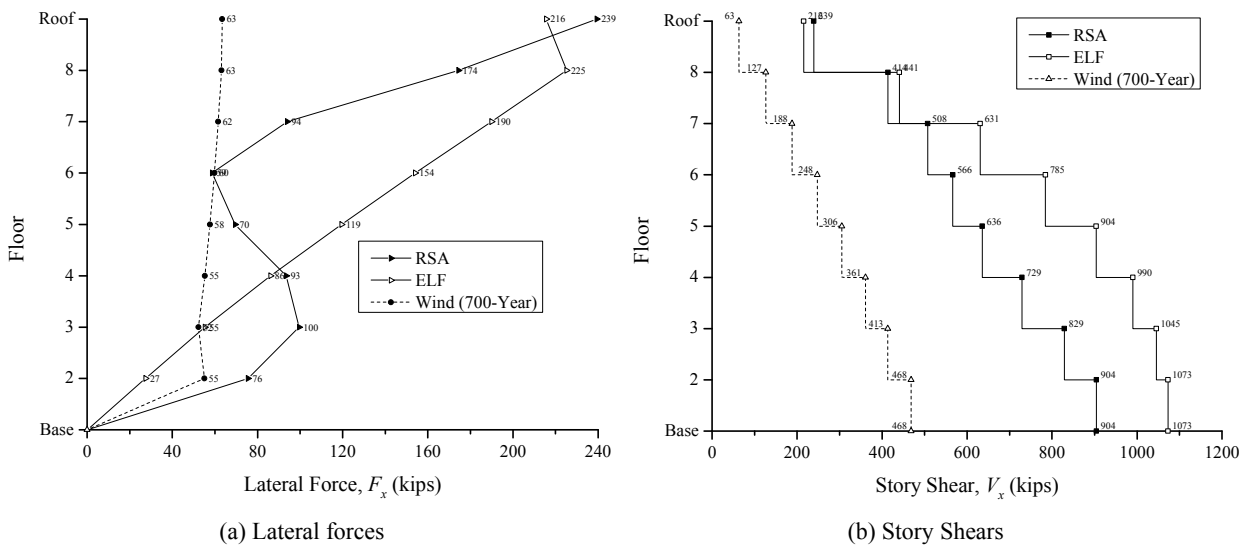


Figure B-13. Strength Design Lateral Forces and Story Shears

Table B-24. Summary of Seismic Drift Forces, N-S MC8

Level, x	F_y (kips)	V_i (kips)	RSA			ELF			Wind (10-Year)			
			δ_x (inch)	Δ_i (inch)	Δ_i / h_{sx}	F_y (kips)	V_i (kips)	δ_x (inch)	Δ_i (inch)	Δ_i / h_{sx}	F_y (kips)	V_i (kips)
Roof	168	168	10.93	1.51	0.009	161	161	14.59	2.03	0.012	18	18
8	122	290	9.42	1.62	0.010	163	324	12.56	2.23	0.013	19	37
7	66	356	7.79	1.68	0.010	133	458	10.33	2.17	0.013	18	55
6	41	397	6.12	1.54	0.009	104	562	8.16	1.99	0.012	17	73
5	49	446	4.58	1.37	0.008	77	638	6.17	2.00	0.012	17	89
4	65	511	3.20	1.10	0.007	52	690	4.17	1.57	0.009	16	105
3	70	581	2.11	1.04	0.006	31	721	2.60	1.39	0.008	15	121
2	53	633	1.06	1.06	0.005	13	735	1.22	1.22	0.006	16	136

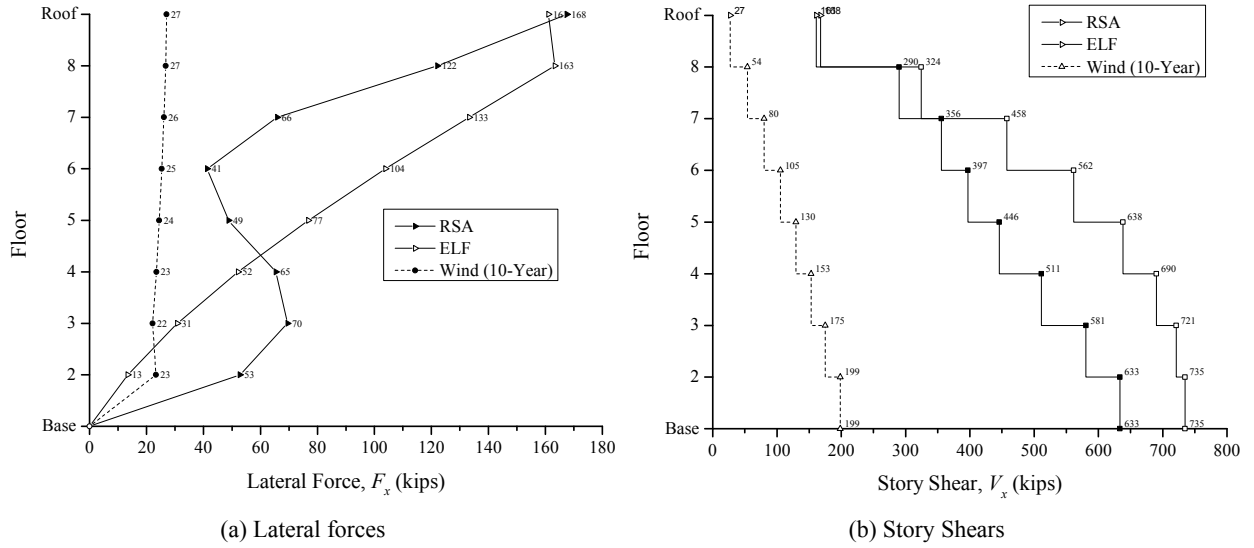


Figure B-14. Drift Design Lateral Forces and Story Shears

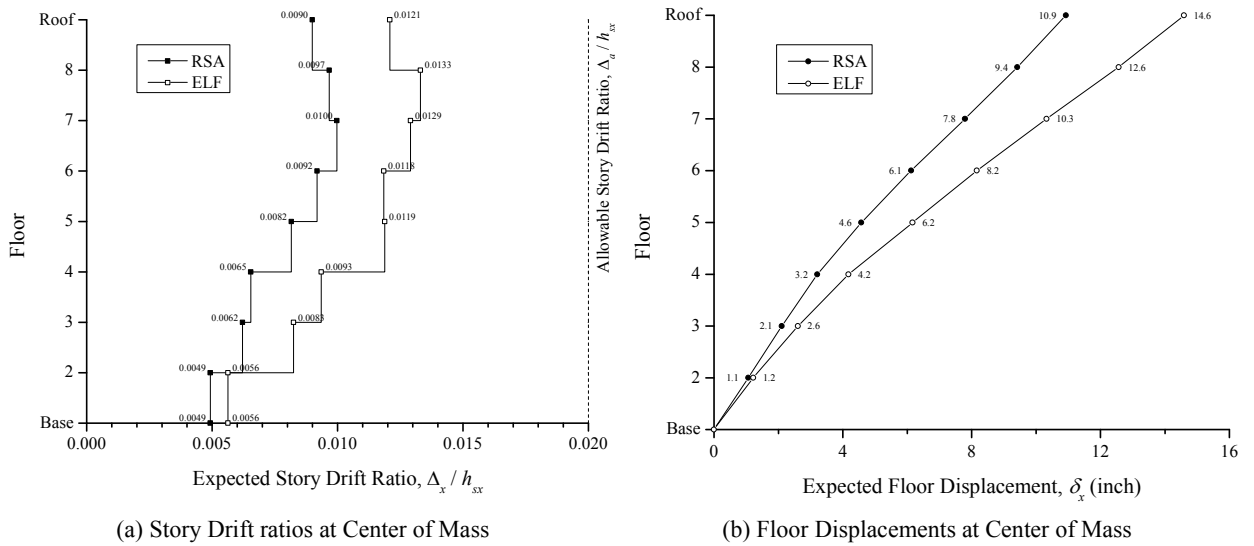


Figure B-15. Story Drift Ratios and Deflected Shape

Table B-25 and Table B-26 provide the tabulated data for verifying the allowable story drifts and the seismic stability coefficient per ASCE 7 §12.8.6 and ASCE §12.8.7 for each archetype building design.

Table B-25. ASCE 7 Allowable Drift and Stability Verification, N-S MC8 RSA

Level, x	$V_i \times C_d$ (kips)	P_x (kips)	Δ_i (inch)	h_{sx} (inch)	Δ_i / h_{sx}	θ_{2i}	θ_{1i}	β_i	$\theta_{max,i}$
ROOF	838	1081	1.51	168	0.009	0.012	0.011	1.00	0.100
8	1449	2443	1.62	168	0.010	0.016	0.016	1.00	0.100
7	1778	3815	1.68	168	0.010	0.021	0.021	1.00	0.100
6	1985	5192	1.54	168	0.009	0.024	0.023	1.00	0.100
5	2229	6580	1.37	168	0.008	0.024	0.024	1.00	0.100
4	2555	7973	1.10	168	0.007	0.020	0.020	1.00	0.100
3	2903	9378	1.04	168	0.006	0.020	0.020	1.00	0.100
2	3167	10807	1.06	216	0.005	0.017	0.017	1.00	0.100

Table B-26. ASCE 7 Allowable Drift and Stability Verification, N-S MC8 ELF

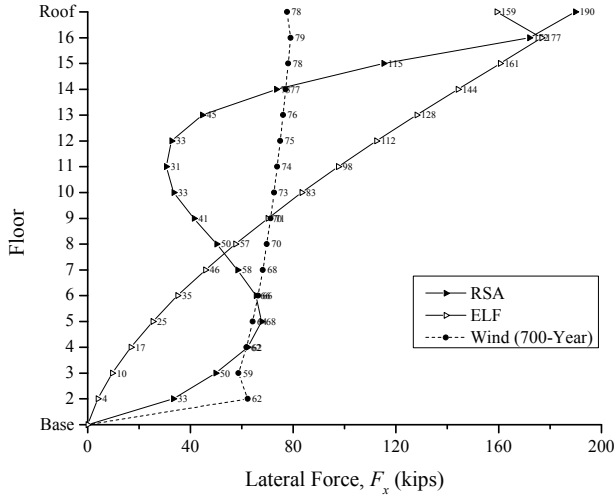
Level, x	$V_i \times C_d$ (kips)	P_x (kips)	Δ_i (inch)	h_{sx} (inch)	Δ_i / h_{sx}	θ_{2i}	θ_{1i}	β_i	$\theta_{max,i}$
ROOF	805	1083	2.03	168	0.012	0.016	0.016	1.00	0.100
8	1622	2450	2.23	168	0.013	0.020	0.020	1.00	0.100
7	2288	3835	2.17	168	0.013	0.022	0.021	1.00	0.100
6	2808	5229	1.99	168	0.012	0.022	0.022	1.00	0.100
5	3192	6631	2.00	168	0.012	0.025	0.024	1.00	0.100
4	3452	8038	1.57	168	0.009	0.022	0.021	1.00	0.100
3	3606	9457	1.39	168	0.008	0.022	0.021	1.00	0.100
2	3673	10898	1.22	216	0.006	0.017	0.016	1.00	0.100

B.1.2.3.3 MC16 (Special Concentrically Braced Frame)

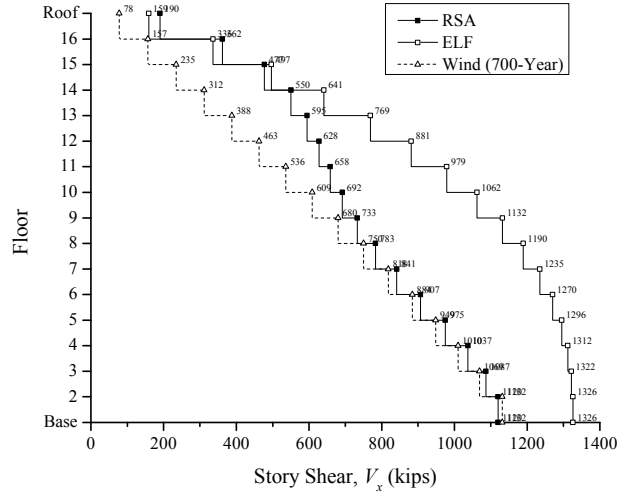
Table B-27 and Table B-28 provide the horizontal seismic forces and story shears for each archetype building design for the seismic strength analysis and the drift analysis. The data are also graphically illustrated in Figure B-16 through Figure B-18. In these tables, F_y represents the seismic forces acting in the N-S direction only. Lastly, the equivalent story forces for the RSA design are backed out from the story shears computed via a modal combination procedure. Although not theoretically correct, the forces provide a comparison basis for evaluating variations in the vertical distribution.

Table B-27. Summary of Seismic Strength Design Forces, N-S MC16

Level, x	RSA		ELF			Wind (700-Year)	
	F_y (kips)	V_i (kips)	F_y (kips)	V_i (kips)	V_{ELF} / V_{RSA}	F_y (kips)	V_i (kips)
Roof	190	190	159	159	1.19	57	57
16	172	362	177	336	1.08	62	119
15	115	477	161	497	0.96	61	180
14	73	550	144	641	0.86	61	241
13	45	595	128	769	0.77	60	301
12	33	628	112	881	0.71	59	360
11	31	658	98	979	0.67	58	417
10	33	692	83	1062	0.65	57	474
9	41	733	70	1132	0.65	56	530
8	50	783	57	1190	0.66	54	584
7	58	841	46	1235	0.68	53	637
6	66	907	35	1270	0.71	51	689
5	68	975	25	1296	0.75	50	738
4	62	1037	17	1312	0.79	48	786
3	50	1087	10	1322	0.82	45	831
2	33	1120	4	1326	0.84	47	878



(a) Lateral forces

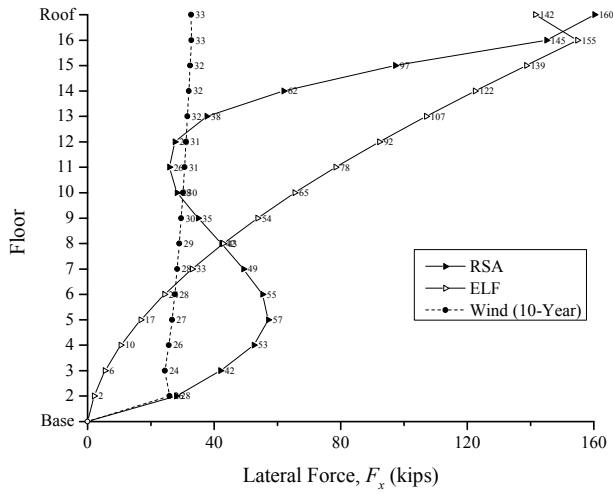


(b) Story Shears

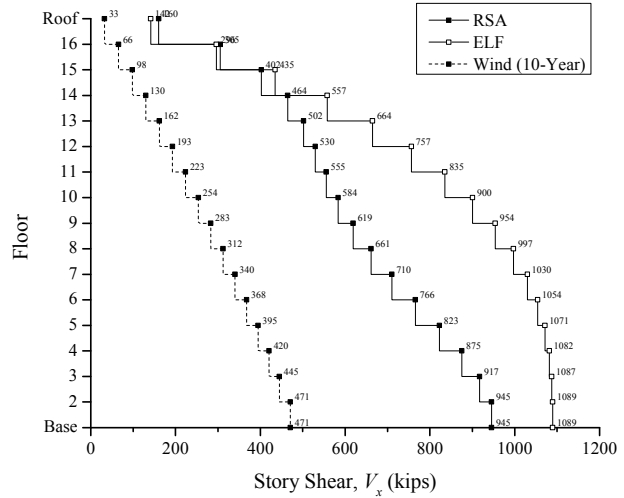
Figure B-16. Strength Design Lateral Forces and Story Shears

Table B-28. Summary of Seismic Drift Forces, N-S MC16

Level, x	RSA					ELF					Wind (10-Year)	
	F_y (kips)	V_i (kips)	δ_x (inch)	Δ_i (inch)	Δ_i / h_{sx}	F_y (kips)	V_i (kips)	δ_x (inch)	Δ_i (inch)	Δ_i / h_{sx}	F_y (kips)	V_i (kips)
Roof	160	160	16.00	1.01	0.006	142	142	24.43	1.53	0.009	23	23
16	145	305	15.00	1.15	0.007	155	296	22.90	1.78	0.011	23	46
15	97	402	13.84	1.21	0.007	139	435	21.12	1.91	0.011	23	69
14	62	464	12.63	1.23	0.007	122	557	19.20	1.99	0.012	23	91
13	38	502	11.41	1.12	0.007	107	664	17.21	1.89	0.011	22	114
12	28	530	10.29	1.08	0.006	92	757	15.32	1.82	0.011	22	136
11	26	555	9.21	1.08	0.006	78	835	13.50	1.74	0.010	22	157
10	28	584	8.13	1.05	0.006	65	900	11.76	1.65	0.010	21	178
9	35	619	7.08	1.05	0.006	54	954	10.11	1.63	0.010	21	199
8	42	661	6.03	1.01	0.006	43	997	8.48	1.53	0.009	20	219
7	49	710	5.02	0.93	0.006	33	1030	6.95	1.48	0.009	20	239
6	55	766	4.09	0.89	0.005	24	1054	5.47	1.36	0.008	19	258
5	57	823	3.20	0.91	0.005	17	1071	4.11	1.29	0.008	19	277
4	53	875	2.29	0.84	0.005	10	1082	2.82	1.11	0.007	18	295
3	42	917	1.45	0.69	0.004	6	1087	1.71	0.86	0.005	17	311
2	28	945	0.76	0.76	0.004	2	1089	0.84	0.84	0.004	18	329

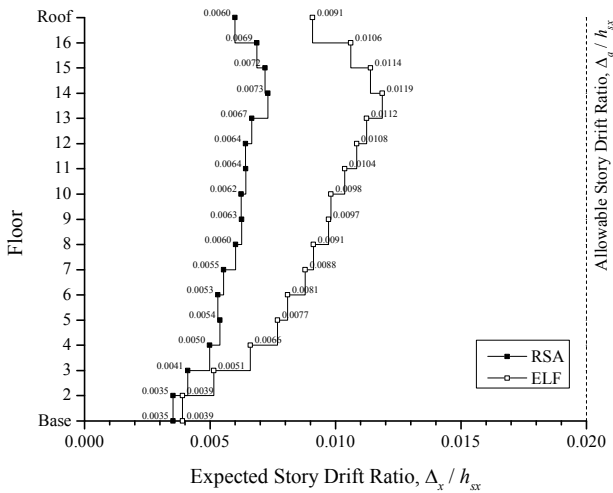


(a) Lateral forces

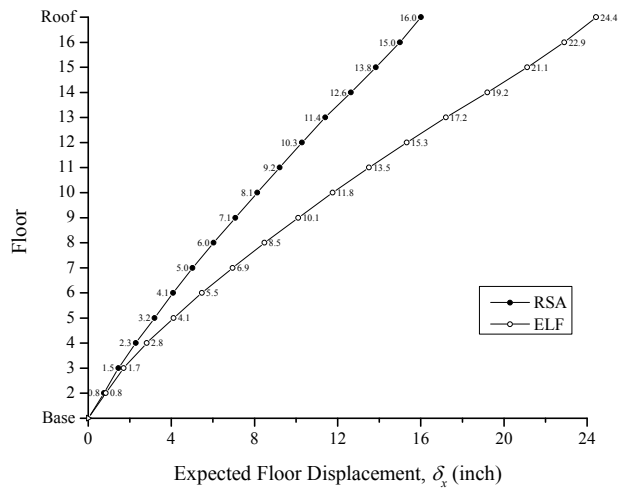


(b) Story Shears

Figure B-17. Drift Design Lateral Forces and Story Shears



(a) Story Drift ratios at Center of Mass



(b) Floor Displacements at Center of Mass

Figure B-18. Story Drift Ratios and Deflected Shape

Table B-29 and Table B-30 provide the tabulated data for verifying the allowable story drifts and the seismic stability coefficient per ASCE 7 §12.8.6 and §12.8.7 for each archetype building design.

Table B-29. ASCE 7 Allowable Drift and Stability Verification, N-S MC16 RSA

Level, x	$V_i \times C_d$ (kips)	P_x (kips)	Δ_i (inch)	h_{sx} (inch)	Δ_i / h_{sx}	θ_{2i}	θ_{1i}	β_i	$\theta_{max,i}$
ROOF	800	1080	1.01	168	0.006	0.008	0.008	1.00	0.100
16	1524	2444	1.15	168	0.007	0.011	0.011	1.00	0.100
15	2010	3812	1.21	168	0.007	0.014	0.013	1.00	0.100
14	2320	5184	1.23	168	0.007	0.016	0.016	1.00	0.100
13	2508	6570	1.12	168	0.007	0.017	0.017	1.00	0.100
12	2646	7960	1.08	168	0.006	0.019	0.019	1.00	0.100
11	2775	9355	1.08	168	0.006	0.022	0.021	1.00	0.100
10	2916	10754	1.05	168	0.006	0.023	0.022	1.00	0.100
9	3090	12160	1.05	168	0.006	0.025	0.024	1.00	0.100
8	3302	13570	1.01	168	0.006	0.025	0.024	1.00	0.100
7	3548	14986	0.93	168	0.006	0.023	0.023	1.00	0.100
6	3824	16406	0.89	168	0.005	0.023	0.022	1.00	0.100
5	4109	17837	0.91	168	0.005	0.023	0.023	1.00	0.100
4	4372	19276	0.84	168	0.005	0.022	0.021	1.00	0.100
3	4581	20726	0.69	168	0.004	0.019	0.018	1.00	0.100
2	4721	22207	0.76	216	0.004	0.017	0.016	1.00	0.100

Table B-30. ASCE 7 Allowable Drift and Stability Verification, N-S MC16 ELF

Level, x	$V_i \times C_d$ (kips)	P_x (kips)	Δ_i (inch)	h_{sx} (inch)	Δ_i / h_{sx}	θ_{2i}	θ_{1i}	β_i	$\theta_{max,i}$
ROOF	706	1080	1.52	168	0.009	0.014	0.014	1.00	0.100
16	1479	2444	1.78	168	0.011	0.017	0.017	1.00	0.100
15	2170	3821	1.91	168	0.011	0.020	0.020	1.00	0.100
14	2782	5206	1.99	168	0.012	0.022	0.022	1.00	0.100
13	3316	6598	1.88	168	0.011	0.022	0.022	1.00	0.100
12	3775	7994	1.82	168	0.011	0.023	0.022	1.00	0.100
11	4167	9396	1.74	168	0.010	0.023	0.023	1.00	0.100
10	4493	10802	1.65	168	0.010	0.024	0.023	1.00	0.100
9	4762	12217	1.63	168	0.010	0.025	0.024	1.00	0.100
8	4975	13636	1.53	168	0.009	0.025	0.024	1.00	0.100
7	5140	15061	1.47	168	0.009	0.026	0.025	1.00	0.100
6	5261	16491	1.36	168	0.008	0.025	0.025	1.00	0.100
5	5345	17929	1.29	168	0.008	0.026	0.025	1.00	0.100
4	5398	19375	1.11	168	0.007	0.024	0.023	1.00	0.100
3	5425	20836	0.86	168	0.005	0.020	0.019	1.00	0.100
2	5435	22334	0.84	216	0.004	0.016	0.016	1.00	0.100

B.2 Horizontal and Vertical Irregularities

B.2.1 Special Moment Frame

Table B-31 through Table B-34 provide the results for the horizontal (type 1) and vertical (type 1 and 5) irregularity verifications.

Table B-31. Horizontal Irregularity Type 1 (a and b) Verification

Floor (x)	$\Delta_{max} / \Delta_{avg}^a$					
	MC4		MC8		MC16	
	ELF	RSA	ELF	RSA	ELF	RSA
Roof MC16	-	-	-	-	1.015	1.012
16	-	-	-	-	1.011	1.009
15	-	-	-	-	1.012	1.008
14	-	-	-	-	1.011	1.007
13	-	-	-	-	1.010	1.008
12	-	-	-	-	1.010	1.007
11	-	-	-	-	1.009	1.007
10	-	-	-	-	1.009	1.007
9 (Roof MC8)	-	-	1.016	1.011	1.008	1.007
8	-	-	1.013	1.009	1.009	1.007
7	-	-	1.012	1.008	1.008	1.006
6	-	-	1.011	1.007	1.008	1.007
5 (Roof MC4)	1.007	1.006	1.009	1.006	1.007	1.006
4	1.006	1.004	1.008	1.005	1.007	1.007
3	1.005	1.004	1.008	1.006	1.011	1.009
2	1.004	1.003	1.006	1.004	1.004	1.005

a. Values include accidental torsion with $A_x = 1.0$.

Table B-32. Vertical Irregularity Type 1 (a and b) Verification (Exception 1)

Floor (x)	$(\Delta / h_{sx})_x / (\Delta / h_{sx})_{x+1}^a$					
	MC4		MC8		MC16	
	ELF	RSA	ELF	RSA	ELF	RSA
Roof MC16	-	-	-	-	-	-
16	-	-	-	-	1.22	1.27
15	-	-	-	-	1.07	1.13
14	-	-	-	-	1.09	0.97
13	-	-	-	-	1.04	0.89
12	-	-	-	-	1.07	1.02
11	-	-	-	-	1.04	1.02
10	-	-	-	-	0.97	0.98
9 (Roof MC8)	-	-	-	-	0.93	0.95
8	-	-	1.26	1.20	0.99	1.00
7	-	-	0.99	1.07	0.99	0.98
6	-	-	1.07	1.02	0.98	0.93
5 (Roof MC4)	-	-	1.02	0.95	0.94	0.88
4	1.32	1.35	1.02	1.00	0.93	0.94
3	1.11	1.19	0.95	0.94	0.83	0.90
2	0.82	0.67	0.77	0.60	0.63	0.67

a. Δ is taken at the center of mass per ASCE 7 §12.8.6.

$$V_{y,i} = \frac{2 \sum_{j=1}^n M_{pr,j}}{h} \quad (\text{B-5})$$

$$h = \frac{h_{sx} + h_{sx+1}}{2} \quad (\text{B-6})$$

Table B-33. Vertical Irregularity Type 5 (a and b) Verification, ELF (kip, feet)

Floor (x)	h^c	MC4			MC8			MC16		
		M_{pr}^a	$V_{y,x}^b$	$V_{y,x+1} / V_{y,x}$	M_{pr}^a	$V_{y,x}^b$	$V_{y,x+1} / V_{y,x}$	M_{pr}^a	$V_{y,x}^b$	$V_{y,x+1} / V_{y,x}$
Roof MC16	7	-	-	-	-	-	-	491.1	421.0	-
16	14	-	-	-	-	-	-	491.1	210.5	0.50
15	14	-	-	-	-	-	-	951.8	407.9	1.94
14	14	-	-	-	-	-	-	951.8	407.9	1.00
13	14	-	-	-	-	-	-	1242.1	532.3	1.31
12	14	-	-	-	-	-	-	1242.1	532.3	1.00
11	14	-	-	-	-	-	-	1242.1	532.3	1.00
10	14	-	-	-	-	-	-	1242.1	532.3	1.00
9 (Roof MC8)	14 / 7	-	-	-	491.1	421.0	-	1662.3	712.4	1.34
8	14	-	-	-	491.1	210.5	0.50	1662.3	712.4	1.00
7	14	-	-	-	951.8	407.9	1.94	1662.3	712.4	1.00
6	14	-	-	-	951.8	407.9	1.00	1662.3	712.4	1.00
5 (Roof MC4)	14 / 7	491.1	421.0	-	1161.6	497.8	1.22	1662.3	712.4	1.00
4	14	679.7	291.3	0.69	1161.6	497.8	1.00	1662.3	712.4	1.00
3	14	754.6	323.4	1.11	1161.6	497.8	1.00	1662.3	712.4	1.00
2	16	754.6	283.0	0.88	1161.6	435.6	0.88	1662.3	623.3	0.88

a. M_{pr} is for a single beam plastic hinge at the center of the RBS.
b. $V_{y,x}$ is computed neglecting the plastic moment strength of the adjacent columns.
c. h is taken as the distance from mid-height of a story to mid-height of the story above ($\neq h_{sx}$).

Table B-34. Vertical Irregularity Type 5 (a and b) Verification, RSA (kip, feet)

Floor (x)	h^c	MC4			MC8			MC16		
		M_{pr}^a	$V_{y,x}^b$	$V_{y,x+1} / V_{y,x}$	M_{pr}^a	$V_{y,x}^b$	$V_{y,x+1} / V_{y,x}$	M_{pr}^a	$V_{y,x}^b$	$V_{y,x+1} / V_{y,x}$
Roof MC16	7	-	-	-	-	-	-	491.1	421.0	-
16	14	-	-	-	-	-	-	491.1	210.5	0.50
15	14	-	-	-	-	-	-	491.1	210.5	1.00
14	14	-	-	-	-	-	-	491.1	210.5	1.00
13	14	-	-	-	-	-	-	951.8	407.9	1.94
12	14	-	-	-	-	-	-	951.8	407.9	1.00
11	14	-	-	-	-	-	-	951.8	407.9	1.00
10	14	-	-	-	-	-	-	951.8	407.9	1.00
9 (Roof MC8)	14 / 7	-	-	-	358.7	307.5	-	1242.1	532.3	1.31
8	14	-	-	-	358.7	153.7	0.50	1242.1	532.3	1.00
7	14	-	-	-	491.1	210.5	1.37	1242.1	532.3	1.00
6	14	-	-	-	491.1	210.5	1.00	1242.1	532.3	1.00
5 (Roof MC4)	14 / 7	491.1	421.0	-	679.7	291.3	1.38	1662.3	712.4	1.34
4	14	491.1	210.5	0.50	679.7	291.3	1.00	1662.3	712.4	1.00
3	14	491.1	210.5	1.00	754.6	323.4	1.11	1662.3	712.4	1.00
2	16	491.1	184.2	0.88	754.6	283.0	0.88	1662.3	623.3	0.88

a. M_{pr} is for a single beam plastic hinge at the center of the RBS.
b. $V_{y,x}$ is computed neglecting the plastic moment strength of the adjacent columns.
c. h is taken as the distance from mid-height of a story to mid-height of the story above ($\neq h_{sx}$).

B.2.2 Special Concentrically Braced Frame

Table B-35 through Table B-38 provide the results for the horizontal (type 1) and vertical (type 1 and 5) irregularity verifications.

Table B-35. Horizontal Irregularity Type 1 (a and b) Verification

Floor (x)	$\Delta_{max} / \Delta_{avg}^a$					
	MC4		MC8		MC16	
	ELF	RSA	ELF	RSA	ELF	RSA
Roof MC16	-	-	-	-	1.097	1.100
16	-	-	-	-	1.073	1.071
15	-	-	-	-	1.072	1.086
14	-	-	-	-	1.079	1.075
13	-	-	-	-	1.077	1.083
12	-	-	-	-	1.073	1.073
11	-	-	-	-	1.089	1.089
10	-	-	-	-	1.063	1.073
9 (Roof MC8)	-	-	1.079	1.084	1.098	1.094
8	-	-	1.081	1.086	1.060	1.070
7	-	-	1.073	1.077	1.102	1.097
6	-	-	1.073	1.082	1.057	1.060
5 (Roof MC4)	1.078	1.096	1.084	1.083	1.103	1.105
4	1.071	1.056	1.069	1.075	1.059	1.056
3	1.040	1.064	1.089	1.091	1.127	1.129
2	1.044	1.045	1.076	1.078	1.077	1.080

a. Values include accidental torsion with $A_x = 1.0$.

Table B-36. Vertical Irregularity Type 1 (a and b) Verification (Using Exception 1)

Floor (x)	$(\Delta / h_{sx})_x / (\Delta / h_{sx})_{x+1}^a$					
	MC4		MC8		MC16	
	ELF	RSA	ELF	RSA	ELF	RSA
Roof MC16	-	-	-	-	-	-
16	-	-	-	-	1.17	1.20
15	-	-	-	-	1.07	1.08
14	-	-	-	-	1.04	1.02
13	-	-	-	-	0.95	0.91
12	-	-	-	-	0.97	0.94
11	-	-	-	-	0.96	1.00
10	-	-	-	-	0.95	0.94
9 (Roof MC8)	-	-	-	-	0.99	0.99
8	-	-	1.10	1.11	0.94	0.93
7	-	-	0.97	1.03	0.96	0.91
6	-	-	0.92	0.91	0.92	0.93
5 (Roof MC4)	-	-	1.00	0.88	0.95	1.01
4	1.26	1.14	0.79	0.77	0.86	0.91
3	0.87	1.02	0.88	0.93	0.78	0.82
2	0.83	0.63	0.68	0.61	0.76	0.85

a. Δ is taken at the center of mass per ASCE 7 §12.8.6.

$$V_{y,i} = (P_{br,C} + P_{br,T}) \frac{b}{2\sqrt{\left(\frac{b}{2}\right)^2 + h_{sx}^2}} \quad (\text{B-7})$$

[$b = 20$ ft. for MC4 and MC8, $b = 30$ ft. for MC16]

Table B-37. Vertical Irregularity Type 5 (a and b) Verification, ELF (kip, feet)

Floor (x)	h_{sx}	MC4				MC8				MC16			
		$P_{br,C}^a$	$P_{br,T}^b$	$V_{y,x}$	$V_{y,x+1} / V_{y,x}$	$P_{br,C}^a$	$P_{br,T}^b$	$V_{y,x}$	$V_{y,x+1} / V_{y,x}$	$P_{br,C}^a$	$P_{br,T}^b$	$V_{y,x}$	$V_{y,x+1} / V_{y,x}$
Roof MC16	14	-	-	-	-	-	-	-	-	99.4	255.9	259.7	-
16	14	-	-	-	-	-	-	-	-	99.4	255.9	259.7	1.00
15	14	-	-	-	-	-	-	-	-	132.7	284.8	305.3	1.18
14	14	-	-	-	-	-	-	-	-	132.7	284.8	305.3	1.00
13	14	-	-	-	-	-	-	-	-	207.5	403.2	446.5	1.46
12	14	-	-	-	-	-	-	-	-	207.5	403.2	446.5	1.00
11	14	-	-	-	-	-	-	-	-	240.2	484.4	529.7	1.19
10	14	-	-	-	-	-	-	-	-	240.2	484.4	529.7	1.00
9 (Roof MC8)	14	-	-	-	-	131.7	255.9	225.3	-	297.9	480.2	568.9	1.07
8	14	-	-	-	-	131.7	255.9	225.3	1.00	297.9	480.2	568.9	1.00
7	14	-	-	-	-	252.8	403.2	381.3	1.69	297.9	480.2	568.9	1.00
6	14	-	-	-	-	252.8	403.2	381.3	1.00	297.9	480.2	568.9	1.00
5 (Roof MC4)	14	78.3	249.2	190.4	-	252.8	403.2	381.3	1.00	297.9	480.2	568.9	1.00
4	14	131.7	255.9	225.3	1.18	252.8	403.2	381.3	1.00	297.9	480.2	568.9	1.00
3	14	252.8	403.2	381.3	1.69	343.3	480.2	478.7	1.26	469.2	679.0	839.4	1.48
2	18	239.0	484.4	351.3	0.92	296.9	480.2	377.4	0.79	419.4	679.0	703.1	0.84

a. Design compression strength.
b. Design tension strength.

Table B-38. Vertical Irregularity Type 5 (a and b) Verification, RSA (kip, feet)

Floor (x)	h_{sx}	MC4				MC8				MC16			
		$P_{br,C}^a$	$P_{br,T}^b$	$V_{y,x}$	$V_{y,x+1} / V_{y,x}$	$P_{br,C}^a$	$P_{br,T}^b$	$V_{y,x}$	$V_{y,x+1} / V_{y,x}$	$P_{br,C}^a$	$P_{br,T}^b$	$V_{y,x}$	$V_{y,x+1} / V_{y,x}$
Roof MC16	14	-	-	-	-	-	-	-	-	99.4	255.9	259.7	-
16	14	-	-	-	-	-	-	-	-	99.4	255.9	259.7	1.00
15	14	-	-	-	-	-	-	-	-	132.7	284.8	305.3	1.18
14	14	-	-	-	-	-	-	-	-	132.7	284.8	305.3	1.00
13	14	-	-	-	-	-	-	-	-	207.5	403.2	446.5	1.46
12	14	-	-	-	-	-	-	-	-	207.5	403.2	446.5	1.00
11	14	-	-	-	-	-	-	-	-	207.5	403.2	446.5	1.00
10	14	-	-	-	-	-	-	-	-	207.5	403.2	446.5	1.00
9 (Roof MC8)	14	-	-	-	-	131.7	255.9	225.3	-	207.5	403.2	446.5	1.00
8	14	-	-	-	-	131.7	255.9	225.3	1.00	207.5	403.2	446.5	1.00
7	14	-	-	-	-	166.5	284.8	262.3	1.16	240.2	484.4	529.7	1.19
6	14	-	-	-	-	166.5	284.8	262.3	1.00	240.2	484.4	529.7	1.00
5 (Roof MC4)	14	67.6	197.9	154.3	-	252.8	403.2	381.3	1.45	297.9	480.2	568.9	1.07
4	14	131.7	255.9	225.3	1.46	252.8	403.2	381.3	1.00	297.9	480.2	568.9	1.00
3	14	166.5	284.8	262.3	1.16	343.3	480.2	478.7	1.26	469.2	679.0	839.4	1.48
2	18	206.6	403.2	296.1	1.13	296.9	480.2	377.4	0.79	419.4	679.0	703.1	0.84

a. Design compression strength
b. Design tension strength.

B.3 SMF AISC Frame Stability (Effective Length Method)

Table B-39 through Table B-44 provide the results from AISC 360, appendix 7 Effective Length Method verifications.

Table B-39. AISC 360 Frame Stability (Effective Length Method), 4-Story SMF ELF (kip, inch)

P_{story}^a	Δ_H^b	H	L	R_m	$P_{e\ story}$	B_2
1314	2.24	499.9	168	0.954	35716	1.04
2936	2.92	897.8	168	0.954	49223	1.06
4574	3.21	1120.0	168	0.954	55854	1.09
6235	3.38	1208.0	216	0.954	73615	1.09

a. P_{story} is computed from $1.2 \times \text{Dead} + 0.25 \times \text{Floor Live}$.

b. Δ_H and H are determined from a first-order static analysis using ASCE 7 §12.8.6.

Table B-40. AISC 360 Frame Stability (Effective Length Method), 4-Story SMF RSA (kip, inch)

P_{story}^a	Δ_H^b	H	L	R_m	$P_{e\ story}$	B_2
1309	2.51	435.5	168	0.954	27764	1.05
2925	3.50	765.8	168	0.954	35055	1.09
4547	3.97	938.0	168	0.954	37806	1.14
6192	4.13	999.6	216	0.954	49870	1.14

a. P_{story} is computed from $1.2 \times \text{Dead} + 0.25 \times \text{Floor Live}$.

b. Δ_H and H are determined from a first-order static analysis using ASCE 7 §12.8.6.

Table B-41. AISC 360 Frame Stability (Effective Length Method), 8-Story SMF ELF (kip, inch)

P_{story}^a	Δ_H^b	H	L	R_m	$P_{e\ story}$	B_2
1300	2.15	392.5	168	0.954	29312	1.05
2901	2.68	764.5	168	0.954	45678	1.07
4525	2.64	1045.2	168	0.954	63361	1.08
6158	2.79	1244.9	168	0.954	71414	1.09
7803	2.81	1377.1	168	0.954	78453	1.11
9452	2.83	1455.0	168	0.954	82282	1.13
11115	2.68	1493.0	168	0.954	89151	1.14
12806	2.66	1505.3	216	0.954	116595	1.12

a. P_{story} is computed from $1.2 \times \text{Dead} + 0.25 \times \text{Floor Live}$.

b. Δ_H and H are determined from a first-order static analysis using ASCE 7 §12.8.6.

Table B-42. AISC 360 Frame Stability (Effective Length Method), 8-Story SMF RSA (kip, inch)

P_{story}^a	Δ_H^b	H	L	R_m	$P_{e\ story}$	B_2
1297	5.76	665.9	168	0.954	18506	1.08
2893	7.62	1297.1	168	0.954	27284	1.12
4501	8.56	1770.7	168	0.954	33134	1.16
6114	8.74	2107.1	168	0.954	38612	1.19
7741	8.11	2330.3	168	0.954	46054	1.20
9373	7.72	2462.1	168	0.954	51065	1.22
11021	6.83	2526.7	168	0.954	59299	1.23
12697	6.44	2547.5	216	0.954	81474	1.18

a. P_{story} is computed from $1.2 \times \text{Dead} + 0.25 \times \text{Floor Live}$.

b. Δ_H and H are determined from a first-order static analysis using ASCE 7 §12.8.6.

Table B-43. AISC 360 Frame Stability (Effective Length Method), 16-Story SMF ELF (kip, inch)

P_{story}^a	Δ_H^b	H	L	R_m	$P_{e\ story}$	B_2
1297	1.62	278.1	168	0.954	27566	1.05
2895	1.97	578.3	168	0.954	47016	1.07
4509	2.09	843.4	168	0.954	64592	1.08
6133	2.26	1073.9	168	0.954	76131	1.09
7766	2.34	1272.1	168	0.954	86953	1.10
9403	2.49	1439.8	168	0.954	92517	1.11
11046	2.57	1579.7	168	0.954	98355	1.13
12695	2.50	1694.0	168	0.954	108744	1.13
14355	2.31	1785.7	168	0.954	123781	1.13
16020	2.27	1856.8	168	0.954	131214	1.14
17691	2.24	1909.9	168	0.954	136851	1.15
19369	2.18	1947.6	168	0.954	143441	1.16
21056	2.05	1972.5	168	0.954	154360	1.16
22754	1.91	1987.2	168	0.954	167096	1.16
24469	1.60	1994.5	168	0.954	199929	1.14
26227	1.32	1996.8	216	0.954	311432	1.09

a. P_{story} is computed from $1.2 \times \text{Dead} + 0.25 \times \text{Floor Live}$.

b. Δ_H and H are determined from a first-order static analysis using ASCE 7 §12.8.6.

Table B-44. AISC 360 Frame Stability (Effective Length Method), 16-Story SMF RSA (kip, inch)

P_{story}^a	Δ_H^b	H	L	R_m	$P_{e\ story}$	B_2
1296	2.83	390.9	168	0.954	22100	1.06
2893	3.88	812.9	168	0.954	33576	1.09
4496	4.75	1182.8	168	0.954	39868	1.13
6105	4.89	1503.8	168	0.954	49305	1.14
7728	4.56	1781.0	168	0.954	62558	1.14
9358	4.71	2015.7	168	0.954	68592	1.16
10993	4.83	2211.3	168	0.954	73302	1.18
12634	4.73	2371.3	168	0.954	80383	1.19
14282	4.45	2499.2	168	0.954	90046	1.19
15936	4.34	2598.5	168	0.954	95899	1.20
17595	4.17	2672.7	168	0.954	102632	1.21
19260	3.78	2725.3	168	0.954	115496	1.20
20939	3.25	2760.2	168	0.954	136170	1.18
22627	2.94	2780.8	168	0.954	151337	1.18
24328	2.50	2790.8	168	0.954	178505	1.16
26067	2.16	2794.1	216	0.954	267012	1.11

a. P_{story} is computed from $1.2 \times \text{Dead} + 0.25 \times \text{Floor Live}$.

b. Δ_H and H are determined from a first-order static analysis using ASCE 7 §12.8.6.

Table B-45. Adjusted Effective Length Factors – 4-Story SMF

Story	ELF		RSA	
	K_{2x} (note a) Exterior	K_{2x} (note a) Interior	K_{2x} (note a) Exterior	K_{2x} (note a) Interior
4	2.23	2.98	2.46	3.08
3	2.44	3.26	2.99	3.74
2	2.54	3.37	3.08	3.86
1	2.42	3.21	2.58	3.23

a. x designates in-plane buckling about x -axis as depicted in AISC 360 Part 1.

Table B-46. Adjusted Effective Length Factors – 8-Story SMF

Story	ELF		RSA	
	K_{2x} (note a)	K_{2x} (note a)	K_{2x} (note a)	K_{2x} (note a)
	Exterior	Interior	Exterior	Interior
8	2.18	2.75	2.59	2.74
7	2.12	2.67	2.61	2.76
6	2.09	2.80	2.26	3.21
5	2.04	2.74	2.16	3.08
4	2.04	2.88	2.20	3.38
3	1.99	2.81	2.27	3.48
2	2.09	3.21	2.44	3.82
1	2.03	3.11	2.24	3.51

a. x designates in-plane buckling about x -axis as depicted in AISC 360 Part 1.

Table B-47. Adjusted Effective Length Factors – 16-Story SMF

Story	ELF		RSA	
	K_{2x} (note a)	K_{2x} (note a)	K_{2x} (note a)	K_{2x} (note a)
	Exterior	Interior	Exterior	Interior
16	3.09	2.46	2.51	2.64
15	3.33	2.65	2.41	2.53
14	2.66	2.80	2.11	2.73
13	2.46	2.59	2.02	2.61
12	2.29	2.52	2.17	2.66
11	2.20	2.43	2.29	2.81
10	2.05	2.49	2.11	2.90
9	2.01	2.43	2.05	2.81
8	1.97	2.70	2.21	2.89
7	2.07	2.84	2.32	3.04
6	2.03	3.21	2.22	3.43
5	1.97	3.12	2.09	3.22
4	2.08	3.21	2.88	3.11
3	2.07	3.20	3.79	4.09
2	2.69	3.25	3.48	4.20
1	2.62	3.17	2.62	3.17

a. x designates in-plane buckling about x -axis as depicted in AISC 360 Part 1.

B.4 Example Design Calculations

The examples presented detail the strength design calculations for the following members and components of each SFRS for the RSA-designed 8-story buildings (MC8):

- SMF beam and beam-to-column connection, MC8 RSA
- SMF column, MC8 RSA
- SMF panel zone, MC8 RSA

Example calculations for components of the SCBF can be found in Volume 2 (Harris and Speicher 2015).

B.4.1 Special Moment Frame Example

B.4.1.1 Member Selection

After several design and analysis iterations, the final member sizes are shown in Figure B-19.

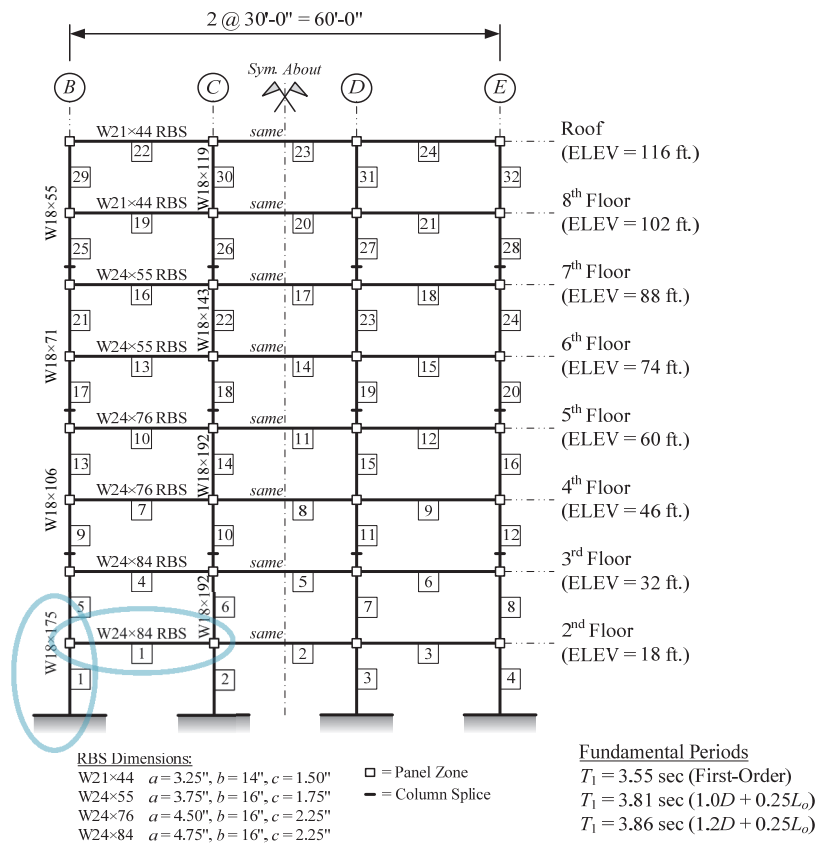


Figure B-19. SMF Member Sizes, 8-story RSA

B.4.1.2 SMF Beam and RBS Beam-to-Column Connection

The second floor frame beam (No. 1) along grid line 1 between grid lines B and C is selected for this example (see circled element in Figure B-19):

- W24×84 with reduced beam sections
- $L = 30$ ft. (centerline)
- A992 Steel: $F_y = 50$ ksi, $R_y = 1.1$, $E = 29000$ ksi, $G = 11200$ ksi

B.4.1.2.1 Flexural Demand

The flexural demand from the controlling load combination from ASCE 7 at the center of the RBS is:

$$M_u = 5696 \text{ kip-in.} = 475 \text{ kip-ft.}$$

B.4.1.2.2 Flexural Strength

The controlling beam strength is at the center of the RBS ($a = 4.75$ in., $b = 16$ in., and $c = 2.25$ in.—see AISC 358). Composite action is neglected in the design for positive moment strength. The effective plastic modulus at the center of the RBS is:

$$Z_e = Z_x - 2ct_f(d - t_f) = 224 - 2(2.25)(0.77)(24.1 - 0.770) = 143.16 \text{ in.}^3$$

The nominal beam capacity at the reduced section is:

$$\phi_b M_n = \phi_b F_y Z_e = 0.9(50)(143.16) = 6442 \text{ kip-in.} = 536 \text{ kip-ft.}$$

$$\therefore \phi_b M_n \geq M_u \text{ (ratio} = 1.12)$$

The beam is braced along its length per AISC 360 and AISC 341.

$$L_b \leq L_p = 1.76r_y \sqrt{\frac{E}{F_{ye}}} = 40.4r_y \leq 0.086r_y \frac{E}{F_{ye}} = 45.3r_y \text{ (note that AISC 360 is more strict)}$$

$$M_p = Z_x F_y = 224(50) = 11200 \text{ kip-in} = 933 \text{ kip-ft.}$$

$$\therefore \phi_b M_n \geq M_u$$

B.4.1.2.3 Fully Restrained Connection

The moment capacity at the face of the column needs to be verified (the expected moment capacity at the face of the column needs to be greater than the probable maximum moment at the center of the fully yielded and strain hardened RBS projected to the face of the column).

The expected moment capacity at the column face is:

$$M_{pe} = Z_b R_y F_y = 224(1.1)(50) = 12320 \text{ kip-in. (AISC 358 Equation 5.8-7)}$$

The probable moment at the RBS is:

$$M_{pr} = C_{pr} R_y F_y Z_e = 1.15(1.1)(50)(143.16) = 9055 \text{ kip-in. (AISC 358 Equation 5.8-5)}$$

The moment at the column face resulting from the M_{pr} at the RBS is:

$$M_f = M_{pr} + V_{RBS} S_h + \frac{w S_h^2}{2} = 9057 + 70.7(12.75) + \frac{0.0829(12.75)^2}{2} = 9962 \text{ kip-in.}$$

$$V_{RBS} = \frac{2M_{pr}}{L'} + \frac{wL'}{2} = \frac{2(9057)}{314.3} + \frac{0.0829(314.3)}{2} = 70.7 \text{ kips}$$

where V_{RBS} is the *probable* shear force at the center of the RBS.

$$\phi_b M_{pe} = 1.0(12320) = 12320 \geq M_f = 9962$$

The shear strength is computed as:

$$\frac{h}{t_w} = 42.5 \leq 2.24 \sqrt{\frac{29000}{50}} = 53.9 \therefore C_v = 1.0$$

$$V_n = 0.6 F_y A_w C_v = 0.6(50)(15.56)(1.0) = 467 \text{ kips}$$

$$\phi_v V_n = 1.0(467) = 467 \geq V_{RBS} = 70.7$$

B.4.1.3 SMF Column

The first story column (No. 1) at the intersection of grid lines 1 and B is selected for this example (see circled element in Figure B-19):

- W18×175
- $h_{sx} = 18 \text{ ft.}$ (L_b of the column is conservatively taken as h_{sx})

- A992 Steel: $F_y = 50$ ksi, $R_y = 1.1$, $E = 29000$ ksi, $G = 11200$ ksi

B.4.1.3.1 Axial and Flexural Demand

The demands in the column from the controlling load combinations from ASCE 7 are presented in Table B-48—maximum/minimum values for an individual action displayed with bolded text.

Table B-48. Controlling Load Combinations (kips, feet)

LC Index	$P_{u,A}$	$P_{u,B}$	$M_{u,A,x}$	$M_{u,B,x}$	Max/Min Action
163	-123.90	-123.90	672.20	168.81	$P_{u,min}$
117	-757.01	-753.18	-689.41	-137.83	$P_{u,max}$
134	-212.09	-209.62	685.32	-140.51	$M_{u,A,min}$
66	-676.27	-672.98	-702.53	171.49	$M_{u,A,max}$
107	-449.00	-445.17	666.02	179.93	$M_{u,B,min}$
173	-433.82	-431.90	-683.23	-148.95	$M_{u,B,max}$

$P_r = 757$ kips and $M_{r,x} = 690$ kip-ft.—from the load combination selected for this example (#117 in Table B-48).

SMF column design is also governed by the capacity design requirements specified in AISC 341 §D1.4a (2), which permits flexural forces resulting from seismic drift of the frame to be neglected in this case.

$$P_{u,\Omega_o} = 1065 \text{ kips}$$

B.4.1.3.2 Axial Strength

The axial compression strength of the column is calculated per AISC 360 §E3.

$$P_n = A_g F_{cr}$$

Flexural Buckling about the y -axis (out-of-plane):

$$\frac{K_y L_y}{r_y} \sqrt{\frac{F_y}{E}} = \frac{1.0(216)}{2.76} \sqrt{\frac{50}{29000}} = 3.25 \leq 4.71$$

$$F_{e,y} = \frac{\pi^2 E}{\left(\frac{K_y L_y}{r_y}\right)^2} = \frac{\pi^2 (29000)}{\left(\frac{1.0(216)}{2.76}\right)^2} = 46.7 \text{ ksi}$$

$$\therefore F_{cr} = \left[0.658^{(F_y/F_{e,y})}\right] F_y = 32.0 \text{ ksi}$$

$$\phi_c P_{n,y} = 0.9(51.3)(32.0) = 0.9(1639) = 1475 \text{ kips} \rightarrow \text{governs}$$

Flexural Buckling about the x -axis (in-plane):

$K_{2x} = 2.59 \rightarrow$ computed using the story buckling method in AISC 360 (assuming only vertical loads triggers story buckling—independently of the stories above and below).

$$\frac{K_x L_x}{r_x} \sqrt{\frac{F_y}{E}} = \frac{2.59(216)}{8.20} \sqrt{\frac{50}{29000}} = 2.83 \leq 4.71$$

$$F_{e,x} = \frac{\pi^2 E}{\left(\frac{K_x L_x}{r_x}\right)^2} = \frac{\pi^2 (29000)}{\left(\frac{2.59(216)}{8.20}\right)^2} = 61.5 \text{ ksi}$$

$$\therefore F_{cr} = \left[0.658^{(F_y/F_{e,x})}\right] F_y = 35.6 \text{ ksi}$$

$$\phi_c P_{n,x} = 0.9(51.3)(35.6) = 0.9(1825) = 1643 \text{ kips} \rightarrow \text{see } \phi_c P_{n,y}$$

B.4.1.3.3 Flexural Strength

The flexural capacity of the column is:

$$M_n = C_b \left[M_p - (M_p - 0.7F_y S_x)(L_b - L_p) / (L_r - L_p) \right] \leq M_p$$

$$M_n = 1.99 \left[1658 - \left(1658 - \frac{0.7(50)(344)}{12} \right) \frac{(15.7 - 9.7)}{(46.8 - 9.7)} \right] = 1.99(1548) = 3080 > M_p = 1658 \text{ kip-ft.}$$

$$\therefore \phi_b M_n = \phi_b M_p = 0.9(1658) \text{ kip-ft.} = 17900 \text{ kip-in.}$$

B.4.1.3.4 Strength Check

The interaction equation check is done using AISC 360 §H1.3.

(a) In-plane stability (AISC 360 Equation H1-1a) using LC #117—see Table B-48

$$\frac{P_r}{P_{n,x}} = \frac{757}{1643} = 0.46$$

For $P_r / P_{n,x} \geq 0.2$, the interaction equation in AISC 360 §H1.1 is:

$$\frac{P_u}{\phi_c P_{n,x}} + \frac{8}{9} \left(\frac{M_{u,x}}{\phi_b M_{n,x}} \right) = \frac{757}{1643} + \frac{8}{9} \left(\frac{8273}{17900} \right) = 0.46 + 0.41 = 0.87 \leq 1.0$$

(b) Out-of-plane stability (AISC 360 Equation H1-2) using LC #117—see Table B-48

$$\frac{P_r}{P_{cy}} = \frac{P_u}{\phi_c P_{n,y}} = \frac{757}{1475} = 0.51$$

$$\begin{aligned} \frac{P_u}{\phi_c P_{n,y}} \left(1.5 - 0.5 \frac{P_u}{\phi_c P_{n,y}} \right) + \left(\frac{M_{u,x}}{C_b \phi_b M_{n,LTB,x}} \right)^2 &= 0.51(1.5 - 0.5(0.51)) + \left(\frac{8273}{1.99(0.9)(18576)} \right)^2 \\ &= 0.63 + 0.062 = 0.69 \leq 1.0 \end{aligned}$$

(c) Amplified seismic load with system overstrength factor from ASCE 7

$$\frac{P_{r,\Omega_o}}{\phi_c P_{n,y}} = \frac{1065}{1475} = 0.72 \leq 1.0$$

B.4.1.4 SMF Panel Zone

The panel zone at the top of the first story column located at the intersection of grid lines 1 and B is selected for this example (see circled element in Figure B-19):

- Column = W18×175 (No. 1)
- Beam = W24×84 (No. 1)
- A992 Steel: $F_y = 50$ ksi, $R_y = 1.1$, $E = 29000$ ksi, $G = 11200$ ksi

B.4.1.4.1 Shear Demand

The panel zone demand is determined using the projected *probable* moment strength at the center of the RBS (AISC 341 E3.6e (1) states *expected* moments; however, most design examples use the *probable* moment because of prequalification testing).

$$M_{pr} = C_{pr} R_y F_y Z_{RBS} = 1.15(1.1)(50)(143.16) = 9057 \text{ kip-in} = 755 \text{ kip-ft.}$$

Projecting this demand to the face of the column:

$$M_f = M_{pr} + V_{RBS} S_h = 9057 + 70.7(12.75) = 9956 \text{ kip-in} = 830 \text{ kip-ft.}$$

The approximate panel zone demand is:

$$V_{u,PZ} = \frac{M_{1f,L}}{(d_1 - t_{f1})} + \frac{M_{1f,R}}{(d_2 - t_{f2})} - V_c$$

$$V_c = \frac{M_{f,L} + M_{f,R}}{\left(\frac{h_b}{2}\right) + \left(\frac{h_t}{2}\right)} = \frac{0 + 9956}{\left(\frac{216}{2}\right) + \left(\frac{168}{2}\right)} = 51.9 \text{ (assumes inflection point at mid-height of columns)}$$

$$V_{u,PZ} = 0 + \frac{9956}{(24.1 - 0.77)} - 51.9 = 375 \text{ kips}$$

$M_{f,R}$ is the moment from the right beam and $M_{f,L} = 0$ since the panel zone is part of a one-sided beam-to-column connection.

Alternatively, the shear demand can be approximated with ASCE 41 §5.4.2.4.2.

$$V_{PZ} = \frac{\sum M_f}{d_b} \left(\frac{L}{L - d_c} \right) \left(\frac{h - d_b}{h} \right) = \frac{830/12}{24.1} \left(\frac{360}{360 - 20} \right) \left(\frac{192 - 24.1}{192} \right) = 382 \text{ kips}$$

B.4.1.4.2 Shear Strength

The panel zone strength is calculated from AISC Equation J10-11:

$$V_n = 0.60F_y d_c t_w \left(1 + \frac{3b_{cf} t_{cf}^2}{d_b d_c t_w} \right) = V_y \left(1 + \frac{3b_{cf} t_{cf}^2}{d_b d_c t_w} \right)$$

$$V_y = 0.60F_y d_c t_w = 0.60(50)(20.0)(0.89) = 534 \text{ kips}$$

$$V_n = V_y \left(1 + \frac{3(11.4)(1.59)^2}{24.1(20.0)(0.89)} \right) = 534(1.2) = 642 \text{ kips}$$

B.4.1.4.3 Strength Check

The panel zone strength check is:

$$\frac{V_r}{\phi V_n} = \frac{375}{1.0(642)} = 0.58 \leq 1.0 \text{ (using probable moment)}$$

Also,

$$\frac{V_r}{V_y} = \frac{375}{534} = 0.7 \leq 1.0 \text{ (using probable moment)}$$

Therefore, the panel zone is not expected to yield at the probable moment.

B.4.1.5 SMF Strong-Column / Weak-Beam

AISC 341 §E3.4a requires that the sum of the nominal flexural strengths of SMF columns at a joint—projected to the joint—be stronger than the expected flexural strengths of the beam-to-column connections at the joint—projected to the joint.

$$\frac{\sum M_{pc}^*}{\sum M_{pb}^*} > 1.0 \text{ (AISC 341 Equation (E3-1))}$$

AISC 341 §E3.4a permits the use of a straight line interaction equation to determine the column flexural strength, M_{pc} (which is a lower-bound nominal plastic section strength). This moment strength is projected to the beam centerline assuming that the shear in column, V_c , is in equilibrium with M_{pc} :

$$\sum M_{pc}^* = Z_{x,top} \left(F_y - \frac{P_{r,top}}{A_g} \right) \left(\frac{h_t}{h_t - \frac{d_b}{2}} \right) + Z_{x,bot} \left(F_y - \frac{P_{r,bot}}{A_g} \right) \left(\frac{h_b}{h_b - \frac{d_b}{2}} \right)$$

Because this is the base column, the assumption that the inflection point occurs at mid-height of the first story is likely invalid due to the fixity of the column-to-base connection. A more accurate estimate can be obtained by a nonlinear static analysis or by taking moments from the elastic analysis. Using Load Combination #117—see Table B-48, the point of inflection, z , from the base is approximately:

$$z = \left(\frac{M_{bot}}{M_{bot} - M_{top}} \right) L' = \left(\frac{689}{689 - (-138)} \right) (192) = 158 \text{ in.}$$

and $h_b = 216 - \frac{24.1}{2} - 158 = 46 \text{ in.}$

The inflection point at the second story is assumed to be at mid-height; therefore,

$$\sum M_{pc}^* = 398 \left(50 - \frac{907}{51.3} \right) \left(\frac{84}{84 - (24.1/2)} \right) + 398 \left(50 - \frac{1065}{51.3} \right) \left(\frac{46}{46 - (24.1/2)} \right) = 30790 \text{ kip-in.}$$

The sum of the projections of the expected flexural strengths of the beams is:

$$\sum M_{pb}^* = \sum (M_{pr} + M_{uv})$$

$\sum M_{pr}$ is the sum of the *probable moments* produced at each RBS centerline determined previously. $\sum M_{uv}$ is the sum of the moments produced at the column centerline by the shear at the plastic hinges:

$$V_{RBS} = \frac{2M_{pr}}{L'} + \frac{wL'}{2} = \frac{2(9057)}{314.3} + \frac{0.0829(314.3)}{2} = 70.7 \text{ kips}$$

$$\sum M_{uv} = \sum \left[V_{RBS} \left(a + \frac{b}{2} + \frac{d_c}{2} \right) \right] = 70.7 \left(4.75 + \frac{16}{2} + \frac{20}{2} \right) = 70.7(22.75) = 1608 \text{ kip-in.}$$

$$\sum M_{pb}^* = 9057 + 1608 = 10665 \text{ kip-in.} = 889 \text{ kip ft.}$$

Therefore,

$$\frac{\sum M_{pc}^*}{\sum M_{pb}^*} = \frac{30790}{10665} = 2.9 > 1.0$$

The previous calculations intend to protect the column against from hinging but does not also check the column against instability at the probable strength of the beam-to-column connection(s). The low ratio result suggests that column instability will not be a concern.

Assuming adequate lateral bracing at the ends of the columns, using AISC 360 Equation H1-2 for out-of-plane buckling with in-plane moments:

$$\frac{P_{r,\Omega_o}}{P_{n,y}} \left(1.5 - 0.5 \frac{P_u}{P_{n,y}} \right) + \left(\frac{M_{u,x}}{C_b M_{n,LTB,x}} \right)^2 = 1.0$$

$$M_{pc,x} = C_b M_{n,LTB,x} \sqrt{1 - \frac{P_{r,\Omega_o}}{P_{n,y}} \left(1.5 - 0.5 \frac{P_{r,\Omega_o}}{P_{n,y}} \right)} = 1.99(18576) \sqrt{1 - \frac{1065}{1638} \left(1.5 - 0.5 \frac{1065}{1638} \right)}$$

$$M_{pc,x} = 36966 \sqrt{1 - 0.65(1.5 - 0.5(0.65))} = 18000 \text{ kip-in} = 1500 \text{ kip-ft.}$$

Similarly, using AISC 360 Equation H1-1a for in-plane buckling with in-plane moments,

$$\frac{P_{r,\Omega_o}}{P_{n,x}} + \frac{8 M_{pc,x}}{9 M_{n,x}} = 1.0 \quad (P_{n,x} \text{ uses } K_x L_x = L_x)$$

$$M_{pc,x} = M_{n,x} \frac{9}{8} \left(1 - \frac{P_{r,\Omega_o}}{P_{n,x}} \right) = (19900) \frac{9}{8} \left(1 - \frac{1065}{1825} \right) = 9323 \text{ kip-in.} = 777 \text{ kip-ft.} \rightarrow \text{governs}$$

Both values for M_{pc} associated with the axis of buckling above must be less than M_{pc} computed from the chosen yield surface, which can be approximated using AISC 360 Equation H1-1a.

$$\frac{P_{r,\Omega_o}}{P_y} + \frac{8 M_{pc,x}}{9 M_{p,x}} = 1.0$$

$$M_{pc,x} = M_{p,x} \frac{9}{8} \left(1 - \frac{P_{r,\Omega_o}}{P_y} \right) = (19900) \frac{9}{8} \left(1 - \frac{1065}{51.3(50)} \right) = 13092 \text{ kip-in.} = 1092 \text{ kip-ft.}$$

For the column above, $M_{pc,x} = 12637$ kip-in. Thus,

$$\sum M_{pc}^* = 12637 \left(\frac{84}{84 - (24.1/2)} \right) + 9323 \left(\frac{46}{46 - (24.1/2)} \right) = 27380 \text{ kip-in.}$$

$$\sum M_{pb}^* = 10665 \text{ kip-in.}$$

$$\frac{\sum M_{pc}^*}{\sum M_{pb}^*} = \frac{27380}{10665} = 2.6 > 1.0$$

The above calculations assume that a plastic hinge formed at the column base does not influence the interaction curves and conservatively assumes K_x for in-plane buckling is invariant to that used for design (which conservatively encompasses all load combinations and load patterns).

Appendix C Example Assessment Calculations

The examples presented in this appendix detail the assessment calculations for the following *primary* members and connections of each SFRS for the RSA-designed 8-story buildings (MC8):

- SMF beam and beam-to-column connection, MC8 RSA
- SMF column, MC8 RSA
- SMF panel zone, MC8 RSA

Linear assessment example calculations are provided in C.1, and examples for the nonlinear assessment example calculations are provided in C.2.

C.1 Linear Assessment Examples

The following example provides guidance to how the linear assessment calculations were conducted in this study. Linear assessment of the selected components is performed for the following criteria:

- Linear Dynamic Procedure (LDP)
- Collapse Prevention (CP) Building Performance Level (BPL) for the BSE-2 Earthquake Hazard Level (EHL)

C.1.1 SMF Frame Beam and RBS Beam-to-Column Connection

The second floor frame beam (No. 1) along grid line 1 between grid lines B and C is selected for this example (see circled element in Figure B-19).

- W24×84 with reduced beam sections
- $L = 30$ ft. (centerline)
- A992 Steel: $F_{y,LB} = F_y = 50$ ksi, $F_{ye} = 55$ ksi, $E = 29000$ ksi, $G = 11154$ ksi

C.1.1.1 Flexural Demand

C.1.1.1.1 Frame Beam

Flexural actions in the beam are *deformation-controlled* (assuming small axial loads); therefore,

$$M_{UD} = M_G \pm M_E \quad (\text{ASCE 41 §3.4.2.1.1})$$

Based on the controlling load combination, the moment at the center of each RBS is:

$$M_{UD,L} = 2336 \text{ kip-ft.} \rightarrow \text{left}$$

$$M_{UD,R} = 2130 \text{ kip-ft.} \rightarrow \text{right}$$

C.1.1.1.2 FR Connection

Flexural action in a FR connection is *deformation-controlled*, therefore:

$$M_{UD} = M_G \pm M_E \quad (\text{ASCE 41 §3.4.2.1.1})$$

Based on the controlling load combination, the moment at the face of each column is:

$$M_{UD,L} = 2533 \text{ kip-ft.} \rightarrow \text{left} \qquad M_{UD,R} = 2327 \text{ kip-ft.} \rightarrow \text{right}$$

C.1.1.2 Flexural Strength

C.1.1.2.1 Beam

Per ASCE 41 §5.4.2.3.2.1, the flexural strength is determined from AISC 360 Chapter F. Because this is new construction designed in accordance with AISC 360 and AISC 341, the beam is braced sufficiently to develop its plastic moment strength.

$$L_b \leq L_p = 1.76r_y \sqrt{\frac{E}{F_{ye}}} = 40.4r_y \leq 0.086r_y \frac{E}{F_{ye}} = 45.3r_y \quad (\text{note that AISC 360 is more strict})$$

$$M_{CE} = M_n = M_p = Z_x F_{ye} = 224(55) = 12320 \text{ kip-in} = 1027 \text{ kip-ft.}$$

The controlling beam strength is at the center of the RBS ($a = 4.75$ in., $b = 16$ in., and $c = 2.25$ in., see AISC 358). The effective plastic modulus at the center of the RBS is:

$$Z_e = Z_x - 2ct_f(d - t_f) = 224 - 2(2.25)(0.77)(24.1 - 0.770) = 143.2 \text{ in.}^3$$

The *expected* plastic moment at the center of the RBS is:

$$M_{CE} = M_{pe} = Z_e F_{ye} = 143.2(55) = 7876 \text{ kip-in.} = 656 \text{ kip-ft.}$$

C.1.1.2.2 Fully Restrained Connection

Per ASCE 41 §5.4.2.4-4, Q_{CE} shall be taken as the capacity of the critical connection component. The acceptance criteria in ASCE 41 for beam-to-column connections are applicable for demands at the face of the column. Thus, Q_{CE} is taken as the expected flexural strength of the RBS projected to the column face.

The corresponding moment strength at the face of the column is:

$$M_{CE} = M_f = M_{pe} \left(\frac{L_{clear}}{L_{clear} - 2 \left(a + \frac{b}{2} \right)} \right) = 7876 \left(\frac{314}{314 - 2 \left(4.75 + \frac{16}{2} \right)} \right) = 8512 \text{ kip-in.} = 709 \text{ kip-ft.}$$

where L_{clear} is the clear distance between column faces.

C.1.1.3 Acceptance Criteria

C.1.1.3.1 Beam

The m -factor for the RBS defined as a beam (primary) is taken from ASCE 41 Table 5-5.

$$\frac{b_f}{2t_f} = 5.86 \leq \frac{52}{\sqrt{F_{ye}}} = 7.01$$

$$\frac{h}{t_w} = 45.9 \leq \frac{418}{\sqrt{F_{ye}}} = 56.4$$

$$\therefore m = 8$$

C.1.1.3.2 Fully Restrained Connection

The *initial* m -factor for the RBS beam-to-column connection (primary) is taken from ASCE 41 Table 5-5.

$$m_i = 6.2 - 0.032d = 6.2 - 0.032(24.1) = 5.43$$

Per ASCE 41 Table 5-4, the RBS is considered a fully restrained (FR) connection and thus the acceptance criteria is subject to the following acceptance criteria modifications in ASCE 41 §5.4.2.4.3 (each modifier is taken as α here).

Continuity Plate Modifier (ASCE 41 §5.4.2.4.2-4.1)

$$t_{cf} = 1.59 \text{ in. and } t_{cp} = 0.5 \text{ in. at both connections, } b_{bf} = 9.02 \text{ in. and } t_{bf} = 0.77 \text{ in.}$$

$$\frac{b_{bf}}{7} \leq t_{cf} < \frac{b_{bf}}{5.2} \text{ and continuity plates with } t \geq \frac{t_{bf}}{2}$$

$$\therefore 1.29 \leq t_{cf} < 1.73 \text{ and } t_{cp} \geq 0.39$$

$$\therefore \alpha_{CP} = 1.0 \text{ for both connections}$$

Panel Zone Strength Modifier (ASCE 41 §5.4.2.4.2-4.2)

The shear demand in the panel zone is:

$$V_{PZ} = \frac{\sum M_{y,beam}}{d} \left(\frac{L}{L-d_c} \right) \left(\frac{h-d_b}{h} \right)$$

where $M_{y,beam}$ is the moment at the face of the column, projected from the flexural *yield* strength of the critical connection component (*i.e.*, $S \times F_{ye}$).

The reduced moment of inertia, I'_x , and the elastic section modulus, S'_x , at the center of the RBS are:

$$I'_x = I_x - \frac{1}{3} c t_f (4 t_f^2 - 6 d t_f + 3 d^2) = 1427 \text{ in.}^4$$

$$S'_x = 2 I'_x / d = 118 \text{ in.}^3$$

$$\therefore M_{y,RBS} = F_{ye} S'_x = 1.1(50)(118) = 6512 \text{ kip-in.} = 543 \text{ kip-ft.}$$

The moment at the column face is—neglecting small gravity load contributions:

$$M_f = M_{y,beam} = M_{y,RBS} \left(\frac{L_{clear}}{L_{clear} - 2(a+b/2)} \right) = 7040 \text{ kip-in.} = 587 \text{ kip-ft.}$$

The average story height of the columns is:

$$h = \frac{168 + 216}{2} = 192 \text{ in.}$$

Therefore, the panel zone demands (left and right) are:

$$V_{PZ,L} = \frac{7040}{24.1} \left(\frac{360}{360-20} \right) \left(\frac{192-24.1}{192} \right) = 271 \text{ kips}$$

$$V_{PZ,R} = \frac{(7040 + 7040)}{24.1} \left(\frac{360}{360-20} \right) \left(\frac{192-24.1}{192} \right) = 541 \text{ kips}$$

The panel zone strengths (left and right) are:

$$V_{y,L} = 0.55 F_{ye} t_{cw} d_c = 538 \text{ kips} \quad V_{y,R} = 0.55 F_{ye} t_{cw} d_c = 592 \text{ kips}$$

The panel zone strength ratios (left and right) are:

$$\left(V_{PZ}/V_y\right)_L = 0.50 < 0.6 \quad \left(V_{PZ}/V_y\right)_R = 0.91 > 0.9$$

$\therefore \alpha_{PZ} = 0.80$ for both connections since the ratios are outside the range of $0.6 \leq V_{PZ}/V_y \leq 0.9$.

Clear Span-to-Depth Modifier (ASCE 41 §5.4.2.4.2-4.3)

$$\frac{L_c}{d} = \frac{340}{24.1} = 14.1 > 10$$

$$\therefore \alpha_{LD} = 1.4 - 0.04 \frac{L_c}{d} = 1.4 - 0.04 \left(\frac{340}{24} \right) = 0.836$$

(The clear span-to-depth ratio is used differently for nonlinear analysis procedures.)

Beam Web and Flange Slenderness Modifier (ASCE 41 §5.4.2.4.2-4.4)

ASCE 41 is not clear if these compactness requirements are applicable at the column face or at the critical connection component (i.e., center of RBS). It is assumed here that the measurements are applicable at the face of the column because such an applicability provides the largest element slenderness values.

$$\frac{b_f}{2t_f} = 5.86 < \frac{52}{\sqrt{F_{ye}}} = 7.01$$

$$\frac{h}{t_w} = 45.9 < \frac{418}{\sqrt{F_{ye}}} = 56.4$$

$$\therefore \alpha_{SL} = 1.0$$

Therefore, the adjusted m -factors for the left and right beam-to-column connection are:

$$m = m_i \alpha_{CP} \alpha_{PZ} \alpha_{LD} \alpha_{SL} = 5.43(1.0)(0.80)(0.836)(1.0) = 3.63$$

C.1.1.4 Acceptance Criteria Check

C.1.1.4.1 Beam

The acceptance criteria check for the beam (done at the center of the RBS) is:

$$DCR_{N,L} = \frac{DCR}{m\kappa} = \frac{M_{UD}}{m\kappa M_{CE}} = \frac{2336}{8(656)} = 0.45 < 1.0$$

$$DCR_{N,R} = \frac{DCR}{m\kappa} = \frac{M_{UD}}{m\kappa M_{CE}} = \frac{2130}{8(656)} = 0.41 < 1.0$$

The left and right beam hinges satisfy the CP BPL acceptance criteria at the BSE-2 EHL.

C.1.1.4.2 Fully Restrained Connection

The acceptance criteria check for the beam-to-column connection (done at the face of the column) is:

$$DCR_{N,L} = \frac{DCR}{m\kappa} = \frac{M_{UD}}{m\kappa M_{CE}} = \frac{2533}{3.63(656 \times 1.08)} = 0.98 < 1.0$$

$$DCR_{N,R} = \frac{DCR}{m\kappa} = \frac{M_{UD}}{m\kappa M_{CE}} = \frac{2326}{3.63(709)} = 0.90 < 1.0$$

To check force-controlled action at the face of the column:

$$Q_{CLc} \geq Q_{CEb} \quad (\text{ASCE 41 Eq. 5-14})$$

$$Q_{CLc} = M_p = 1027 \left(\frac{50}{55} \right) = 934 \text{ kip-ft.}$$

$$Q_{CEb} = 830 \text{ kip-ft. } (= M_f \text{— see previous beam-to-column connection calculation})$$

$$\therefore Q_{CLc} > Q_{CEb} \text{ OK}$$

In general, the deformation-control check at the center of the RBS (or converted to the face of the column as illustrated above) will control over the force-control check because of the strength requirements in AISC 358 at the face of the column. ASCE 41 should clarify this provision. For example, should the material strength change when the same member is used for the beam and connection calculations.

The left and right beam-to-column connections satisfy the CP BPL acceptance criteria at the BSE-2 EHL.

C.1.2 SMF Column

The first story column (No. 1) at the intersection of grid lines 1 and B is selected for this example (see circled element in Figure B-19):

- W18×175
- $h_{sx} = 18 \text{ ft.}$ (L_b of the column is conservatively taken as h_{sx})
- A992 Steel: $F_{y,LB} = F_y = 50 \text{ ksi}$, $F_{ye} = 55 \text{ ksi}$, $E = 29000 \text{ ksi}$, $G = 11154 \text{ ksi}$

C.1.2.1 Axial Demand

The axial force in the column is *force-controlled* by default per ASCE 41:

$$P_{UF} = P_G \pm \frac{P_E}{C_1 C_2 J} \quad (\text{ASCE 41 } \S 3.4.2.1.2)$$

where

$$C_1 = 1.0 \quad (T > 1.0 \text{ sec.}) \text{ per ASCE 41 } \S 3.3.1.3.1$$

$$C_2 = 1.0 \quad (T > 0.7 \text{ sec.}) \text{ per ASCE 41 } \S 3.3.1.3.1$$

$$J = \max \left\{ \begin{array}{l} \min(DCR) \\ 2.0 \end{array} \right. = 2.05 \quad (\min(DCR) \text{ roof beam} = 0.83 \times 2.47 = 2.05) \quad (\text{ASCE 41 } \S 3.4.2.1.2)$$

where *DCR* is the demand-to-capacity ratio of any component in the load path delivering force to the column. For the column in this example, this is interpreted to be all beam-to-column connection DCRs on the column line at and above the second floor. The minimum value of 2.0 allowed in ASCE 41 was selected because the building is considered to be in a zone with a high level of seismicity.

Based on the controlling load combination, the demand on the column is:

$$P_G = 1.1(P_D + 0.25P_L + P_S) = 1.1(400 + 0.25(217) + 0) = 499 \text{ kips}$$

$$P_E = \pm 1.0E_x \pm 0.3E_y = 869 \text{ kips}$$

$$\therefore P_{UF} = 499 + \frac{869}{1.0(1.0)(2.05)} = 926 \text{ kips}$$

C.1.2.2 Axial Strength

In accordance with ASCE 41 §5.4.2.4.2, the lower-bound compression strength is determined as P_n from AISC 360 §E3 using $\phi_c = 1$ and $F_y = F_{y,LB} = 50$ ksi. Flexural buckling about the minor axis (*y*-axis) governs.

$$P_{CL} = P_{n,y} = A_g F_{cr,y}$$

$$\frac{K_y L_y}{r_y} \sqrt{\frac{F_{y,LB}}{E}} = \frac{1.0(216)}{2.76} \sqrt{\frac{50}{29000}} = 3.25 \leq 4.71$$

$$F_{e,y} = \frac{\pi^2 E}{\left(\frac{K_y L_y}{r_y}\right)^2} = \frac{\pi^2 (29000)}{\left(\frac{1.0(216)}{2.76}\right)^2} = 46.7 \text{ ksi}$$

$$\therefore F_{cr,y} = \left[0.658^{(F_y/F_e)}\right] F_y = 32.0 \text{ ksi}$$

$$P_{CL} = 51.3(32.0) = 1639 \text{ kips}$$

$$\frac{P_{UF}}{P_{CL}} = \frac{926}{1639} = 0.56 > 0.50 \rightarrow \text{column is } \textit{force-controlled} \text{ for flexure}$$

$$\frac{P_{UF,G}}{P_{CL}} = \frac{499}{1639} = 0.30 > \frac{P_{UF}}{P_{CL}} = 0.20 \rightarrow m \text{ is reduced for } P\text{-}M \text{ interaction}$$

$$\frac{P_{UF}}{P_{ye}} = \frac{926}{1.1(50)51.3} = 0.33 \rightarrow \text{column would be } \textit{deformation-controlled} \text{ for flexure per}$$

FEMA 273

C.1.2.3 Flexural Demand

The *force-controlled* flexure in the column is:

$$M_{UF} = M_G \pm \frac{M_E}{C_1 C_2 J} \quad (\text{ASCE 41 } \S 3.4.2.1.2)$$

Based on the controlling load combination, the moment at the bottom of the column is:

$$M_{UF} = 10 + \frac{47052}{1.0(1.0)(2.05)} = 23087 \text{ kip-in.} = 1924 \text{ kip-ft.}$$

C.1.2.4 Flexural Strength

Per ASCE 4 Section 5.4.6.4.3.2.2, the lower-bound flexural strength, M_{CL} , is determined as M_n from AISC 360 §F1 and §F2 using $\phi_b = 1.0$ and $F_y = F_{y,LB} = 50 \text{ ksi}$.

$$M_{CL} = M_n = C_b \left[M_p - (M_p - 0.7F_{y,LB}S_x)(L_b - L_p) / (L_r - L_p) \right] \leq M_p$$

$$M_{CL} = 1.44 \left[1658 - \left(1658 - \frac{0.7(50)(344)}{12} \right) \frac{(15.7 - 9.7)}{(46.8 - 9.7)} \right] = 1.44(1548) = 2229 \text{ kip-ft}$$

$$\therefore M_{CL} = M_p = 1658 \text{ kip-ft.}$$

C.1.2.5 Acceptance Criteria Check

The column acceptance criteria check is:

$$DCR_N = \frac{P_{UF}}{P_{CL}} + \frac{M_{UF}}{M_{CL}} = \frac{926}{1639} + \frac{1924}{1658} = 0.56 + 1.16 = 1.72 > 1.0 \quad (\text{ASCE 41 §5.4.2.4})$$

Therefore, the column fails to satisfy the CP BPL acceptance criteria at the BSE-2 EHL. However, it is uncertain what physical phenomenon is represented by this result—does a plastic hinge form in the column or does the column buckle out-of-plane.

C.1.3 SMF Panel Zone

The panel zone at the top of the first story column at the intersection of grid lines 1 and B is selected for this example (see circled elements in Figure B-19):

- Column = W18×175 (No. 1)
- Beam = W24×84 (No. 1)
- A992 Steel: $F_{y,LB} = F_y = 50$ ksi, $F_{ye} = 55$ ksi, $E = 29000$ ksi, $G = 11154$ ksi

C.1.3.1 Shear Demand

The panel zone demand is obtained from summing the beam moments framing into the panel zone and then subtracting out the associated column shear—gravity loads are ignored for simplicity:

$$V_{UD} = \frac{M_1}{(d_1 - t_{f1})} + \frac{M_2}{(d_2 - t_{f2})} - V_c = \frac{29835}{(24.1 - 0.77)} + 0 - 180 = 1099 \text{ kips}$$

M_1 is the moment from the right beam and $M_2 = 0$ because this panel zone is part of a one-sided beam-to-column connection.

C.1.3.2 Shear Strength

The panel zone strength is calculated from ASCE 41 Equation 5-5:

$$V_{CE} = V_{ye} = 0.55F_{ye}t_{cw}d_c = 538 \text{ kips (recall that no doubler plates are used in this study)}$$

C.1.3.3 Acceptance Criteria

The m -factor is taken from ASCE 41 Table 5-5:

$$m = 11$$

C.1.3.4 Acceptance Criteria Check

The panel zone acceptance criteria check is:

$$DCR_N = \frac{DCR}{\kappa m} = \frac{V_{UD}}{\kappa m V_{CE}} = \frac{1099}{11(538)} = 0.19 < 1.0$$

Therefore, the panel zone satisfies the CP BPL acceptance criteria at the BSE-2 EHL.

C.2 Nonlinear Assessment Examples

The following example provides guidance to how the nonlinear assessment calculations were conducted in this study. Nonlinear assessment of the selected components is performed for the following criteria:

- Nonlinear Dynamic Procedure (NDP) or Nonlinear Static Procedure (NSP)
- Median value of the record set is used for the NDP
- Collapse Prevention Building Performance Level for the BSE-2 EHL

C.2.1 SMF Beam

The second floor beam along grid line 1 between grid lines B and C is selected for this example (see circled element in Figure B-19).

- W24×84 with reduced beam sections
- $L = 30$ ft. (centerline)
- A992 Steel: $F_{y, LB} = F_y = 50$ ksi, $F_{ye} = 55$ ksi, $E = 29000$ ksi, $G = 11154$ ksi

The demands for the SMF beam are taken from the median value of the record set from the NDP.

C.2.1.1 Deformation Demand

Total curvature demand (plastic plus elastic) in the beam-to-column connection (measured at the center of the RBS) is obtained directly from the moment-curvature response of the beam hinge in the PERFORM-3D model. The total curvature demand for the left connections is:

$$\phi_{UD,L} = 0.02842 \text{ in./in.}$$

Additionally, the moment demand is:

$$M_{UD,L} = 9056 \text{ kip-in.}$$

C.2.1.2 Acceptance Criteria

The acceptance criteria in terms of plastic rotation are given in ASCE 41, Table 5-6. To compare against the moment-curvature results coming from PERFORM-3D, the plastic rotation is converted to total curvature:

$$\phi_{total,AC} = \alpha\beta \overbrace{\frac{\phi_{p,AC}}{l_p}}^{plastic} + \overbrace{\phi_y + \phi_{pe}}^{elastic}$$

$$\phi_y = \left(\frac{M_{pe}}{EI} \right)_{RBS}$$

$$\phi_{pe} = \left(\frac{M_{UD} - M_{pe}}{EI} \right)_{RBS}$$

where l_p is the plastic hinge length (taken as the length of the RBS), α is the total FR connection modifier considering the items described below, and β is the modifier that shifts the acceptance criteria from the face of the column to the centerline of the RBS. Per ASCE 41 Table 5-6, the *initial* plastic rotation acceptance criterion for a primary member with a RBS connection is:

$$\theta_{p,AC} = 0.05 - 0.00030d = 0.05 - 0.00030(24.1) = 0.0428 \text{ rad.}$$

Per ASCE 41 Table 5-4, the RBS is considered an FR connection and thus the acceptance criteria is subject to the following acceptance criteria modifications in ASCE 41 §5.4.2.4.3 (each modifier is taken as α here).

Continuity Plate Modifier (ASCE 41 § 5.4.2.4.3-4.1)

Refer to the linear analysis calculations above.

$$\alpha_{CP} = 1.0 \text{ for both connections}$$

Panel Zone Strength Modifier (ASCE 41 § 5.4.2.4.3-4.2)

Refer to the linear analysis calculations above.

$$\alpha_{PZ} = 0.80 \text{ for both connections since the ratio is outside the range of } 0.6 \leq V_{PZ}/V_y \leq 0.9 .$$

Clear Span-to-Depth Modifier (ASCE 41 § 5.4.2.4.2-4.3)

$$\frac{L_c}{d} = \frac{340}{24.1} = 14.1 > 8$$

$$\therefore \alpha_{LD} = 1.0$$

Beam Web and Flange Slenderness Modifier (ASCE 41 § 5.4.2.4-4.4)

Refer to the linear analysis calculations above.

$$\therefore \alpha_{SL} = 1.0$$

Therefore, the adjusted m-factors for the left and right beam-to-column connections are:

$$\alpha = \alpha_{CP} \alpha_{PZ} \alpha_{LD} \alpha_{SL} = (1.0)(0.80)(1.0)(1.0) = 0.8$$

Additionally, β is:

$$\beta = \frac{L_{clear}}{L'} = \frac{28.32}{26.19} = 1.081$$

where L' is the distance between RBS centerlines. This can be determined by using a simple cantilever model to convert rotation to the RBS to keep the same tip displacement.

Therefore, the acceptance criterion is:

$$\phi_p = 0.8(1.081) \left(\frac{0.0428}{16} \right) = 0.002313 \text{ in/in.}$$

$$M_{pe} = ZF_{ye} = 7874 \text{ kip-in.}$$

$$\phi_y = \frac{7874}{29000(1397)} = 0.000194 \text{ in/in.}$$

$$\phi_{pe} = \frac{9056 - 7874}{29000(1397)} = 0.0000292 \text{ in/in.}$$

$$\phi_{total,AC} = 0.002313 + 0.000194 + 0.0000292 = 0.002535 \text{ in/in.}$$

C.2.1.3 Acceptance Criteria Check

The beam-to-column connection acceptance criteria check is (based on the median of the record set):

$$DCR_{N,L} = \frac{\phi_{plastic} + \phi_{elastic}}{\kappa(\phi_y + \phi_{pe} + \phi_{p,AC})} = \frac{0.02842}{1.0(0.002535)} = 11.1 > 1.0$$

The left beam-to-column connection does not satisfy the CP BPL acceptance criteria at the BSE-2 EHL.

C.2.2 SMF Column

The first story column (No. 1) at the intersection of grid lines 1 and B is selected for this example (see circled element in Figure B-19):

- W18×175
- $h_{sx} = 18$ ft. (L_b of the column is conservatively taken as h_{sx})
- A992 Steel: $F_{y,LB} = F_y = 50$ ksi, $F_{ye} = 55$ ksi, $E = 29000$ ksi, $G = 11154$ ksi

Given that the axial-moment demand changes for each earthquake record when doing the NDP, the demands for this example are taken from the NSP at the target displacement.

C.2.2.1 Axial Demand

The compressive axial load in the column at the target displacement is:

$$P = 780.1 \text{ kips}$$

C.2.2.2 Axial Strength

In accordance with ASCE 41 §5.4.2.4.2, the lower-bound compression strength is determined as P_n from AISC 360 §E3 using $\phi_c = 1$ and $F_y = F_{y,LB} = 50$ ksi. Flexural buckling about the minor axis (y -axis) governs.

$$P_{CL} = P_{n,y} = 51.3(32.0) = 1639 \text{ kips} \rightarrow \text{refer to the linear analysis calculations above}$$

$$\frac{P}{P_{CL}} = \frac{780.1}{1639} = 0.48 < 0.50 \rightarrow \text{column is considered } \textit{deformation-controlled} \text{ for flexure}$$

C.2.2.3 Deformation Demand

Total curvature demand (plastic plus elastic) in the column hinge is obtained directly from the moment-curvature response of the column hinge in the PERFORM-3D model. The total curvature demand is:

$$\phi_{UD} = 0.00123 \text{ in./in.}$$

C.2.2.4 Acceptance Criteria

The acceptance criteria in terms of plastic rotation are given in ASCE 41 Table 5-6. To compare against the moment-curvature results coming from PERFORM-3D, the plastic rotation is converted to total curvature:

$$\frac{P}{P_{CL}} = 0.48 > 0.2$$

$$\frac{b_f}{2t_f} = 3.58 \leq \frac{52}{\sqrt{F_{ye}}} = 7.01$$

$$\frac{h}{t_w} = 18.0 \leq \frac{260}{\sqrt{F_{ye}}} = 35.1$$

$$\therefore \theta_{p,AC} = 11 \left(1 - \frac{5}{3} \frac{P}{P_{CL}} \right) \theta_y = 2.27 \theta_y$$

From ASCE 41 Equation 5-2:

$$P_{ye} = F_{ye} A = 55(51.3) = 2822 \text{ kips}$$

$$\theta_y = \frac{\overbrace{ZF_{ye} I_c}^{\theta_{y@P=0}}}{6EI_c} \left(1 - \frac{P}{P_{ye}} \right) = 0.00788 \left(1 - \frac{780.1}{2822} \right) = 0.00570 \text{ rad.}$$

However, to be consistent with the P - M interaction curve used to model the plastic hinge response, θ_y , is taken as:

$$\theta_y = \theta_{y@P=0} \beta \sqrt[1 - \left(\frac{P}{P_{ye}} \right)^\alpha]{} = 0.00788 \sqrt[1 - 0.276^{1.5}]{} = 0.00683 \text{ rad. (a 20% increase from ASCE 41)}$$

Therefore:

$$\theta_{p,AC} = 2.27(0.00683) = 0.0155 \text{ rad.}$$

Therefore, the acceptance criterion is:

$$\phi_{total,AC} = \frac{\overbrace{\theta_{p,AC}}^{plastic}}{l_p} + \overbrace{\phi_y + \phi_{pe}}^{elastic}$$

$$\phi_{y@P=0} = \frac{M_{pe}}{EI} = \frac{21890}{29000(3450)} = 0.000219 \text{ in./in.}$$

$$M_{CE} = 1.18 \left(1 - \frac{P}{P_{ye}} \right) M_{pe} = 1.18(1 - 0.276)(21890) = 18701 \text{ kip-in} \quad (\text{ASCE 41 Eq 5-4})$$

However, ASCE 41 Equation 5-4 is impossible to implement in PERFORM-3D. Thus to be consistent with the P - M interaction curve used to model the plastic hinge response, the following is used:

$$M_{CE} = M_{pe} \times \beta \sqrt[1.5]{1 - \left(\frac{P}{P_{ye}} \right)^\alpha} = 21890 \times 1.1 \sqrt[1.5]{1 - 0.276^{1.5}} = 18984 \text{ kip-in.} \quad (\text{see PERFORM-3D})$$

$$\phi_y = \frac{M_{CE}}{EI} = \frac{18984}{29000(3450)} = 0.000190 \text{ in./in.}$$

$$\phi_{pe} = \frac{M_t - M_{CE}}{EI} = \frac{20205 - 18984}{29000(3450)} = 0.0000122 \text{ in./in.}$$

Therefore,

$$\phi_{total,AC} = \frac{\overbrace{0.0155}^{plastic}}{20.0} + \overbrace{0.000190 + 0.0000122}^{elastic} = 0.0009783 \text{ in./in.}$$

C.2.2.5 Acceptance Criteria Check

The column hinge acceptance criteria check is:

$$DCR_N = \frac{\phi_{plastic} + \phi_{elastic}}{\kappa(\phi_y + \phi_{pe} + \phi_{p,AC})} = \frac{0.00123}{1.0(0.000978)} = 1.26 > 1.0$$

Therefore, the column fails to satisfy CP BPL acceptance criteria at the BSE-2 EHL—for the NSP.

C.2.3 SMF Panel Zone

The panel zone at the top of the first story column at the intersection of grid lines 1 and B is selected for this example (see circled element in Figure B-19).

- Column = W18×175 (No. 1)
- Beam = W24×84 (No. 1)
- A992 Steel: $F_{y,LB} = F_y = 50 \text{ ksi}$, $F_{ye} = 55 \text{ ksi}$, $E = 29000 \text{ ksi}$, $G = 11154 \text{ ksi}$

The demands for the panel zone are taken from the NSP at the target displacement.

C.2.3.1 Deformation Demand

The panel zone demand taken as the total shear deformation (plastic plus elastic) is obtained directly from the shear-shear strain response of the shear hinge in the PERFORM-3D model. The total shear strain demand is:

$$\gamma_{UD} = 0.00187 \text{ rad.}$$

C.2.3.2 Acceptance Criteria

The acceptance criteria in terms of plastic shear angle are given in ASCE 41 Table 5-6. To compare against the strain results coming from PERFORM-3D, the plastic shear angle is converted to total shear angle:

$$\gamma_{p,AC} = 11\theta_y \text{ rad.}$$

where θ_y is the angular shear deformation of the panel zone.

$$\theta_y \equiv \gamma_y = \frac{\tau_y}{G} = \frac{0.55F_{ye}}{G} = \frac{0.55(55)}{11154} = 0.00271 \text{ rad.}$$

$$\therefore \gamma_{p,AC} = 11(0.00271) = 0.0298$$

$$\therefore \gamma_{total,AC} = 0.00271 + 0.0298 = 0.0325$$

C.2.3.3 Acceptance Criteria Check

The panel zone acceptance criteria check is:

$$DCR_N = \frac{\gamma_{UD}}{\kappa \gamma_{AC}} = \frac{0.00187}{0.0325} = 0.057 < 1.0$$

Therefore, the panel zone satisfies the CP BPL acceptance criteria at the BSE-2 EHL—for the NSP.

Appendix D References

AISC (1989). *Specification for Structural Steel Buildings: Allowable Stress Design and Plastic Design*. American Institute of Steel Construction, Chicago, IL.

AISC (1999). *Wide-Flange Column Stiffening at Moment Connections – Design Guide 13*. American Institute of Steel Construction, Chicago, IL.

AISC (2002). *Seismic Provisions for Structural Steel Buildings – ANSI/AISC 341-02*. American Institute of Steel Construction, Chicago, IL.

AISC (2005). *Specification for Structural Steel Buildings – ANSI/AISC 360-05*. American Institute of Steel Construction, Chicago, IL.

AISC (2010a). *Specification for Structural Steel Buildings – ANSI/AISC 360-10*. American Institute of Steel Construction, Chicago, IL.

AISC (2010b). *Seismic Provisions for Structural Steel Buildings – ANSI/AISC 341-10*. American Institute of Steel Construction, Chicago, IL.

AISC (2010c). *Prequalified Connections for Special and Intermediate Steel Moment Frames for Seismic Applications – ANSI/AISC 358-10*. American Institute of Steel Construction, Chicago, IL.

AISC (2013). *Stability Design of Steel Buildings – Design Guide 28*. American Institute of Steel Construction, Chicago, IL.

ASCE (2005). *Minimum Design Loads for Buildings and Other Structures – ASCE/SEI 7-05*. American Society of Civil Engineers, Reston, VA.

ASCE (2006). *Seismic Rehabilitation of Existing Buildings – ASCE/SEI 41-06*. American Society of Civil Engineers, Reston, VA.

ASCE (2010). *Minimum Design Loads for Buildings and Other Structures – ASCE/SEI 7-10*. American Society of Civil Engineers, Reston, VA.

ASCE (2014). *Seismic Evaluation and Retrofit of Existing Buildings – ASCE/SEI 41-13*. American Society of Civil Engineers, Reston, VA.

ASCE (2016). *Minimum Design Loads for Buildings and Other Structures – ASCE/SEI 7-16*. American Society of Civil Engineers, Reston, VA. *In Progress*.

CBSC (2010) *California Code of Regulations, Part 2 – California Building Standards Code – Title 24*. California Building Standards Commission, Sacramento, California.

CSI (2011a). ETABS (Version 9.7.4) [Computer Software]. Computers and Structures, Inc., Berkeley, CA.

CSI (2011b). PERFORM-3D (Version 5.0) [Computer Software]. Computers and Structures, Inc., Berkeley, CA.

CSI (2011c). *Components and Elements for PERFORM-3D and PERFORM-COLLAPSE* (Version 5.0). Computers and Structures, Inc., Berkeley, CA.

CSI (2011d). *User Guide PERFORM-3D* (Version 5.0). Computers and Structures, Inc., Berkeley, CA.

Engelhardt, M.D., Winneberger, T., Zekany, A.J., and Potyraj, T.J. (1998). “Experimental Investigation of Dogbone Moment Connections”. *Engineering Journal*, AISC, 4th Quarter, pp. 128-139.

FEMA (1997). *NEHRP Guidelines for the Seismic Rehabilitation of Buildings – FEMA 273*. Federal Emergency Management Agency, Washington, D.C.

FEMA (2000a). *Recommended Seismic Design Criteria for New Steel Moment Frame Buildings – FEMA 350*. Federal Emergency Management Agency, Washington, D.C.

FEMA (2000b). *Recommended Seismic Evaluation and Upgrade Criteria for Existing Welded Steel Moment Frame Buildings – FEMA 351*. Federal Emergency Management Agency, Washington, D.C.

FEMA (2000c). *State of the Art Report on Connection Performance – FEMA 355D*. Federal Emergency Management Agency, Washington, D.C.

FEMA (2000d). *State of the Art Report on Performance Prediction and Evaluation – FEMA 355F*. Federal Emergency Management Agency, Washington, D.C.

FEMA (2000e). *Prestandard and Commentary for the Seismic Rehabilitation of Buildings – FEMA 356*. Federal Emergency Management Agency, Washington, D.C.

FEMA (2000f). *Global Topics Report on the Prestandard and Commentary for the Seismic Rehabilitation of Buildings – FEMA 357*. Federal Emergency Management Agency, Washington, D.C.

FEMA (2005). *Improvements of Nonlinear Static Seismic Analysis Procedures – FEMA 440*. Federal Emergency Management Agency, Washington, D.C.

FEMA (2009a). *Quantification of Building Seismic Performance Factors – FEMA P695*. Federal Emergency Management Agency, Washington, D.C.

FEMA (2009b). *NEHRP Recommended Seismic Provisions for New Buildings and Other Structures – FEMA P-750*. Federal Emergency Management Agency, Washington, D.C.

FEMA (2009c). *Effects of Strength and Stiffness Degradation on Seismic Response* – FEMA P-440A. Federal Emergency Management Agency, Washington, D.C.

FEMA (2012). *Seismic Performance Assessment of Buildings* – FEMA P-58. Federal Emergency Management Agency, Washington, D.C.

FEMA (2015). *NEHRP Recommended Seismic Provisions for New Buildings and Other Structures*. Federal Emergency Management Agency, Washington, D.C. *In Progress*.

GSA (2012). *Facilities Standards for the Public Buildings Service* – PBS-P100. U.S. General Services Administration, Washington, D.C.

Harris, J.L. and Speicher, M.S. (2015). *Assessment of First Generation Performance-Based Design Methods for New Steel Buildings, Volume 2: Special Concentrically Braced Frames* – NIST TN 1863-2. National Institute of Standards and Technology, Gaithersburg, MD.

Haselton, C.B., Kircher, C.A., and Liel, A.B. (2009). “Concept Paper on Utilizing the FEMA P695 (ATC-63) Ground Motion Spectral Shape Guidelines to Adjust the Target Displacement in the ASCE/SEI 41 Nonlinear Static Procedure” *Proc.*: ATC & SEI 2009 Conference on Improving the Seismic Performance of Existing Buildings and Other Structures, San Francisco, CA Dec. 9-11, 2009.

ICC (2012a). *International Existing Building Code (IEBC)*. International Code Council, Washington, DC.

ICC (2012b). *International Building Code (IBC)*. International Code Council, Washington, DC.

Krawinkler, H., Bertero, V.V., and Popov, E.P. (1971). *Inelastic Behavior of Steel Beam-to-Column Subassemblages* – Report No. UCB/EERC-71/07. Earthquake Engineering Research Center, University of California, Berkeley, CA, October 1971.

Krawinkler, H. (1978). “Shear in Beam Column Joints in Seismic Design of Steel Frames”. *Engineering Journal*, AISC, 3rd Quarter, pp. 82-91.

Lee, D., Cotton, S.C., Dexter, R.J., Hajjar, J.F., Ye, Y. and Ojard, S.D. (2002). *Column Stiffener Detailing and Panel Zone Behavior of Steel Moment Frame Connections* – Report No. ST-01-3.2. Dept. of Civil Engineering, University of Minnesota, Minneapolis, MN, 2002.

NIBS (2013). *National Performance-Based Design Guide for Buildings*. National Institute of Building Sciences, Washington, D.C.

NIST (2009a). *Research Required to Support Full Implementation of Performance-Based Seismic Design* – NIST GCR 09-917-2. Produced by the Building Seismic Safety Council for the National Institute of Standards and Technology, Gaithersburg, MD.

NIST (2009b). *Seismic Design of Steel Special Moment Frames: A Guide for Practicing Engineers*, NEHRP Seismic Design Technical Brief No. 2 – NIST GCR 09-917-3. Produced by the NEHRP Consultants Joint

Venture, a partnership of the Applied Technology Council and the Consortium of Universities for Research in Earthquake Engineering, for the National Institute of Standards and Technology, Gaithersburg, MD.

NIST (2010a). *Nonlinear Structural Analysis for Seismic Design: A Guide for Practicing Engineers*, NEHRP Seismic Design Technical Brief No. 4 – NIST GCR 10-917-5. Produced by the NEHRP Consultants Joint Venture, a partnership of the Applied Technology Council and the Consortium of Universities for Research in Earthquake Engineering, for the National Institute of Standards and Technology, Gaithersburg, MD.

NIST (2010b). *Evaluation of the FEMA P-695 Methodology for Quantification of Building Seismic Performance Factors* – NIST GCR 10-917-8. Produced by the NEHRP Consultants Joint Venture, a partnership of the Applied Technology Council and the Consortium of Universities for Research in Earthquake Engineering, for the National Institute of Standards and Technology, Gaithersburg, MD.

NIST (2010c). *Applicability of Nonlinear Multi-Degree-of-Freedom Modeling for Design* – NIST GCR 10-917-9. Produced by the NEHRP Consultants Joint Venture, a partnership of the Applied Technology Council and the Consortium of Universities for Research in Earthquake Engineering, for the National Institute of Standards and Technology, Gaithersburg, MD.

NIST (2011a). *Standards of Seismic Safety for Existing Federally Owned and Leased Buildings: ICSSC Recommended Practice 8 (RP 8)* – NIST GCR 11-917-12. Produced by the Building Seismic Safety Council of the National Institute of Building Sciences for the National Institute of Standards and Technology, Gaithersburg, MD.

NIST (2011b). *Seismic Design of Composite Steel Deck and Concrete-filled Diaphragms: A Guide for Practicing Engineers*, NEHRP Seismic Design Technical Brief No. 5 – NIST GCR 11-917-10. Produced by the NEHRP Consultants Joint Venture, a partnership of the Applied Technology Council and the Consortium of Universities for Research in Earthquake Engineering, for the National Institute of Standards and Technology, Gaithersburg, MD.

NIST (2011c). *Research Plan for the Study of Seismic Behavior and Design of Deep, Slender Wide-Flange Structural Steel Beam-Column Members* – NIST GCR 11-917-13. Produced by the NEHRP Consultants Joint Venture, a partnership of the Applied Technology Council and the Consortium of Universities for Research in Earthquake Engineering, for the National Institute of Standards and Technology, Gaithersburg, MD.

NIST (2011d). *Selecting and Scaling Earthquake Ground Motions for Performing Response-History Analyses* – NIST GCR 11-917-15. Produced by the NEHRP Consultants Joint Venture, a partnership of the Applied Technology Council and the Consortium of Universities for Research in Earthquake Engineering, for the National Institute of Standards and Technology, Gaithersburg, MD.

NIST (2012). *Tentative Framework for Development of Advanced Seismic Design Criteria for New Buildings* – NIST GCR 12-917-20. Produced by the NEHRP Consultants Joint Venture, a partnership of

the Applied Technology Council and the Consortium of Universities for Research in Earthquake Engineering, for the National Institute of Standards and Technology, Gaithersburg, MD.

NIST (2013). *Seismic Design of Steel Special Concentrically Braced Frame Systems: A Guide for Practicing Engineers*, NEHRP Seismic Design Technical Brief No. 8 – NIST GCR 13-917-24. Produced by the NEHRP Consultants Joint Venture, a partnership of the Applied Technology Council and the Consortium of Universities for Research in Earthquake Engineering, for the National Institute of Standards and Technology, Gaithersburg, MD.

Paret, T.F., Searer, G.R., and Freeman, S.A. (2011). “ASCE 31 and 41: Apocalypse Now”. *Proc.: Structures Congress 2011*, Las Vegas, NV, April 14-16, 2011.

Pekelnicky, R. and Poland, C. (2012). “ASCE 41-13: Seismic Evaluation and Retrofit Rehabilitation of Existing Buildings”. *Proc.: 2012 SEAOC-SEANM Convention*, Santa Fe, NM, Sept. 12-15, 2012.

SEAONC (2010) “Perspectives on ASCE 41 for Seismic Rehabilitation of Building – Survey by the Structural Engineers Association of Northern California”. *Structures Magazine*, Oct. 2010.

Toranzo-Dianderas, L.A. (2009). “Evaluation of the ASCE 41 Linear Elastic Procedure for Seismic Retrofit of Existing Structures: Pros and Cons of the Method.” *Proc.: ATC & SEI 2009 Conference on Improving the Seismic Performance of Existing Buildings and Other Structures*, San Francisco, CA Dec. 9-11, 2009.

Troup, E. (1999). “Effective Contract and Shop Drawings for Structural Steel”. *Proc.: North American Steel Construction Conference*, Toronto, Ontario, Canada, May 19-21, 1999.

White, D.W. and Hajjar, J.F. (1997). “Design of Steel Frames without Consideration of Effective Length”. *Engineering Structures*, Vol. 19(10), pp. 797-810.